UNIVERSITY OF OKLAHOMA

GRADUATE COLLEGE

WOODFORD SHALE ENCLOSED MINI-BASIN FILL ON THE HUNTON PALEO SHELF. A DEPOSITIONAL MODEL FOR UNCONVENTIONAL RESOURCE SHALES

A DISSERTATION

SUBMITTED TO THE GRADUATE FACULTY

in partial fulfillment of the requirements for the

Degree of

DOCTOR OF PHILOSOPHY

By

EMILIO J. TORRES-PARADA

Norman, Oklahoma
2020

WOODFORD SHALE ENCLOSED MINI-BASIN FILL ON THE HUNTON PALEO SHELF. A DEPOSITIONAL MODEL FOR UNCONVENTIONAL RESOURCE SHALES

A DISSERTATION APPROVED FOR THE

UNIVERSITY OF OKLAHOMA

SCHOOL OF GEOSCIENCES

BY THE COMMITTEE CONSISTING OF

Dr. Kurt J. Marfurt, Chair

Dr. Roger M. Slatt, Co-chair

Dr. Deepak Devegowda

Dr. Michael Engel

Dr. R. Paul Philp

To Heydi, Simón, Antonia, Lorenzo and all my family

With them on my side, everything is possible!

In memoriam of Jose M. Torres-Mantilla (1954-2012), my beloved Dad
In memoriam of Dr. Roger Slatt. It's been an awesome ride! "at any rate!..."

"Con Dios todo y sin el nada"

Acknowledgments

I want to express my highest gratitude to many different people who supported and encouraged me to pursue my goals and dreams. I have really enjoyed my years as a sooner.

I would like to express my deepest gratitude to Dr. Roger M. Slatt, who very generously accepted to be my advisor. I am very grateful for his guidance, mentoring, friendship and support throughout many years. He has always believed in me and been a constant support to all my research projects. He has kindly advised and helped my family and myself for coming to OU during the past ten years and also nicely accepted to be leading my faculty committee and supported "*Emilio's ideas."* He is more than a friend and mentor. I will continue your legacy.

To Dr. Kurt Marfurt, "*El Cacique!".* Many thanks for all your help and constant support. For influencing and encouraging me the passion of the quantitative seismic analyses. Many thanks for your reviews, suggestions, talks and co-authoring my work.

To Dr. R. Paul Philp, for serving on my committee, for your kind and constant support. Many thanks for guiding me all these years in my petroleum geochemistry learning curve. I highly appreciate the time and dedication of co-authoring my technical products and review of this manuscript.

I wish to extend my gratitude to Dr. Michael Engel and R. Deepak Devegowda for serving as committee members and helping me in reviewing my technical products and guiding my research.

My most profound appreciation to 89 Energy, it has been a great ride! To John-Mark Beaver, Kyle Shipley, Farsheed Rock, Darien Whitehurst, Ryan Rickett, Brian Collins, Lexy Sikes, James Head, Kurt Hibbard, Jacob Hendrickson, Adam Chapman, Andrew Haraway, Kevin Manning, Kim McAuliffe, and Megan Honeycutt. I have learned and accomplished a lot that without your kind support, it couldn't be possible. I miss the MEP challenges and the "the thirsty kids."

Special thanks to the American Association of Petroleum Geologist AAPG grants-in-aid program (GIA), to The Society of Exploration Geophysicists SEG scholarship foundation and to the OU Colombian Student Association COLSA COUAA foundation. To all of them for honoring me as an active member and as a recipient of scholarship awards, which provided me financial support to conduct and conclude my doctoral studies.

My special gratitude to the OU Institute of Reservoir Characterization (IRC) staff and students, for their financial and technical support. Also, I would like to thank IRC current and former members and sponsors for all the technical discussions and recommendations during my doctoral research experience and field trips that I was able to lead. Special thanks to Henry Galvis-Portilla and Daniela Becerra-Rondon for their friendship, technical data sets and support.

My thankfulness to the people from the OU Organic Geochemistry Laboratories, in particular to Mr. Jon Allen for his helpful technical support; to Dr. Xiaolei Liu, Dr. Tomaz Kurder, Dr. Than Nguyen, Carl Symcox, Cecilia Lopez-Gamundi, Lydia Jones, Gregory T. Connock, Britney Tamborello, Larry Hayde and Tara Putri for their assistance; special thanks to Dr. Andreina Liborius-Parada for her time, advice and recommendations.

My special appreciation to the OU AASPI consortium director, staff, students, and sponsors. It has been an enjoyable experience to learn geophysics with them. Special thanks to Humble Geological Services for the Rock-Eval pyrolysis analyses and to Schlumberger and CGG for their software academic licenses and support.

I want to acknowledge the entire directors, faculty, and staff members of the OU Mewbourne college of earth and energy (MCEE) and Mewbourne school of geosciences. For honoring me with student award recognitions, scholarships, helping me to continually grow as a professional and contributing to achieving my doctoral degree. I also would like to show my special appreciation to Mrs. Rebeca Fay, Mrs. Nancy Leonard, and Mrs. Yoana Walschap.

Many thanks to all my friends from the University, COLSA, and outside OU, who have accompanied me during this journey. For their joy, help, and support to the *"Emilio's team":* Saurabh Sinha, Dr. Lennon Infante-Paez, Dr. Jing Zhang, David Duarte, David Prado, Dr. Rafael Pires Da Lima, Dr. Benmadi Milad, Dr. Sayantan Ghosh, Carolina Mayorga, Dr. Antonio Cervantes, Alexandro Vera, Gustavo Leon, Maria Cofano, Andres Hernan Ruiz, Thang Ha, Dr. Fuge Zhou, Jean Amorocho, Hernando Delgado, Marco Vignali, Juan Ramon Torres, Jose Moreno, Michael Mendez, Sergio Mendez, Dr. Carlos Molinares, Luis Castillo, Dr. Richard Brito, Dr. Gabriel Machado, and Dr. Andreina Liborius-Parada. In memoriam of Mr. Jerry Wilson.

My most special thanks extended to my mom Ana Mercedes, brother Jose Manuel Jr., sister Laura, nephews Sebastian, and Camilo. To my family-in-law Rodrigo, Gladys, Laura and Thomas. Both families are the dearest people in my life. Thank you for your love, patience, support, and for always trusting in me. In the loving memory of my father, Jose Manuel Torres-Mantilla, who always believed, advised and encouraged me. *Viejito,* I am still missing you a lot!

Last but never least, a special dedication to my lovely, energetic, caring and wonderful wife, **Heydi Rodriguez-Cardenas**, for her priceless love and support. For believing that coming to OU has been the best journey of our lives. For co-authoring in my technical work and also and for always encouraging me through each step of the way. You are a fantastic person for giving me the best things I ever had, our kids Simon and Antonia. Heydi, *"you are the real MVP!"*. Simon and Antonia, when you read this, I hope you feel proud of your dad. This journey has always been planning about the best for you guys. This journey is made with lots of love for you, my beloved kids. Also, a special dedication to our puppy Lorenzo!

Thanks, *y'all* very much!!!

"Gracias, totales!!!"

Table of contents

List of figures

List of tables

Abstract

The exploration of unconventional hydrocarbon resources of the Woodford Shale in Oklahoma (USA) has focused on characterizing this formation as an entirely open marine deposit. The impact of recognizing the enclosed mini-basin fill settings remains under-explored. To better understand these effects, I propose a detailed integrated study to highlight how these depositional variations occur. It is necessary to perform a workflow that involves multidisciplinary integration of geological, geochemical (both organic and inorganic) and geophysical characterizations to identify the characteristics of these deposits, how they vary vertically in the stratigraphic section of the Woodford Shale (internal variations in organic matter content and type; variability of the major heavy elements; and differences in mineralogy), and how they are laterally dissimilar by analyzing and comparing different Woodford locations in the Oklahoman petroleum provinces.

The enclosed mini-basin fill settings occur locally in areas of thicker (gross thickness greater than 200 ft) and more organic-rich Woodford Shale (greater than 5.5 % on average of total organic carbon TOC). By understanding the context of regional sea-level fluctuations in the Upper Devonian time, it is observed that the Woodford Shale is deposited upon a pre-existent carbonate platform, where this platform was previously eroded by karstification or incised valley development during regional sea level drops at the pre-Woodford time. These karst/incised valley-forming processes formed a regional erosional unconformity, which allowed the development of sinkholes, pockets, and pods with more accommodation space for Woodford Shale sediment deposition in enclosed mini-basin fill settings. These erosional unconformities can be identified in outcrops, cores, well logs, and on 3D seismic data sets. I propose that the localized and discontinuous enclosed mini-basin fills settings represented silled constricted oceanic circulation with higher bottom-water euxinia (high free sulfur), which had better conditions for accumulation

and preservation of clay and organic matter particles than did the well-circulated, open marine settings. I interpret that these depositional differences provide recognizable patterns in bed thickness and organic matter variations inside the Woodford Shale. I propose that areas in Oklahoma with thicker Woodford enclosed mini-basin fill settings are stratigraphical variations that could economically produce more oil and gas than other areas deposited under more open marine conditions or thinner enclosed mini-basin fill intervals. I capture these intervals by determining which ones contain more organic matter, more hydrogen, lower oxygen, more amorphous organic matter (more oil-prone than gas prone), the differences in paleo water chemistry (water column stratification, higher water salinity, higher levels of anoxia and euxinia). I recognize that these enclosed mini-basin fill geochemical characteristics are combined with the identification of enrichments in detrital quartz and relatively high depletions in the clay content of the lithofacies. The enclosed mini-basin fill deposits not only accumulate more organic matter but present different petrophysical and mechanical characteristics that, when modeled, simulated and compared with reported production, recover higher volumes of hydrocarbons under the standard unconventional petroleum industry operational practices.

Introduction

Four sections and integrated conclusions are presented in this manuscript. These represent the description, interpretations, and applications of detailed geological, geochemical, and geophysical analyses of Woodford Shale's successions in different provinces of Oklahoma, USA. By integrating a series of discrete methodologies and data sets, I describe and interpret some of the Woodford rock intervals as enclosed mini-basin fill deposits within an overall open marine setting. This document builds on the premise that the Woodford Shale is not entirely an open marine deposit and is not homogeneous in its vertical stratigraphy or lateral continuity. I propose a consistent way to build robust, reliable geological, geochemical, and petrophysical data sets and combine them with quantitative 3D seismic interpretations and estimations of inorganic composition, organic matter, and rock mechanic properties. These data sets can be used to interpret sequence stratigraphy relationships, build regional sequence stratigraphic correlations, and highlight environmental conditions that can be used to identify targets for hydrocarbon exploration. Also, the applicability is to evaluate how the depositional environment and resulting deposits changed through geologic time within a dominantly marine shale and simulate the hydrocarbon production and recovery in these areas under standard unconventional shale practices.

Significance of Chapter I: This section is the introduction to the Woodford Shale, the internal member subdivision, and previous characterizations of the Woodford Shale. It also presents the definition of enclosed mini-basin fill settings and their relationship within the depositional stages of the Woodford Shale under major marine conditions. This section of the dissertation introduces a critical component, the scientific importance of identifying the features of the Woodford enclosed mini-basin fill deposits from commonly considered open marine deposits in the rock record. This research is the first to be made with an unconventional marine

shale to evaluate the internal occurrence of enclosed mini-basin fill deposits and might lead to the unconventional shale resource assessment for further considerations of these unconventional reservoirs.

Significance of Chapter II: This section shows how stratigraphic sequence frameworks built from seismic data sets compare to sequence stratigraphic interpretations made from lithostratigraphy and well log information in a study area with poor well control and unavailable core samples (drilling cutting samples were the only samples available). The study area is in the Cherokee platform, Seminole County, Oklahoma. This chapter explains the workflow for performing a detailed quantitative 3D seismic analysis that allows the identification of pre-Woodford eroded strata, and the calculation and quantification of total organic matter (%TOC) volumes using machine learning probabilistic workflows. The vertical and lateral variability of Woodford Shale %TOC volumes, purely identified from high vertical resolution 3D seismic, combined with the interpreted lateral and vertical seismic stratigraphic variations, allowed to understand the areas where enclosed mini-basin fill settings might occur at seismic scale, and concentrate more %TOC.

Significance of Chapter III: This section is the detailed characterization of geological and geochemical (organic-inorganic) properties in a 314 ft type section of the Woodford Shale, named the Speake Ranch outcrop. This outcrop is in Murray County, at the south end of the SCOOP Oklahoma petroleum province. I characterize in this section both open marine and enclosed mini-basin fill intervals. The geological characterization in this part of the dissertation was complemented to that previously made in this outcrop by Becerra-Rondon (2017), Galvis (2017), and Galvis et al. (2017). This chapter helps to establish in detail the significance and relationship of different organic compounds (biomarkers), when correctly identified and measured, to the

vertical variability within a stratigraphic profile. When geochemistry is representative of basin conditions at the time of deposition, it is useful as the basis for a regional sequence stratigraphic framework of the Woodford Shale. I correlate the outcrop rock mechanics characteristics and lateral extent of these geological-geochemical profiles to subsurface wells. Additionally, I present the regional state-wide mapping of subsea structure, gross thickness, average organic matter content, and average thermal maturity of thousands of sampled wells with Woodford Shale penetrations in Oklahoma.

Significance of Chapter IV: This chapter shows the identification of enclosed mini-basin fill settings in northern Oklahoma. Also, this chapter displays how a detailed geological-geochemical-seismic-geomechanics machine learning-oriented characterization serves as the guide of unconventional static reservoir models, and input for the production simulation of Woodford Shale resources. The static reservoir model and simulation was performed in areas identified as restricted enclosed mini-basin fill, compared with areas designated as open marine within the 3D seismic survey with known cumulative production data. The simulation part supports current unconventional horizontal production and operation plans. The vertical and lateral variability of Woodford Shale %TOC, density, and rock mechanics (Young's modulus, Poisson ratio, shear modulus, Biot's modulus, fracture gradient, fracture toughness) volumes, combined with the interpreted seismic attribute lateral and vertical stratigraphic variations, allowed to understand the areas where enclosed mini-basin fill settings occur at seismic scale and where they produced more hydrocarbons under similar operational drilling and completion practices.

Appendix A: Refers to the methodology applied in Chapter III and Chapter V for estimating the dynamic rock mechanics properties in the Woodford Shale (Young's modulus,

Poisson ratio, shear modulus, Biot's modulus, fracture gradient, fracture toughness), from literature considerations using sonic and density well logs.

Appendix B: Explains the analytical techniques and workflows for the Chapter III organic matter extractions to Woodford Shale rock samples, the organic compound separation, and analysis of the different biomarker compounds.

Appendix C: This appendix corresponds to the Rock-Eval analysis of the Woodford Shale at different locations in the state of Oklahoma from masters and doctoral thesis data sets of the Institute of Reservoir Characterization (IRC) at The University of Oklahoma. This characterization serves to compare the variability of the Woodford Shale organic matter content and maturity levels at different locations of the Oklahoman petroleum provinces.

Appendix D: This appendix shows the organic compound structures of the applied biomarkers in Chapter III.

Chapter I: The concept of enclosed mini-basin fill

Over the last decade, unconventional resources (coalbed methane, tight gas, shale gas, shale oil, gas hydrates, and deep-basin gas systems) have become significant providers of natural gas and oil in the United States basins (Figure 1.1). The most useful resource, the gas/oil shale, has been developed and used to test exploratory concepts. Unconventional shale systems have proved that the generation of resources and storage occur within the same formation (Cardott 2014), establishing the concept of a self-sourced system. These successful exploratory concepts have brought considerable interest in hydrocarbon source rocks characterization where these fine-grained, organic-rich rocks are both the source and the reservoir (EIA, 2016).

Most of the North American resource shale systems are the Marcellus, Utica-Point Pleasant, Eagle Ford, Barnett, Horn River, Niobrara, Mowry, Spraberry, Bone Spring, and Wolfcamp Shales (Figure 1.1; EIA, 2016). The Woodford Shale in the Oklahoman basins (Figure 1.2 and Figure 1.3) has been characterized as a set of marine unconventional shale sequences with the common characteristic of being deposited above a carbonate formation where the paleo sea-level fluctuations allowed the formation of erosional surfaces (Figure 1.4; Comer and Hinch, 1987; Johnson and Cardott, 1990; Comer 1992 and 2005). The erosional events which occurred before the Woodford Shale layers were deposited (Figure 1.4) produced paleo depressions by the interactions of physical weathering, incised valley formation, and karstification processes, causing chemical reactions and de-watering effects of the carbonate (Hunton Group) pre-existing strata (Johnson and Cardott, 1990; Comer, 2005; Slatt et al., 2012; Slatt, 2016). The combination of these processes produced a regional erosional surface maker at the base of the Woodford Shale, as is shown in Figure 1.4, and these depocenters of water “pools” are referred in this study as the enclosed mini-basin fill settings (Figure 1.5).

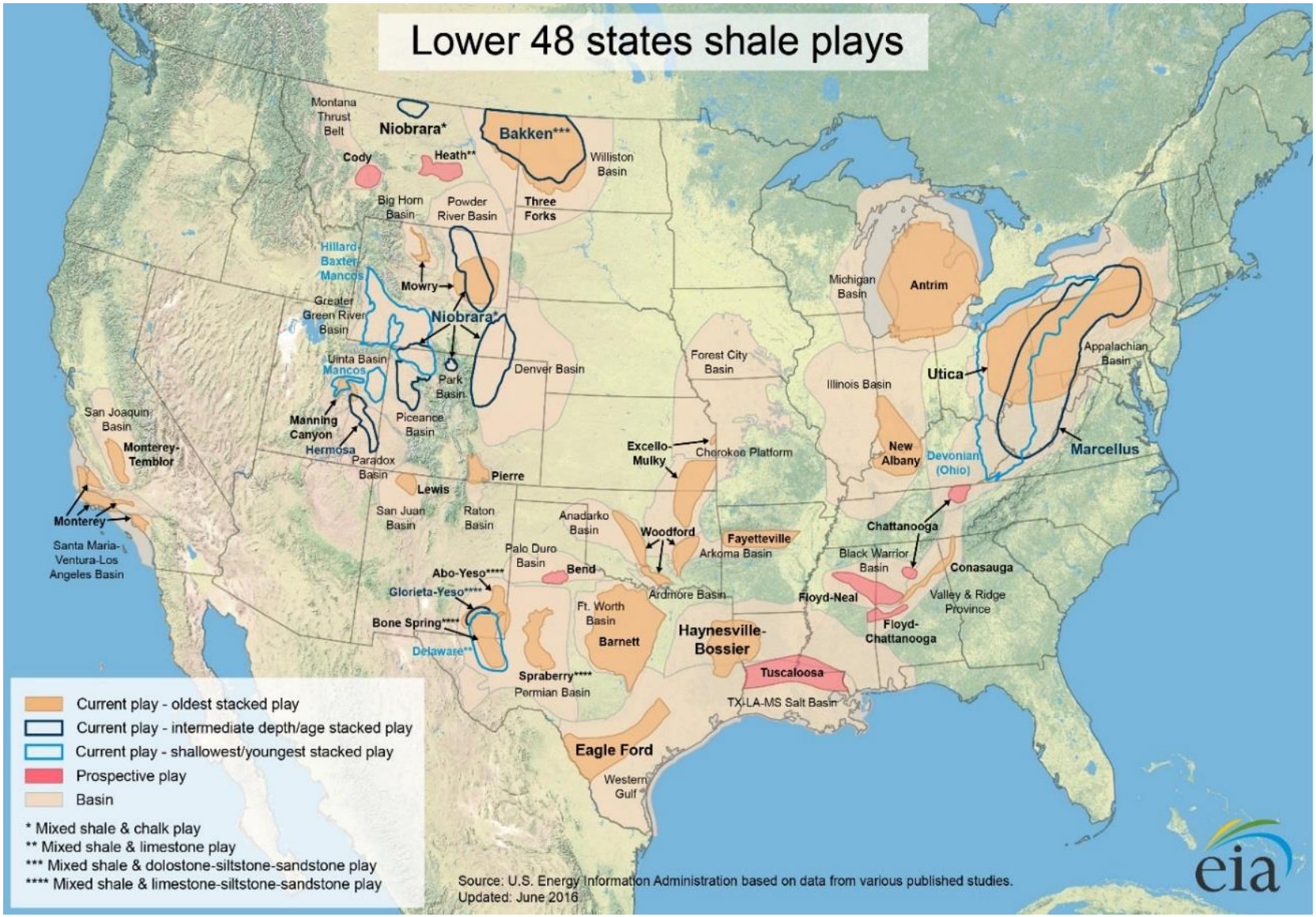

Figure 1.1. U.S. shale gas plays, Lower 48 states (EIA June 30, 2016). Source: Energy Information Administration (EIA), 2016.

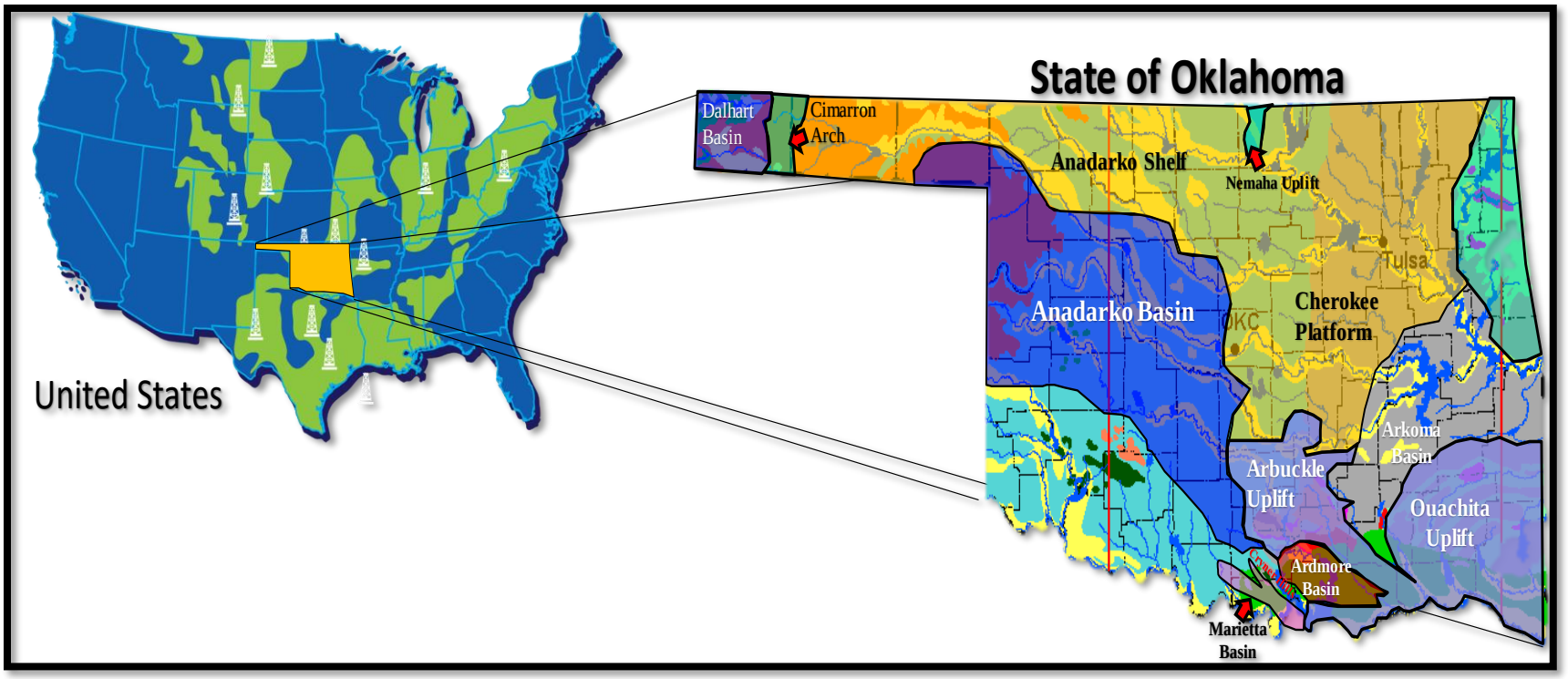

Figure 1.2. State of Oklahoma Sedimentary basins. Modified after Energy Information Administration (2016), and Liborius et al. (2017).

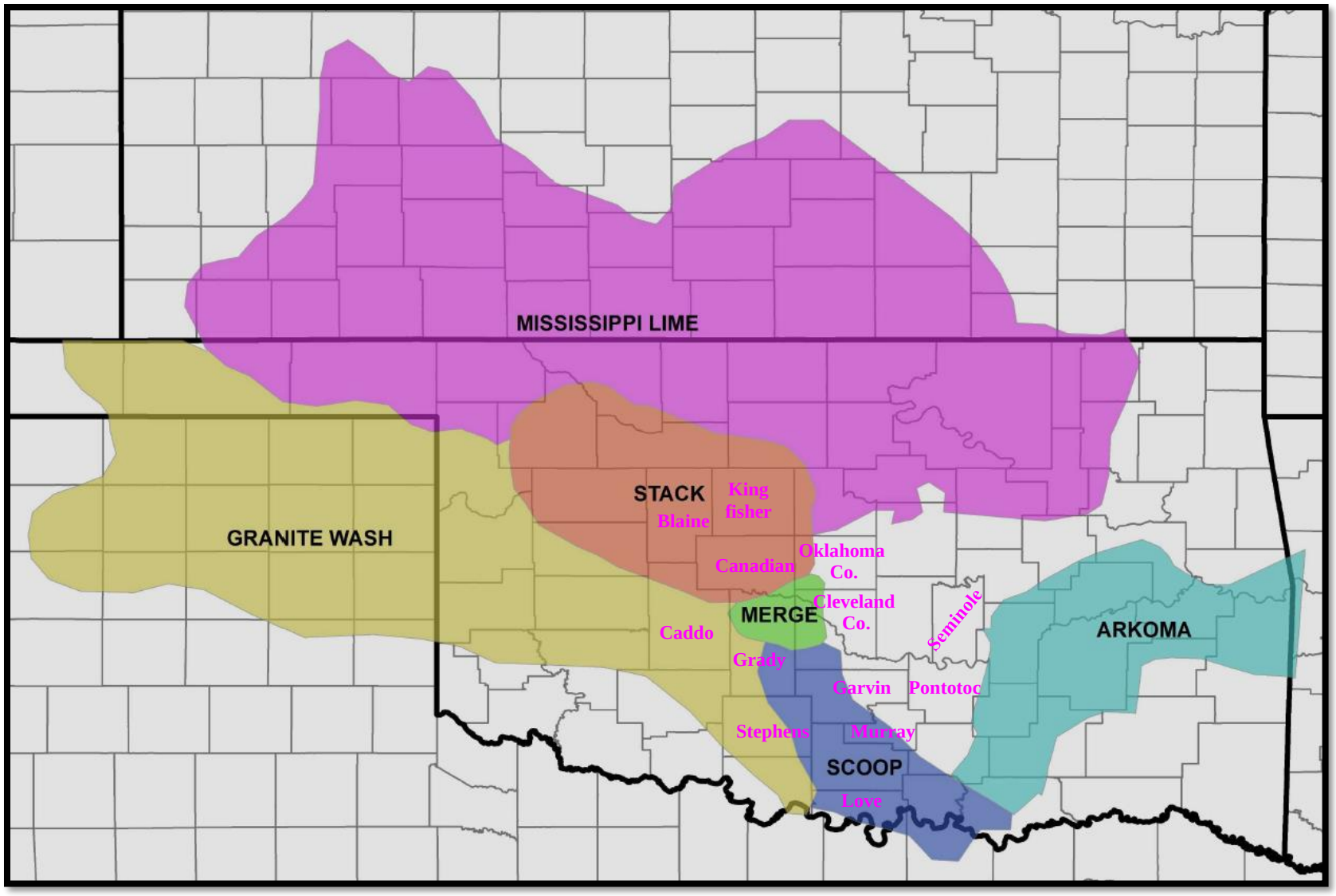

Figure 1.3. Mid-Continent USA, Oklahoman petroleum provinces. This study mainly relies on the STACK-SCOOP-Cherokee platform areas. Modified from Liborius et al. (2017).

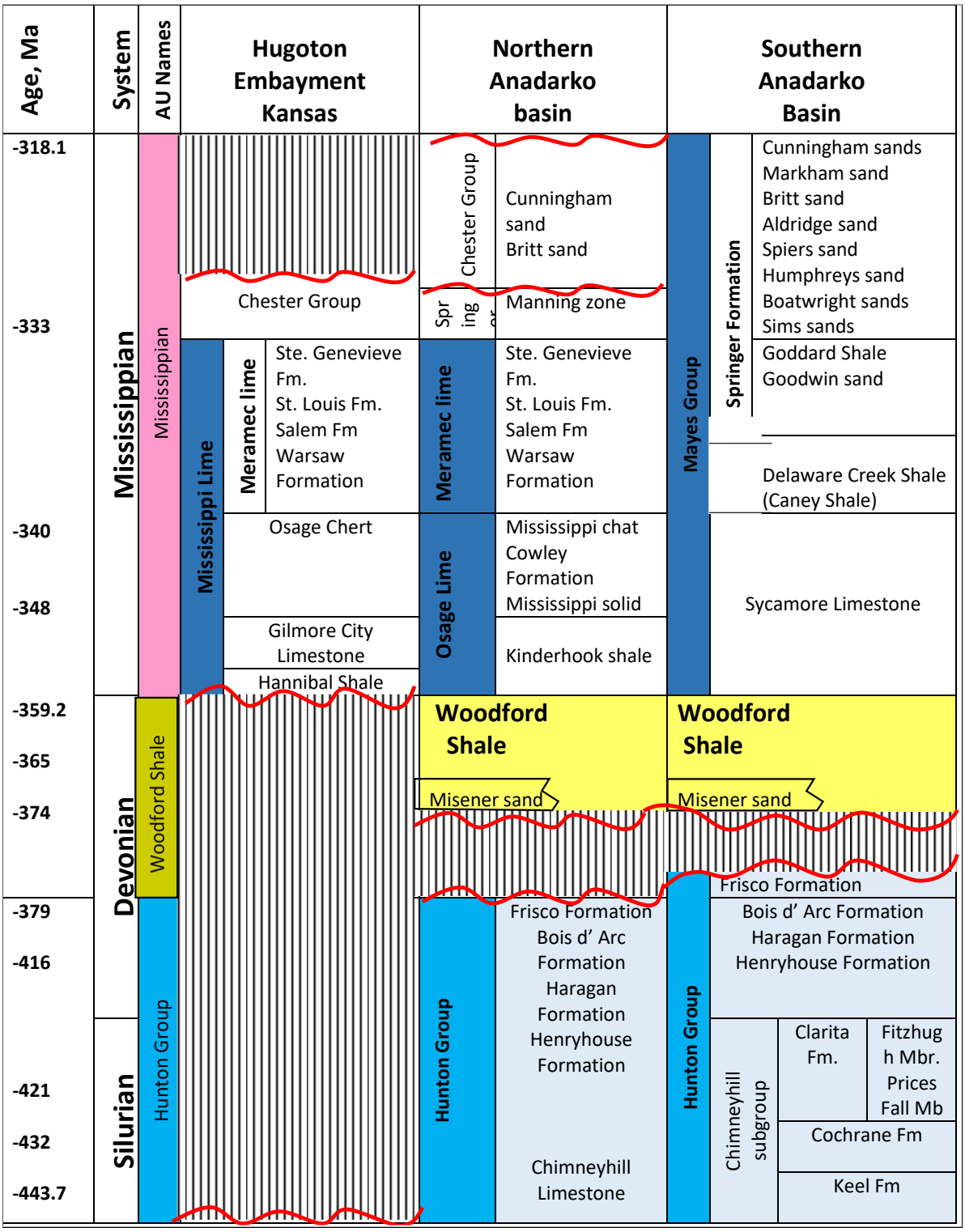

Figure 1.4. Woodford Shale general stratigraphic chart that highlights the significant unconformities at the base of the formation in the Oklahoman basins. Modified from Slatt (2016), and Liborius et al. (2017).

1.1.Geological definition of mini-basin fill

The geological definition of a mini-basin depression formed on a carbonate shelf was provided by the American Geological Institute (AGI, 1960). This concept mentions that it corresponds to "*A down-warped area containing stratified rocks, either sedimentary or volcanic or both, that extends into a terrain of other rocks, e.g., the Mississippi sinkhole fill over the carbonate platforms of the U.S. Gulf Coast*." In this study, we interpret based on Pyles and Slatt (2000) that in the marine settings, the enclosed mini-basin fill settings can occur in water depths below the sea wave base level (>500 ft below the sea level) and are in a transitional paralic environment towards the deeper ocean.

1.2.Geological definition of a paralic depositional environment

The depositional environments referred to as paralic correspond to coastal and marine siliciclastic settings where sediments accumulate under a significant marine influence (Pyles and Slatt, 2000). Hampson et al. (2017) mention that the paralic environments include coastal settings characterized by both marine and freshwater influences, specifically to transitional estuary/bay environments and lagoonal environments (Figure 1.5). It is essential to mention that these settings can form a mixture of lagoons and enclosed bodies of water capable of hosting deposition in parallel to the shore, or estuaries where the deposits are elongated mainly perpendicular to the shoreline (Hampson et al., 2017).

The direct identification of these deposits is tricky to recognize in the rock record because the estuary/bay and platform systems are tripartite (have an inner, middle and outer zone), with an outer zone dominated by the strong wave and tidal currents (Hampson et al., 2017). The paralic deposits have an extensive mud deposition typically in the middle region of the system, and the inner area is commonly dominated by fluvial flows within bayhead deltas (Pyles and Slatt, 2000;

Hampson et al., 2017). These distinctions are currently not used to describe the Woodford Shale, but the transition between an open marine environment towards shallower waters leads into sediment and organic-matter supply from the continent (Zhang and Slatt, 2019). Both estuary/bay and lagoon systems can range in salinity from hypersaline to regular marine, to hyposaline, and its variations in the stratigraphic record will reflect critical features in the organic matter facies (Hampson et al., 2017). The organic matter, minerals, and heavy elements formed under these paralic environments can be transported towards the deeper basin where the Woodford Shale enclosed mini-basin fill settings are formed by cycles of seaward stepping (Slatt, 2016).

1.3.The enclosed mini-basin fill system

In the present study, the definition of an "enclosed mini-basin fill" consists of a geological area with a shape resembling a concave downward pod-shaped structure with a deeper water level than most estuaries and embayment deposits (Slatt, 2016). The enclosed mini-basin fill settings correspond to the formation of isolated-restricted saline water masses in the middle to the outer shelf of the paralic environment (Figure 1.5). These depression shapes are due to the aerial/subaerial exposure of the pre-existing strata, commonly an eroded/karstified carbonate platform, which allow the creation of downhole depressions that subsequently permit water and sediments to concentrate (McCullough and Slatt, 2014; Zhang and Slatt, 2019). These mini-basins are then filled paleo depressions in an initial transgressive stage (sea level landward stepping from the deeper basin). Once these enclosed depocenters are filled, the shale deposits occur in a widespread blanket manner, as is typical of an open marine system (McCullough and Slatt, 2014; Slatt, 2016). In this study, the enclosed mini-basin fill system is presented as a distal part of the paralic system because this is also a marine deposit that occurs in the transitional parts from the

platform towards the open ocean (middle to outer shelf, before the shelf break; Figure 1.5) but without a substantial detrital coarse-grained sediment input.

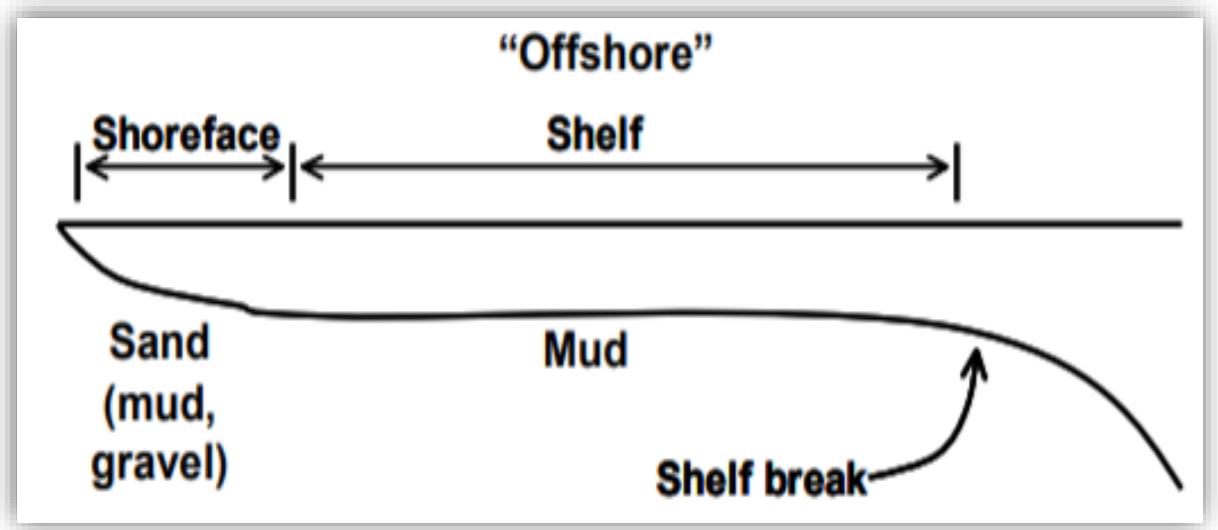

Figure 1.5. A schematic cross-section that shows the transition of a marine platform from shoreface deposits (more sand, mud, and gravel content), towards the transitional shelf (more mud deposits) and deeper open ocean waters beyond the shelf break. Hampson et al. (2017).

For the enclosed mini-basin fill, these specific characteristics of confinement by a silled barrier allow the concentration of a large body of salt-water, which is partially enclosed by land (eroded pre-strata; Slatt, 2016; Zhang and Slatt, 2019). These sills and barriers prevent the high energy open water circulation and oxidation processes (Figure 1.6). This study proposes that these factors provide areas of organic matter and sediments that concentrate when sea level rises and fill these depressions, or when influxes from the continent reach these depressions with higher availability of accommodation space (Figure 1.6; McCullough and Slatt, 2014). To date, the exploration and development of all unconventional resource shale systems have focused on shales interpreted as predominantly open marine depositional systems, deposited in a wide-spread blanket manner. The occurrence and the detailed characterization of the enclosed mini-basin fill under mostly open marine conditions have been untested.

These types of intervals within the shales might be bypassed or not focused during the application of the screening techniques in the exploration phase of these rocks (Slatt, 2016). The significance about understanding the marine shale variation into enclosed mini-basin fill is that the marine organic matter is oil and gas prone, and possible deposition and preservation of amorphous organic matter (lacustrine, type I kerogen) inside the enclosed mini-basin fills can lead into the generation of more oil than gas for some Woodford Shale intervals (Cardott, 2012; Katz and Lin, 2014; Slatt, 2016). The organic matter of terrestrial and lacustrine origin can be transported from the continent towards the enclosed mini-basin fill, and the deposits with this type of organic matter, especially for the lacustrine sourced one, might generate higher prospectivity for these intervals (Slatt, 2016). Lacustrine kerogens typically highlight more oil-prone source intervals from the amorphous organic matter, which are more resistant to thermal cracking and degradation than the open marine sourced organic matter (Katz and Lin, 2014).

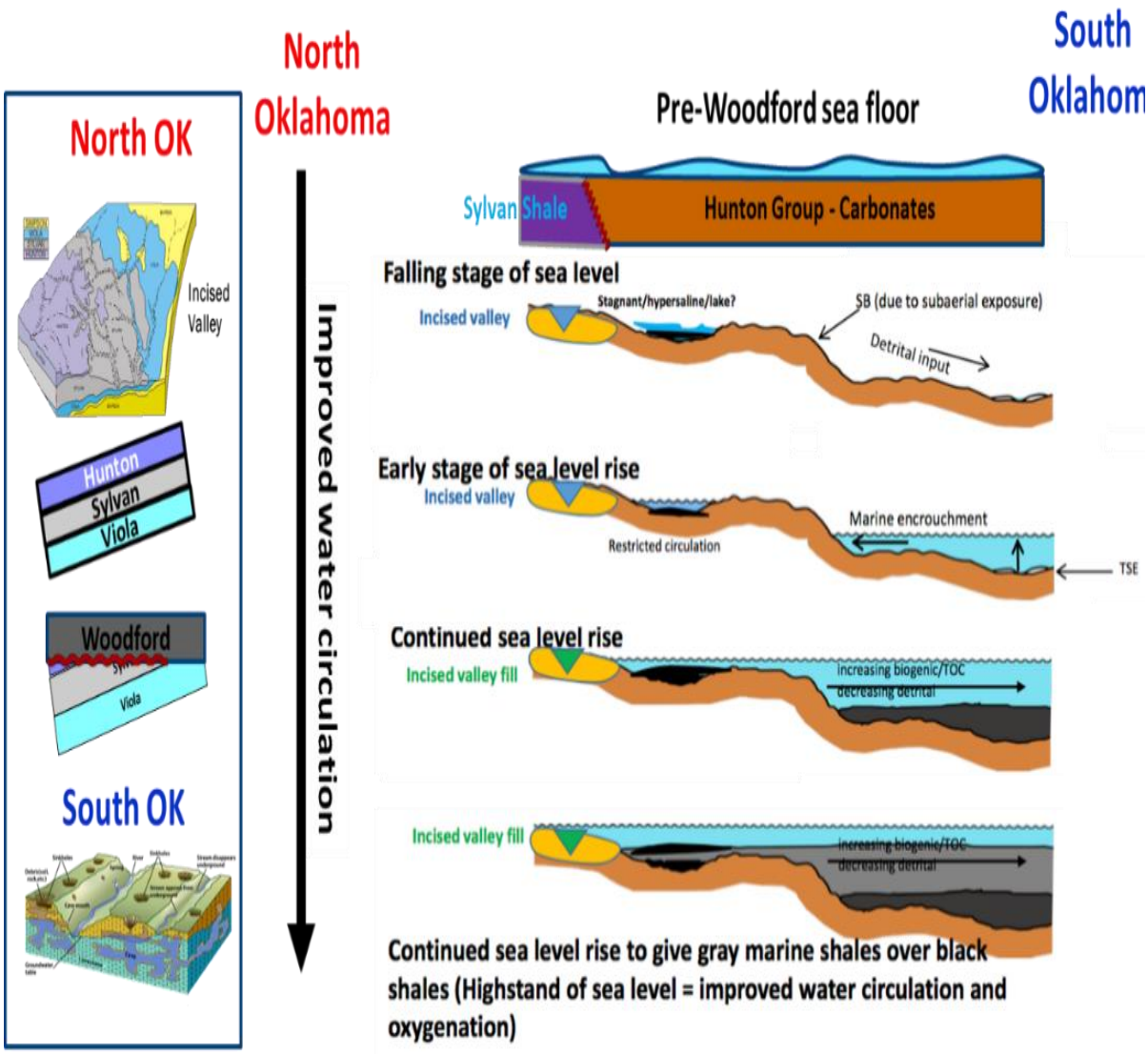

Figure 1.6. Depositional Model of the Woodford Shale through the Devonian sea-level variation (Slatt 2016; Torres-Parada et al., 2017). Note at the initial stages of falling sea levels the water isolation and restricted circulation over valley/karst filled areas. SB = sequence boundary; TSE = transgressive surface of erosion. Modified from Bauernfeind (1980) and Slatt (2016).

The Woodford Shale formation is broadly studied at the University of Oklahoma, Institute of Reservoir Characterization (IRC). This formation is the starting point of a marine unconventional shale system with the probable occurrence of enclosed mini-basin fill. This study focuses on identifying for this formation the critical geological, stratigraphical, geochemical (organic and inorganic), and seismic characteristics that support the recognition of enclosed mini-basin fill rock intervals deposited within the formation (Slatt, 2016).

As stated by Slatt and Rodriguez (2012), Slatt (2016), and Zhang and Slatt (2019), these highly restricted depositional parameters can also be related to other marine shale systems which have been deposited on a carbonate shelf. The identification of the erosional processes over the carbonate platform is crucial for evaluating the applicability and impact in other unconventional systems such as the Eagle Ford, Niobrara, Wolfcamp, Haynesville, Horn River, and Marcellus, which are recognized to be predominantly open marine deposits (Slatt and Rodriguez, 2012; Slatt and Zhang, 2019).

1.4.Geological and geochemical characterization of unconventional systems

The comparison of geochemical characteristics (organic and inorganic) of unconventional systems has revealed that all unconventional resource shales present a different unique set of features that make each oil and gas system distinctive (Slatt and Rodriguez, 2012; Slatt, 2016). The key aspects this research considers for characterizing the enclosed mini-basin fill are:

1.4.1. Organic richness and type

Slatt and Rodriguez (2012) characterized the prolific unconventional marine shale systems having a high organic abundance (usually greater than 3% total organic carbon –%TOC-), and hydrogen index (HI) values greater than 350 mg HC/g. These values are more significant than the threshold values typical of gas generation from conventional gas-prone source rocks and are more similar to typical characteristics of type II kerogen-rich, oil, and gas prone source rocks. The %TOC values generally track well log API gamma-ray log values (Cardott, 2012). Visual kerogen analyses of several shales indicate a predominance of type II kerogen (marine) within marine deposits (Cardott 2009 and 2012). Amorphous (lacustrine related) organic matter content of up to 93% and H/C ratios of 1.41 have been reported for the Barnett Shale (Hill et al., 2007). Likewise,

values of up to 80% amorphous organic matter were reported by Lewan (1987) for some immature Woodford Shale samples.

1.4.2. Biomarker characterization that serves as indicators of anoxic and oxic depositional environmental conditions.

Miceli-Romero (2010), Rodriguez and Philp (2010), Miceli-Romero and Philp (2012), Slatt and Rodriguez (2012), Jones (2017), Connock et al. (2018) and Philp and DeGarmo (2020), proposed that biomarker analyses are also in agreement with the hypothesis of fluctuating oxic conditions during deposition of the Woodford Shale. In general, for unconventional resource shales, Rodriguez (2007) and Slatt and Rodriguez (2012) suggested that variations in the pristane/phytane ratio (Pr/Ph) and C_{13}-C_{20} regular isoprenoids measured in core extracts are associated with changes in redox conditions as well as variations in terrigenous input during deposition of the Barnett Shale. Similarly, Miceli-Romero and Philp (2012) differentiated the Upper and Middle Woodford Shale members based on the distribution of several biomarker ratios: pristane/phytane, hopanes/steranes, C_{23} tricyclic/C_{30} hopane, and C_{18} aryl isoprenoids (Figure 1.7). Miceli-Romero (2010) and Miceli-Romero and Philp (2012) state that more oxic conditions prevailed during the deposition of the ‘cleaner, organic poor' Upper Woodford, as indicated by higher concentrations of C_{29} steranes (Figure 1.7). Dysaerobic to anaerobic environments prevailed during the deposition of the Middle Woodford Shale member as indicated by higher levels of aryl isoprenoids derived from the green sulfur bacteria *Chlorobiaceae* (Miceli-Romero and Philp, 2012; Connock et al., 2018; Figure 1.7). Aryl isoprenoid ratios also indicated that photic zone anoxia was episodic in the Woodford Shale (Miceli-Romero and Philp, 2012; Connock et al., 2018).

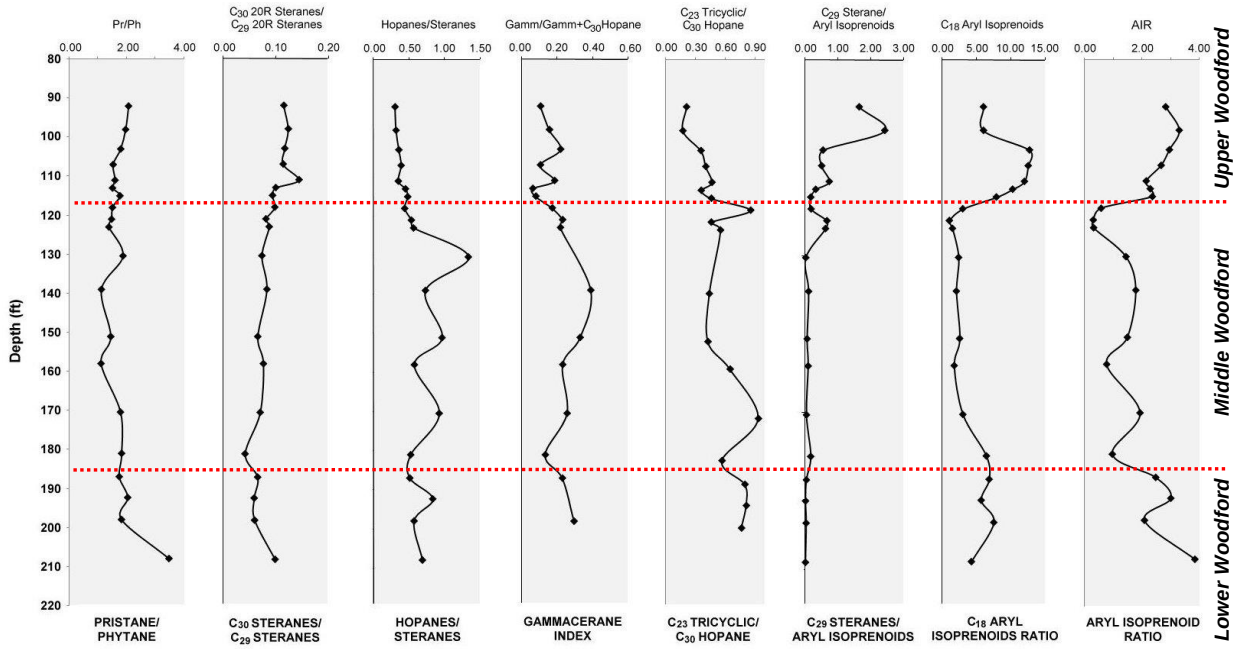

Figure 1.7. Stratigraphic variations in various biomarker ratios for the Woodford Shale in the Wyche Quarry, Oklahoma (Miceli-Romero, 2010).

1.5.The Woodford Shale in Oklahoma, USA.

The Late Devonian-Early Mississippian Woodford Shale was deposited in the Anadarko-Arkoma-Ardmore basins, in the mid-continent USA over a 33My (359-392My) time (Paxton et al., 2006; Slatt et al., 2012; Molinares, 2013). It is comprised of three members: The Lower Woodford black shale, which unconformably overlies Hunton group carbonates, the Middle Woodford organic-rich, black, pyritic shale, and the more quartzose-phosphatic Upper Woodford (Figure 1.8; Paxton et al., 2006).

The stratigraphic studies of the Woodford conducted by drilling a borehole just behind a quarry wall (Sierra-Perez, 2011; Slatt et al., 2012; Molinares, 2013; Turner et al., 2015) have provided excellent correlation with subsurface wells for improved understanding of both subsurface stratigraphy and natural fracture distribution. The Wyche-1 core is characterized to be

at lower levels of thermal maturity, where the organic matter is carefully preserved close to original conditions and in this dissertation is described as the starting stage for evaluating the enclosed mini-basin fill deposits within a marine system (Figure 1.9; Connock et al., 2018; Molinares, 2019).

According to Slatt et al. (2012), the Woodford Shale was deposited during a 2nd order sea-level cycle, but a superimposed 3rd order sequence stratigraphic framework has been developed, which was identified at the Henry House Creek outcrop (Paxton et al., 2006), Speake Ranch outcrop (Galvis, 2017), I-35S outcrop (Becerra-Rondon, 2017; Jones 2017), Arbuckle Mountains Wilderness outcrop (Bontempi, 2015; Ghosh 2017), McAlester quarry outcrop (Serna-Bernal, 2013; DeGarmo, 2015; Ekwunife, 2017), and Wyche Farm quarry (Miceli-Romero, 2010; Miceli-Romero and Philp, 2012; Sierra-Perez, 2011; Slatt et al., 2012; Molinares 2013; Turner et al., 2015; Connock et al., 2018; Molinares, 2019). All of these authors mentioned that the Woodford Shale stratigraphic sections consist of several parasequences composed of a basal, high API gamma-ray response [counts per second] overlain by a lower API section (Figure 1.8). The interpreted outcrop stratigraphy was correlated to subsurface wells initially by Paxton et al. (2006) and summarized in Slatt et al. (2012; Figure 1.8). Paxton et al. (2006) emphasized that the outcrop features are very distinctive and are similarly present in the geological characteristic of subsurface well logs and core samples. Similar sequence stratigraphy has been interpreted at the Wyche Farm quarry by Slatt et al. (2012) and Molinares (2013), and for the Speake Ranch outcrop and subsurface wells by Galvis (2017). The Woodford Shale downlapping clinoforms can sometimes be identified on seismic reflection records (Althoff, 2012; Amorocho-Sanchez, 2012; Cardona-Valencia, 2014; Infante-Paez et al., 2016; Milad, 2019; Figure 1.9).

At a smaller stratigraphic scale, some intervals contain interbedded chert and fissile shale, giving rise to a very intricate Gamma-ray log pattern (Molinares, 2013; Turner et al., 2015). The chert beds are composed mainly of diagenetically-recrystallized radiolarians, providing a rigid, brittle framework, while the more ductile shale interbeds contain both detrital and authigenic quartz, clay (mainly illite), feldspar and >10wt %TOC, contain more amorphous organic matter and *Tasmanites* cysts (Fishman et al., 2013; Cecil, 2016; Molinares, 2013; Becerra-Rondon, 2017; Galvis, 2017).

A 190 ft research borehole drilled just behind a quarry wall has provided an excellent correlation with subsurface wells for improved understanding of both subsurface stratigraphy and natural fracture distribution (Portas, 2009; Slatt et al., 2012; Molinares, 2013; Figure 1.9). Geochemical analysis indicates this core is at lower levels of thermal maturity (vitrinite reflectance values –Ro%- <0.60%) where the organic matter is preserved to its nearly original thermal condition (Miceli-Romero, 2010; Miceli-Romero and Philp, 2012; Connock et al., 2018). Because this quarry is a surface or close-to-surface exposure, the rocks can have suffered chemical and mechanical weathering that might alter the interpretation of the original organic matter conditions (Miceli-Romero and Philp, 2012).

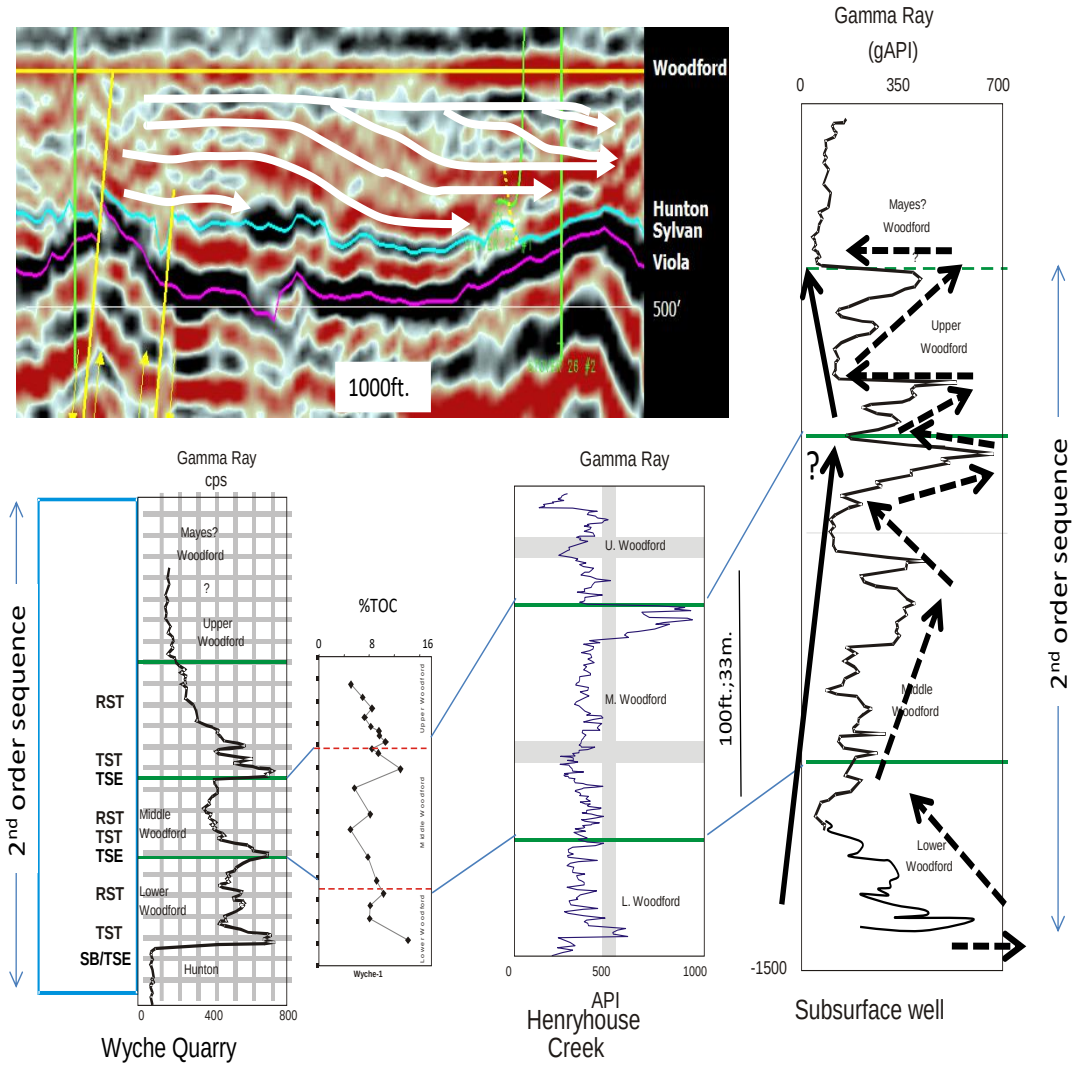

Figure 1.8. Gamma-ray, TOC profile, and sequence stratigraphy of the Woodford Shale from the Wyche quarry, Oklahoma (modified from Slatt et al., 2012), correlated with a nearby subsurface well. The Woodford is a 2nd order sequence with many higher frequency sequences superimposed. Inset shows the downlap pattern of the 2nd order HST/RST onto the lowermost Woodford (after May and Anderson, 2010).

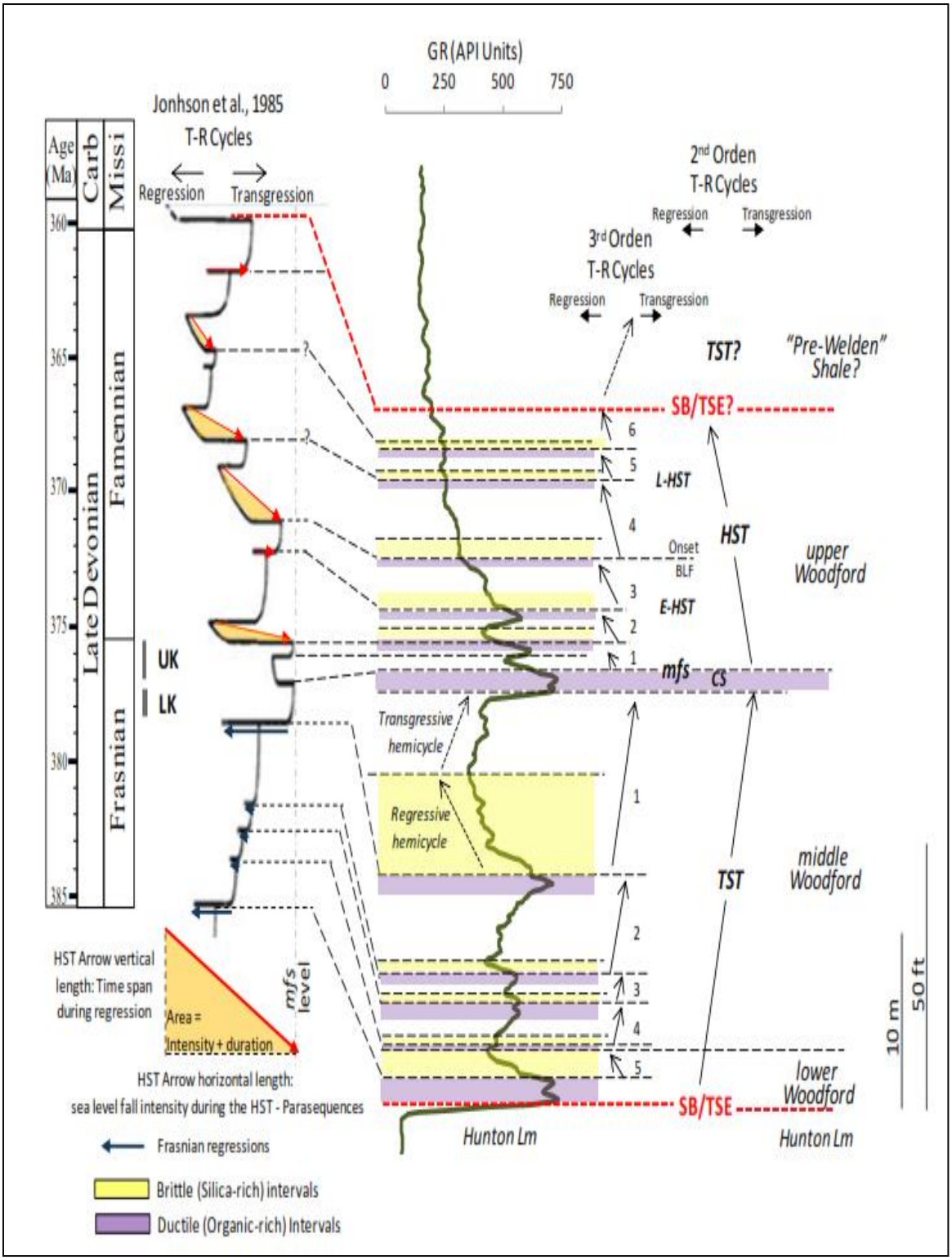

Figure 1.9. Interpreted sequence stratigraphy and third-order cycles of the Woodford Shale in Pontotoc County, Oklahoma, proposed by Serna-Bernal (2012) and Molinares (2013). SB= sequence boundary; TSE=transgressive surface of erosion; TST= transgressive system tract; HST= highstand system tracts; CS= condensed section; MFS= maximum flooding surface.

This *Wyche Farm* core served as the starting stage for evaluating the Woodford Shale at The University of Oklahoma, Institute of Reservoir Characterization (IRC). This Wyche-1 core was also the starting point to interpret whether the enclosed mini-basin fill deposits occur within this predominantly marine deposit. The Wyche-1 core stratigraphic framework (Figure 1.9) was developed by Slatt et al. (2012, and 2018), Molinares (2013), Connock (2015), Turner et al. (2015), Galvis et al. (2017), and Connock et al. (2018). These sequence stratigraphy interpretations are then correlated to the study areas of this dissertation (Cherokee Platform in Chapter II; south SCOOP in Chapter III; and STACK in Chapter IV) and served as a reference for the integrated stratigraphic analysis of The Speake Ranch (SR) outcrop presented in Chapter III. As mentioned by Slatt et al. (2012), the Woodford Shale was deposited during a 2nd order sea-level cycle. In the SR, Galvis (2017) and Galvis et al. (2017) interpreted a superimposed third-order sequence stratigraphic framework which has been developed by several parasequences composed of a basal, high API gamma-ray response condensed section, overlain by a lower gamma-ray regressive systems tract. All of these stratigraphic features have been correlated to the subsurface (Paxton et al., 2006; Molinares 2013; Galvis, 2017; Galvis et al., 2017) and are common in all of the Oklahoma petroleum provinces (Figure 1.3; Chapter II; Chapter III; Chapter IV).

The regional thickness map of the Woodford Shale in the state of Oklahoma is shown in Chapter III of this manuscript. In summary, this regional map shows that the Woodford strata tend to be thicker in paleotopographic lows upon the depositional sequence boundary (Hunton Group thickness depressions by erosion and karstification processes; Milad, 2019). This fact is coupled with the basal Woodford often being organic-rich (Figure 1.7 and Figure 1.10) and provides an opportunity for localized accumulation of highly restricted and highly anoxic prone facies,

proposed to be found in the enclosed mini-basin fill, and which are different from an open marine depositional system.

1.6.Geological framework of enclosed mini-basin fill in unconventional systems

For his study, the characterization of enclosed paleo depressions deposits is defined as "*enclosed mini-basin fill,"* which are hosts of marine organic matter, but can also host continental and lacustrine organic matter and preserve these particles in a better manner than the open marine intervals (Slatt, 2016). The higher preservation of the organic matter occurred when the barriers in the depressions act as sills that prevent open water circulation, oxidation, and physicochemical destruction (McCullough and Slatt, 2014; Zhang and Slatt, 2019). When mentioning the occurrence of lacustrine and continental organic matter, it is essential to highlight that the depositional environment is different from the frequent lacustrine freshwater deposits, where the presence of this type of organic matter indicates that these continental particles can be transported and deposited seaward, towards the deeper basinal areas (McCullough and Slatt, 2014; Brito, 2019). According to Bohacs (2012) and Brito (2014), lacustrine deposits are entirely inland, and enclosed systems, where the rate of water evaporation exceeds the rates of water precipitation (water column recharge) and more continental strata and continental organic matter is deposited.

This enclosed mini-basin fill characterization focuses on oceanic environments where the sea level floor has accommodation space in concave downward pod-shaped areas, which have restricted oceanic water circulation (Zhang and Slatt, 2019). Also, where the sediment and organic matter particle deposition occurs much deeper than the wave base level (>500 ft). In this enclosed fill, it is proposed that there are restricted-energy variations, and rapid and persistent development of anoxic conditions is present and crucial to preserve the accumulation of organic matter. For all these reasons, it is essential to review the literature for the characteristics of common lacustrine

geological deposits, and the type of organic matter that can be transported towards the enclosed mini-basin fill, which are proposed to occur in the transitional paralic area (mud shelf deposits before the shelf-break, towards the deeper ocean slope) and different than the open marine deep basinal shale deposits (Slatt, 2016).

A systematic exploration for recognizing the enclosed mini-basin fill rock intervals within the marine mudstone deposits has a starting point of considering these as highly restricted marine deposits within open marine depositional settings (Slatt, 2016). This definition requires the understanding of both the stratigraphy and geochemistry conditions of the minerals and organic matter that constitute the different lithologies in the enclosed fill deposits (sea-level variations, development of accommodation space, sediment supply, water chemistry, and heavy elements supply; Slatt, 2016). It is essential to rely on the organic geochemistry characterization for recognizing the existence and persistence of different organisms that formed different types of organic matter (organic facies), and inputs from the continent (Chapter III).

Additionally, the integration with mineralogical and elemental concentrations permit the recognition of essential characteristics deposited in the stratigraphic intervals of these shales (Slatt, 2016). The variations in organic matter content, type, and alterations that support the development of *"lacustrine"* type source intervals, also an indicator of supply of continental organic matter particles towards a deeper basin (Brito, 2014), which can be identified by different organic marker tracers in the sedimentary record (biomarkers; Chapter III). Although quantitative predictions about this enclosed mini-basin fill have not been conducted within the North American shale systems, previous qualitative assessments might indicate the probability of these type of intervals to be present as isolated areas within the unconventional marine deposits (Figure 1.10; Althoff, 2012; Brito, 2014; Infante-Paez et al., 2016; Torres-Parada et al., 2017).

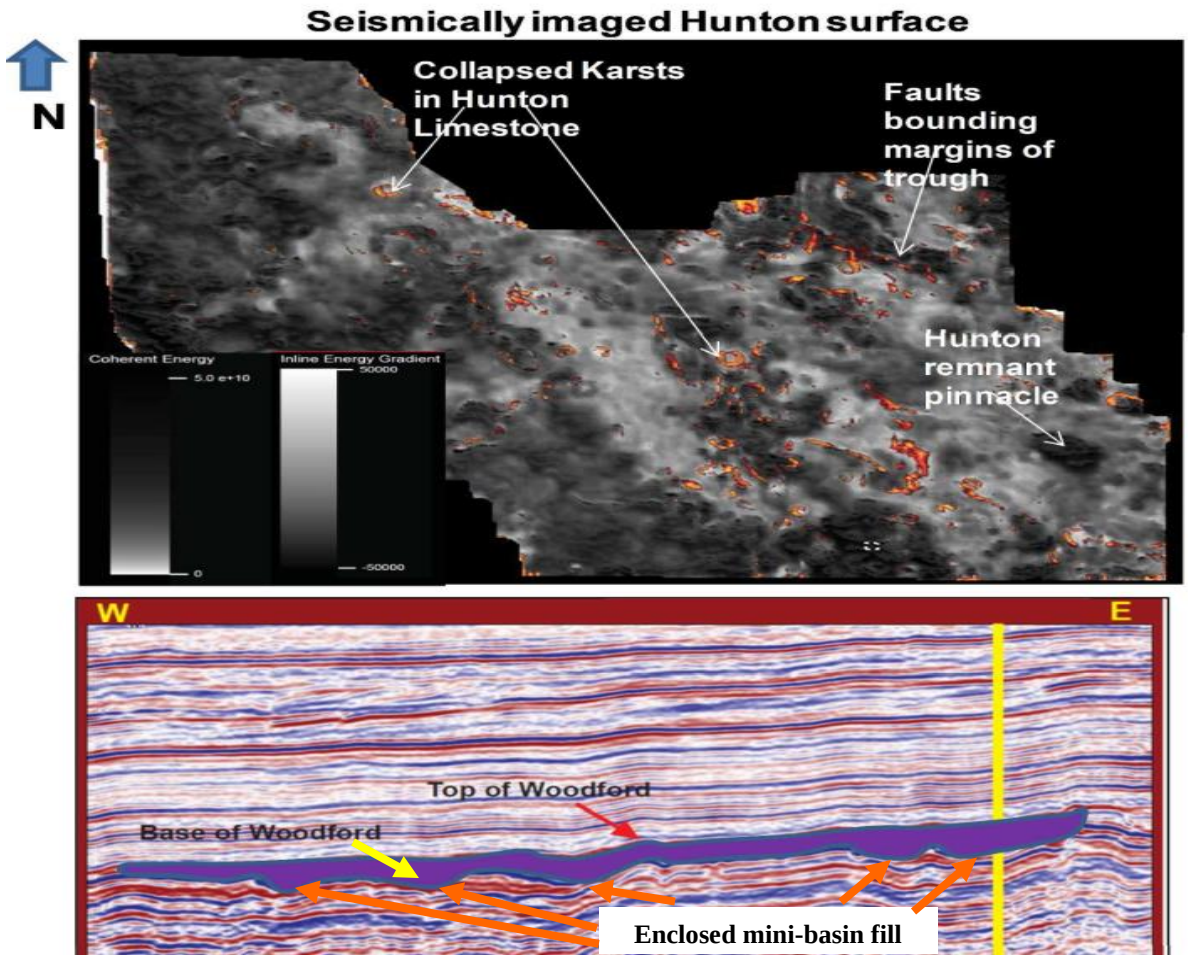

Figure 1.10. Irregular unconformity surface at the base of the Woodford Shale (top of the Hunton), and an overlying incised valley or collapsed cave fill was sitting on the unconformity (purple color), identified by Althoff (2012) and Infante-Paez et al. (2016). These local depocenters are proposed as mini-basin fill (indicated by the orange arrows).

For characterizing the highly restricted deposits settings, the analog of a restricted marine environment is proposed and based on Bohacs (2012), and Katz and Lin (2014). Bohacs (2012) mentioned that for defining a stratigraphic deposit as restricted, it requires the understanding of the distribution of topographic depressions, the paleoclimate conditions and the paleo water chemistry. The saltwater body needs to be areally dispersed and long-lived to allow the development of significant volumes of organic-rich sediments (Bohacs, 2012). Katz (1990) and Katz and Liro (1993) recognized that water chemistry controls the nature and level of organic

products in any depositional environment, which influences the preservation or alteration of the organic matter.

Organic matter preservation or alteration occurs by alternating water density and oxygen solubility and the availability of other chemical oxidizing agents such as sulfates and nitrates in the restricted system, where the identification of sulfur-rich conditions are crucial to address these highly restricted deposit characteristics (Katz and Liro, 1993). Slatt and Rodriguez (2012), Brito (2014), Katz and Lin (2014), and Slatt (2016) mentioned that rapid sea-level fluctuations might lead to rapid changes in the filling levels of an open marine basin. These changes occur rapidly on a geological scale and may reduce the areal extent of potentially thick source rock development to only the areas in a basin where permanent deep depressions were present (pre-existing available accommodation space for sediments to accumulate; Katz and Lin, 2014). The unconventional target area of the enclosed mini-basin fill might be geographically limited compared with entirely marine deposit counterparts because these open marine mudstones are deposited in a more widespread blanket manner (Slatt, 2016).

As the sea level fluctuates at the beginning of the deposition of the Woodford Shale, it is very probable that continental and lacustrine organic matter is deposited in these enclosed depressions (Slatt, 2016). It is essential to mention the published literature that refers to the characterization of hydrocarbon products that are sourced from lacustrine deposits and lacustrine organic facies has been principally focused on systems that are enclosed and have a limited water recharge, where the rates of water evaporation exceeds the rates of water precipitation (Espitalié et al., 1977; Bohacs et al., 2000). These evaporation conditions can occur when filling these enclosed mini-basin depressions, as when these pockets are being filled the water depth should be changing in addition to sea-level fluctuations (Espitalié et al., 1977; Tissot et al., 1987; Burnham

et al., 1990; Pepper et al., 1995; Bohacs et al., 2000; Zhao et al., 2010; Burnett et al., 2011; Bohacs, 2012; Katz and Lin, 2014).

There are several different properties when comparing rocks rich in lacustrine organic matter to source rocks with only marine organic matter: kerogens, the precursors of oil and gas, in lacustrine-rich source rocks tend to be more hydrogen-enriched than their marine-rich counterparts displaying elevated atomic H/C ratios and hydrogen indices from Rock-Eval pyrolysis data (Espitalié et al., 1977; Tissot et al., 1987; Burnham et al., 1990; Pepper et al., 1995; Bohacs et al., 2000).

Other key differences when comparing an organic matter particle of marine origin against an organic matter particle formed from lacustrine kerogen are that the level of "waxiness" and paraffin content in the generated hydrocarbon liquid fraction in both marine and lacustrine sources differ significantly (Katz and Lin, 2014). The liquid fractions in lacustrine oils are commonly waxier and display different hydrocarbon generation yields and mobility properties (Scheck et al., 1997), where high wax oil might display different flow and viscosity characteristics (Bohacs, 2012). The cracking kinetics of lacustrine-rich source intervals is different from the marine ones in the timing of gas generation, resulting in different thermal maturity yields for marine and lacustrine deposits, where the oil and gas windows are shifted towards higher thermal maturity levels (Katz, 1990; Scheck et al., 1997; Bohacs, 2012).

The temperature ranges of activation energy required for hydrocarbon generation in lacustrine kerogens are narrower than the one required for the marine kerogens, and the lacustrine sourced oils and bitumens are more resistant to start to generate gas than the marine sourced oil and bitumens (Burnham et al., 1990; Pepper et al., 1995; Bohacs, 2012). There are not only differences in generation kinetics, but there are also differences in cracking kinetics for lacustrine-

derived and marine-derived hydrocarbons (Burnham et al., 1990; Pepper et al., 1995). Scheck et al. (1997), proved by laboratory simulations that the cracking of marine-derived organic matter occurs at earlier thermal maturity levels than the lacustrine counterparts. These conclusions by Scheck et al. (1997) indicate that the marine oils may have higher gas yields than the lacustrine oils. Jarvie et al. (2005 and 2007) and Katz and Lin (2014) suggested that the published thermal maturity methodologies for risk ranking the unconventional marine systems might not be valid for lacustrine rock intervals and need to be developed in marine rock intervals rich in lacustrine-sourced organic matter.

1.7. The scientific hypothesis of an enclosed mini-basin fill deposit within a marine shale

Typical marine hydrocarbon source rocks have been characterized as the primary target for unconventional oil/gas shale systems (EIA, 2016). In the North America Lower 48, most of the marine shale systems are deposited above carbonate platforms (Woodford Shale, Barnett Shale, Eagle Ford Shale, Marcellus Shale, Haynesville Shale, and Horn River Shale; Slatt and Rodriguez, 2012). The sea-level fluctuations during the deposition of these systems allowed aerial exposure and subsequent erosion of the pre-existing carbonate platforms (Slatt, 2016). The creation of the eroded sink surfaces as isolated areas allow seawater body masses to accumulate and restrict the organic matter from oxidation processes, preserving more oil-prone source rock intervals (higher hydrogen content, which is preserved in the organic matter; Slatt and Rodriguez, 2012; Zhang and Slatt, 2019). This study proposes that the enclosed mini-basin fill rock intervals are stratigraphical variations that could economically produce more oil than gas by determining the intervals which might contain amorphous organic matter with large molecular organic compounds, higher levels of water salinity, high levels of anoxia, enriched in quartz and have relatively low clay content.

1.7.1. Minerals as indicators of anoxic and oxic depositional environmental conditions

The lithological and organic facies variations within individual marine shale systems have been documented (Loucks and Ruppel, 2007; Singh, 2008; Buckner et al., 2009), and typical mineral indicators of marine depositional environments have been identified. Phosphatic nodules are usually present within organic-rich intervals in the Barnett (Singh et al., 2008), Woodford (Buckner et al., 2009), and Montney (Adams, 2009) shale systems. These are usually interpreted as characteristics of sea-level regression during deposition (Slatt, 2016). Reducing conditions are also proposed as characteristics of the environments of deposition of shale systems (Slatt and Rodriguez, 2012). The presence of pyrite has been reported in Barnett (Singh, 2008), Haynesville (Hammes and Carr, 2009), Marcellus (Nyahay et al., 2007), Woodford (Buckner et al., 2009) and Horn River (McPhail et al., 2009) shales, attesting to reducing conditions. The recognized pyrite dissemination in discrete intervals indicates that anoxic conditions were not persistent throughout shale deposition.

The conclusions by Turner et al. (2015), Becerra-Rondon (2017), Galvis et al. (2017) and Brito (2019), proposed specific element proxies for local depositional and environmental conditions during sedimentation for the Woodford Shale. The principal elements used in the Woodford Shale by Turner et al. (2015) and Galvis et al. (2017) are titanium (Ti), zirconium (Zr), silicon (Si), Calcium (Ca), strontium (Sr), phosphorous (P), aluminum (Al), potassium (K), molybdenum (Mo), and vanadium (V). Turner et al. (2015) notes that Ti and Zr are strongly associated with continentally derived sediment; Ca and Sr are both related to carbonate accumulation; Al and K are connected with feldspars and clays; Mo and V can be used as an indication of redox conditions and additionally that Si is found in biogenic quartz, detrital quartz, feldspars, and clays and is useful to evaluate the type of Silica source using a ratio of Si/Al (Turner

et al., 2015; Galvis et al., 2017). When evaluating the elemental Al content related to the Si concentration, the Si/Al ratio provides an approximation for the amount of biogenic quartz present within a stratigraphic layer and the changes in the trends of these elements can be used to interpret changes in the local sea level shoreline trajectory (Turner et al., 2015; Molinares, 2019). The result of changes in sediment supply and accommodation space can be correlated across the Oklahoman basins by identifying areas of restricted sediment influx (Turner et al., 2015; Brito, 2019).

1.8.Sustainability of project and main objectives

The scope of this project involves the primary stage of the characterization in the Woodford Shale (Oklahoma) for the identification of crucial geological, stratigraphical, geochemical (organic and inorganic), and 3D seismic tools that support the assessment of the presence of enclosed mini-basin fill within the marine depositional system (Torres-Parada et al., 2017). The Woodford unconventional oil/gas marine shale is a mature shale play under active exploration and production and is known for its hydrocarbon source rock and reservoir rock attributes (Jarvie et al., 2007; Cardott, 2014). However, its enclosed mini-basin fill intervals have not been studied in detail in the depositional models (Slatt, 2016). This study relies on outcrop and subsurface core samples to establish the high-resolution sedimentology, stratigraphy, and geochemistry of the Woodford Shale in different Oklahoma petroleum provinces.

Because of accumulated knowledge of the Late Devonian-Early Mississippian Woodford Shale in Oklahoma, it will be used as the first test for the presence/absence of restricted, enclosed mini-basin fill. The Woodford Shale is comprised of three members: The Lower Woodford black shale which unconformably overlies the Hunton Group carbonates with considerable topographic relief (Infante-Paez et al., 2017; Milad, 2019), the Middle Woodford organic-rich, black, pyritic shale, and the more quartzose-phosphatic Upper Woodford (Figure 1.9).

The Woodford strata tend to be thicker and more organic-rich in paleo-topographic lows upon the Hunton unconformity (Infante-Paez et al., 2017; Torres-Parada et al., 2017; Milad, 2019). The inorganic geochemistry data coupled with Rock-Eval pyrolysis data that served for pre-selection of the possible enclosed mini-basin fill rock intervals are based on the screening for anoxic restricted redox conditions: the initial measurements of high hydrogen indices (HI) and very low oxygen indices (OI) under low maturity conditions, related to high molybdenum (Mo) and vanadium (V) content (element analysis are independent to the maturity levels), are used to identify initial suspects of salt-water lacustrine deposits.

The laboratory work phase consisted of selecting rock samples on an immature (0.56 Ro%) and complete >314 ft stratigraphic section of The Woodford Shale: The Speake Ranch outcrop (Chapter III). This outcrop was selected because it reflected the complete stratigraphic properties of the formation and was discovered, described, and analyzed by Becerra-Rondon (2017), Galvis (2017) and Galvis et al. (2017). In this study, the Speake Ranch section is integrated and complemented with the additional integration of mineralogical, sedimentological, sequence stratigraphic, geophysical, petrophysical, geostatistical, organic, and inorganic geomechanical properties. These are the key parameters to understand the occurrence of enclosed mini-basin fill deposits within the Woodford Shale depositional model from local to regional petroleum province scales. The laboratory phase is mainly focused on the quantification of the organic geochemistry properties by biomarkers with gas chromatography, and mass spectrometry for detecting the organic matter precursors and depositional environment properties. The restricted organic-rich and anoxic intervals were analyzed in the OU organic geochemistry group (OG2) laboratories (Chapter III). The rock samples were selected based on geostatistical analysis of the 536 samples collected by Galvis (2017) and Galvis et al. (2017).

The geostatistical analysis of these samples collected by Galvis (2017), consists of the integration of XRF data of the major heavy elements, combined with the Rock-Eval pyrolysis data in a "one-to-one" manner for obtaining unsupervised facies classification by K-means and compare with previous hierarchical cluster analyses classification by Galvis (2017). The clusters, or "*machine learning facies*," obtained after these classification methodologies, served as the criteria for selecting the samples that have biomarker analyses of their saturate and aromatic fractions, selecting at least one sample per representative K-means facies. Details about the methodologies, hypothesis, and selected biomarkers for identifying the presence of enclosed mini-basin fill deposits and their variability along the Woodford Shale stratigraphic column are in Chapter III of this manuscript.

The geochemical attributes of the Woodford are tied with the stratigraphy by correlation with lithologies, element, and mineral contents. The organic geochemistry phase is complemented with mineralogy analysis via X-ray diffraction (XRD) for clay mineral recognition and scanning electron microscopy (SEM) for interpreting the nano-scale mineralogical arrangements and structures. Sample characterization is correlated to well log responses and seismic subsurface reflections through identifying regional tracers of the enclosed mini-basin fill indicators (Chapter II and Chapter IV). This correlation with subsurface data is critical for understanding the factors that control the occurrence of enclosed mini-basin fill intervals within a primary marine depositional environment.

1.9. Petroleum industry relevance

This research is the first to be reported with an unconventional marine shale to evaluate the detailed characterization of enclosed mini-basin fill deposits and might lead the unconventional assessment for further considerations of these shales. The depressions of pre-Woodford Shale

strata can be systematically recognized, but the rock intervals that constitute these fills might not have been studied in detail (Slatt, 2016). The products of this research can be useful and applicable to determining if rocks of a marine environment under very controlled conditions can additionally support the accumulation of lacustrine-source organic matter (more oil-prone) under these types of depressions and paleo sea-level fluctuations.

1.10. Cited References

- Adams, C., 2009. Shale gas activity in British Columbia, exploration, and development of BC's shale gas areas. Ministry of energy, mines and petroleum resources, resource development, and geoscience branch. 3rd Annual unconventional gas technical forum, Canada.
- Althoff, C., 2012. Characterization of depositional megacycles in the Woodford trough of Central Oklahoma. M.Sc. thesis manuscript, The University of Oklahoma, p. 167.
- American Geological Institute AGI, 1960. Glossary of geology and related sciences 1957, Washington, DC., p. 325. Supplement, 1960, p. 72.
- Amorocho-Sanchez, J.D., 2012. Sequence stratigraphy and seismic interpretation of the Upper Devonian- Lower Mississippian Woodford Shale in the Cherokee platform: a characterization approach for unconventional resources. M.Sc. thesis manuscript, The University of Oklahoma, p. 153.
- Bauernfeind, P.E., 1980. The Misener sandstone in portions of Lincoln and Creek Counties, Oklahoma. Oklahoma City Geological Society, Shale Shaker Digest, 30, 1-30.
- Bohacs, K.K., 2012. Relation of hydrocarbon reservoir potential to lake-basin type: an integrated approach to unraveling complex genetic relations among fluvial, lake-plain, lake margin, and lake center strata. In: Baganz, O.W., Bartov, Y., Bohacs, K., Nummedal, D., eds., Lacustrine sandstone reservoirs and hydrocarbon systems. AAPG Memoir 95, 13-56.
- Bohacs, K.M., Carroll, A.R., Neal, J.E., Mankiewicz, P.J., 2000. Lake-basin type, source potential, and hydrocarbon character: an integrated-sequence-stratigraphic geochemical framework. In: Gierlowski-Kordesch, E.H., and Kelts, K.R., eds., Lake basins through space and time. AAPG Studies in Geology 46, 3-34.

- Bontempi, C., 2015. High-resolution stratigraphy of thin-bedded shales/radiolarians, Woodford Shale, Arbuckle wilderness area, Murray County, Oklahoma: A new correlation tool. M.Sc. thesis manuscript, The University of Oklahoma, p. 98.
- Brito, R.J., 2014. Geological characterization and sequence stratigraphic framework of the Brown Shale, Central Sumatra basin, Indonesia: implications as an unconventional resource. M.Sc. thesis manuscript, The University of Oklahoma, p. 106.
- Brito, R.J., 2019. The Woodford Shale in the Marietta basin: Oklahoma and North Texas. Doctoral dissertation manuscript, The University of Oklahoma, p. 182.
- Buckner, N., Slatt, R.M., Coffey, B., Davis, R.J., 2009. Stratigraphy of the Woodford Shale from behind-outcrop drilling, logging, and coring: AAPG Annual convention, San Antonio, TX. AAPG Search and Discovery Article 50147.
- Burnett, A.P., Soreghan, M.J., Scholz, C.A., Brown, E.T., 2011. Tropical East African climate change and its relation to global climate: a record from Lake Tanganyika, tropical East Africa, over the past 90+ kyr. Palaeogeography, Palaeoclimatology, Palaeoecology 303, 1-4, 155-167.
- Burnham, A.K., Braun, R.L., 1990. Development of a detailed model of petroleum formation, destruction, and expulsion from lacustrine and marine source rocks. Organic Geochemistry, 16, 27-39.
- Cardott B. J., 2009. Woodford gas-shale plays of Oklahoma. Louisiana oil & gas symposium, May 20, 2009. Oklahoma Geological Survey OGS.
- Cardott, B.J., 2012, Thermal maturity of Woodford Shale gas and oil plays, Oklahoma, USA. International Journal of Coal Geology 103, 109-119.
- Cardott, B.J., 2014. Woodford Shale play update: Expanded in the oil window. American Association of Petroleum Geologists, Search and Discovery article 80409.
- Cecil, K.A, 2016. Origin and characteristics of Devonian-Mississippian novaculitic chert in Oklahoma. M.Sc. thesis manuscript, Oklahoma State University, p. 166.
- Comer, J.B., Hinch, H.H., 1987. Recognizing and quantifying expulsion of oil from the Woodford formation and age-equivalent rocks in Oklahoma and Arkansas. AAPG Bulletin 71, 844-858.
- Comer, J.B., 1992. Organic geochemistry and paleogeography of Upper Devonian formations in Oklahoma and northwestern Arkansas. In: Johnson, K.S., Cardott, B.J., eds., Source rocks in the southern Midcontinent, 1990 symposium. OGS Circular 93, 70-93.

- Comer, J.B., 2005, Facies distributions and hydrocarbon production potential of the Woodford Shale in the southern midcontinent: in B.J. Cardott, eds., Unconventional energy resources in the southern Midcontinent, 2004 symposium. Oklahoma Geological Survey, Circular 110, 51-62.
- Connock, G.T., 2015. Paleoenvironmental Interpretation of the Woodford Shale, Wyche Farm shale pit, Pontotoc County, Arkoma Basin, Oklahoma with Primary Focus on Water Column Structure. M.Sc. thesis manuscript, The University of Oklahoma, p. 266.
- Connock, GT., Nguyen, T.X., Philp, R.P., 2018. The development and extent of photic-zone euxinia concomitant with Woodford Shale deposition. AAPG Bulletin 102, 6, 959-986.
- DeGarmo, D., 2015. Geochemical characterization of the Woodford Shale (Devonian-Mississippian), McAlister cemetery quarry, Criner Hills uplift, Ardmore basin, Oklahoma. M.Sc. thesis manuscript, The University of Oklahoma, p. 223.
- Ekwunife, I.C., 2017. Assessing mudrock characteristics, high-resolution Chemostratigraphy, and sequence stratigraphy of the Woodford Shale in the McAlister cemetery quarry, Ardmore basin, Oklahoma. M.Sc. Thesis manuscript, The University of Oklahoma, p. 167.
- Energy Information Administration EIA, 2016. U.S. Lower 48 states shale plays map. http://www.eia.gov/analysis/studies/usshalegas/images/shalemap-sm.png
- Espitalié, J., Laporte, J.L., Madec, M., Marquis, F., Leplat, P., Poulet, J., Boutefeu, A., 1977. Méthode rapide de caractérisation des roches mères de leur potential pétrolier et de leur degré d'évolution. Revue de I'Institute Francais du Pétrole 32, 23-42.
- Fishman, N.S., Ellis, G.S., Boehlke, A.R., Paxton, S.T., Egenhoff, S.O., 2013. Gas storage in the Upper Devonian-Lower Mississippian Woodford Shale, Arbuckle Mountains, Oklahoma: How much of a role do chert beds play? In: Chatellier, J.Y., Jarvie, D.M., eds., Critical assessment of shale resource plays. AAPG Memoir 103, 81-107.
- Galvis, H., 2017. Detailed lithostratigraphic characterization and sequence stratigraphy of a complete Woodford Shale outcrop section in southern Oklahoma. M.Sc. thesis manuscript, The University of Oklahoma, p. 170.
- Galvis, H., Becerra-Rondon, D., Slatt, R.M., 2017. Lithofacies and stratigraphy of a complete Woodford Shale outcrop section in south-central Oklahoma: Geologic considerations for the evaluation of unconventional shale reservoirs. Interpretation 2017, 6, 1, SC15-SC27.

- Ghosh, S., 2017. Integrated studies on Woodford Shale's natural fracture attributes, origin, and their relation to hydraulic fracturing. Doctorate dissertation manuscript, The University of Oklahoma, p. 264.
- Grotzinger, J.G, Jordan, T.H., 2010. Understanding earth. In: Freeman, W.H., Sixth Edition, p. 672.
- Hammes, U., Carr, D. L., 2009. Sequence stratigraphy, depositional environments, and production fairways of the Haynesville Shale gas play in East Texas. Search and Discovery article 110084.
- Hampson, G.J., Reynolds, A.D., Kostic, B., Wells, M.R., 2017. Sedimentology of paralic reservoirs: Recent advances. Geological Society of London, Special Publications 444, 7-34.
- Hill, R., Jarvie, D., Zumberge, J., Henry, M., Pollastro, R., 2007. Oil and gas geochemistry and petroleum systems of the Fort Worth basin: AAPG Bulletin 91, 4, 445–473.
- Infante-Paez, L.E., Cardona, L.F., McCullough, B., Slatt, R.M., 2016. Seismic analysis of paleo topography and stratigraphic controls on total organic carbon: Rich sweet spot distribution in the Woodford Shale, Oklahoma, USA. Interpretation 5, 1, T33-T47.
- Jarvie, D.M., Hill, R.J., Pollastro, R.M., 2005. Assessment of the gas potential and yields from shales: the Barnett Shale model. In: Cadott, B., eds., Oklahoma Geological Survey Circular 110: Unconventional gas of the southern mid-continent symposium, March 2005. Oklahoma City, Oklahoma, p. 37-50.
- Jarvie, D.M., Hill, R.J., Ruble, T.E., Pollastro, R.M., 2007. Unconventional shale-gas systems: the Mississippian Barnett Shale of North-Central Texas as one model for thermogenic shale-gas assessment. AAPG Bulletin 91, 4, 475-499.
- Johnson, K.S., Cardott, B.K., 1992. Geologic framework and hydrocarbon source rocks of Oklahoma, In: Johnson, K.S., Cardott, B.J., eds., Source rocks in the southern Midcontinent, 1990 symposium. OGS Circular 93, 21-37.
- Jones, L.C., 2017. An integrated analysis of sequence stratigraphy, petroleum geochemistry, and Devonian mass extinction events in the Woodford Shale, southern Oklahoma. M.Sc. thesis manuscript, The University of Oklahoma, p. 219.
- Katz, B.J., 1990. Controls on the distribution of lacustrine source rocks through time and space. In: Katz, B.J., eds., Lacustrine basin exploration-case studies, and modern analogs. AAPG Memoir 50, 61-76.

- Katz, B.J., Liro, L.M., 1993. The Waltman Shale member, Fort Union formation, Wind River basin: A Paleocene classics lacustrine source rock system. In: Keefer, W.R., Metzger, W.J., and Godwin, L.H., eds., Oil and gas and other resources of the Wind River basin Wyoming. Wyoming Geological Association, Casper, WY, 163-174.
- Katz, B.J., Lin, F., 2014. Lacustrine basin unconventional resource plays key differences. Marine and Petroleum Geology 56, 255-265.
- Lewan, M.D., 1987. Petrographic study of primary petroleum migration in the Woodford Shale and related rock units, in Doligez, B., eds., Migration of hydrocarbons in sedimentary basins. Paris, Editions Technip, 113-130.
- Loucks, R.G., Ruppel, S.C., 2007. Mississippian Barnett shale: Lithofacies and depositional setting of a deep–water shale-gas succession in the Fort Worth basin, Texas. AAPG Bulletin 91, 4, 579-601.
- May, J.A., Anderson, D.S., 2010. Mudrock reservoir description and stratigraphy: not homogenous, not boring. In: Critical assessment of shale resource plays. AAPG Hedberg Research Conference, December 2010. Austin, Texas.
- McCullough, B., Slatt, R.M., 2014. Paleotopographic control on the variability of Woodford Shale strata across the southern Cherokee platform area of central Oklahoma: A mechanism for increased preservation-potential of organic content: AAPG Search and Discovery article 1125.
- McPhail, S., Walsh, W., Lee, C., Monahan, P.A., 2009. Shale units of the Horn River formation, Horn River basin, and Cordova embayment, Northeastern British Columbia. British Columbia Ministry of energy, mines, and petroleum resources.
- Miceli-Romero, A.A, 2010. Geochemical characterization of the Woodford Shale, central and southeastern Oklahoma. M.Sc. thesis manuscript, The University of Oklahoma, p. 149.
- Miceli-Romero, A.A., Philp, R.P., 2012. Organic geochemistry of the Woodford Shale, southeastern Oklahoma: How variable can shales be? AAPG Bulletin, 96, 3, 493-517.
- Molinares, C.E., 2013. Stratigraphy and palynomorphs composition of the Woodford Shale in the Wyche Farm shale pit, Pontotoc County, Oklahoma. M.Sc. thesis manuscript, The University of Oklahoma, p. 104.

- Molinares, C.E., 2019. The Frasnian/Famennian (F/F) transition in the Woodford Shale, south-central Oklahoma – a multiproxy approach. Doctoral dissertation manuscript, The University of Oklahoma, p. 117
- Nyahay, R., Leone, J., Smith, l., Martin, J., Jarvie, D., 2007. Update on the regional assessment of gas potential in the Devonian Marcellus and Ordovician Utica shale in New York. AAPG Search and Discovery article 10136.
- Paxton, S.T., Cruise, A.M., Krystyniak, A.M., 2006. Fingerprints of global sea-level change revealed in Upper Devonian/Lower Mississippian Woodford Shale of south-central Oklahoma. AAPG Search and Discovery article 4021.
- Pepper, A.S., Corvi, P.J., 1995. Simple kinetic models of petroleum formation. Part 1: Oil and gas generation from kerogen. Marine and Petroleum Geology 12, 291-319.
- Pyles, D.R., Slatt, R.M., 2000. A high-frequency sequence stratigraphic framework for shallow through deep-water deposits of the Lewis Shale and Fox Hills sandstone, Great Divide, and Washakie basins, Wyoming. In: Weimer, P., eds., GCS-SEPM Deep-water reservoirs of the world. SEPM 2000, 20.
- Rodríguez, N.D., Philp, R.P., 2010. Geochemical characterization of gases from the Mississippian Barnett Shale, Fort Worth basin, Texas. AAPG Bulletin 94, 11, 1641-1656.
- Schenk, H.J., di Primio, R., Horsefield, B., 1997. The conversion of oil into gas in petroleum reservoirs. Part 1: a comparative kinetic investigation of gas generation from crude oils of lacustrine, marine, and fluvio-deltaic origin by programmed temperature closed-system pyrolysis. Organic Geochemistry 26, 467-481.
- Sefein, K.J., Nguyen, T.X., Philp, R.P., 2017. Organic geochemical and paleoenvironmental characterization of the Brown Shale formation, Kiliran sub-basin, Central Sumatra basin, Indonesia. Organic Geochemistry, 112, October 2017, 137-157.
- Singh, P., 2008. Lithofacies and sequence stratigraphic framework of the Barnett Shale, Northeast Texas. Doctoral dissertation manuscript. The University of Oklahoma, p. 227.
- Sierra-Perez, R., 2011. Integrated geomechanics and geological characterization of the Devonian-Mississippian Woodford Shale. M.Sc. thesis manuscript, The University of Oklahoma, p. 123.
- Slatt, R. M., Buckner, N., Abousleiman, Y., Sierra, R., Philp, R.P., Miceli-Romero, A., Portas, R., O'Brien, N., Tran, M., Davis, R., Wawrzyniec, T., 2012. Outcrop/behind outcrop (quarry),

multiscale characterization of the Woodford gas shale, Oklahoma, in J. Breyer, eds., Shale reservoirs-giant resources for the 21st century: American Association of Petroleum Geologists AAPG Memoir 97, 1–21.

- Slatt, R.M., Philp, P.R., Abousleiman, Y., Singh, P., Perez-Altamar, R., Portas, R., Marfurt, K.J., Madrid-Arroyo, S., O'Brien, N., Eslinger E.V., Baruch, E.T., 2012. Pore-to regional-scale integrated characterization workflow for unconventional gas shales: in J.A. Breyer, eds., Shale reservoirs-giant resources for the 21st Century. AAPG Memoir 97, 127-150.
- Slatt, R. M., Rodríguez, N.D., 2012. Comparative sequence stratigraphy and organic geochemistry of gas shales: Commonality or coincidence? Journal of Natural Gas Science and Engineering, 8, 68-84.
- Slatt, R.M., 2016. Institute of Reservoir Characterization (IRC), Woodford-Mississippian consortium, phase III technical report. The University of Oklahoma, p. 202.
- Slatt, R.M., Zhang, J., Molinares, C.E., Torres-Parada, E.J., Duarte, D., Milad, B., Galvis-Portilla, H., Becerra-Rondon, D., Ekwunife, I.C., Brito, R., 2018. Outcrop and subsurface geology applied to drilling, sweet spot, and target zone detection of resource shales: the Woodford example. Unconventional Resources Technology Conference, Houston, Texas, 2018. 2018 SEG Global meeting abstracts, 319-335.
- Tissot, B., Durand, B., Espitalié, J., Combaz, A., 1974. Influence of nature and diagenesis of organic matter in the formation of petroleum. American Association of Petroleum Geologists Bulletin 58, 3, 499-506.
- Tissot, B.P., Pelet, R., Ungerer, P.H., 1987. Thermal history of sedimentary basins, maturation indices, and kinetics of oil and gas generation. AAPG Bulletin 71, 1445-1466.
- Totten, M. W., 2011. Electron probe micro-analysis of the Woodford Shale, south-central Oklahoma, M.S. thesis manuscript, The University of Oklahoma, p. 137.
- Trenton, J., 2014. Outcrop-derived Chemostratigraphy of the Woodford Shale, Murray County, Oklahoma. The University of Oklahoma, M.Sc. thesis manuscript, p. 138.
- Turner, B., 2015. The use of Chemostratigraphy to refine ambiguous sequence stratigraphic correlations in marine shales: An example of the Woodford Shale, Oklahoma. AAPG education directorate, Woodford Shale forum: Focus on optimization. Oklahoma City, Oklahoma, 2015. AAPG Datapages Search and Discovery article 90241.

- Turner, B., Molinares, C., Slatt, R.M., 2015. Chemo stratigraphic, palynostratigraphic, and sequence stratigraphic analysis of the Woodford Shale, Wyche Farm quarry, Pontotoc County, Oklahoma. Interpretation 3, 1, SH1-SH9.
- Widayat, A.H., 2011. Paleoenvironmental and paleoecological changes during the deposition of the Late Eocene Kiliran oil shale, Central Sumatra basin, Indonesia. Johann Wolfgang Goethe University in Frankfurt am Main, Germany. Doctorate dissertation manuscript, 144 p.
- Zhao, W., Wang, H., Yuan, X., Zecheng, W., Zhu, G., 2009. Petroleum systems of Chinese nonmarine basins. Basin Research 22, 4 - 16.
- Zhang, J., Slatt R. M., 2019. The significance of karst unconformities on overlying resource shales: Lessons learned from the Devonian Woodford formation applied to the Permian Wolfcamp Shale. AAPG-SEG Interpretation, 7, 4, SK33-SK43.

Chapter II: 3D seismic identification of enclosed mini-basin fill, and their role as organic matter catchment areas for the Woodford Shale, Oklahoma, USA.

Publication Title: Torres-Parada, E.J., Slatt, R.M., Marfurt, K.J., Infante-Paez, L.E., Castillo, L.A., 2018. Identification of potential lacustrine-embayment stratigraphic intervals in the Woodford Shale, Oklahoma, using multi-attribute 3-D seismic displays and a supervised probabilistic neural network. Houston Geophysical Society Bulletin. January 2018 8, 5, 13-25.

2.1 Abstract

Several of the North American resource shales have been characterized as open marine sequences with the common characteristic of being deposited unconformably above a carbonate formation. The fluctuations in paleo sea-level during the deposition of these resource shales allowed the development of erosional topography that may have led to highly restricted depositional settings over the eroded pre-existing shallower carbonate platforms. Identifying the presence of these deposits is crucial to understand the differences in the amounts of the organic matter accumulated and preserved under these highly restricted geological conditions.

For this study, the highly restricted depositional conditions over the eroded pre-existing carbonate platform are identified as enclosed mini-basin fill settings. The main purpose is to calculate for the Woodford Shale in the Cherokee platform, South-Central Oklahoma, U.S.A, the lateral and vertical variations of total organic carbon (%TOC) under the enclose mini-basin fill settings. The analyzed data set corresponds to a post-stack 3D seismic volume with six wells with vertical penetrations and sonic log recorded for the complete Woodford Shale stratigraphy. The %TOC estimations were calculated and calibrated using rock cutting measurements of %TOC, density, resistivity and sonic logs. For predicting the %TOC lateral and vertical variations, a

model-based post-stack seismic acoustic impedance inversion and a supervised neural network analysis (probabilistic neural network, PNN) of 3D seismic attributes were applied. These analyses confirmed the hypothesis that the seismic impedance anomalies seen in the Woodford Shale correspond to internal lateral and vertical %TOC-bearing facies variation. In the study area, the Woodford Shale is both thicker and more %TOC-rich, where the underlying Hunton group (shallow carbonate platform) is completely eroded, and the topographic relief is high. Seismic analysis at and above the unconformity surface produced by the erosion of the Hunton group reveals pod-shaped intervals of high %TOC that may have been deposited as very restricted intervals in mini-basin fill settings. These results are tied to the Woodford Shale regional context for the identification of geological differences that potentially allowed the deposition of rock intervals under this enclosed mini-basin fill settings.

2.2.Introduction

Geoscientific research in Oklahoma has mainly focused over the past few years on the stratigraphy and sedimentology of the Upper Devonian-Lower Mississippian Woodford Shale (Comer 2005 and 2008; Cardott 2009 and 2014; Slatt, 2016). The Woodford is not only an excellent mid-continent (U.S.A.) oil and gas producer but also a good analog for other 'siliceous' unconventional resource shales, particularly if they are underlain by carbonates (Comer 2005 and 2008; Slatt and Rodriguez, 2012). The studies in the Cherokee platform, Oklahoma, have emphasized in the detailed mapping and stratigraphic characterization of the Woodford Shale (Castillo, 2013; McCullough, 2014; Ali; 2015; Figure 2.1- 2.3), but have also provided a foundation for relating the Woodford Shale stratigraphy to its geophysical, geochemical, and geomechanical properties (Amorocho-Sanchez, 2012; Cardona-Valencia, 2014; Figure 2.4). Shale researchers commonly interpret that the Woodford (and most analog resource shales) are wholly

of open marine origin (Slatt and Rodriguez, 2012). For the Woodford Shale, the Rock-Eval pyrolysis analyses usually indicate type II kerogen (Cardott, 2012); however, occasionally, a type I kerogen is detected (Cardott, 2009 and 2014). Other unconventional resource shales show a similar pattern, but these anomalies are often shrugged off as analytical errors (Slatt and Rodriguez, 2012).

Regional isopach maps of the Woodford Shale and Hunton Group in the Cherokee platform (McCullough, 2014; McCullough and Slatt, 2014; Ali, 2015; Figure 2.2) and the utilized 3D seismic survey in south-east Cherokee platform, Seminole County Oklahoma, reveal an unconformity surface on top of the Woodford Shale underlying carbonate rocks (Hunton Group). This unconformity surface has considerable karst topography and ~ >100m of vertical eroded relief (Milad, 2019; Figure 2.5 - 2.8). From these regional maps and from the identification of the unconformities at the base of the Woodford Shale, a geological model by Slatt (2016) claims that during a low stand of sea level, karst topography forms an irregular surface, which can provide discontinuous catchment areas for ponding of enclosed mini-basin fill water masses, creating restricted water circulation and establishing conditions for higher deposition and preservation of organic matter (Figure 2.2 and Figure 2.3). The 3D seismic survey is inverted to predict %TOC variability that shows discontinuous "pod-like" areas of local anomalously high %TOC in the deeper paleo-topographic Woodford Shale zones, contrasting with the conventional thinking that organic-rich strata are deposit from marine waters in a blanket fashion.

2.3.Geological background of the seismic study area

According to Cardott (2009, 2012 and 2014) and Jarvie et al. (2005 and 2007), the Woodford Shale is a very active and prolific gas and oil shale reservoir, that even in a mature exploration and production phase is still attractive. Therefore, there is a specific interest to characterize the possible

occurrence of internal enclosed mini-basin fill or highly restricted intervals within this open marine mudstone. This novel concept of enclosed mini-basin fill settings might provide untested internal horizons or areas where it is thought that the Woodford has a limited GOR (gas-oil-ratio) fluid production (more oil production over natural gas production; Katz and Lin, 2014). The Woodford Shale age is from Upper Devonian-Lower Mississippian and its principal lithologies are organic-rich black shale with intercalations of chert, siltstone, dolostones, and light-colored siliceous mudstones (Kirkland et al., 1992; Comer, 2008; Slatt et al., 2012; Molinares, 2013; Turner et al., 2015; Maynard, 2016). There are general assumptions that the whole Woodford Shale was deposited under a similar setting or regime, in local, regional and statewide scales (McCullough and Slatt, 2014).

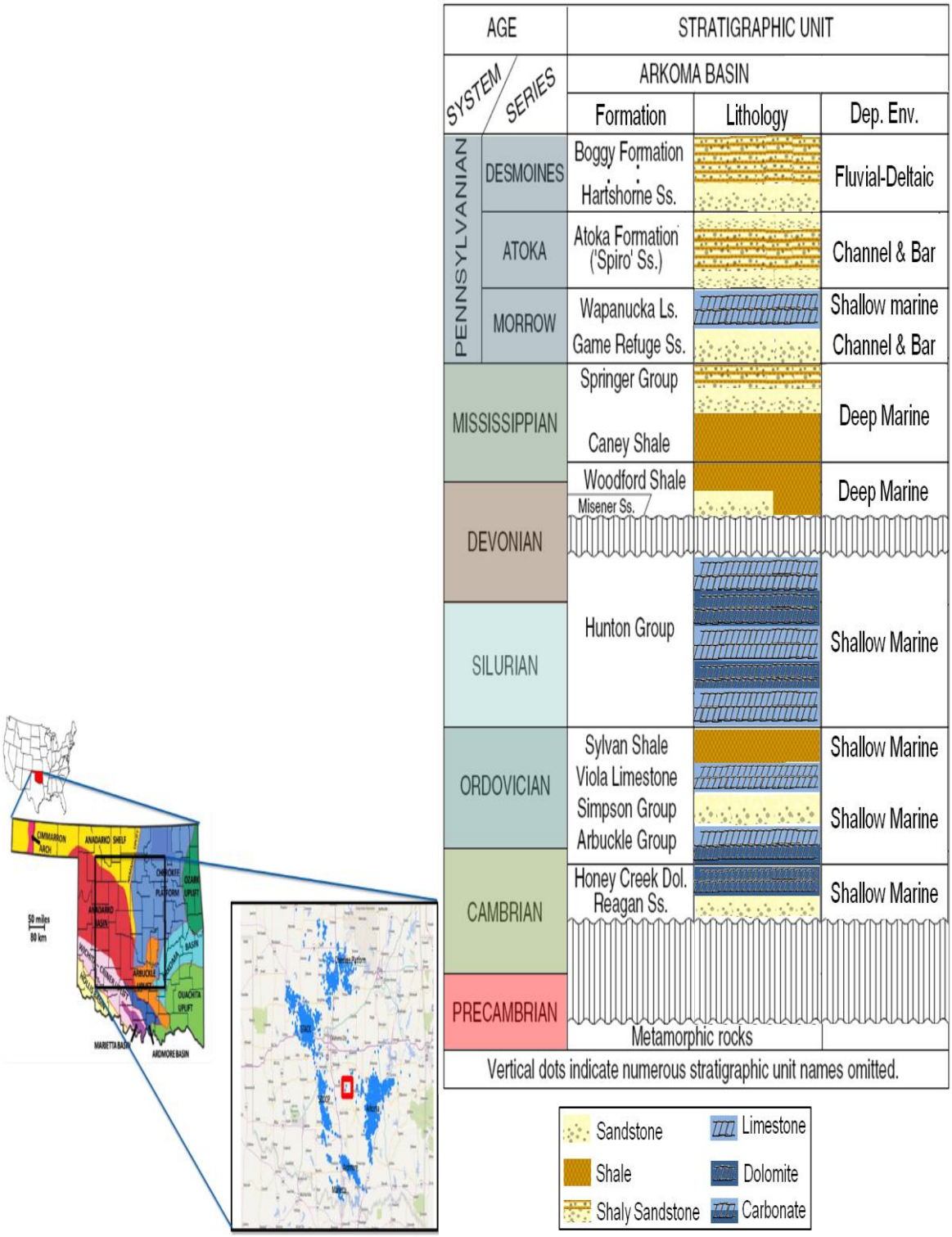

Figure 2.1. Location map of the Cherokee platform (res square of the map), and principal geologic provinces in Oklahoma (in light blue; after Northcutt et al., 2001); Image on the right corresponds to the stratigraphic chart for the Arkoma basin, southeastern Oklahoma (Modified after Perry, 1995).

The Woodford Shale unconformably overlies the limestones and dolomites of the Hunton group (Silurian-Devonian age) and grades conformably into fine-grained silty limestones interbedded with thin layers of dark-gray shales from the Sycamore formation (Figure 2.1; Modified after Perry, 1995; Slatt et al., 2012). Cardott (2012 and 2014) emphasizes that the Woodford Shale has a series of stratigraphic equivalents that extend over central and Eastern United States (e.g., Chattanooga Shale, Arkansas Novaculite, Antrim Shale, Bakken Shale, New Albany Shale, Marcellus Shale) that represent the global marine transgression which occurred during the Late Devonian (Figure 2.3; Sullivan, 1985; Kirkland et al., 1992; Northcutt et al., 2001; Comer, 2005; Slatt et al., 2012; Cardott, 2014).

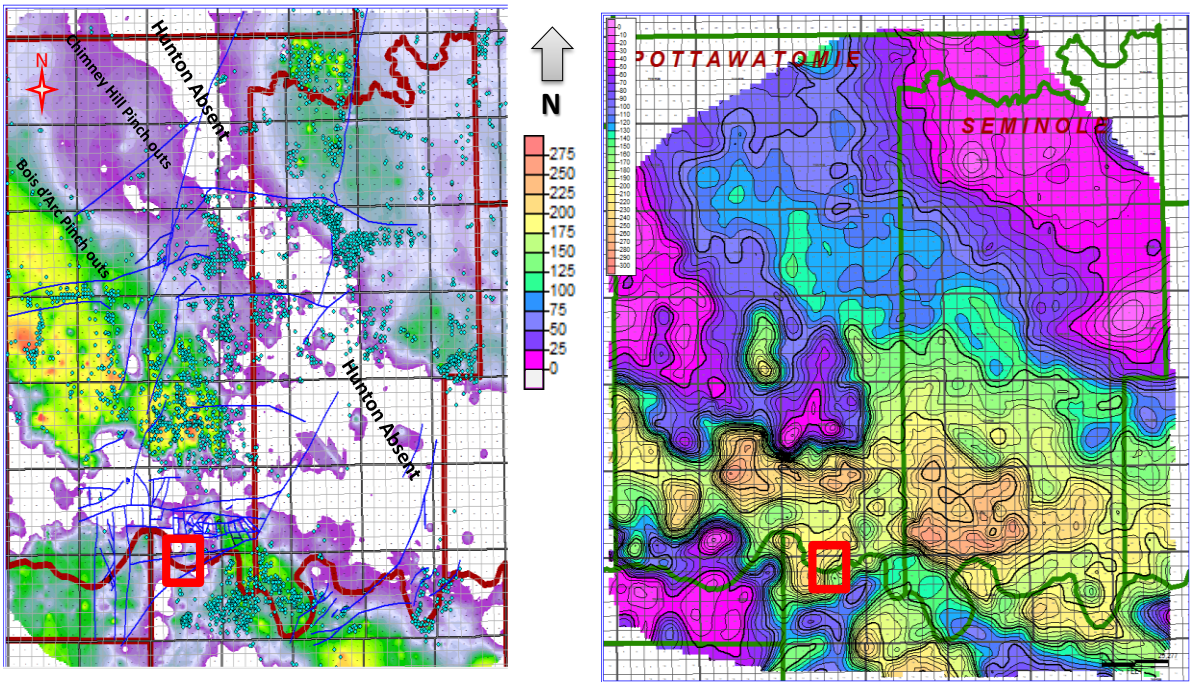

Hunton Regional Isopach Map

Woodford Regional Isopach Map

Figure 2.2. Regional isopach maps created from well tops by McCullough (2014). On the left, the Hunton group regional thickness map. On the right, the Woodford Shale regional thickness map. The study area is located in the red box of the southeast Pottawatomie and Pontotoc border, Oklahoma U.S.A. Note the inverse correlation of the formation thickness, where the Hunton is eroded the Woodford Shale is thicker than the areas where the Hunton is thick and preserve; this is attributed to the depositional model of the Woodford Shale where karstifications and lowstand incised valley formation occur to the Hunton exposure leading into more accumulation space for the Woodford depositional fairway.

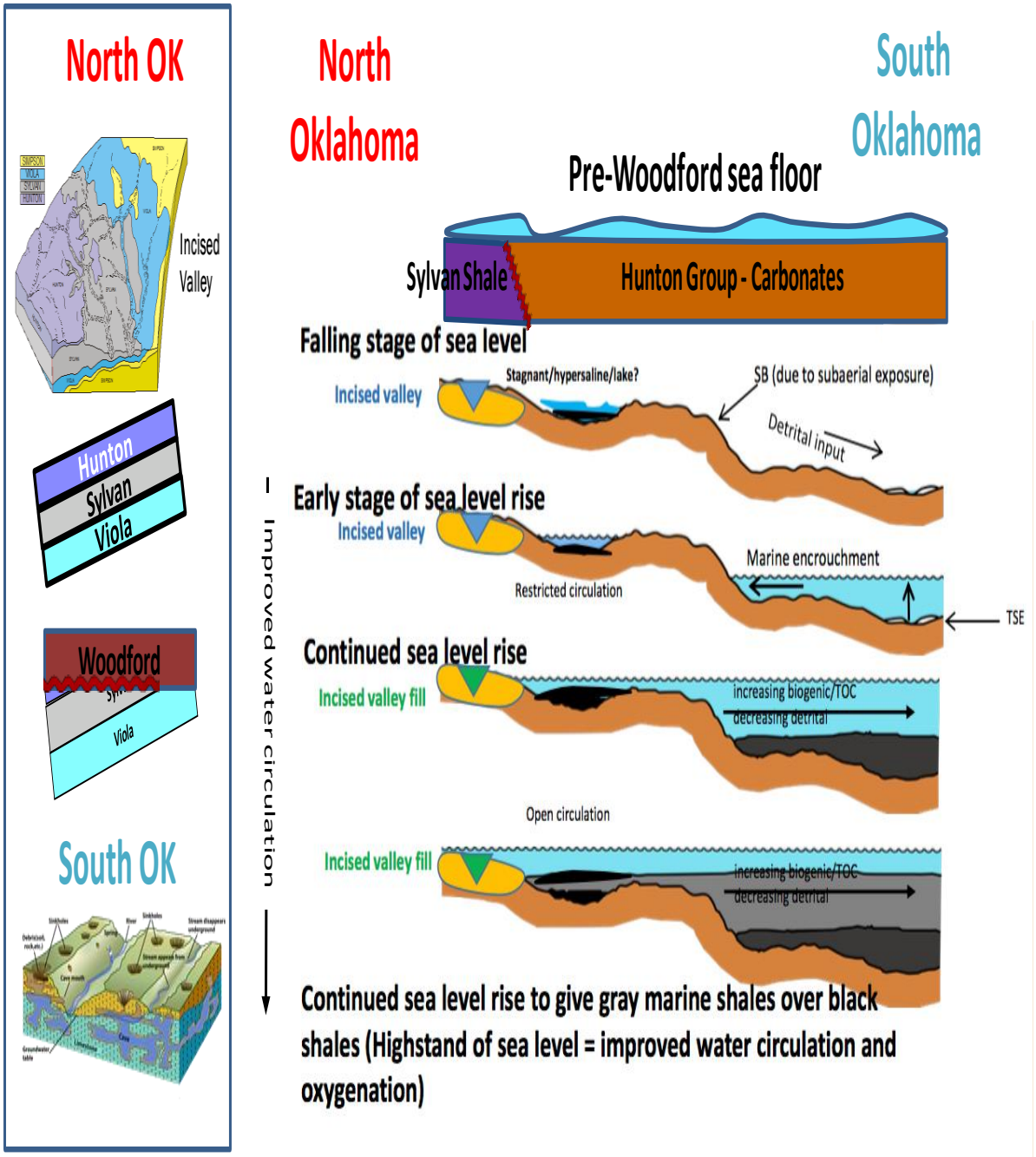

Figure 2.3. Depositional model of the Woodford Shale through one eustatic sea-level cycle (Torres-Parada et al., 2017; modified after Bauernfeind [1990], Grotzinger and Jordan [2010] and Slatt [2016]). The early stage of falling sea level may result in water mass isolation and restricted water circulation over topographic depressions left by karst/incised valley development on the underlying carbonate surface (Hunton limestone in the case of the Woodford). TSE= Transgressive surface of erosion; SB= Sequence boundary.

2.4. 3D Seismic multi-attribute analysis, organic facies (%TOC) identification, and low-frequency background model seismic inversion

For the Cherokee platform in Oklahoma, U.S.A., Althoff (2012), Amorocho-Sanchez (2012), Castillo et al. (2012), Cardona-Valencia (2014), and Infante-Paez et al. (2016) have proposed that a complete 3D seismic characterization is an essential part in the understanding of the Woodford Shale unconventional resource plays. Initially, the main objective of a 3D seismic characterization in their study areas was to identify geo-hazards such as faults, fractures, and karsting, which would negatively impact the drilling and completion operational practices of the wells, as recommended by Sena et al. (2011).

This study integrates a multi-attribute seismic analysis in combination with post-stack seismic inversion (P-impedance inversion, Z_p). The incorporation of seismic volumes with Z_p data is helpful for analyzing not only the significant geologic features such as faults, fracture zones, or folds but also to identify vertical and lateral changes in rock properties related to the impedance.

Hampson et al. (2001), Verma (2014) and Verma et al. (2016) proposed that there is a Z_p correlation with rock compositional properties, such as the total porosity and the organic matter %TOC. These correlations with Z_p help to understand the depositional conditions and variabilities of the rocks of interest, but additionally, to propose how to place horizontal wells in strata with higher potential for unconventional oil and gas production (rock intervals with higher %TOC and higher total porosity; applied workflow in Figure 2.4; Infante et al., 2016; Verma et al., 2016).

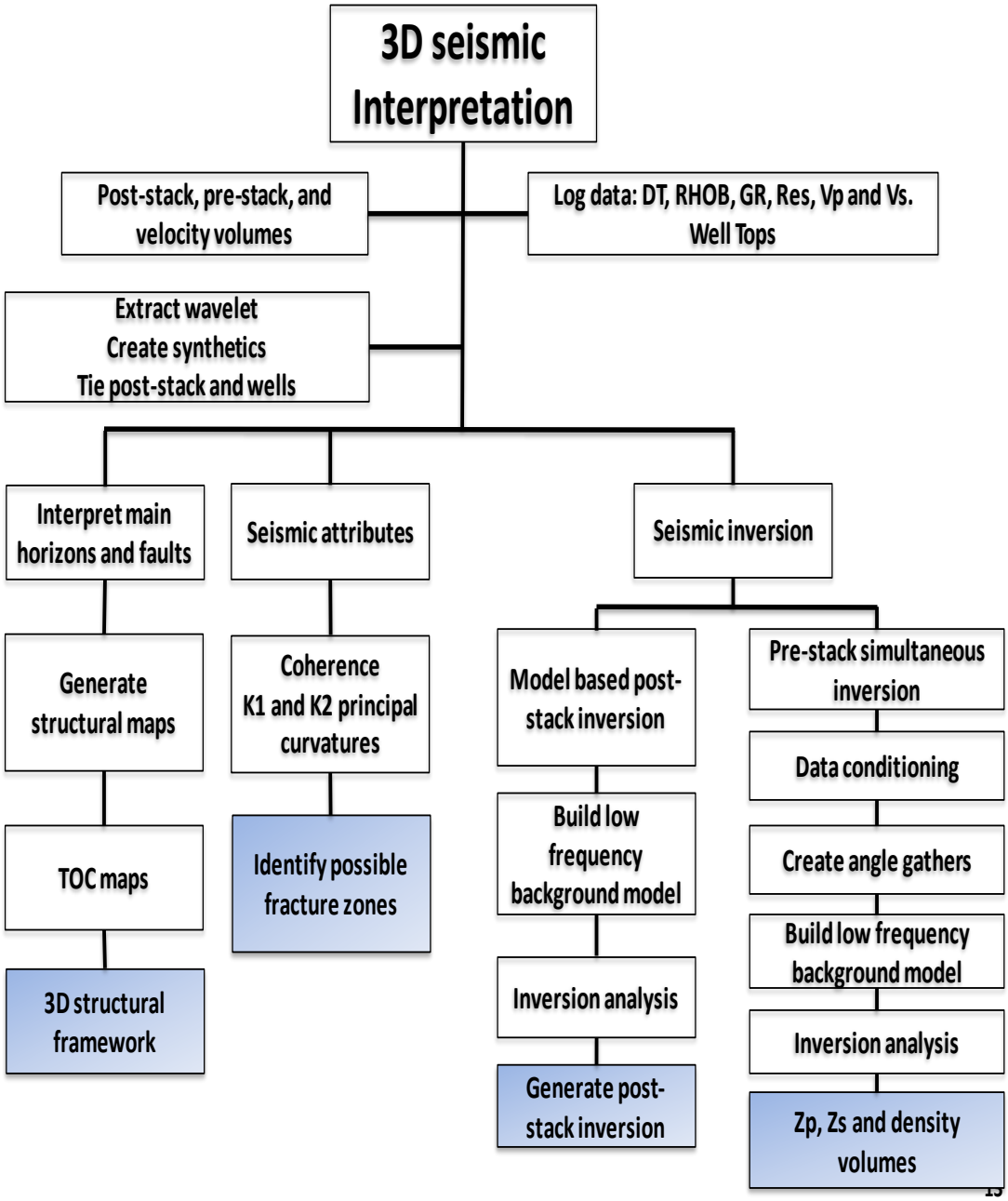

Figure 2.4. OU IRC-AASPI consortium 3D seismic interpretation and inversion workflow. Only post-stack data was available for inversion.

In order to highlight the presence of potential “enclosed mini-basin fill” type deposits, time thickness interpretation, coherent energy, most-positive, and most-negative curvature volumes were computed and interpreted for the Hunton Group horizon which represents the base of the Woodford Shale (Figure 2.2, Figure 2.5., Figure 2.7 - 2.11). By using coherent energy attributes, negative response features were identified as karsts and faults (Figure 2.10 and Figure 2.11).

In the study area, the Hunton group is almost completely eroded and characterized by low seismic energy values (Figure 2.10 and Figure 2.11). Also, the most positive and most negative curvature seismic attributes were a useful tool in identifying karst features (Figure 2.9 and Figure 2.11). These collapse features can be recognized as negative values of most-positive curvature (Figure 2.5, Figure 2.9 – 2.11; Baruch et al., 2009; Gupta, 2012). Also, the Hunton isochron map shows in the central and north part of the study area a concave downward pod-shaped structure topography (Figure 2.5, Figure 2.9 and Figure 2.11).

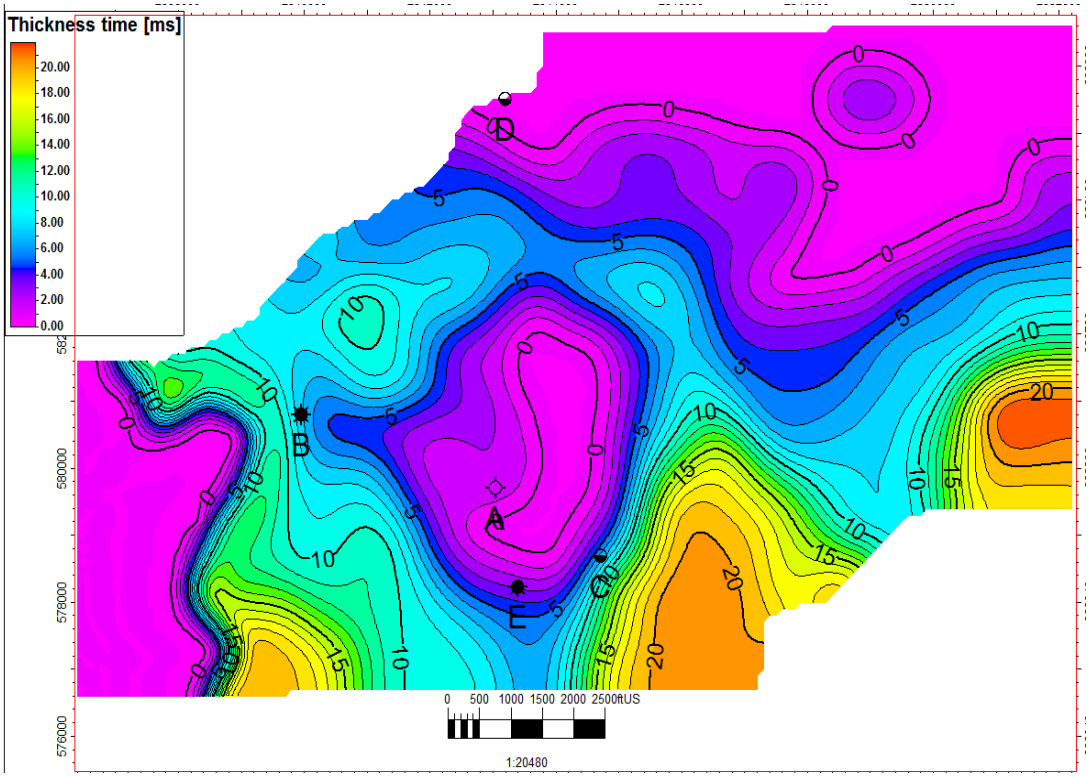

Figure 2.5. Time thickness map in milliseconds [ms] of the Hunton Group. Low isochron areas with the potential of enclosed mini-basin fill type deposits.

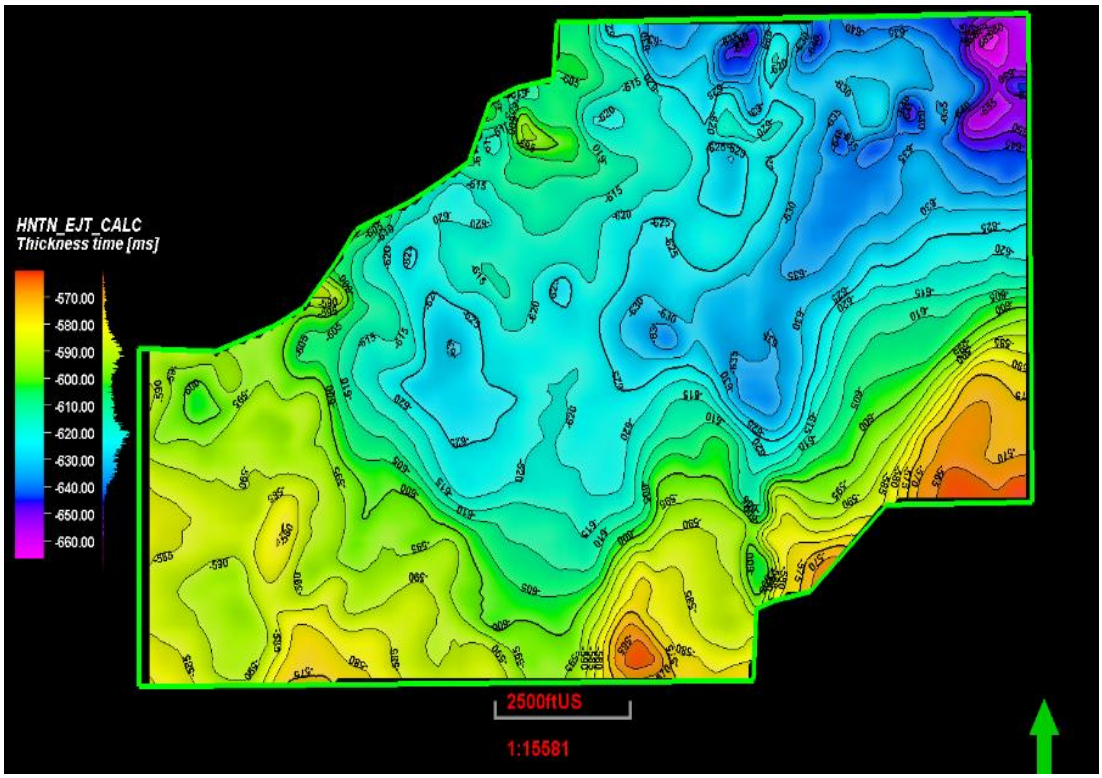

Figure 2.6. Time structure map in milliseconds [ms] of the Hunton group

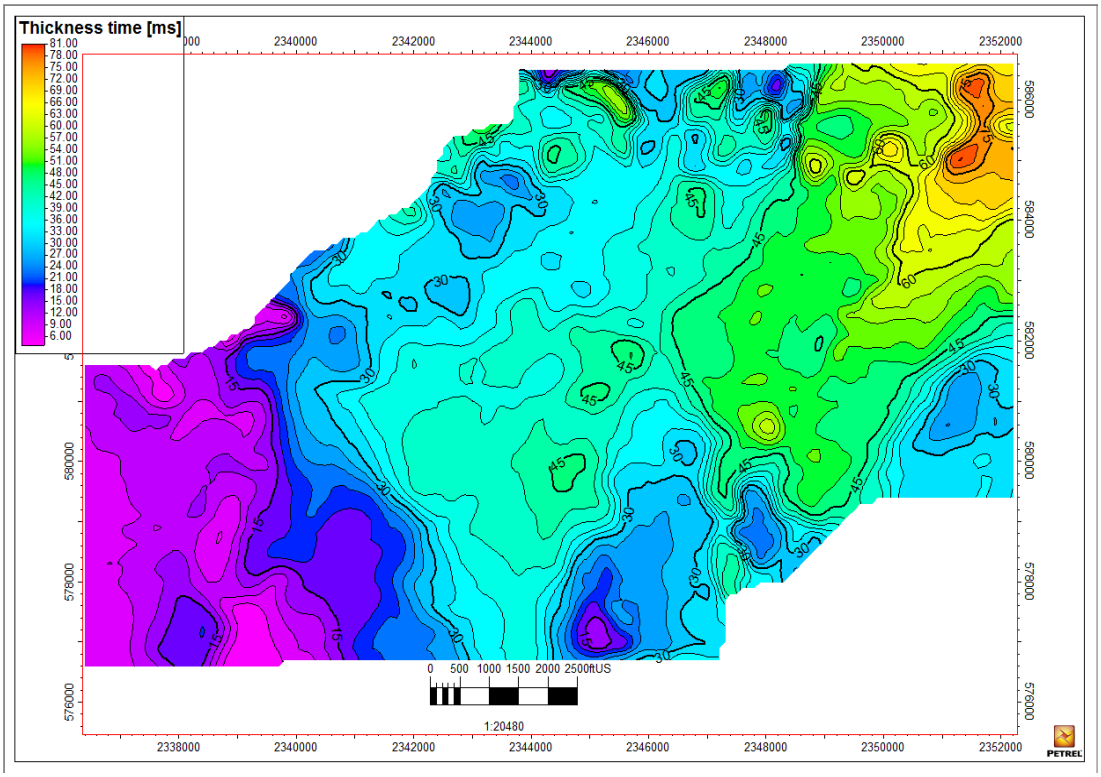

Figure 2.7. Time thickness map of the Woodford Shale [ms]. Note the thicker area in the middle part of the study area, where the Hunton isochron values (time thickness) are zero (Figure 4).

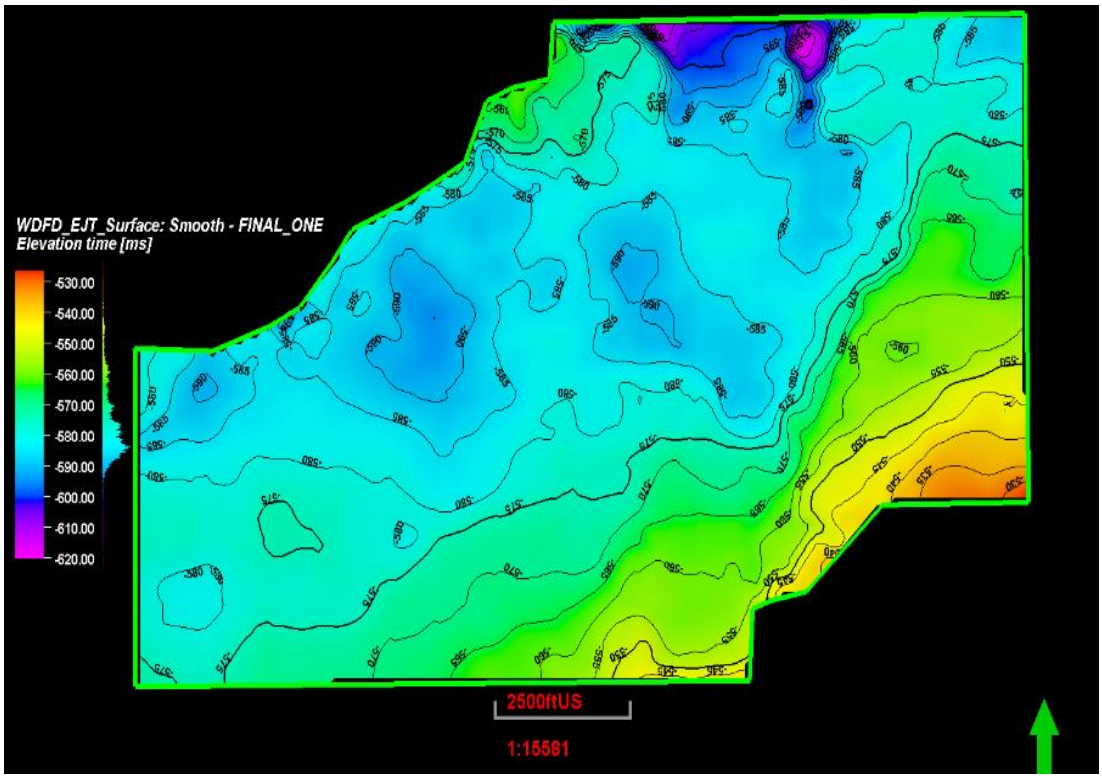

Figure 2.8. Time Structure map [ms] of the Hunton Group.

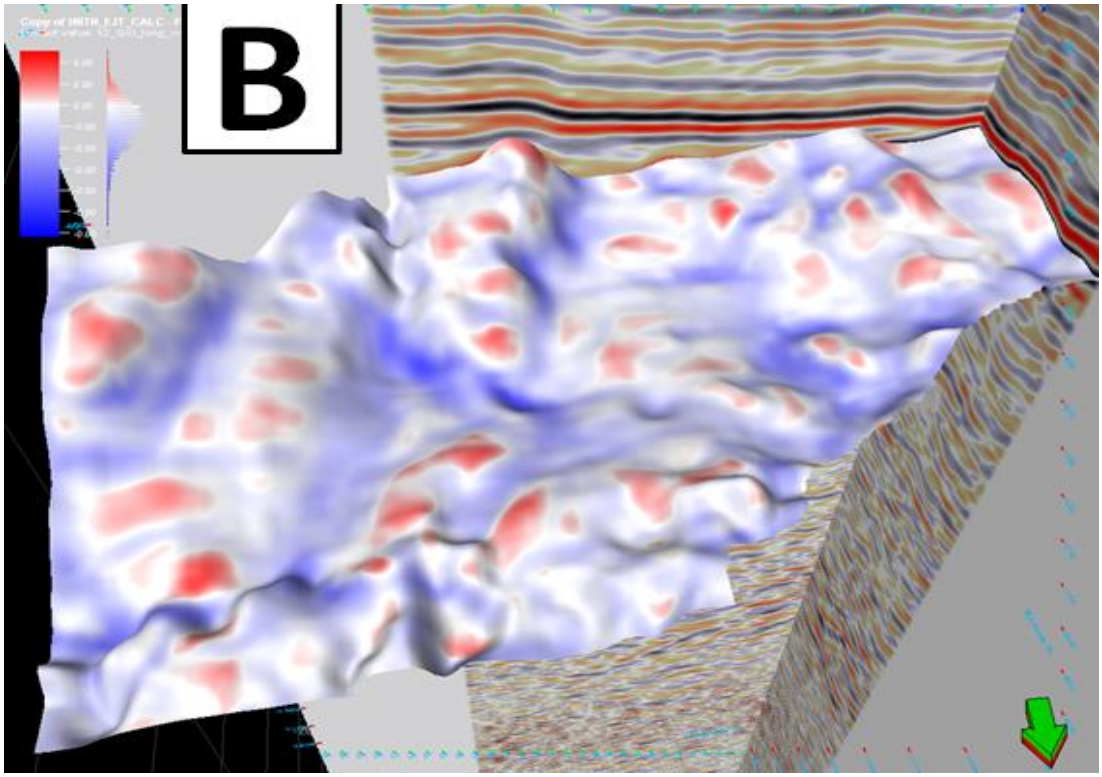

Figure 2.9. Horizon slice along the top Hunton through the most positive curvature and most negative curvature volume. Most negative curvature (blue areas) associated with significant karstifications and concave-down areas that can lead to an enclosed mini-basins fill.

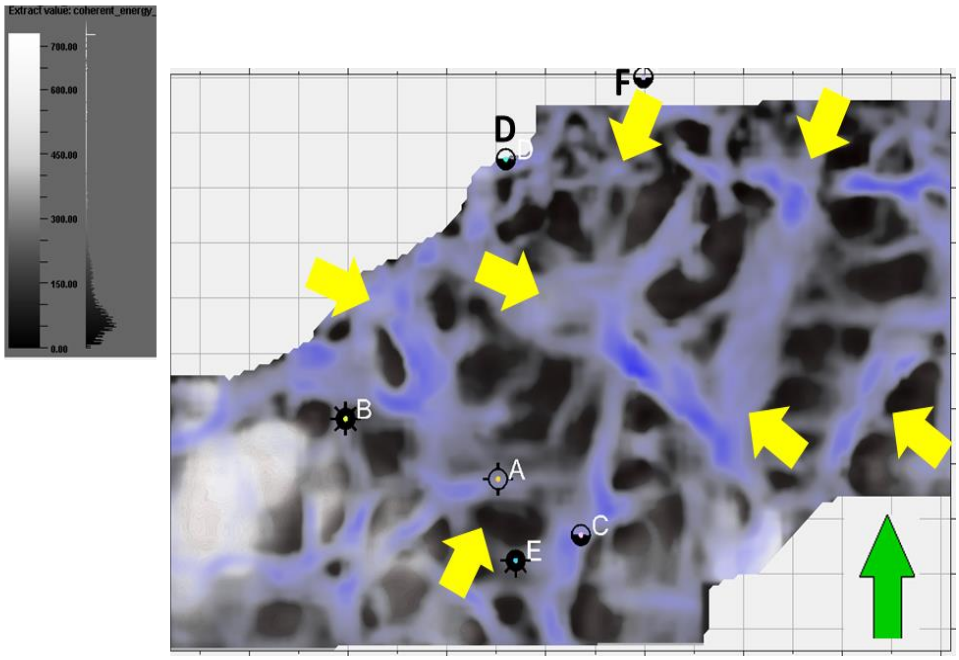

Figure 2.10. Hunton Group time-structure co-rendered with coherent energy, and most negative curvature. The yellow arrows indicate karst features and possible pod depressions; the Hunton Group is eroded (almost gone) in the study area.

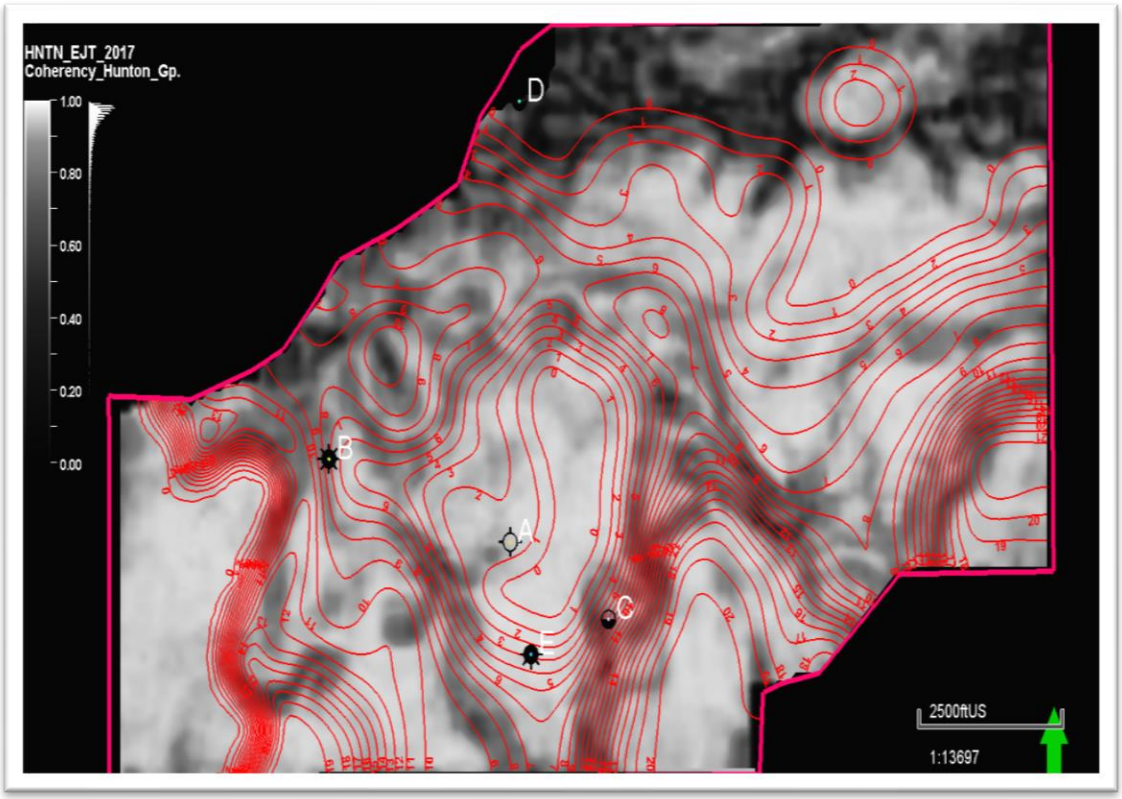

Figure 2.11. Hunton time-thickness co-rendered with coherent energy (zero and near-zero that correlate with dark coherency features contours indicate karst features and possible lake pods). Note that the Hunton group is eroded (almost gone) in the study area.

The Z_p is the product of rock density and P-wave velocity; therefore, it is a derived rock property (Hampson et al., 2001). The Z_p inversion is the transformation of seismic data into pseudo-Z_p logs at every seismic trace (Latimer et al., 2000). Latimer et al. (2000) and Verma et al. (2016) list some advantages of using impedance data in quantitative 3D seismic calculations, including:

- A good impedance model contains more information than seismic data since it is the result of integrating seismic, well log, and velocity data.
- Z_p is closely related to lithology and porosity, providing the basis for the generation of 3D facies and petrophysical models.

- The Z_p concept is generalized to handle the inversion of angle or offset stack data to elastic impedance or elastic parameters. This kind of data analysis can improve the ability to discriminate lithology and fluids.

Verma (2014), Infante-Paez et al. (2016), Verma et al. (2016), and Torres-Parada et al. (2017), report that since Z_p is an indirect measurement of the bulk density properties in rock lithologies, the impedance volumes are an excellent correlation factor with organic matter content in rocks (high %TOC correlates with low Z_p, and vice versa). As proposed by Amorocho-Sanchez (2012), Verma (2015) and Verma et al. (2016), for determining the geological and internal organic facies variations in unconventional shales, a model-based Zp should be estimated. This model-based inversion workflow begins with a low-frequency background geological model that is modified until the error has been minimized between the synthetic seismic trace created by that model and the original seismic data (Infante et al., 2016; Verma et al., 2016).

The main objective for generating a model-based inversion of the Woodford Shale was to identify vertical and lateral facies changes that may help to delineate the "enclosed mini-basin fill" deposits (Figure 2.3 and Figure 2.11). All the six wells in the study area (Figure 2.12) were used for the initial model (Figure 2.13 and Figure 2.14), and the statistical wavelet extracted from the wells was used on the model-based inversion. The Woodford Shale has the lowest impedance due to its low velocities and low densities (Figure 2.14). The initial inversion model revealed a higher vertical resolution and lateral impedance changes within the Woodford Shale (Figure 2.14 - 2.16).

The work of Verma (2014) proposed the quantitative seismic analysis of unconventional shales, and that several well logs could measure the presence of %TOC. The high Gamma-ray log response can be correlated to high uranium content in the organic matter (Fertl and Chilingar, 1988), but can also be attributed to heavy elements deposited within mudstones due to upwelling

currents (Turner et al., 2015). Additionally, a common characteristic is that the organic matter is less dense than to the mineral matrix resulting in a low measurement on bulk density log (Schmoker and Hester, 1983; Verma 2014). The transit times recorded on the P-sonic log may increase in the presence of organic matter (Passey, 1990; Sondergeld et al., 2010; Verma, 2014) but also can be indicators of zones with overpressure regimes.

The neutron logs (PHIN, NPHI, PHIS) may provide a high response in the presence of organic matter (Sondergeld et al., 2010; Verma, 2014). Passey (1990) states that as the organic matter is non- conductive, the resistivity logs read high values for high %TOC in immature source rock intervals. For this reason, Verma (2014) for the Barnett Shale, and Altoff (2012), Amorocho-Sanchez (2012), Infante-Paez et al. (2016) and Torres-Parada et al. (2017) propose for the Woodford Shale that the structural lows may have been isolated or semi-isolated lakes-embayments represented by locally increased accommodation space, and in the study areas might correspond to restricted Woodford Shale organic-rich deposits, therefore providing opportunities for more innovative unconventionals exploration targeting.

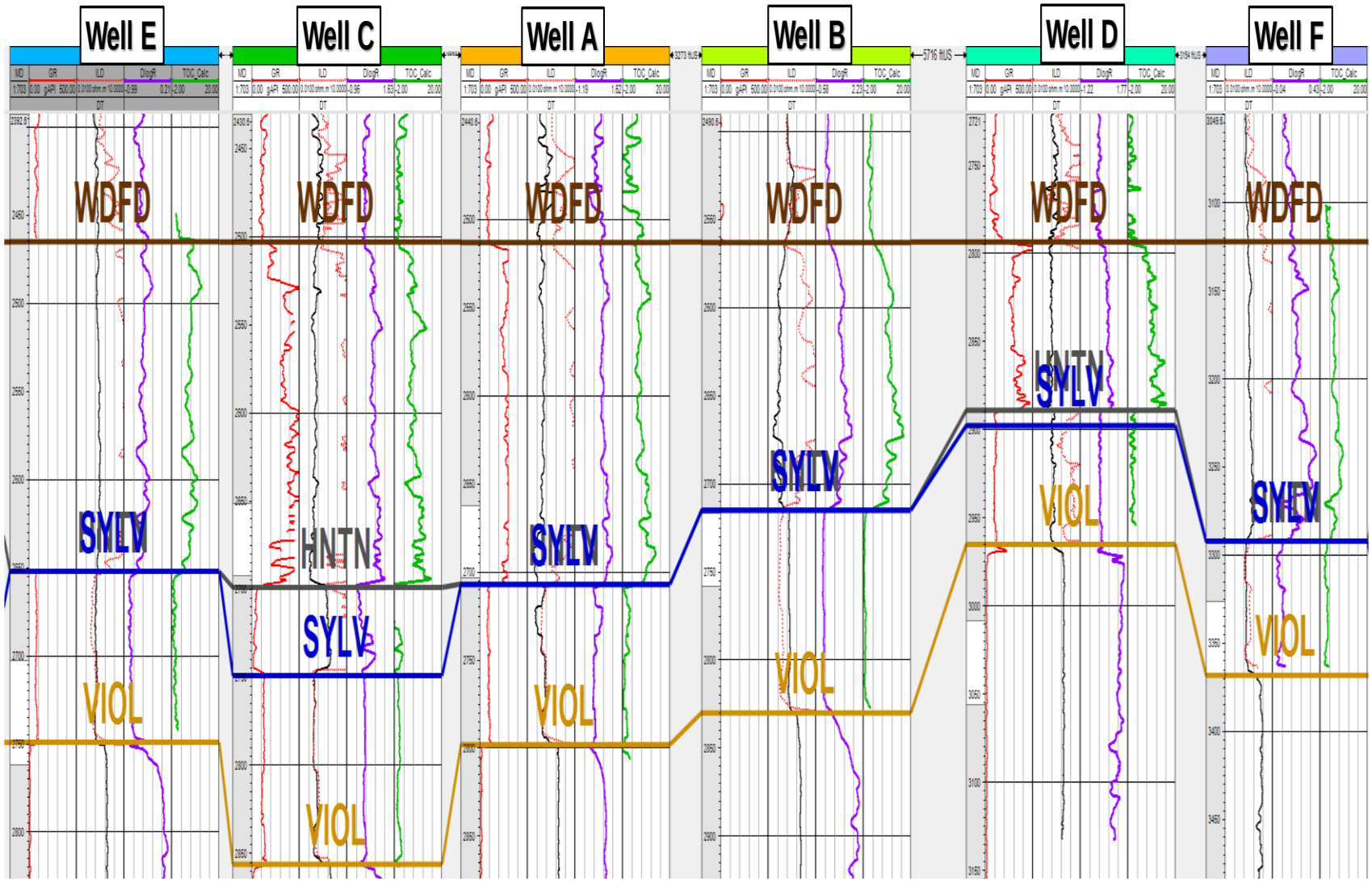

Figure 2.12. Stratigraphic correlation of the wells in the study area flattened at the Woodford Shale top. Note the thickness variations of the Hunton group and where it is absent, and the Woodford Shale has the highest thickness. These restricted intervals served as %TOC catchment areas, as it can be observed that the lowermost Woodford Shale has the highest %TOC in all wells (green curve).

2.4.1. Details of %TOC estimation using Passey's well log methodology

According to Passey et al. (1990), the presence of organic matter and the presence of generated hydrocarbons can have a tremendous response on the resistivity well log. The technique presented by Passey et al. (1990 and 2013) uses the overlap of a porosity log, usually the sonic on a deep resistivity curve (Figure 2.13). Passey et al. (1990 and 2013) attribute this well-log separation in high organic-rich intervals as the result of the low density/low-velocity kerogen, where the resistivity responds to the formation fluid.

To be able to calculate the %TOC content using this method, the level of organic metamorphism (LOM) reached by the organic matter in the rock must be known or estimated. In this case, the previous work by Miceli-Romero (2010) and conclusions by Cardott (2012) for the southeast Cherokee platform were assumed to be valid LOM of 8 in order to calculate the %TOC for the wells in the study area (Figure 2.13).

Passey's (1990 and 2013) method is also called "Delta log R" method (Figure 2.13), and it requires a resistivity log along with a porosity log e.g. P-sonic, density or neutron log in order to estimate %TOC log:

$$\Delta\log R = \log10\,(RTD / RTD\_Base) - 2.5 * (RHOB - RHOB\_base) \quad (3.1)$$

$$\%TOC = (\Delta\log R * 10\,a), \quad (3.2)$$

where,

$$a=0.297 - 0.1688 * LOM, \text{ and} \quad (3.3)$$

RTD: deep resistivity in any zone (ohm-m)

RTD_Base: deep resistivity baseline in non-source rock (ohm-m)

RHOB: bulk density (g/cm3)

RHOB_base: bulk density baseline in non-source rock (g/cm3)

LOM: Level of Maturity. Assumed 8 because is an immature area.

The LOM has been correlated to vitrinite reflectance (Ro%) (Passey et al., 1990), which also indicates the maturity of the rock. The %TOC computed with LOM=8 provides the best match with cuttings %TOC measurements. Therefore, the same values of RTD_Base, RHOB_base, and LOM were for all the wells in the survey area. The revised graphic relation of logR vs. derived %TOC published by Passey et al. (2010) was used for the calculations. A baseline was drawn at the Sylvan Shale (which is a low %TOC shale; Figure 2.13), and a LOM of 8 was applied, which is equivalent to a vitrinite reflectance (%Ro) value of 0.56% to honor the published %Ro data of the study area (Cardott, 2012). The calculated %TOC curve (Figure 2.13) was included in the seismic well-tie (Figure 2.14) of all wells in the study area.

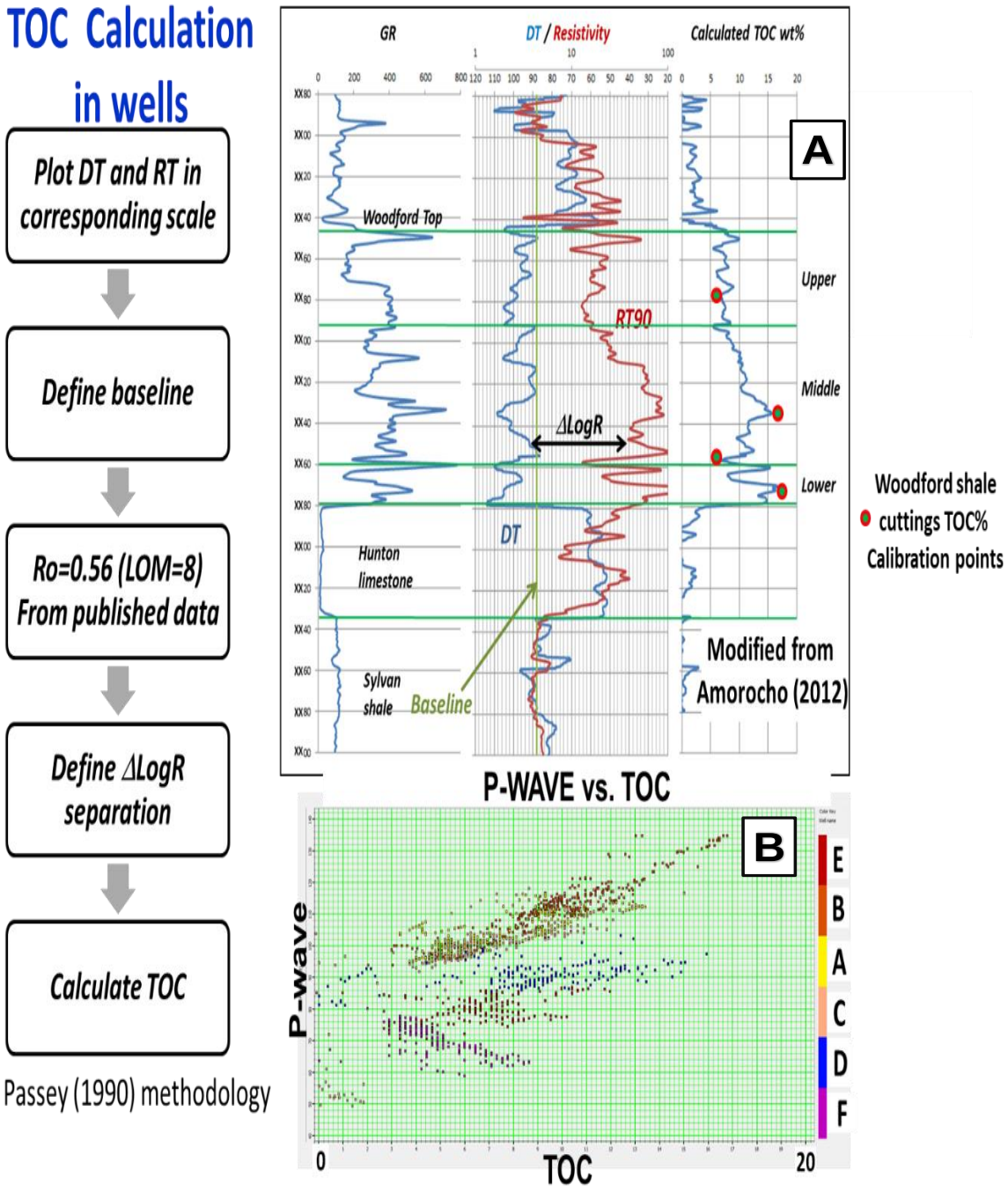

Figure 2.13. A) %TOC calculation process using Passey et al. (1990) methodology; **B)** Cross-plot of calculated %TOC (wt.) in wellbores and the P-impedance (calculated in all wells), the data points are color-coded according to each well. Modified after Amorocho, 2012.

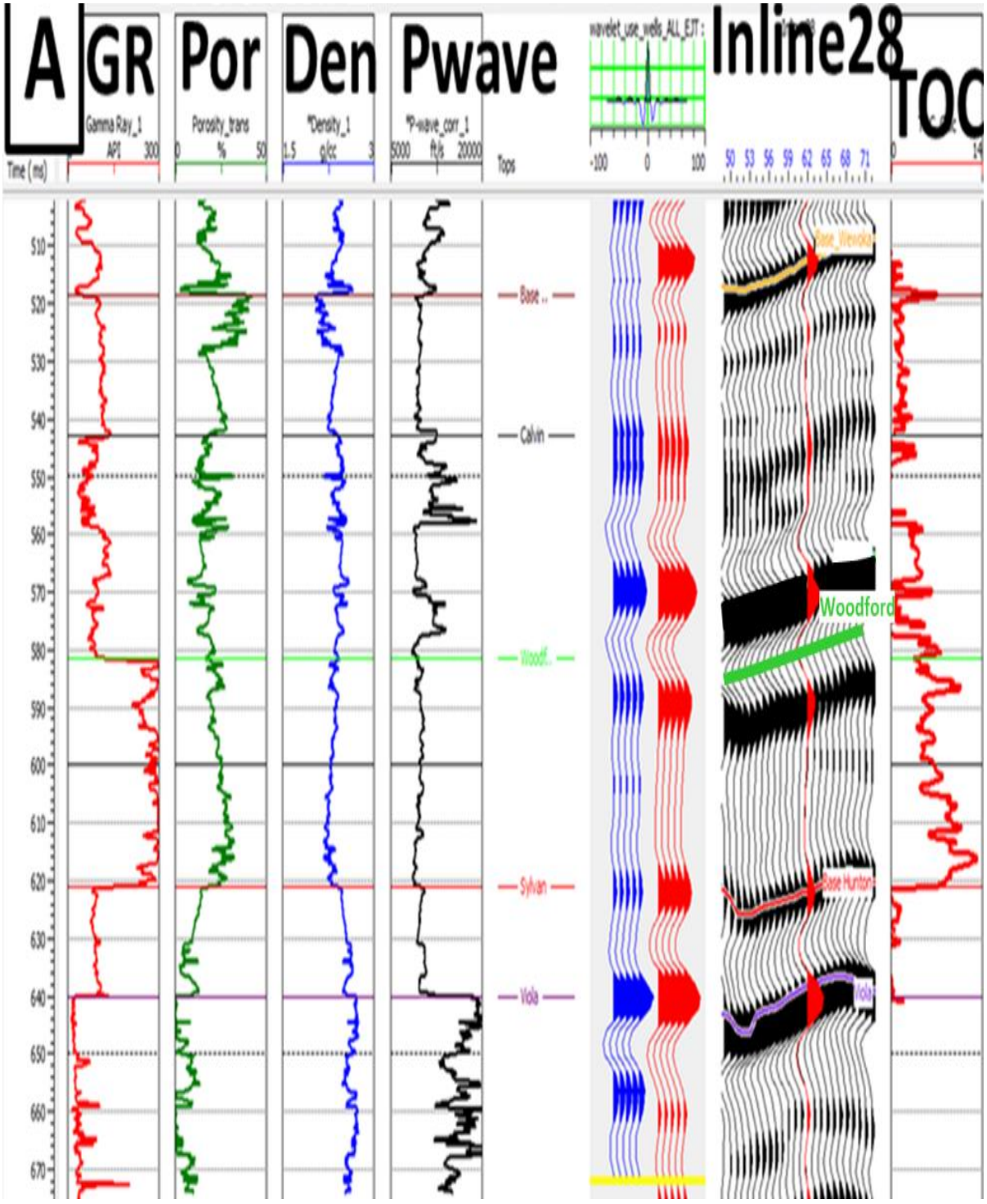

Figure 2.14. %TOC (wt.) calculation and seismic tie for well A using the Passey et al. (1990) method and the seismic well-tie and synthetic seismogram generated. A statistical wavelet using all wells was applied. The Woodford Shale top is the light green horizon, and the base is the red horizon (Sylvan Shale).

The RTD baseline is interpreter-dependent (Passey et al., 2010). The RTD_Base= 5 ohm-m was used, and a RHOB_base =2.53 g/cm3 for shaly intervals (Figure 2.13). For providing an input to the probabilistic neural network (PNN) and then estimate %TOC in three dimensions across the seismic survey, the calculated Passey-methodology %TOC (which is an estimated %TOC) is referred as "actual TOC" in the PNN (Figure 2.14, the red curve on the top right track). The calculated %TOC form the PNN is computed after estimating the non-linear relationships with the 3D seismic attributes. The PNN estimated %TOC is referred to as "modeled TOC" (Figure 2.14).

2.5.Results: Post-stack seismic inversion and supervised neural network analysis

To distribute %TOC in the study area, a supervised PNN workflow was applied to incorporate the post-stack 3D seismic data in combination with the calculated Z_p from the seismic inversion (Figure 2.5, Figure 2.16, and Figure 2.17). Similarly, to the methodology applied by Infante et al. (2016), principal components analysis (PCA) of spectral decomposition data every 5Hz, combined with the Z_p, coherent energy and similarity volumes were used as inputs to the PNN. All these seismic calculated volumes acted as external attributes for the supervised neural network analysis (Figure 2.18, and Figure 2.19).

The input attributes applied in the workflow for training the neural network are shown in Figure 2.4, Figure 2.18 and Figure 2.19. During the supervised neural network training (Figure 2.18), the weighting function is adjusted to optimize the prediction of %TOC as a direct indicator of organic facies variations and for avoiding the neural network overtraining (Figure 2.19, Figure 2.20, and Figure 2.21). High %TOC zones correlate with the location of karst features, and potential restricted enclosed mini-basin fill deposits (Figure 2.22, Figure 2.23, and Figure 2.24).

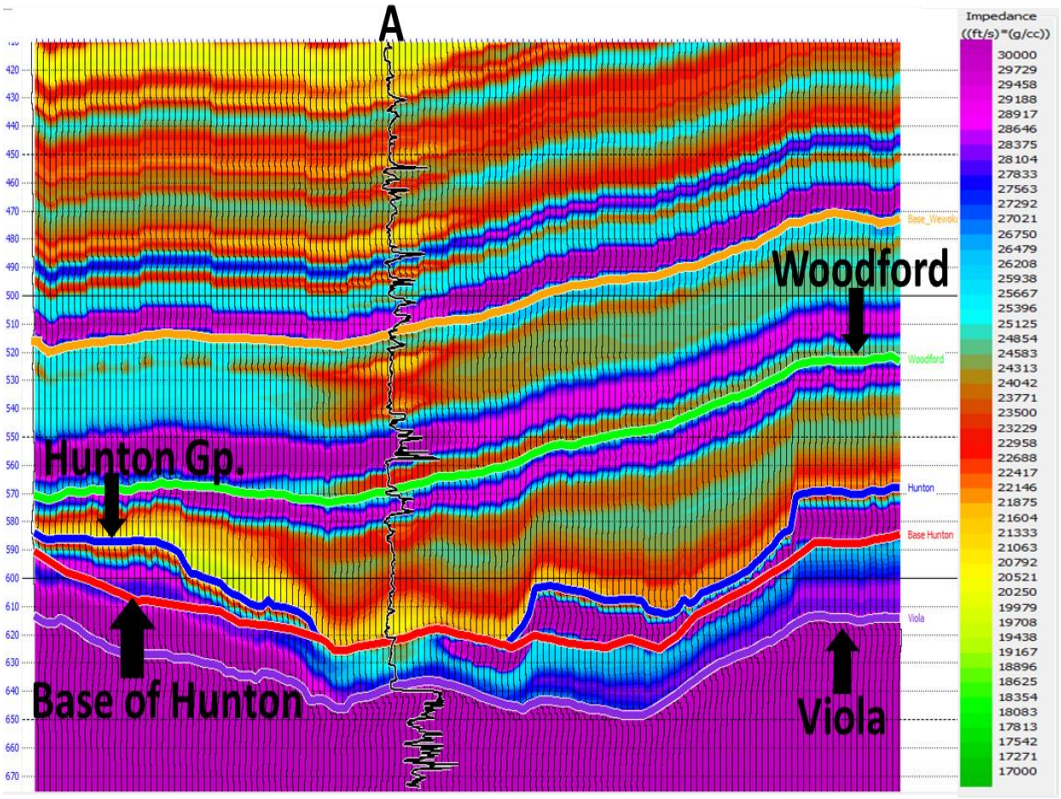

Figure 2.15. Initial low-frequency background model on an in-line passing through well A.

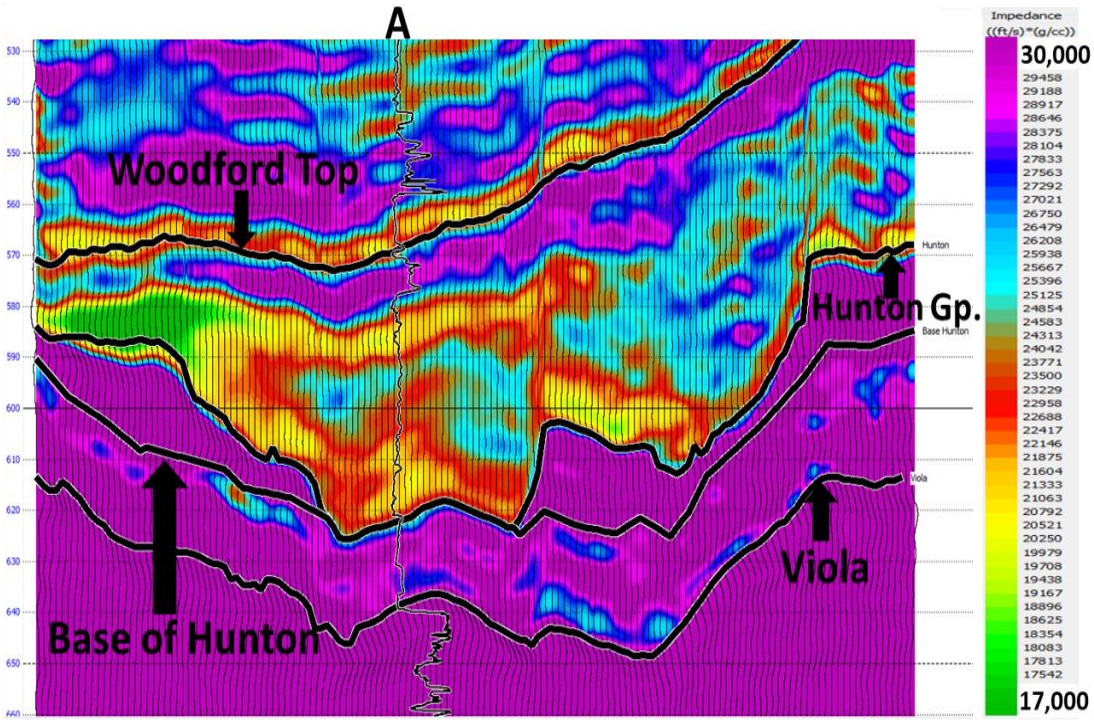

Figure 2.16. Inversion Zp results in an arbitrary impedance in-line showing well A.

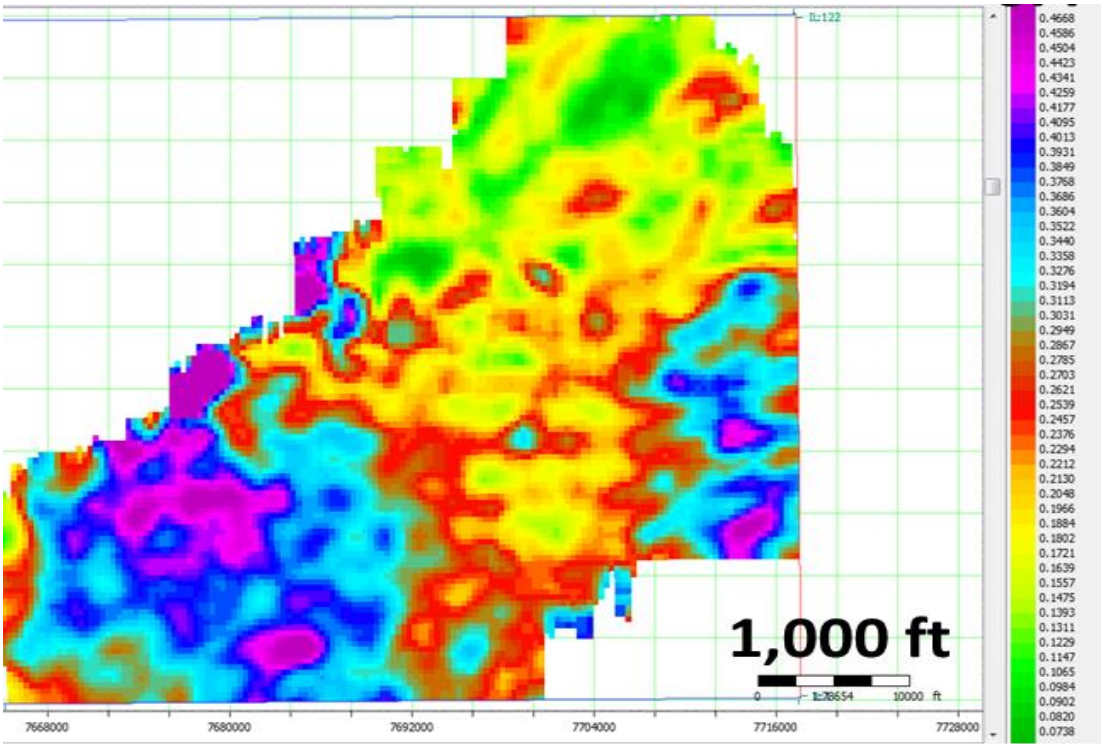

Figure 2.17. Data-error slice calculated two milli-seconds [ms] below the Woodford Shale top seismic horizon. A higher error in the SW of the study is due to the probable tuning effect, where the Woodford Shale and Hunton seismic horizons are very close, and the time thickness for both formations are minimal.

The applied seismic analysis window of the PNN training and calculations were limited only to the Woodford Shale seismic window (±50 milliseconds [ms] from Woodford Shale top and base) and were aimed to be within the stratigraphic zone of interest to obtain a better correlation in the calculations and %TOC seismic modeling (Figure 2.14 and 2.21). The PNN performed the non-linear relationship calculation process at every sample location in the seismic volume (Heggland, 2004). Each PNN sample point was compared to each data sample of the calculated %TOC-log in wells, with nine data samples of each of the three selected seismic attributes (Zp, coherency and principal component analysis vector1 [PC1]; Figure 2.19).

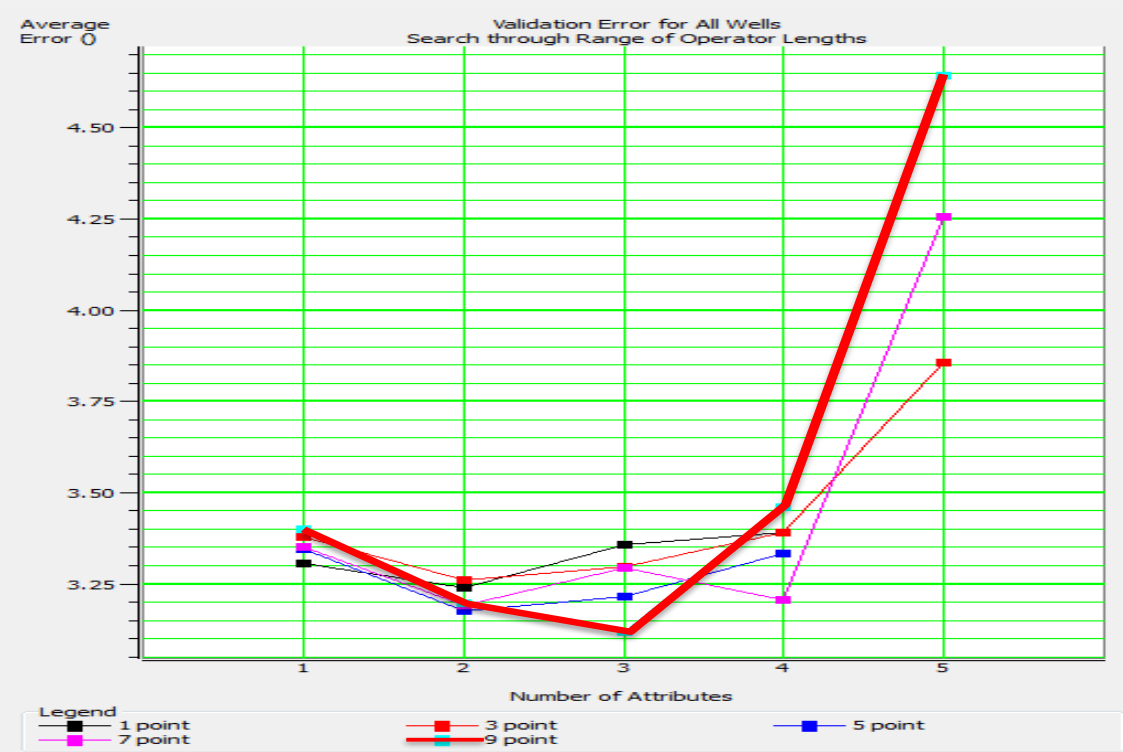

Figure 2.18. Probabilistic neural network (PNN) training operator length and attribute selection.

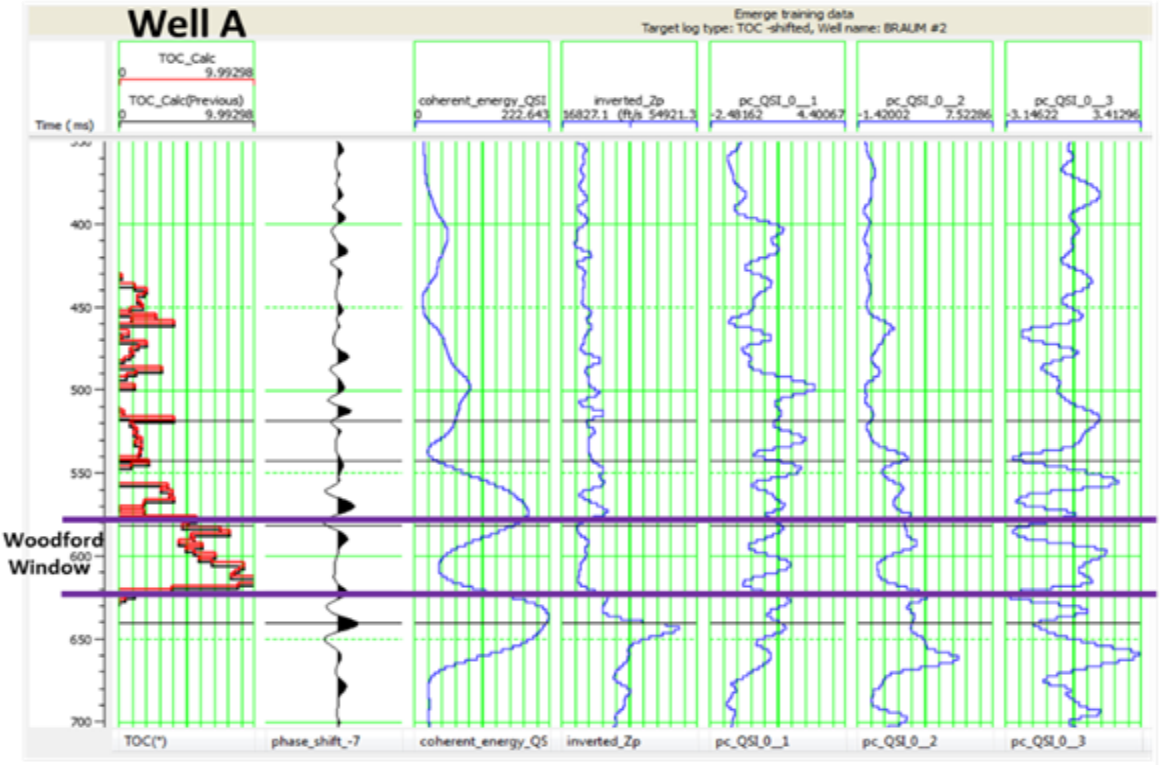

Figure 2.19. PNN training data. %TOC (red) with extracted seismic data, coherent Energy and Zp from seismic inversion, spectral decomposition every 5Hz principal components 1, 2, and 3.

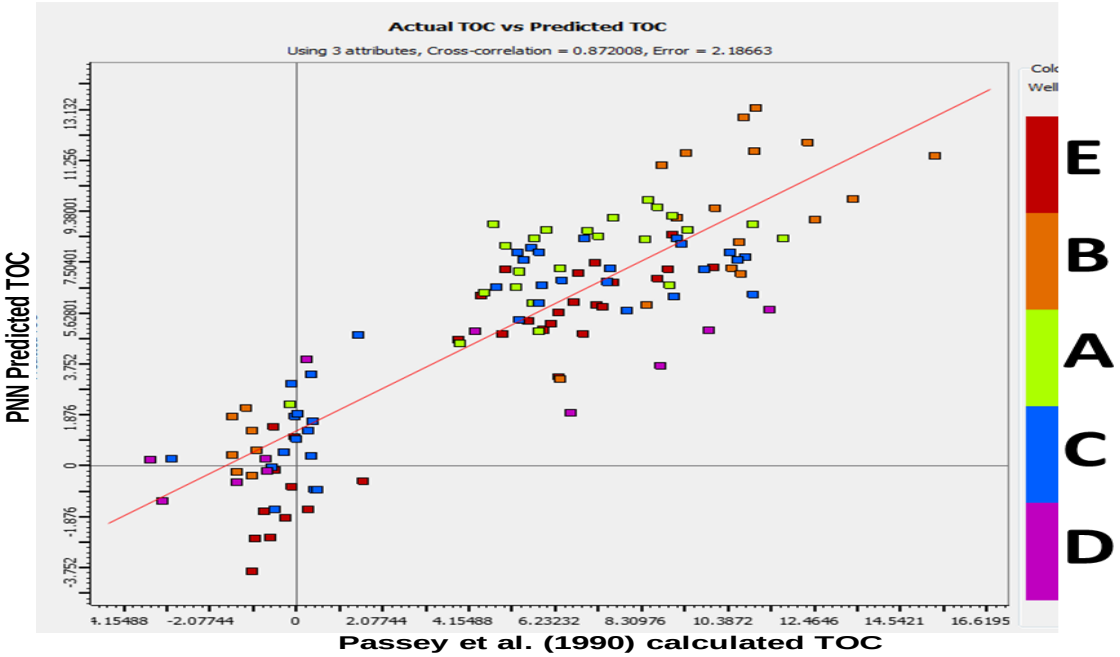

Figure 2.20. Multi-attribute regression of actual %TOC (Passey et al. [1990] method calculated) vs. predicted %TOC. Three attributes were used in the regression: Z_p, coherent energy, and spectral PC 2. Negative %TOC values correspond to the Hunton Group.

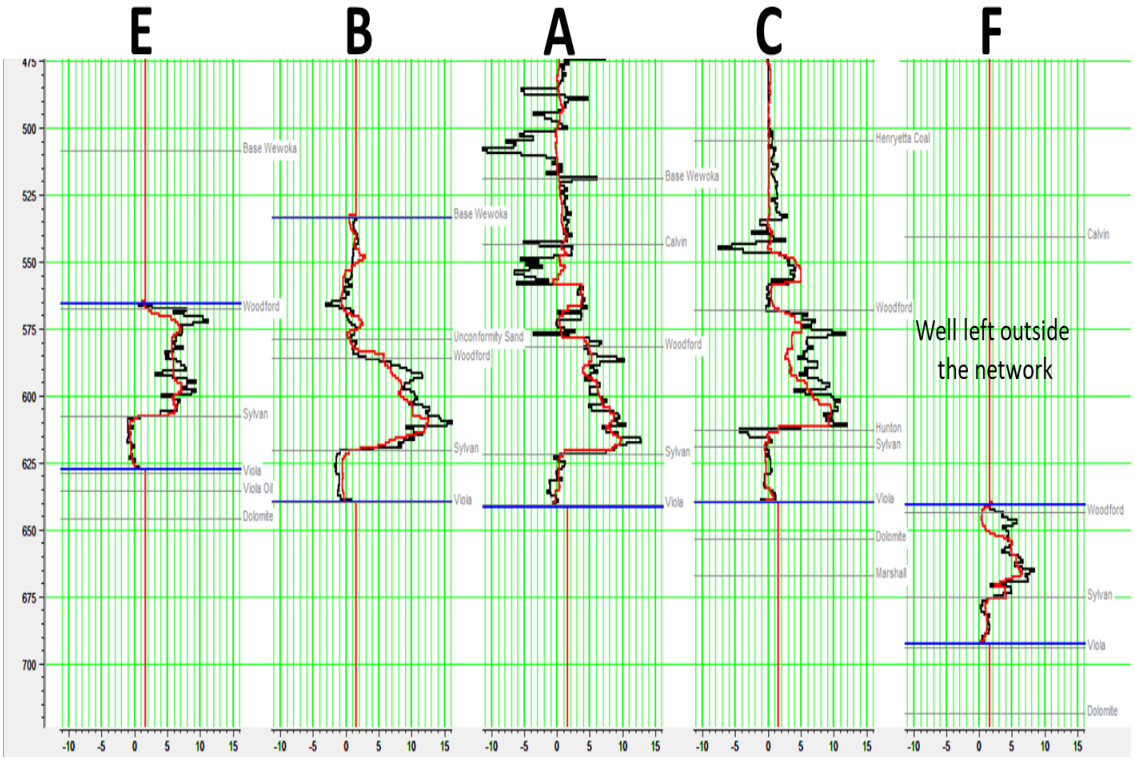

Figure 2.21. Probabilistic neural network using three attributes. %TOC calculated with Passey et al. (1990) methodology in a black curve, %TOC modeled from the supervised neural network in the red curves.

The PNN modeled %TOC results show that the Woodford Shale is thicker and with more %TOC where the Hunton Group is entirely or significantly eroded, and structural features allow the identification of concave-down enclosed mini-basins produced by karstification or wide incised valley processes of the Hunton Group paleo platform (Figure 2.24).

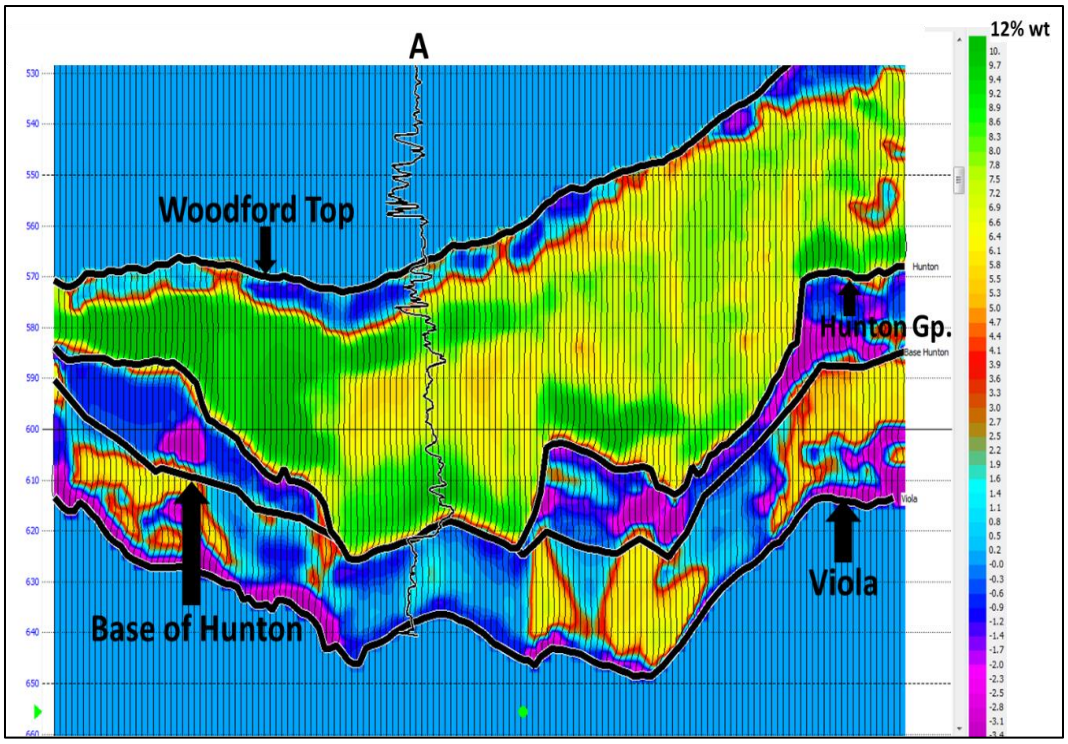

Figure 2.22. Inline of the %TOC cross-section extracted along the Woodford Shale. Note the lake-pod shape of the Woodford where the well is located. Higher %TOC is computed for these enclosed areas.

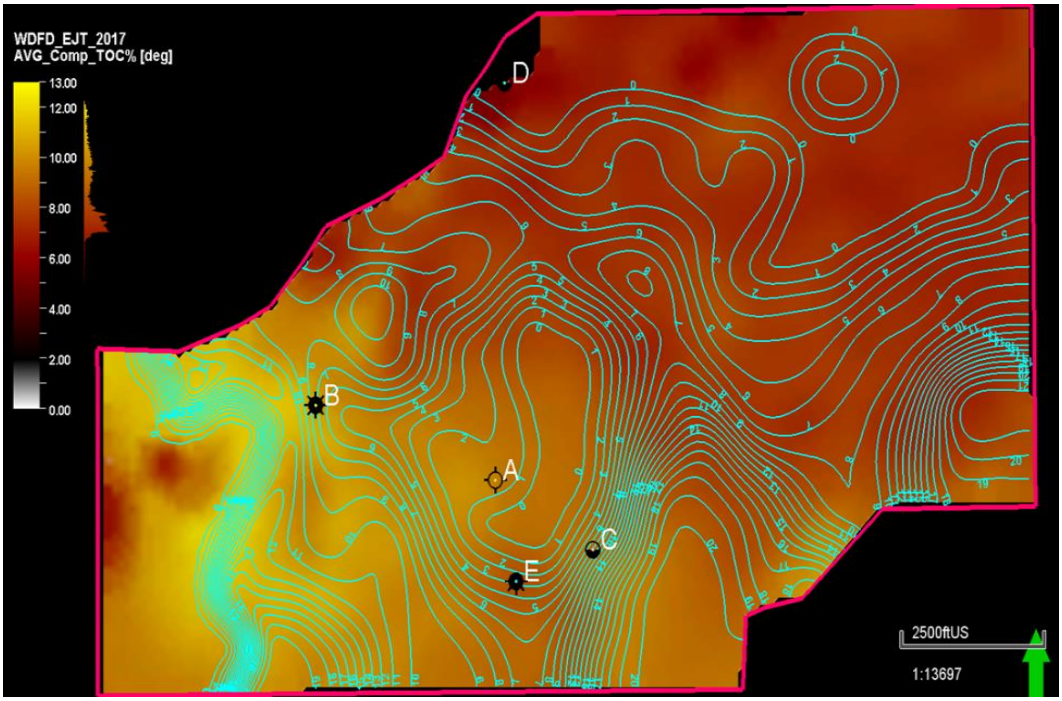

Figure 2.23. Calculated %TOC from the supervised neural network analysis. Average %TOC values are extracted for the Woodford Shale stratigraphic interval and are shown in the display colors of the map. The contours correspond to the Hunton Group seismic isochrones in milliseconds [ms].

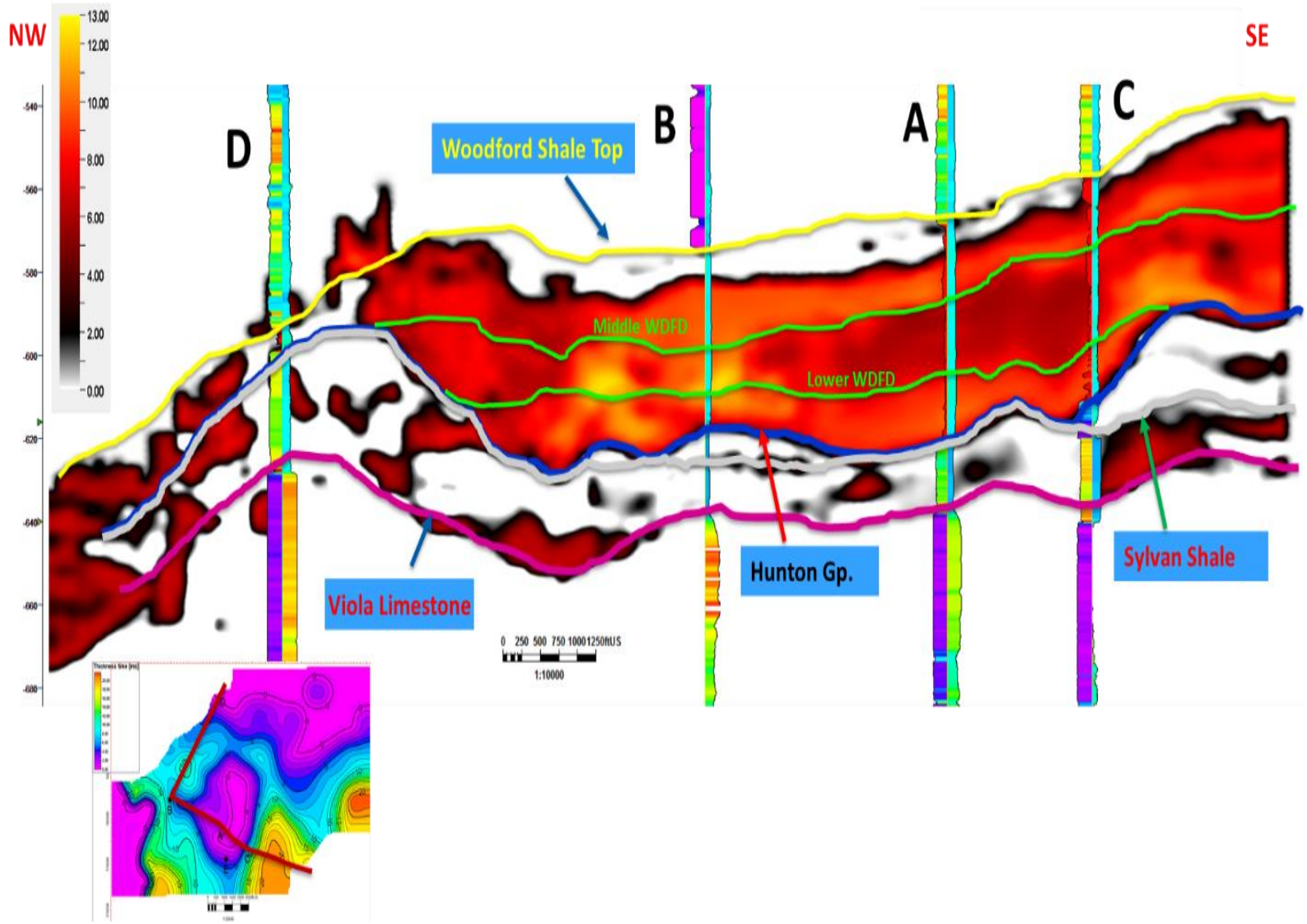

Figure 2.24. A composite section that correlates all wells in the study area and their %TOC calculation for the Woodford Shale seismic window. Note the concave-down pod shape of the Woodford Shale where the well A and C are located; these correspond to enclosed mini-basin deposits with higher computed %TOC from the PNN.

2.6. Conclusions and discussion

The 3D seismic multi-attribute interpretation, seismic post-stack inversion, and probabilistic neural network %TOC modeling supported the hypothesis that the Z_p anomalies seen in the Woodford Shale correspond to internal lateral and vertical facies variation (Figure 2.16, Figure 2.22, Figure 2.23 and Figure 2.24). The Woodford Shale is thicker and with more %TOC where the Hunton Group is completely or significantly eroded (Figure 2.5, Figure 2.11, Figure 2.23 and Figure 2.24). The seismic structural features allow the identification of concave-down enclosed mini-basin fill settings produced by karstification or wide incised valley processes of the Hunton Group paleo platform. The recognized enclosed mini-basin fill intervals suggest highly restricted deposits that contributed to the formation of Woodford Shale organic-rich deposits. These are identified by the computed %TOC with the PNN (Figure, Figure 2.22, Figure 2.23, and Figure 2.24), thereby providing opportunities for more innovative exploration strategies.

The recognized seismic characteristics of enclosed mini-basin fill deposits are:

- Thicker basal sections that trend to pinch out towards paleo structural height of the pre-existing strata. In this case, the seismic resolution was enough to image internal reflectors of the Woodford Shale.
- Incoherent seismic data at the base of the formation, caused by erosion or karstification of pre-existing strata
- Most negative curvature values in the areas of these deposits that indicate accommodation space-filling these pockets.
- Low (or the lowest) acoustic impedance that correlates with higher accumulations of organic matter, due to deeper water column in these areas and more restricted water circulation and upwelling currents (Figures 2.16, 2.22, 2.23, 2.24).

For future analysis, the pre-stack simultaneous inversion is suggested for estimating the elastic properties, and therefore reduce the inversion error which can provide better %TOC

estimates and understand reservoir properties with seismic such as porosity, density, and geomechanical parameters (*Lamé* parameters), which are not possible with a post-stack survey that was only available for this study.

2.7.Acknowledgments

Special thanks to Pathfinder Exploration LLC., **Mr. Gerald "Jerry!" Wilson (*in-memoriam*),** and the Wilson family, for providing the 3D seismic surveys and the well-log data for this exercise. We want to thank the kind assistance of the geophysicists and sponsors of both the University of Oklahoma Institute of Reservoir Characterization (IRC) and Attribute Assisted Seismic Processing and Interpretation (AASPI) consortiums.

2.8. Cited References

- Ali, E.E., 2015. Integrated characterization of the Woodford Shale in southwest Cherokee platform, Oklahoma. M.Sc. thesis manuscript, The University of Oklahoma, p. 104.
- Althoff, C., 2012. Characterization of depositional megacycles in the Woodford trough of Central Oklahoma. M.Sc. thesis manuscript, The University of Oklahoma, p. 167.
- Amorocho-Sanchez, J.D., 2012. Sequence stratigraphy and seismic interpretation of the Upper Devonian- Lower Mississippian Woodford Shale in the Cherokee platform: a characterization approach for unconventional resources. M.Sc. thesis manuscript, The University of Oklahoma, p. 153.
- Baruch, E., Elebiju, O., Pérez, R., 2009. Geophysical evidence of basement-controlled faulting in the Ellenberger group and Viola Limestone, Fort Worth basin, Texas. 79th Annual International Meeting, SEG, Expanded Abstracts, 995–999.
- Cardona-Valencia, L.F., 2014. Integrated characterization of the Woodford Shale in the southern Cherokee platform, Oklahoma. M.Sc. thesis manuscript, The University of Oklahoma, p. 98.
- Cardott B. J., 2009. Woodford gas-shale plays of Oklahoma. Louisiana oil & gas symposium, May 20, 2009. Oklahoma Geological Survey OGS.

- Cardott, B. J., 2012. Thermal maturity of Woodford Shale gas and oil plays, Oklahoma, USA. International Journal of Coal Geology, 1-13.
- Cardott, B.J., 2014. Woodford Shale play update: Expanded in the oil window. American Association of Petroleum Geologists, Search and Discovery article 80409.
- Castillo, L.A, 2013. Integrated reservoir characterization of the Ordovician-Silurian Hunton carbonate, north Cherokee platform, Oklahoma. M.Sc. thesis manuscript, The University of Oklahoma, p. 90.
- Comer, J.B., 2005. Facies distributions and hydrocarbon production potential of the Woodford Shale in the southern midcontinent: in B.J. Cardott, eds., Unconventional energy resources in the southern mid-continent, 2004 symposium. Oklahoma Geological Survey, Circular 110, 51-62.
- Comer, J.B., 2008. Woodford Shale in southern mid-continent, USA, transgressive system tract marine source rocks on an arid passive continental margin with persistent oceanic upwelling. American Association of Petroleum Geologists Annual Convention, Search and Discovery Article 404026.
- Grotzinger, J.G, Jordan, T.H., 2010. Understanding earth. In: Freeman, W.H., Sixth Edition, p. 672.
- Gupta, N., 2012. Multi-scale characterization of the Woodford Shale in West-central Oklahoma: From scanning electron microscope to 3D seismic. Doctorate dissertation manuscript, The University of Oklahoma, p. 148.
- Hampson, D. J., S. Schuelke, J. Quirein, 2001. Use of multiattribute transforms to predict log properties from seismic data. Geophysics 66, 220- 236.
- Heggland, R., 2004. Definition of geohazards in exploration 3-D seismic data using attributes and neural network analysis. AAPG Bulletin, 88, 857–868.
- Jarvie, D.M., Hill, R.J., Pollastro, R.M., 2005. Assessment of the gas potential and yields from shales: the Barnett Shale model. In: Cadott, B., eds., Oklahoma Geological Survey Circular 110: Unconventional gas of the southern mid-continent symposium, March 2005. Oklahoma City, Oklahoma, p. 37-50.
- Jarvie, D.M., Hill, R.J., Ruble, T.E., Pollastro, R.M., 2007. Unconventional shale-gas systems: the Mississippian Barnett Shale of North-Central Texas as one model for thermogenic shale-gas assessment. AAPG Bulletin 91, 4, 475-499.

- Katz, B.J., Lin, F., 2014. Lacustrine basin unconventional resource plays key differences. Marine and Petroleum Geology 56, 255-265.
- Kirkland D.W., Denison, R.E., Summers, D.M., Gormly, J.R., 1992. Geology and organic geochemistry of the Woodford Shale in the Criner Hills and western Arbuckle Mountains, Oklahoma. Oklahoma Geological Survey, Circular 93, 38-69.
- Latimer, R.B., Davison, R., van Riel, P., 2000. An interpreter's guide to understanding and working with seismic-derived acoustic impedance data. The Leading Edge 19, 242-256.
- Maynard, S., 2016. Correlation of bioturbated facies, chemostratigraphy, total organic carbon, and sequence stratigraphy in the Woodford Shale of south-central Oklahoma. M.Sc. thesis manuscript, The University of Oklahoma, p. 119.
- McCullough, B.J., 2014. Sequence-stratigraphic framework and characterization of the Woodford Shale on the southern Cherokee platform of Central Oklahoma. M.Sc. thesis manuscript, The University of Oklahoma, p. 212.
- McCullough, B., Slatt, R.M., 2014. Paleotopographic control on the variability of Woodford Shale strata across the southern Cherokee platform area of central Oklahoma: A mechanism for increased preservation-potential of organic content: AAPG Search and Discovery article 1125.
- Miceli-Romero, A.A, 2010. Geochemical characterization of the Woodford Shale, central and southeastern Oklahoma. M.Sc. thesis manuscript, The University of Oklahoma, p. 149.
- Molinares, C.E., 2013. Stratigraphy and palynomorphs composition of the Woodford Shale in the Wyche Farm shale pit, Pontotoc County, Oklahoma. M.Sc. thesis manuscript, The University of Oklahoma, p. 104.
- Northcutt, R.A., Johnson, K. S., Hinshaw, G. C., 2001. Geology and petroleum reservoirs in Silurian, Devonian, and Mississippian rocks in Oklahoma. In: Johnson K. S., eds., Silurian, Devonian, and Mississippian geology and petroleum in the southern Midcontinent, 1999 symposium. Oklahoma Geological Survey Circular 105, 1-29.
- Passey, Q.R., Creaney, S., Kulla, J.B., Moretti, F.J., Stroud, J.D., 1990. A practical model for organic richness from porosity and resistivity logs. AAPG Bulletin 74, 1777-1794.
- Passey, Q.R., Bohacs, K. M., Esch, W. L., Klimentidis, R., Sinha, S., 2010. From oil-prone source rock to gas-producing shale reservoir-geologic and petrophysical characterization

of unconventional shale-gas reservoirs. 2010 CPS/SPE International Oil and Gas Conference and Exhibition in China, 29 p.

- Perry, W.J., 1995. USGS 1995 National oil and gas assessment – Arkoma basin province. United States Geological Survey 62, p. 134.
- Portas, R., 2009. Characterization and origin of fracture patterns in the Woodford Shale in southeastern Oklahoma for application to exploration and development. M.Sc. thesis manuscript, The University of Oklahoma, p. 113.
- Sena, A., Castillo, G., Chesser, K., 2011. Seismic reservoir characterization in resource shale plays: Stress analysis and sweet spot discrimination. SEG The Leading Edge, 30, 7, 758-764.
- Slatt, R.M., Buckner, N., Abousleiman, Y., Sierra, R., Philp, R.P., Miceli-Romero, A., Portas, R., O'Brien, N., Tran, M., Davis, R., Wawrzyniec, T., 2012. Outcrop/behind outcrop (quarry), multiscale characterization of the Woodford gas shale, Oklahoma, in J. Breyer, eds., Shale reservoirs-giant resources for the 21st century: American Association of Petroleum Geologists AAPG Memoir 97, 1–21.
- Slatt, R.M., 2016. Institute of Reservoir Characterization (IRC), Woodford-Mississippian consortium, phase III technical report. The University of Oklahoma, p. 202.
- Turner, B., 2015. The use of chemostratigraphy to refine ambiguous sequence stratigraphic correlations in marine shales: An example of the Woodford Shale, Oklahoma. AAPG education directorate, Woodford Shale forum: Focus on optimization. Oklahoma City, Oklahoma, 2015. AAPG Datapages Search and Discovery article 90241.
- Verma, S., 2014. Seismic data conditioning for quantitative interpretation of unconventional reservoirs. Doctoral dissertation manuscript, The University of Oklahoma, p. 195.
- Verma, S., Zhao, T., Marfurt, K.J., Devegowda, D., 2016. Estimation of total organic carbon and brittleness volume. Interpretation 4, 3, T373-T385.

Chapter III: Integration of geochemical and stratigraphic properties for characterizing the enclosed mini-basin fills in the Woodford Shale Speake Ranch outcrop.

3.1 Abstract

Since the early 2010s, the exploitation of unconventional resources in the Woodford Shale has become very active because of its historical recognition as a significant source of high volumes of hydrocarbons to Oklahoma reservoirs and its potential storage capacity as a self-sourced tight reservoir. One of the parameters which make the Woodford Shale one of the best source rocks in the world is its deposition during a major extensive transgressive and dysaerobic setting, which created the optimal conditions for the productivity and preservation of the organic matter. In recent years, southern Oklahoma has become a very active petroleum province due to the interest in unexplored Woodford Shale acreage. The Speake Ranch (SR) in southern Oklahoma is a crucial outcrop with a complete Woodford Shale stratigraphic section. The SR was initially described by Becerra-Rondon (2017) and Galvis et al. (2017a and 2017b). This chapter focuses on complementing the previous analyses with the full use of geological, inorganic (X-ray fluorescence XRF) and organic (total organic carbon %TOC, Rock-Eval pyrolysis and biomarkers) geochemical parameters. These parameters are used to better understand the vertical variability of the depositional conditions, variations in the organic matter source material, thermal maturity and the presence and impact of enclosed mini-basin fill deposits in the SR. Also, this chapter compares these characteristics with other areas in Oklahoma by performing regional mapping of the Woodford Shale and how these characteristics correlate with subsurface geological interpretations. This combined evaluation indicates the excellent potential of the enclosed mini-basin fill as prolific oil and gas intervals in unconventional resource shales. These characterizations show the tremendous value that biomarkers provide in the exploration of prospective unconventional resource shales. Not only

do the biomarkers assist in identifying paleoenvironmental changes and redox conditions, but they also represent the best organo-facies that define the economic hydrocarbon producing intervals.

The principal indicators for a highly restricted enclosed mini-basin fill in the SR are:

- The SR is located in an area of the Ardmore basin (south Oklahoma) where the Woodford Shale thickness is greater than 300ft (typically the Woodford is 50-200 ft in Oklahoma), and the Hunton Group thickness is less than 200ft (usually this group is 400-600 ft). These differences in gross thickness are related to thicker Lower and Middle member intervals, associated with higher pre-Woodford accommodation space filled under enclosed mini-basin fill settings. This chapter shows the regional mapping and cross-sections from subsurface well-log interpretations of nearby areas for supporting these comparisons.
- The Lower Woodford member thickness in the SR is 120 ft. This is a thick stratigraphic section of this member when compared to other Woodford locations in Oklahoma petroleum provinces; therefore, more accommodation space was available for these basal Woodford Shale deposits and suggested enclosed mini-basin fill settings.
- Several faulted provinces surround the SR that, according to Ghosh (2017) and Galvis (2017), are the reactivation of pre-existing fault grabens that could have acted as paleo structural lows. These grabens allowed more accommodation space for basal Woodford Shale deposits. This outcrop presents higher sedimentation rates and sediment supply due to the proximity to the paleo Wichita uplifts (Galvis et al., 2017a). All these combined structural and depositional factors favored the development of restricted conditions to the water chemocline for preventing open water circulation processes.

- Biomarker analyses indicating an increase in the gammacerane index, decrease in sterane/hopane ratios, increase in aryl isoprenoids concentrations and an increase in C_{40} carotenoid concentrations suggest that the Lower Woodford and upper portions of the Middle Woodford members have isolated and persistent episodes of photic-zone euxinia (PZE) and oxygen minimum zones. These persistent PZE conditions suggest highly restricted anoxic depositional settings for organic matter preservation. When combined with the structural and sedimentological interpretations, such as the present in the SR, the persistent PZE suggest the enclosed mini-basin fill settings (from 14ft to 210 ft of the outcrop stratigraphic section).
- For the uppermost Middle member and complete Upper Woodford member, the biomarker analyses have provided evidence for a potential mechanism for mass extinctions involving eutrophication of shallow marine settings. These eutrophication events are followed by increased bio-productivity, oxygen consumption and subsequent global euxinic oceanic conditions. The start of the maximum flooding surface (MFS) in the SR defines that these mass extinction events occurred during the beginning of a highstand system tract (HST). The SR HST is an interval of typical open marine deposits.
- The development of enclosed mini-basin fill settings in the Woodford Shale at the SR is critical for allowing the higher accumulation, restriction and preservation of organic matter. The higher total organic carbon (%TOC), higher hydrogen index (HI), and low oxygen index (OI) values in the Lower Woodford member and basal to middle parts of the Middle Woodford member indicate more preservation of the organic matter. Also, the regional bulk %TOC maps indicate that the SR has higher average %TOC values for the Woodford Shale. The SR has higher average %TOC on a regional scale when compared to other

Oklahoman petroleum provinces under similar Woodford Shale gross thickness and thermal maturity levels.

- The Lower, Middle, and Upper Woodford members present in the SR might geologically vary in the state of Oklahoma. A direct one-to-one detailed comparison of Woodford Shale members must be made when interpreting if the same enclosed mini-basin fill settings are present in other areas of Oklahoma. Commonly, the Woodford members are identified or labeled with the same nomenclature in all of the Oklahoma petroleum provinces. The Lower and Middle Woodford Shale members might be lithologically different and thinner, or not present, in other areas of Oklahoma.
- The enrichment in the Upper Woodford member of organically related proxies U, Mo, V, are likely to relate to more open water circulation conditions. These upwelling deposits occur under typical open marine sediments, that captured these heavy elements via upwelling current supply and concentrated these elements principally in the phosphate concretions and chert-rich lithofacies.

3.2. The Woodford Shale Speake Ranch outcrop location

The SR is located along the southern flank of the Arbuckle Mountains in the south of Oklahoma, USA (Figure 3.1). It covers portions of Carter and Murray Counties in south-central Oklahoma and correlates with the subsurface Woodford present in the southern parts of the SCOOP region (Figure 3.1), where the unconventional resource drilling activity is focused on economic Woodford hydrocarbon production and Mississippian reservoirs sourced from the Woodford Shale.

The surface geology mapping of the area reveals a nearly east-west outcrop trend, where the Woodford Shale outcrops through roadcuts, creeks, and quarries (Kirkland et al., 1992). Within this structural trend, some of the most visited Woodford Shale exposures occur along the southbound side of Interstate 35 (Johnson et al. 1989; Bontempi, 2015; Galvis et al., 2016; Becerra-Rondon, 2017; Ghosh, 2017; Jones, 2017; Milad and Slatt, 2018; Milad, 2019; Figure 3.1), including Henry House Falls quarry and the Arbuckle anticline (OHMEGCO) quarry (Turner and Slatt, 2016; Galvis, 2017; Brito 2019; Figure 3.1). According to Johnson et al. (1972), Johnson and Cardott (1992), Johnson (2008); Paxton et al. (2015) and Slatt (2016), most of the outcrops that are exposed in the Arbuckle Mountains of Oklahoma are useful for recognizing the unique characteristics of the Woodford Shale, because all of these locations, as well as the McAlester Cemetery quarry (Ekwunife, 2017), present the complete stratigraphic intervals of the formation and have a dipping exposure that allows walking along the vertical stratigraphic sections (Figure 3.1).

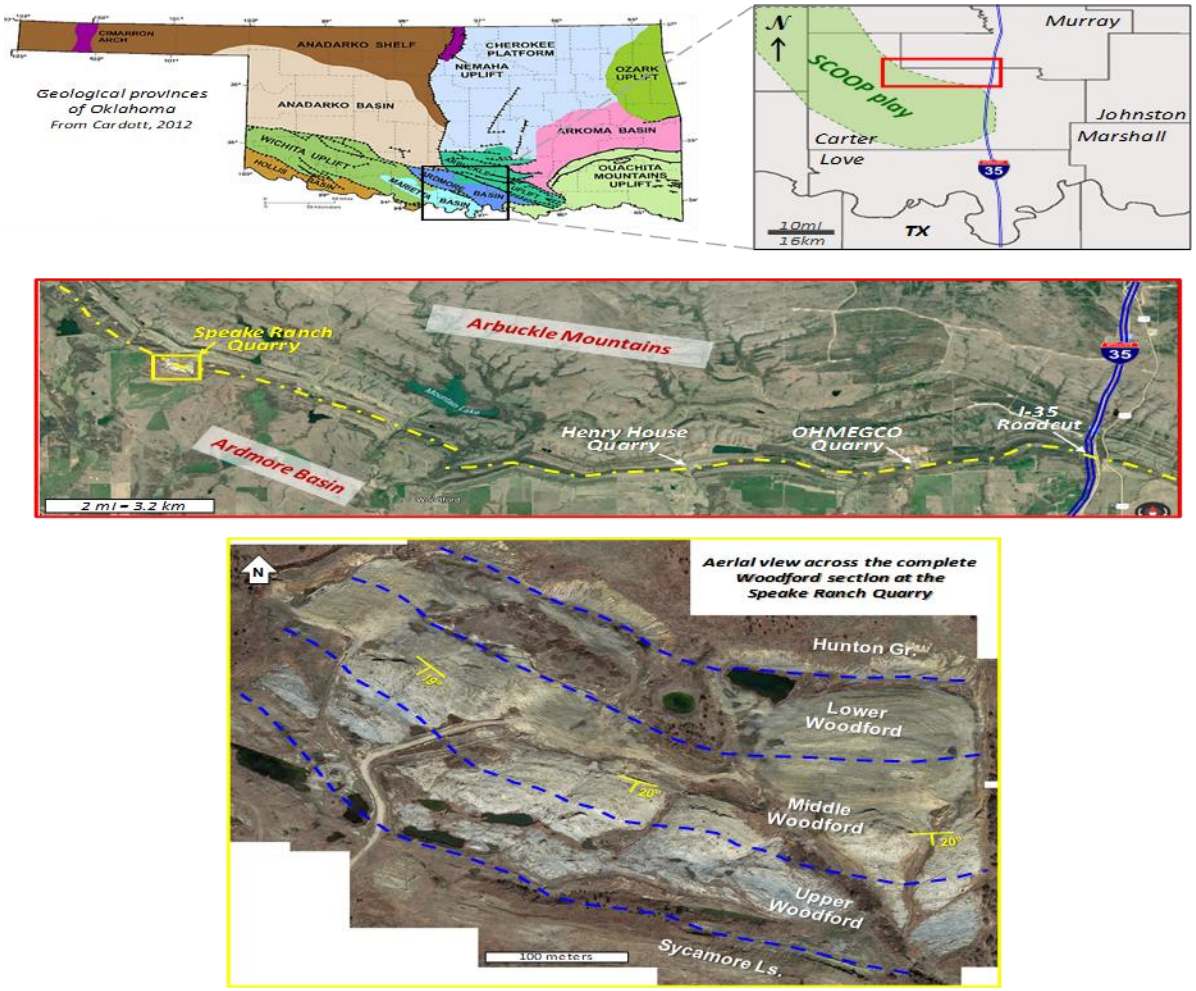

Figure 3.1. Location of the study area, images courtesy from Galvis (2017), and modified from Galvis et al. (2017a). Upper left: Geological provinces of Oklahoma highlighting a portion of south-central Oklahoma and the Arbuckle Mountains (Cardott, 2012 in Galvis, 2017). Middle: Location of Woodford Shale outcrops along the nearly E-W outcrop belt. The Speake Ranch quarry is the westernmost outcrop of this belt in the Arbuckle Mountains. Lower: Aerial view of Speake Ranch quarry across the complete Woodford section. The bedding strike is about N47-55°W and dips around 20°SW. Images courtesy of Galvis in Galvis (2017), and Galvis et al. (2017a).

The Speake Ranch was selected as the best outcrop characterized by the OU Institute of Reservoir Characterization (IRC) by Slatt (2016), Becerra-Rondon (2017) and Galvis (2017), because this presents a complete Woodford Shale section in this region, and has a vast lateral extent of the rock exposure, allowing observation of lateral bed and fault attributes (Figure 3.2). This outcrop is located in a private quarry under the name 'Speake Creed Ranch,' with geographic coordinates SE ¼ Section 18, Township 2S, Range 1W.

The geological and sedimentological characterization of the Woodford Shale in the SR was performed by Becerra-Rondon (2017), Galvis (2017), and Galvis et al. (2017a and 2017b). The geochemical characterization is complemented in this present study, focusing on the integration of the previous work with new key selected biomarker analyses. The integration with previous studies is crucial for recognizing the origin and variations of the organic facies through the vertical stratigraphic column and their relationship with the lithofacies, paleo-water conditions, and regional depositional models that correlate with the present-day subsurface Woodford Shale reservoir conditions. This multi-scale data integration is crucial for understanding how the organic matter variations are from enclosed mini-basin fills in the basal Woodford towards a more open marine system in the Upper sections of the Woodford Shale.

The SR total vertical stratigraphic exposure is approximately 355 ft thick, comprising the entire Lower, Middle and Upper members of the Woodford Shale (~314 ft), the uppermost portion of the underlying Hunton Group (28 ft; including the unconformity surface) and the lowermost parts of the overlying Sycamore limestone (25 ft). Thus, it offers a unique and complete Woodford Shale section that preserves the stratigraphic relations with its units in the stratigraphic base and top, which allows understanding the transition of the poor organic matter content of pre-Woodford and post-Woodford Shale strata (Figure 3.2).

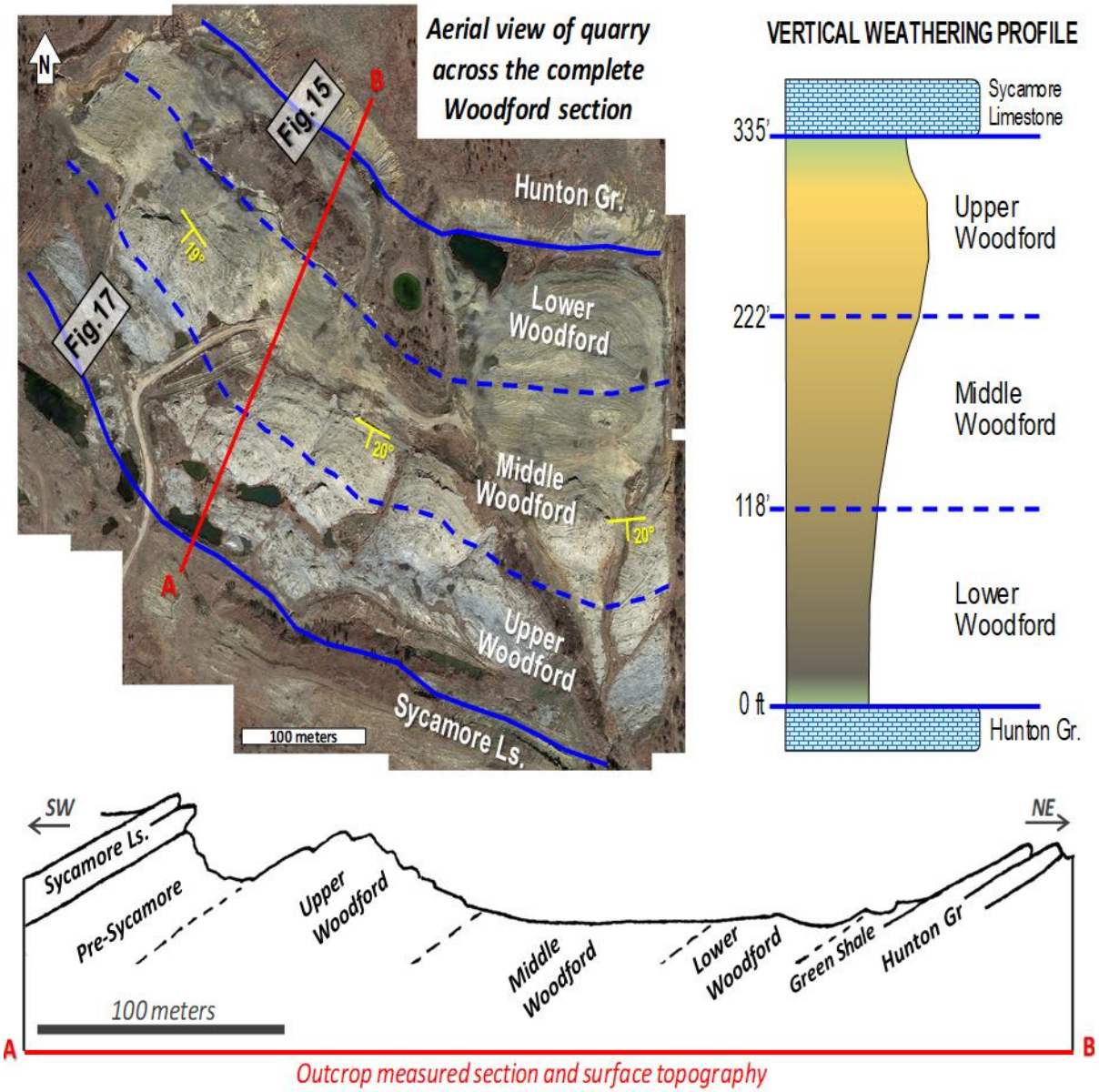

Figure 3.2. Weathering response of the Woodford Shale of south-central Oklahoma described by Galvis et al. (2017a). Upper left: aerial view of Speake Ranch outcrop quarry outlining the Woodford formational contacts with its underlying Hunton Group and overlying Pre-Sycamore limestone. Upper right and lower images: schematic weathering profiles made by Galvis (2017), highlighting large-scale variations in the resistance of the Woodford Shale strata; the Lower Woodford and Middle Woodford members are less resistant when compared with the Upper Woodford member, which is more competent and usually develops creeks on outcrops. Images courtesy of Galvis in Galvis (2017), and Galvis et al. (2017a).

3.3.The Woodford Shale geological characteristics in the outcrop

For presenting the characterization of the Woodford Shale in this region of Oklahoma, this document refers to the most accepted formation subdivision into the Lower, Middle, and Upper members, as initially adopted by Sullivan (1985), Hester et al. (1988 and 1990), and Lambert (1993). This terminology can be counterproductive in terms of time-rock stratigraphy as correctly discussed by Turner et al. (2015), Becerra-Rondon (2017) and Galvis et al. (2017a and 2017b), but this informal subdivision has demonstrated consistency among industry and academia, finding it useful for communication and reference of the main internal Woodford subdivisions as also reported in other Woodford Shale literature by Portas (2009), Miceli-Romero (2010), Badra (2011), Kilian (2011), Sierra-Perez (2011), Totten (2011), Althoff (2012), Amorocho (2012), Cardott (2012 and 2014), Chain (2012), Gupta (2012), Miceli-Romero and Philp (2012), Slatt et al. (2012), Castillo (2013), Molinares (2013, 2019), Serna-Bernal (2013), Cardona-Valencia (2014), McCullough (2014), McCullough and Slatt (2014), Ali (2015), Bontempi (2015), Connock (2015), DeGarmo (2015), Infante-Paez et al. (2016), Maynard (2016), Turner (2016), Villalba (2016), Wang (2016), Zhang (2016, and 2019), Becerra-Rondon (2017), Galvis (2017), Galvis et al. (2017a and 2017b), Ghosh (2017), Jones (2017), Connock et al. (2018), Liborius-Parada et al. (2017), Brito (2019), Milad (2019), Zhang and Slatt (2019), and Philp and DeGarmo (2020).

As an outstanding characteristic, the Woodford Shale at the SR outcrop exhibits unique visible repetitions of alternations in mechanical stratigraphy (coupling of hard [brittle] and soft [ductile, less brittle] rock bed intervals). These sets of repetitions were defined in the SR by Becerra-Rondon (2017) and for the southern Oklahoma Woodford Shale I-35 section. Becerra-Rondon (2017), and Galvis (2017) recognized the soft-to-hard ratio every half foot (Figure 3.3 and Figure 3.4). Galvis (2017) observed that the outcrop measured Gamma-ray responses correlate

with the rock beds' soft-to-hard ratios. Becerra-Rondon (2017) reports the softer a rock interval, the higher is the radioactivity (higher values) from the Gamma-ray log response (Figure 3.4).

Additionally, in the SR, the higher the organic matter content correlates with softer beds and a higher Gamma-ray response log (Galvis et al., 2017a and 2017 b). In the Woodford Shale, these observations can be consistently explained according to Slatt (2016), Becerra-Rondon (2017), and Galvis (2017a and 2017b). These studies mentioned that soft beds are the ones that present more clay minerals and higher preservation of total organic carbon (%TOC), and the hard bed counterparts show more silica content (quartz of both detrital and biogenic origin). The hard beds in the SR cause the rock to be more resistant to stresses, fracturing, and deformation than the clay-rich and organic-rich fraction (Becerra-Rondon, 2017).

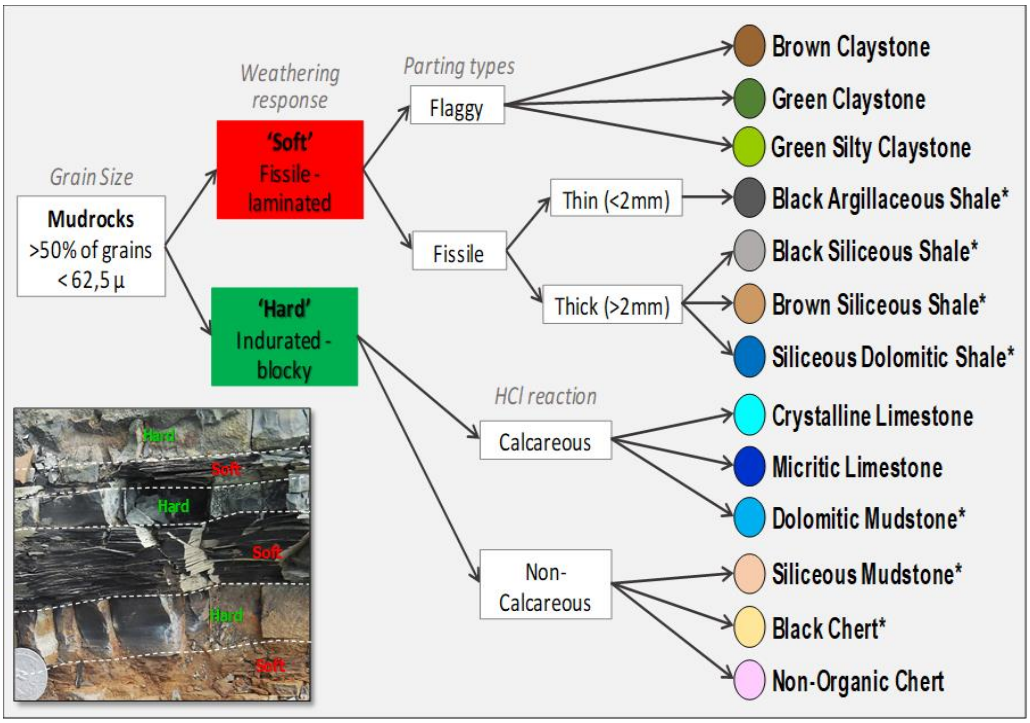

Figure 3.3. Field-based lithofacies classification of Woodford Shale mudrocks in the Speake Ranch outcrop and their classification based on mechanical stratigraphy (Galvis, 2017). The first criterion by Galvis (2017) distinguishes between hard and soft (i.e., less hard) beds based on weathering responses, then textural and compositional descriptors are added based on parting responses and HCl reaction. Image courtesy of Galvis in Becerra-Rendon (2017) and Galvis (2017).

3.3.1. The Lower Woodford member (LW)

Galvis (2017) and Galvis et al. (2017a) report the measured section of LW member at the SR as about 105 ft thick (~32 meters, Figure 3.4.). This member has the characteristics that generate topographic lows throughout the section because it is less resistant to weathering and reworking by surface exposure. In this member, the softer beds dominate, making soft-to-hard ratios varying from 70/30 to 100/0, along with very high outcrop Gamma-ray responses ranging from 600 to 1300 counts per second [cps,] averaging 800 cps (Galvis et al., 2017a and 2017b; Figure 3.4 and Figure 3.6).

The 'soft' component identified in this member described by Galvis (2017) is mostly represented by his proposed lithofacies named "*argillaceous, siliceous, and dolomitic shales"* that, when compared with other members in this Woodford outcrop, are the most abundant lithofacies within the Lower Woodford (Figure 3.5 and Figure 3.6). The "hard" lithofacies counterpart was described by Galvis (2017) as mainly composed of siliceous rich mudstones and cherts, and these harder rock intervals only account for less than 30% of the stratigraphic thickness within this LW member (Figure 3.4). The distribution of bed thicknesses in the LW has a preference of soft beds being much thicker (>12 inches) than the hard beds (0.25- 2 inches on average; Figure 3.4). Galvis (2017) and Galvis et al. (2017a) report that the contact between the Lower and Middle Woodford members is represented by a significant turnaround point in the Gamma-ray profile (Figure 3.4). As reported by Galvis (2017), this change of member distinction coincides lithologically in the outcrop with a zone of bioturbated dolomitic mudstones.

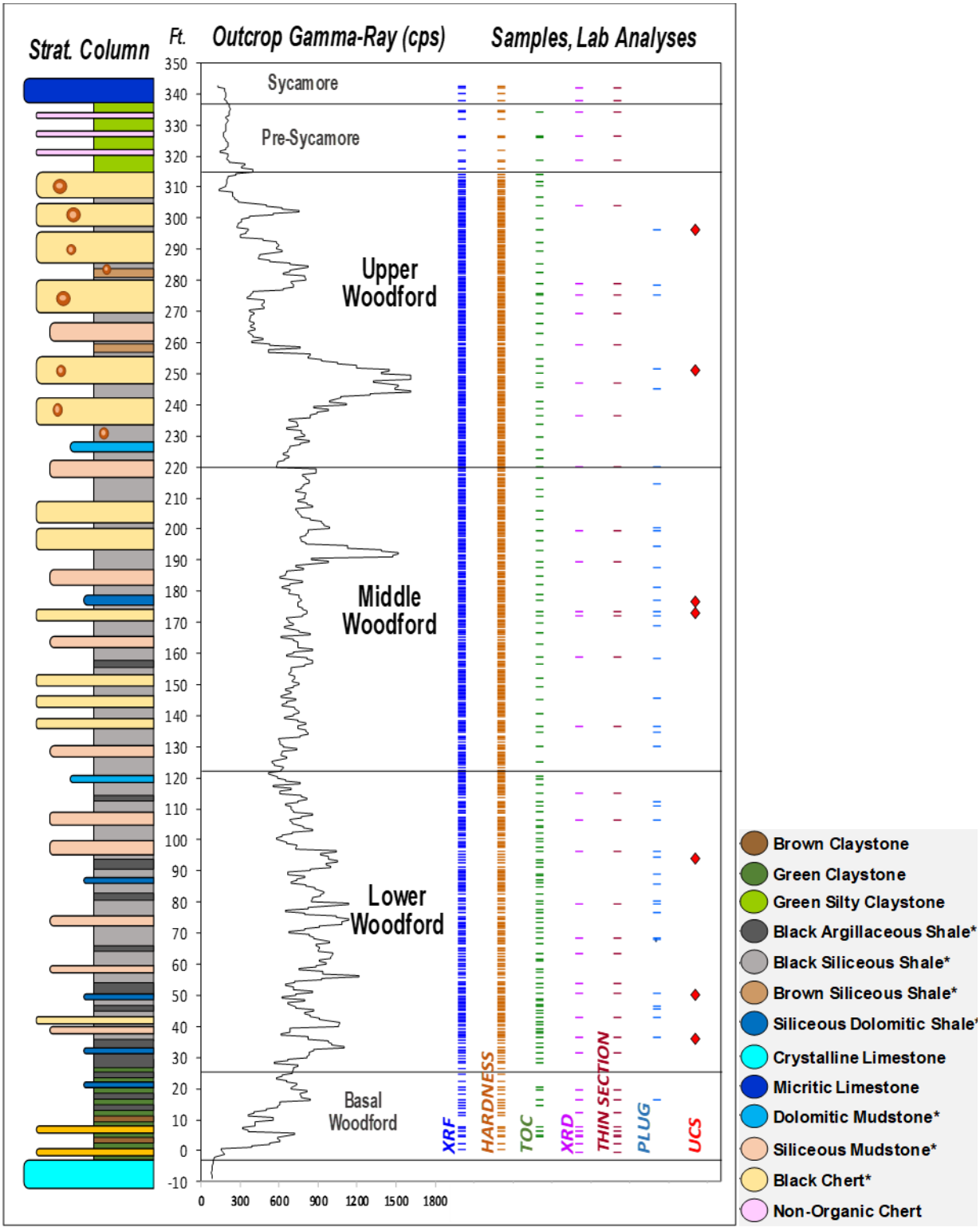

Figure 3.4. The thirteen lithofacies that were recognized throughout the section by Becerra-Rendon (2017) and Galvis et al. (2017a). Image courtesy of Galvis in Galvis (2017).

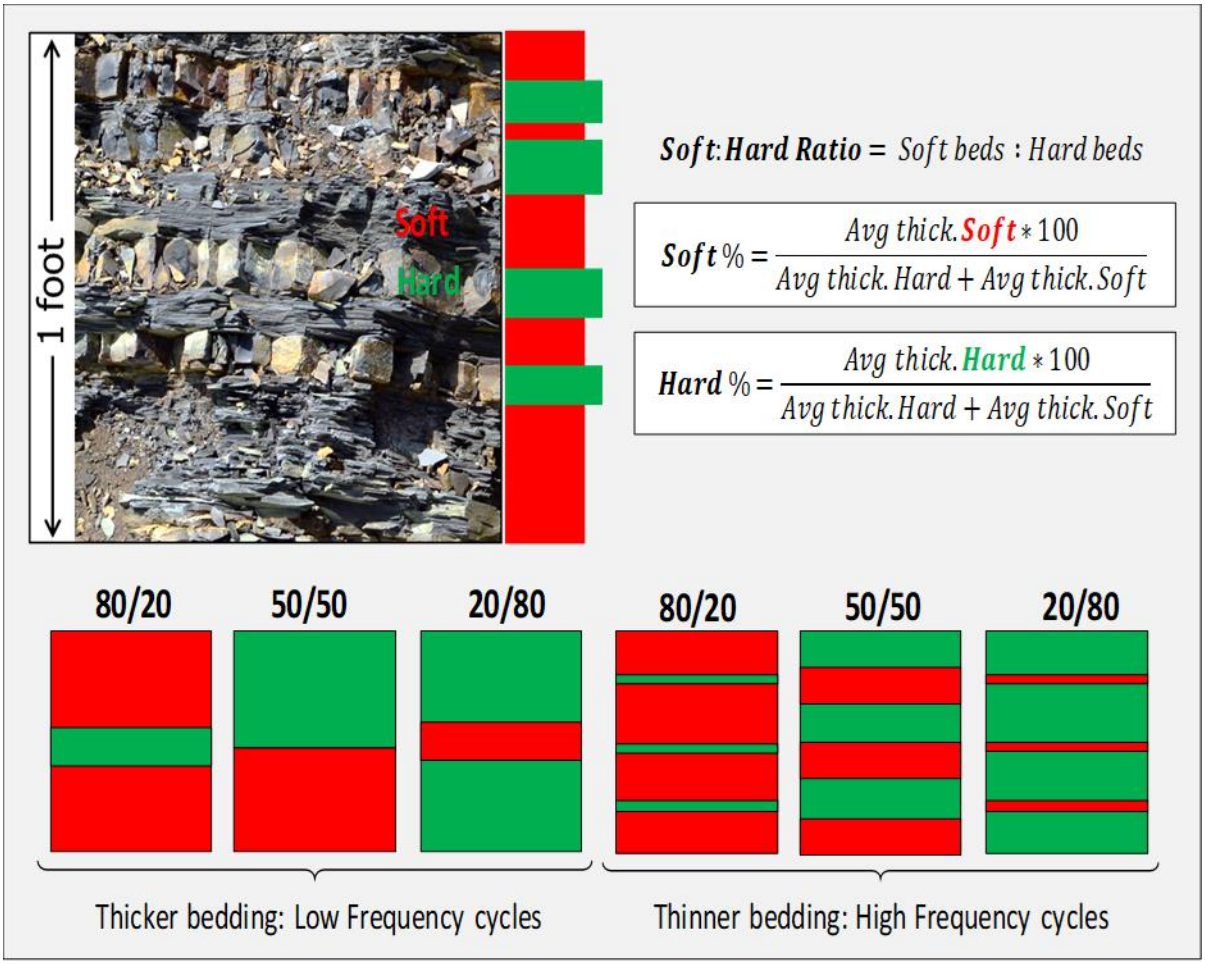

Figure 3.5. Cyclical heterogeneity between soft and hard beds for the Woodford Shale proposed by Becerra-Rondon (2017) and Galvis (2017). Soft beds are laminated and fissile, while hard beds are blocky with more vertical fractures. The soft-to-hard ratio is measured by extracting the average bed thickness per bed per unit foot. Image courtesy of Galvis in Galvis (2017).

3.3.2. **The Middle Woodford member (MW)**

Galvis (2017) and Galvis et al. (2017a and 2017b) reported that the MW member at the SR outcrop is about 104 ft thick (~31,6 meters) and is dominated by soft-to-hard ratios between 85/15 to 50/50. This mechanical stratigraphy ratio indicates that when compared with the LW, the proportion of hard beds increases gradually upward, while the soft ones decrease (Figure 3.4 and Figure 3.6). The outcrop Gamma-ray radioactivity readings in this member were reported by Galvis (2017) as being more homogenous, mostly ranging from 650 to 900 cps (Figure 3.3).

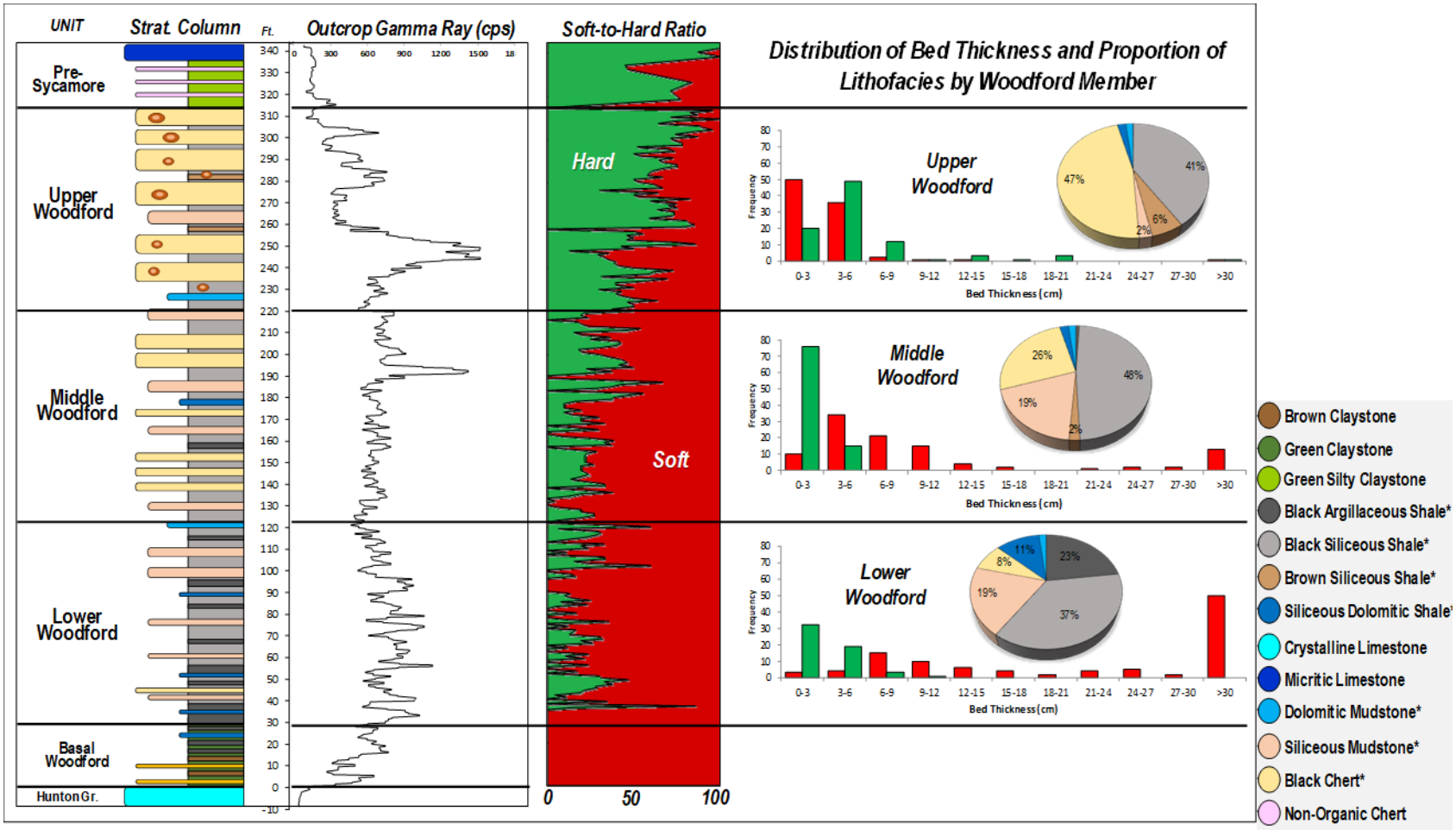

Figure 3.6. Summarized outcrop description by Galvis (2017). Integration of vertical distribution of lithofacies, soft-to-hard ratios, and distribution of bed thicknesses by the three Woodford members. Galvis (2017) identified four main components in this section: 1) the increasing upward trend of the hard beds; 2) The LW is dominated by thick, soft beds of argillaceous and siliceous shales; 3) The MW is characterized by a nearly 50/50 mix of soft and hard beds of siliceous shales and cherts; 4) The UW is dominated by higher contents of hard beds of thick-bedded cherts, which Galvis (2017) identified of being intercalated with thin beds of siliceous rich mudstones. Image Courtesy of Galvis in Galvis (2017) and Galvis et al. (2017a).

According to Becerra-Rondon (2017) and Galvis et al. (2017a and 2017b), the average bed thickness between soft and hard beds varies from 1-12 cm, and in some cases, the layering occurs in 1-6 cm intervals (Figure 3.3). Galvis et al. (2017a and 2017b) interpreted this as the occurrence of high-frequency cycles of soft and hard bed deposition and rapid changes in sedimentation rates and organic-inorganic factors. Galvis (2017) and Galvis et al. (2017a and 2017b) recognized that the lithofacies within this member are primarily represented by siliceous shales, cherts, and siliceous mudstones (Figure 3.3) and that the clay-rich and dolomitic lithofacies, as well as the argillaceous and dolomitic shales, decrease upward abruptly from its underlying Lower Woodford member boundary. The contact between the Middle and Upper Woodford members is reported by Galvis (2017), and Galvis et al. (2017a), as being located at about 220.5 ft from the bottom of the SR stratigraphic section. As described by Galvis (2017), this contact is marked by the first occurrence of phosphate nodules and concretions, which are of variable diameter (2-5cm) and shape. A log curve trough also marks this contact in the outcrop Gamma-ray radioactivity log response (Figure 3.4). According to Turner et al. (2015), Jones (2017), Molinares (2019) and Philp and DeGarmo (2020), in the south of Oklahoma, the Frasnian-Fammenian (F-F) mass extinction boundary occurs near the top of the MW.

3.3.3. The Upper Woodford member (UW)

Galvis (2017) and Galvis et al. (2017a and 2017b) describe this member at the SR as about 92 ft thick (~28 meters) and generally more competent (harder beds) than its preceding members, and usually develops scarp slopes on the SR ranchlands (Figure 3.4 - 3.6). The radioactivity responses in the outcrop Gamma-ray log measurements by Galvis (2017) are highly variable, ranging from 450 to 900 cps, with outlier values higher than 1200 cps near the most phosphatic-rich zone. According to Molinares (2013, and 2019), these high Gamma-ray values for the

Woodford Shale are directly related to the higher uranium content in the phosphatic concretions rather than in the clay-rich beds (Figure 3.4 - 3.7).

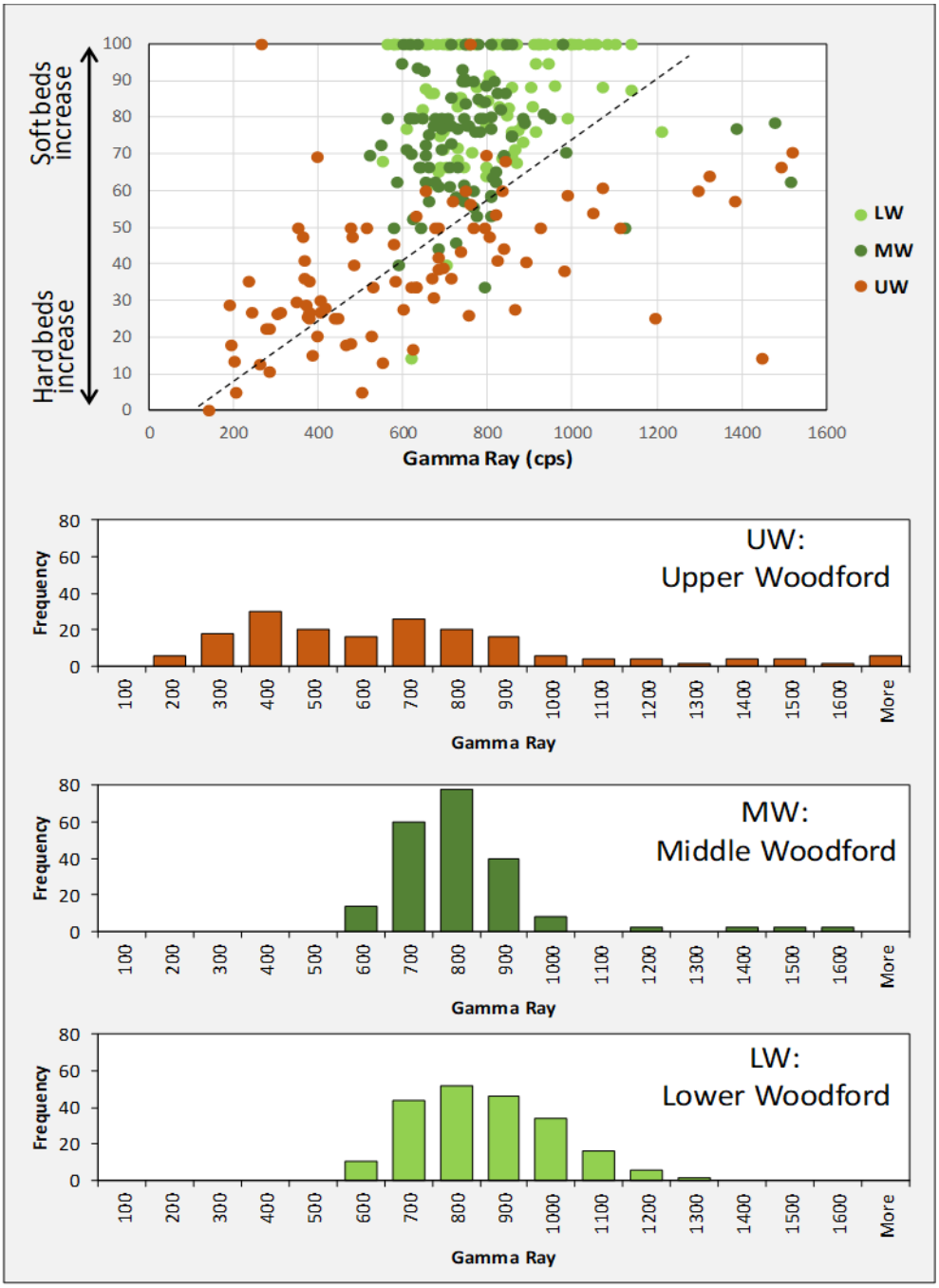

Figure 3.7. Identified correlation by Becerra-Rondon (2017) and Galvis et al. (2017) between Gamma-ray responses and the Soft-to-Hard ratios per foot by Woodford member in southern Oklahoma. Galvis (2017) highlights the positive correlation between these two variables, implying a generalized increase in radioactivity with more soft beds per foot. Image Courtesy of Galvis in Galvis (2017).

The average soft-to-hard ratios in the UW identified by Becerra-Rondon (2017), and Galvis et al. (2017a and 2017b) range from 40/60 to 5/95, with the regional characteristic that this is the hardest and most brittle interval among the Woodford members (Figure 3.6 and Figure 3.7). The crucial highlight for this UW made by Galvis (2017), and Galvis et al. (2017a and 2017b) is that the distributions of bed thickness reveal the dominance of thicker hard beds (2-8 inches) compared to the soft intervals (<2 inches). The cherts and siliceous shale rich beds are the most abundant lithofacies (Figure 3.6), and according to Galvis (2017), that make up about 80% of the lithofacies in this member. Galvis (2017) notes in the SR that other field-scale features of this Upper Woodford member include the abundant occurrence of phosphate nodules and concretions of variable diameter and shapes (0.5 – 10 inches), and also observed bitumen filled microfractures.

3.4. Geochemical characterization

A comprehensive series of geochemical analyses was performed on 536 Woodford Shale outcrop samples, including Rock-Eval pyrolysis, total organic carbon (%TOC), some measurements of vitrinite reflectance (%R_o), and organic fluid inclusions (by courtesy of The Oklahoma Geological Survey -OGS- and directed by organic petrologist Mr. Brian Cardott). Additionally, crushed rock extracts were subjected to gas chromatography (GC) and gas chromatography-mass spectrometry (GC-MS) for biomarker analyses. Rock-Eval pyrolysis and %TOC determination were performed at GeoMark™ Geochemical Services in Humble, Texas, and their results are very applicable in the screening process of organic parameters variability along with the vertical stratigraphy of a shale system. The biomarker analyses were performed at the University of Oklahoma Organic Geochemistry Laboratories under the supervision of Dr. R. Paul Philp. The details about the applied instrumental biomarker methodologies are described in Appendix B.

The data obtained for the reservoir quality analyses of the SR outcrop samples include the measured stratigraphic section, the lithostratigraphic descriptions, the calculated scanning electron microscopy (SEM) porosity, thin section analyses, and X-ray diffraction (XRD) mineral content analyses by Galvis (2017). In addition, this study includes and complements the measured X-ray fluorescence (XRF) for each of the 536 samples, with an integrated geochemical characterization (%TOC, relative hydrocarbon potential (RHP), biomarker contents, and inorganic geochemistry elemental distribution profiles). For integrating all of the multi-scale data set, an unsupervised machine learning *K-means* clustering technique is utilized for performing geostatistical sorting and correlation of all these properties in each sample acquired in the SR outcrop. This unsupervised clustering allowed us to interpret and group the SR samples with statistical similarities as "*K-means facies*."

3.4.1. Organic geochemistry %TOC and RHP profiling

Rock-Eval pyrolysis results include weight %TOC, S1, S2, S3, Tmax, hydrogen index (HI), oxygen index (OI), and a pseudo Van Krevelen kerogen type plot. The %TOC results are graphically represented next to the outcrop Gamma-ray response, as typically performed in other shale systems (Figure 3.8). The relative hydrocarbon potential (RHP) has been proposed as a screening tool for indications of anoxic and oxic depositional environmental conditions (Fang et al., 1993). According to Fang et al. (1993), the fluctuations in oxygenation conditions are reflected by variations in the relative hydrocarbon potential ratio, which is calculated using the following equation (3.1):

$$\mathrm{RHP} = \frac{\mathrm{S1\ mg\ HC/g + S2\ mg\ HC/g}}{\%\mathrm{TOC\ [wt.\%]}} \quad \text{Fang et al., (1993)} \qquad (3.1)$$

Fang et al. (1993), Miceli-Romero (2010), Rodriguez and Philp (2010), Slatt and Rodriguez (2012), Albaghdady (2013), Slatt (2013a, 2013b), Torres-Parada (2013), Rodriguez and Katz (2017), and Liborius-Parada (2019), all noted stratigraphic variations in the RHP in the La Luna Shale, Barnett Shale, and Woodford Shale with their organic matter and mineralogy content. In the case of the Barnett Shale (Singh, 2008; Slatt and Rodriguez, 2012; Figure 3.8), it was observed that changes in oxygen levels, as indicated by the RHP, showed a good correlation with changes in relative sea-level fluctuations derived from the stratigraphic interpretations. The depths with maximum RHP values (anoxic conditions) correspond with interpreted stratigraphic flooding surfaces, while minimum RHP values (oxic conditions) correlate with oxidizing conditions due to lowered sea level (Slatt and Rodriguez, 2012).

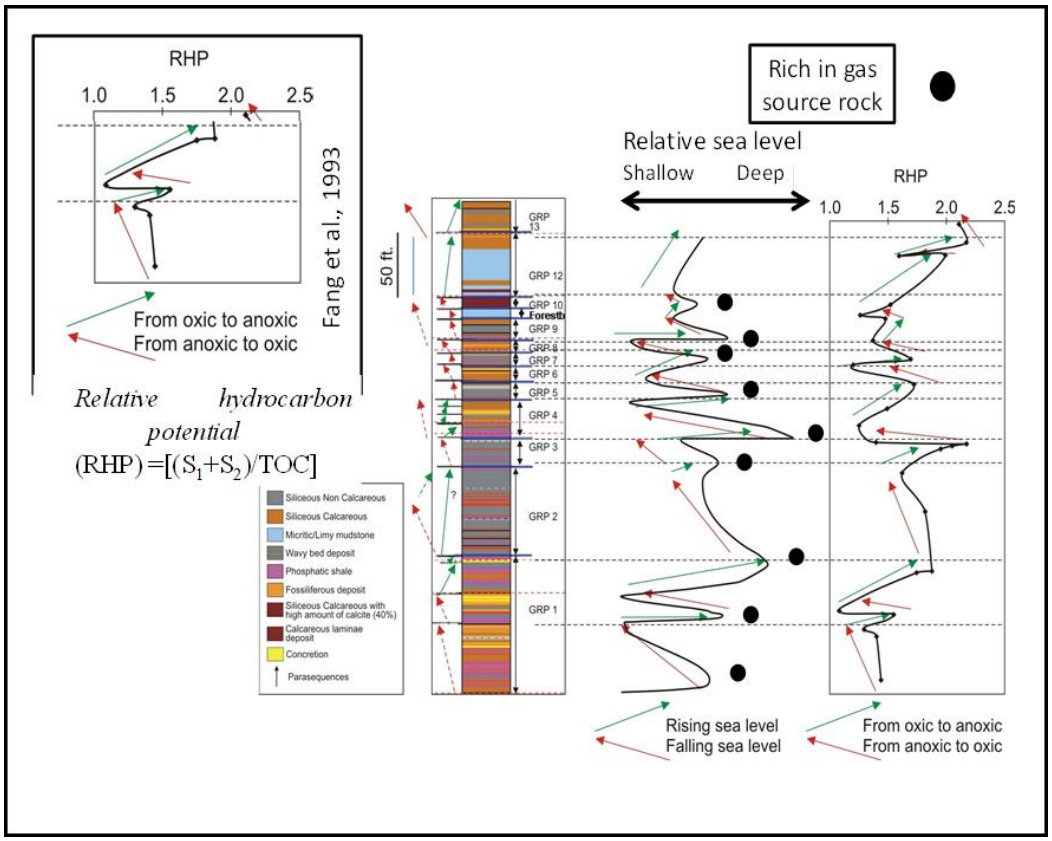

Figure 3.8. Comparison of relative sea level and RHP curves for the Barnett Shale. Changes in oxic conditions, as indicated by the RHP, show a positive correlation with fluctuations in relative sea level. Modified from Miceli-Romero (2010), Singh (2008), and Slatt and Rodriguez (2012).

For the SR section, the RHP shows a lot of variabilities that occur through all of the Woodford Shale members (Figure 3.9). The pre-Woodford section has an initial cycle of rising-falling-rising of sea level (Figure 3.9). The lowermost Woodford Shale starts with a relative sea-level falling stage and fluctuates with rising-falling cycles towards the maximum flooding surface (MFS), covering the Lower and Middle Woodford members (Figure 3.9, from 30 to 194.5 ft). The basal Upper Woodford member starts at 220.5 ft with a general trend of the sea-level drop, and then drastic variable rising-falling cycles occur in the uppermost Upper Woodford member (Figure 3.9, 250-314 ft.). This Upper Woodford RHP variability, when compared to the %TOC and S1 curves in Figure 3.9, is not representative of rising and falling sea-level stages. It is representing that RHP in the Upper member is affected by the high S1 peak from the migrated hydrocarbons that charge this member. In the SR outcrop, these RHP variabilities in the Upper Woodford member correlate to the high %TOC and S1 values that are associated with migrated hydrocarbons charging the microfractures in the Upper Woodford siliceous and chert rich shales (Figure 3.9, values higher than 10% from 250-310 ft). The Upper Woodford member has an overall falling sea level, as interpreted by Miceli-Romero and Philp (2012), Turner et al. (2015), Connock et al. (2018), Molinares (2019), and Philp and DeGarmo (2020). In this SR Woodford section, these RHP values are anomalous for this Upper member.

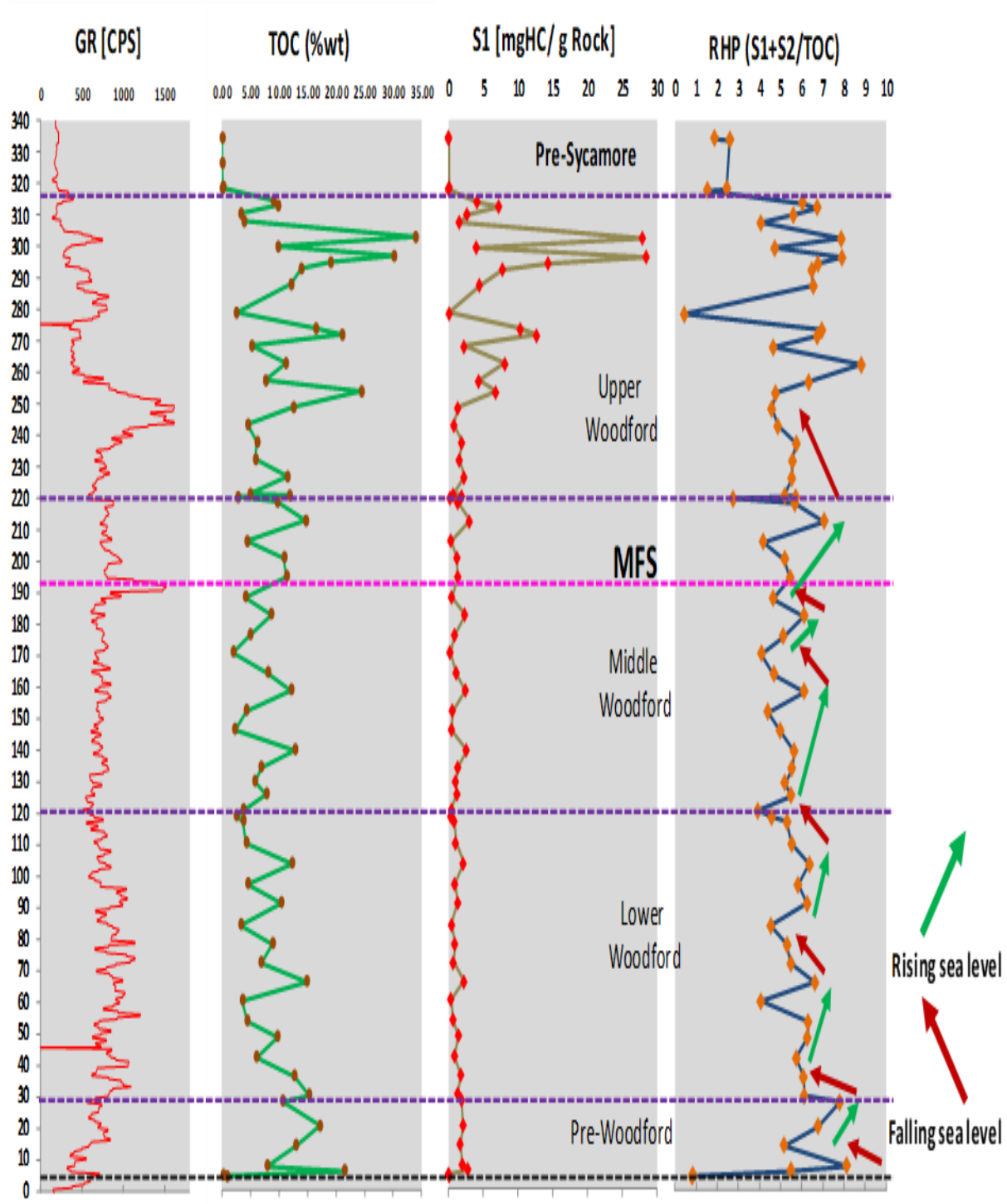

Figure 3.9. RHP curve in the Speake Ranch outcrop. MFS = maximum flooding surface.

3.4.2. Sample handling and preparation

Forty-five outcrop samples, out of the 536 collected by Galvis (2017), were taken from the SR section for the Woodford Shale. For compound recognition and comparison of the polycyclic aromatic hydrocarbons, an international coal tar standard was analyzed (coal tar standard reference material #1597). Between 50 and 100g of rock were taken for each sample at approximately 1ft back into the outcrop from the surface by Galvis (2017) and used in this study.

3.4.3. Rock-Eval pyrolysis, total organic carbon (%TOC), and X-Ray fluorescence (XRF).

For performing the screening analysis of organic matter content in the acquired samples at the SR, one gram of each of the 536 samples in the Ranch was crushed and sent to GeoMark™ (Houston, TX) for courtesy Rock-Eval pyrolysis and %TOC measurements. The studies of Galvis (2017) and Galvis et al. (2017a) included Rock-Eval pyrolysis analyses on 120 samples out of the 536 from this SR section; therefore, this study presents a high-resolution, more detailed characterization of the organic matter content (OM), hydrogen index (HI), oxygen index (OI), and relative hydrocarbon potential (RHP) in each sample collected within the 314ft Woodford stratigraphic section (one sample was collected every half foot, including pre-Woodford and Post-Woodford strata). Peters and Cassa (1994) described that to determine the %TOC content in a rock sample. The ground rock is acidified with hydrochloric acid (HCl) to remove carbonate material, then combusted in a Leco carbon analyzer at 1,000 °C. The CO_2 released from the combustion is detected by infrared detectors and used to calculate %TOC.

For the pyrolysis measurements, the samples were heated at a programmed temperature rate of 25 °C per minute, and a flame ionization detector measured the released hydrocarbons. As a part of the screening methodology, many bulk data measurements were made percent carbonate

(wt.%), %TOC (wt.%), Rock-Eval S1 (mg HC/g), S2 (mg HC/g), S3 (mg CO2/g), and Tmax (°C). From these measurements, specific calculations were undertaken to obtain other meaningful values: calculated relative maturity levels of vitrinite reflectance (%Ro), hydrogen index (HI; S2*100/%TOC), oxygen index (OI; S3*100/%TOC), S2/S3 concentration (mg HC/mg CO2), S1/%TOC normal oil content, and production index (PI=S1/[S1+S2]).

The pseudo van Krevelen diagrams (Figure 3.10 - 3.12) were applied for screening the organic matter content and variability along with the Woodford Shale members and lithofacies described by Galvis (2017). The %TOC content for the Lower Woodford member varies from 0 to 20%, the HI from 300-780 (mg HC/g), and the OI from 0-20 (mg HC/g); for the Middle Woodford member, the %TOC varies from 0 to 16%, the HI from 40-600(mg HC/g), and the OI from 5-200 (mg HC/g); and for the Upper Woodford member, the %TOC varies from 0 to 35%, the HI from 2-700 (mg HC/g), and the OI from 8-180 (mg HC/g). The samples in the Upper Woodford of %TOC higher than 15% and HI higher than 550 in this member are suspected of possibly containing migrated hydrocarbons charging the silica-rich lithologies through microfractures filled with bitumen, as described by Galvis (2017), and Milad and Slatt (2018) for the Upper Woodford member.

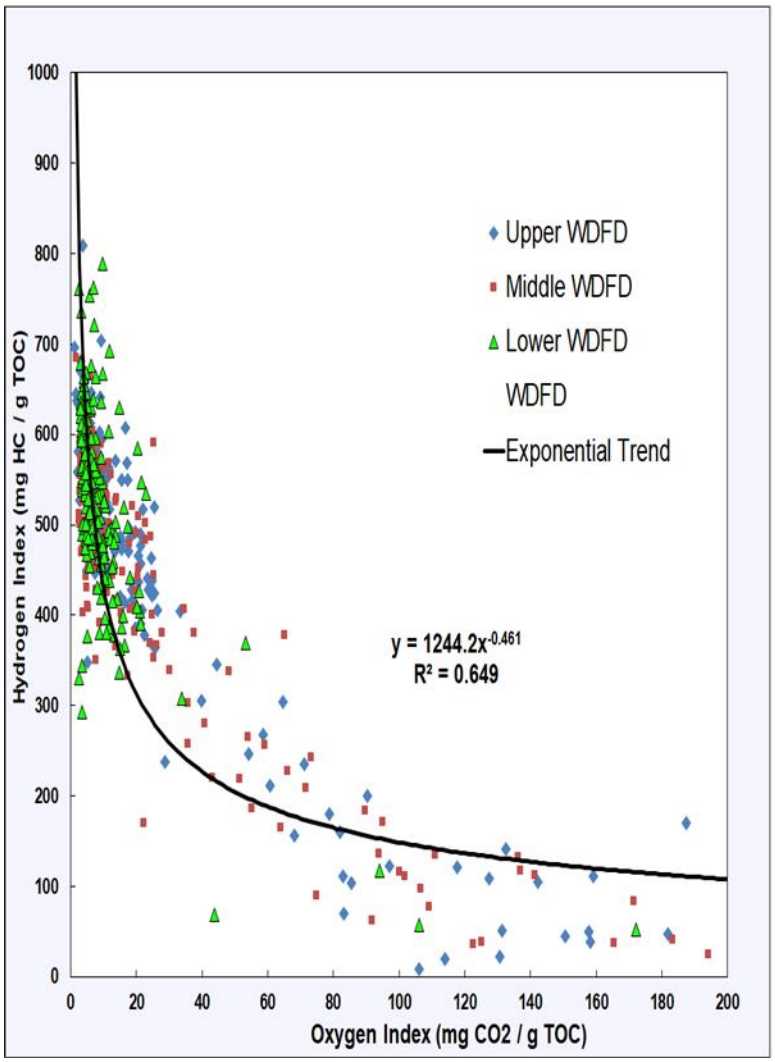

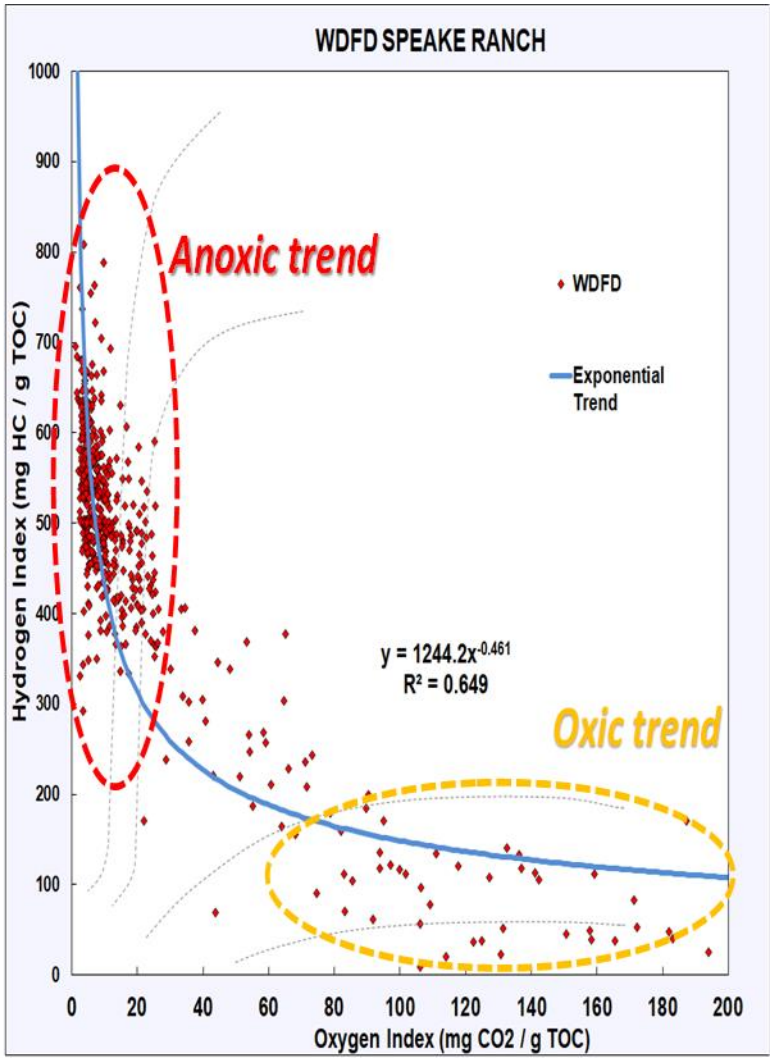

Figure 3.10. Modified pseudo van Krevelen plot for the 536 Speake Ranch samples. There are two trends in this plot, where high HI content and low OI are associated with anoxic restricted intervals and correspond to mostly the Lower and Middle Woodford member samples. Some of the Middle Woodford and Upper Woodford samples are transitional (in between these two significant clusters), and most of the Upper Woodford member samples yield in the cluster of more oxic conditions (HI<200 mg HC/g, and OI>60 mg HC/g).

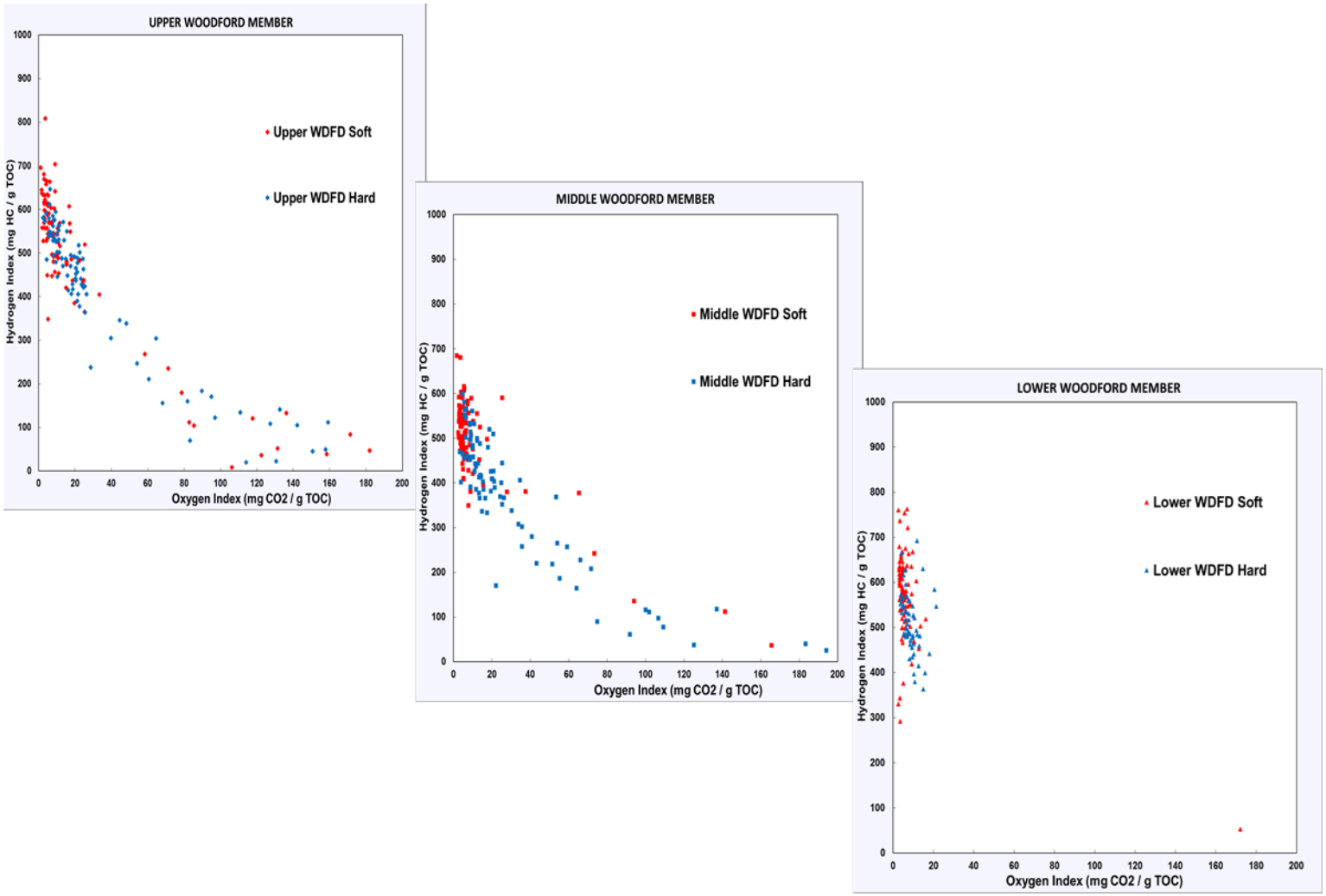

Figure 3.11. Modified pseudo van Krevelen plot for the 536 Speake Ranch samples grouped per member. Mostly all of the Lower Woodford member samples have high HI (>400) and low OI (<20). Some of the Middle Woodford and Upper Woodford samples are transitional (in between low OI and high OI areas), and most of the Upper Woodford member samples yield in the cluster of more oxic conditions (HI<300, and OI>60). The hard shale samples in the Middle and Upper members are the ones with a higher content of OI.

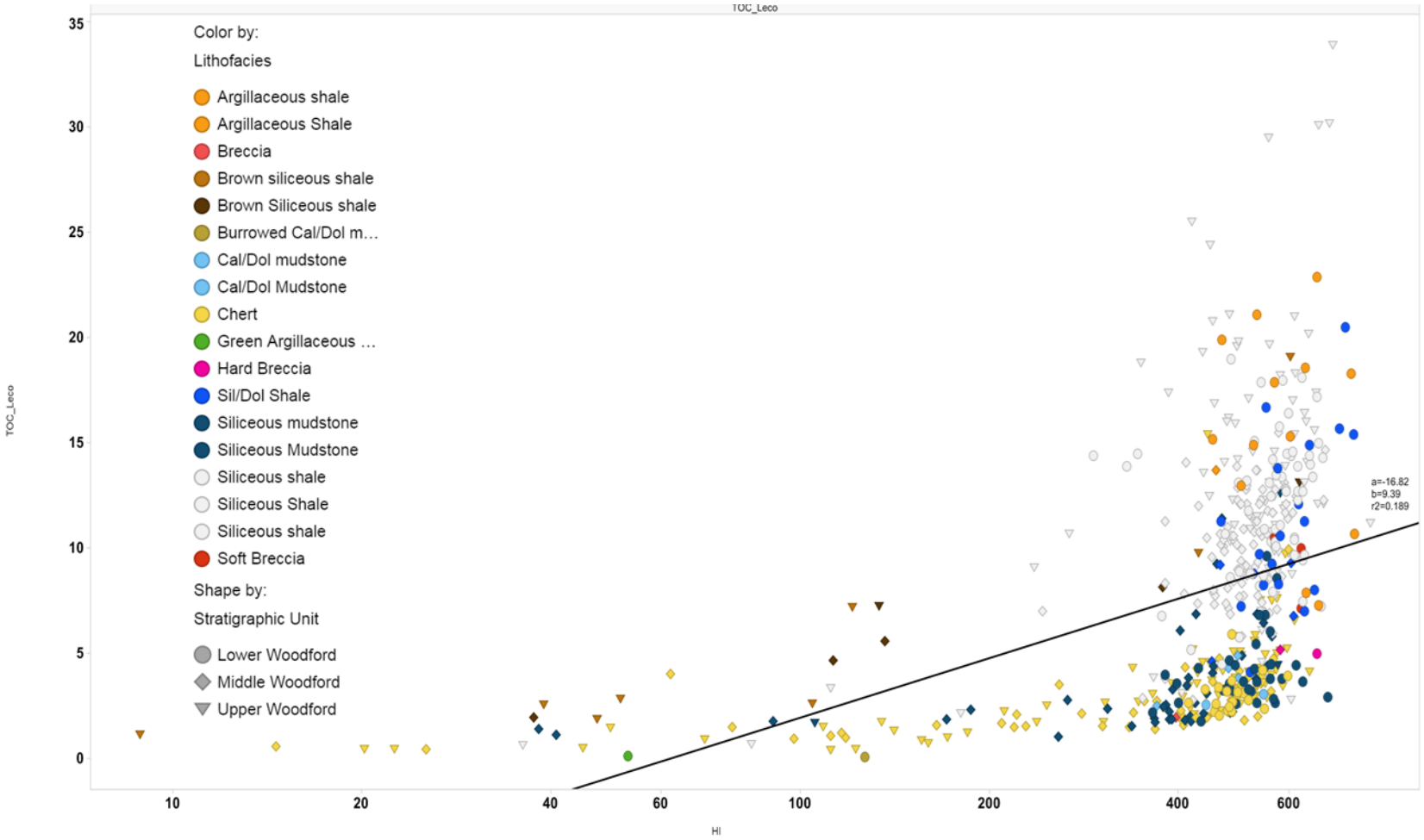

Figure 3.12. Relationship of %TOC and HI content with lithofacies described by Galvis (2017). Note that the highest %TOC is associated with the Upper Woodford siliceous shales that can be possibly hosting migrated hydrocarbons (%TOC higher than 20%, S1>5 mg HC/g, S2<80 mg HC/g), and, the Lower Woodford samples (circle shapes) of argillaceous shale and siliceous shale lithofacies. There is a weak correlation between %TOC and HI, because of the lower %TOC (<5%) samples in the Middle and Lower members present high HI values (>400). The black line corresponds to the weak linear correlation (18%) of %TOC and HI (mg H/g Rock).

The XRF characterization of elemental proxies recognized by Becerra-Rondon (2017), and Galvis (2017) were complemented with proxies made from the Rock-Eval pyrolysis data and coupled with the hardness log for understanding the mechanical stratigraphic response and variations of each rock interval (Figure 3.13 - 3.17). There is a weak correlation between %TOC and HI, due to the lower %TOC (<5%) in the samples of the Middle and Lower members with high HI values (>400 mg HC/g), as can be observed in Figure 3.12 and Figure 3.13.

As interpreted for the Woodford Shale by Turner et al. (2015), Becerra-Rondon (2017), Galvis et al. (2017a), the high response of the XRF proxy Si/Al indicates biogenic silica over detrital silica. Galvis et al. (2017a) proposed that the higher V and Mo/Al suggests more upwelling currents that deposited these heavy minerals rather than the concentration of these elements in the anoxic organic matter-rich intervals. A proposed normalized iron content (Fe ppm averaged by the percentage of soft vs. hard ratio per stratigraphic foot), marks the difference from the maximum flooding surface (MFS) towards the Woodford Shale top (Figure 3.16). The Fe difference indicates the association of Fe^{+2} and Fe^{+3} to the depositional anoxic conditions for organic matter preservation (Molinares et al., 2019). In the Upper Woodford member, the high V/Ni and U/Al also indicates more upwelling currents that deposited these heavy elements (Turner et al., 2015; Molinares, 2019).

%TOC upscaled was calculated using a weighted average of the percentage of rock hardness in one stratigraphic foot. Galvis (2017) reported for every stratigraphic foot in the SR the percentage of soft and hard beds. The upscaled %TOC is obtained by multiplying a %TOC value, which is previously identified as soft or hard, with the percentage of that hardness in a stratigraphic foot (e.g., a %TOC point in a hard bed will be multiplied for the %hard in that stratigraphic foot were the sample was collected). This calculation is simplified using the following equation 3.2:

$$\text{Upscaled\%TOC} = (\%TOC_{soft} * \%\ soft) + (\%TOC_{hard} * \%\ hard) \text{ in the same stratigraphic foot} \quad (3.2)$$

Note how after calculating the weighted average %TOC (upscaled %TOC), the obtained %TOC curve now shows a clear common trend of %TOC decreasing from the Lowermost Woodford Shale (15-20%) towards the Upper Woodford Shale (<4%; Figure 3.17).

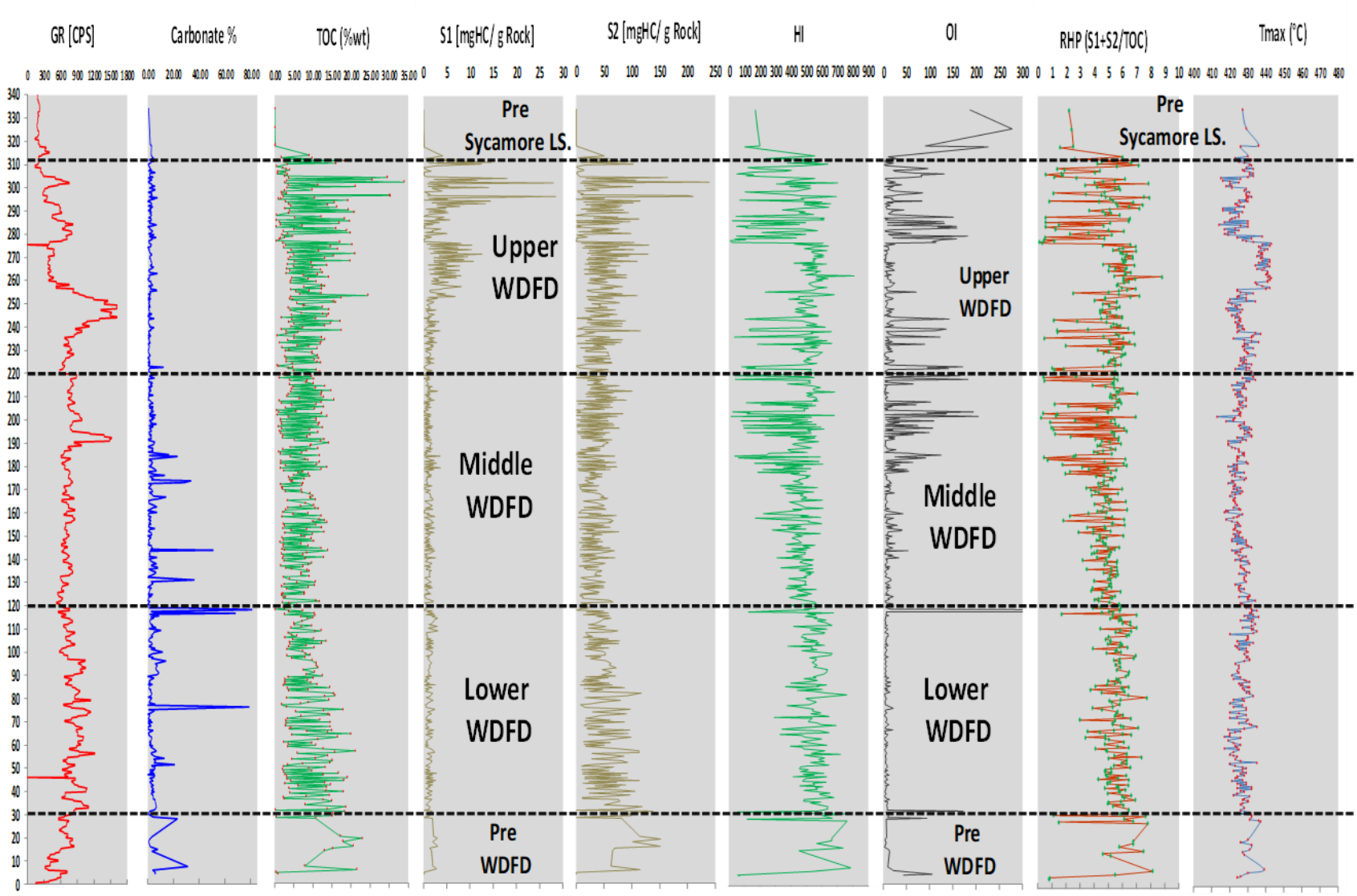

Figure 3.13. Depth plots of Gamma-ray and Rock-Eval pyrolysis data for the 536 Speake Ranch samples.

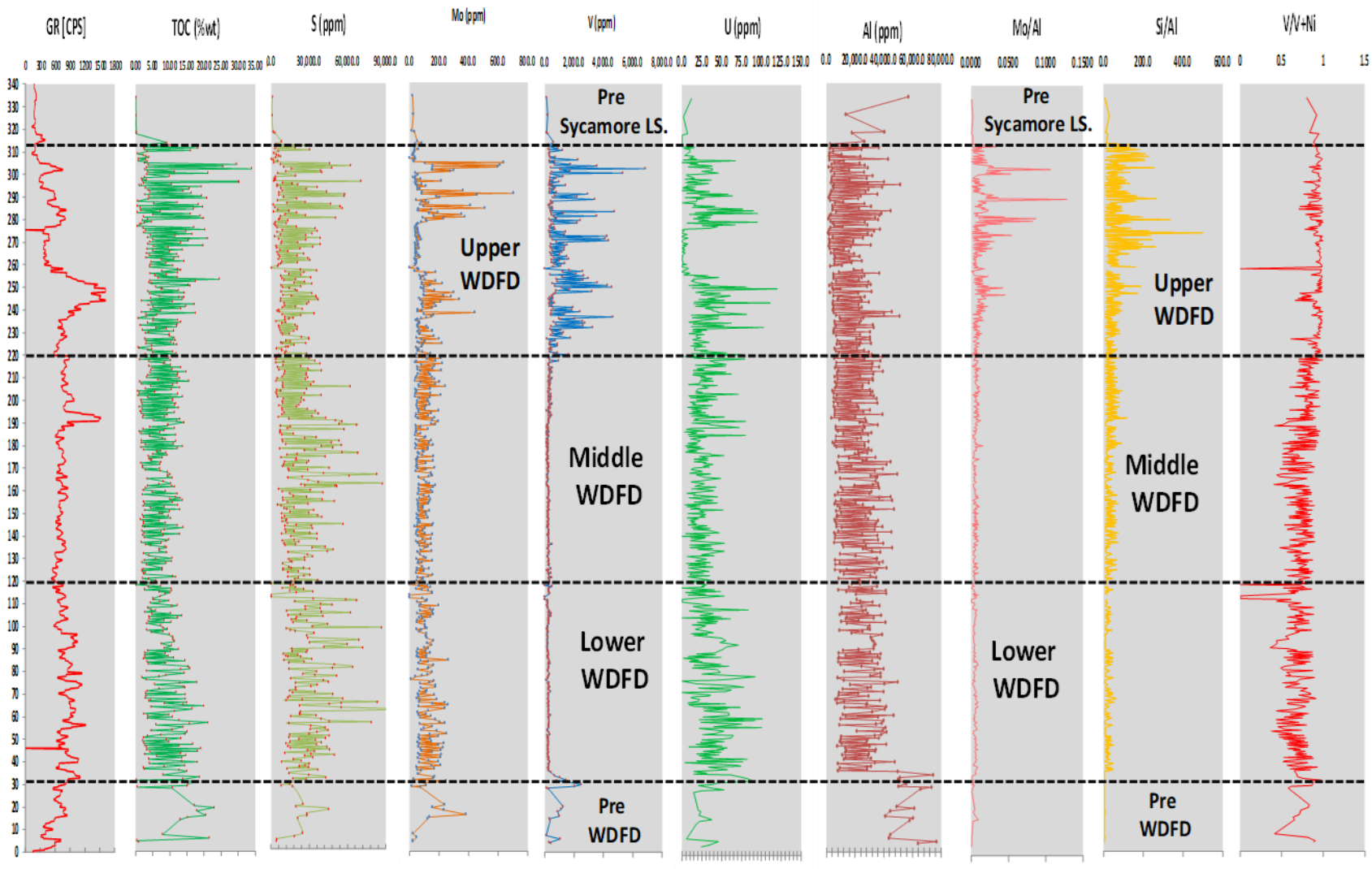

Figure 3.14. Depth plots of Gamma-ray, %TOC, and Galvis (2017) XRF data for the 536 Speake Ranch samples. High Si/Al indicates biogenic silica over detrital silica, and higher V and Mo/Al indicate upwelling currents that deposited these heavy minerals rather than concentration of these significant elements in the organic matter associated with clay-rich deposits.

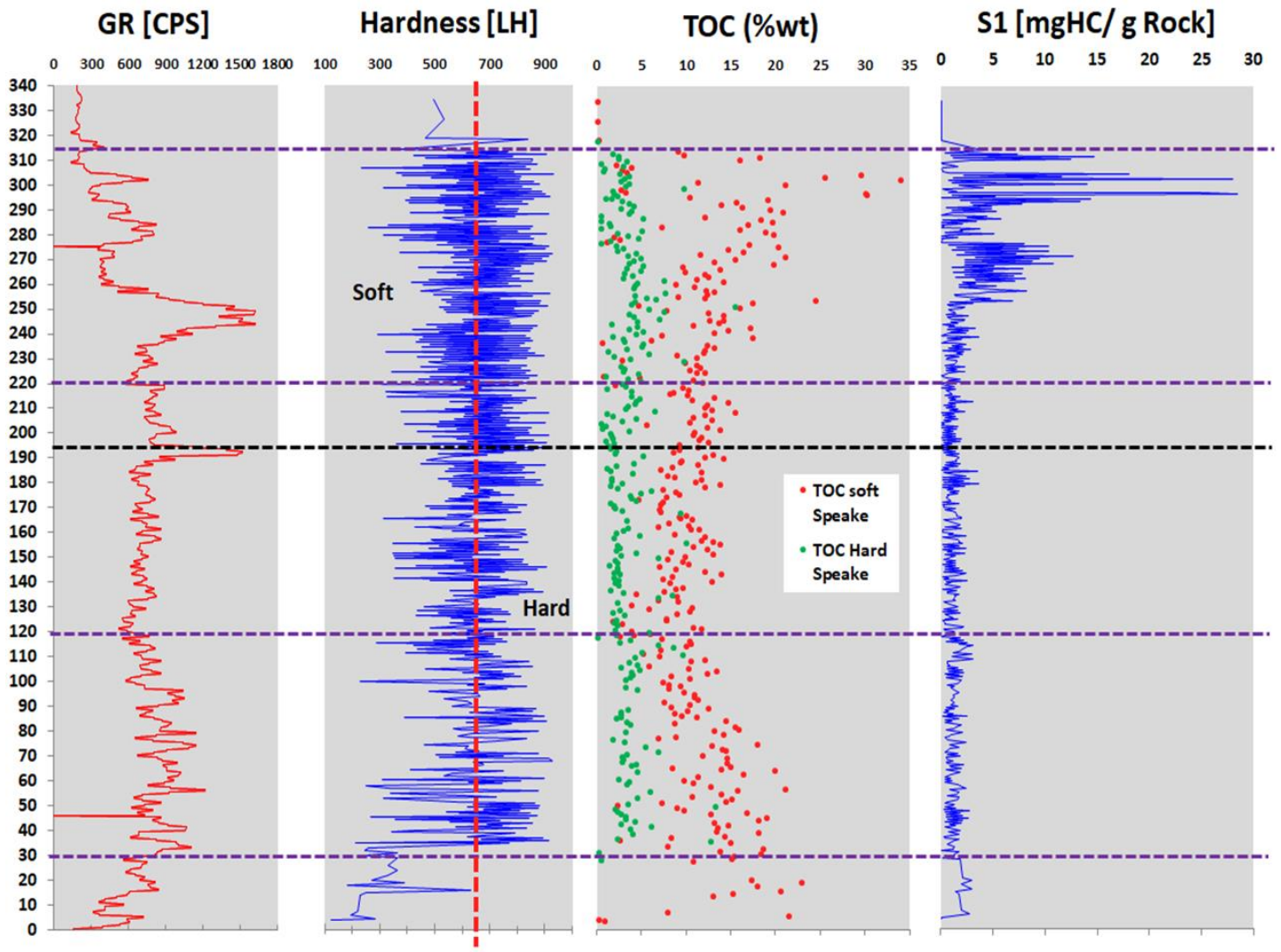

Figure 3.15. Depth plots of Gamma-ray, %TOC, S1, and Galvis' (2017) XRF-hardness data for the 536 Speake Ranch samples (dashed vertical line is the separation between a soft or a hard regime). Possible migration of hydrocarbons in the Upper Woodford member due to the high %TOC (5 to 35%), and S1>5 (mg HC/g).

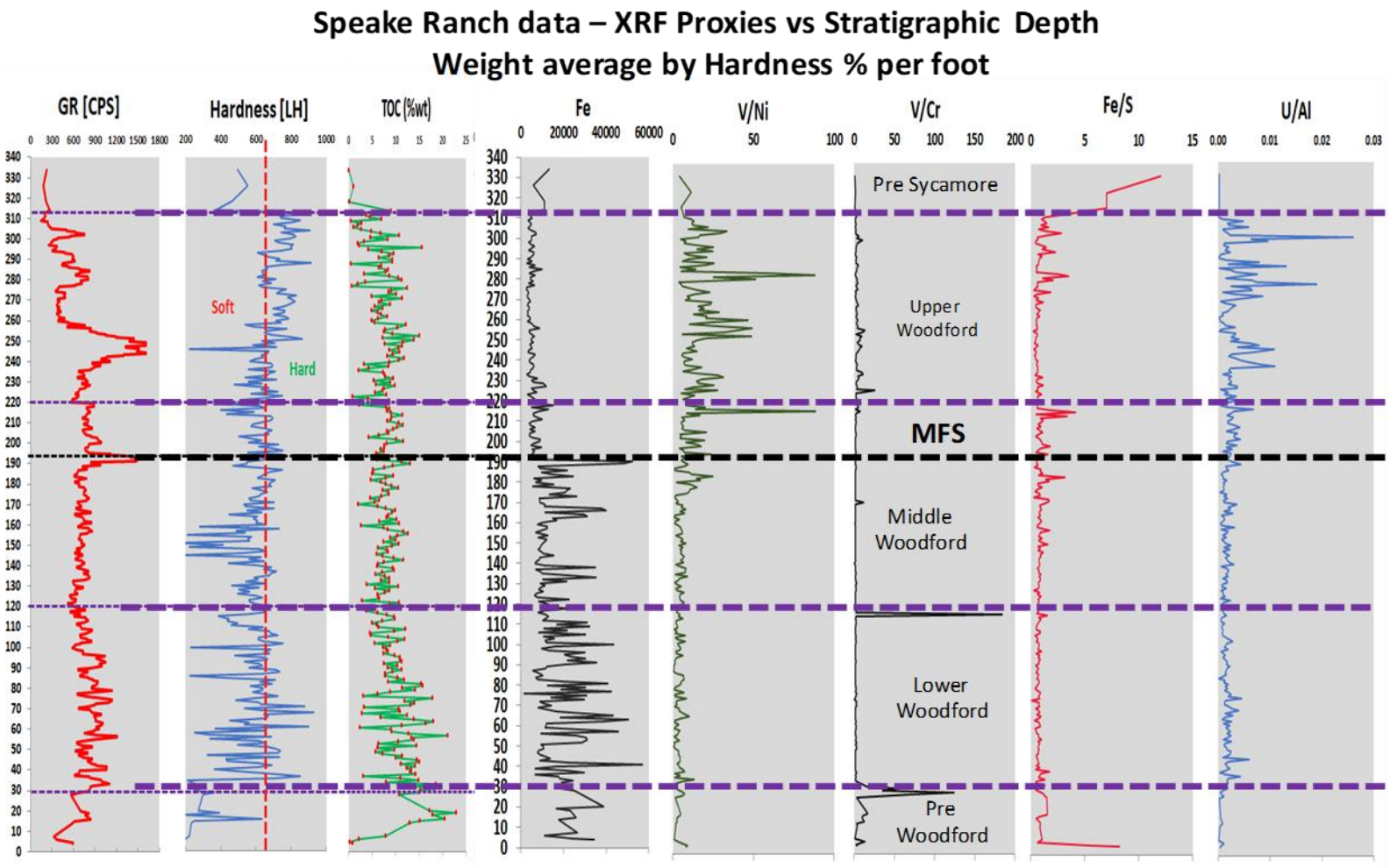

Figure 3.16. Depth plots of Gamma-ray, %TOC, S1, and Galvis (2017) XRF-hardness data for the 536 Speake Ranch samples. Migrated hydrocarbons in the Upper Woodford member are a product of high %TOC (5 to 35%) and S1>5 (mg HC/g). Note how hardness increases after the Middle Woodford top, and the %TOC trend decreases. Also, a normalized iron content marks the difference from the maximum flooding surface (MFS) to the Woodford top. High V/Ni and U/Al indicates more upwelling currents that deposited these heavy minerals rather than the concentration of these elements in the clay-rich deposits organic matter.

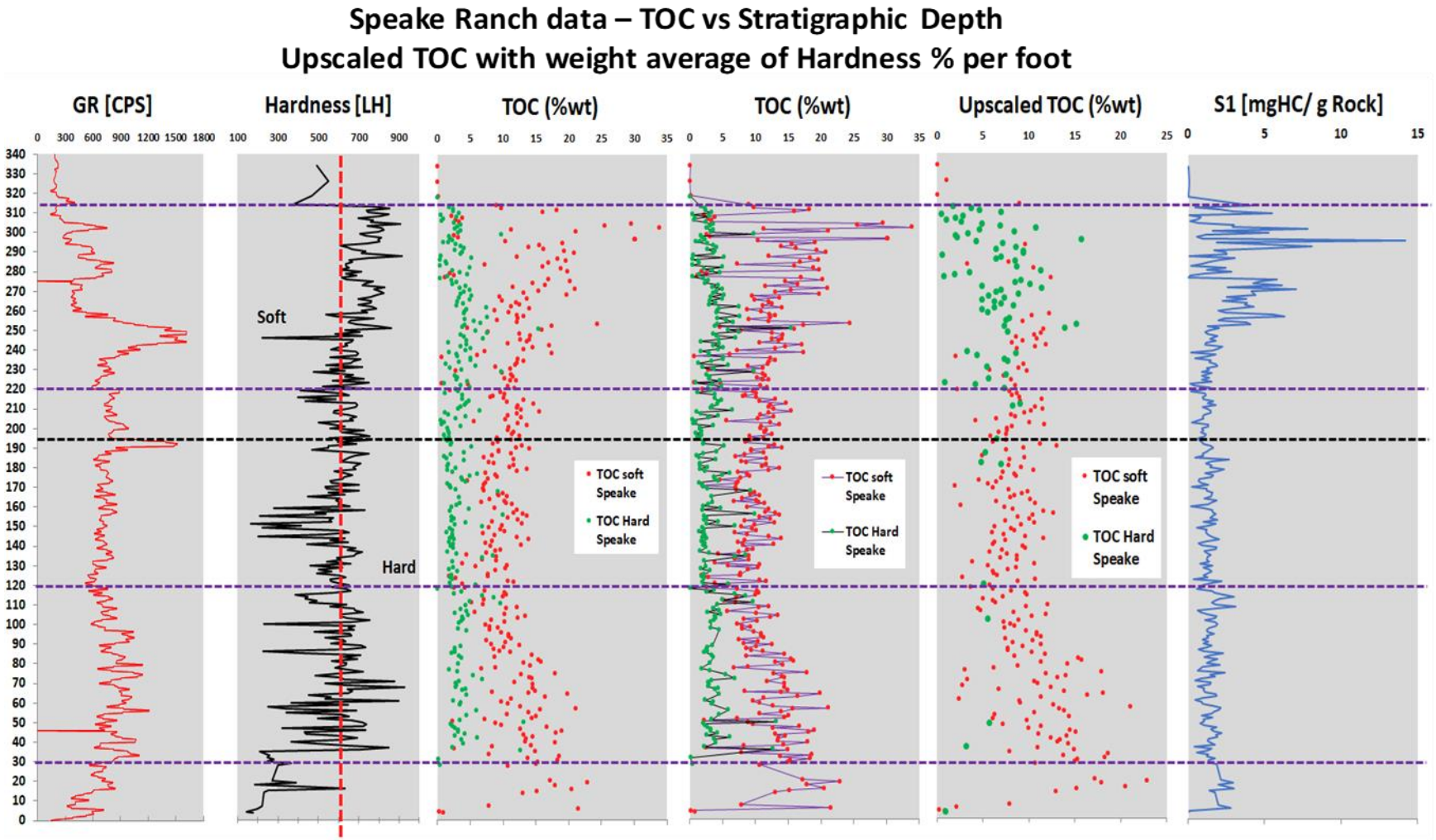

Figure 3.17. Depth plots of weighted average per percentage of mechanical stratigraphy in each stratigraphic foot. Logs of Gamma-ray, %TOC, S1, and Galvis' (2017) XRF-hardness data for the 536 Speake Ranch samples. Possible migrated hydrocarbons in the Upper Woodford member resulted in the high %TOC (5 to 35%) and S1>5. Note how the average %TOC (Upscaled %TOC) shows a clear common trend of %TOC decreasing from the lowermost Woodford Shale (15-20%) to the Upper Woodford Shale (<4%). The %TOC track with lines shows the data variability in rocks under similar mechanical stratigraphic settings (soft and hard beds).

As proposed by Molinares et al. (2019) for the Woodford Shale in the Wyche quarry, the enrichment factors were calculated for U, Mo, V, and Fe for understanding oxic and higher dilution trends (Figure 3.18) which are identified to be much lower in the Middle and Lower Woodford than in the Upper member. Aluminum (Al) was used as a normalization concentration factor to reduce the effects of the detrital and authigenic dilution (Calvert and Pederson, 1993; Tribovillard et al., 2006; Molinares, 2019). Al normalized values of trace elements are usually given as $x10^{-4}$ notation, and it was applicable in this case because Al resides principally within the detrital clay fraction and their presence has not been identified as an evidence of significant remobilization during diagenesis (Elmore et al., 2016; Turner, 2016; Ekwunife, 2017; Molinares, 2019). The normalized aluminum concentration was used to calculate the enrichment factor (EF) plots, as proposed for the Woodford Shale by Ekwunife (2017) and Molinares (2019), and the results are obtained after applying the equation 3.3. and are shown in Figure 3.18:

Enrichment factor (EF) of an element X = ([X]/Al sample) /([X]/Al average shale), (3.3)

The EF compares the elemental concentration of the analyzed sample in terms of international standards (Algeo and Scheckler, 1998; Turner, 2016; Ekwunife, 2017; Molinares, 2019). A specific element enrichment is considered when the ppm values of that specific element are greater than one to the standards statistical mean (Tribovillard et al., 2006; Molinares, 2019). The values that are less than one to the standard are associated with depletions (Tribovillard et al., 2006; Algeo and Rowe, 2012; Molinares, 2019). The standard values are corresponding with the international average values for the average shale lithologies and upper continental crust compiled by Tribovillard et al. (2006). The Average EF from four modern anoxic basins analogs (Black Sea, Cariaco, Framvaren Fjord, and Saanich Inlet basins) complied by Tribovillard et al. (2006) are used for element enrichment factor comparison of the SR with average shales and modern anoxic

basins (Table 3.1). The results of EF in the SR are shown in Figure 3.18, indicating a higher enrichment factor in Ti, Zn, Zr and Fe for the Upper Woodford member and also in the Middle Woodford member at the maximum flooding surface area (MFS) which indicates that the continental and detrital inputs were increasing from this part of the stratigraphic section.

The enrichment in the Upper Woodford member of organically related proxies U, Mo, V, are likely to relate to more open water circulation conditions that captured these heavy elements via upwelling currents supply and concentrated these elements principally in the phosphate concretions (similarly as proposed by Galvis, 2017). Also, the possible migrated oil in the Upper Woodford siliceous rich lithologies (Figure 3.19 and Figure 3.20) should be able to carry some heavy elements in their high molecular polarity fractions that can be detected by the XRF beam, since the migrated bitumen provides saturation of the rock matrix.

Figure 3.20 summarizes the three lithofacies described by Galvis et al. (2017) as the ones which constitute the SR Upper member and are the lithologies capable of hosting the migrated hydrocarbons. For the chert lithofacies, the matrix is made of microcrystalline quartz aggregates; well-preserved radiolarian tests and *Tasmanite*s are replaced by chalcedony quartz; vertical microfractures are common, these are filled with bitumen and quartz (Galvis et al., 2017). For the siliceous mudstone lithologies, the micro fabric is slightly laminated to massive; the shale matrix is made of aggregates of micro-crystalline quartz (no visible discrete grains contacts); radiolarian and *Tasmanites* are scattered through the matrix, abundant, well-preserved and filled with chalcedony and pyrite (Figure 3.20). For the siliceous shale lithofacies, the shale matrix is mostly made of microcrystalline authigenic quartz and clays; embedded coarser particles include silt-sized detrital quartz in laminae and flattened *Tasmanites*; siltier microlenses seem to provide better primary porosities within this lithofacies (Galvis, 2017; Figure 3.20).

			Black Sea		Saanich Inlet		Framvaren		Cariaco Trench	
	Average Shale	Average Continental Crust	X/Al (10^4)	EF	X/Al (10^4)	EF	X/Al (10^4)	EF	X/Al (10^4)	EF
Cu	45.0	25.0	7.1	1.4	12.3	2.4	37.5	7.3	5.3	1.0
Mn	850.0	600.0	132.6	1.4	106.3	1.1	160.0	1.7	31.2	0.3
Mo	1.3	1.5	4.3	14.3	18.0	60.0	100.0	33.3	11.1	37.0
Ni	68.0	44.0	19.8	2.6	7.4	1.0	90.6	11.8	5.8	0.8
U	3.0	2.8	3.3	8.2	1.4	3.5	8.1	20.2	2.2	5.5
Ti	2000	5700	NA	NA	NA	NA	NA	NA	NA	NA
Zr	70	165	NA	NA	NA	NA	NA	NA	NA	NA
Al	88,900	80,400	NA	NA	NA	NA	NA	NA	NA	NA

Table 3.1. EF Factors of international standards for calculating the enrichment factors of trace elements in Tribovillard et al. (2006).

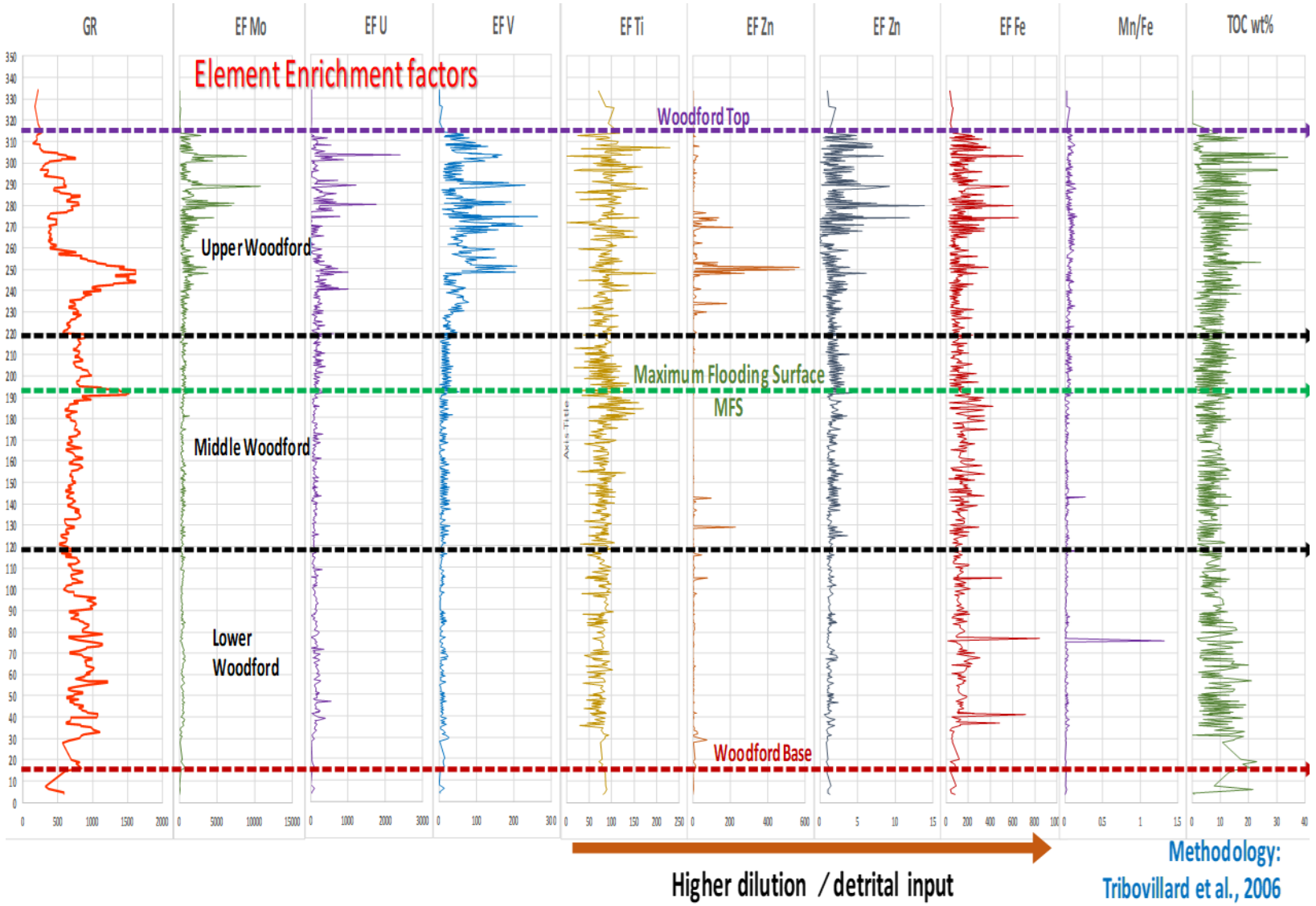

Figure 3.18. Enrichment factors calculated for U, Mo, V, and Fe for understanding oxic and higher dilution trends, which are identified to be much lower in the Middle and Lower Woodford (detrital input of sediments) than in the Upper member.

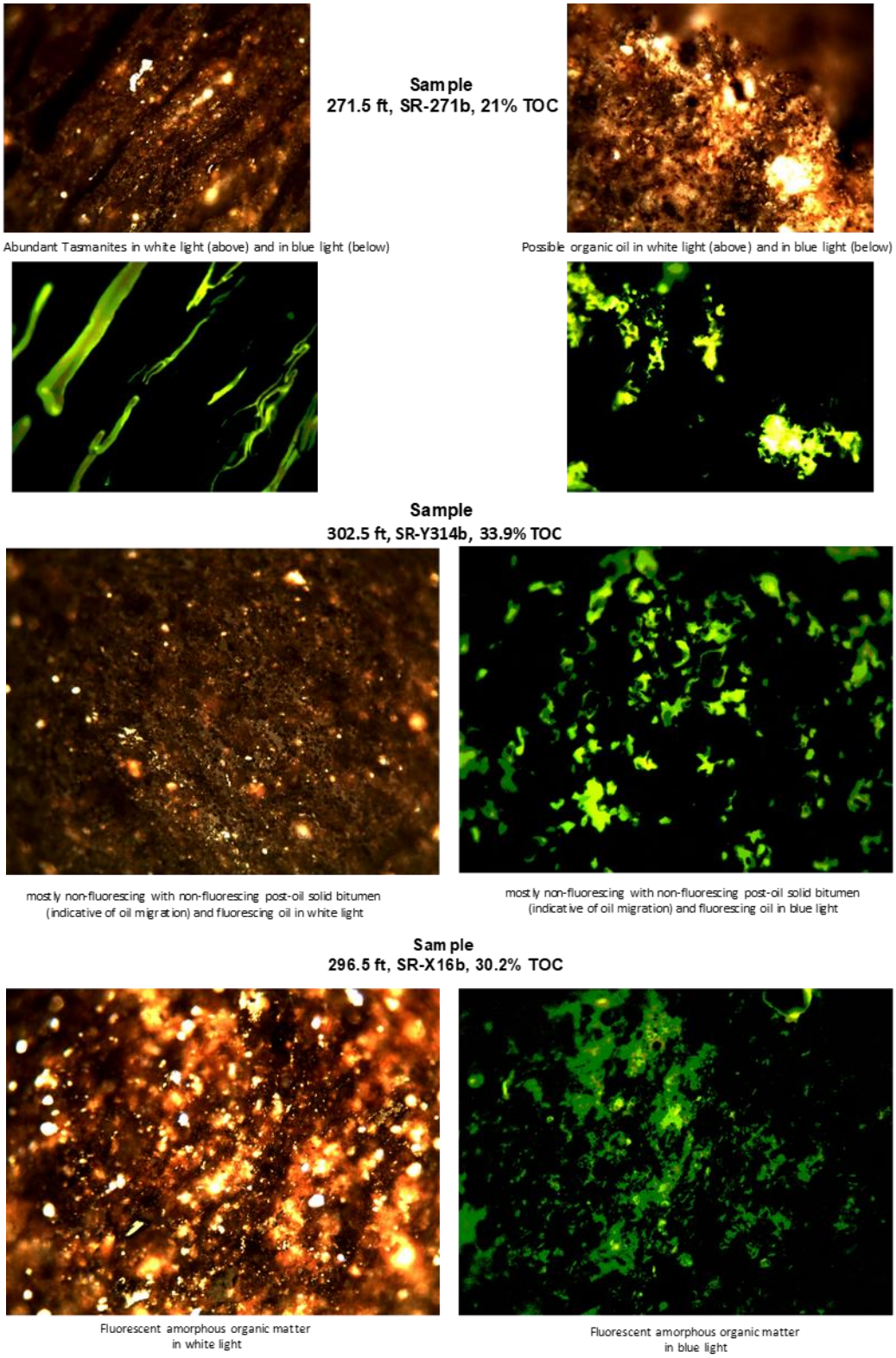

Figure 3.19. Photomicrograph analysis by courtesy of Mr. Brian Cardott, Oklahoma Geological Survey (OGS). He comments that the high S1 peak is undoubtedly from a migrated oil. Note that the fluorescence is not seen very well in the photomicrographs (better under the microscope).

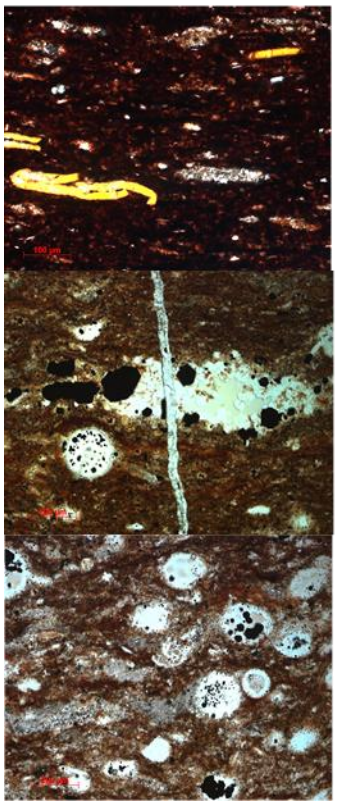

Siliceous shale lithofacies description from Galvis (2017)

The shale matrix is largely made of microcrystalline authigenic quartz and clays; embedded coarser particles include silt-sized detrital quartz in laminae and flattened *Tasmanites*.

Siliceous mudstone lithofacies description

The shale matrix is made of aggregates of micro-crystalline quartz (no visible discrete grains contacts). Scattered through the matrix there are abundant well-preserved radiolarian and *Tasmanites* filled with chalcedony and pyrite.

Chert lithofacies description

The matrix is made of micro-crystalline quartz aggregates.
Well-preserved radiolarian tests and *Tasmanites* are replaced by chalcedony quartz.

Figure 3.20. Siliceous shale, siliceous mudstone and chert-rich lithofacies proposed and described by Galvis (2017) in the Woodford Shale that served as hosting lithologies of migrated hydrocarbons identified by the fluid inclusion analyses.

3.4.4. Sample selection criteria for biomarker analysis

The selection of the samples for biomarker analysis was based on the recognition of intervals with higher %TOC content, higher HI, and statistical cluster analysis using unsupervised K-means facies classification to incorporate the inorganic geochemical properties by the elemental composition analysis of XRF data. This clustering technique was applied in an unsupervised manner, as suggested by Franti and Sieranoja (2019), and Qiao et al. (2019) for big data clustering analytics. Unsupervised clustering means that no user interpretation was applied, and each data site point at each sample was compared, and their statistical centroid correlation factors were

identified and grouped in clusters (Qiao et al., 2019). The result clusters are interpreted as "facies" and referred to as *"K-means facies."*

The K-means unsupervised machine learning classification obtained ten different clusters that were interpreted as *K-means facies.* The biomarker analyses are proposed to be conducted on at least one sample of each of these ten *K-means facies* for covering the different rock types in the stratigraphic section. More samples were selected systematically, trying to expand every 20ft intervals of stratigraphic variations, and were interpreted to be representative for the 314 ft SR section, since typical Woodford Shale layers along the section are very likely to present a variable concentration of elemental Mo and V (from XRF), high hydrogen index, and low oxygen index (from Rock-Eval pyrolysis). The K-means facies clustering results are in Table 3.2, under the column named *"K-means Facies,"* with values from 0 to 9. For K-means facies, each similar number corresponding to similar geostatistical facies. The computational theory defines K-means as a clustering tool that classifies related or unrelated data into *n* observations $X(x_1, x_2, \ldots, x_n)$ into k clusters to minimize the cluster center. The K-means algorithm and the most common steps are the following:

$$Distance = \sum_{i=1}^{k} \sum_{j=1}^{n} x_{ij} - C_i^2$$

Where $C_i = \frac{1}{N_i} \sum_{x \in x_i} x, \quad i = 1, 2, \ldots, k$ represents the *i*th. ; (3.4)

1. Initialize cluster centroids Ci with k random samples;

2. Assign each observation xi to the nearest cluster center;

3. Recalculate and update each cluster center $C_i = \frac{1}{N_i} \sum_{x \in x_i} x, \quad i = 1, 2, \ldots, k$; where Ni is the element in the i^{th} cluster; (3.5)

4. Repeat steps 2 and 3 until Ci does not change.

In the results of this unsupervised clustering methodology, the facies have been assigned as voxels into ten groups that are labeled from 0 to 9 and represent a direct dependent relation between the elemental content from XRF and the organic matter characteristics provided by the Rock-eval pyrolysis into this unsupervised geometrical statistical technique (Table 3.2).

Details about the organic geochemistry analytical sample preparation, molecular fractionations, and instrumental analysis settings are provided in Appendix B of this manuscript. A summary of the entire laboratory workflow used to analyze samples is illustrated in Figure 3.21.

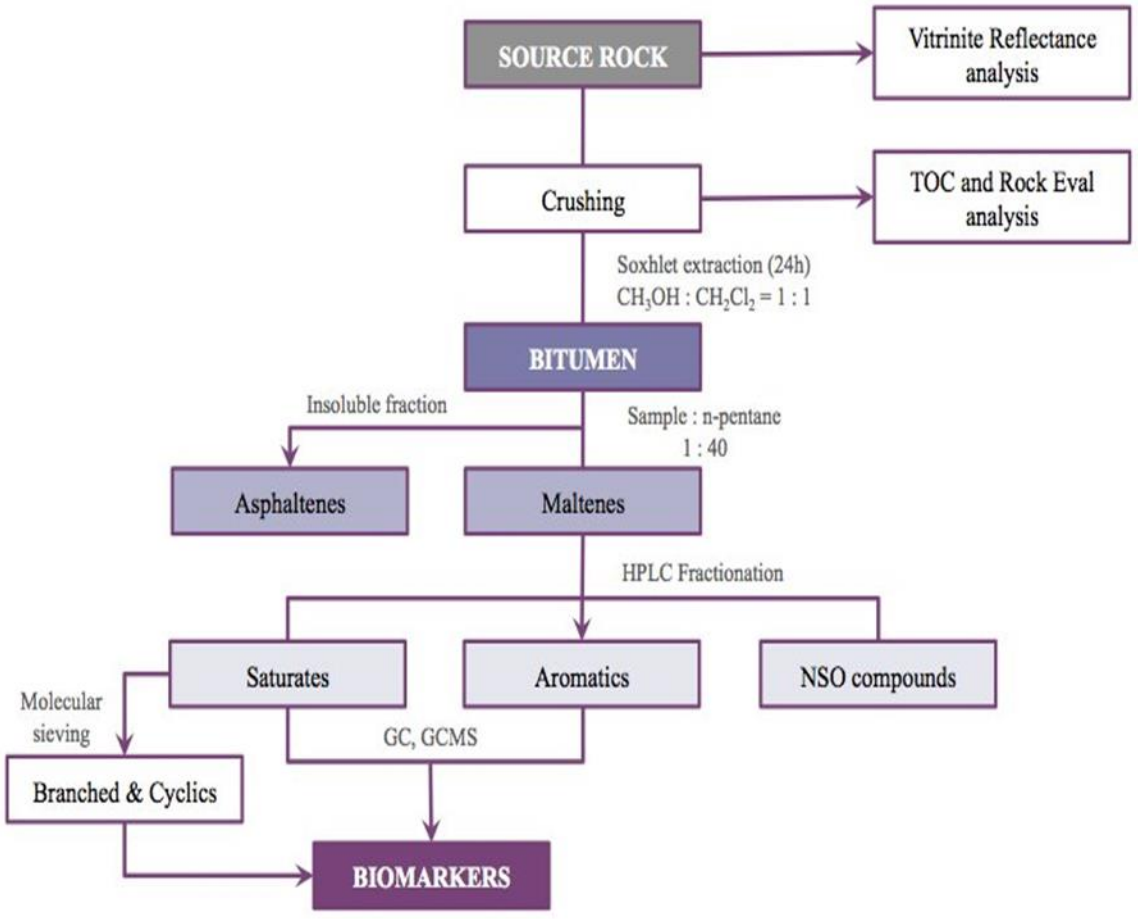

Figure 3.21. Schematic workflow used in the laboratory analysis. Methodology from the OU Organic Geochemistry Group (OG2). Diagram modified from Miceli-Romero (2014).

Sample ID	Formation	Outcrop Depth	Kmeans Facies	TOC Leco	S1	S2	S3	Tmax	RHP	Calc. Ro%	HI	OI	S2/S3	S1/TOC	PI	Si/Al	Si/Ti	V (ppm)	Mo (ppm)	U (ppm)	S (ppm)	Fe (ppm)	TOC vol%	GR CPS	Soft vs Hard	Hardness
SR-Y326	Upper Woodford	314.0	1	9.04	4.12	50.34	0.95	430	6.02	0.58	556.86	10.51	52.99	45.58	0.08	13.54	152.68	593.09	52.52	0.00	8112.40	11015.70	18.08	267.20	Soft	676.3
SR-X16b	Upper Woodford	296.5	6	30.20	28.49	210.08	0.37	432	7.90	0.62	695.63	1.23	567.78	94.34	0.12	5.48	431.14	964.84	216.53	33.29	70463.39	21293.86	60.40	363.80	Soft	578.4
SR-X7b	Upper Woodford	287.5	1	12.10	4.48	74.67	0.38	423	6.54	0.45	617.11	3.14	196.50	37.02	0.06	33.46	426.88	558.74	112.47	17.28	26599.98	12802.67	24.20	441.00	Soft	538.8
SR-271b	Upper Woodford	271.5	6	21.00	12.66	128.62	0.66	438	6.73	0.72	612.48	3.14	194.88	60.29	0.09	13.83	276.42	4119.44	72.93	0.00	38420.81	4959.74	42.00	485.60	Soft	820.5
SR-243a	Upper Woodford	243.0	0	4.50	0.78	21.16	0.79	426	4.88	0.51	470.22	17.56	26.78	17.33	0.04	11.11	142.47	683.87	211.01	35.18	29535.69	5801.83	9.00	1298.40	Hard	750.2
SR-230b	Upper Woodford	230.5	1	11.10	1.72	54.47	1.15	428	5.06	0.54	490.72	10.36	47.37	15.50	0.03	81.26	1115.34	490.36	66.23	8.77	6930.43	7900.28	22.20	798.00	Soft	541.5
SR-229a	Upper Woodford	229.0	0	9.74	1.47	57.62	0.40	430	6.07	0.58	591.58	4.11	144.05	15.09	0.02	15.97	262.03	1189.35	73.42	18.01	14247.70	6604.68	19.48	717.00	Hard	865.1
SR-227b	Upper Woodford	227.5	1	11.20	1.25	59.20	0.48	428	5.40	0.54	528.57	4.29	123.33	11.16	0.02	12.61	146.28	1747.58	164.98	13.43	23646.01	10402.90	22.40	833.20	Soft	897.4
SR-226b	Upper Woodford	226.5	1	11.50	2.28	61.33	0.54	429	5.53	0.56	533.30	4.70	113.57	19.83	0.04	11.86	188.92	733.86	200.11	34.32	29632.28	20597.87	23.00	759.40	Soft	834.6
SR-224b	Upper Woodford	224.5	1	12.00	1.66	64.21	0.43	432	5.49	0.62	535.08	3.58	149.33	13.83	0.03	55.82	1212.67	356.80	67.52	24.09	8705.16	5811.52	24.00	630.20	Soft	546.8
SR-223a	Upper Woodford	223.0	7	1.00	0.12	1.71	0.95	431	1.83	0.60	171.00	95.00	1.80	12.00	0.07	17.28	255.77	407.19	85.12	31.91	13483.91	8256.24	2.00	675.20	Hard	815.0
SR-221b	Upper Woodford	221.5	1	10.80	1.82	56.96	0.46	432	5.44	0.62	527.41	4.26	123.83	16.85	0.03	59.58	886.87	332.21	66.60	12.16	8326.24	5178.09	21.60	587.20	Soft	341.5
SR-220b	Upper Woodford	220.5	1	11.80	1.96	65.38	0.35	435	5.71	0.67	554.07	2.97	186.80	16.61	0.03	46.01	770.57	621.67	88.64	3.56	10709.29	6714.13	23.60	577.60	Soft	628.9
SR-220a	Middle Woodford	220.0	0	2.82	0.20	7.50	1.52	431	2.73	0.60	265.96	53.90	4.93	7.09	0.03	11.46	183.42	1619.35	142.41	22.38	27710.71	14643.41	5.64	577.60	Hard	873.8
SR-219a	Middle Woodford	219.0	0	3.16	0.68	16.44	0.59	433	5.42	0.63	520.25	18.67	27.86	21.52	0.04	7.50	135.46	277.26	122.10	79.00	3530.33	34972.20	6.32	885.80	Hard	844.8
SR-217b	Middle Woodford	217.5	4	10.20	1.38	53.69	0.37	429	5.40	0.56	526.37	3.63	145.11	13.53	0.03	28.65	426.30	956.06	118.55	40.30	3681.19	15245.64	20.40	780.40	Soft	630.4
SR-211b	Middle Woodford	211.5	1	12.30	1.45	66.65	0.36	423	5.54	0.45	541.87	2.93	185.14	11.79	0.02	11.16	174.74	381.99	130.82	30.04	27512.97	10880.14	24.60	809.20	Soft	866.8
SR-210b	Middle Woodford	210.5	1	12.10	1.38	62.24	0.77	424	5.26	0.47	514.38	6.36	80.83	11.40	0.02	15.65	234.28	339.28	141.51	38.14	27540.69	17899.98	24.20	794.40	Soft	832.8
SR-209a	Middle Woodford	209.0	0	6.46	0.86	35.32	0.42	429	5.60	0.56	546.75	6.50	84.10	13.31	0.02	50.97	907.52	286.82	42.69	22.40	4607.19	3962.30	12.92	743.40	Hard	634.4
SR-208b	Middle Woodford	208.5	1	15.50	2.32	89.58	1.14	425	5.93	0.49	577.94	7.35	78.58	14.97	0.03	9.47	130.91	387.07	171.72	21.89	26955.15	9539.12	31.00	810.40	Soft	747.2
SR-206a	Middle Woodford	206.0	0	4.36	0.37	17.85	0.87	427	4.18	0.53	409.40	19.95	20.52	8.49	0.02	58.09	1504.55	310.67	63.14	20.40	8969.86	4298.48	8.72	725.60	Hard	376.4
SR-205a	Middle Woodford	205.0	0	2.79	0.26	13.52	0.27	425	4.94	0.49	484.59	9.68	50.07	9.32	0.02	66.37	1815.13	273.24	66.15	17.76	9443.37	6800.84	5.58	745.60	Hard	611.9
SR-195b	Middle Woodford	195.5	1	9.13	1.12	48.39	0.34	430	5.42	0.58	530.01	3.72	142.32	12.27	0.02	11.63	117.57	119.44	106.62	29.54	28332.70	7882.23	18.26	808.40	Soft	790.9
SR-194b	Middle Woodford	194.5	1	11.30	1.33	60.15	0.46	428	5.44	0.54	532.30	4.07	130.76	11.77	0.02	13.60	153.53	390.53	199.16	33.26	34806.95	18945.55	22.60	1125.60	Soft	859.9
SR-193b	Middle Woodford	193.5	4	9.22	1.08	52.06	0.31	432	5.76	0.62	564.64	3.36	167.94	11.71	0.02	8.48	128.21	475.60	147.73	53.40	37180.08	22223.06	18.44	1387.40	Soft	905.2
SR-191a	Middle Woodford	191.0	0	5.19	0.50	30.14	0.29	426	5.90	0.51	580.73	5.59	103.93	9.63	0.02	43.60	1731.28	302.60	58.06	12.51	14065.28	4913.37	10.38	1478.40	Hard	517.4
SR-190b	Middle Woodford	190.5	4	12.00	1.55	51.68	0.59	419	4.44	0.38	430.67	4.92	87.59	12.92	0.03	12.28	170.36	273.31	156.88	34.68	50254.13	30219.33	24.00	846.80	Soft	861.2
SR-185b	Middle Woodford	185.5	3	7.04	0.72	17.11	5.16	428	2.53	0.54	243.04	73.30	3.32	10.23	0.04	11.38	116.13	127.16	48.42	79.72	7142.21	7784.39	14.08	652.80	Soft	796.5
SR-182b	Middle Woodford	182.5	1	8.65	2.37	50.49	0.62	429	6.11	0.56	583.70	7.17	81.44	27.40	0.04	17.73	155.70	159.73	104.35	19.27	26329.95	13253.94	17.30	778.40	Soft	551.8
SR-170b	Middle Woodford	170.5	0	1.95	0.25	7.73	0.30	424	4.09	0.47	396.41	15.38	25.77	12.82	0.03	22.43	388.88	240.32	54.32	11.49	17390.11	21090.64	3.90	655.00	Soft	640.2
SR-159b	Middle Woodford	159.5	4	8.71	1.24	44.70	0.49	425	5.27	0.49	513.20	5.63	91.22	14.24	0.03	11.32	160.76	312.18	144.75	16.82	30811.02	27229.00	17.42	661.20	Soft	426.0
SR-152b	Middle Woodford	152.5	3	8.33	1.13	31.72	3.12	426	3.94	0.51	380.79	37.45	10.17	13.57	0.03	11.07	169.32	225.13	93.42	51.93	7846.62	16396.93	16.66	715.00	Soft	515.4
SR-142b	Middle Woodford	142.5	5	8.42	1.38	41.17	0.30	425	5.05	0.49	488.95	3.56	137.23	16.39	0.03	10.84	182.97	309.13	105.16	46.97	32540.79	27696.90	16.84	716.00	Soft	749.8
SR-134b	Middle Woodford	134.5	4	8.97	1.28	44.60	0.35	425	5.11	0.49	497.21	3.90	127.43	14.27	0.03	6.34	110.87	206.19	126.70	53.58	42238.63	34451.41	17.94	824.00	D	806.4
SR-129a	Middle Woodford	129.0	7	2.49	0.28	9.41	0.33	425	3.89	0.49	377.91	13.25	28.52	11.24	0.03	67.68	1770.87	286.54	47.51	5.80	13545.56	11347.09	4.98	739.60	Hard	611.4
SR-120b	Lower Woodford	120.5	1	3.79	0.43	14.44	0.33	429	3.92	0.56	381.00	8.71	43.76	11.35	0.03	15.62	237.45	317.05	94.03	22.77	21453.44	14608.84	7.58	588.60	Soft	864.5
SR-118c	Lower Woodford	118.8	9	4.15	0.67	21.56	0.67	435	5.36	0.67	519.52	16.14	32.18	16.14	0.03	9.56	160.10	334.07	38.19	28.55	19425.27	16225.22	8.30	762.60	Soft	707.8
SR-110b	Lower Woodford	110.5	4	7.00	2.02	44.40	0.34	432	6.63	0.62	634.29	4.86	130.59	28.86	0.04	7.53	102.30	175.87	110.42	36.56	66870.14	18273.60	14.00	696.80	Soft	392.9
SR-90	Lower Woodford	90.0	4	8.28	0.98	45.26	0.53	426	5.58	0.51	546.62	6.40	85.40	11.84	0.02	8.39	126.94	170.52	101.62	43.54	41414.96	20501.16	16.56	838.40	Soft	618.9
SR-72b	Lower Woodford	72.5	1	14.40	0.88	42.14	0.51	420	2.99	0.40	292.64	3.54	82.63	6.11	0.02	10.64	172.18	237.39	176.30	55.01	31186.73	27435.05	28.80	906.20	Soft	624.3
SR-60a	Lower Woodford	60.0	0	3.58	0.40	14.21	0.37	424	4.08	0.47	396.93	10.34	38.41	11.17	0.03	28.83	612.20	258.16	62.59	21.84	22529.19	11847.58	7.16	960.60	Hard	898.2
SR-42b	Lower Woodford	42.5	1	14.60	1.97	88.77	0.67	424	6.22	0.47	608.01	4.59	132.49	13.49	0.02	11.01	171.95	241.24	214.93	82.24	31221.93	19266.11	29.20	913.60	Soft	555.0
SR-30	Lower Woodford	30.0	5	15.30	1.30	92.32	1.76	432	6.12	0.62	603.40	11.50	52.45	8.50	0.01	4.24	66.60	2474.80	94.79	37.44	15697.68	17984.00	30.60	813.20	Soft	365.1
SR-28a	Lower Woodford	28.0	4	10.70	1.88	81.66	0.74	437	7.81	0.71	763.18	6.92	110.35	17.57	0.02	3.71	65.36	276.45	75.31	14.90	16869.98	25024.29	21.40	564.40	Soft	331.0
SR-14	Lower Woodford	14.0	1	13.00	1.73	65.47	1.76	428	5.17	0.54	503.62	13.54	37.20	13.31	0.03	4.30	67.05	375.33	122.59	17.96	20879.85	17700.96	26.00	587.20	Soft	230.8

Table 3.2. Samples selected for biomarker analysis. Total of forty-five samples representing the different ten K-means facies along with the Woodford Shale Speake Ranch vertical stratigraphic variability. Data selection by the integration of Rock-Eval pyrolysis data, X-ray fluorescence (XRF) major elements analysis, outcrop measured Gamma-ray log, and hardness measurements by Galvis (2017).

3.5. Proposed biomarkers as indicators of anoxic and oxic depositional environmental conditions between open marine and highly restricted enclosed fills.

As mentioned in Chapter I, Rodriguez and Philp (2010), Miceli-Romero and Philp (2012), Slatt and Rodriguez (2012), Torres-Parada (2013), Miceli-Romero (2014), Connock et al. (2017), Jones (2017), Miceli-Romero et al. (2018), and Liborius-Parada (2019), proposed that biomarker analyses could detect fluctuating oxic/anoxic conditions during the deposition of unconventional resource shales of different geological ages and depositional environments (Barnett, Woodford, Eagle Ford, and La Luna Shales).

This section presents the biomarker families that are correlated with the already established sequence stratigraphic framework for the SR in order to identify the relationships between the organic geochemistry trends and the SR stratigraphic sequences. For the characterization of enclosed mini-basin fill settings, these observations focused on the geochemical identification of anoxic and restricted conditions during the deposition for the Woodford Shale members. The biomarker compound families that are analyzed for 47 SR samples are the n-alkanes, steranes, monoaromatic steroids, diasteranes, pregnanes and homopregnanes, terpanes, tetracyclic polyprenoids (TPP), C_{40} aromatic carotenoid and aryl isoprenoids, polycyclic aromatic hydrocarbons (PAHs). An analysis of the biodegradation effect on the samples is mentioned at the end of this SR geochemical characterization.

3.5.1. n-Alkanes

The n-alkane distributions are commonly obtained for crude oils, and source rock extracts by gas chromatography of the saturate fractions and are a useful correlation tool and organic matter source indicator (Waples, 1985; Peters et al., 2005). The origin of such compounds stems primarily

from lipids in living organisms derived from lipids present in waxes of higher-order plants (Eglinton and Hamilton, 1967), or algae in the case of lower carbon chain homologs (Smith, 1968).

The gas chromatography fingerprints for the saturate fractions of the Woodford Shale SR samples (Figure 3.22) do not show significant presence of n-alkanes, indicating weathering and subsequent depletion and any analysis based on the n-alkanes can lead to misinterpretations. Weathering and n-alkane removal were observed in all the samples of the SR stratigraphic section, and Figure 3.22 shows representative chromatograms for extracts of the Woodford Shale members of the SR.

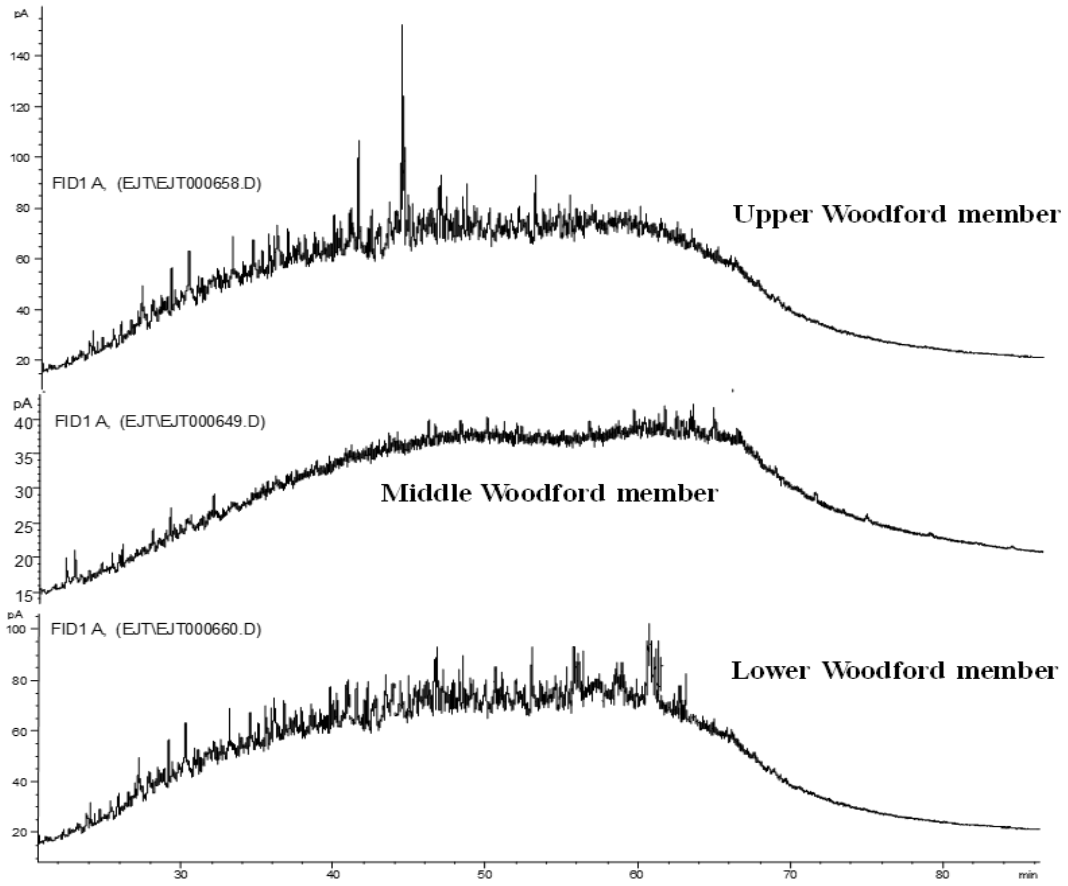

Figure 3.22. Gas chromatograms of saturate fractions from bitumen extracts of Speake Ranch Woodford Shale members. Note the severe biodegradation level evidenced by the humps and the removal of n-alkane and depletion of isoprenoids.

Due to the preferential removal of alkanes by intense biodegradation processes and constant surface water recharge in the outcrop, the isoprenoids were relatively more abundant than the n-alkanes in the more degraded samples. In this study, it was not possible to determine the pristane/phytane ratio consistently since the peaks in many samples were too low to identify the compounds or make any meaningful measurements in an accurate manner, but it is assumed that the ratio should fluctuate from 0.9 to 1.1 according to Jones (2017) who analyzed the less weathered Woodford section in the nearby Arbuckle Mountains structural trend.

3.5.2. Steranes

The sterane distributions for the Woodford Shale SR samples were determined through analysis of the saturate, and branched and cyclic (B&C), fractions by single ion monitoring gas chromatography-mass spectrometry (SIM/GCMS) using the m/z 217 ion (Figure 3.23 - 3.26). The resulting fragmentograms (Figure 3.24 and Figure 3.25) show the C_{27}, $C_{28,}$ and C_{29} regular steranes (peak identifications are presented in Table 3.3). This group of biomarkers is derived from sterols of eukaryotic organisms, principally algae, and higher plants (Blumer et al., 1971; Peters et al., 2005) but are rare or absent in prokaryotic organisms (Volkman, 1986). Huang and Meinschein (1979) used C_{27}, $C_{28,}$ and C_{29} sterol distributions and plotted them on a ternary diagram to define ecosystems. Moldowan et al. (1985) used this diagram to plot regular sterane distributions from crude oils and source rock extracts in order to assess depositional environments. Other authors (Dzou et al., 1995; Duan et al., 2006; Hodairi, 2012) have applied the same principle to determine organic matter source and for correlation studies.

The C_{27} steranes (cholestanes) are derived from sterols that are abundant in plankton and marine invertebrates. The C_{28} (ergostanes) are also derived from similar precursors, although they can also be generated from terrigenous organisms (Huang and Meinschein, 1979; Peters et al.,

2005). C_{29} Steranes (stigmastanes) originate from sterols present in terrigenous organic matter, but also marine algae (Volkman, 1986). Generally, oils generated from kerogens containing organic matter derived from marine phytoplankton display enhanced amounts of C_{27} relative to C_{29} steranes (Mackenzie et al., 1982; Waples and Machihara, 1991). The presence of C_{30} steranes (24-n-propylcholestanes) in oils and extracts is principally related to *pelagophyte* algae, which indicate a contribution from marine phytoplankton organic matter (Moldowan, 1984; Moldowan et al., 1990; Summons et al., 1992; Peters and Moldowan, 1993; Peters et al., 2005). From the ternary plot in Figure 3.23and the fragmentograms analyzed for the SR samples (Table 3.3; Figure 3.24 and Figure 3.25), it can be seen that C_{29} steranes are in relatively higher proportions (Figure 3.25; Table 3.3).

Sterane ratios (Moldowan et al., 1985) (3.6)

$\%C_{27} = C_{27}$ steranes / (C_{27} steranes + C_{28} steranes + C_{29} steranes) *100,

$\%C_{28} = C_{28}$ steranes / (C_{27} steranes + C_{28} steranes + C_{29} steranes) *100,

$\%C_{29} = C_{29}$ steranes / (C_{27} steranes + C_{28} steranes + C_{29} steranes) *100,

Where,

C_{27} steranes = [14α(H),17α(H) + 14β(H),17β(H)-Cholestane (20S+ 20R)]),

C_{28} steranes = 24-Methyl-[14α(H),17α(H) + 14β(H),17β(H)-Cholestane (20S+ 20R)]),

C_{29} steranes = 24-Ethyl-[14α(H),17α(H) + 14β(H),17β(H)-Cholestane (20S+ 20R)]).

According to Zumberge (1984), Grantham (1986), Volkman (1986), Grantham and Wakefield (1988), and Peters et al. (2005), this higher C_{29} sterane distribution in a source rock

extract indicates a contribution of terrestrial organic matter input. Caution must be considered when interpreting a land-plant source from C_{29} steranes alone, as there are recognized instances of C_{29} predominance in Precambrian rocks, which has been attributed to algae because land plants had not fully evolved yet (Grantham, 1986; Volkman et al., 1986). The relative proportion of the C_{27}, C_{28} and C_{29} regular steranes was plotted on a ternary diagram (Figure 3.23) to determine possible variations in the SR Woodford Shale members after analyzing the fragmentograms summarized in Figure 3.25. The C_{29} steranes are in relative higher abundance to the C_{27} steranes, directly comparing each type of isomers (e.g., C_{29} ααα**R** in a relative higher peak height and peak area than the C_{27} ααα**R**; C_{29} ααα**S** in a relative higher peak height and peak area than the C_{27} ααα**S**), for the Lower and Middle members, but for the samples of the Upper Woodford member that are suspected with migrated hydrocarbons (samples 2.71.5 and 287.5 ft in Figure 3.25) the C_{27} steranes predominate over the C_{29} steranes.

According to the regular sterane ternary diagram developed by Moldowan et al. (1985), most of SR samples are clustered in a restricted area of the plot, where the marine shale and marine carbonate in origin yields overlap, but with the integration with other biomarker parameters and recognized lithofacies, the samples are interpreted as marine shale source rocks with contributions of terrestrial organic matter. This interpretation of the organic matter principally of marine origin in the SR is also in agreement with the conclusions in the Woodford Shale of Comer and Hinch (1987), Kirkland et al. (1992), Lo and Cardott (1995), Miceli-Romero and Philp (2012), Connock et al. (2018), and Philp and DeGarmo (2020).

Seifert and Moldowan (1986) proposed that geochemical ratios of C_{29} steranes isomers provide a useful tool for identifying the thermal maturity variations. Peters et al. (2005) support these ideas when identifying that the steroid precursors in nature have only an R configuration at

C-20, that with increasing maturation are progressively converted to mixtures of R (biological) and S (thermal). For the C_{29} 20S/(20S+20R) sterane ratio, this increases with thermal maturity from 0 reaching equilibrium at 0.52 to 0.55 (Seifert and Moldowan, 1986; Peters et al., 2005). Peters et al. (2005) also proposed that the C_{29} ββ/(ββ+αα) steranes ratio is not influenced by organic matter source, and its mixture is reached at higher maturity levels compared to the C_{29} 20S/(20S+20R) steranes. With increasing thermal maturation isomerization at C-14 and C-17 in the C_{29} 20S and 20R regular steranes increases the ββ/(ββ+αα) ratio from near-zero values to about 0.7 (Miceli-Romero and Philp, 2012; Miceli-Romero et al. 2018). For the SR, there are differences in maturity levels based on the C_{29} 20S/(20S+20R) vs. C_{29} ββ/(ββ+αα) steranes ratio (Figure 3.25). This maturity assessment suggests a higher maturity level in the Upper and some uppermost Middle Woodford member samples, which correspond to the samples with suspected migrated hydrocarbons (Figure 3.25). Peters et al. (2005) suggested that the organic facies changes, weathering, and biodegradation may affect this maturity parameter. For this reason, it is interpreted that the lower maturity in the basal part of the SR stratigraphy, the Lower member, can be due to a more mature Woodford oil is charging the upper part of the Middle member and the Upper Woodford member (Figure 3.25 and Figure 3.26). Figure 3.25 shows the steranes ααα R vs. ααα S isomer predominance (C_{27}, C_{28}, C_{29} steranes). These isomer thermal maturity differences are not expected because the outcrop suffered the same burial and uplifting events, therefore, all the rock intervals should have been exposed to similar thermal regimes. Samples in both the Lower and Middle Woodford members present a general trend of higher C_{27} and C_{29} ααα R isomer predominance over the ααα S (Figure 3.26), indicating low thermal maturity as expected from the vitrinite reflectance values of 0.58 Ro% reported by Galvis et al. (2017a).

Peak #	Compound
1	Diapregnane
2	14β(H),17β(H)-Pregnane
3	Diahomopregnane
4	14β(H),17β(H)-Homopregnane
5	13β(H),17α(H)-Diacholestane (20S)
6	13β(H),17α(H)-Diacholestane (20R)
7	13α(H),17β(H)-Diacholestane (20S)
8	13α(H),17β(H)-Diacholestane (20R)
9	24-Methyl-13β(H),17α(H)-Diacholestane (20S)
10	24-Methyl-13β(H),17α(H)-Diacholestane (20R)
11	24-Methyl-13α(H),17β(H)-Diacholestane (20S) + 14α(H),17α(H)-Cholestane (20S)
12	24-Ethyl-13β(H),17α(H)-Diacholestane (20S) + 14β(H),17β(H)-Cholestane (20R)
13	14β(H),17β(H)-Cholestane (20S) + 24-Methyl-13α(H),17β(H)-Diacholestane (20R)
14	14α(H),17α(H)-Cholestane (20R)
15	24-Ethyl-13β(H),17α(H)-Diacholestane (20R)
16	24-Ethyl-13α(H),17β(H)-Diacholestane (20S)
17	24-Methyl-14α(H),17α(H)-Cholestane (20S)
18	24-Methyl-14β(H),17β(H)-Cholestane (20R) + 24-Ethyl-13α(H),17β(H)-Diacholestane (20R)
19	24-Methyl-14β(H),17β(H)-Cholestane (20S)
20	24-Methyl-14α(H),17α(H)-Cholestane (20R)
21	24-Ethyl-14α(H),17α(H)-Cholestane (20S)
22	24-Ethyl-14β(H),17β(H)-Cholestane (20R)
23	24-Ethyl-14β(H),17β(H)-Cholestane (20S)
24	24-Ethyl-14α(H),17α(H)-Cholestane (20R)
25	24-Propyl-14α(H),17α(H)-Cholestane (20S)
26	24-Propyl-14β(H),17β(H)-Cholestane (20R)
27	24-Propyl-14β(H),17β(H)-Cholestane (20S)
28	24-Propyl-14α(H),17α(H)-Cholestane (20R)

Table 3.3. Identification of steranes in the m/z 217.3 fragmentogram. Compound nomenclature from Peters et al. (2005), and Miceli-Romero et al. (2018). Names refer to peaks identified in Figure 3.24 and Figure 3.25.

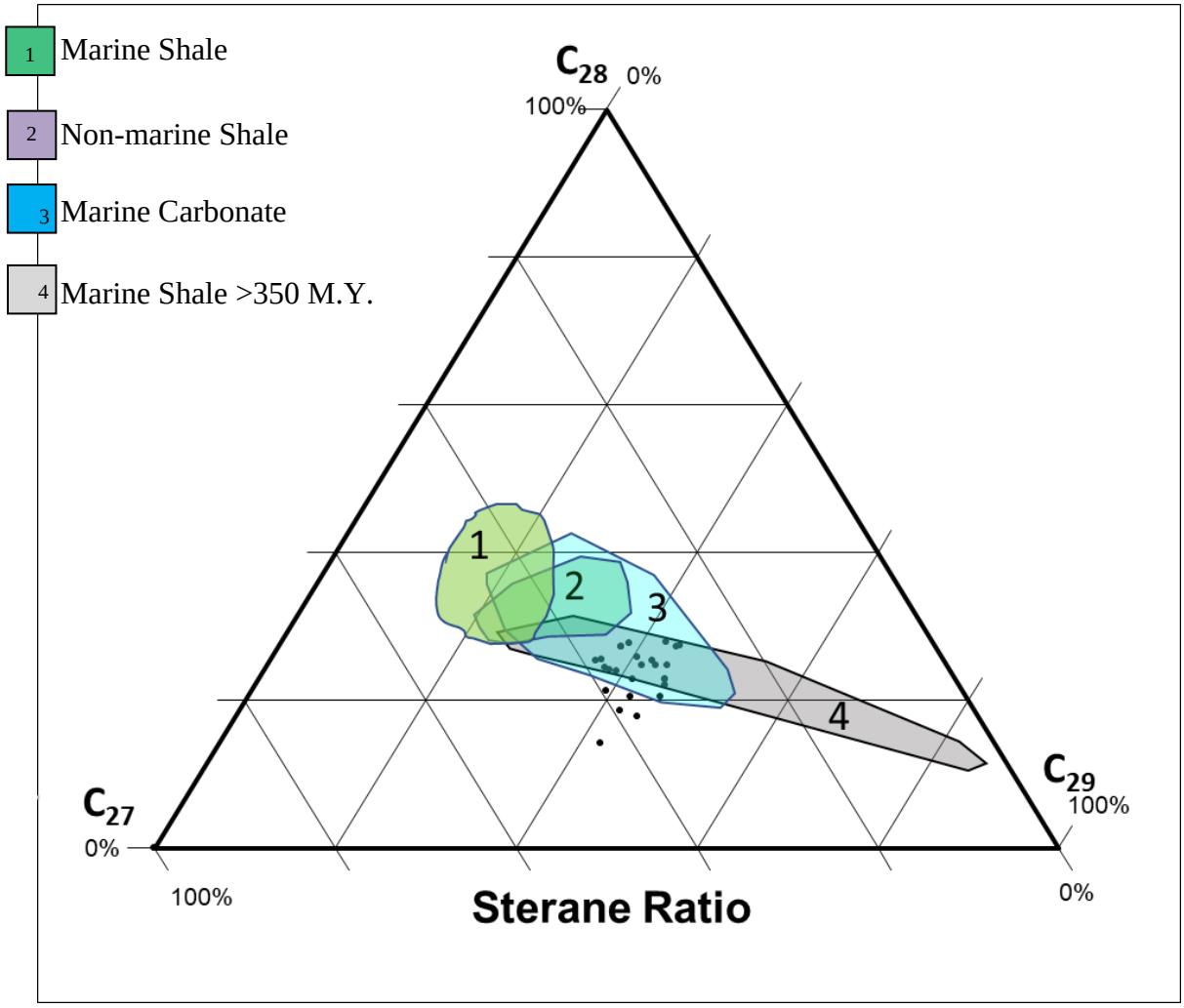

Figure 3.23. Ternary plot showing the relative proportions of the C_{27}:C_{28}: C_{29} steranes compared to distributions originally proposed by Moldowan (1985) for source rocks of varying ages.

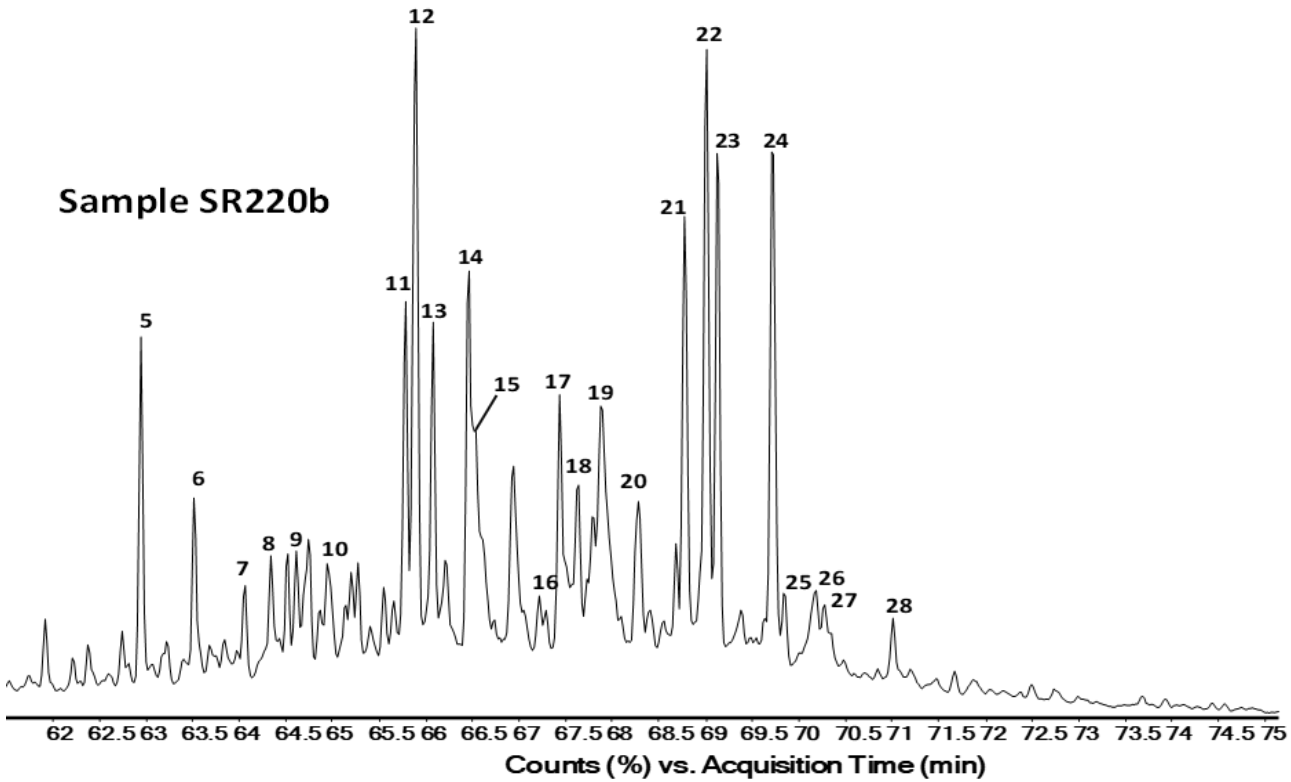

Figure 3.24. GC-MS m/z 217.3 fragmentogram identifying C_{27}-C_{30} steranes and diasteranes in a Middle-Upper Woodford boundary sample. Peak identities in Table 3.3.

a

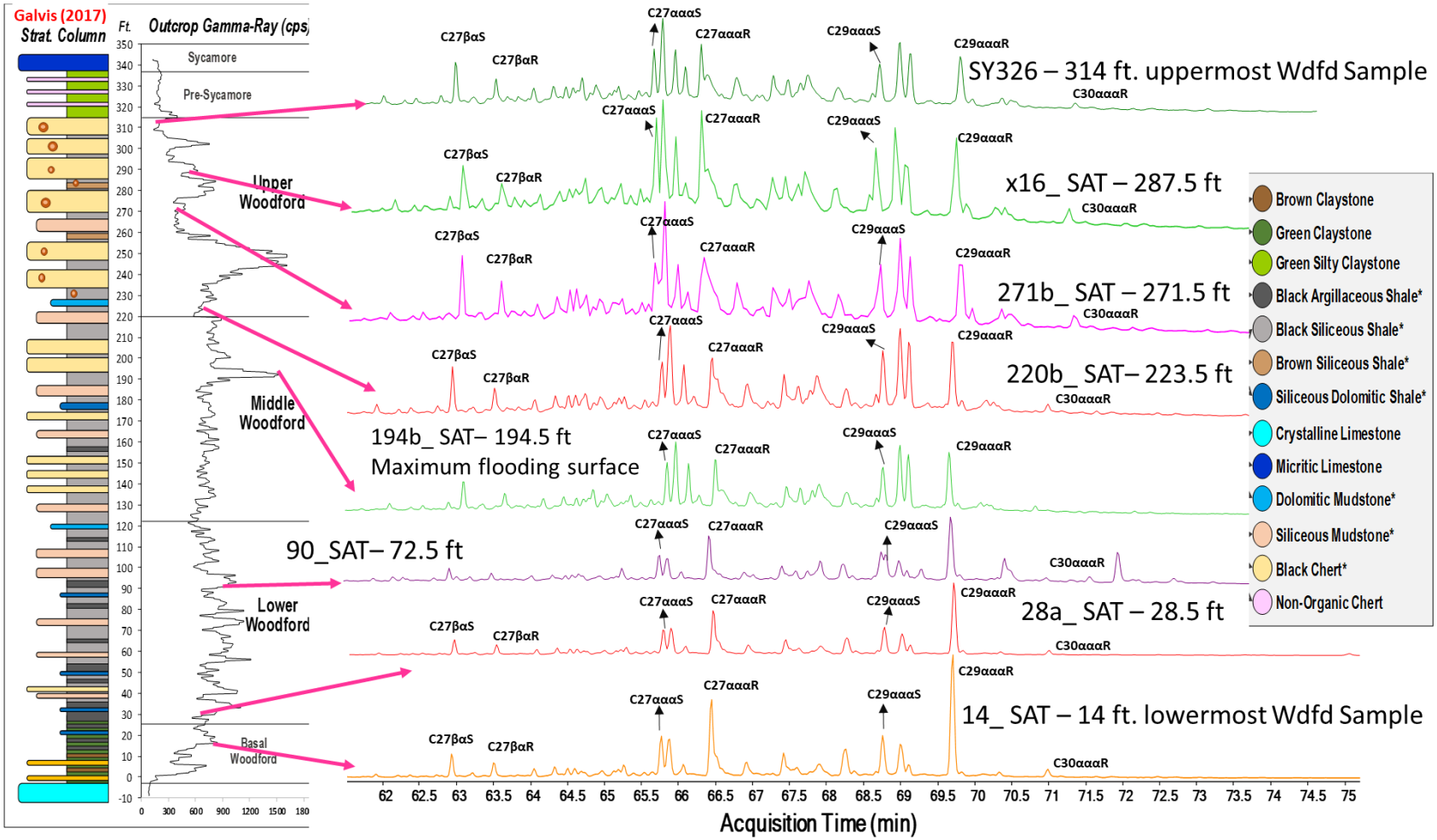

Figure 3.25. M/z 217.3 showing the steranes variations in the vertical stratigraphic section of the Woodford Shale. Peak identification in Table 3.3.

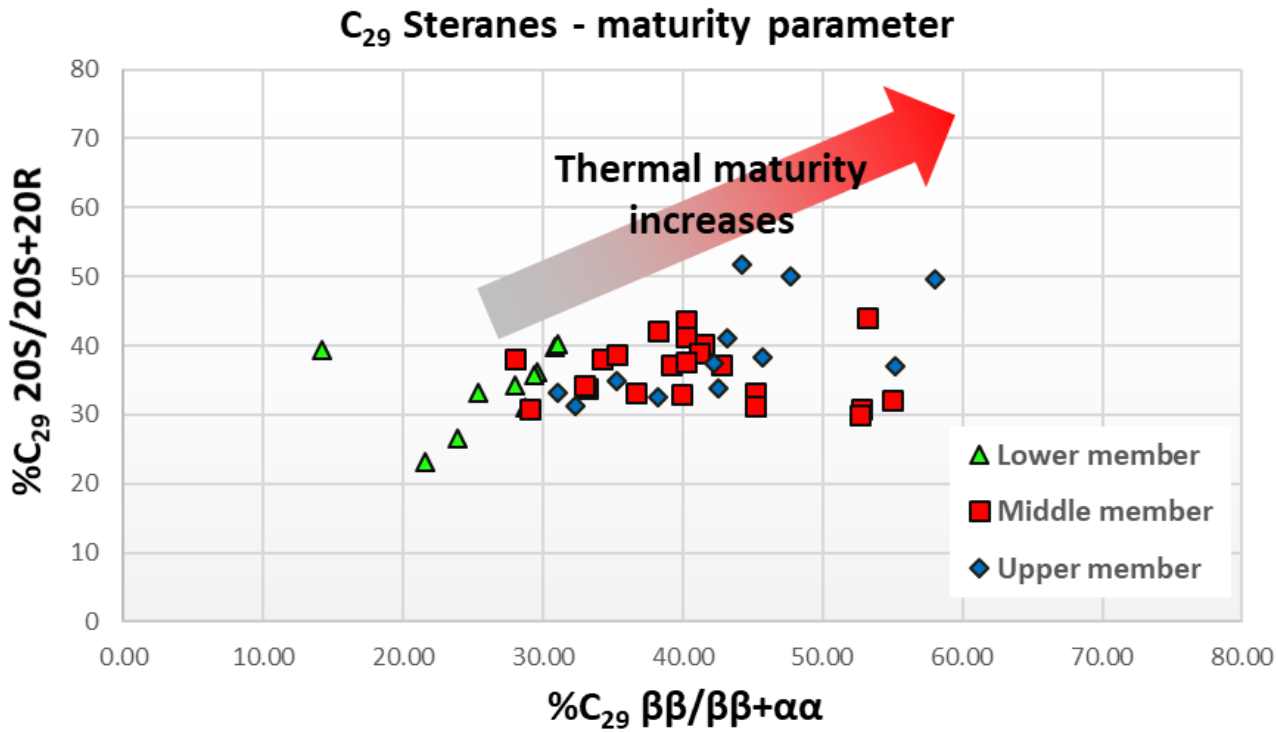

Figure 3.26. Plot of C_{29} ββ/(ββ+αα) steranes versus C_{29} 20S/(20S+20R) steranes showing variations in thermal maturity for Woodford Shale SR members. Plot modified from Peters, 1999). Lower maturity in the Lower member caused for probable re-working the organic matter. Higher maturity levels in the Upper and Middle Woodford member samples correspond to the samples with suspected migrated hydrocarbons.

3.5.3. Monoaromatic steroids (MAS)

The C_{27}, C_{28}, and C_{29} monoaromatic steroids (MAS) can also be used to provide a characterization of the variations in the sources of these compounds (Moldowan et al., 1985; Riolo et al. 1985; Miceli-Romero and Philp, 2012; Miceli-Romero et al. 2018; Liborius-Parada, 2019). Moldowan et al. (1985) also reported that oils and bitumens derived from marine organic matter contain higher amounts of C_{28} MAS than those of nonmarine origin, and some oils derived from marine carbonate source rocks contain higher amounts of C_{29} MAS than oils derived from marine shales. The MAS presence in the SR was determined in the B&C fraction through GCMS/SIM by analysis of the m/z 253.3 ion (Figure 3.27; Table 3.4). All the samples analyzed have a higher concentration of C_{28} MAS, followed by C_{27} and C_{29} MAS, indicating a relatively homogeneous marine source rock facies (Figure 3.27; Table 3.4). Moldowan and Fago (1985) reported the maturation effects on the preservation of the MAS, but in the SR outcrop, the thermal maturity is very low, so any changes observed here will not be related to maturity changes but related to changes in sources and changes in the depositional environment. Lin et al. (1989) and Philp et al. (1989) reported for the southern Oklahoma shallow reservoirs and outcrops the preservation of MAS after identifying severe biodegradation processes in their bitumen samples. For this reason, the higher C_{28} MAS concentrations are reliable indicators of major marine depositional settings for all the SR samples.

Peak number	Compounds name
1	C_{21} Pregnane
2	C_{22} 20-Methylpregnane
3	5β-Cholestane 20S
4	Diacholestane 20S
5	5β-Cholestane 20R + Diacholestane 20R
6	5β-Ergostane 20S + Diaergostane 20S
7	5α-Cholestane 20R
8	5α-Ergostane 20S
9	5β-Ergostane 20R + Diaergostane 20R
10	5β-Stigmastane 20S + Diastigmastane 20S
11	5α-Stigmastane 20S
12	5α-Ergostane 20R
13	5β-Stigmastane 20R + Diastigmastane 20R
14	5α-Stigmastane 20R

Table 3.4. Identification of monoaromatic steroids (MAS) in the m/z 253.3. Compound nomenclature from Peters et al. (2005), and Miceli-Romero et al. (2018).

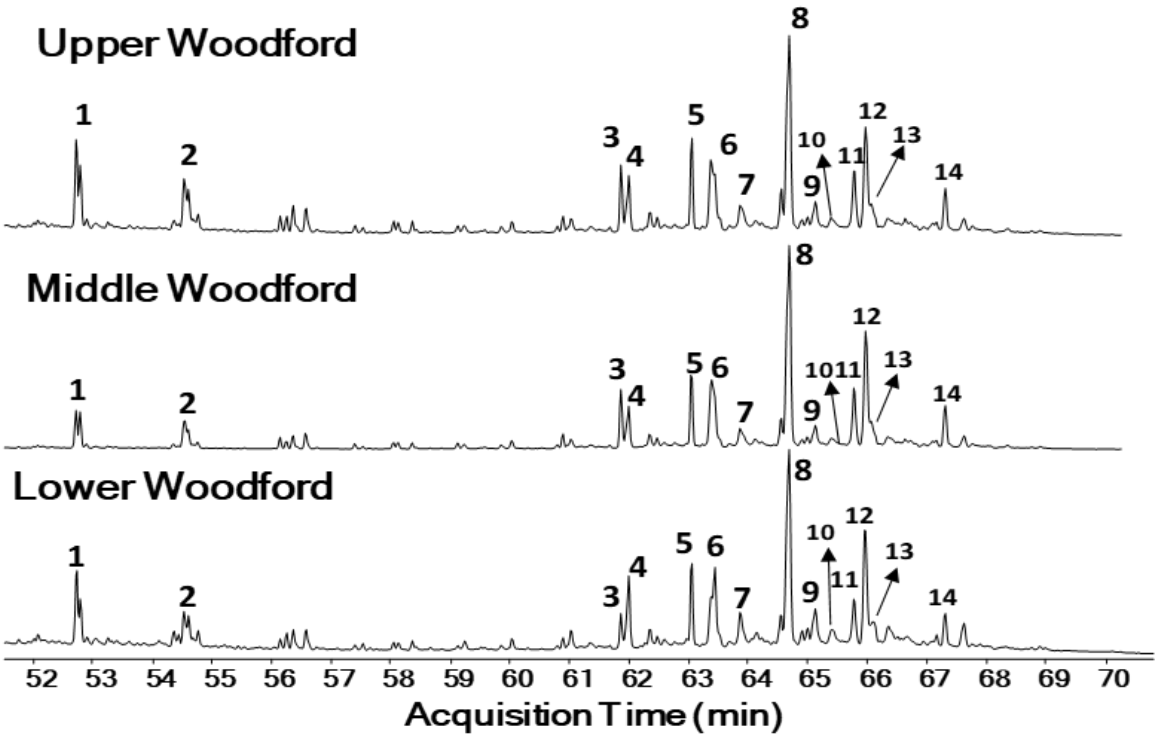

Figure 3.27. Fragmentograms of the m/z 253.3 ion showing distribution of the monoaromatic steroids (MAS) in the branched and cyclic (B&C) fractions of the Speake Ranch samples. Peak identification is presented in Table 3.4.

3.5.4. Diasteranes

The diasterane/sterane ratios are commonly used to discriminate carbonate from clay-rich source rocks, where low diasterane/sterane ratios indicate anoxic clay-poor or carbonate source rocks (Clark and Philp, 1989), and high ratios are usually a feature of source rocks containing abundant clays (Mello et al., 1988). During diagenesis, acidic sites on clays catalyze the conversion of steranes to diasteranes (Grantham, 1986; Grantham and Wakefield, 1988). It is also proposed that the proportion of diasteranes compared with regular steranes is known to be dependent upon maturity as well because the original steranes are converted gradually to mixtures of diasteranes and steranes (Hughes et al., 1985; Goodarzi et al., 1989). Seifert and Moldowan (1986) also suggested that high proportions of diasteranes compared with regular steranes in oils are consistent with substantial biodegradation, resulting in the elimination of steranes relative to diasteranes.

3.5.5. Pregnanes and Homopregnanes

The precursors of pregnanes ($C_{21}H_{36}$) and homopregnanes ($C_{22}H_{38}$) are pregnol and homopregnol, which exist in protozoans (Yang, 1991; Wang, 1993; Wang et al., 2015). Wang (1993) analyzed extracts from the Springer formation in the Anadarko basin, Oklahoma, and found that pregnanes were more resistant to weathering compared to regular steranes and diasteranes. ten Haven et al. (1985 and 1988), and Jiamo et al. (1988) encountered them in higher concentration in rock samples from to hypersaline environments, but they can also be a result of the thermal cracking of C_{27}-C_{29} steranes (Mueller et al., 1995; Wang et al., 2015; Miceli-Romero et al., 2018). According to Peters et al. (2005) and Wang et al. (2015), the pregnanes and homopregnanes being resistant to biodegradation can be associated with a change of the redox conditions, lithofacies, and mineral contents in the source rocks when compared with regular steranes and diasteranes. These compounds were identified for all samples and in a relatively lower abundance in the Upper Woodford member. This recognition allowed to estimate intervals of higher salinity relatively with other intervals by the pregnanes/(pregnanes+steranes+diasteranes) ratio (Wang et al., 2015; Liborius-Parada, 2019). For the case of a sample with a high concentration of diasteranes and a lower concentration of pregnanes, this can be associated with oxic conditions, terrigenous input, and high clay content (ten-Haven et al., 1985; Wang et al., 2015; Liborius-Parada, 2019). For the cases of low diasteranes and high pregnanes concentration, high salinity in the oceanic waters of the depositional environment and clastic-starved, non-terrigenous, sulfur-rich conditions are likely to occur (ten-Haven et al., 1985; Wang et al., 2015; Liborius-Parada, 2019). In the low maturity SR samples, these conditions of low diasteranes and high pregnanes are interpreted as higher salinity in the paleo Woodford oceanic water.

3.5.6. Terpanes

Hopanes are pentacyclic triterpanes whose precursors are derived from bacterial membrane lipids (bacteria and cyanobacteria; Ourisson et al., 1982; Peters et al., 2005). In the SR Woodford samples, the hopanes distributions were analyzed by SIM/GCMS using mainly the m/z 191 ion (Figure 3.28 and Figure 3.29). Peak identifications are given in Table 3.5, and biomarker ratios based on the tricyclic terpanes and hopanes are presented in Table 3.6. The ratios of tricyclic terpanes vs. hopanes are a petroleum industry-standard tool to predict the source rock characteristics and to evaluate the extent of thermal maturity and biodegradation in oils and source rocks (Seifert and Moldowan, 1980; Zumberge, 1984; Peters and Moldowan, 1993; Wenger et al., 2002).

The widespread occurrences of tricyclic terpanes are believed to result from precursors produced by algae (Seifert and Moldowan, 1980; Philp and Gilbert, 1986; Philp et al., 1992) and are typically absent, or occur in small amounts, in oils from terrigenous source materials (Robinson, 1987; Peters et al., 2005). Philp et al. (1992) pointed out that tricyclic terpanes have also been reported in saline lacustrine oils from China and suggested a salinity-controlled occurrence of these compounds. The tricyclic terpanes are generally more abundant in highly mature oils and/or source rocks because they are thermally more stable than other terpanes (Peters and Moldowan, 1993), and thus the ratio of tricyclic terpanes to 17α-hopanes will rise with increasing maturity (Waples and Machihara, 1990). The high abundance of extended tricyclic terpanes relative to hopanes in oils and/or source rocks may also be related to maturity effects and is also probably due to marine-influenced depositional conditions (Seifert and Moldowan, 1980; Philp et al., 1992).

Peak #	Compound
1	**C_{20}** Tricyclic terpane
2	**C_{21}** Tricyclic terpane
3	**C_{22}** Tricyclic terpane
4	**C_{23}** Tricyclic terpane
5	**C_{24}** Tricyclic terpane
6	**C_{25}** Tricyclic terpanes (22S and 22R)
7	**C_{24}** Tetracyclic terpane
8	**C_{26}** Tricyclic terpanes (22S and 22R)
9	**C_{28}** Tricyclic terpanes (22S and 22R)
10	**C_{29}** Tricyclic terpanes (22S and 22R)
11	**C_{27}** 18α(H)-22,29,30-Trisnorneohopane (Ts)
12	**C_{27}** 17α(H)-22,29,30-Trisnorhopane (Tm)
13	**C_{29}** 17α(H),21β(H)-30-Norhopane
14	**C_{29}Ts** 18α(H)-30-Norneohopane
15	**C_{30}D** 15α-methyl-17α(H)-27-Norhopane (Diahopane)
16	**C_{29}** 17β(H),21α(H)-30-Normoretane
17	**C_{30}** 17α(H),21β(H)-Hopane
18	**C_{30}** 17β(H),21α(H)-Moretane
19	**C_{31}** 17α(H),21β(H)-Homohopanes (22S and 22R)
20	**C_{32}** 17α(H),21β(H)-Bishomohopane (22S and 22R)
21	**C_{33}** 17α(H),21β(H)-Trishomohopane (22S and 22R)
22	**C_{34}** 17α(H),21β(H)-Tetrakishomohopane (22S and 22R)
23	**C_{35}** 17α(H),21β(H)-Pentakishomohopane (22S and 22R)
G	Gammacerane

Table 3.5. Identity of terpanes in the m/z 191 fragmentograms. Compound nomenclature from Peters et al. (2005), and Miceli-Romero et al. (2018).

Sample ID	Outcrop Depth	Kmeans Facies	%TOC	C26TT/C 25TT	C31R/ C30HH	G/ (G+C30HH)	Ts/ Ts+Tm	regular steranes/17α-hopanes	C35S/C34S	C27%	C28%	C29%	DIAST IND	STERANE IND	C30TPP/ C30Steranes	TPP RATIO	%C29 20S/ [20S+20R)	%C29(ββ/ ββ+αα)
SR-Y326	314.0	1	9.04	0.50	0.09	0.03	0.30	0.11	0.11	36.84	24.03	39.13	0.29	0.09	0.47		33.92	42.50
SR-X16b	296.5	6	30.20	1.16	0.33	0.11	0.33	0.09	0.37	32.14	24.72	43.13	0.25	0.17	0.09		50.01	47.67
SR-X7b	287.5	1	12.10	0.44	0.30	0.13	0.30	0.14	0.98	37.51	24.17	38.31	0.26	0.11	0.40	0.11	37.05	55.14
SR-271b	271.5	6	21.00	1.62	0.34	0.17	0.36	0.25	0.88	28.64	27.26	44.10	0.25	0.13	0.11	0.002	49.65	58.01
SR-243a	243.0	0	4.50	0.46	0.28	0.11	0.34	0.10	0.23	37.97	24.41	37.62	0.20	0.19	0.31		51.73	44.19
SR-230b	230.5	1	11.10	0.61	0.29	0.09	0.29	0.45	0.43	39.42	23.25	37.33	0.21	0.17	0.29		31.21	32.33
SR-229a	229.0	0	9.74	0.56	0.39	0.17	0.26	0.78	0.52	32.23	25.30	42.47	0.25	0.14	0.29		34.89	35.23
SR-227b	227.5	1	11.20	0.48	0.40	0.12	0.22	0.65	0.65	36.81	24.86	38.33	0.25	0.12	0.25		33.22	31.01
SR-226b	226.5	1	11.50	0.49	0.42	0.10	0.18	0.55	0.30	36.83	23.96	39.21	0.26	0.13	0.24		32.45	38.24
SR-224b	224.5	1	12.00	0.40	0.36	0.10	0.20	0.52	0.32	36.00	23.46	40.55	0.28	0.11	0.32		41.02	43.22
SR-223a	223.0	7	1.00	0.34	0.05	0.09	0.13	0.10	0.20	38.45	25.41	36.14	0.31	0.10	0.21		38.39	45.75
SR-221b	221.5	1	10.80	0.39	0.35	0.14	0.19	0.11	0.41	34.98	25.84	39.17	0.28	0.10	0.52		37.45	42.22
SR-220b	220.5	1	11.80	0.36	0.44	0.16	0.25	0.13	0.78	32.05	22.88	45.06	0.24	0.11	0.63	0.182	42.02	53.14
SR-220a	220.0	0	2.82	0.54	0.41	0.14	0.24	0.27	0.99	30.86	24.78	44.37	0.25	0.12	0.48		43.95	52.77
SR-219a	219.0	0	3.16	0.59	0.37	0.19	0.24	0.07	0.80	33.61	25.83	40.56	0.24	0.16	0.09		30.76	52.64
SR-217b	217.5	4	10.20	0.74	0.38	0.20	0.18	0.14	0.60	37.13	20.46	42.41	0.26	0.15	0.05		30.08	54.95
SR-211b	211.5	1	12.30	0.76	0.32	0.19	0.17	0.25	0.49	37.02	21.84	41.13	0.25	0.09	0.12		32.11	34.23
SR-210b	210.5	1	12.10	0.69	0.33	0.21	0.20	0.35	0.42	37.11	21.03	41.86	0.25	0.11	0.21		38.14	33.12
SR-209a	209.0	0	6.46	0.54	0.30	0.22	0.17	0.45	0.52	38.26	19.75	41.99	0.24	0.11	0.25		33.88	39.12
SR-208b	208.5	1	15.50	0.52	0.36	0.21	0.19	0.33	0.49	35.65	22.84	41.51	0.24	0.12	0.31		37.25	45.14
SR-206a	206.0	0	4.36	0.50	0.30	0.20	0.24	0.52	0.59	37.94	21.32	40.74	0.23	0.14	0.29		33.12	45.22
SR-205a	205.0	0	2.79	0.31	0.29	0.19	0.28	0.55	0.62	35.44	20.10	44.46	0.21	0.16	0.24		31.25	39.87
SR-195b	195.5	1	9.13	0.30	0.34	0.26	0.33	0.76	0.70	35.99	19.22	44.79	0.21	0.15	0.29		32.96	40.25
SR-194b	194.5	1	11.30	0.29	0.48	0.19	0.25	0.96	0.74	32.52	22.00	45.48	0.23	0.18	0.38	0.101	43.68	41.50
SR-193b	193.5	4	9.22	0.26	0.35	0.25	0.32	0.94	0.76	31.04	29.33	39.63	0.21	0.20	0.35		40.12	42.77
SR-191a	191.0	0	5.19	0.12	0.21	0.18	0.33	1.12	0.80	32.14	28.74	39.12	0.22	0.21	0.31		37.33	40.23
SR-190b	190.5	4	12.00	0.33	0.19	0.29	0.20	0.84	0.83	31.02	24.53	44.45	0.25	0.23	0.29		41.35	38.25
SR-185b	185.5	3	7.04	0.36	0.12	0.21	0.24	0.63	0.85	38.11	22.13	39.76	0.24	0.26	0.30		42.24	41.14
SR-182b	182.5	1	8.65	0.43	0.28	0.21	0.25	0.57	0.98	39.36	21.26	39.38	0.22	0.11	0.28	0.095	39.01	40.22
SR-170b	170.5	0	1.95	0.34	0.30	0.11	0.28	0.31	0.92	43.53	14.23	42.24	0.25	0.20	0.38		37.57	36.66
SR-159b	159.5	4	8.71	0.38	0.29	0.09	0.25	0.38	0.95	34.72	27.31	37.96	0.30	0.13	0.44		33.25	35.31
SR-152b	152.5	3	8.33	0.30	0.39	0.12	0.11	0.44	0.99	37.72	25.52	36.76	0.24	0.06	0.34		38.63	32.96
SR-142b	142.5	5	8.42	0.37	0.26	0.09	0.19	0.41	0.74	37.70	17.84	44.46	0.20	0.15	0.27		34.24	29.01
SR-134b	134.5	4	8.97	0.41	0.24	0.11	0.23	0.49	0.99	34.72	27.31	37.96	0.20	0.13	0.74	0.553	30.75	27.99
SR-129a	129.0	7	2.49	0.40	0.09	0.16	0.24	0.49	0.77	33.75	20.48	45.77	0.22	0.26	0.34	0.164	38.01	26.59
SR-120b	120.5	1	3.79	0.48	0.13	0.11	0.22	0.52	0.68	32.15	21.50	46.35	0.13	0.23	0.13		39.87	30.83
SR-118c	118.8	9	4.15	0.55	0.29	0.09	0.11	0.62	0.67	28.07	27.48	44.45	0.21	0.20	0.15		40.11	31.02
SR-110b	110.5	4	7.00	0.54	0.27	0.10	0.22	0.43	0.74	28.96	26.11	44.93	0.17	0.18	0.14		34.24	27.99
SR-90	90.0	4	8.28	0.57	0.30	0.19	0.10	0.53	0.76	29.44	27.90	42.66	0.19	0.17	0.18		39.41	14.20
SR-72b	72.5	1	14.40	0.45	0.25	0.20	0.21	0.82	0.85	28.35	29.53	42.12	0.12	0.16	0.14		36.24	29.54
SR-60a	60.0	0	3.58	0.52	0.15	0.11	0.09	0.82	0.74	34.53	27.55	37.92	0.18	0.13	0.12		33.12	25.32
SR-42b	42.5	1	14.60	0.69	0.28	0.20	0.15	0.77	0.92	33.54	27.80	38.67	0.20	0.11	0.12		35.81	29.34
SR-30	30.0	5	15.30	0.45	0.45	0.25	0.18	1.33	0.87	27.90	25.36	46.74	0.20	0.13	0.11		31.08	28.78
SR-28a	28.0	4	10.70	0.56	0.34	0.16	0.13	0.56	0.82	32.05	22.88	45.06	0.24	0.11	0.09	0.004	26.60	23.85
SR-14	14.0	1	13.00	0.61	0.33	0.13	0.15	0.23	0.64	39.27	18.53	42.19	0.23	0.10	0.08	0.003	23.08	21.59

Table 3.6. Steranes, terpanes, and hopanes ratios in the Speake Ranch Woodford 314 ft stratigraphic section with the respective K-means facies and %TOC. Kmeans Facies = unsupervised cluster analysis that generated statistical facies. C26TT/C25TT= C_{26}/C_{25} tricyclic terpanes ratio; $C_{31}R/C_{30}HH$= $C_{31}R/C_{30}$ hopane ratio; G/G+$C_{30}HH$= gammacerane index; Ts/Ts+Tm= Ts vs Tm ratio; C35HH/C34HH = C35S/C34 hopanes ratio; regular steranes/17α-hopanes = regular steranes/hopanes; C_{27}%= %C_{27} steranes; C_{28}%= %C_{28} steranes; C_{29}% = %C_{29} steranes; DIAST IND = diasteranes index; STERANE IND = steranes index.

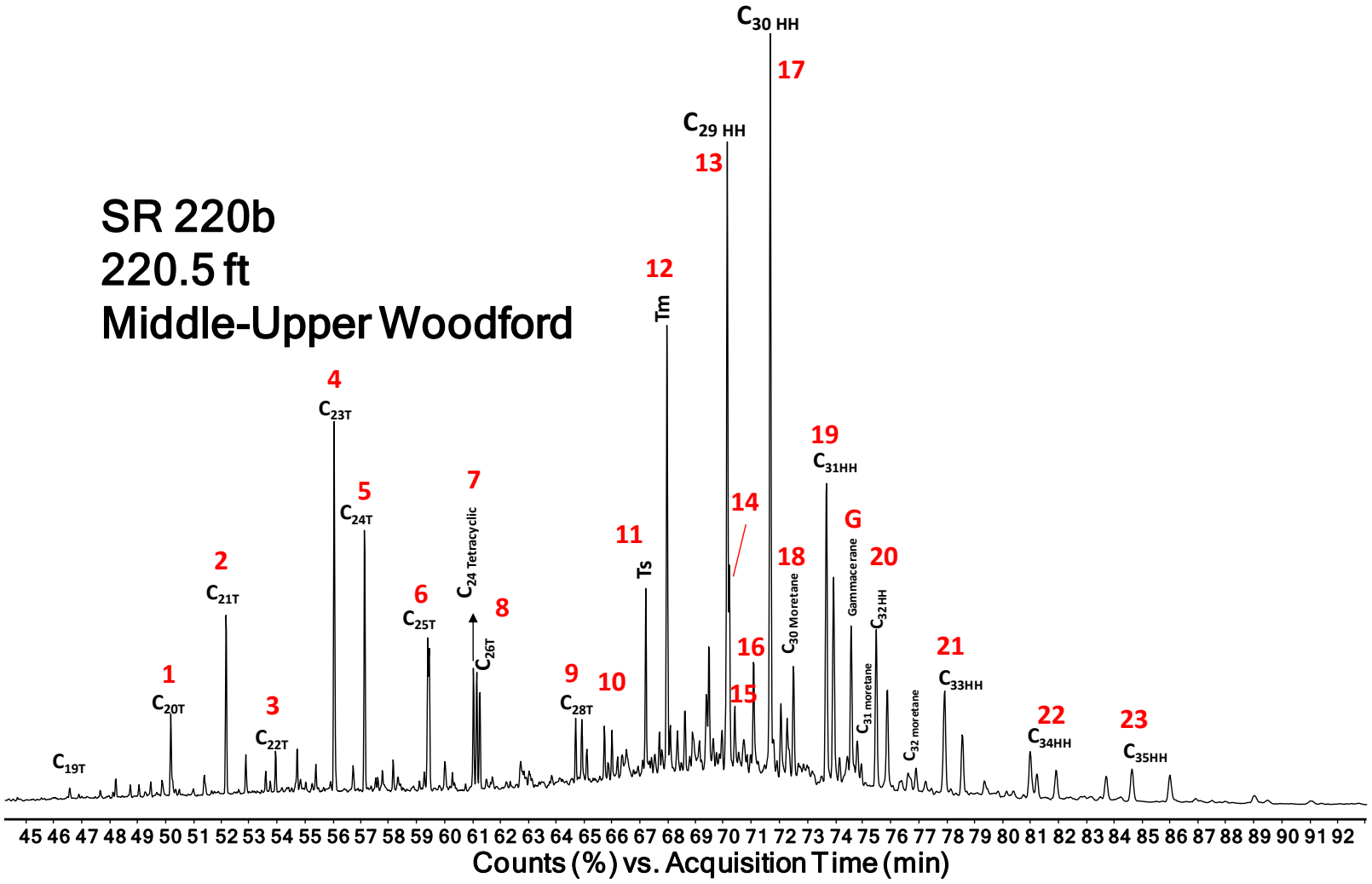

Figure 3.28. Tricyclic terpanes and hopanes identification using m/z 191.3 plot of sample 220b, Middle-Upper Woodford 220.5 ft boundary. Peaks nomenclature in Table 3.5.

For the SR, the regular steranes/17α-hopanes ratio is, on average, 0.48. This ratio is frequently used to evaluate eukaryote (plankton and/or benthic algae) versus prokaryote (bacteria) organic matter input in sediments (Peters et al., 2005). High values of this ratio are indicative of marine depositional environments, whereas low, near-zero values are associated with terrigenous and/or reworked organic matter (Peters et al., 2005). For the Lower Woodford member, the values range from 0.46 to 1.33 (Table 3.6), indicating that the rates vary from organic matter in marine deposits with high values of the ratio, to a more prokaryotic input in the depositional conditions of samples with low values of the ratio (Miceli-Romero and Philp, 2012). For the Middle member, the ratio ranges from 0.31 to 1.13, with a similar interpretation of marine deposits with higher values located at the maximum flooding surface (MFS located at 194.5 ft in Figure 3.29 and Figure 3.30) and decreasing upwards with more transitional deposits manifested by the low values for the ratio in the Upper Woodford member. For the Upper member, the regular steranes/17α-hopanes ratio ranges from 0.09 to 0.78 (Table 3.6), indicating a more terrigenous and/or reworked organic matter deposited in silica-rich and chertier rock matrix (from identified lithofacies).

Hopanes are derived primarily from hopanoid compounds present in the cell membranes of prokaryotes bacteria and cyanobacteria (Ourisson et al., 1982). The C_{29} 17α(H)-norhopane (30-Norhopane) and C_{30} 17α(H)-hopanes are the predominant triterpanes commonly found as major peaks in the m/z 191 (Waples and Machihara, 1991; Peters et al., 2005). The C_{29}/C_{30} hopane ratio is commonly used to distinguish carbonate from clastic lithology (Palacas et al., 1984; Peters and Moldowan, 1993). Oils sourced from organic-rich carbonates and evaporites are generally characterized by high values (>1) for the C_{29}/C_{30} hopane ratio while low values of C_{29}/C_{30} hopane ratios are characteristic of siliceous shale deposits (Zumberge, 1984; Price et al., 1987; Clark and

Philp, 1989; Figure 3.29 and Figure 3.30). For all the SR outcrop samples, the C_{29}/C_{30} hopane ratio ranged from 0.7 to 1 (Table 3.6).

Tricyclic terpanes (cheilanthanes) are thought to be derived from algae and bacterial precursors (Seifert and Moldowan, 1980; Aquino Neto et al., 1982; Ourisson et al., 1982; Peters et al., 2005). Volkman et al. (1989) found significant amounts of tricyclic terpanes in bitumen from rocks containing *Tasmanites*, suggesting an origin from these organisms. Philp and Gilbert (1986) determined that tricyclic terpanes are abundant in marine oils. The C_{22}/C_{21} and the C_{24}/C_{23} tricyclic terpane ratios assist in the identification of oils derived from carbonate rocks (Philp and Gilbert, 1986; Peters et al., 2005; Miceli-Romero et al., 2018). Extracts and oils derived from these source rocks typically show high C_{22}/C_{21} (>0.50) and low C_{24}/C_{23} (< 0.50) tricyclic terpanes ratios, while marine source rocks show low C_{22}/C_{21} (0.20-0.50) and high C_{24}/C_{23} (0.50-1.00) tricyclic terpanes (Peters et al., 2005). For the SR, all samples show low C_{22}/C_{21} (0.10-0.40) and variable C_{24}/C_{23} (0.25-0.60), but the C_{22}/C_{21} being lower than 0.50 for all the samples indicates that are marine shales than marine carbonates (Figure 3.29 and 3.30).

Connan et al. (1986) and Clark and Philp (1989) reported the occurrence of the C_{24} tetracyclic terpanes in samples from high salinity depositional environments. Other authors (Palacas et al., 1984; Connan et al., 1986) mention that C_{24} tetracyclic terpanes are usually found in relatively high concentrations in oils from evaporite-carbonate sequences and typically dominate the terpane distribution. The high preservation rate of organic matter in evaporitic (higher salinity) environments is predominantly due to the decrease in solubility of oxygen with increasing salinity and limited water recharge caused by enclosed water circulations (Sammy, 1985). Also, tetracyclic terpanes are more resistant to biodegradation than hopanes (Aquino Neto et al., 1983). Because of the mudstone lithofacies identified for all the Woodford Shale members

in the SR (varying from argillaceous, siliceous to chert-rich), it is unlikely that the presence of the C_{24} tetracyclic terpane is related to a significant carbonate evaporitic condition. The C_{24} tetracyclic terpane/C_{30} hopane ratio show values and minor variations for all the SR samples (0.2-0.3).

The homohopanes index (HHI) is used as an indicator of redox potential (Eh) in marine sediments during diagenesis (Moldowan et al., 1991). The homohopanes (C_{31} to C_{35}) are believed to be derived from bacteriopolyhopanol present in prokaryotic cell membranes (Peters and Moldowan, 1991; Waples and Machihara, 1991; Peters et al., 2005). The higher proportions of the C_{35} homohopane with respect to its C_{34} homolog are associated with anoxic marine depositional environments due to preferential preservation of the C_{35} homolog (Peters and Moldowan, 1991; Moldowan et al., 1992). According to Peters and Moldowan (1993) and Dahl et al. (1994), low ratios of $C_{35}S$ to $C_{34}S$ homohopanes (0.38–0.65) suggest prevailing oxic to sub-oxic (high Eh) conditions during deposition and hence low preservation of organic matter. Values of this ratio greater than 0.8 are frequently related to marine carbonate source rocks (Peters et al., 2005; Miceli-Romero et al., 2018). For the SR samples, the $C_{35}S/C_{34}S$ ratio is higher than 0.65 but less than 0.8, indicating a predominantly anoxic depositional environment, hence high preservation of the C_{35} homohopane and %TOC values (Table 3.6; Figure 3.28 - 3.30).

The Ts vs. Tm ratio is suggested as dependent on the depositional environment and the source of organic material (Philp et al., 1992; Peters et al., 2005). The ratio is also affected by lithology and oxicity of the depositional environment, where bitumen from many high-salinity source rocks show high Ts/ (Ts+Tm) ratios (Fan Pu et al., 1987; Peters et al., 2005). Moldowan et al. (1986) and Peters et al. (2005) observed that the Ts/Tm ratio increases at lower Eh and decreases at higher pH for the depositional environment of a series of Lower Toarcian marine shales from southwestern Germany. It is reported in unusual cases that the ratio decreases in an anoxic (low

Eh) section (McKirdy et al., 1983, and 1984; Rullkötter et al., 1985; Price et al., 1987). All of the SR samples show relatively low Ts/Ts+Tm values (less than 0.3, Figure 3.29 and Figure 3.30). Even if the Ts/Ts+Tm values are low, the relative vertical changes of this ratio in the stratigraphic column of the SR section (Figure 3.28) show the trends of change in anoxia.

Increasing trends in the SR the Ts/Ts+Tm are related to more saline deposits at the Lower Woodford member, and base of the Middle Woodford member, as suggested for the ratio by Moldowan et al. (1986) and Peters et al. (2005). The ratio is slightly high for the uppermost Middle member and decreases in the Upper member, indicating more transitional deposits and suboxic depositional environments for the uppermost Woodford Shale.

The presence of gammacerane (peak gammacerane in Figure 3.28 and Figure 3.29) in the SR samples was determined by SIM/GCMS using the m/z 191 ion. Its presence suggests some variations in the depositional environment. Gammacerane is a C_{30} triterpane derived from diagenesis of tetrahymanol, a compound biologically related to the freshwater *ciliated protozoan Tetrahymena* (ten Haven et al., 1989). Gammacerane is an excellent indicator of water-column stratification during sedimentation in marine and non-marine environments, and is usually associated with hypersaline conditions at depth, especially in alkaline lakes and lagoonal carbonate-evaporite environments; however, it is not restricted to this type of setting (Sinninghe Damsté et al., 1995; Schreiber et al., 2001). The presence of gammacerane has been interpreted as an indicator of the existence of a saline stratified water column deposition of strata at the SR section.

The geochemical log for the gammacerane index (gammacerane/gammacerane + C_{30} hopanes) in the SR is illustrated in Figure 3.29, which shows a higher proportion of gammacerane in the base of the Lower, Middle, and Upper members. These observations suggest that water

stratification and salinity played an essential role in the transitions of all members, where the transgressive sequences were starting to be deposited and very likely to fill the pre-existent enclosed mini-basins as the Lower member and basal Middle member deposits. Peters et al. (2005) indicate that values of the gammacerane index higher than 0.20 are resulting from water salinity and stratification, which correlates with a decrease in pristane/phytane ratios due to low oxygen content in bottom waters. This relationship between gammacerane and pristane/phytane ratios could not be estimated due to the high degradation of these isoprenoids in the n-alkane fractions. For the SR, in the Lower and Middle members, the gammacerane index values vary from 0.13-0.25), indicating a stratified water column, and fort the Upper Woodford members, the values drop from 0.14-0.09 (Table 3.6).

For the SR, the most abundant terpane in the majority of the samples is the C_{30} hopane (C_{30} 17α(H),21β(H)-hopane), followed by the C_{23} tricyclic terpane (Figure 3.28 and Figure 3.29). The C_{30} hopane is thought to be derived from diploptene or diplopterol present in bacteria (Ourisson et al., 1982). Dzou et al. (1995) also suggested an origin from bacteriohopanetetrol, a compound present in bacterial membranes. A microbial and/or algal source has been proposed for the tricyclic terpanes, although it is thought that their bacterial origin is different from that of the C_{30} hopanes (Ourisson et al., 1982). The ratios C_{23} tricyclic/C_{30} hopanes have been used to determine organic matter input and maturation; however, care must be taken when assessing which parameter has more influence on the samples analyzed, especially for immature samples (Seifert and Moldowan, 1980; Dzou et al., 1995). This ratio has been used to evaluate biomarkers derived from bacterial or algal sources (tricyclics) against biomarkers derived from prokaryotes (hopanes; Peters et al., 2005).

For all three Woodford members in the SR, this C_{23} tricyclic/C_{30} hopanes parameter shows significant variations (Figure 3.29 and Figure 3.30; Table 3.6), where the ratio generally decreases with depth on the section, possibly indicating a higher input of marine algae going up in the sequence. The relatively low abundance of the tricyclic terpanes, the predominance of C_{27} and C_{30} steranes, the strong presence of C_{24} tetracyclic, relative higher pregnanes and homopregnanes, all support the organic matter has a predominant anoxic, saline to high salinity marine depositional environment for samples of the Lower and Middle Woodford Shale member, and for the siliceous mudstones at the basal Upper Woodford member (Table 3.6; Figure 3.29).

The C_{31} 22R/C_{30} hopane ratio (31R/30H) is applied to differentiate source rocks of marine versus lacustrine origin. C_{31} 22R/C_{30} hopane ratios greater than 0.25 are associated with marine shale, carbonate, and marl source rocks (Peters et al., 2005). In the Sr, the values for this ratio (Figure 3.31) do not show much variation between the different members, and the majority of samples have values of 31R/30H vs. C_{26}TT/C_{25}TT are indicative of a marine origin. Only two Upper member samples are in an apparent lacustrine depositional setting, but these samples are the suspected migrated bitumen towards the outcrop location that fill the upper Woodford silica-rich lithologies (Figure 3.20).

Tm and Ts are frequently used to assess maturation from immature to post mature stage (Peters et al., 2005). Tm becomes less stable than Ts with increasing thermal maturity; therefore, the Ts/(Ts+Tm) ratio can be used as a maturity indicator, particularly for samples of similar lithology and organic facies (Moldowan et al., 1994; Peters et al., 2005). Differences in thermal maturity within the SR Woodford Shale samples can be observed when analyzing the differences in Ts, Tm (Figure 3.29 and Figure 3.32). From the beginning of the Upper Woodford member

(220.5 ft), a decrease can be observed in Tm over Ts (Figure 3.29 and Figure 3.32), and a much higher ratio of C_{23} tricyclic terpane over C_{30} hopane.

Samples in both the Lower and Middle Woodford members present a general trend of high Tm (Figure 3.29 and Figure 3.32), indicating low thermal maturity as expected from the vitrinite reflectance values of 0.58 Ro% reported by Galvis et al. (2017a). These differences are probably indicating that the extracted organic matter has a higher value of thermal maturity in the Upper Woodford member than in the lower portions of the SR. These maturity differences might indicate that the Upper Woodford member lithofacies can be hosting migrated hydrocarbons (more mature Woodford oil charging the SR Upper Woodford microfractures), supported by the extremely high Rock-Eval pyrolysis S1 peak (free volatile hydrocarbons in the sample; Figure 3.19 and Figure 3.30).

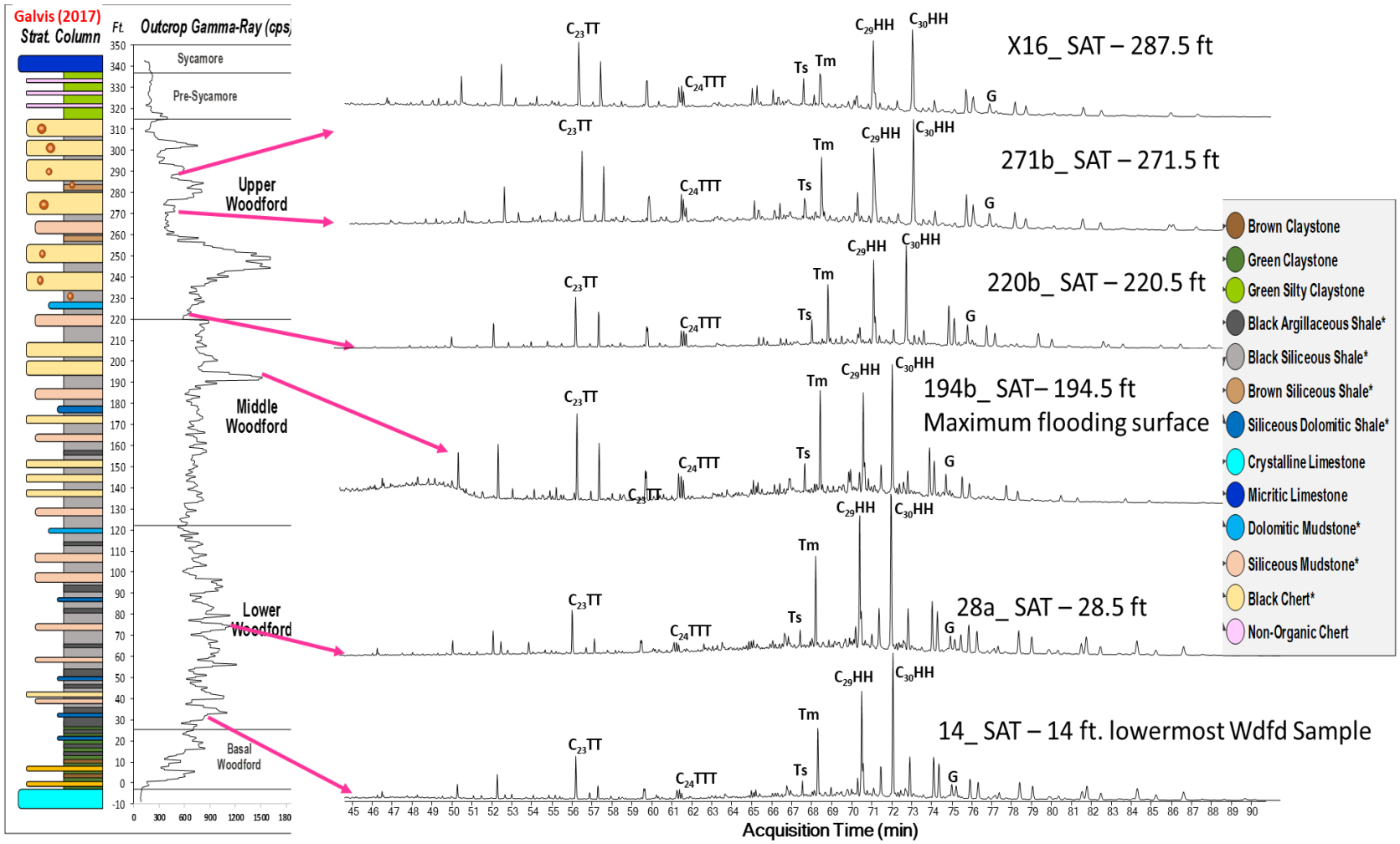

Figure 3.29. Tricyclic terpanes and hopanes identification using m/z 191.3 plot of sample 220b, Middle-Upper Woodford members boundary at 220.5 ft. Peak identification in Table 3.5.

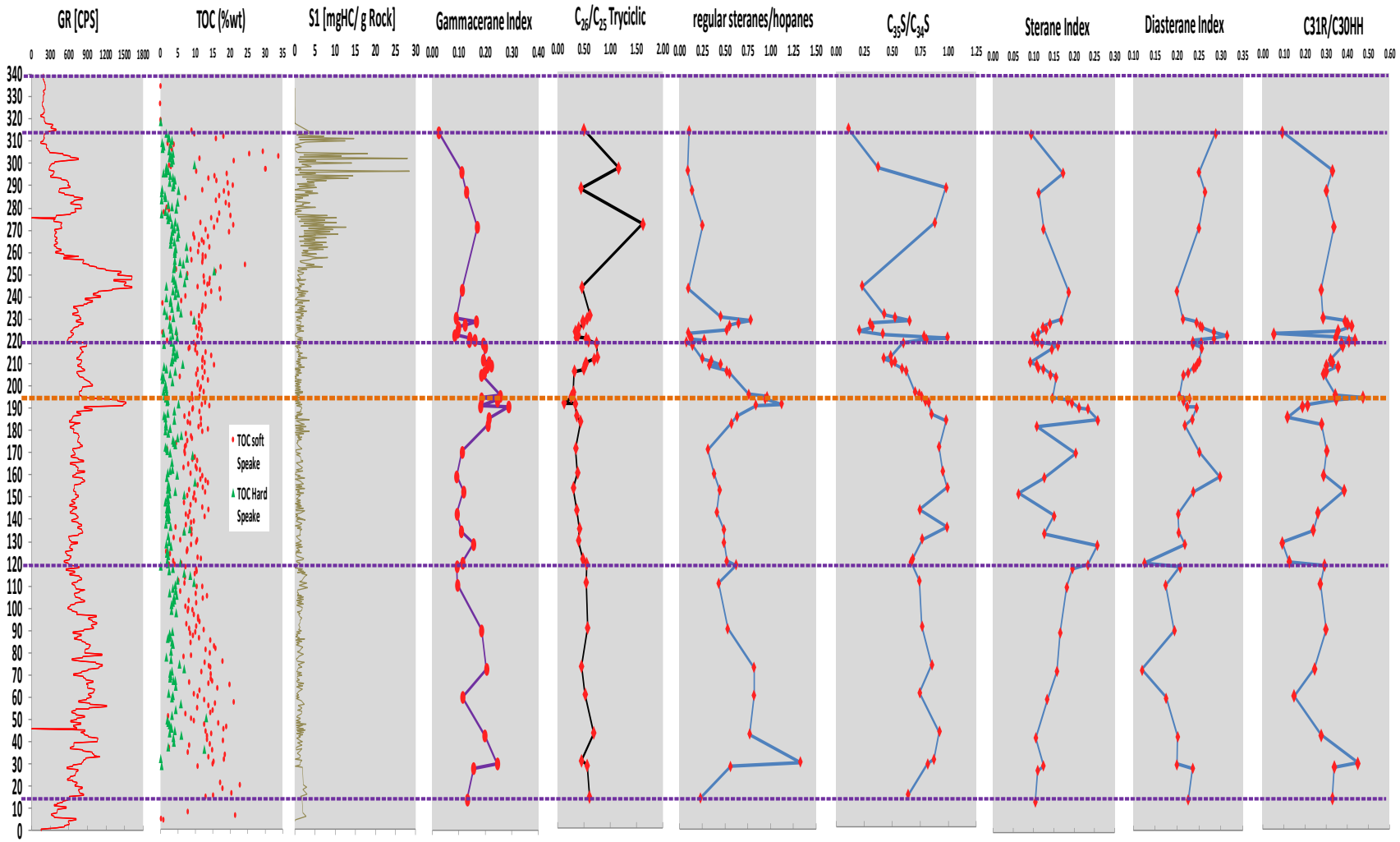

Figure 3.30. Comparison of tricyclic terpanes and hopanes abundance, as compared to Gamma-Ray log and %TOC classified by the mechanical stratigraphy of the rock layers (soft vs. hard; Galvis, 2017). (Tricyclic terpane / hopanes ratio = [C_{28}-C_{29} tricyclic terpanes / C_{29}-C_{33} hopanes]; gammacerane index = 10* gammacerane / [gammacerane + C_{30} hopane]; C_{26}/C_{25} TT = C_{26}/C_{25} tricyclic terpanes; $C_{31}R/ C_{30}$ = $C_{31}R/ C_{30}$ hopanes; TT/Hop = [C_{28} + C_{29} tricyclic terpanes] / [C_{29} –C_{33} hopanes]; C_{30} TPP/C_{30} steranes).

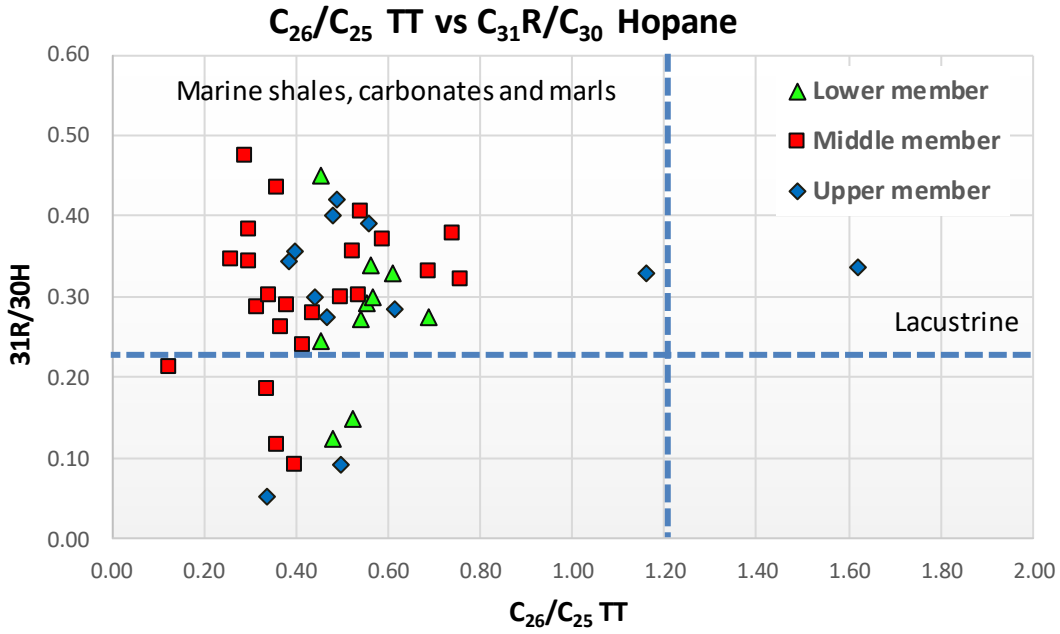

Figure 3.31. C_{26}/C_{25} vs. $C_{31}R/C_{30}$ Hopane shows that the Woodford Shale samples are mainly of marine origin (Dotted lines are used as a guide and do not represent fixed fields on the diagram. Plot modified from Peters et al., 2005). Only two Upper member samples are in an apparent lacustrine depositional setting, but these samples are the suspected migrated bitumen towards the outcrop.

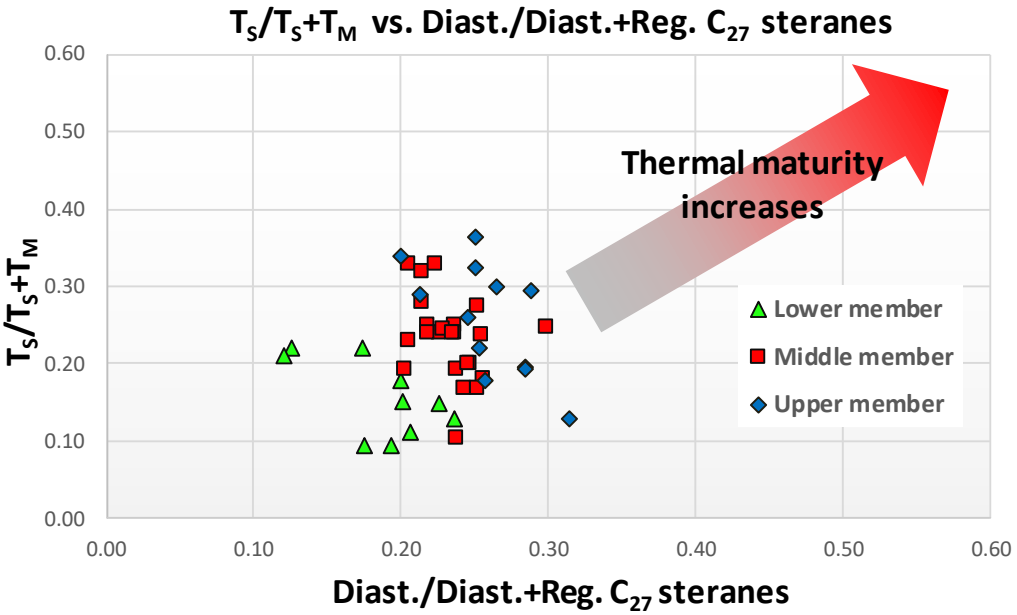

Figure 3.32. A plot of diasteranes/(diasteranes+regular) C_{27} Steranes vs. Ts/(Ts+Tm) ratios shows differences in thermal maturity (Plot modified from Moldowan et al., 1994).

3.5.7. Tetracyclic polyprenoids (TPP)

These biomarkers are highly specialized for lacustrine brackish environments, but also from freshwater algae species (Holba et al., 2000 and 2003; Figure 3.33). Holba et al. (2003) encountered high levels of TPP in near-shore facies of samples that have no marine palynomorphs but abundant *Chlorococcalean* (Green) algal nonmarine palynomorphs. Holba et al. (2003) suggested that green algae (or *Chlorophyta*) are a possible source for the TPP compounds. Holba (2000) compared the TPP ratio with the most consistent indicator of marine algal input, the 24-n-propylcholestanes (C_{30} steranes) derived from marine algae, according to Moldowan et al., (1990). Holba et al. (2000 and 2003) concluded that marine oils have low TPP ratios and a high percentage of 24-n-propylcholestanes, whereas pure non-marine oils presented no detectable 24-n-propylcholestanes. Holba et al. (1998) mentioned that mixed inputs present a non-zero percentage of 24-n-propylcholestanes and elevated TPP ratios. Holba et al. (2000 and 2003) defined the TPP ratio (equation 3.7; Figure 3.33) using the peaks recognized in m/z 414→259 and m/z 358→217 (Figure 3.33 – 3.36) as the following:

$$\text{TPP ratio} = (2 * \text{21R TPP})/[(2 * \text{21R TPP}+(\Sigma\text{27-norcholestane isomers})] \quad (3.7)$$

Σ27-norcholestane isomers = (13β,17α,20S-27-nordiacholestane + 13β,17α,20R-27-nordiacholestane + 5α,14α,17α,20S-27-norcholestane + 5α,14β,17β,20R-27-norcholestane+ 5α, 14β, 17β, 20S-27-norcholestane+ 5α, 14α, 17α, 20R-27-norcholestane).

Schaeffer et al. (1994), Poinsot et al. (1997 and 1998), and Holba et al. (2003) mentioned that under reducing non-marine conditions, which are usually low in free sulfate content, the parent backbone of the TPP precursors is probably preserved as saturate hydrocarbons in the bitumen and kerogens, whereas under anoxic, sulfate-rich conditions like the marine deposits. Poinsot et al. (1997 and 1998) mentioned that the functionalized C_{30} TPP precursors are likely to undergo sulfurization, thus preserving them as heterocyclic compounds bound to kerogen. TPPs were tentatively identified for the SR using GC-MS analysis on saturate fractions, the m/z 259.3, and m/z 217.3 fragmentogram comparisons (Figure 3.34). Precise identification and confirmation were made using the GC/MS/MS m/z 414→259 transitions, as suggested by Holba et al. (2000, and 2003; Figure 3.33 - 3.36).

Figure 3.35 illustrates the TPP vs. %C30 regular steranes plot and shows the yields proposed by Holba et al. (2000 and 2003) for the lacustrine, mixed facies and marine depositional settings. The values of Holba et al. (2003) for lacustrine settings in Figure 3.35 are from 0.2 – 1 in the TPP ratio and near-to-zero values of the $\%C_{30}$ regular sterane. The marine settings in the Holba et al. (2003) plot is for TPP ratios of less than 0.2 and $\%C_{30}$ regular steranes higher than 2% (Figure 3.35). The mixed facies are for TPP 0.2 – 0.4 And $\%C_{30}$ regular steranes for 0-2% (Figure 3.35). In some of the SR samples, the TPPs were found in relatively high levels that can be distinguished on GC-MS (Figure 3.33) and are reliable indicators that lacustrine kerogen particles reached the paleo Woodford ocean, where continental inputs were transported towards deeper basinal deposits. Figure 3.36 illustrates the Holba et al. (2003) plot for depositional settings identification using the TPP ratio vs. $\%C_{30}$ regular steranes in the SR. Note that despite recognizing TPP ratio values higher than 0.2, the $\%C_{30}$ regular steranes plot for all the Woodford Shale members as marine depositional settings and mixed facies (Figure 3.36).

Holba et al. (2003) mentioned that the C_{30}TPP/C_{30}steranes higher than 0.4 correspond to their identified lacustrine and brackish facies. There are values of this ratio in the same range for the SR, but when comparing higher values of the TPP ratio (Figure 3.37 - 3.42) with the TPP ratio vs. %C_{30} regular steranes (>0.2; Figure 3.36 and Figure 3.42) for the Middle and Upper members, suggest that depositional mechanisms brought the brackish TPPs towards the basin in a progradational manner (seaward stepping). These identified TPPs were preserved, surviving the mechanical reworking that occurs during sediment transport (Figure 3.33, and Figure 3.37). For the Lower Woodford member, the TPP ratio is low (Figure 3.40 – 3.42), as expected due to a principal transgressive system tract regime (Figure 3.36 and Figure 3.42). The identification of TPPs in the SR might look relatively large, but a direct interpretation of these high peaks in the chromatograms (Figure 3.37 – 3.41) might be misleading since the chromatograms are normalized and then the TPPs are calculated as relative concentrations (TPP ratio; TPP ratio vs. %C_{30} regular steranes) and not as absolute concentrations.

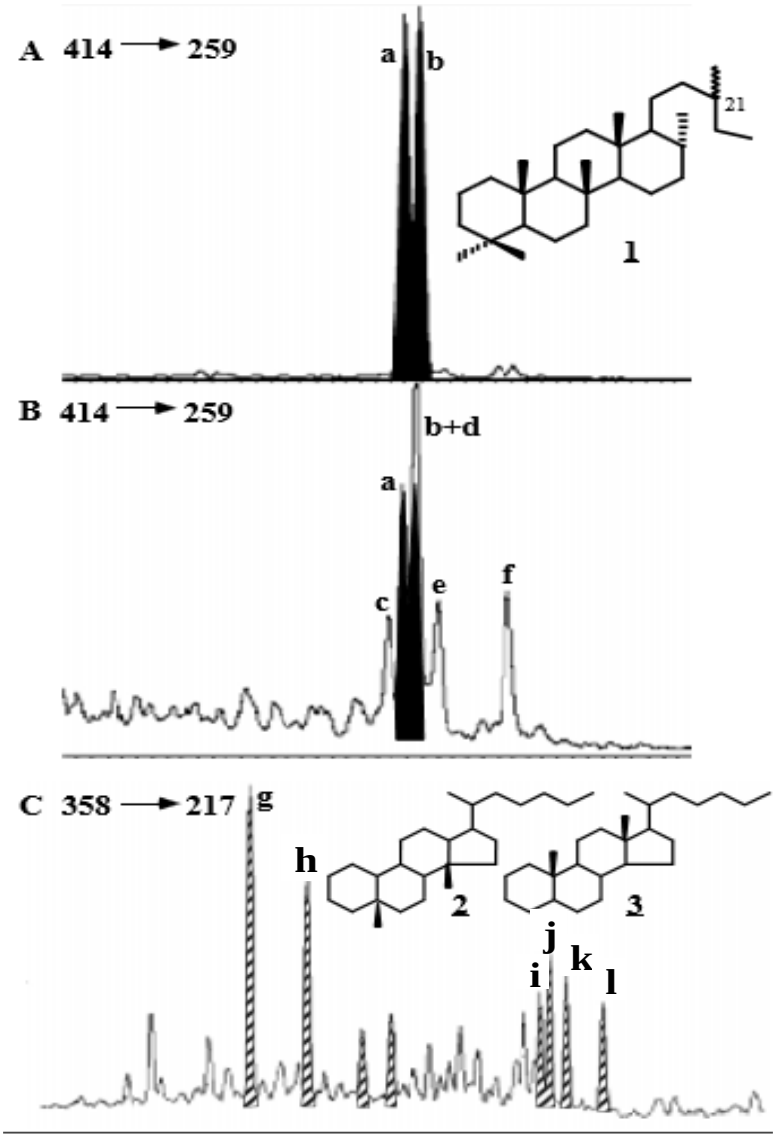

Figure 3.33. GC/MS/MS mass chromatograms of Holba et al. (2000 and 2003) TPP identification samples. A: 414 ➔ 259 lacustrine source-rock extract from Triassic Cacheuta Shale, Cuyo basin, Argentina. B: 414 ➔ 259 from Jurassic marine oil, Ekofisk field, North Sea, Norway. C: 358 ➔ 217 norcholestanes from Jurassic marine oil, Cook Inlet, Alaska. Compound structures and nomenclature: compound 1, peaks a = C_{30} TPP 18α(h),21R; b = C_{30} TPP 18α(h),21S; c = 14α,17α,20S-3β-propylcholestane; d = 14β,17β,20R-3β-propylcholestane; e = 14β,17β,20S-3β-propylcholestane, f = 14α,17α,20R-3β-propylcholestane. For compound 2: g = 13β,17α,20S-27-nordiacholestane; h = 13β,17α,20R-27-nordiacholestane. For compound 3: peaks i = 5α,14α,17α,20S-27-norcholestane; j = 5α,14β,17β,20R-27-norcholestane; k = 5α, 14β, 17β, 20S-27-norcholestane; l = 5α, 14α, 17α, 20R-27-norcholestane. Modified from Holba et al. (2003).

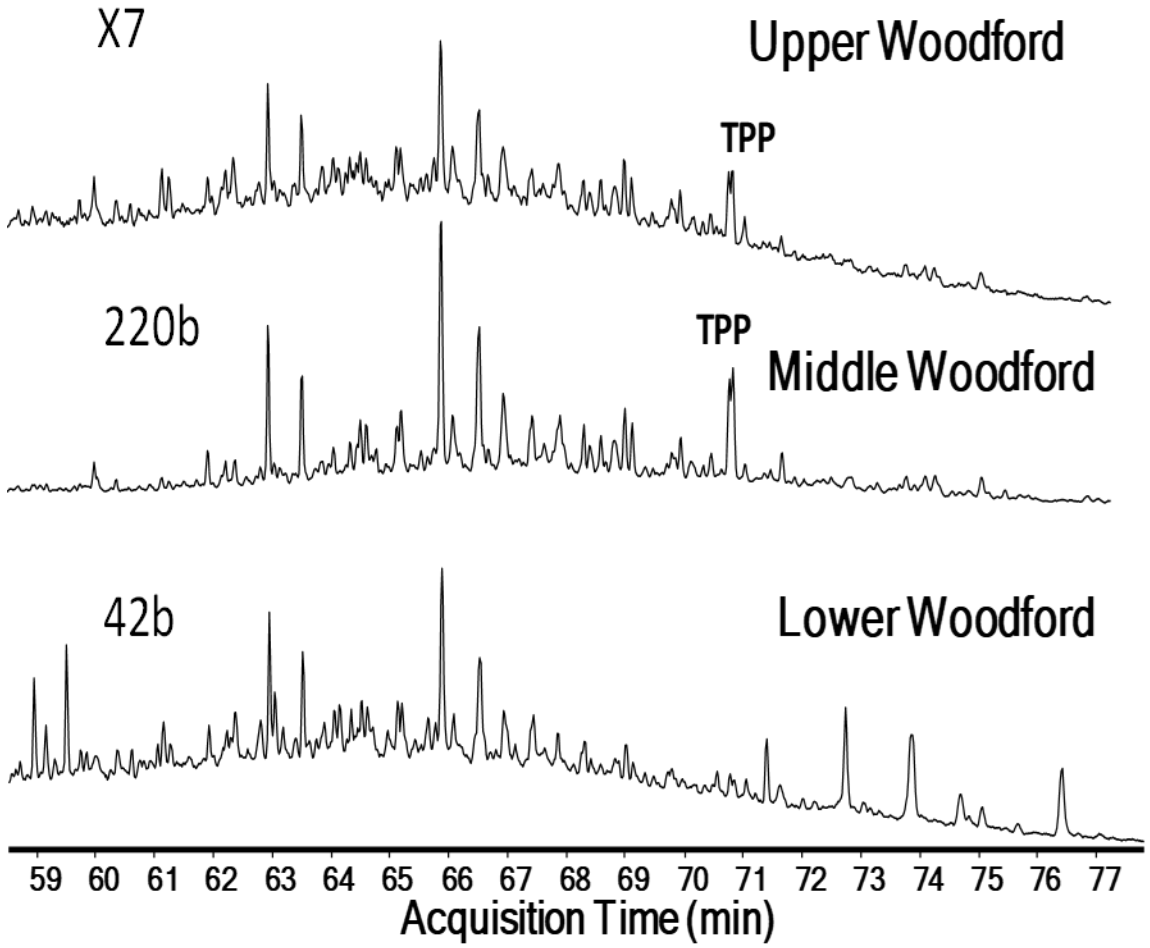

Figure 3.34. GC-MS saturate fraction of one sample in the Upper, one in the Middle, and one in the Lower Woodford members for screening in the m/z 259.3 the possible presence of TPP, confirmed with GC-MS/MS in Figure 3.37 – 3.39.

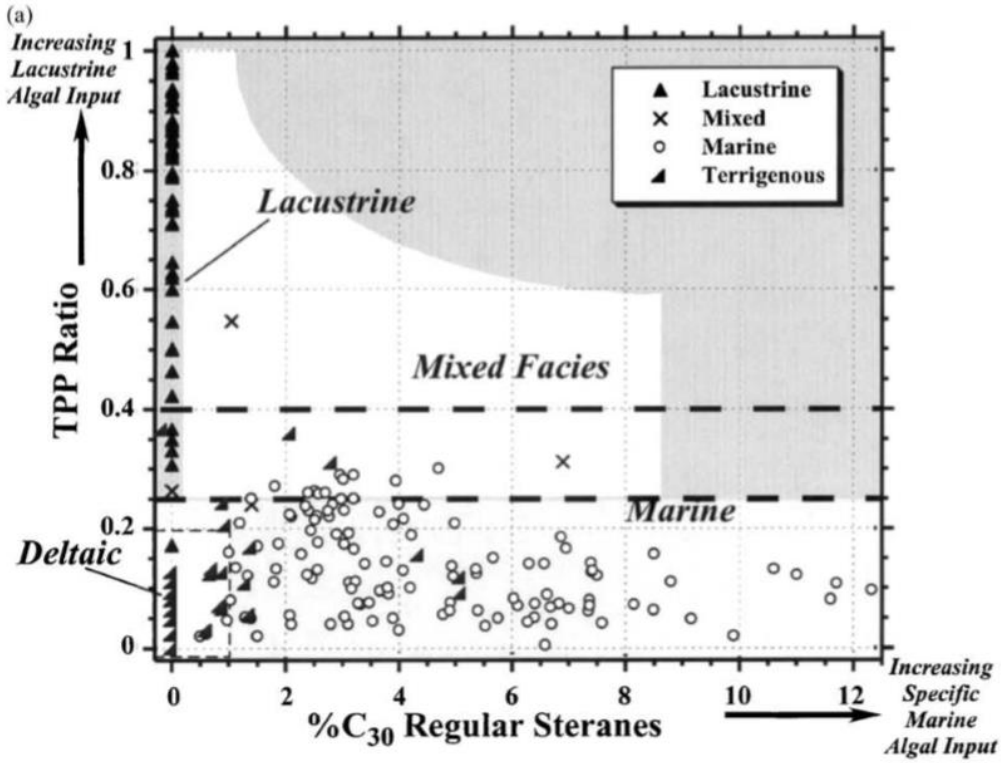

Figure 3.35. Plots of biomarker indicators of depositional environment and biological input (Holba et al., 2003). Holba et al. (2000 and 2003) proposed the TPP ratio (an indicator of fresh/ brackish water algal input) vs. $\%C_{30}$ 24-propylcholestanes (an indicator of marine algal input).

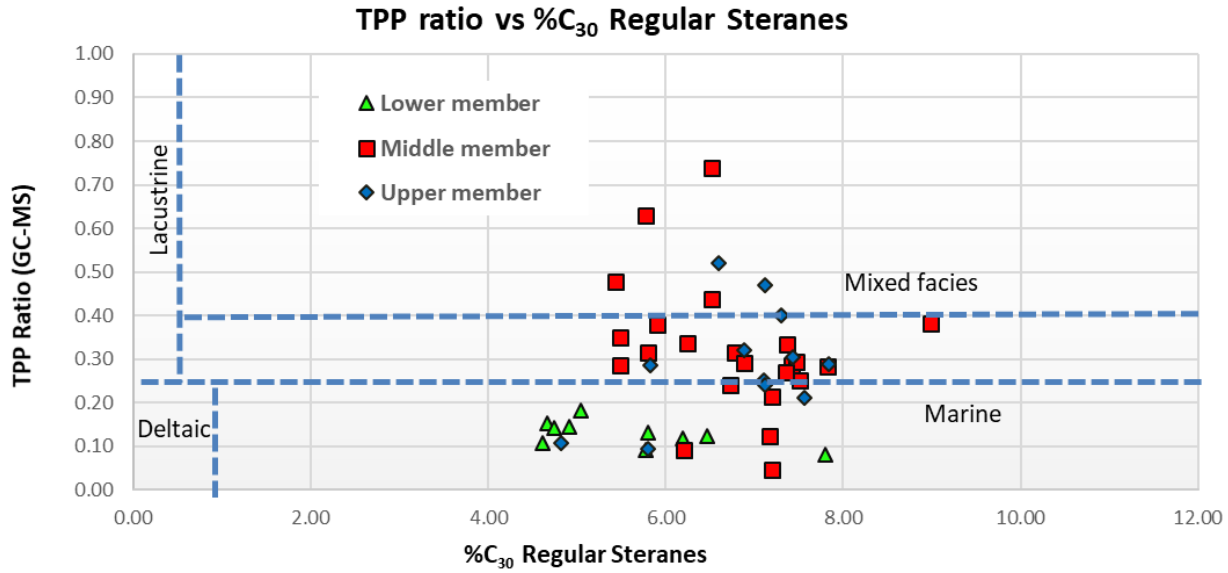

Figure 3.36. Plots of biomarker indicators of depositional environment and biological input for the SR using TPPs (Holba et al., 2003). Note that no samples yield in the lacustrine interval proposed by Holba et al. (2000 and 2003). Some upper Woodford and Middle Woodford samples are in the mixed organic matter according to this plot modified after Holba et al. (2003).

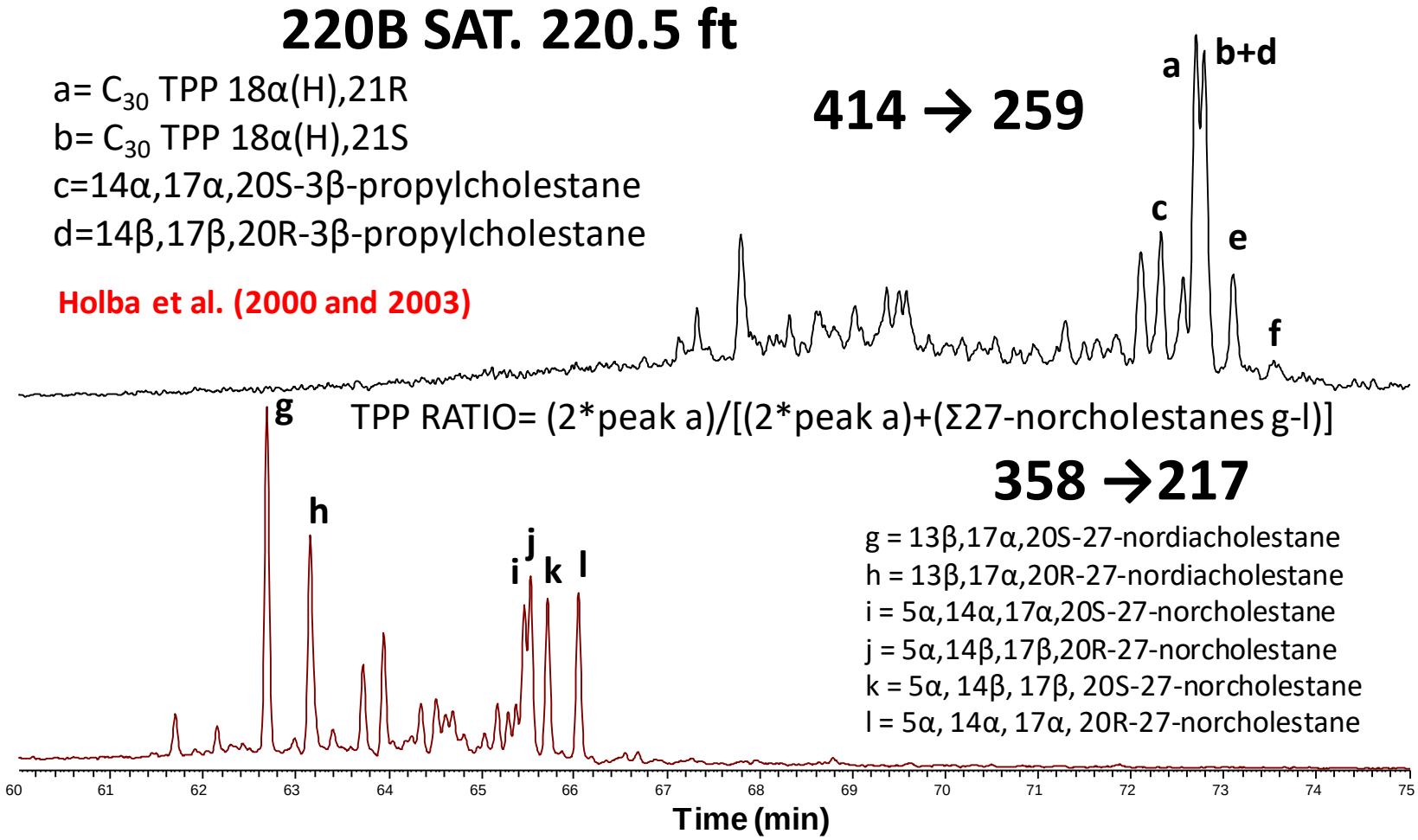

Figure 3.37. GC-MS/MS in a Middle Woodford Shale sample, 220.5 ft. M/z 414→259 and m/z 358→217 for recognizing the presence of tetracyclic polyprenoids (TPP) and the TPP ratio when compared to the 27-norcholestanes using the methodology of Holba et al. (2000 and 2003). TPP Ratio of 0.18. Compound structures in Figure 3.30.

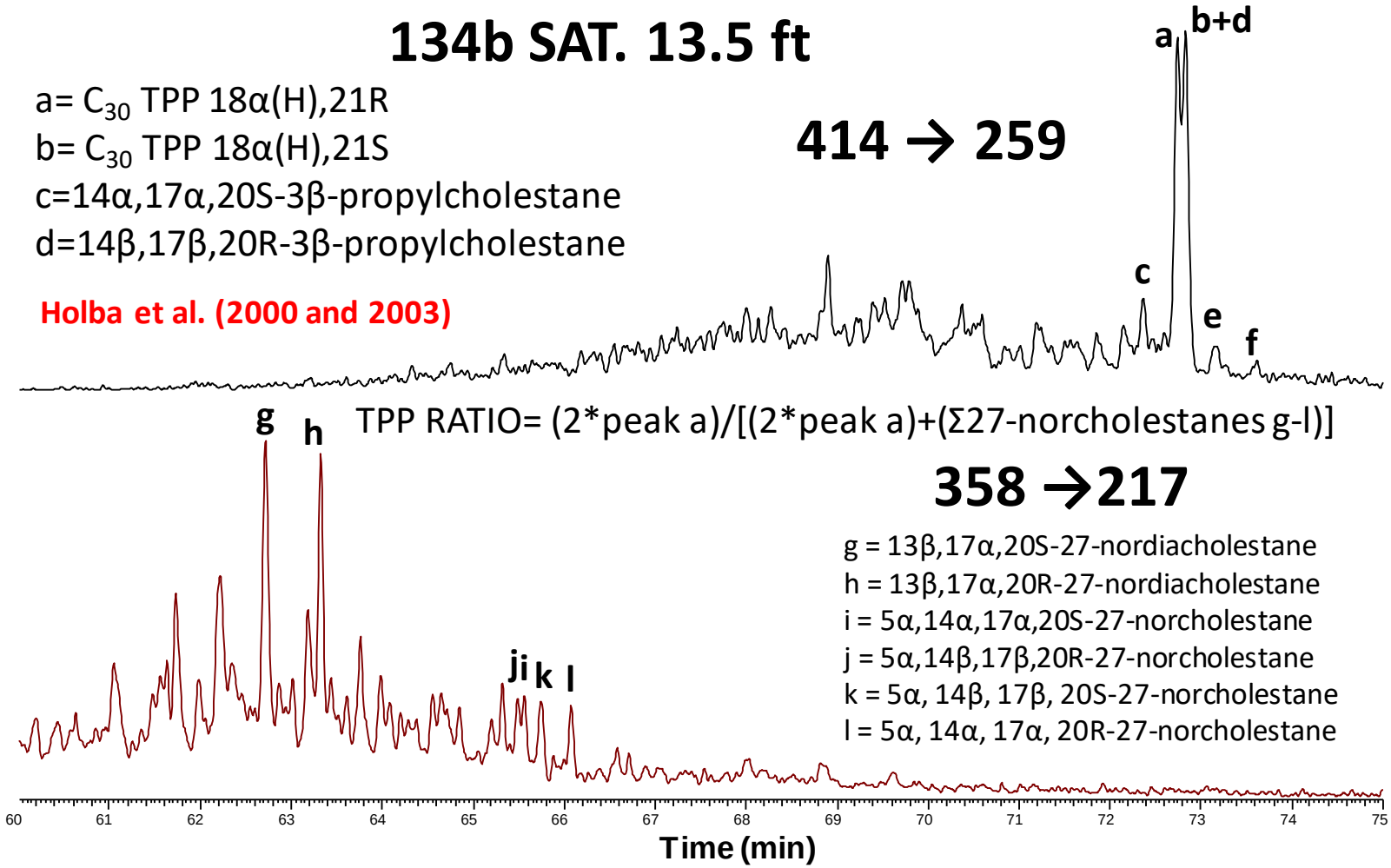

Figure 3.38. GC-MS/MS in a Middle Woodford Shale sample, 134.5 ft. M/z 414→259 and m/z 358→217 for recognizing the presence of tetracyclic polyprenoids (TPP) and the TPP ratio when compared to the 27-norcholestanes using the methodology of Holba et al. (2000 and 2003). TPP ratio 0.55, is the highest found in the Speake Ranch. Compound structures in Figure 3.30.

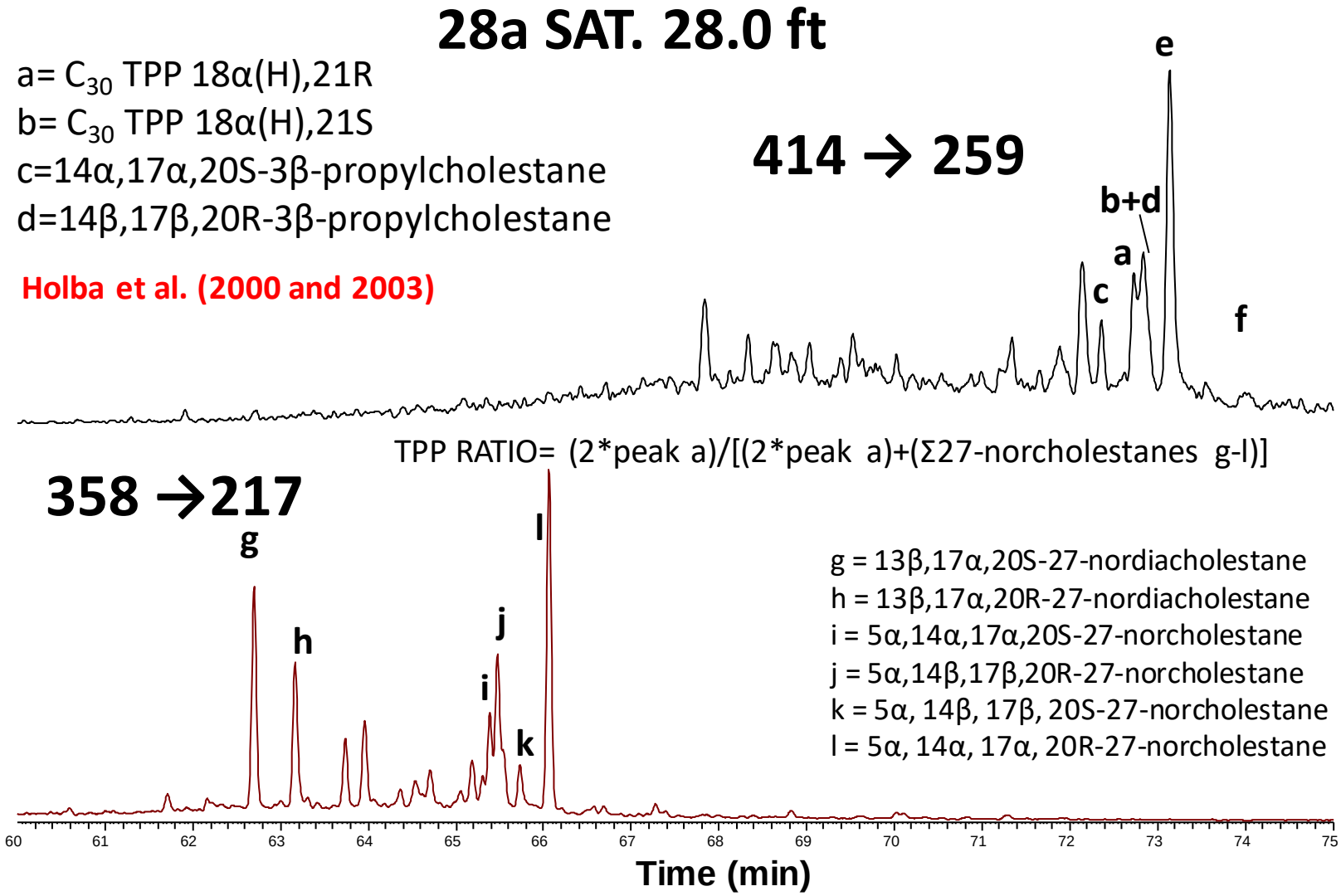

Figure 3.39. GC-MS/MS in a Lower Woodford Shale sample, 28.0 ft. M/z 414→259 and m/z 358→217 for recognizing the presence of tetracyclic polyprenoids (TPP) and the TPP ratio when compared to the 27-norcholestanes using the methodology of Holba et al. (2000 and 2003). TPP ratio 0.004, is the lowest found in the Speake Ranch. Compound structures in Figure 3.30.

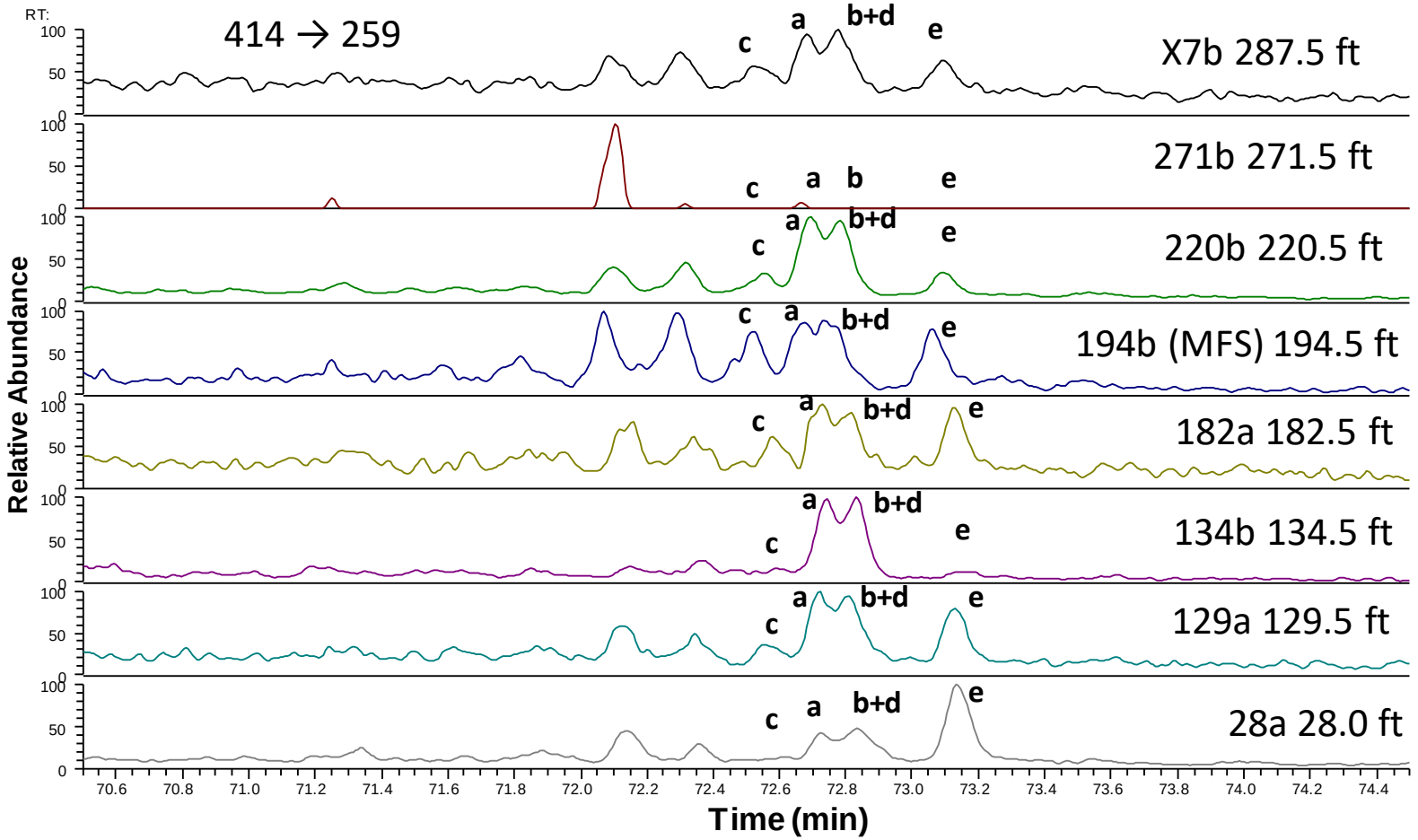

Figure 3.40. GC-MS/MS of the m/z 414→259 for recognizing the presence of tetracyclic polyprenoids (TPP) in eight samples of the Speake Ranch. Peak recognition criteria from Holba et al. (2000 and 2003): a = C_{30} TPP 18α(h),21R; b = C_{30} TPP 18α(h),21S; c = 14α,17α,20S-3β-propylcholestane; d = 14β,17β,20R-3β-propylcholestane; e = 14β,17β,20S-3β-propylcholestane. Upper Woodford samples are the X7b and 271b; the Lower Woodford sample is the 28a. Others correspond to the Middle Woodford member. Compound structures in Figure 3.30.

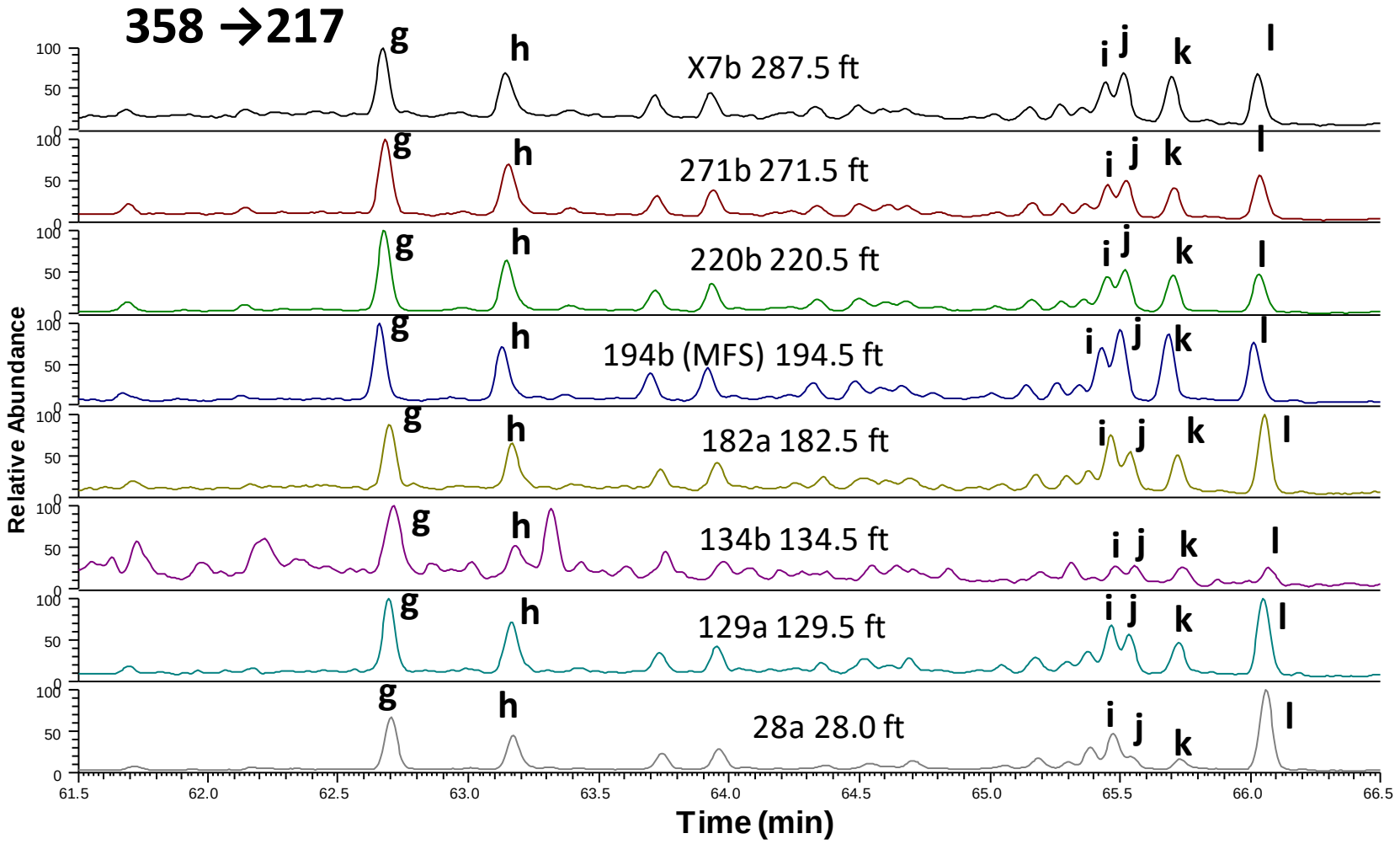

Figure 3.41. GC-MS/MS of the m/z 358→217 for recognizing the presence of tetracyclic polyprenoids (TPP) in eight samples of the Speake Ranch. Peak recognition criteria from Holba et al. (2000 and 2003): g = 13β,17α,20S-27-nordiacholestane; h = 13β,17α,20R-27-nordiacholestane; i = 5α,14α,17α,20S-27-norcholestane; j = 5α,14β,17β,20R-27-norcholestane; k = 5α, 14β, 17β, 20S-27-norcholestane; l = 5α, 14α, 17α, 20R-27-norcholestane. Upper Woodford samples are the X7b and 271b; the Lower Woodford sample is the 28a. Others correspond to the Middle Woodford member. Compound structures in Figure 3.30.

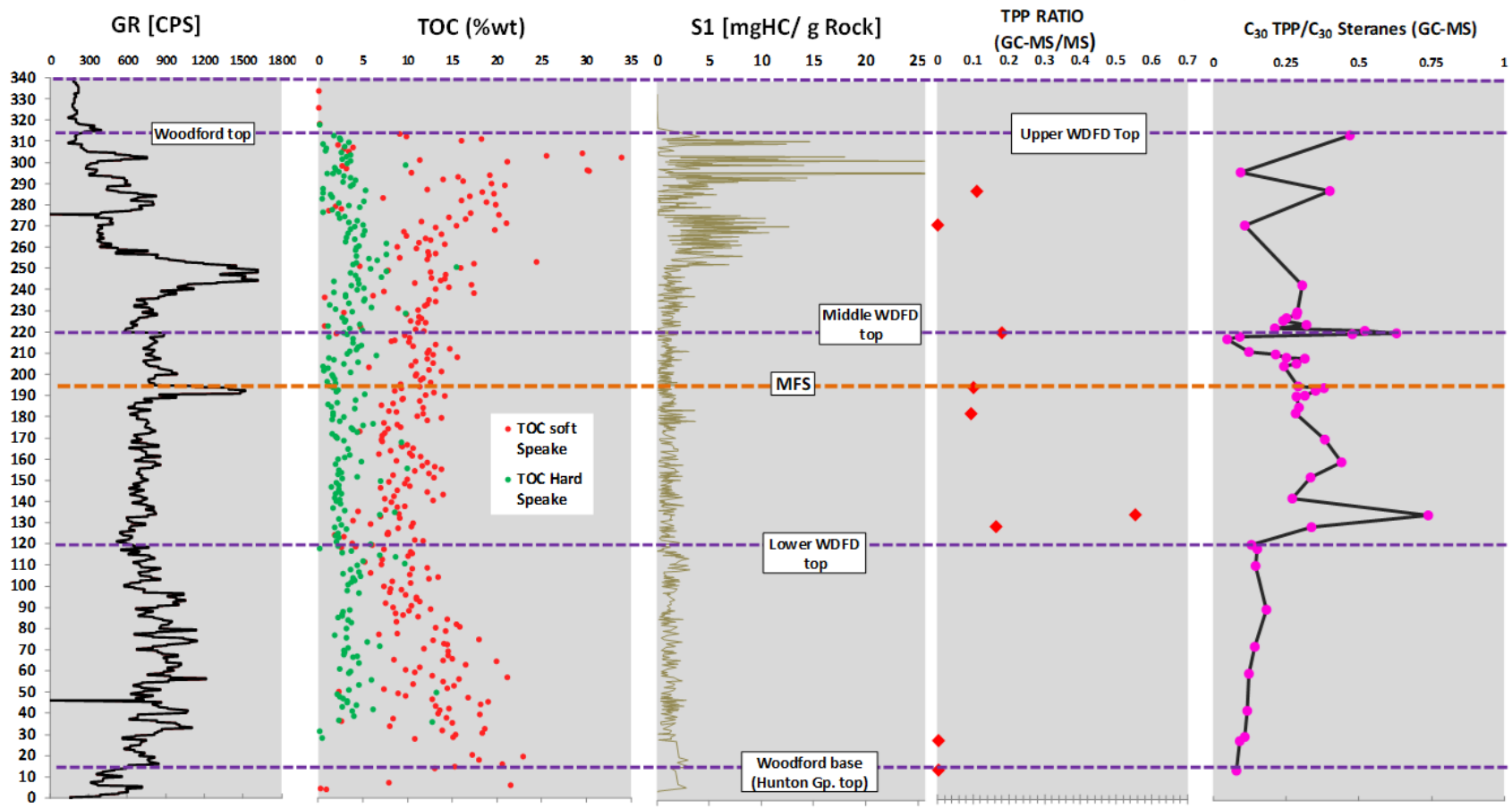

Figure 3.42. Comparison of tricyclic polyprenoid (TPP) abundance (calculated as TPP ratio, with the methodology of Holba et al., 2000 and 2003) from the GC-MS/MS m/z 414→259 and m/z 358→217 ions. TPP ratio as compared to Gamma-Ray log, %TOC (classified by the mechanical stratigraphy of the rock layers, soft vs. hard; Galvis et al., 2017a), Rock-Eval pyrolysis S1 peak, and TPP ratio to C_{30} steranes from the GC-MS /z 191 and m/z 217 ions. Note the low TPP ratio in the Lower Woodford Shale for both TPP ratio points and TPP/C_{30} steranes curve, then both TPP ratio and TPP/C_{30} steranes are increasing from the start of the Middle Woodford member, and the values of the TPP ratio are higher in the uppermost portion of the Upper Woodford member.

3.5.8. C_{40} Aromatic carotenoids and aryl isoprenoids

Isorenieratane, a C_{40} diaromatic carotenoid pigment, is generally thought to be produced by the green sulfur bacteria (GSB) *Chlorobiaceae* (Brown and Kenig, 2004; Schwark and Frimmel, 2004; Brocks et al., 2005; Bryant and Dahl, 2006; Brocks and Summons, 2014). The importance of recognizing these carotenoids is that *Chlorobiaceae* performs photosynthesis under light-penetrated, H_2S-saturated, anoxic waters (Figure 3.43). Frigaard and Dahl, (2008) mentioned that *Chlorobiaceae* are phototrophic and autotrophic anaerobes which exclusively produce the carotenoids isorenieratane (**I**, brown strain), chlorobactene (**VI**, green strain), paleorenieratane (**II**, origin unknown; see Figure 3.44 for structures by Connock, 2015).

Isorenieratane and other diagenetic products of isorenieratane are excellent proxies for the assessment of past photic zone euxinia (PZE) present in the water column (Summons and Powell, 1986; Sinninghe Damsté et al., 1987, 1995; Requejo et al., 1992; Koopmans et al., 1996a and 1996b; Schwark and Frimmel, 2004; Sinninghe Damsté and Schouten, 2006). These carotenoids are usually used as indicators of past sedimentary conditions (Brown and Kenig, 2004; Grice et al., 2005; Marynowski and Filipiak, 2007; Hays et al., 2007; Table 3.7; Figures 3.43 and 3.44).

The GSB possesses a unique organelle, the chlorosome, composed of bacteriochlorophyll (Hartgers et al., 1994; Frigaard and Dahl, 2008; Connock et al., 2018). According to Connock (2015), the chlorosomes assist in the proliferation of GSB at extreme depths of the anaerobic photic zone, which was over 300 ft deep for the Woodford Shale in southern Oklahoma. The development of this deep PZE is proposed in this SR study as an additional indicator of enclosed mini-basin fill settings because the erosion of pre-Woodford strata allowed the development of deep concave down depocenters. These depocenters are silled and these barriers prevented the oxygen recharge by open oceanic water circulations. In mini-basin fill settings, the restriction should have permitted

thicker chemocline development, which can be identified for the Woodford Shale by analyzing the fluctuations of the PZE conditions (Connock, 2015; Connock et al., 2018). Overman et al. (1992) and Overman (2008) mentioned that at extreme depths of the PZE, the light intensities are low, which is essential for the development of GSB which lack flagella (characteristic of *Chromatiaceae*, purple sulfur bacteria), and instead utilize gas vacuoles for propulsion. van Gemerden (1983) and Connock (2015) mentioned that the GSB capable light scavengers, require H_2S as an electron donor in addition to light to sustain metabolic function.

Sirevåg and Ormerod (1970), Summons and Powell (1986), and Connock et al. (2018) emphasized that in the photosynthetic cycle of green sulfur bacteria, the molecule of carbon is fixed via the reductive tricarboxylic acid cycle (reverse TCA). This reverse TCA results in the biomass becoming enriched in ^{13}C as mentioned by Quandt et al. (1977), Sirevåg et al. (1977), Summons and Powell (1986), van der Meer et al. (2001), and Connock et al. (2018). The GSB retains its isotopic signature despite structural changes during burial and diagenesis (Grice et al., 1996; Koopmans et al., 1996a; Williford et al., 2016; Connock et al., 2018). This isotopic effect assists the correlation of particular biomarkers to the GSB, and Connock et al. (2018) emphasized that it is useful from a paleoenvironmental perspective due to the specific and unique requirements of GSB for the Woodford Shale and the development of PZE and variations in the euxinic conditions. The basal Woodford sea, which was relatively shallow in Oklahoma (Comer, 2008), went through periods of restricted circulation, giving way to conditions that would cause PZE (Comer, 2008; Connock, 2015; Jones, 2017), and these PZE conditions are proposed to be persistent in enclosed mini-basin fills systems.

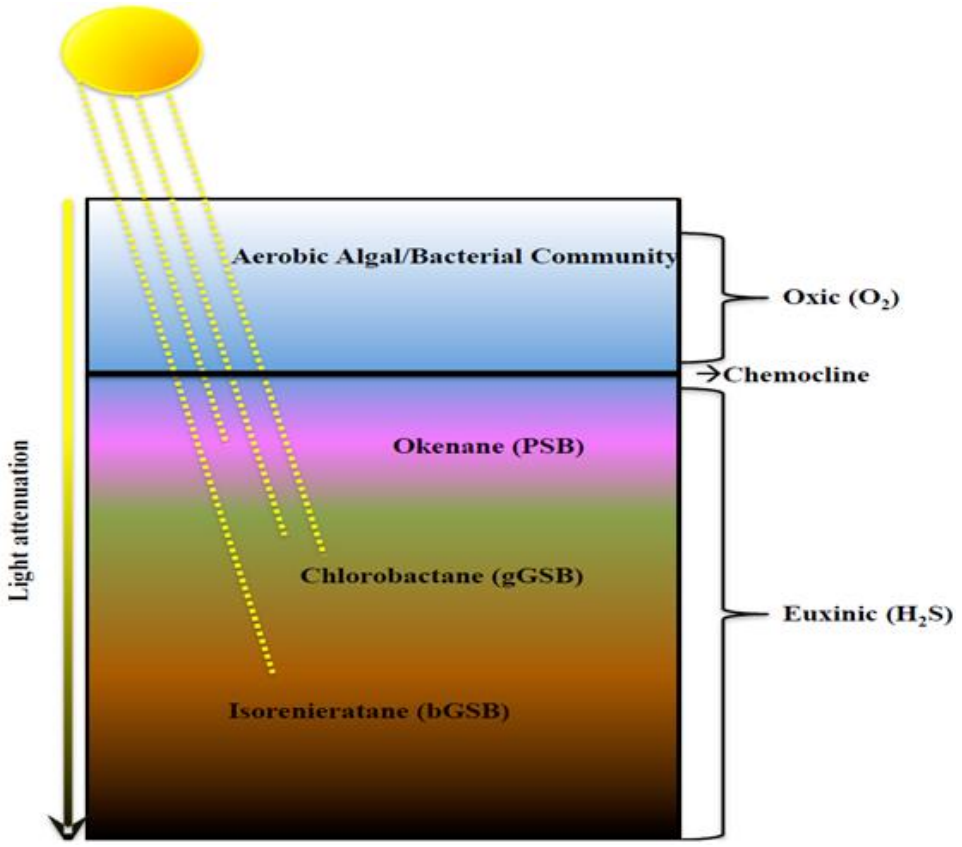

Figure 3.43. Water column biological composition and structure during periods of euxinia proposed by Connock (2015). Jones (2017) and Connock et al. (2018) mentioned that for the Woodford Shale, the invasion of the photic zone by H_2S (PZE) could be identified with the C_{40} carotenoids. The persistent PZE conditions are proposed to be indicators of enclosed mini-basin fills for the SR.

Aryl isoprenoids are generally proposed to be derived from isorenieratane similarly to the C_{40} carotenoids (Summons and Powell, 1987; Brown and Kenig, 2004; Schwark and Frimmel, 2004; Widayat, 2011; Widayat et al., 2016). The distribution and identification of aryl isoprenoids and carotenoids using the m/z 133 and m/z 134 ions in previous studies are shown in Figure 3.45 (Marynowski and Filipiak, 2007). The identification of aryl isoprenoids and carotenoids in the SR in Figure 3.46 - 3.48. For the SR, the C_{13}-C_{31}, the C_{32}+ aryl isoprenoids, and C_{40} carotenoids appear in the aromatic fractions (Figure 3.46 and Figure 3.47).

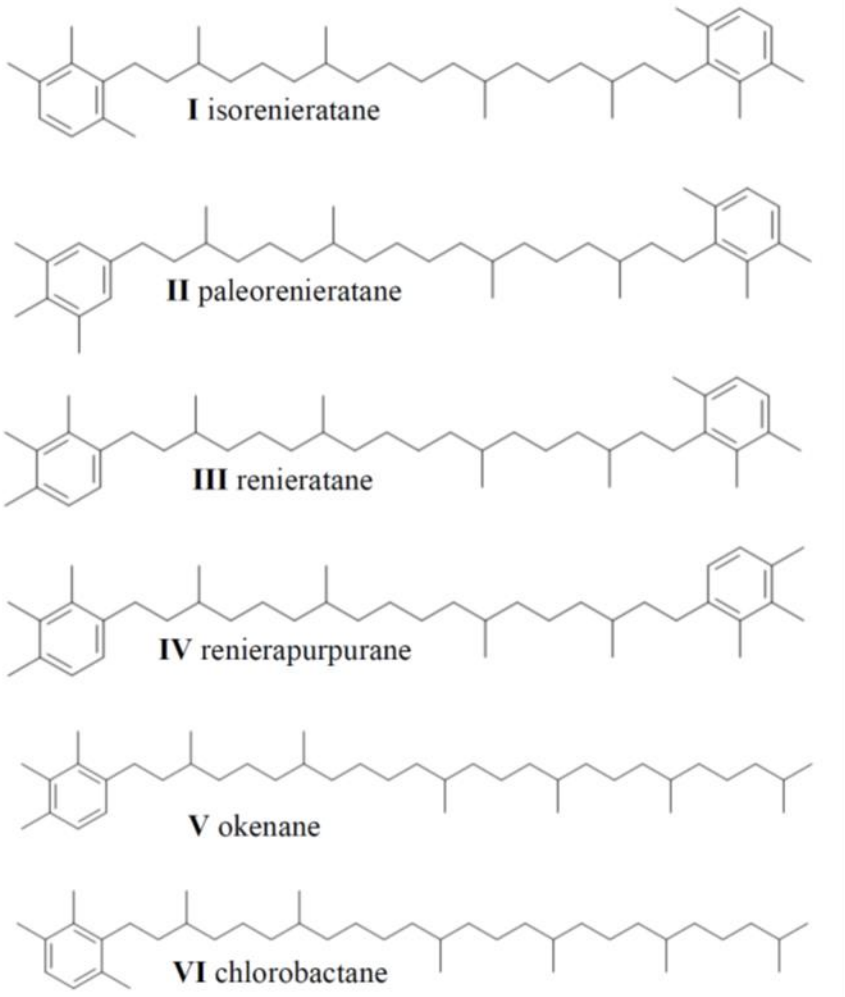

Figure 3.44. C_{40} carotenoid molecular structure. From Connock, 2015.

The 2,3,6 trimethyl-substituted aryl isoprenoids (m/z 133) are derived from both β-isorenieratane and β-carotane, which come from green sulfur bacteria and cyanobacteria, respectively (Koopmans et al., 1996a; Brown and Kenig, 2004). The 3,4,5 trimethyl-substituted aryl isoprenoids are derived solely from isorenieratane from *Chlorobiaceae* and therefore make for a more direct indicator of euxinia (Summons and Powell, 1987; Koopmans et al., 1996a; Brown and Kenig, 2004; Miceli-Romero and Philp, 2012). The identification of the 2,3,6 trimethyl-

substituted and 3,4,5 trimethyl-substituted aryl isoprenoids, as derived from these bacteria, can be specific indicators of photic zone anoxia (PZA; Schwark and Frimmel, 2004).

The aryl isoprenoid ratio (AIR: 2,3,6/3,4,5 trimethyl-substituted aryl isoprenoids; Figure 3.46 and Figure 3.47) can be utilized to assess relative amounts of aryl isoprenoids from *Chlorobiaceae*, where lower values correspond with more green sulfur bacteria input, as opposed to cyanobacteria input (Schwark and Frimmel, 2004; Marynowski and Filipiak, 2007). Schwark and Frimmel (2004) introduced this ratio by analyzing the proportions of the short-chain (C_{13}-C_{17}) and intermediate-chain (C_{18}-C_{22}) aryl isoprenoids. High AIR (3.0) is associated with episodic PZA, which leads to alteration of the long- and intermediate-chain aryl isoprenoids. On the contrary, low AIR (0.5) indicates persistent PZA, which contributes to the preservation of the long-chain aryl isoprenoids (Schwark and Frimmel, 2004; Miceli-Romero and Philp, 2012). Usually, a lower value of AIR corresponds to more anoxic conditions and lower Pr/Ph ratios (Schwark and Frimmel, 2004). A depth plot of 3,4,5 trimethyl-substituted aryl isoprenoids, 2,3,6 trimethyl-substituted aryl isoprenoids, and the total sum of aryl isoprenoids demonstrate similar covariations from the base of the outcrop (Figure 3.48). This may imply that the source of the 2,3,6 trimethyl-substituted aryl isoprenoids in the zone that covaries may also be mainly from isorenieratane and, therefore, a sign of PZE.

Previous AIR calculations for the Woodford Shale have also encountered high values in the Upper Woodford member (6.09-12.80) by Miceli-Romero (2010) and Jones (2017), which were attributed to relatively oxic conditions (Miceli-Romero and Philp, 2012), but the high preservation of aryl isoprenoids and carotenoids between the lower portion of the Upper member in the SR outcrop would suggest otherwise. In the case of the Upper Woodford, differences in the

AIR between this and previous studies may arise from regional differences in the organic deposition, since the SR section is a restricted and anoxic Woodford deposit (Figure 3.48).

Figure 3.48 illustrates the SR variation of AIR for each Woodford member. For the Lower member, it can be observed at the base (10 to 40 ft) an AIR value of 2.0 – 5.0, indicating that the PZA was episodic, then PZA was more persistent for the middle and upper parts of the Lower member (60 – 120 ft). At the lower part of the Middle member, PZA is persistent but increases from 120.5 – 182.5 ft (Figure 3.48). At the MFS (194.5 ft) the AIR has a sharp increase (1.5 – 3.0) and is interpreted that the PZA was episodic, then after the MFS, the PZA is variable, with a general low trend of AIR value (0.5-1.5) indicating variable episodic PZA (Figure 3.48). The Upper Woodford member has higher AIR values and PZA is interpreted as episodic (Figure 3.48).

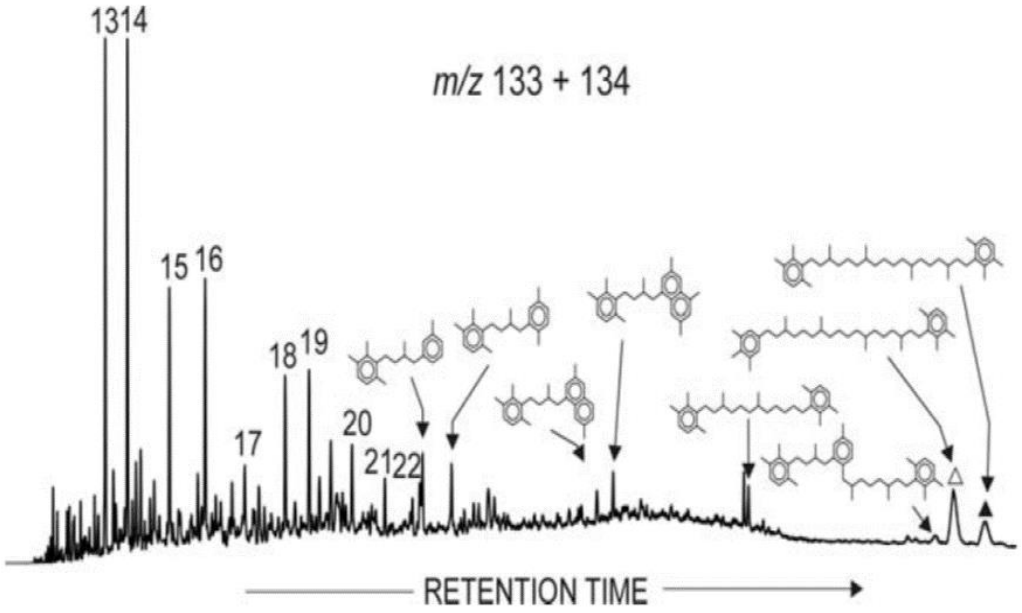

Figure 3.45. Summed mass chromatogram m/z 133 + 134 of the organic-rich Devonian shale sample in Marynowski and Filipiak (2007), showing the distribution of isorenieratane (filled triangle), 2,3,6-/3,4,5-TM substituted diaryl-isoprenoid (white triangle) and their related derivatives including aryl isoprenoids (numbers identify individual carbon number pseudohomologues).

Sample ID	Outcrop Depth	Kmeans Facies	Leco TOC%	Gamm. Index	AIR	Isorenieratane µg/g EOM	Paleorenieratane µg/g EOM	Renierapurpurane µg/g EOM
SR-Y326	314.0	1	9.04	0.03	0.58	1.22	10.54	0.20
SR-X16b	296.5	6	30.20	0.11	2.05	5.42	46.81	0.88
SR-X7b	287.5	1	12.10	0.13	1.61	8.78	53.98	1.01
SR-271b	271.5	6	21.00	0.17	0.90	5.31	71.69	1.34
SR-243a	243.0	0	4.50	0.11	1.43	0.88	11.22	0.21
SR-230b	230.5	1	11.10	0.09	1.25	1.46	37.95	0.71
SR-229a	229.0	0	9.74	0.17	1.21	2.36	30.84	0.58
SR-227b	227.5	1	11.20	0.12	0.84	2.61	36.36	0.68
SR-226b	226.5	1	11.50	0.10	0.71	0.62	41.66	0.78
SR-224b	224.5	1	12.00	0.10	1.61	0.83	40.14	0.75
SR-223a	223.0	7	1.00	0.09	0.39	0.54	35.84	0.67
SR-221b	221.5	1	10.80	0.14	1.13	1.35	29.46	0.55
SR-220b	220.5	1	11.80	0.16	0.12	1.62	37.90	0.71
SR-220a	220.0	0	2.82	0.14	0.38	1.24	39.04	0.73
SR-219a	219.0	0	3.16	0.19	0.96	1.37	33.41	0.63
SR-217b	217.5	4	10.20	0.20	1.47	0.21	35.26	0.66
SR-211b	211.5	1	12.30	0.19	0.62	3.18	81.39	1.53
SR-210b	210.5	1	12.10	0.21	0.41	5.53	90.24	1.69
SR-209a	209.0	0	6.46	0.22	0.84	6.51	94.04	1.76
SR-208b	208.5	1	15.50	0.21	1.54	8.11	86.87	1.63
SR-206a	206.0	0	4.36	0.20	1.21	7.36	82.23	1.54
SR-205a	205.0	0	2.79	0.19	0.72	6.25	78.01	1.46
SR-195b	195.5	1	9.13	0.26	2.87	7.54	107.95	2.02
SR-194b	194.5	1	11.30	0.19	2.73	9.79	78.43	1.47
SR-193b	193.5	4	9.22	0.25	2.36	10.84	93.34	1.94
SR-191a	191.0	0	5.19	0.18	2.50	12.33	76.96	1.44
SR-190b	190.5	4	12.00	0.29	2.36	11.85	108.69	1.22
SR-185b	185.5	3	7.04	0.21	2.45	9.20	89.82	1.68
SR-182b	182.5	1	8.65	0.21	1.55	9.34	88.85	1.67
SR-170b	170.5	0	1.95	0.11	1.21	9.87	47.23	0.89
SR-159b	159.5	4	8.71	0.09	0.97	11.34	38.80	0.73
SR-152b	152.5	3	8.33	0.12	0.77	8.66	49.76	0.93
SR-142b	142.5	5	8.42	0.09	0.45	7.00	39.22	0.73
SR-134b	134.5	4	8.97	0.11	0.38	19.09	46.39	0.87
SR-129a	129.0	7	2.49	0.16	0.63	8.71	65.78	1.23
SR-120b	120.5	1	3.79	0.11	0.41	3.41	48.07	0.90
SR-118c	118.8	9	4.15	0.09	0.29	3.93	39.22	0.73
SR-110b	110.5	4	7.00	0.10	0.38	3.72	40.06	0.75
SR-90	90.0	4	8.28	0.19	0.36	4.73	78.43	1.47
SR-72b	72.5	1	14.40	0.20	0.91	5.64	86.02	1.61
SR-60a	60.0	0	3.58	0.11	0.73	3.18	48.07	0.90
SR-42b	42.5	1	14.60	0.20	2.58	3.02	83.49	1.56
SR-30	30.0	5	15.30	0.25	3.65	5.80	103.31	1.94
SR-28a	28.0	4	10.70	0.16	2.42	2.33	65.78	1.23
SR-14	14.0	1	13.00	0.13	0.91	5.56	19.20	0.36

Table 3.7. Aryl-isoprenoid and C_{40} carotenoid concentrations in the Speake Ranch Woodford 314 ft stratigraphic section with the respective K-means facies and %TOC (Leco column). C_{40} carotenoid concentration normalized with amounts of extracted organic matter (EOM) after Soxhlet extractions (not to %TOC).

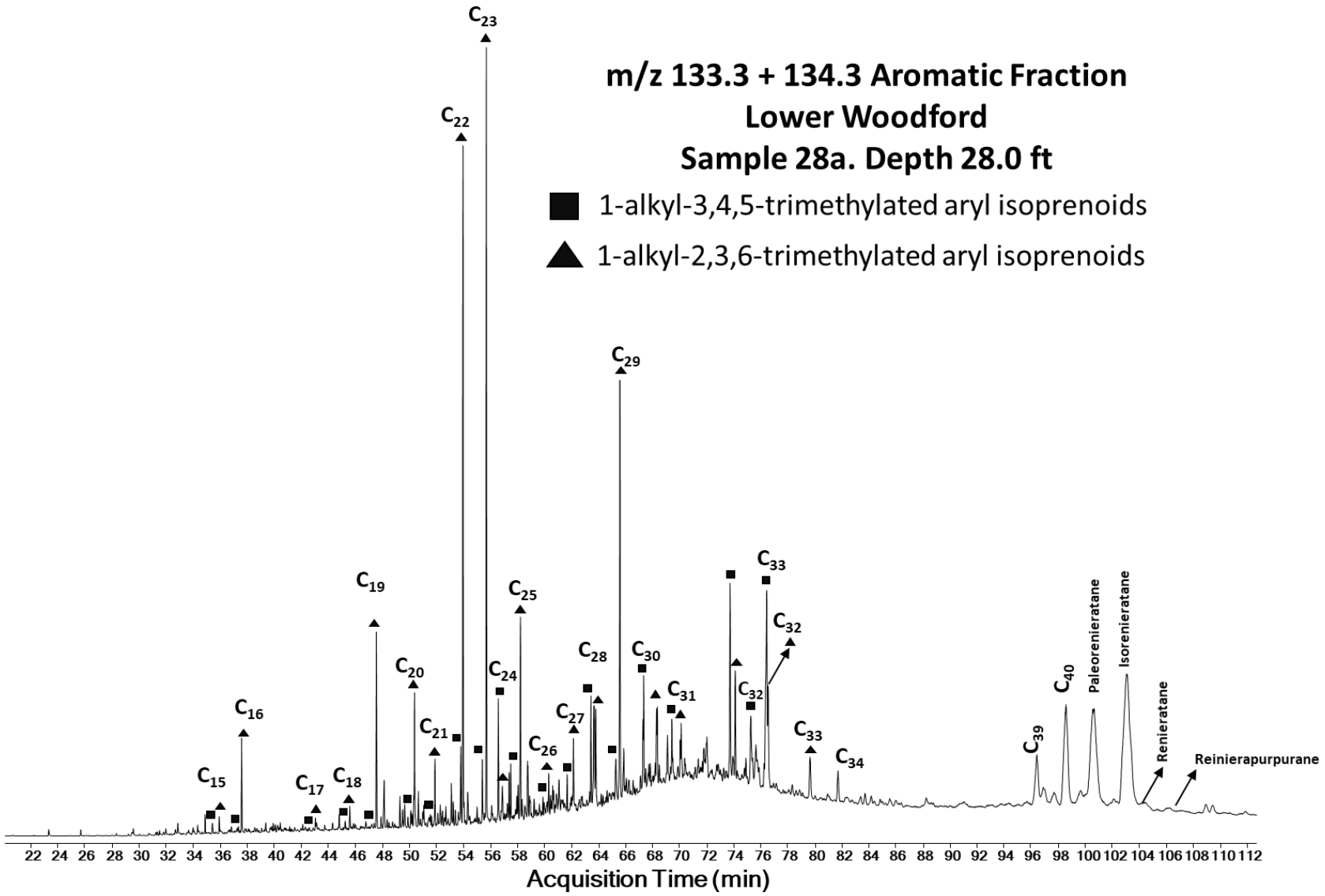

Figure 3.46. Identification of aryl isoprenoids, and C_{40} carotenoids using m/z 133 + 134. Depth 28.0, Lower Woodford member.

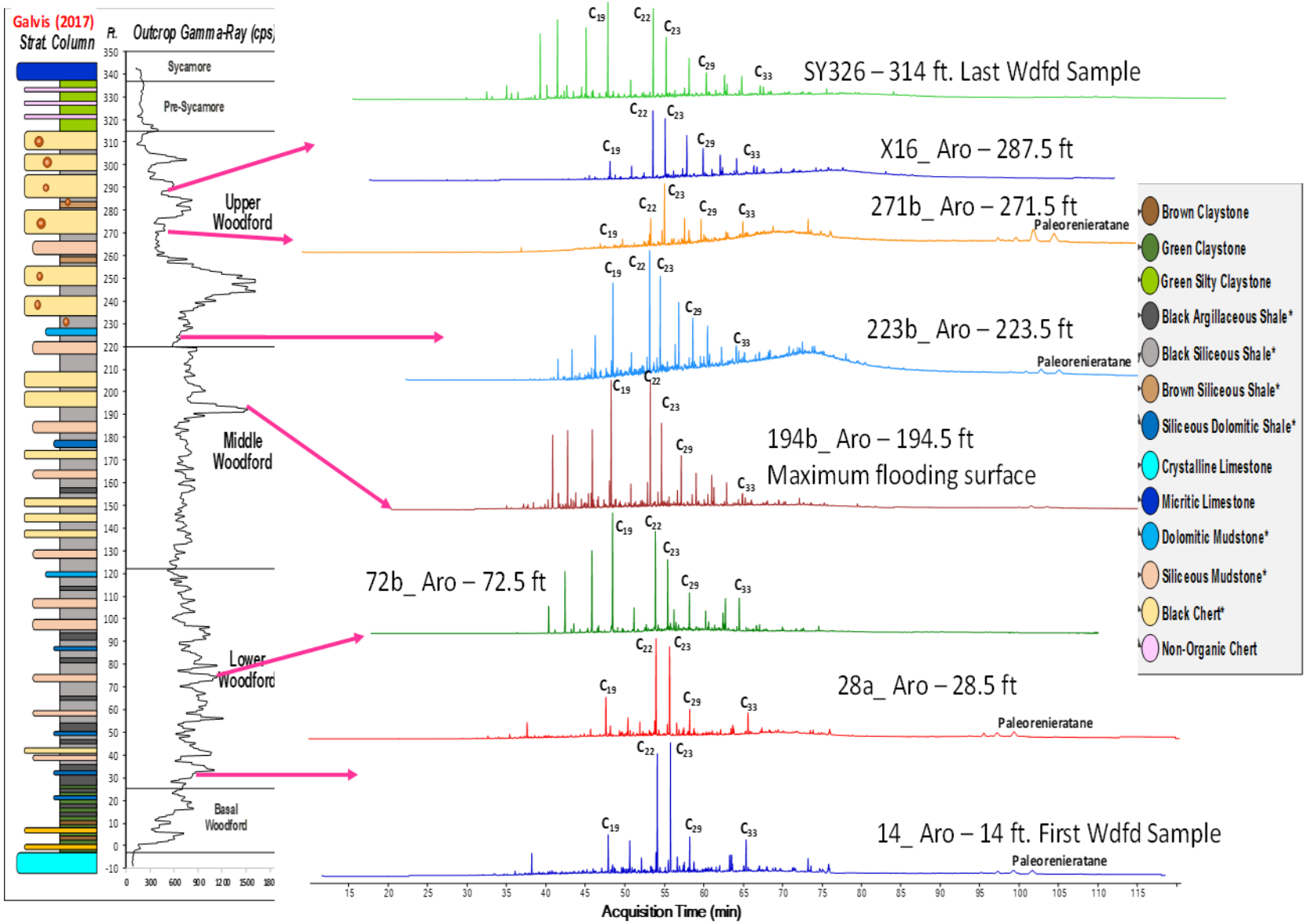

Figure 3.47. Aryl-isoprenoids and C_{40} carotenoids identified in the m/z 133+134 fraction of different Woodford member samples.

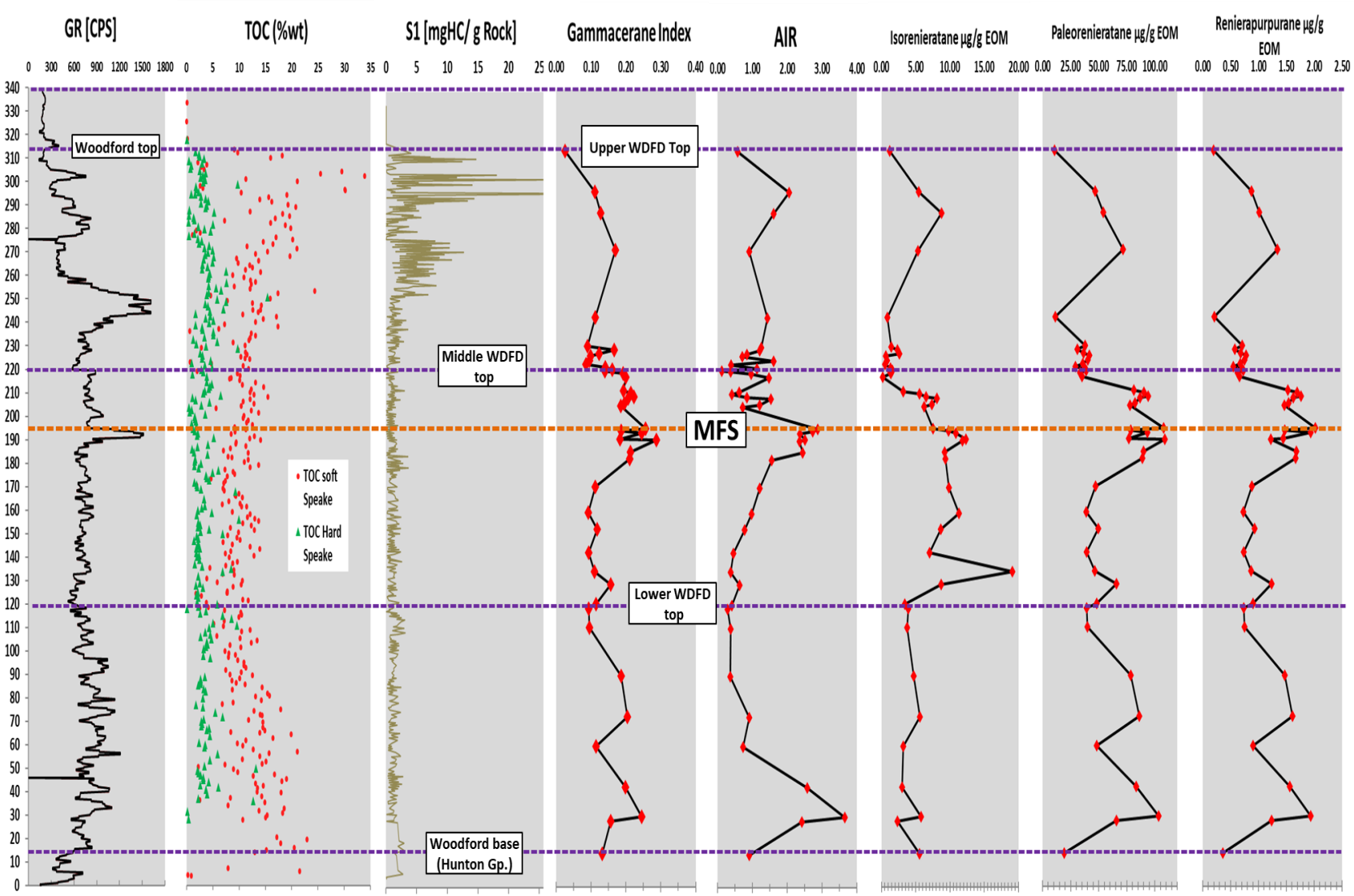

Figure 3.48. Comparison of gammacerane index and C_{40} carotenoids abundance, as compared to Gamma-Ray log and %TOC classified by the mechanical stratigraphy of the rock layers (soft vs. hard; Galvis, 2017).

3.5.9. Polycyclic aromatic hydrocarbons (PAHs)

Polycyclic aromatic hydrocarbons (PAHs) are the result of diagenetic and catagenic processes, which cause the aromatization of organic compounds prevalent in sediments and oils. As such PAHs do not precisely meet the definition of biomarkers (Alexander et al., 1992; Stout et al., 2015). The PAHs can be identified in the SR section, and as discussed by DeGarmo (2015), Jones (2017), and Philp and DeGarmo (2020) are useful for addressing potential terrestrial inputs to the Woodford Shale in southern Oklahoma. These PAHs include phenanthrenes, dibenzothiophenes, dibenzofurans, fluoranthene, benzofluoranthenes, perylenes, benzoperylenes, pyrenes, benzopyrenes, biphenyl, cadalene, chrysene, benzoanthracene, and triphenylene. If these terrestrial organic matter compounds are present or mixed with marine-sourced organic matter, the mechanisms that formed this mixture requires (1) transport of material from the continent to the marine setting, and (2) preservation of organic material after transport mechanical reworking and physical degradation (Connan et al., 1980; Tissot and Welte, 1984; Jiang, 1998; Widayat, 2011, Li et al., 2012; DeGarmo, 2015; Fang et al., 2015; Widayat et al., 2016; Jones, 2017).

The occurrence of the terrestrial plant biomarkers in a marine setting would require transportation of continental material from river runoff, progradation, or transgression onto a previously exposed soil horizon where PAHs may have accumulated. These events are possible during sea-level fluctuations (drops in sea-level) during the depositional periods of the Woodford Shale. Fluoranthene, pyrene, perylene, benzo (e)pyrene, benzo(a)pyrene, benzo (g,h,i) pyrene have been identified in the Middle and Upper members SR Woodford samples SR as terrestrial indicators (Table 3.8; Figure 3.49). The identification of high concentrations of these PAHs is a direct implication for the sequence stratigraphic framework of the SR, as higher concentrations would be expected during a transition from transgressive system tract (TST) to highstand system

tract (HST) settings (sea-level drop that leads to progradational depositions towards the paleo basin). DeGarmo (2015) and Jones (2017) provided an example for the Woodford Shale in southern Oklahoma and Marynowski et al. (2000 and 2015) for other Devonian shales, that indicated dibenzofuran was a prototypical biomarker that could be used to identify plant input from continental sources (Figure 3.50). Septhon et al. (2005), and Mizukami et al. (2013 and 2014) recognized dibenzofuran (DBF) as a product of weathered terrestrial organic matter, and for this reason, it is proposed for the Woodford Shale in the SR as a possible indicator of soil erosion material transported towards the deeper basinal deposits via progadational events.

Other PAHs detected in the Woodford Shale in southern Oklahoma, and proposed for the SR, which are also known to be derived from similar terrestrial plant origins include cadalene (a bicyclic compound derived from sesquiterpenoids; Jones, 2017) and perylene, which is not thought of as a direct product of higher plants (DeGarmo, 2015; Marynowski et al., 2015; Jones, 2017), but is instead considered a product of wood-degrading fungus, thus making it an indicator of terrestrial plant input (Marynowski et al., 2015; Figure 3.50 and Figure 3.51).

The PAHs tied to decomposed terrestrial plants, including pyrene, chrysene, DBF, and cadalene, showed increased concentrations in the Upper-Middle Woodford members boundary, followed by diminishing values towards the Upper Woodford member (Figure 3.51). This trend was also observed by DeGarmo (2015), Jones (2017), and Philp and DeGarmo (2020) for the Woodford Shale in other southern Oklahoma outcrops. Pyrene and perylene are frequently found with a suite of PAHs related to the partial combustion of organic matter from both forest fires and petroleum, including (but not limited to) fluorene, benzo(e)pyrene (BeP), benzo(a)pyrene (BaP), and benzo (g, h, i) perylene (BghiP) (Aizenshtat, 1973; Laflamme and Hites, 1978; Lichtfouse et al., 1997; Nabbefeld et al., 2010). Marynowski and Filipiak (2007), and Marynowski et al. (2015)

used artificial maturation to track the transformation and degradation of perylene into its thermal products. Figure 3.51 shows the higher content towards the end of the Middle Woodford Shale member and increasing in the uppermost upper Woodford member, which coincides with the start of the drop of sea level at the end of Woodford Shale and more progradation deposits into the basin.

Sample ID	Outcrop Depth	Kmeans Facies	Leco TOC%	DBT µg/g EOM	Cadalene µg/g EOM	Perylene µg/g EOM	DBF µg/g EOM	benzo a + chrysene µg/g EOM
SR-Y326	314.0	1	9.04	0.58	0.70	8.24	0.65	0.22
SR-X16b	296.5	6	30.20	2.59	0.77	9.10	2.89	1.00
SR-X7b	287.5	1	12.10	4.20	0.51	6.01	4.68	1.62
SR-271b	271.5	6	21.00	2.54	0.56	6.60	2.83	0.98
SR-243a	243.0	0	4.50	0.42	0.48	5.66	0.47	1.16
SR-230b	230.5	1	11.10	0.70	0.69	8.10	0.78	0.76
SR-229a	229.0	0	9.74	1.13	0.55	6.47	1.26	0.43
SR-227b	227.5	1	11.20	1.25	0.85	10.04	1.39	0.48
SR-226b	226.5	1	11.50	0.30	0.75	8.88	0.33	0.41
SR-224b	224.5	1	12.00	0.40	0.16	1.87	0.44	0.52
SR-223a	223.0	7	1.00	0.26	0.31	3.63	0.29	0.61
SR-221b	221.5	1	10.80	0.64	0.46	5.41	0.72	0.55
SR-220b	220.5	1	11.80	0.77	0.59	6.98	0.86	0.49
SR-220a	220.0	0	2.82	0.59	0.57	6.67	0.66	0.23
SR-219a	219.0	0	3.16	0.65	0.45	5.33	0.73	0.25
SR-217b	217.5	4	10.20	0.10	0.37	4.30	0.11	0.04
SR-211b	211.5	1	12.30	1.52	0.24	2.83	1.69	0.59
SR-210b	210.5	1	12.10	2.64	0.59	6.92	2.95	1.02
SR-209a	209.0	0	6.46	3.11	0.40	4.75	3.47	1.20
SR-208b	208.5	1	15.50	3.88	0.46	5.39	4.32	1.49
SR-206a	206.0	0	4.36	3.52	0.57	6.70	3.92	1.36
SR-205a	205.0	0	2.79	2.99	0.66	7.82	3.33	1.15
SR-195b	195.5	1	9.13	3.61	0.78	9.22	4.02	1.05
SR-194b	194.5	1	11.30	4.68	0.58	6.84	5.22	0.75
SR-193b	193.5	4	9.22	5.18	0.76	8.94	5.78	0.98
SR-191a	191.0	0	5.19	5.89	0.83	9.73	6.57	0.63
SR-190b	190.5	4	12.00	5.66	0.49	5.72	6.32	0.60
SR-185b	185.5	3	7.04	4.40	0.33	3.83	4.90	0.47
SR-182b	182.5	1	8.65	4.46	0.42	4.99	4.98	0.48
SR-170b	170.5	0	1.95	4.72	0.53	6.27	5.26	0.50
SR-159b	159.5	4	8.71	5.42	0.33	3.83	6.05	0.58
SR-152b	152.5	3	8.33	4.14	0.25	2.93	4.61	0.44
SR-142b	142.5	5	8.42	3.35	0.46	5.42	3.73	0.36
SR-134b	134.5	4	8.97	9.13	0.26	3.05	10.18	0.97
SR-129a	129.0	7	2.49	4.16	0.25	2.92	4.64	0.44
SR-120b	120.5	1	3.79	1.63	0.16	1.87	1.82	0.17
SR-118c	118.8	9	4.15	1.88	0.27	3.13	2.09	0.20
SR-110b	110.5	4	7.00	1.78	0.12	1.45	1.98	0.19
SR-90	90.0	4	8.28	2.26	0.23	2.68	2.52	0.24
SR-72b	72.5	1	14.40	2.70	0.05	0.64	3.01	0.29
SR-60a	60.0	0	3.58	1.52	0.24	2.78	1.69	0.16
SR-42b	42.5	1	14.60	1.44	0.36	4.22	1.61	0.15
SR-30	30.0	5	15.30	2.77	0.12	1.36	3.09	0.30
SR-28a	28.0	4	10.70	1.12	0.16	1.84	1.24	0.12
SR-14	14.0	1	13.00	2.66	0.06	0.71	2.97	0.28

Table 3.8. Applied polycyclic aromatic hydrocarbons (PAHs) in the Speake Ranch Woodford 314 ft stratigraphic section. K means corresponds to each geostatistical analysis of Rock-Eval data with XRF data for defining unsupervised facies clustering. Ten facies from 0 – 9 are identified. PAHs data comparison with the respective K-means facies and %TOC (Leco column) for identifying progadational terrestrial organic matter inputs towards deeper basinal deposits of the Woodford Shale. PAHs concentrations in µg/g EOM.

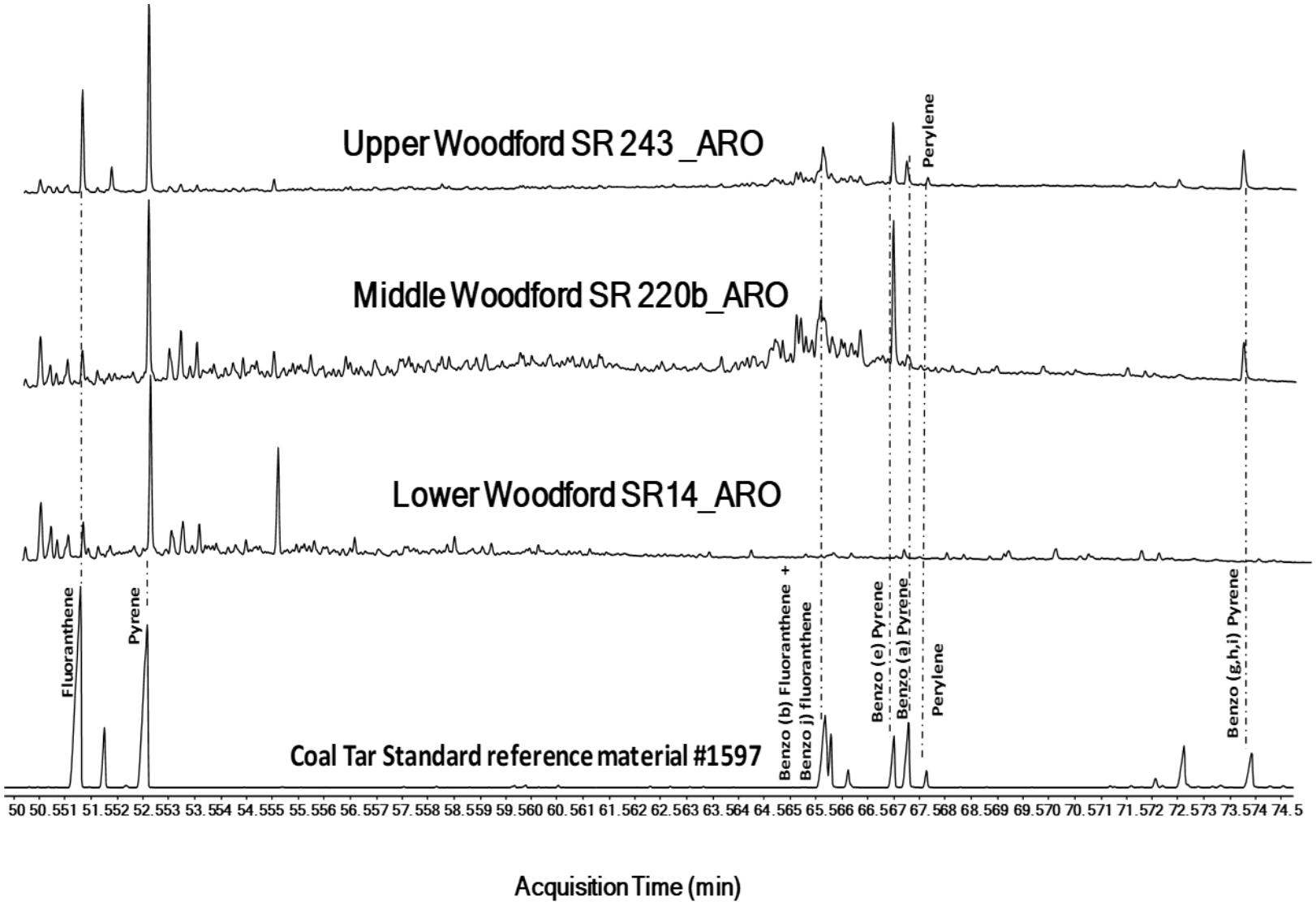

Figure 3.49. GC-MS identification of fluoranthene, pyrene, benzofluoranthenes, benzopyrenes, and perylene, by comparing previously identified peaks for the coal tar standard with peaks in the Lower, Middle, and Upper Woodford member samples. M/z 202+252+276

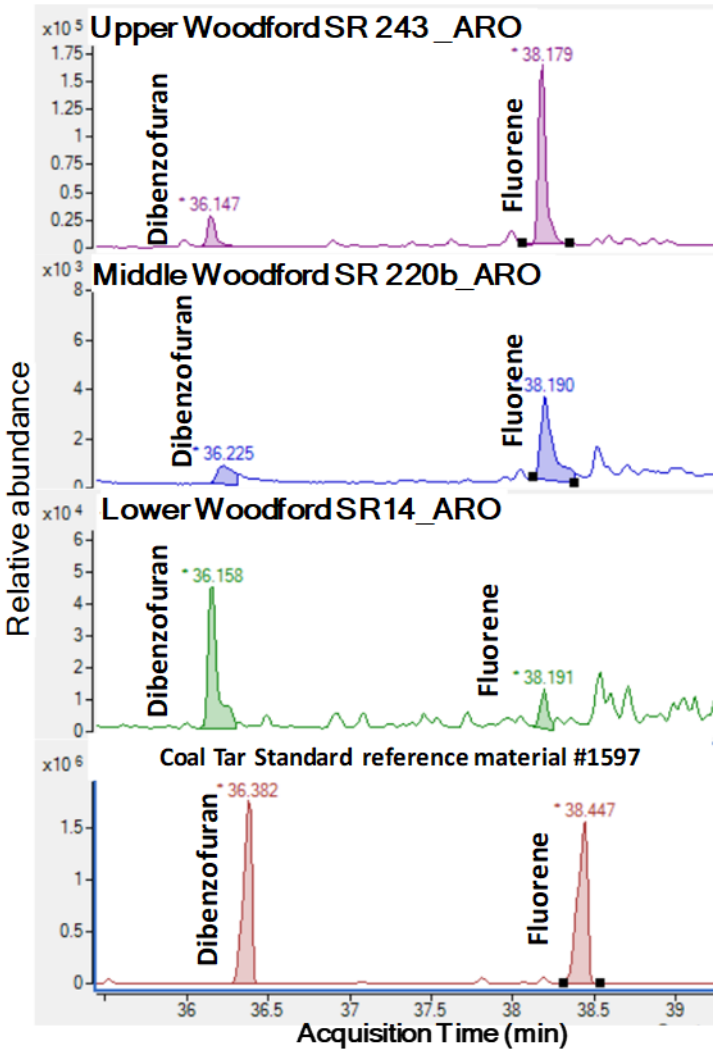

Figure 3.50. GC-MS identification of dibenzofuran and fluorene by comparing previously identified peaks for the coal tar standard reference material #1597 with peaks in the Lower, Middle, and Upper Woodford members samples. M/z 166.3+168.3 ions. Retention times of the compounds shown with their relative abundance. Differences in the retention times of the standard vs. the samples are related to a change of the GC column length that affected in a difference of 0.3 minutes of the retention times.

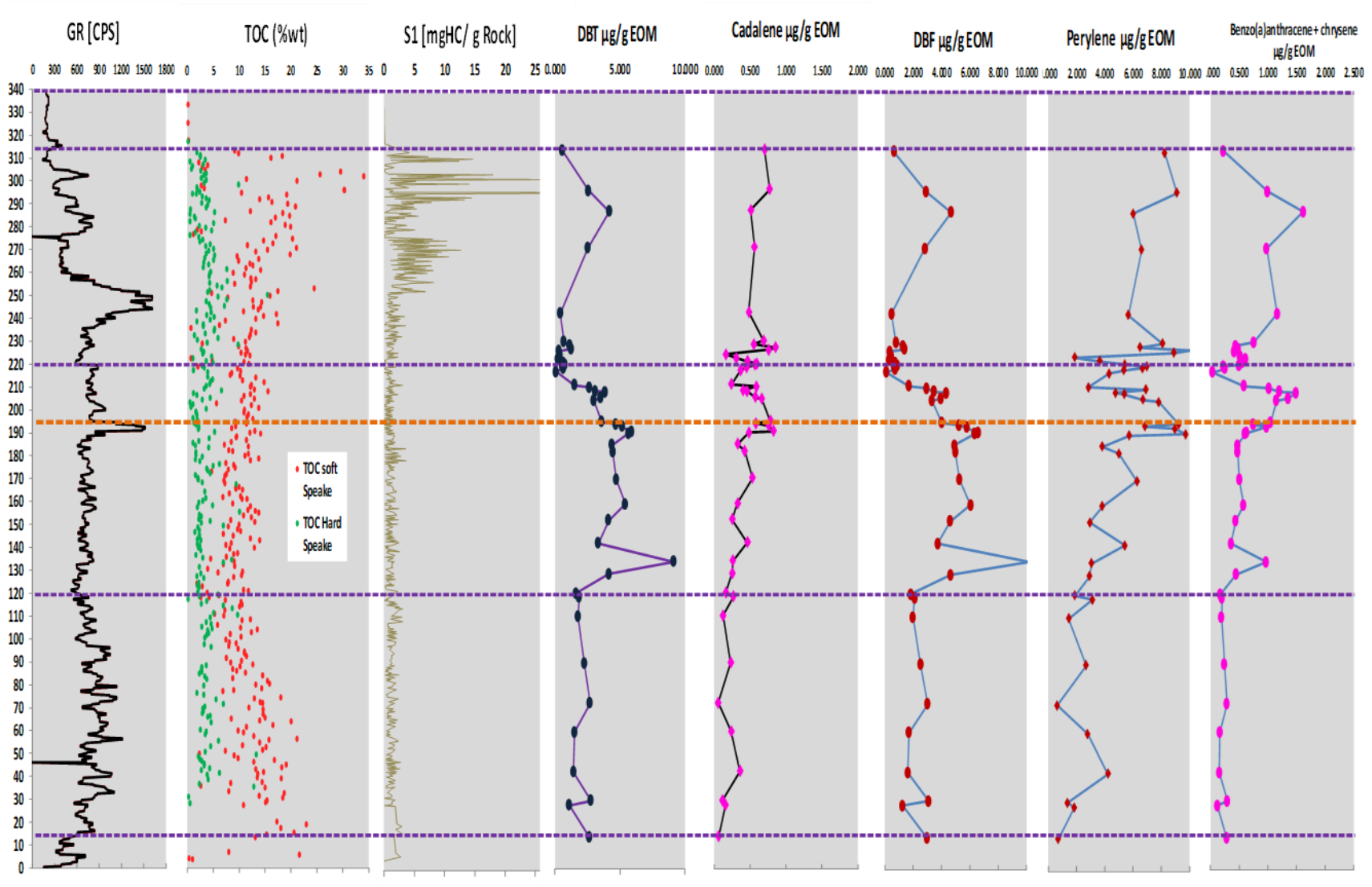

Figure 3.51. Comparison of polycyclic aromatic hydrocarbons (PAHs) concentrations to the Gamma-ray log and %TOC classified by the mechanical stratigraphy of the rock layers (soft vs. hard; Galvis, 2017).

3.5.10. Possible mass extinction events in the Speake Ranch stratigraphic section

The higher gammacerane index, high isorenieratane, and paleorenieratane concentrations, coupled with high DBT, DBF, all increasing in abundance towards the bottom of the outcrop suggests water column stratification, high salinity in the paleo-water conditions, and H_2S abundance. These factors are typically associated with restricted, reducing conditions, and match the pre-criteria for enclosed mini-basin fill settings within a marine depositional system. Additionally, aryl isoprenoids and carotenoids from *Chlorobiaceae*, which require PZE for habitation, demonstrate instances of euxinia in the basin, which starts at the base of the Lower member, ending in the lower part of the Woodford Upper member deposition. An interval of persistent PZE conditions is associated with a significant period of established water column stratification within this section of the Woodford Shale. It can be observed that at least on seven occasions (three times in the Lower, twice in the Middle Woodford member, and twice in the Upper Woodford member), these cyclical periods demonstrate prominent stratification (~15-40 feet of gross thickness of these intervals).

The abundances of aryl isoprenoids, carotenoids, DBT and gammacerane, coincide and point to a distinct period of persistent PZE mostly for the Lower Woodford and Middle Woodford members, and slightly in the Upper Woodford member. Moreover, this study proposes high concentrations of high isorenieratane and paleorenieratane, coupled with high concentrations of DBT, DBF pyrene, chrysene, and cadalene as evidence of ecologic stress that characterized the primary extinctions of the Devonian period. The extinction events in the Late Devonian period proposed for the SR are the Kellwasser and Hangenberg (K&H) events. The K&H events have been recognized for the Devonian period by McGhee (1981 and 1996), Sandberg et al. (1988), Nabbefeld et al. (2000), Nowaczewski (2011), Becker et al. (2012), and Kaiser et al., (2015).

Galvis et al. (2017a and 2017b), and Becerra-Rondon (2017) proposed these K&H events in the SR after a stratigraphic correlation to subsurface wells, locating the K&H in the interval of 190-240 ft. Jones (2017) proposed the K&H events to be present in the Woodford Shale, in a nearby section of the SR Arbuckle Mountains structural trend. Connock et al. (2018) using biomarker analyses, and Molinares (2019) using palynology analyses, identified the K&H as well for the Woodford Shale in the Arkoma basin, Oklahoma.

In the Woodford Shale SR section, the biomarker indicators of terrestrial organic matter and pyrogenic origins, coupled with PZE conditions, suggest the K&H extinction events are present in the south SCOOP Oklahoma petroleum province. These lines of evidence of the K&H events are principally based on the increased abundance of PAHs such as cadalene, perylene, fluorene, dibenzofuran, etc. These PAH abundances suggest that the increased terrestrial input from land plants during the late Devonian, likely upset marine life by contributing to harsh, anoxic conditions that killed off many species between the Frasnian-Famennian (F-F) and Devonian-Carboniferous (D-C) boundaries. From the biomarker analysis, it is interpreted that the F-F event is located between 194.5 to 210 ft of SR (Figure 3.48 and Figure 3.51). This interpretation narrows the stratigraphic interval proposed by Galvis (2017), and Galvis et al. (2017a and 2017b), but the precise location of these F-F and D-C boundaries within the 314 ft of Woodford Shale SR stratigraphic section will require a much more detailed biomarker analysis coupled with biostratigraphic end of species recognitions, that should cover a closer vertical sample spacing than the one applied in this study.

It is proposed that for the Middle, and Lower Woodford Shale, the intervals with the excessive terrestrial organic matter was accumulated due to the diversification of land plants, which likely suppressed the marine ecosystem, and eventually led to a significant destruction of

the existing Devonian biota. The increased nutrients available caused the blooming of marine fauna, followed by over-consumption of oxygen, and therefore O_2-poor waters. At these intervals, high amounts of organic matter are preserved under euxinic conditions, and when found, may point to specific, regionally correlative units within the Woodford Shale that could be rich in hydrocarbons.

3.5.11. Biodegradation

The SR sampled areas correspond to an old open quarry that floods during the rainy season. According to Ghosh (2017), the SR has outcrops over millions of years, with the significant tectonic uplifts starting after the end of the Mississippian-Pennsylvanian orogeny of the Arbuckle Mountains in southern Oklahoma. Also, the sampled rocks are in some small creeks and streams that cut the rocks of the SR (Galvis, 2017). These creeks provide outcrop exposure, and the rock samples have likely suffered chemical alterations from surface exposure, constant water recharge, and weathering over these long periods. The term "biodegradation" has been most commonly and extensively used for reservoirs and crude oils, rather than for soluble bitumen in source rock cores and outcrops. The occurrence of biodegradation affecting outcrops is enhanced by weathering and the different events of freshwater washing, as has been reported in the Woodford Shale outcrops in southern Oklahoma by Lin et al. (1989), Michael et al. (1989), Philp et al. (1989), Lo and Cardott (1995), DeGarmo (2015) and Jones (2017).

Biodegradation is a process where anaerobic bacteria are the primary factors in subsurface degradation of crude oil (Wilkes et al., 2000; Wenger et al., 2002; Grasby et al., 2009). Peters and Moldowan (1993) stated that oil could be catabolized (break down of large molecules) by aerobic and anaerobic bacteria only if several requirements are satisfied. These are: (i) access to surface

recharge waters containing oxygen; (ii) temperatures no more than about 65 to 80°C; (iii) the crude oil must be free of H_2S, which poisons the bacteria (Peters and Moldowan, 1993).

The constant water recharge and prolonged surface exposure of the SR probably are the main elements that stimulated the weathering and biodegradation processes in the outcrop. Biodegradation can be understood as sequential because some of the less resistant organic compound classes can be attacked before the destruction of the more resistant classes (Lin et al., 1989; Peters and Moldowan, 1993). The general sequence of increasing resistance to biodegradation of biomarkers is *n*-alkanes, isoprenoids, steranes, hopanes/diasteranes, aromatic steroids, and porphyrins (Lin et al., 1989; Philp et al., 1989; Chosson et al., 1992; Moldowan et al., 1992; Wenger et al., 2002).

Because of their differential resistance to biodegradation, a comparison of the amounts of biomarker types in crude oils ranks the relative extent of biodegradation (Wenger et al., 2002). The removal of biomarker groups like the n-alkane and isoprenoids recognizes the level of biodegradation for the soluble bitumen extracts of the SR samples as moderate (Figure 3.52), according to Lin et al. (1989) and Philp et al. (1989) for southern Oklahoma bitumens and the ranking proposed by Wenger et al. (2002). Wenger et al. (2002) developed a scale based on Volkman et al. (1986) and Moldowan et al. (1992) to assess the extent of biodegradation based on the relative abundance of various hydrocarbon classes (Figure 3.52). For this level of biodegradation, the biomarker interpretations of the SR samples focus on the steranes, terpanes, and aromatic hydrocarbons, and do not include precise n-alkane interpretations.

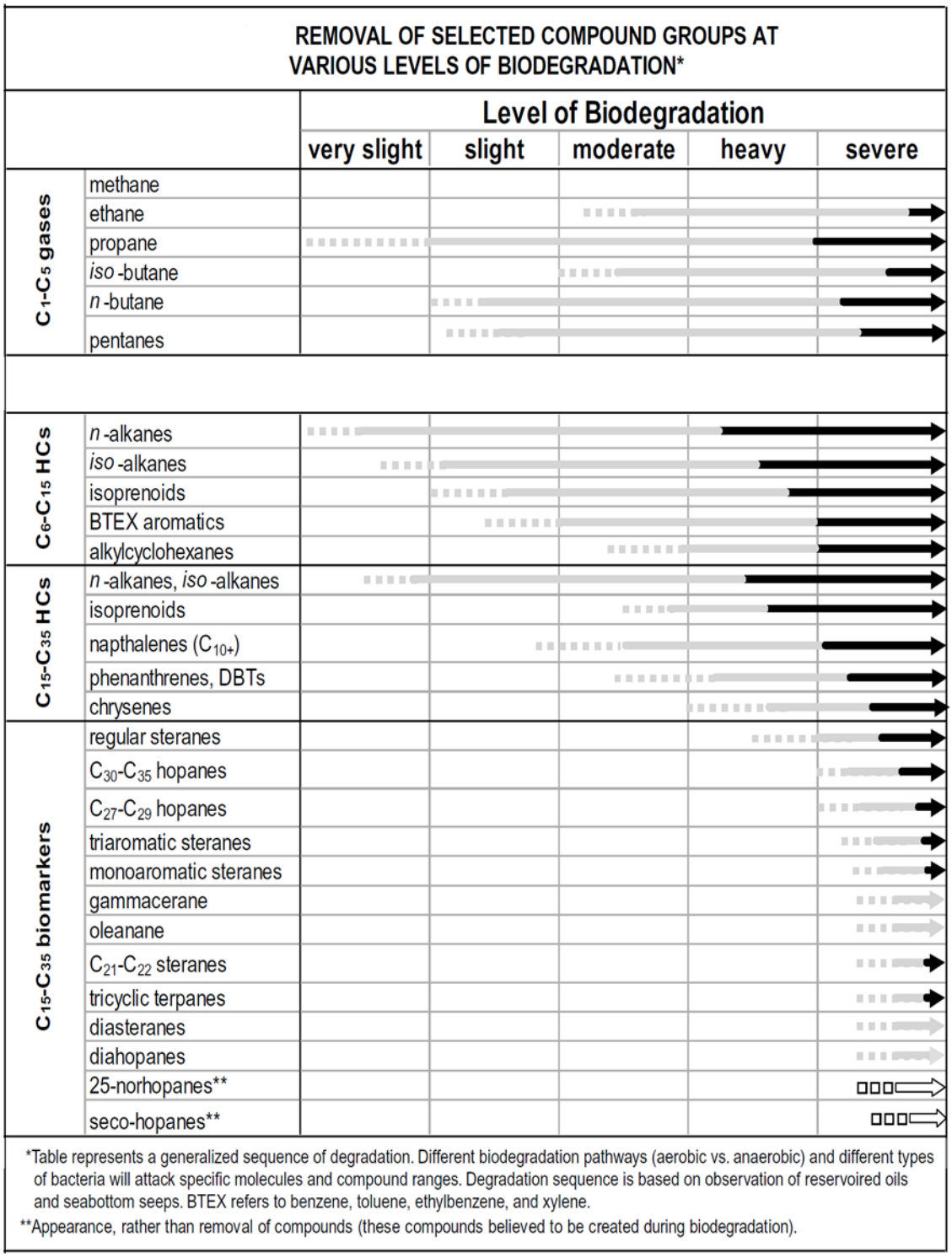

Figure 3.52. Ranking of biodegradation levels proposed by Wenger et al. (2002). This chart represents the extent of biodegradation of mature crude oil based on differing resistance of compound classes to microbial attack. Dashed lines indicate where compound classes are initially

altered, the solid gray lines indicate substantial depletion, and the black arrows indicate those that indicate complete depletion.

3.6. Geological, geochemical, and regional stratigraphic integrations in the SR.

For supplementing the organic and inorganic geochemistry analysis towards the identification of potential enclosed mini-basin fill depositional settings, a series of regional Woodford maps constructed with regional geological cross-sections are integrated into this study. One of the interpreted stratigraphic cross-sections is illustrated in Figure 3.53. This cross-section includes the SR outcrop Gamma-Ray log and allows identification of similarities in the outcrop and the subsurface wells nearby to the SR (Figure 3.53). When flattened the well log correlation cross-section on the Woodford stratigraphic top, the thickness variation of the Woodford Shale is higher where the Hunton Group thins (Figure 3.53). This paleo structural highs and lows of the Hunton group allowed the formation of silled areas and pockets and are interpreted as structural indicators that the SR locates in the flank of a significant enclosed mini-basin fill setting, with the thickest Woodford Shale in the central part of the cross-section (Figure 3.53).

The rock mechanics brittleness is much lower in the identified highly restricted intervals of the Lower and Middle Woodford members, as calculated and illustrated in Figure 3.54. Brittleness increases in the layers of more open water conditions and less anoxia (Figure 3.54; red-colored log intervals of the brittleness index track). Also, as stated by Slatt and Abousleiman (2011), in unconventional shales, this is due to a higher concentration of quartz as the principal component that provides the hardness level of individual rock layers. Figure 3.55 illustrates the rock mechanics variations and much higher brittleness index for the post-Woodford Shale Mississippian strata than the Woodford Shale layers (in Figure 3.54).

The maps of the Woodford Shale present-day depth (Figure 3.56), Woodford Shale gross thickness (Figure 3.57), Hunton group gross thickness (Figure 3.58), Woodford Shale average organic matter content (%TOC; Figure 3.59) and average maturity (Tmax ℃; Figure 3.60), were constructed with the database information of the Institute of Reservoir Characterization at the University of Oklahoma (IRC). This database consists of stratigraphic tops of thousands of vertically drilled wells, and hundreds of analyses performed on outcrop, core, and cutting rock samples. These datasets are unified into a state-wide database and published as the local to regional integration of the SR with subsurface data and nearby petroleum provinces. For the SR area, the outcrop is located in the area of highest average %TOC content (Figure 3.59), the Hunton group thins (Figure 3.58), and the Woodford Shale thickens towards the southwest (Figure 3.57).

The SR is also surrounded by a lot of faulted provinces that according to Ghosh (2017) and Galvis (2017) are the reactivation of pre-existing fault grabens that could have acted as paleo structural lows that allowed more accommodation space, higher sedimentation rates due to the proximity to the paleo Wichita uplifts sediment supply to the basin, favoring these factors to the development of restricted conditions to the water chemocline for preventing open water circulation. Ham et al. (1967), Suneson (1996 and 1997), Johnson (2008), and Ghosh (2017) mentioned that the Wichita and Ouachita orogenies occurred syn-depositionally with the Woodford Shale (410-330 My) and concluded in mid to late Mississippian.

The Wichita and Ouachita orogenies were the major period of faulting and mountain building in southern Oklahoma and western Arkansas (Suneson 1996 and 1997). The driving force behind this orogeny was the collision of the North American and Gondwanan plates (Ham 1964; Ham et al., 1967; Suneson, 1996 and 2012). The Ouachita orogeny also initiated the formation of the Arkoma basin, which is an arcuate foreland basin (Byrnes and Lawyer, 1999; Ghosh, 2017). These

mentioned tectonic events allowed the availability of accommodation space and, combined with erosion and karstification of pre-Woodford Shale strata, might allow the development of silled restricted areas in the basin that acted as highly restricted areas principally for the Lower and Middle Woodford members.

All of these mentioned characteristics are crucial factors for recognizing enclosed mini-basin fills settings within an open marine mudstone system. As observed with the different biomarker ratios integrated with the geological characterizations, the Lower and Middle members of the Woodford Shale were more anoxic and restricted. The upper part of the Middle member (after the Maximum flooding surface -MFS) and the lower part of the Upper member still have some intermittent episodes of anoxia and high sulfur (PZE), that subsequently ceased towards the uppermost Upper Woodford member. Finally, the organic matter fabric shut down in the Pre-Sycamore sections (post-Woodford Shale strata).

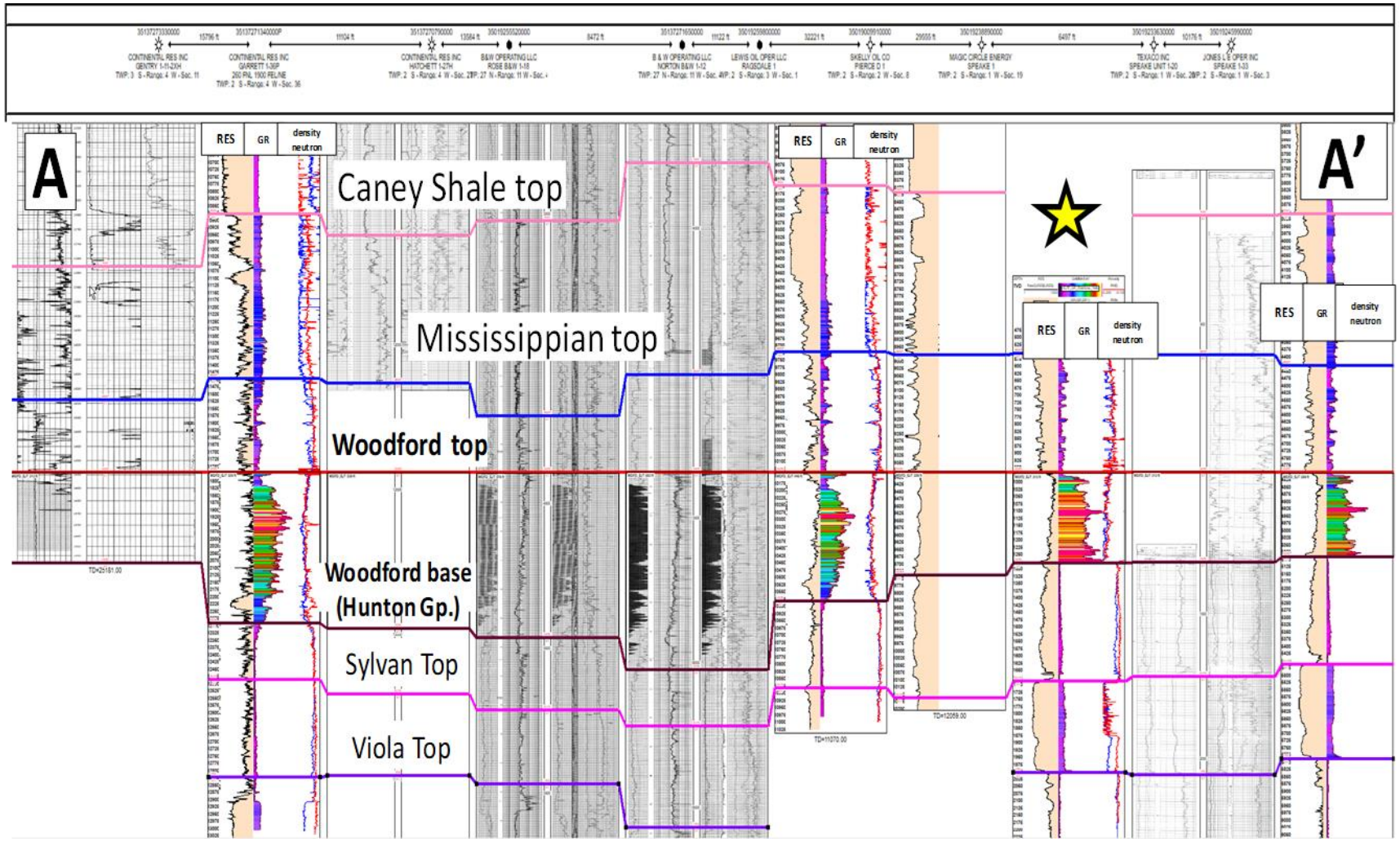

Figure 3.53. The stratigraphic cross-section in the Speake Ranch subsurface areas. The outcrop corresponds to the yellow star. The location map of this section is in Figure 3.56. When flattened on the Woodford stratigraphic top, the thickness variation of the Woodford Shale is highlighted where the Hunton Group thins. This area in the south of Oklahoma likely corresponds with the basal Woodford deposits being in an enclosed mini-basin fills paleo-topographic setting (erosion of Hunton Group and accumulation of high %TOC and restricted anoxic strata).

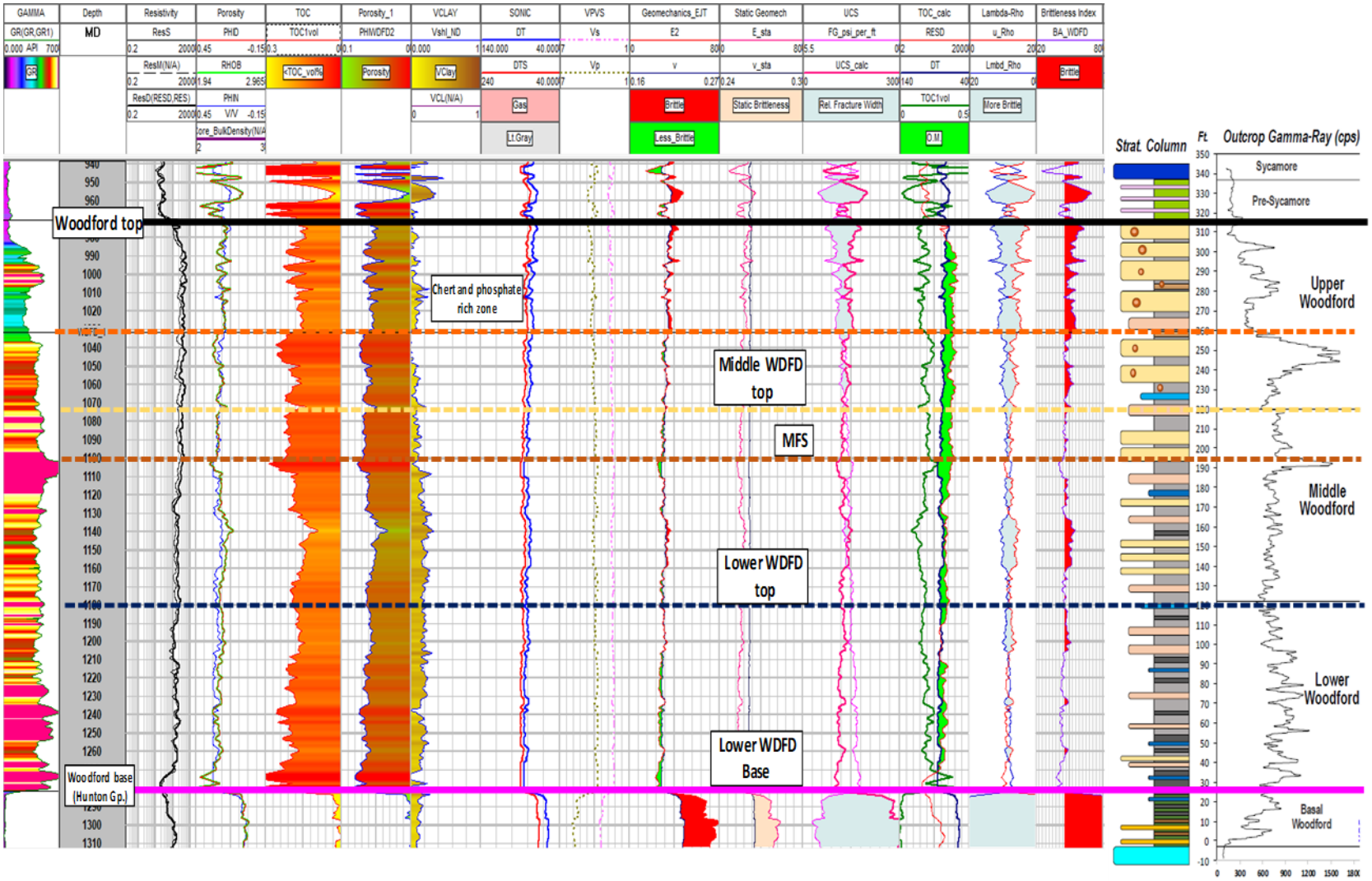

Figure 3.54. Geomechanical characterization of dynamic properties (the methodology is detailed in **Appendix 8.1**.) of the Woodford Shale strata nearby the Speake Ranch. Speake-1 well is the subsurface reference of the ranch outcrop, as is referenced in the image (similar Woodford thickness in the Speake Ranch outcrop and Speake-1 well).

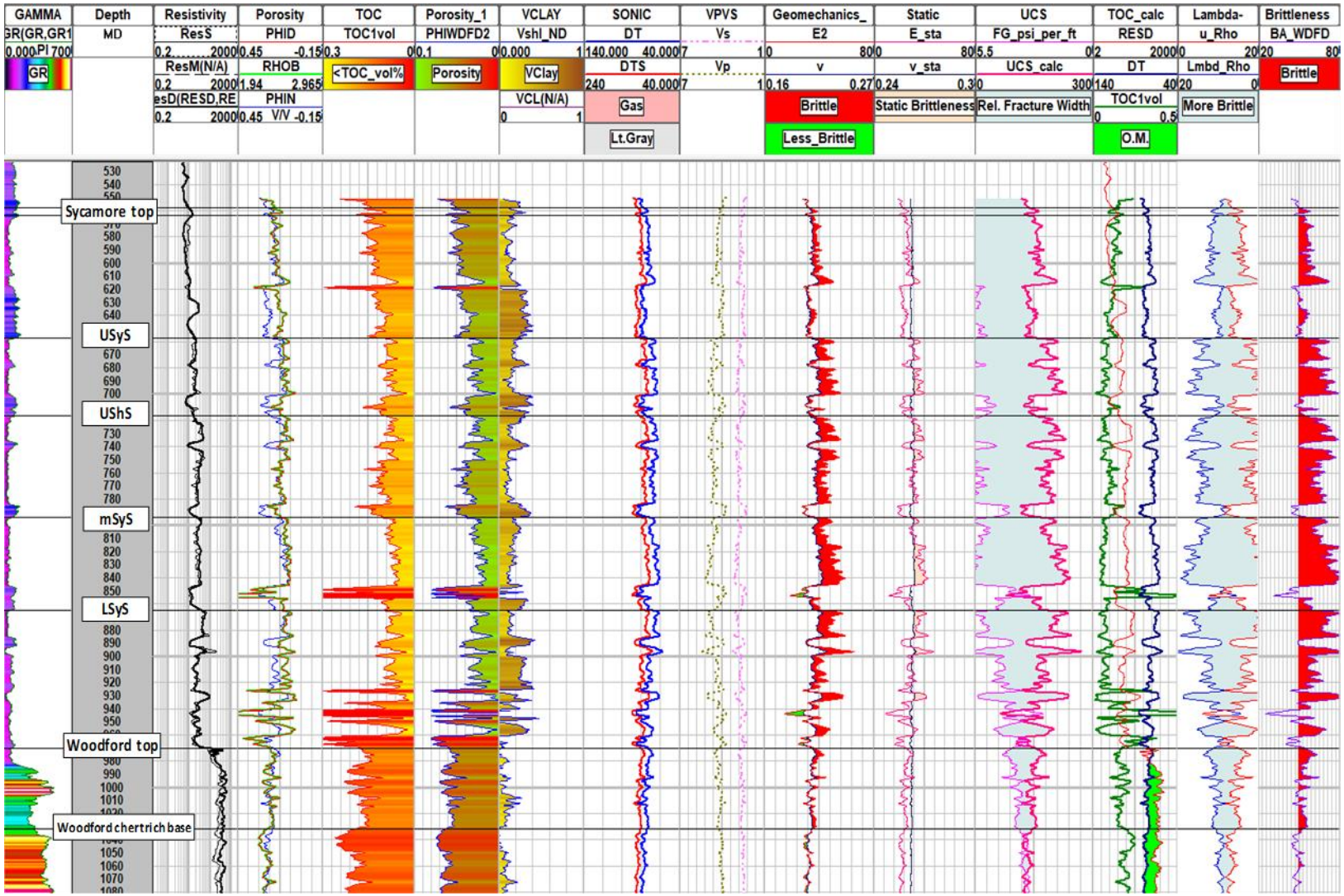

Figure 3.55. Geomechanical characterization of dynamic properties (Methodology is detailed in **Appendix 8.1.)** of the Mississippian strata nearby the Speake Ranch. Speake-1 well is the subsurface reference of the Ranch outcrop. Sycamore subdivision and labeling based on the intervals described in Milad (2019) for the southern Oklahoma I-35 Sycamore outcrop.

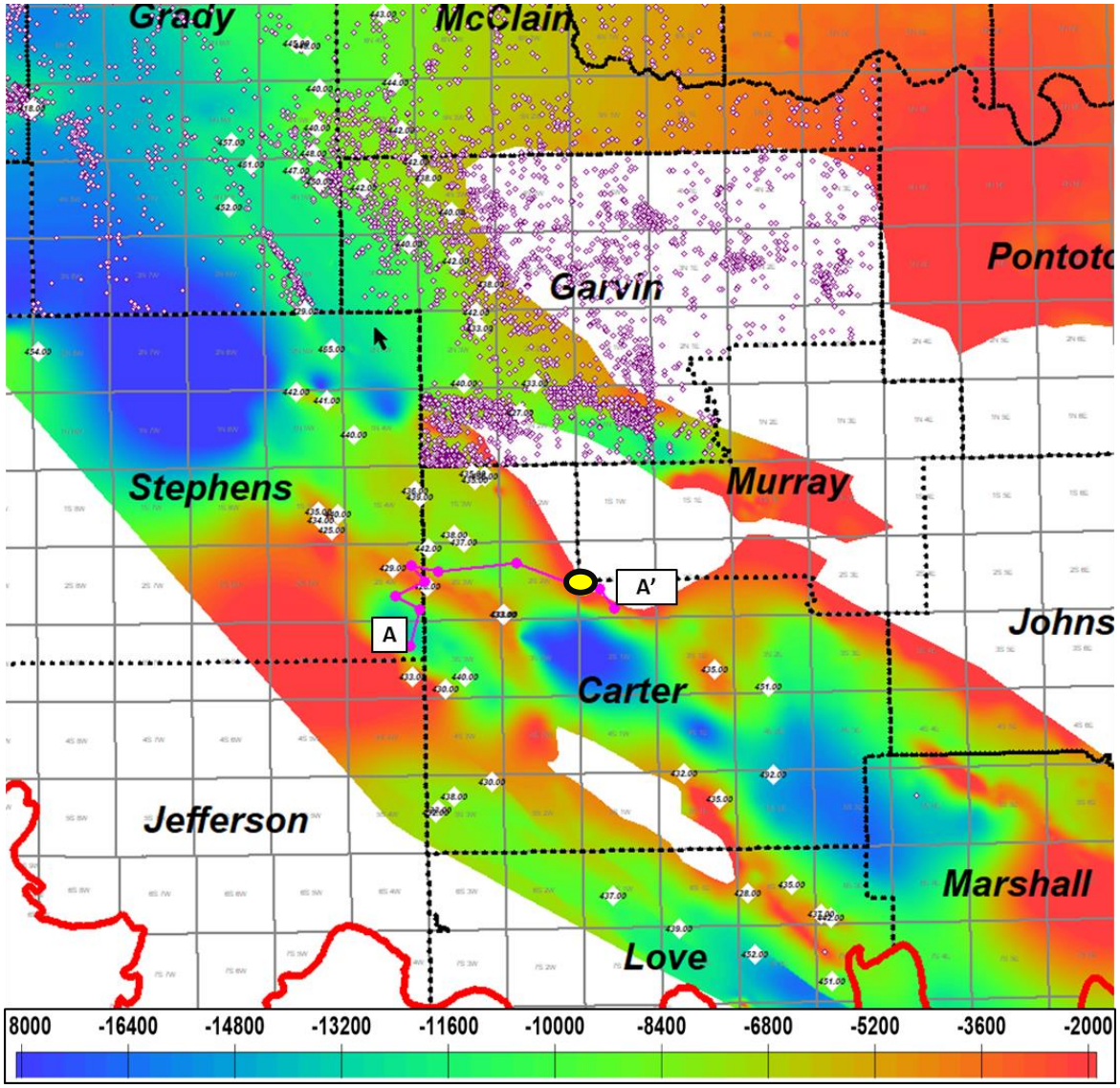

Figure 3.56. Woodford Shale structure map [TVD-feet] in the regional areas nearby the Speake Ranch. The Speake Ranch location is highlighted in the yellow spot. White diamonds and values correspond to average T-max [°C] maturity values for the Woodford Shale from the IRC Woodford-Mississippian consortium database.

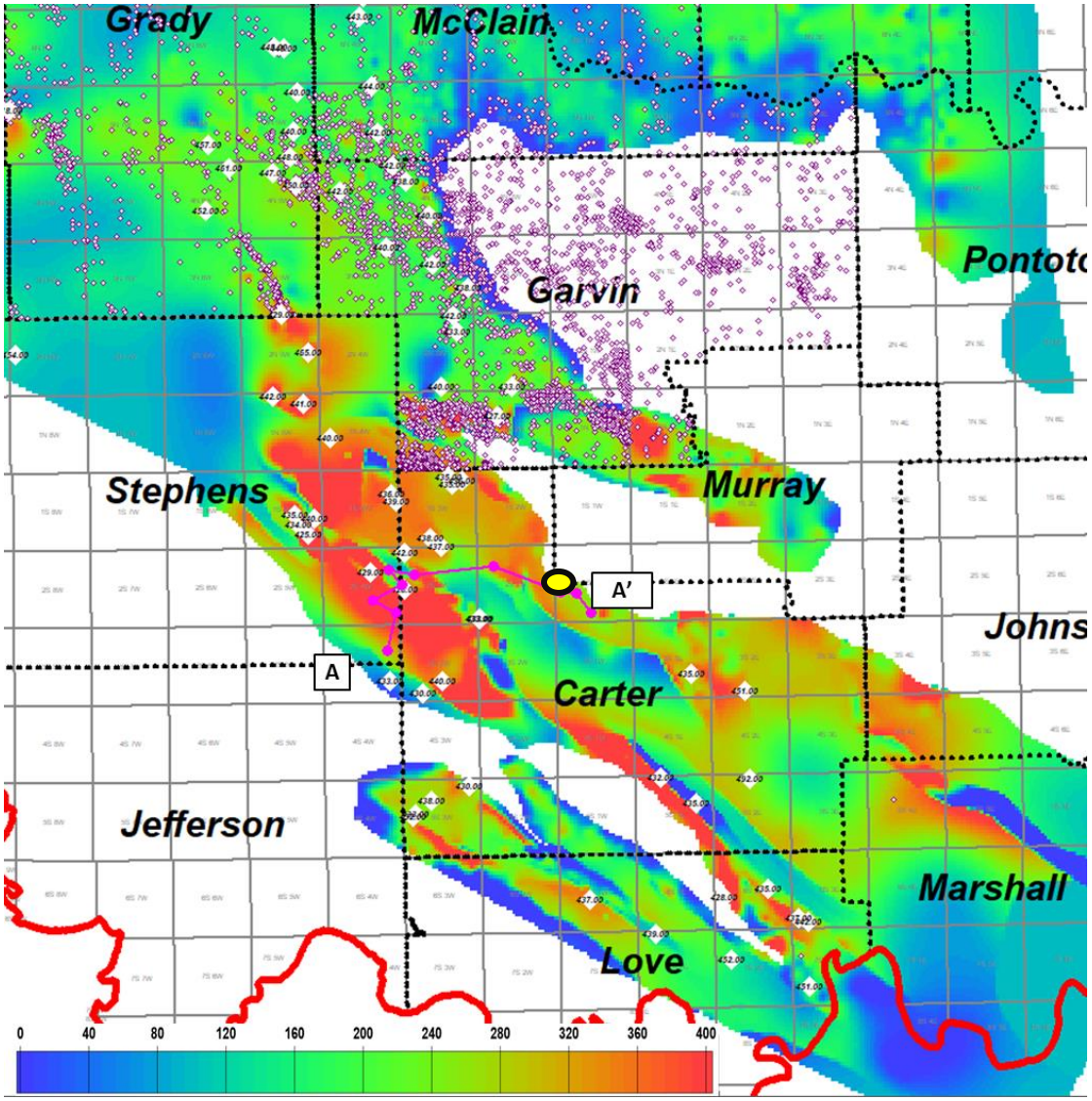

Figure 3.57. Woodford Shale thickness [feet] map in the regional areas nearby the Speake Ranch. The Speake Ranch location is highlighted in the yellow spot. White diamonds and values correspond to average T-max [°C] maturity values for the Woodford Shale from the IRC Woodford-Mississippian consortium database. Thickness values from 0 to 400 ft.

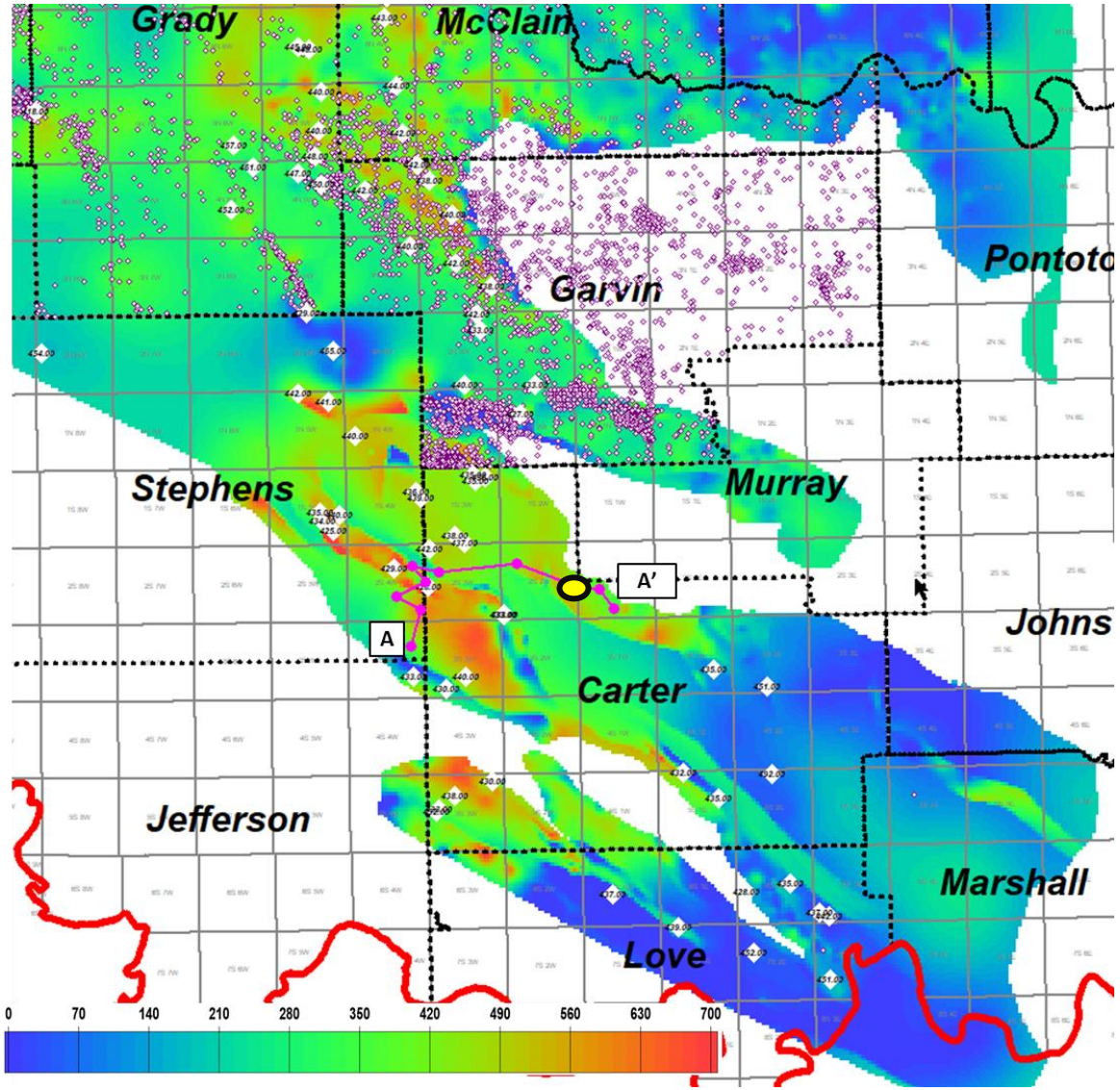

Figure 3.58. Hunton group thickness [feet] map in the regional areas nearby the Speake Ranch. The Speake Ranch location is highlighted in the yellow spot. White diamonds and values correspond to average T-max [°C] maturity values for the Woodford Shale from the IRC Woodford-Mississippian consortium database. Thickness values from 0 to 700 ft.

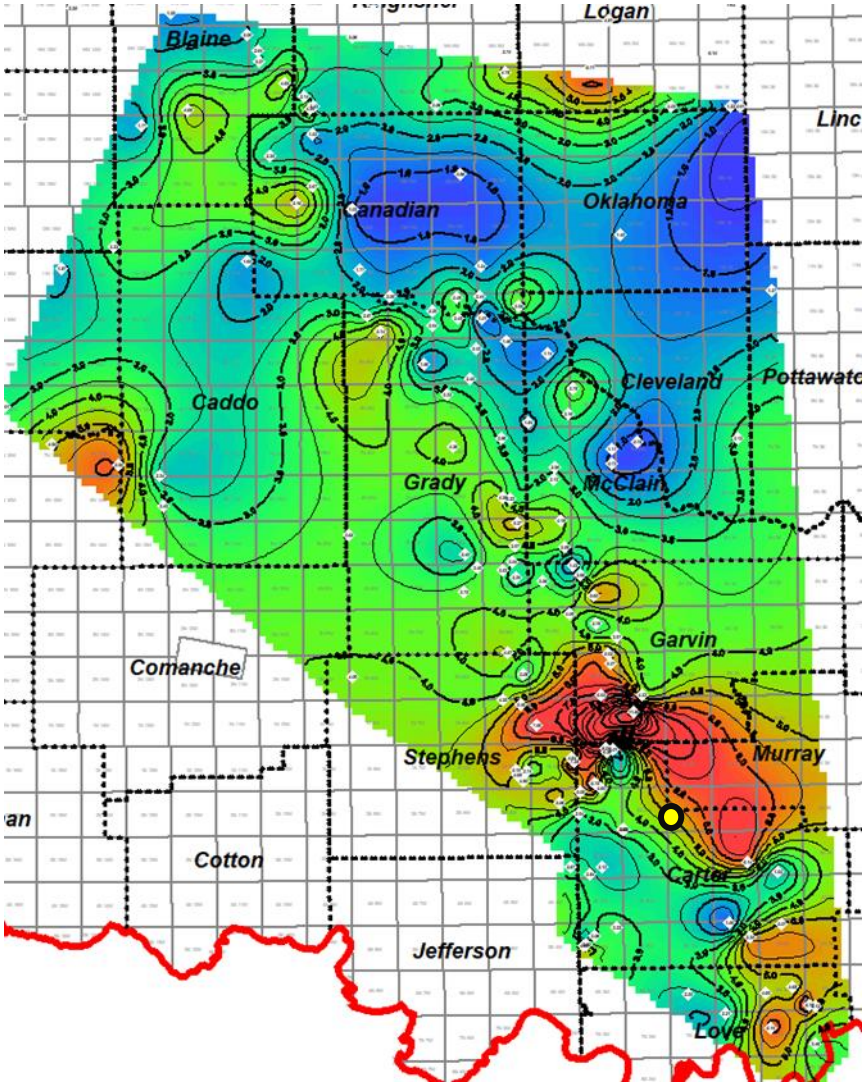

Figure 3.59. Woodford Shale average total organic carbon [%TOC] map on the regional scale of Oklahoma. The Speake Ranch location is highlighted in the yellow spot. White diamonds and values correspond to average T-max [°C] maturity values for the Woodford Shale from the IRC Woodford-Mississippian consortium database.

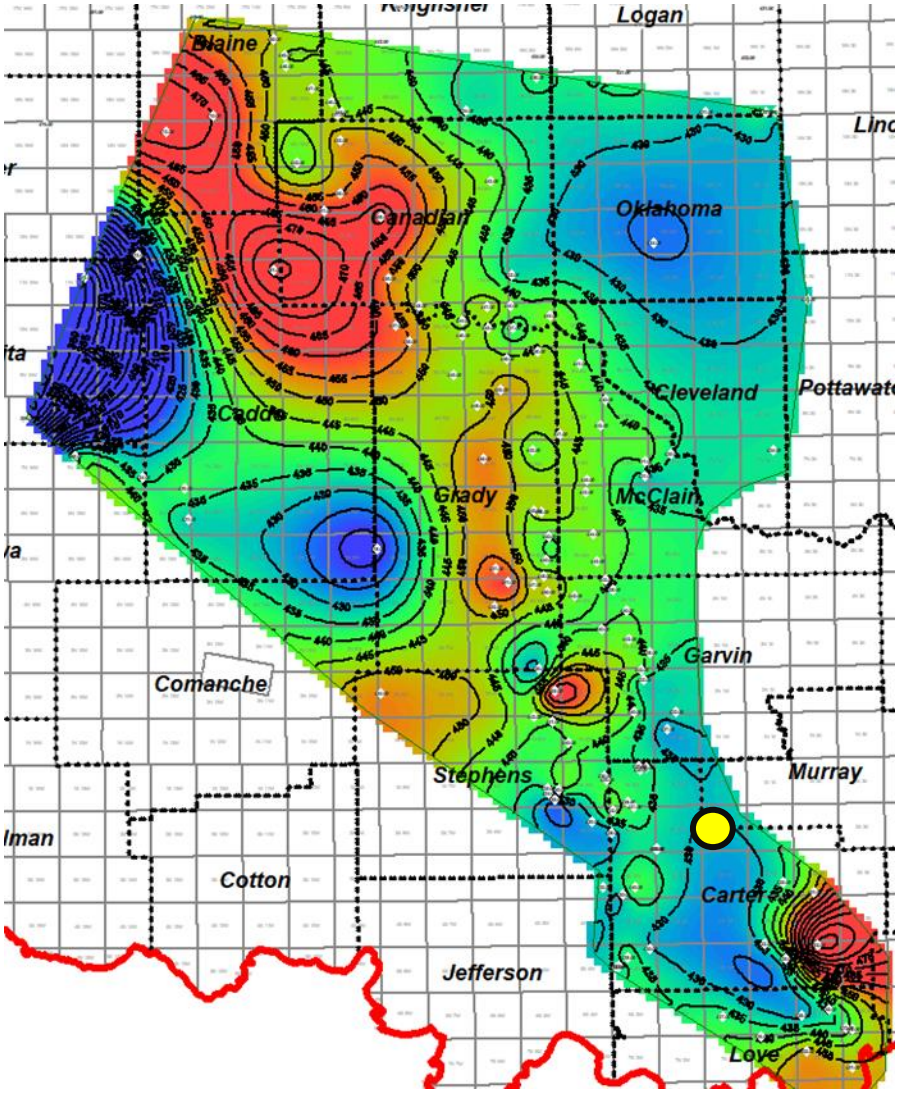

Figure 3.60. Woodford Shale average Tmax maturity [°C] map on the regional scale of Oklahoma. The Speake Ranch location is highlighted in the yellow spot. White diamonds and values correspond to average T-max maturity values for the Woodford Shale from the IRC Woodford-Mississippian consortium database.

3.7. Conclusions

Previous integrated studies (Serna-Bernal, 2013; Connock, 2015 DeGarmo, 2015; Becerra-Rondon, 2017; Ekwunife, 2017; Galvis et al., 2017a and 2017b; Jones 2017; Connock et al. 2018; Philp and DeGarmo, 2020) of lithostratigraphy and sequence stratigraphy of the Woodford Shale in southern Oklahoma have shown similar conclusions for evidence of photic zone euxinia, with terrestrial organic inputs at the Woodford Shale top culminating in the collapse of both the terrestrial and marine ecosystems for the post-Woodford Shale Mississippian strata. This study is the first one to correlate the Woodford Shale SR outcrop integrated geological and geochemical characterization with nearby subsurface well log data corresponding to the south SCOOP Oklahoma petroleum province.

For the Middle and Upper Woodford, the biomarker analyses provided evidence for a potential mechanism for mass extinctions involving eutrophication of shallow marine settings, followed by increased bioproductivity, oxygen consumption, and subsequent global euxinic seas. Based on sequence stratigraphic models by Slatt (2016), combined with the biomarker analyses and XRF proxy interpretations it can be concluded that at the start of the maximum flooding surface, it would define this Woodford section as an HST interval with a type II marine kerogen (Slatt et al., 2011) and a typical open marine deposit. The Rock-Eval data, steranes ratios, as well as the presence of 24-n-propylcholestanes, demonstrate the anticipated marine organic signature but with high levels of anoxic intervals overall in the SR section. The relatively higher amounts of C_{29} steranes demonstrate the inclusion of some terrestrial input, and this occurs in depositional cycles that include the upper part of the Lower Woodford member as well. But the general higher concentration of C_{28} MAS over the C_{27} and C_{29} MAS indicates that the principal depositional environment is marine. For this reason, the recognition of biomarkers related to terrestrial organic

matter inputs (PAHs and TPPs) are proposed as progradational processes that deposited these compounds from the continent towards deeper basinal areas.

The proposed and identified specific biomarkers gave insight into the lithologic features of the Woodford Shale. Relatively higher concentrations of diasteranes were observed in units with the highest shale content, as expected and correlated with the lithologies described by Galvis (2017) and Galvis et al. (2017a and 2017b) and were particularly predominant in all the Lower and Middle Woodford Shale argillaceous rich mudstones facies. On the other hand, the silica and chert-rich rock intervals were characterized by relatively high amounts of tricyclic terpanes, which are indicative of *Tasmanites* and algal input. *Tasmanites* are also identified in the lithologies of the SR by the petrographic analyses of Galvis (2017). Upwellings causing chert deposition also provided nutrient-rich waters, causing algal and planktonic blooms, as seen by the tricyclic terpane signature, the increase of the TPP ratio and the integration with the XRF, XRF-EF data of U, Mo, V, Fe, S, and the ratios of Si/Al, Mo/Al.

By applying the regional sequence stratigraphic model of the Woodford Shale in Oklahoma proposed by Slatt (2016), and integrating this into the SR section analysis, it can be concluded that there were high levels of oxygenation and open marine circulation with shallower sea level after the end of the maximum flooding surface (MFS), towards the deposition of the Upper Woodford member layers. However, biomarkers from this analysis point to some instances of anoxia and marine restriction in the Upper Woodford, but with less preservation of the organic matter.

Based on the increased abundances of PAHs such as cadalene, perylene, fluorene, dibenzofuran, there is an indication of increased terrestrial input from land plants during the Late Devonian, which likely upset marine life by contributing to harsh, anoxic conditions that killed off many species between the F-F and Devonian-Carboniferous boundaries at the uppermost

Woodford Shale. It is interpreted that the F-F event is located between 202 ft to 220 ft of the section, but the precise location of these boundaries within the 314 ft of Woodford stratigraphic section will require a much more detailed analysis that covers a closer vertical sample spacing of biomarker samples than the one applied in this study and the combination with detailed biostratigraphic analysis.

The recognition and fluctuations in PZE through the vertical stratigraphy of the Woodford Shale might indicate that the conditions for an enclosed mini-basin fill setting were very likely to be present for the entire Lower Woodford member and the middle and lower parts of the Middle member in this location of Oklahoma. These enclosed mini-basin fill settings are critical for allowing the higher accumulation, restriction, and preservation of organic matter, which has a subsequent formation of rock beds principally in the intervals deposited below the maximum flooding surface (MFS). More increasing oxicity in the organic matter after the MFS is proposed to be an indicator of less restricted conditions. The biomarker indicators of terrestrial organic matter input and decrease in PZE conditions, combined with the XRF proxies of upwelling current effects, are reliable signals of open marine depositional settings for the uppermost Woodford Shale intervals (upper part of the Middle member, and entire Upper member).

Additionally, on a more areally dispersed scale, the regional maps show areas of thinner pre-Woodford strata (Hunton Group) thicker Woodford intervals, and higher average bulk %TOC content under immature (low average Tmax, <435 °C) conditions. It is essential to clarify that the Lower, Middle and Upper Woodford members present in this section might vary across the state of Oklahoma, so a direct one-to-one detailed comparison must be made when interpreting if the same enclosed mini-basin fills deposits are present in other areas where the Woodford members are identified or labeled with the same nomenclature (e.g., the Lower and Middle Woodford Shale

members might be lithologically different and thinner, or not present, in other areas of Oklahoma, and present lower %TOC content because of depletion caused by higher maturity levels).

Geochemical attribute	Characteristic
SR stratigraphic depth	14.0 - 208.5 ft
n-Alkanes distribution	Not detected
Steranes	C_{29} Steranes > C_{27} steranes
Regular steranes / hopanes	> 0.3
Sterane index	> 0.15
MAS	5α-Ergostane 20S is the highest MAS
C35S/C34S	> 0.55
Gammacerane index	> 0.13
AIR	0 - 2
Isorenieratane	> 5 μg/g EOM
Paleorenieratane	> 40 μg/g EOM
Renierapurpurane	> 0.6 μg/g EOM
DBF	> 2.5 μg/g EOM
DBT	> 3.0 μg/g EOM
TPP ratio	0.2 - 0.4

Table 3.10. Summary of biomarker characteristics in the SR interval interpreted as an enclosed mini-basin fill setting.

3.8. Cited References

- Aizenshtat, Z., 1973. Perylene and its geochemical significance. Geochimica et Cosmochimica Acta 37, 559-567.
- Aizenshtat, Z., 1973. Perylene and its geochemical significance. Geochimica et Cosmochimica Acta 37, 559-567.
- Albaghdady, A., 2013.Organic geochemical characterization of source rocks (Sirt Shale) and crude oils from the Central Sirt basin, Lybia. Doctoral dissertation manuscript, The University of Oklahoma, p. 259.
- Alexander, R., Larcher, A.V., Kagi, R.I., Price, P.L., 1992. An oil-source correlation study using age-specific plant-derived aromatic biomarkers. In: Moldowan, J.M., Albrecht, P., Philp, R.P., eds., Biological markers in sediments and petroleum, 1992. Prentice-Hall, Englewood Cliffs, New Jersey, 201-221.
- Algeo, T.J., Scheckler, S.E., 1998. Terrestrial-marine teleconnections in the Devonian: links between the evolution of land plants, weathering processes, and marine anoxic events. Philosophical Translations of the Royal Society of London 1998, 353, 113-30.
- Algeo, T.J., Rowe, H., 2012. Paleoceanographic applications of trace-metal concentration data. Chemical Geology 324-325, 6-18.
- Ali, E.E., 2015. Integrated characterization of the Woodford Shale in southwest Cherokee platform, Oklahoma. M.Sc. thesis manuscript, The University of Oklahoma, p. 104.
- Althoff, C., 2012. Characterization of depositional megacycles in the Woodford trough of Central Oklahoma. M.Sc. thesis manuscript, The University of Oklahoma, p. 167.
- Amorocho-Sanchez, J.D., 2012. Sequence stratigraphy and seismic interpretation of the Upper Devonian- Lower Mississippian Woodford Shale in the Cherokee platform: a characterization approach for unconventional resources. M.Sc. thesis manuscript, The University of Oklahoma, p. 153.
- Aquino Neto, F.R., Restle, A., Connan, J., Albrecht P., Ourisson, G., 1982. Novel tricyclic terpanes (C_{19}, C_{20}) in sediments and petroleums. Tetrahedron Letters, 23, 2027-30.
- Aquino Neto, F.R., Trendel, J.M., Restle, A., Connan, J., Albrecht, P.A., 1983. Occurrence and formation of tricyclic terpanes in sediments and petroleums. In: M. Bjorøy, eds.,

Advances in organic geochemistry 1981. International Conference Proceedings John & Sons, New York, p. 659-76.

- Badra, H., 2011. Field characterization and analog modeling of natural fractures in the Woodford Shale, southeast Oklahoma. M.Sc. thesis manuscript, The University of Oklahoma, p. 156.
- Becerra-Rondon, D., 2017. Integrated geological characterization at the bed scale of the Woodford Shale at the I-35 outcrop, southern Oklahoma. M.Sc. thesis manuscript, The University of Oklahoma, p. 202.
- Becker, R.T., Gradstein, F.M., Hammer, O., 2012. The Devonian period. In: Gradstein, F.M. Ogg, J.G., Schmitz, M.D., Ogg, G.M., eds., The Geologic Time Scale 2012. Elsevier, Amsterdam, 2, 559-601.
- Blumer, M., Guillard, R.R.L., Chase, T., 1971. Hydrocarbons of marine plankton. Marine Biology, 8, 183-9.
- Bontempi, C., 2015. High-resolution stratigraphy of thin-bedded shales/radiolarians, Woodford Shale, Arbuckle wilderness area, Murray County, Oklahoma: A new correlation tool. M.Sc. thesis manuscript, The University of Oklahoma, p. 98.
- Brito, R.J., 2014. Geological characterization and stratigraphic sequence framework of the Brown Shale, Central Sumatra basin, Indonesia: implications as an unconventional resource. M.Sc. thesis manuscript, The University of Oklahoma, p. 106.
- Brito, R.J., 2019. The Woodford Shale in the Marietta basin: Oklahoma and North Texas. Doctoral dissertation manuscript, The University of Oklahoma, p. 182.
- Brocks, J.J., Love, G.D., Summons, R.E., Knoll, A.H., Logan, G.A., Bowden, S.A., 2005. Biomarker evidence for green and purple sulfur bacteria in a stratified Palaeoproterozoic sea. Nature 437, 866-870.
- Brocks, J.J., Summons, R.E., 2014. Sedimentary hydrocarbons, biomarkers for early life. In: Turekian, K., Holland, H., eds., Elsevier Treatise on Geochemistry 2nd Edition 8, 61-103.
- Brown, T.C., Kenig, F., 2004. Water column structure during deposition of Middle Devonian-Lower Mississippian black and green/gray shales of the Illinois and Michigan basins: A biomarker approach. Paleogeography, Palaeoclimatology, Palaeoecology 215, 59-85.

- Byrnes, A.P., Lawyer, G., 1999. Burial, Maturation, and Petroleum Generation History of the Arkoma Basin and Ouachita Foldbelt, Oklahoma and Arkansas. Natural Resources Research, 8, 1.
- Calvert, S.E., Pedersen, T.F., 1993. Geochemistry of recent oxic and anoxic marine sediments: Implications for the geological record. Marine Geology 113, 67–88.
- Cardona-Valencia, L.F., 2014. Integrated characterization of the Woodford Shale in the southern Cherokee platform, Oklahoma. M.Sc. thesis manuscript, The University of Oklahoma, p. 98.
- Cardott, B. J., 2012. Thermal maturity of Woodford Shale gas and oil plays, Oklahoma, USA. International Journal of Coal Geology, 1-13.
- Cardott, B.J., 2014. Woodford Shale play update: Expanded in the oil window. American Association of Petroleum Geologists, Search and Discovery article 80409.
- Castillo, L.A, 2013. Integrated reservoir characterization of the Ordovician-Silurian Hunton carbonate, north Cherokee platform, Oklahoma. M.Sc. thesis manuscript, The University of Oklahoma, p. 90.
- Chain, A.R., 2012. Stratigraphy and composition of the Woodford Shale in depositionally updip and downdip wells, Anadarko Basin, Oklahoma. M.Sc. thesis manuscript, The University of Oklahoma, p. 138.
- Chosson, P., Connan, J., Dessort, D., Lanau, C., 1992. In vitro biodegradation of steranes and terpanes: a clue to understanding geological situations. In: Moldowan, J.M., Albrecht, P., Philp, R.P., eds., Biological Markers in Sediments and Petroleum. Prentice-Hall, 320-349.
- Clark, J.P., Philp, R.P., 1989. Geochemical characterization of evaporate and carbonate depositional environments and correlation of associated crude oils in the black Creek Basin, Alberta. Bulletin of Canadian Petroleum Geology 37, 401–416.
- Comer J. B., Hinch, H. H., 1987. Recognizing and quantifying expulsion of oil from the Woodford Shale and age-equivalent rocks in Oklahoma and Arkansas. American Association of Petroleum Geologists Bulletin 71, 844-858.
- Comer, J.B., 2005. Facies distributions and hydrocarbon production potential of the Woodford Shale in the southern midcontinent: in B.J. Cardott, eds., Unconventional energy

resources in the southern mid-continent, 2004 symposium. Oklahoma Geological Survey, Circular 110, 51-62.

- Comer, J.B., 2008. Woodford Shale in southern mid-continent, USA, transgressive system tract marine source rocks on an arid passive continental margin with persistent oceanic upwelling. American Association of Petroleum Geologists Annual Convention, Search and Discovery Article 404026.
- Connan, J., Restle, A., Albrecht, P., 1980. Biodegradation of crude oil in the Aquitane basin. In: Douglas, D.G., and Maxwell, J. R., eds., Advances in Organic Geochemistry 1979, Pergamon Press, Oxford 12, 1-17.
- Connock, G.T., 2015. Paleoenvironmental interpretation of the Woodford Shale, Wyche farm shale pit, Pontotoc County, Arkoma basin, Oklahoma with a primary focus on water column structure. M.Sc. thesis manuscript, The University of Oklahoma, p. 266.
- Connock, GT., Nguyen, T.X., Philp, R.P., 2018. The development and extent of photic-zone euxinia concomitant with Woodford Shale deposition. AAPG Bulletin 102, 6, 959-986.
- Dahl, J.E., Moldowan, J.M., Teerman, S.C., McCaffrey, M.A., P., S., Pena, M., Stelting, C.E., 1994. Source rock quality determination from oil biomarkers I. – An example from the Aspen Shale, Scully's Gap, Wyoming. American Association of Petroleum Geologists AAPG Bulletin 78, 1507-1526.
- DeGarmo, D., 2015. Geochemical characterization of the Woodford Shale (Devonian-Mississippian), McAlister cemetery quarry, Criner Hills uplift, Ardmore basin, Oklahoma. M.Sc. thesis manuscript, The University of Oklahoma, p. 223.
- Duan, Y., Zheng C., Wang Z., Wu B., Wang C., Zhang H., Qian Y., Zheng G., 2006. Biomarker geochemistry of crude oils from the Qaidam Basin, NW China. Journal of Petroleum Geology 29, 2, 175-188.
- Dzou, L.I.P., Noble R.A., Senftle J.T., 1995. Maturation effects on absolute biomarker concentration in a suite of coals and associated vitrinite concentrates. Organic Geochemistry 23, 7, 681-697.
- Ekwunife, I.C., 2017. Assessing mudrock characteristics, high-resolution chemostratigraphy, and sequence stratigraphy of the Woodford Shale in the McAlister

cemetery quarry, Ardmore basin, Oklahoma. M.Sc. thesis manuscript, The University of Oklahoma, p. 167.

- Elmore, R.D., Heij, G.W., Wickard, A.K., 2016. Paragenesis of mineralized fractures and diagenesis of prominent North American shales: The sedimentary record. SEPM 14, 4-10.
- Fang H., Jianyu C., Yongchuan S. and Yaozong L., 1993. Application of organic facies studies to sedimentary basin analysis: a case study from the Yitong Graben, China. Organic Geochemistry 20, 1, 27-42.
- Fang, R., Li, M., Wang, T.G., Zhang, L., Shi, S., 2015. Identification and distribution of pyrene, methylpyrenes, and their isomers in rock extracts and crude oils. Organic Geochemistry 83-84, 65-76.
- Franti, P., Sieranoja, S., 2019. How much can k-means be improved by using better initialization and repeats? Journal of Pattern Recognition, 93, 2019, 95-112.
- Frigaard, N.U., Dahl, C., 2008. Sulfur metabolism in phototrophic sulfur bacteria. Elsevier Masson SAAS, p. 134.
- Galvis-Portilla, H., Becerra-Rondon, D., Duarte, D., Slatt, R.M., 2016. Rock and fracture characterization of the Woodford Shale along the I-35 Outcrop. American Association of Petroleum Geologists Search and Discovery Article #51240.
- Galvis, H., 2017. Detailed lithostratigraphic characterization and sequence stratigraphy of a complete Woodford Shale outcrop section in southern Oklahoma. M.Sc. thesis manuscript, The University of Oklahoma, p. 170.
- Galvis, H., D. Becerra-Rondon, R.M. Slatt, 2017a. Lithofacies and stratigraphy of a complete Woodford Shale outcrop section in south Central Oklahoma: Geologic considerations for the evaluation of unconventional shale reservoirs. Interpretation 2017, 6, 1 SC15-SC27.
- Galvis, H., Becerra-Rondon, D., Slatt, R.M., 2017b. Let’s make outcrops recover their value, understanding the rock on the surface for predicting into the subsurface: Woodford Shale case study, Ardmore basin, Oklahoma. American Association of Petroleum Geologists, Search and Discovery Article 10907.
- Ghosh, S., 2017. Integrated studies on Woodford Shale's natural fracture attributes, origin, and their relation to hydraulic fracturing. Doctorate dissertation manuscript, The University of Oklahoma, p. 264.

- Goodarzi, F., Brooks, P.W., Embry, P.F., 1989. Regional maturity as determined by organic petrology and geochemistry of the Schei Point Group (Triassic) in Western Sverdrup Basin, Canadian Archipelago. Marine and Petroleum Geology 6, 290-302.
- Grantham, P.J., 1986. The occurrence of unusual C_{27} and C_{29} sterane predominances in two types of Oman crude oil. Organic Geochemistry 9, 1-10.
- Grantham, P.J., Wakefield, L.L., 1988. Variations in the sterane carbon number distributions of marine source rock derived crude oils through geological time. Organic Geochemistry 12, 61-73.
- Grasby, S.E., Chen, Z., Issler, D., Stasiuk, L., 2009. Evidence for deep anaerobic biodegradation associated with rapid sedimentation and burial in the Beaufort-Mackenzie basin, Canada. Applied Geochemistry 24, 536-542.
- Grice K., Cao C., Love G.D., Bottcher M. E., Twitchett R. J., Grosjean E., Summons R. E., Turgeon S. C., Dunning W., Jin Y., 2005. Photic zone euxinia during the Permian-Triassic Superanoxic Event. Science 307, 706-708.
- Gupta, N., 2012. Multi-scale characterization of the Woodford Shale in West-central Oklahoma: From scanning electron microscope to 3D seismic. Doctorate dissertation manuscript, The University of Oklahoma, p. 148.
- Ham, W.E., Denison, R.E., Merritt, C.A., 1964. Basement rocks and structural evolution of southern Oklahoma. Oklahoma Geological Survey Bulletin 95, 1-302.
- Ham, W.E., Wilson, J.L., 1967. Paleozoic epeirogeny and orogeny in the central United States. American Journal of Science 265, 332-407.
- Hartgers, W., Sinninghe Damsté, J. S., Requejo, A.G., Allan, J., Hayes, J. M., Ling, Y., Xie, T.M., Primack J., De Leeuw, J.W., 1994. A molecular and carbon isotopic study towards the origin and diagenetic fate of diaromatic carotenoids. Organic Geochemistry 22, 703-725.
- Hays, L.E., Beatty, T., Henderson, C.M., Love, G.D., Summons, R.E., 2007. Evidence for photic zone euxinia through the end-Permian mass extinction in the Panthalassic Ocean (Peace River basin, Western Canada). Paleo world 16, 1-3, 39-50.
- Hester, T.C., Sahl, H.L., Schmoker, J.W., 1988. Cross-sections based on Gamma-ray, density, and resistivity logs showing stratigraphic units of the Woodford Shale, Anadarko basin, Oklahoma. United States Geological Survey Bulletin 1866-D, 1-38.

- Hester, T.C., Schmoker, J.W., Sahl, H.L., 1990. Log-derived regional source rock characteristics of the Woodford Shale, Anadarko basin, Oklahoma. U.S. Geological Survey Bulletin 1866-D, p. 38.
- Holba, A.G., Dzou, L.I.P., Masterson, W.D., Hughes, W.B., Huizinga, B.J., Singletary, M. S., Moldowan, J.M., Mello, M.R., Tegelaar, E., 1998. Application of 24-norcholestanes for constraining source age of petroleum. Organic Geochemistry 29, 5-7, 1269-1283.
- Holba, A.G., Tegelaar, E., Ellis, L., Singletary, M.S., Albrecht, P., 2000. Tetracyclic polyprenoids: indicators of freshwater (lacustrine) algal input. Geology 28, 251-254.
- Holba, A.G., Dzou, L.I., Wood, G.D., Ellis, L., Adam, P., Schaeffer, P., Albrecht, P., Greene, T., Hughes, W.B., 2003. Application of tetracyclic polyprenoids as indicators of input from fresh-brackish water environments. Organic Geochemistry 34, 441–469.
- Huang, W.Y., Meinschein, W.G., 1979. Sterols as ecological indicators. Geochimica et Cosmochimica Acta 43, 739-745.
- Hughes, W.B., Holba, A.G., Miller, D.E., Richardson, J.S., 1985. Geochemistry of greater Ekofisk crude oils. In: Thomas, B. M., Dore´, A.G., Eggen, S.S., Home, P.C. & Larsen, R.M. (Eds.) Petroleum Geochemistry in Exploration of the Norwegian Shelf. Graham and Trotman, London, p. 75–92.
- Infante-Paez, L.E., Cardona, L.F., McCullough, B., Slatt, R.M., 2016. Seismic analysis of paleo topography and stratigraphic controls on total organic carbon: Rich sweet spot distribution in the Woodford Shale, Oklahoma, USA. Interpretation 5, 1, T33-T47.
- Jiamo, F., Guoying, S., Dehan, L., 1988. Organic geochemical characteristics of major types of terrestrial petroleum source rocks in China. In: Fleet, A.J., Klets, K., Talbot, M.R., eds., Lacustrine petroleum source rocks. Geological Society of London Special Publications 40, 279-289.
- Jiang, C., Alexander, R., Kagi, R.I., Murray, A.P., 1998. Polycyclic aromatic hydrocarbons in ancient sediments and their relationships to paleoclimate. Organic Geochemistry 29, 5-7, 1721-1735.
- Johnson, K.S, Branson C.C., Curtis, N.M., Ham, W.E., 1972. Geology and earth resources of Oklahoma. An atlas of maps and cross-sections. Oklahoma Geological Survey OGS, Educational Publication 1, 1-8.

- Johnson, K.S., Cardott, B. J., 1992. Geologic framework and hydrocarbon source rocks of Oklahoma. Oklahoma Geological Survey Circular 93, 21-37.
- Johnson, K. S., Amsden, T.W., Denison, R. E., Dutton, S.P., Goldstein, A. G., Rascoe Jr., B., Sutherland, P.K., Thompson, D.M., 1989. Geology of the southern Midcontinent. Oklahoma Geological Survey Special Publication 89-2, 1-53.
- Johnson, K.S., 2008. The geologic history of Oklahoma. Oklahoma Geological Survey. Educational Publication 9, 2-9.
- Jones, L.C., 2017. An integrated analysis of sequence stratigraphy, petroleum geochemistry, and Devonian mass extinction events in the Woodford Shale, southern Oklahoma. M.Sc. thesis manuscript, The University of Oklahoma, p. 219.
- Kaiser, S.I., Aretz, M., Becker, R.T., 2015. The global Hangenberg crisis (Devonian-Carboniferous transition): a review of first-order mass extinction. Geological Society of London, Special Publications 2015, 423, 387-437.
- Kilian, B.J., 2012. Sequence Stratigraphy of the Woodford Shale, Anadarko basin, Oklahoma: Implications on regional Woodford target correlation. M.Sc. thesis manuscript, The University of Oklahoma, p. 102.
- Kirkland D.W., Denison, R.E., Summers, D.M., Gormly, J.R., 1992. Geology and organic geochemistry of the Woodford Shale in the Criner Hills and western Arbuckle Mountains, Oklahoma. Oklahoma Geological Survey, Circular 93, 38-69.
- Koopmans, M.P., Koster, J., Van Kaam-Peters, H. M. E., Kenig, F., Schouten, S., Hartgers, W.A., De Leeuw, J.Q., Sinninghe Damsté, J.S., 1996a. Diagenetic and catagenetic products of isorenieratane: Molecular indicators for photic zone anoxia. Geochimica Cosmochimica Acta 60, 4467-4496.
- Koopmans, M.P., Schouten, S., Kohnen, M.E.L, Sinninghe Damsté, J.S., 1996b. The restricted utility of aryl isoprenoids as indicators for photic zone anoxicity. Geochimica et Cosmochimica Acta 60, 4873-4876.
- Laflamme, R.E., Hites, R.A., 1978. The global distribution of polycyclic aromatic hydrocarbons in recent sediments. Geochimica et Cosmochimica Acta 42, 289-303.
- Lambert, M.W., 1993. Internal stratigraphy and organic facies of the Devonian-Mississippian Chattanooga (Woodford) Shale in Oklahoma and Kansas. In: Katz, B.J.,

Pratt, L.M., eds., Source rocks in a sequence stratigraphic framework. AAPG Studies in Geology 37, 163-176.

- Li, M., Shi, S., Wang, T.G., 2012. Identification and distribution of chrysene, methyl chrysenes, and their isomers in crude oils and rock extracts. Organic Geochemistry 52, 55-66.
- Liborius-Parada, A.D.L., Sneddon, A., Wu, S., 2017. Geochemical insights into the Oswego formation in Kingfisher County, Oklahoma. Oklahoma City Geological Society, Shale Saker 68, 4, p. 176.
- Liborius-Parada, A.D.L., 2019. Applied petroleum source rock evaluation and high-resolution sequence stratigraphy for unconventional reservoirs in La Luna formation (Cenomanian-Santonian) Northwest Maracaibo basin, Venezuela. Doctoral dissertation manuscript. The University of Oklahoma, p. 379.
- Lichtfouse, E., Budzinski, H., Garrigues, P., Eglinton, T.I., 1997. Ancient polycyclic aromatic hydrocarbons in modern soils: 13C, 14C and biomarker evidence. Organic Geochemistry 26, 353-359.
- Lo, H.B., Cardott, B.J., 1995. Detection of natural weathering of upper McAlester coal and Woodford Shale, Oklahoma, U.S.A. Organic Geochemistry 22, 73-83.
- Mackenzie, A.S., Lamb, N.A., Maxwell, J.R., 1982. Steroid hydrocarbons and the thermal history of sediments. Nature 295, 223-6.
- Marynowski, L., Narkiewicz, M., Grelowski, C., 2000. Biomarkers as environmental indicators in a carbonate complex, examples from the Middle Devonian, the Holy Cross Mountains, Poland. Sedimentary Geology 137, 187–212.
- Marynowski, L., Filipiak, P., 2007. Water column euxinia and wildfire evidence during the deposition of the Upper Famennian Hangenberg event horizon from the Holy Cross Mountains (Central Poland). Geology Magazine 144, 569-595.
- Marynowski, L., Smolarek, J., Hautevelle, Y., 2015. Perylene degradation during the gradual onset of organic matter maturation. International Journal of Coal Geology 139, 17-25.
- Maynard, S., 2016. Correlation of bioturbated facies, chemostratigraphy, total organic carbon, and sequence stratigraphy in the Woodford Shale of south-central Oklahoma. M.Sc. thesis manuscript, The University of Oklahoma, p. 119.

- McCullough, B.J., 2014. Sequence-stratigraphic framework and characterization of the Woodford Shale on the southern Cherokee platform of Central Oklahoma. M.Sc. thesis manuscript, The University of Oklahoma, p. 212.
- McCullough, B., Slatt, R.M., 2014. Paleotopographic control on the variability of Woodford Shale strata across the southern Cherokee platform area of central Oklahoma: A mechanism for increased preservation-potential of organic content: AAPG Search and Discovery article 1125.
- McKirdy, D.M., Aldridge, A.K., Ypma, P.J.M., 1983. A geochemical comparison of some crude oils from pre-Ordovician carbonate rocks. In: Bjorøy, M., eds., Advances in Organic Geochemistry 1981. Organic Geochemistry, London: Wiley, p. 99-107.
- McGhee, G.R., 1981. Evolutionary replacement of ecological equivalents in late Devonian benthic marine communities. Paleogeography, Palaeoclimatology, Palaeoecology 34, 267-283.
- McGhee, G. R., 1996. The late Devonian mass extinction: The Frasnian/Famennian crisis. Columbia University Press, 303.
- Mello, M.R., Telnaes, N., P.C., G., Chicarelli, M.I., Brassell, S.C., Maxwell, J.R., 1988. Organic geochemical characterization of depositional environment in Brazilian marginal basins. Organic Geochemistry 13, 31-46.
- Miceli-Romero, A.A, 2010. Geochemical characterization of the Woodford Shale, central and southeastern Oklahoma. M.Sc. thesis manuscript, The University of Oklahoma, p. 149.
- Miceli-Romero, A.A., Philp, R.P., 2012. Organic geochemistry of the Woodford Shale, southeastern Oklahoma: How variable can shales be? AAPG Bulletin 96, 3, 493-517.
- Miceli-Romero, A.A., Nguyen, T., Philp, R.P., 2018. Organic geochemistry of the Eagle Ford group in Texas. AAPG Bulletin 107, 7, 1379-1412.
- Milad, B., Slatt, R.M., 2018. Impact of lithofacies variations and structural changes on natural fracture distributions. Interpretation, 6, 4, 1-15.
- Milad., B., 2019. Integrated reservoir characterization and geological upscaling for reservoir flow simulations of the Sycamore/Meramec and Hunton plays in Oklahoma. Doctoral dissertation manuscript, The University of Oklahoma, p. 179.

- Mizukami, T., Kaiho, K., Oba, M., 2013. Significant changes in land vegetation and oceanic redox across the Cretaceous/Paleogene boundary. Palaeogeography, Palaeoclimatology, Palaeoecology 369, 41-47.
- Mizukami, T., Kaiho, K., Oba, M., 2014. A spike of woody plant biomarkers in the deep-sea iridium layer at the Cretaceous/Paleogene boundary. Palaeogeography, Palaeoclimatology, Palaeoecology 412, 241-248.
- Moldowan, J. M., Seifert, W. K., 1979. Head-to-head linked isoprenoid hydrocarbons in petroleum. Science 204, 169-71.
- Moldowan, J.M., 1984. C30-steranes, novel markers for marine petroleums and sedimentary rocks. Geochimica et Cosmochimica Acta 48, 2767-2768.
- Moldowan, J.M., Fago, F., 1985. Structure and significance of a novel rearranged monoaromatic steroid hydrocarbon in petroleum. Geochimica et Cosmochimica Acta 50, 3, 343-351.
- Moldowan, J.M., Seifert, W. K., Gallegos, E.J., 1985. Relationship between petroleum composition and depositional environment of petroleum source rocks. American Association of Petroleum Geologists Bulletin 69, 1255-68.
- Moldowan, J.M., Fago, F.J., Lee, C.Y., Jacobson, S.R., Watt, D.S., Slougui, N.E., Jeganathan, A., Young, D.C., 1990. Sedimentary 24-n-propylcholestanes, molecular fossils diagnostic of marine algae. Science 247, 309-312.
- Moldowan, J.M., Lee, C.Y., Sundararaman, P., 1992. Source correlation and maturity of select oils and rocks from the Central Adriatic basin (Italy and Yugoslavia). In: Moldowan. J.M., Albrecht, P., Philp, R.P., eds., Biological Markers in Sediments and Petroleum. Prentice-Hall, Englewood Cliffs, New Jersey, 370-401.
- Molinares, C.E., 2013. Stratigraphy and palynomorphs composition of the Woodford Shale in the Wyche Farm shale pit, Pontotoc County, Oklahoma. M.Sc. thesis manuscript, The University of Oklahoma, p. 104.
- Molinares, C.E., 2019. The Frasnian/Famennian (F/F) transition in the Woodford Shale, south-central Oklahoma – a multiproxy approach. Doctoral dissertation manuscript, The University of Oklahoma, p. 117.

- Nabbefeld, B., Grice, K., Summons, R.E., Lindsay, E.H., Cao, C., 2010. Significance of polycyclic aromatic hydrocarbons (PAHs) in Permian/Triassic boundary sections. Applied Geochemistry 25, 1374-1382.
- Nowaczewski, V., 2011. Biomarker and paleontological investigations of the Late Devonian extinctions, Woodford Shale, southern Oklahoma. M.Sc. thesis manuscript, University of Kansas, p. 96.
- Ourisson, G., Albrecht, P., Rohmer, M., 1982. Predictive microbial biochemistry – from molecular fossils to prokaryotic membranes. Trends in Biochemical Sciences 7, 236-239.
- Overmann, J., 2008. Ecology of phototrophic sulfur bacteria. In: Sulfur Metabolism in Phototrophic Organisms 2, 375-396.
- Overmann, J., Cypionka, H., Pfennig, N., 1992. An extremely low-light adapted phototrophic sulfur bacterium from the Black Sea. Oceanography 37, 150155.
- Paxton, S.T., Olsen, T., Price, C., Gross, E., Allison, S. 2015. Spectral Gamma-Ray profile of Woodford Shale - OHMEGCO locality, Oklahoma. Ardmore Geological Society Presentations, 2015, p. 108.
- Peters, K.E., 1986. Guidelines for evaluating petroleum source rock using programmed pyrolysis. American Association of Petroleum Geologists Bulletin, 70, 318-29.
- Peters, K.E., Moldowan, J.M., 1993. The Biomarker Guide: Interpreting Molecular Fossils in Petroleum and Ancient Sediments. Prentice-Hall, Englewood Cliffs, N.J., p. 363.
- Peters, K.E., Cassa, M.R., 1994. Applied source rock geochemistry. In: Magoon, L.B., and Dow, W.G., eds., The petroleum system – from source to trap, American Association of Petroleum Geologists Memoir 94, 93-117.
- Peters, K.E., Walters, C.C., Moldowan, J.W., 2005. The biomarker guide, Volume 1, Biomarkers, and isotopes in the environment and human history. Cambridge University Press, New York, second edition, p. 1155. Volume 2, Biomarkers, and isotopes in petroleum exploration and earth history. Cambridge University Press, New York, second edition, p. 471.
- Philp, R.P., Gilbert, T.D., 1986. Biomarker distributions in Australian oils predominantly derived from terrigenous source material. In: Leythauser D., Rullkötter J., eds., Advances in Organic Geochemistry 1985. Pergamon Press, Oxford, 73-84.

- Philp, R.P., Chen, J.H., Fu, J.M., Sheng, G.Y., 1992. A geochemical investigation of crude oils and source rocks from Biyang Basin, China. Organic Geochemistry 18, 933-945.
- Philp, R.P., DeGarmo, C.D., 2020. Geochemical characterization of the Devonian-Mississippian Woodford Shale from the McAlister Cemetery Quarry, Criner Hills Uplift, Ardmore basin, Oklahoma. Marine and Petroleum Geology 112, February 2020, 104078.
- Poinsot, J., Schneckenburger, P., Adam, P., Schaeffer, P., Trendel, J., Albrecht, P., 1997. Novel polycyclic polyprenoid sulfides in sediments. Chemical Communications, 2191–2192.
- Poinsot, J., Schneckenburger, P., Adam, P., Schaeffer, P., Trendel, J.M., Riva, A., Albrecht, P., 1998. Novel polycyclic sulfides derived from regular polyprenoids in sediments: characterization, distribution, and geochemical significance. Geochimica et Cosmochimica Acta 62, 5, 805–814.
- Portas, R. M., 2009. Characterization and Origin of Fracture Patterns in the Woodford Shale in Southeastern Oklahoma for Application to Exploration and Development. M. S. thesis manuscript, University of Oklahoma, p. 110.
- Price, P.L., O'Sullivan, T., Alexander, R., 1987. The nature and occurrence of oil in Seram, Indonesia. In: Proceedings of the Indonesian Petroleum Association, 16th Annual Convention. Indonesian Petroleum Association Jakarta 1, 141-173.
- Qiao, J., Cai, X., Xiao, Q., Chen, Z., Kulkarni, P., Ferris, C., Kamarthi, S., Sridhar, S., 2019. Data on MRI brain lesion segmentation using K-means and Gaussian Mixture model-expectation maximization. Journal Data 27, 2019, 104628, p. 9.
- Quandt, L., Gottschalk, G., Ziegler, H., Stichler, W., 1977. Isotope discrimination by photosynthetic bacteria. FEMS Microbiology Letters, 1, 125-128.
- Requejo, A. G., Allan, J., Creaney, S., Gray, N. R., Cole, K. S., 1992. Aryl isoprenoids and diaromatic carotenoids in Paleozoic source rocks and oils from the Western Canada and Williston basins. Organic Geochemistry 19, 245-264.
- Riolo, J., Ludwig, B., Albrecht, P., 1985. Synthesis of ring C monoaromatic steroid hydrocarbons occurring in Geological samples. Tetrahedron Letters 26, 22, 2697-2700.
- Rodriguez, N.D., Katz, B. J., 2017. The effect of oil-based drilling mud (OBM) on the assessment of hydrocarbon charge potential: Are we underestimating source rock

potential? Annual Meeting of the American Association of Petroleum Geologists, Search and Discovery Article 90291.

- Rullkötter, J., Spiro, B., Nissenbaum, A., 1985. Biological marker characteristics of oils and asphalts from carbonate source rocks in a rapidly subsiding graben, Dead Sea. Geochimica et Cosmochimica Acta 49, 1357-1370.
- Sammy, N., 1985. Biological systems in northern Australia solar salt and fields. In: Schreiber, B.C., Harner, L., eds., 6th International Symposium on Salt. Salt Institute, Alexandria, Virginia 1, 207-215.
- Sandberg, C.A., Ziegler, W., Dreesen, R., Butler, J.L., 1988. Part 3: Late Frasnian mass extinction: conodont event stratigraphy, global changes, and possible causes. Courier Forschung-Institut Senckenberg 102, 263-307.
- Schaeffer, P., Poinsot, J., Hauke, V., Adam, P., Wehrung, P., Trendel, J.M., Albrecht, P., Dessort, D., Connan, J., 1994. Novel optically active hydrocarbons in sediments: evidence for an extensive biological cyclization of higher regular polyprenols. Angewandte Chemie International Edition 33, 11, 1166–1169.
- Schreiber, B.C., Philp, R.P., Benali, S., Helman, M.L., De la Peña, J.A., Marfil, R., Kendall, C.S., 2001. Characterization of organic matter formed in hypersaline carbonate/evaporite environments: Hydrocarbon potential and biomarkers obtained through artificial maturation studies. Journal of Petroleum Geology, 24, 3, 309-338.
- Schwark, L., Frimmel, A., 2004. Chemostratigraphy of the Posidonia Black Shale, SW Germany II. Assessment of extent and persistence of photic-zone anoxia using aryl isoprenoids distributions. Chemical Geology 206, 231-248.
- Seifert, W.K., Moldowan, J.M., 1979. The effect of biodegradation on steranes and terpanes in crude oils. Geochimica et Cosmochimica Acta 43, 111-126.
- Seifert, W.K., Moldowan, J.M., 1980. The effect of thermal stress on source-rock quality as measured by hopane stereochemistry. Physics and Chemistry of the Earth 12, 229-237.
- Seifert, W.K., Moldowan, J.M., Jones, R.W., 1980. Application of biological marker chemistry to petroleum exploration. In Proc. Tenth World Petroleum Congress, Bucharest, Romania. September 1979. Paper SP8, 425-440.
- Seifert, W.K., Moldowan, J.M., 1986. Use of biological markers in petroleum exploration. In: Johns, R.B., eds., Methods in Geochemistry and Geophysics 24, 261-290.

- Sephton, M.A., Looy C.V., Brinkhuis, H., Wignall, P.B., de Leeuw, J.W., Visscher, H., 2005. Catastrophic soil erosion during the end-Permian biotic crisis. Geology 33, 41-944.
- Serna-Bernal, A., 2013. Geological characterization of the Woodford Shale, McAlister Cemetery quarry, Criner Hills, Ardmore basin, Oklahoma. M.S. Thesis manuscript, The University of Oklahoma, p. 141.
- Singh, P., 2008. Lithofacies and sequence stratigraphic framework of the Barnett Shale, Northeast Texas. Doctoral dissertation manuscript. The University of Oklahoma, p. 227
- Sierra-Perez, R., 2011. Integrated geomechanics and geological characterization of the Devonian-Mississippian Woodford Shale. M.Sc. thesis manuscript, The University of Oklahoma, p. 123.
- Sinninghe Damsté, J.S., de Leeuw, J.W., 1990. Analysis, structure, and geochemical significance of organically-bound sulfur in the geosphere: State of the art and future research. Organic Geochemistry 16, 1077–1101.
- Sinninghe Damsté, J.S., Kock-Van Dalen, A.C., de Leeuw, Schneck, P.A., Sheng, G., Brassell, S.C., 1987. The identification of mono-, di-, and trimethyl 2-methyl-2-(4,8,12-trimethyltricedyl) chromans and their occurrence in the geosphere. Geochimica et Cosmochimica Acta, 51, 2393-2400.
- Sinninghe Damsté, J.S., Kenig, F., Koopmans, M.P., 1995. Evidence of Gammacerane as an indicator of water column stratification. Geochimica et Cosmochimica Acta 59, 9, 1895-1900.
- Sinninghe Damsté, J.S., Schouten, S., 2006. Biological markers for anoxia in the photic zone of the water column. In: Volkman, J., eds., Marine organic matter: Biomarkers, isotopes, and DNA. The Handbook of Environmental Chemistry, 127-163.
- Sirevåg, R., Ormerod, J.G, 1070. Carbon dioxide fixation in green sulfur bacteria. Biochemistry Journal 120, 399-408.
- Sirevåg, R., Buchanan, B.B., Berry J., Troughton, J.H., 1977. Mechanisms of CO_2 fixation in bacterial photosynthesis studied by the carbon isotope fractionation technique. Archaea Microbiology 112, 35-38.
- Slatt, R.M., Abousleiman, Y., 2011. Merging sequence stratigraphy and geomechanics. SEG The Leading Edge, 2001, 274-282.

- Slatt, R. M., Buckner, N., Abousleiman, Y., Sierra, R., Philp, R.P., Miceli-Romero, A., Portas, R., O'Brien, N., Tran, M., Davis, R., Wawrzyniec, T., 2012. Outcrop/behind outcrop (quarry), multiscale characterization of the Woodford gas shale, Oklahoma, in J. Breyer, eds., Shale reservoirs-giant resources for the 21st century: American Association of Petroleum Geologists AAPG Memoir 97, 1–21.
- Slatt, R. M., Rodriguez, N. D., 2012. Comparative sequence stratigraphy and organic geochemistry of gas shales: Commonality or coincidence? Journal of Natural Gas Science and Engineering 8, 68-84.
- Slatt R.M., 2013. Paleotopographic and depositional environment control on 'sweet spot' locations in some unconventional resource shales. Houston Geological Society Presentations, 2013.
- Slatt, R.M., 2013b. Stratigraphic reservoir characterization for petroleum geologists, geophysicists, and engineers: Origin, recognition, initiation, and reservoir quality. In: Developments in Petroleum Science. Second Edition, Elsevier, Netherlands, 1-671.
- Slatt, R.M., Molinares-Blanco, C., Amorocho, J.D., Cabarcas, C.L., Torres-Parada, E., 2014. Sequence stratigraphy, geomechanics, micro seismicity, and geochemistry relationships in unconventional resource shales. Proceedings from the 2nd Unconventional Resources Technology Conference URTeC 1934195.
- Slatt, R.M., Philp, P.R., Abousleiman, Y., Singh, P., Perez-Altamar, R., Portas, R., Marfurt, K.J., Madrid-Arroyo, S., O'Brien, N., Eslinger E.V., Baruch, E.T., 2012. Pore-to regional-scale integrated characterization workflow for unconventional gas shales: in J.A. Breyer, eds., Shale reservoirs-giant resources for the 21st Century. AAPG Memoir 97, 127-150.
- Slatt, R.M., 2016. Institute of Reservoir Characterization (IRC), Woodford-Mississippian consortium, Phase III technical report. The University of Oklahoma, p. 202.
- Smith, H.M., 1968. Qualitative and quantitative aspects of crude oil composition. US Bureau of Mines Bulletin 642, 1-136.
- Stout, S.A., Emsbo-Mattingly, S.D., Douglas, G.S., Uhler, A.D., McCarthy, K.J., 2015. Beyond 16 Priority Pollutant PAHs: A Review of PACs used in Environmental Forensic Chemistry. Polycyclic Aromatic Compounds 35, 285-315.
- Sullivan, K.L., 1985. Organic facies variation of the Woodford Shale in western Oklahoma. Shale Shaker 35, 76-89.

- Summons, R.E., Powell, T.G., 1986. Chlorobiaceae in Paleozoic seas revealed by biological markers, isotopes, and geology. Nature 319, 763-765.
- Summons, R.E., Powell, T.G., 1987. Identification of aryl isoprenoids in source rocks and crude oils: Biological markers for the green sulfur bacteria. Geochimica et Cosmochimica Acta 51, 3, 557-566.
- Summons, R.E., Thomas, J., Maxwell, J.R., Boreham, C.J., 1992. Secular and environmental constraints on the occurrence of dinosterane in sediments. Geochimica et Cosmochimica Acta 56, 2437–2444.
- ten Haven, H.L., de Leeuw, J.W., Schenck, P.A., 1985. Organic geochemical studies of a Messinian evaporitic basin, northern Apennines (Italy). Hydrocarbon biological markers for a hypersaline environment. Geochimica et Cosmochimica Acta 49, 2181-2191.
- ten Haven, H.L., de Leeuw, J.W., Sinninghe Damsté, J.S., Schenck, P.A., Palmer, S.E., Zumberge, J.E., 1988. Application of biological markers in the recognition of palaeohypersaline environments. In: Fleet, A.J., Klets, K., Talbot, M.R., eds., Lacustrine petroleum source rocks. Geological Society of London Special Publications 40, 123-130.
- ten Haven, H.L., Rohmer, M., Rullkötter, J., Bisseret, P., 1989.Tetrahymanol, the most likely precursor of Gammacerane, occurs ubiquitously in marine sediments. Geochimica et Cosmochimica Acta 53, 3073-3079.
- Tissot, B.P., Welte, D.H., 1984. Petroleum formation and occurrence. Berlin Springer-Verlag, p. 699.
- Tribovillard, N., Algeo, T.J., Lyons, T.W., Riboulleau, A., 2006. Trace metals as paleoredox and paleoproductivity proxies: an update. Chemical Geology 232, 12–32.
- Totten, M. W., 2011. Electron probe micro-analysis of the Woodford Shale, southcentral Oklahoma, M.S. thesis manuscript, The University of Oklahoma, p. 137.
- Turner, B., Molinares, C., Slatt, R.M., 2015. Chemostratigraphic, palynostratigraphic, and sequence stratigraphic analysis of the Woodford Shale, Wyche Farm quarry, Pontotoc County, Oklahoma. Interpretation 3, 1, SH1-SH9.
- Turner, B.W., 2016. Utilization of Chemostratigraphic Proxies for generating and refining sequence stratigraphic frameworks in mudrocks and shales. Doctoral dissertation manuscript, The University of Oklahoma, p. 135.

- Turner, B.W., Slatt, R.M., 2016. Assessing bottom water anoxia within the late Devonian Woodford Shale in the Arkoma basin, southern Oklahoma. Marine and Petroleum Geology 78, 536-546.
- van der Meer, M.T.J., Schouten, S., van Dongen, B.E., 2001. Biosynthetic controls on the ^{13}C contents of organic components in photoautotrophic bacterium Chloroflexus aurantiacus. The Journal of Biological Chemistry 276, 10971-10976.
- van Gemerden, H., 1983. Physiological ecology of purple and green bacteria. Anm Microbiology 134, 203-229.
- van Krevelen, D.W., 1961. Coal. Elsevier, New York, 113-120.
- Villalba, D.M., 2016. Organic geochemistry of the Woodford Shale, Cherokee platform, Oklahoma, and its role in a complex petroleum system. M.Sc. thesis manuscript, The University of Oklahoma, p. 126.
- Volkman, J.K., Allen, D.I., Stevenson, P.L., Burton, H.R., 1986. Bacterial and algal hydrocarbons in sediments from a saline Antarctic lake, Ace lake. Organic Geochemistry 10, 671-81.
- Volkman, J.K., Banks, M.R., Denwer, K., Aquino Neto, F.R., 1989. Biomarker composition and depositional setting of Tasmanite oil shale from northern Tasmania, Australia. Presentation at the 14th International Meeting on Organic Geochemistry, September 18-22, Paris, 1989.
- Wang, H.D., 1993. A geochemical study of potential source rocks and crude oils in the Anadarko basin, Oklahoma. Doctoral dissertation manuscript, The University of Oklahoma, p. 326.
- Wang, G., Chang, X., Wang, T.G., Simoneit, B. R., 2015. Pregnanes as molecular indicators for depositional environments of sediments and petroleum source rocks. Organic Geochemistry, 78, 110-120.
- Wang, T., 2016. An organic geochemical study of Woodford Shale and Woodford-Mississippian tight oil from Central Oklahoma. Doctoral thesis manuscript, The University of Oklahoma, p. 297.
- Waples, D.W., 1985. Geochemistry in petroleum exploration. International Human Resources Development Corporation, p. 178.

- Waples, D.W., Machihara, T., 1991. Biomarkers for geologists. AAPG Methods in Exploration Series 9, p. 91.
- Wenger, L.M., Davis, C.L., Isaksen, G.H., 2002. Multiple controls on petroleum biodegradation and impact on oil quality. Society of Petroleum Engineering (SPE) Reservoir Evaluation and Engineering 5, 375-383.
- Widayat, A.H., 2011. Paleoenviromental and paleoecological changes during the deposition of the Late Eocene Kiliran oil shale, Central Sumatra basin, Indonesia. Doctorate dissertation manuscript, Johann Wolfgang Goethe University in Frankfurt am Main, Germany, p. 144.
- Widayat, A.H., van de Schootbrugge, B., Oschmann, W., Anggayana, K., Püttmann, W., 2016. Climatic control on primary productivity changes during development of the Late Eocene Kiliran Jao lake, Central Sumatra Basin, Indonesia. International Journal of Coal Geology 165, 1, 133-141.
- Wilkes, H., Boreham, C., Harms, G., Zengler, K., Rabus, R., 2000. Anaerobic degradation and carbon isotopic fractionation of alkylbenzenes in crude oil by sulfate-reducing bacteria. Organic Geochemistry 31, 101-115.
- Williford, K.H., Ushikubo, T., Lepot, K., Kitajima, K., Hallmann, C., Spicuzza, M.J., Valley, J.W., 2016. Carbon and sulfur isotopic signatures of ancient life and environment at the microbial scale: Neoarchean shales and carbonates. Geobiology, 14, 2, 105–28.
- Yang, B., 1991. Geochemical characteristics of oil from well Shacan 2 in the Tarim basin. Journal of Southeast Asian Earth Sciences 5, 1–4, 401-406.
- Zhang, J., 2016. Comprehensive reservoir characterization of the Woodford Shale in parts of Garfield and Kingfisher Counties, Oklahoma. M.Sc. thesis manuscript, The University of Oklahoma, p. 144.
- Zhang, J., Slatt R.M., 2019. The significance of karst unconformities on overlying resource shales: Lessons learned from the Devonian Woodford formation applied to the Permian Wolfcamp Shale. Interpretation, 7, 4, SK33-SK-43.
- Zumberge, J.E., 1984. Source rock of the La Luna Formation (U. Cretaceous) in the Middle Magdalena Valley, Columbia. Studies in Geology 18, 127-134.

Chapter IV: Machine learning applications in unconventional reservoir characterization and simulation: Woodford Shale case study.

Torres-Parada, E.J., Sinha, S., Infante-Paez L.E., Slatt, R.M., and Marfurt, K.J.

4.1. Abstract

Estimations of geological, geochemical, and geomechanical properties are vital to maximizing production and minimizing cost in the development of shale resource assets like the Woodford Shale of Oklahoma. Whenever possible, such estimates should be made under subsurface temperature and pressure conditions, using both laboratory rock-mechanics measurements and well log control. In this paper, we couple machine learning Kohonen Self-Organizing Maps (SOM) and acoustic impedance (Z_p) to construct a static geocellular model including estimates of porosity, total organic carbon (%TOC), Young's modulus, shear modulus, Biot's coefficient, Poisson's ratio, and stress orientations. We couple the static geological models with reservoir simulator software and history matching to construct a suite of common production type curves areas. These type curve areas help to estimate the expected ultimate recovery for non-produced areas of the seismic survey. The resulting unconventional reservoir model provides geologically consistent type curve areas, which we find to be in excellent agreement with existing production data for the enclosed mini-basin fill areas of the Woodford Shale in the north of Oklahoma.

4.2.Introduction

Geoscientists have used geostatistical analysis to help construct reservoir models for over 20 years (Yarus, 1994; Kelkar and Perez, 2001; Deutsch, 2002; Shepherd, 2009). In conventional reservoir models, we assume that geological data are spatially correlated, thereby allowing us to integrate sparse measurements from wells with more continuously measured data from surface

seismic surveys (Kelkar and Perez, 2001; Deutsch, 2002). These workflows allow us to construct models of the vertical and lateral lithofacies variation of rock lithofacies as well as their associated petrophysical properties of oil saturation, water saturation, porosity, and permeability. Geostatistics provides a means to quantify the spatial correlation of these petrophysical properties and thereby populate cells between wells using sequential indicator simulation or sequential Gaussian simulation methods (Goovaerts, 1994, 1997; Kelkar and Perez, 2001; Deutsch, 2002; Pranter et al., 2004; Coburn et al., 2006; Shepherd, 2009; Manchuk and Deutsch, 2012; Babak et al., 2013; Allen and Pranter, 2016). For the unconventional static reservoir model, we apply well logs and inter-well calculations of industry-standard geological and geomechanical properties: total organic carbon (%TOC), Young's modulus, shear modulus, Biot's coefficient, Poisson's ratio, and stress orientations (Baree and Gilbert, 2009; Mullen et al., 2007; Ghassemi et al., 2013; Kumar and Ghassemi, 2018; Ye et al., 2018).

The machine learning applications of 3D seismic data in geological studies focus on comparing different methods for estimating seismic facies and their distribution (Chopra and Marfurt, 2014; Zhao et al., 2015; Infante-Paez and Marfurt, 2018). These methodologies are commonly (but not limited to) the multilayer perceptron network, self-organizing maps, support vector machine, K-means, generative topographic maps (Meldahl et al., 2011; Roy and Marfurt, 2013; Snyder, 2016; Zhao et al., 2016; Qi et al., 2016). In seismic interpretation, self-organizing maps (SOM) is a clustering technique that extracts similar patterns across multiple seismic attribute volumes and displays those similarities as a color-coded map, with the same colors representing clusters that a human interpreter can visualize as similar facies (Zhao et al., 2016). Infante-Paez and Marfurt (2018) highlight that the input attributes to feed the SOM should be of three types: attributes that highlight the continuity of the reflectors, how layer cake the reflectors

are (GLCM homogeneity and entropy); attributes that highlight the amplitude (peak spectral magnitude); attributes that recognize the frequency (peak spectral frequency) of the target patterns.

The petroleum industry standards of reservoir engineering analyses for production forecasts and reserve calculations are based on declining type curve analysis (Issaka and Ambastha, 1996). A type curve is a statistical average declining production curve of oil, gas and water, that is used to assign the hydrocarbons expected ultimate recovery (EUR) and to evaluate the proved developed producing (PDP) and proved undeveloped non-producing (PDNP) reserves (Issaka and Ambastha, 1996; Fetkovic et al., 1996; Joshi and Lee, 2013; Muralidhara and Joshi, 2018; Joshi et al., 2019). In unconventional resource shale, the type curves are used to represent the expected results for all the wells to be drilled under similar reservoir conditions in a specified area, using the EUR data from previously drilled and producing wells and therefore, defining a type curve area (Joshi and Lee, 2013; Muralidhara and Joshi, 2018; Joshi et al., 2019).

For our case study, we lack a dense data set of well EUR inventory to calculate type curve areas. For this reason, we use static models of geological and geomechanical properties guided by SOM clusters as input to the unconventional shale reservoir flow simulation to estimate the needed type curve areas and EURs. The results of our simulations are compared with reported reserves by the operator in PDP areas that are inside our seismic survey.

We begin our paper with a review of the geology of the Woodford Shale of Oklahoma. We then describe our methodology, calculations and conclude with a discussion of the impact of our simulation results as well as of the value and limitations of our workflow.

4.3.Geology of Woodford shale in the Northern part of Oklahoma

The Upper Devonian-Lower Mississippian age Woodford Shale is present in the Oklahoman geological provinces Anadarko basin, Cherokee platform, Ardmore basin and Arkoma basin (Figure 4.1 and Figure 4.2) and consists of organic-rich black shale with intercalations of chert, siltstone, sandstone, dolostone, and light-colored shale (Slatt et al., 2012; Molinares, 2013; Turner et al., 2015). Laminations of reddish-brown clay, greenish clay and organic matter with scattered siliceous concretions are also present in the formation (Kirkland et al., 1992; Comer, 2005).

Although the Woodford Shale is a prolific gas and oil shale reservoir, Jarvie et al. (2005 and 2007) and Cardott (2009 and 2012) stated that it is essential to recognize its internal vertical and lateral stratigraphic variations. Such detailed characterization can identify enclosed highly restricted mini-basin fill deposits that catch and preserve more organic matter and clay content than more open marine Woodford Shale layers. The more open marine layers will exhibit higher silica content and thus higher brittleness, as well as higher total porosity.

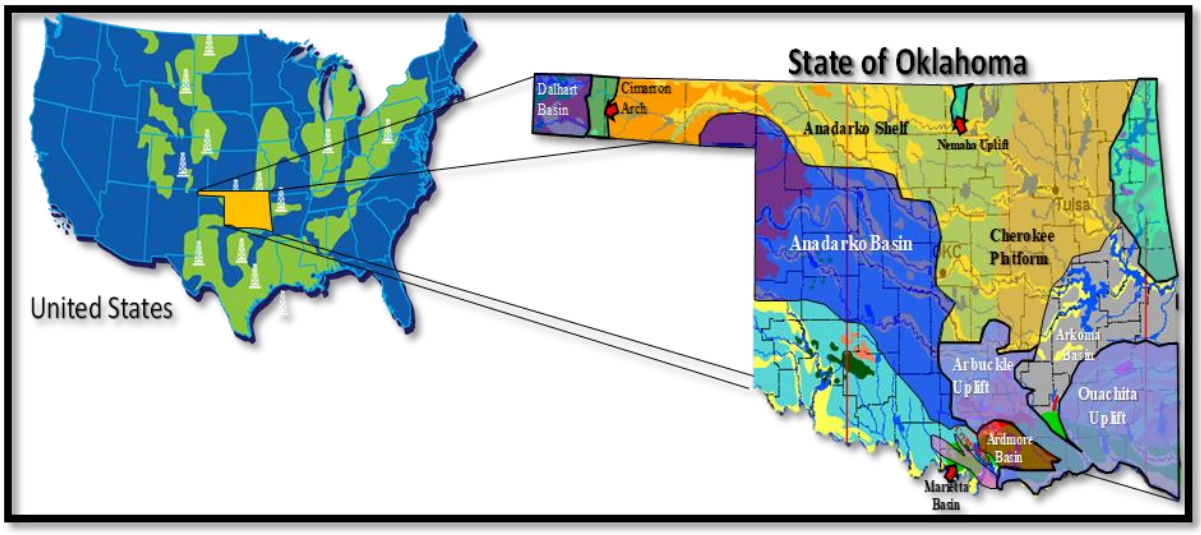

Figure 4.1. State of Oklahoma geological provinces and sedimentary basins (modified after Northcutt et al. [2001], Liborius et al. [2018] and Energy Information Administration [2016]). The study area is a 3D seismic survey in the Anadarko basin, Oklahoma.

The Woodford Shale unconformably overlies the limestones and dolomites of the Silurian-Devonian age Hunton group and grades conformably into fine-grained silty limestones interbedded with thin layers of dark-grey shales from the Sycamore formation (Figure 4.2; Portas, 2009; Slatt et al., 2012). Cardott (2012) emphasized that the Woodford Shale has a series of stratigraphic equivalents that extend over the central and eastern United States (e.g., Chattanooga Shale, Arkansas Novaculite, Antrim Shale, Bakken Shale, New Albany Shale, and Marcellus Shale). It has been proposed that the Woodford Shale represents a global major marine transgression which occurred during the Late Devonian (Figure 4.2, Figure 4.3; Sullivan, 1985; Kirkland et al., 1992; Northcutt et al., 2001; Comer, 2005; Slatt et al., 2012; Cardott,2012).

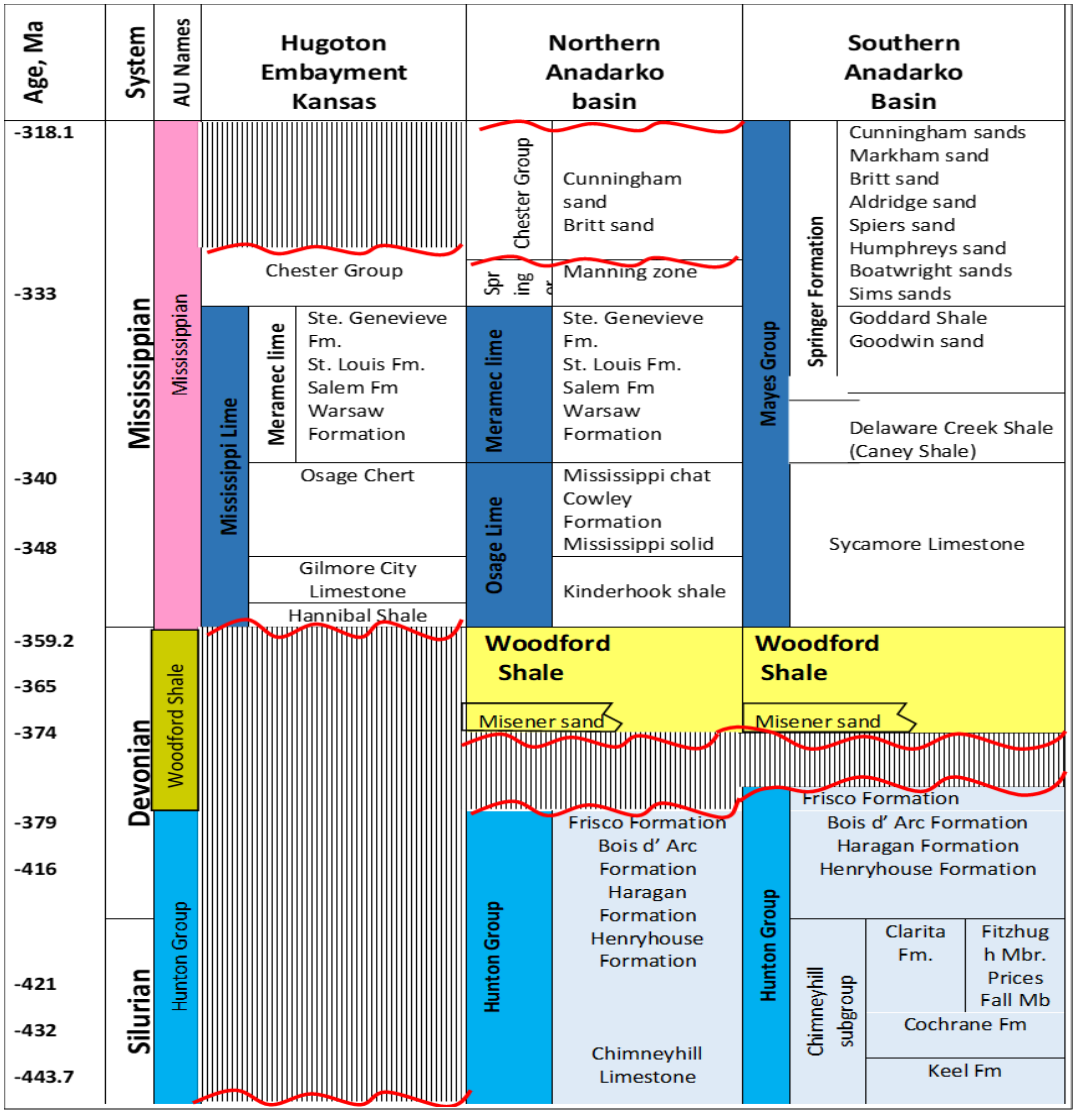

Figure 4.2. A general stratigraphic chart that highlights the significant unconformities at the base of the Woodford Shale in the Oklahoman basins (modified after Liborius et al. [2018] and Slatt [2016]).

We identify the enclosed mini-basin fill settings in this study area by mapping the structure of the Woodford Shale and Hunton group tops. We then use the resulting time-thickness [ms] variations, combined with the identification of unconformities at the base of the Woodford Shale by using 3D seismic attributes of coherence, most positive and most negative curvature to delineate local variations of the regional Woodford Shale depositional model (Figure 4.3) proposed by Slatt (2016).

The interpreted depositional trend suggests that during a low stand of sea-level, incised valley and karst topography modified the paleo Hunton group carbonate shelf, resulting in an irregular surface (Figure 4.3). These processes create areas with paleo topographic barriers, which can provide discontinuous catchment areas for ponding of enclosed mini-basin fill water masses, creating restricted water circulation and establishing conditions for higher deposition and preservation of organic matter (Figure 4.3). In these enclosed mini-basin fill settings, the Woodford Shale is often thicker than the underlying Hunton group carbonates.

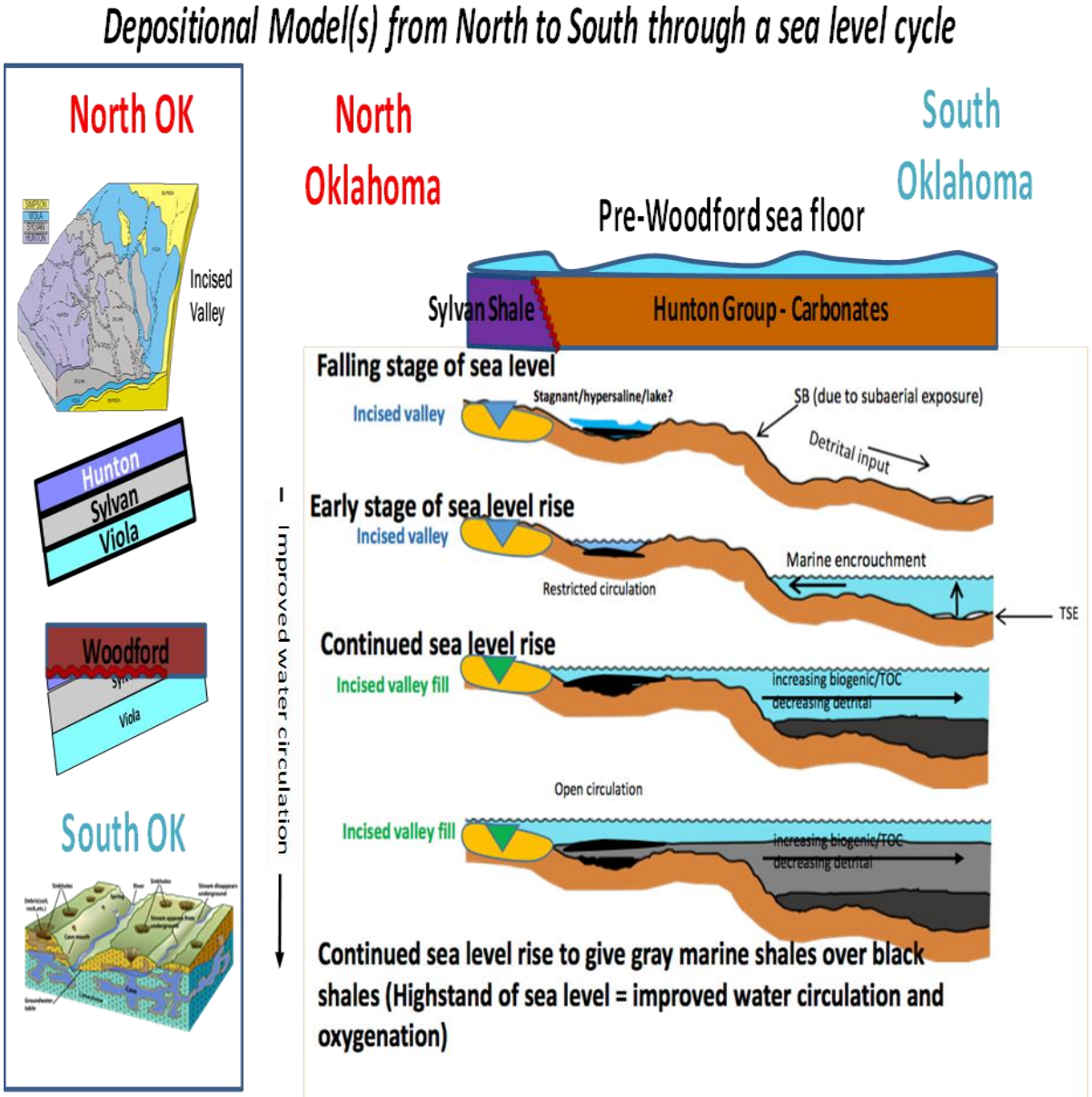

Figure 4.3. Depositional model of the Woodford Shale through one eustatic sea-level cycle (Torres-Parada et al., 2017; modified after Bauernfeind [1990], Grotzinger and Jordan [2010] and Slatt [2016]). The early stage of falling sea level may result in water mass isolation and restricted water circulation over topographic depressions left by karst/incised valley development on the underlying carbonate surface (Hunton limestone in the case of the Woodford). TSE= Transgressive surface of erosion; SB= Sequence boundary.

4.4.Methodology

In this study, we select a total of 21 wells with the criteria that these have well logs that cover the complete Woodford Shale stratigraphic section, including density, density-porosity, and P-wave (compressional sonic) logs to allow a precise tie with the seismic volume. The geomechanics poroelastic properties were determined by combining petroleum industry-accepted dynamic methods for unconventional resource shales (Zoback et al., 2003; Mullen et al., 2007; Rickman et al., 2008; Barree and Gilbert, 2009; Ghassemi et al., 2009, 2013). The geomechanics calculations are then calibrated with the results of static laboratory experiments conducted by Sierra-Perez (2011) for a Woodford Shale core in south Oklahoma. These sets of equations allowed the calculation and determination of Young's modulus (E), Poisson's ratio (v), bulk modulus (K) and the shear modulus (G). We provide a detailed methodology of the geomechanics calculations in Appendix A. Figure 4.4 summarizes the applied workflow, using well logs to derive geomechanical and petrophysical properties. We use the seismic acoustic inversion (calculated impedance volume) to guide the well log derived features in a 3D geocellular static model as recommended by Hampson et al. (2001).

The inversion and multi-attribute volumes serve as inputs to volumetric unsupervised clustering algorithms SOM, GTM and K-means (Chopra and Marfurt, 2007; Roy et al., 2013; Infante-Paez and Marfurt, 2018). Unsupervised clustering means that no user interpretation is applied (Roy et al., 2013; Zhao et al., 2015; Infante-Paez and Marfurt, 2018; Qiao et al., 2019).

K-means is a clustering algorithm that uses an iterative workflow that minimizes the sum of distances from each sample to its cluster centroid over all clusters (Sabeti et al., 2009; Franti and Sieranoja, 2019; Qiao et al., 2019). This algorithm moves samples between clusters until the

sum of distances is a minimum (Sabeti et al., 2009). An elbow plot workflow allows one to estimate the number of clusters that are as compact and well-separated as possible (Qiao et al., 2019).

SOM is a methodology that projects the multi-dimensional data (where each attribute volume adds a dimension) onto a much lower dimensional defined mathematical surface or "manifold" that preserves the geometrical relationship among the data points (Kohonen, 2001; Strecker and Uden, 2002). By construction, this deformed surface is, in turn, mapped to simpler undeformed latent space . Each SOM unit within the latent space preserves the metric relationships and topologies of the multidimensional input data (Kohonen, 2001; Roy et al., 2013; Zhao et al., 2015). The result is that voxels with similar attribute expressions will be mapped to near locations in the latent space. The latent space 2D mapping color bar provides a color-coded image amenable for seismic facies analysis (Strecker and Uden, 2002; Chopra and Marfurt, 2014; Zhao et al., 2015; Infante-Paez and Marfurt, 2018).

GTM is a technique developed as an alternative to solve the shortcomings of SOM. Although SOM assigns each voxel to the cluster (and hence a color) that best represents it, it does not provide a measure of how well that cluster (or any other cluster) represents the voxel. While we know which is the most likely cluster (facies), we do not know how confident the prediction is. GTM is and represents a nonlinear dimension reduction method based on Bayesian principles, providing a probabilistic representation of the data vectors in latent space (Bishop et al., 1998; Roy et al., 2014; Chopra and Marfurt, 2014). Roy et al. (2014) and Zhao et al. (2015) concluded that in 3D seismic application, the GTM is a probabilistic reformulation of SOM that takes care of most of the SOM shortcomings related to the selection of the training radius and the learning rate of the data sets for obtaining a measurement of confidence.

For constructing the geocellular static models, we guide each property in between the vertical wells using a Gaussian random function simulation (GRFS) with collocated cokriging of the SOM and Z_p volumes. This GRFS was used as suggested by Daly et al. (2010), Xiao et al. (2018) and Cervantes-Velasquez (2019) for interpolating the geological properties using multiple seismic volumes as a derived property probability volume. The first variable in the GRFS collocated cokriging was the SOM volume, and the second variable was the Z_p volume. Regularly, geocellular models propagate properties by a previously defined lateral variogram by the user (Kelkar and Perez, 2001), which is defined by comparing the average property value in each vertical control point and the relative distances between these points. In our case, our geocellular modeling of geological properties was guided using the SOM and Zp as probability volumes.

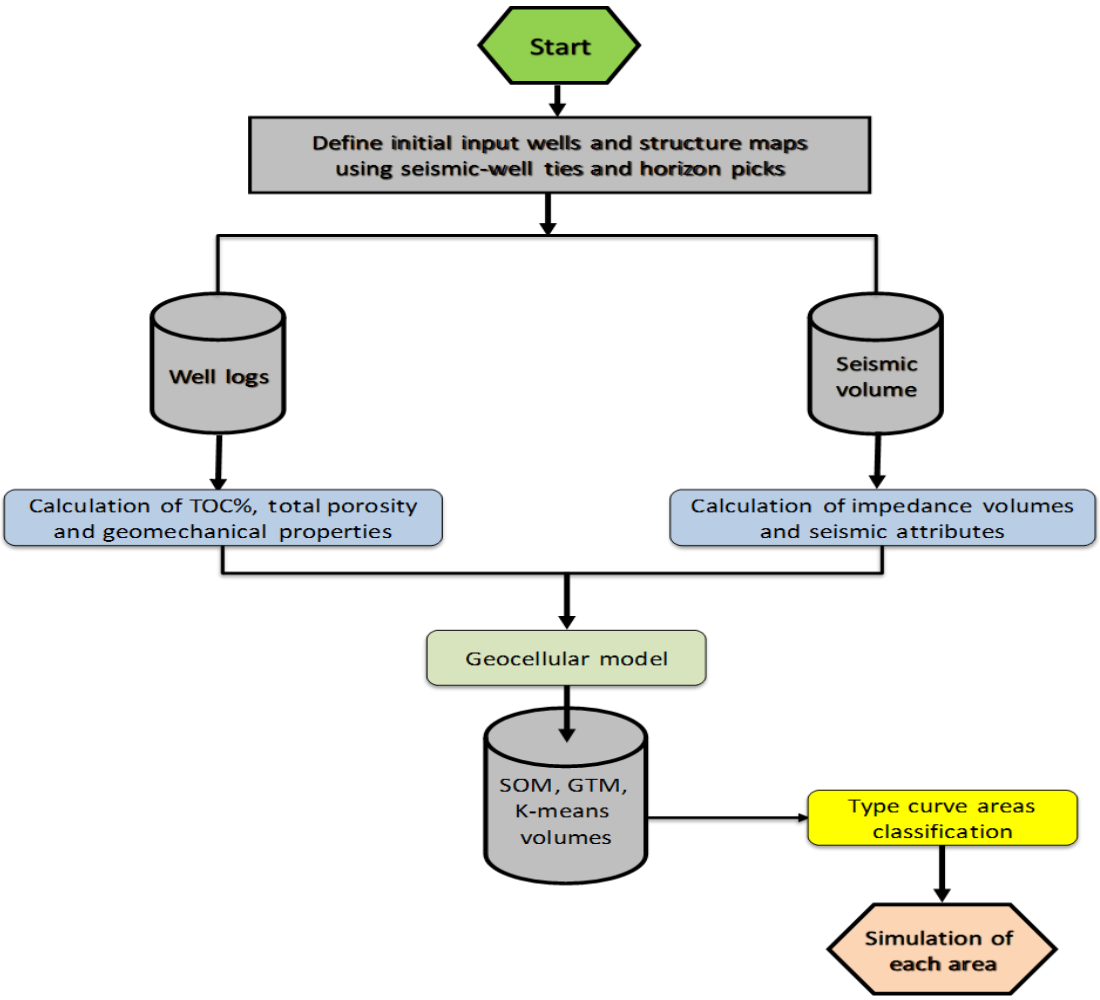

Figure 4.4. Workflow used in this study. We compute the petrophysical and geomechanical properties from the density and P-wave well logs as described in Appendix A. We then use the seismic amplitude volume in two ways, first to define horizons and faults necessary to construct our geocellular model, and second as input for the post-stack seismic impedance inversion which we propagate with collocated cokriging to construct probability of the geomechanical and petrophysical properties at each cell of the static model. These properties, along with the seismic amplitude volume, are input to SOM, GTM, and K-means clustering algorithms. We use the resulting clusters to define type curve areas for subsequent simulation.

4.4.1. Computing the geomechanical properties

Reservoir geomechanical analysis requires the integration of the state of stress, pore pressure, physical properties of reservoirs, natural fractures, major and minor faults, and cap rocks, as well as the formations forming the comprising overburden (Zoback et al., 2003). Geomechanical analysis allows us to understand the interactions between geological conditions, engineering and production practices (Ghassemi et al., 2009, 2013).

The primary parameters controlling these interactions are the state of *in-situ* stress, rock strength, bedding orientation, poroelastic properties (*E, v*), pore pressure, distribution of fractures and faults, wellbore trajectory and mud weight (Liu, 2017; Kumar and Ghassemi, 2018). We define the state of stress in an unconventional reservoir in terms of the vertical stress (*Sv*) and two horizontal stresses (S_{hmax} and S_{hmin}) that occur perpendicularly (Ghassemi et al., 2009, 2013; Sierra-Perez, 2011; Kumar and Ghassemi, 2018). We adopt the geomechanics methodology proposed by Yale and Jamieson (1994) and Yasar and Erdogan (2004), which was modified by Sierra-Perez (2011) for the Woodford Shale Wyche-1 core analysis. This methodology is explained in detail in Appendix A. In our specific study, we estimate *E, v, Sv,* S_{hmax} and S_{hmin}, by computing the P-wave (*Vp*) and S-wave (*Vs*) velocities using the Castagna relationship (1986; 1993). We then calibrate the calculations with measured *Vs* in three wells in the study area.

4.4.2. Computing dynamic moduli from velocities

Surface seismic estimates of density require high quality and high incident angle migrated data gathers (Li et al., 2016; Verma et al., 2016). For our seismic survey, we calculate the rock sample density (ρ) directly from the density well log and then use the seismically derived P- and S-wave impedances to compute the required elastic properties. For the P-wave velocity calculation, 21 wells had the compressional sonic log, three of these with a measured shear sonic

log. All the wells were tied to the seismic volume. Using the density well log, the P-wave velocity (*Vp*) and S-wave velocity (*Vs*) we calculated Young's modulus (E), Poisson's ratio (v), bulk modulus (K) and shear modulus (G) using the Yale and Jamieson (1994) and Yasar and Erdogan (2004) equations:

$$E = \frac{\rho V_s^2 \left(3V_p^2 - 4V_s^2\right)}{\left(V_p^2 - V_s^2\right)}, \tag{4.1}$$

$$v = \frac{\left(V_p^2 - 2V_s^2\right)}{2\left(V_p^2 - V_s^2\right)}, \tag{4.2}$$

$$K = \rho V_p^2 - \frac{4}{3}\rho V_s^2, \tag{4.3}$$

and $$G = \rho V_s^2. \tag{4.4}$$

We compute the uniaxial confined stress (UCS) using Wang's (2000) equations, calibrated with Sierra-Perez's (2011) dynamic and static relationships for the Woodford Shale with *E* and *v*.

$$UCS(MPa) = 7.22E^{0.712}, \quad \text{for shale intervals,} \tag{4.5}$$

$$UCS(MPa) = 25.1E^{0.3}, \quad \text{for dolomite-rich intervals, and} \tag{4.6}$$

$$T_o = 10\%UCS, \quad \text{for Tensile Stress.} \tag{4.7}$$

The computed fracture gradient and the fracture toughness variations for the zones of interest using the methodologies of Havens et al. (2010) and Wang et al. (2011):

Fracture Toughness: $$S_h = \left(\frac{v}{1-v}\right) S_v + \left(\frac{1-2v}{1-v}\right) \alpha\rho, \tag{4.8}$$

minimum horizontal Stress: $$FG = \frac{S_h + T_o}{Z}, \tag{4.9}$$

and

Fracture Gradient:

$$K_{ic} = 0.05E, \tag{4.10}$$

where the depth (Z) is measured in meters.

4.4.3. Computing the dynamic fracture gradient

The *in-situ* pore pressure (PP) within unconventional resource shale, like the Woodford shale, is challenging to measure accurately due to its very low intrinsic permeability using conventional means of well testing (Kumar and Ghassemi, 2018). Specifically, the transient pressures cannot be stabilized in a reasonable amount of time using a modular dynamic test (MDT) commonly used for conventional reservoirs (Kumar and Ghassemi, 2018). In conventional reservoirs, the pore pressure is often approximated by the mud weight when there is neither gas intrusion nor lost - circulation condition, i.e., underbalanced or above fracture gradient (Liu, 2017). We applied the same assumptions using the mud weight information at the reservoir depth and estimated a constant pressure of 3,500 PSI.

4.4.4. Total organic carbon (%TOC) calculations

We compute internal organic facies variations in the Woodford Shale, calculating the %TOC [wt.%] in the wells of the study area using both the Passey (1990) and Schmoker (1979 and 1981) methodologies (Figure 4.5). The well S-A of the study area provides a complete cored Woodford Shale section that allowed us to measure %TOC in the laboratory (Figure 4.5). These %TOC measurements then served as calibration points for the estimations of organic matter using well logs (Figure 4.5).

We extract the seismic attributes in the seismic window between the Woodford Shale seismic top and base (Figure 4.6 - 4.8), and then we compute the acoustic impedance (Z_P) inversion to obtain a %TOC volume estimate, which varies depending upon rock properties (Hampson et al., 2001; Chopra and Marfurt, 2007; Verma et al., 2013). The model-based inversion workflow begins with a low-frequency background geological model of the acoustic impedance (Verma et al., 2013; Infante-Paez et al., 2017), where the low frequencies (0 -10 Hz) are obtained from Z_P measurements at each of the well locations.

We then correlate each individual low-frequency volume with instantaneous 3D seismic attributes from the seismic amplitude volume. The applied instantaneous seismic attributes in the multi-linear regression are the RMS amplitude, peak frequency magnitude, peak amplitude, and instantaneous frequency. These calculations produce a smoothed low-frequency Z_P model (Figure 4.9), which was iteratively modified until we minimized the error between the calculated Z_P by that model and the original seismic data Z_P volume (Figure 4.10). In addition, we observe the Woodford Shale has the lowest impedance when compared to the pre-Woodford Hunton group and post-Woodford Mississippian strata (Meramec and Osage formations; Figure 4.9, Figure 4.10).

When comparing the calculations of %TOC using the Passey et al. (1990) methodology based on resistivity, *Vp* logs and the S-A core %TOC measurements, we obtained estimates that were too large for the low %TOC pre-Woodford and post-Woodford strata (Figure 4.5). In contrast, we found the %TOC calculations obtained based on Schmoker (1979 and 1981) methodology provides a more accurate pre and post-Woodford strata estimates (blue well log curve in Figure 4.5). We attribute this improvement to Schmoker's (1979 and 1981) use of the bulk density log (equation 4.12), which for our rocks has an inverse correlation with the organic matter content. When calibrating the calculated %TOC against Rock-Eval measurements we obtain:

$$\%TOC\ [wt.\%] = [(-56.547*RHOB) + 154.867] / 2. \quad (4.12)$$

Using the model-based impedance inversion of the Woodford Shale to identify vertical and lateral facies changes helped the delineation of higher %TOC layers (Figure 4.9 and Figure 4.10), where high %TOC correlates with low Z_p.

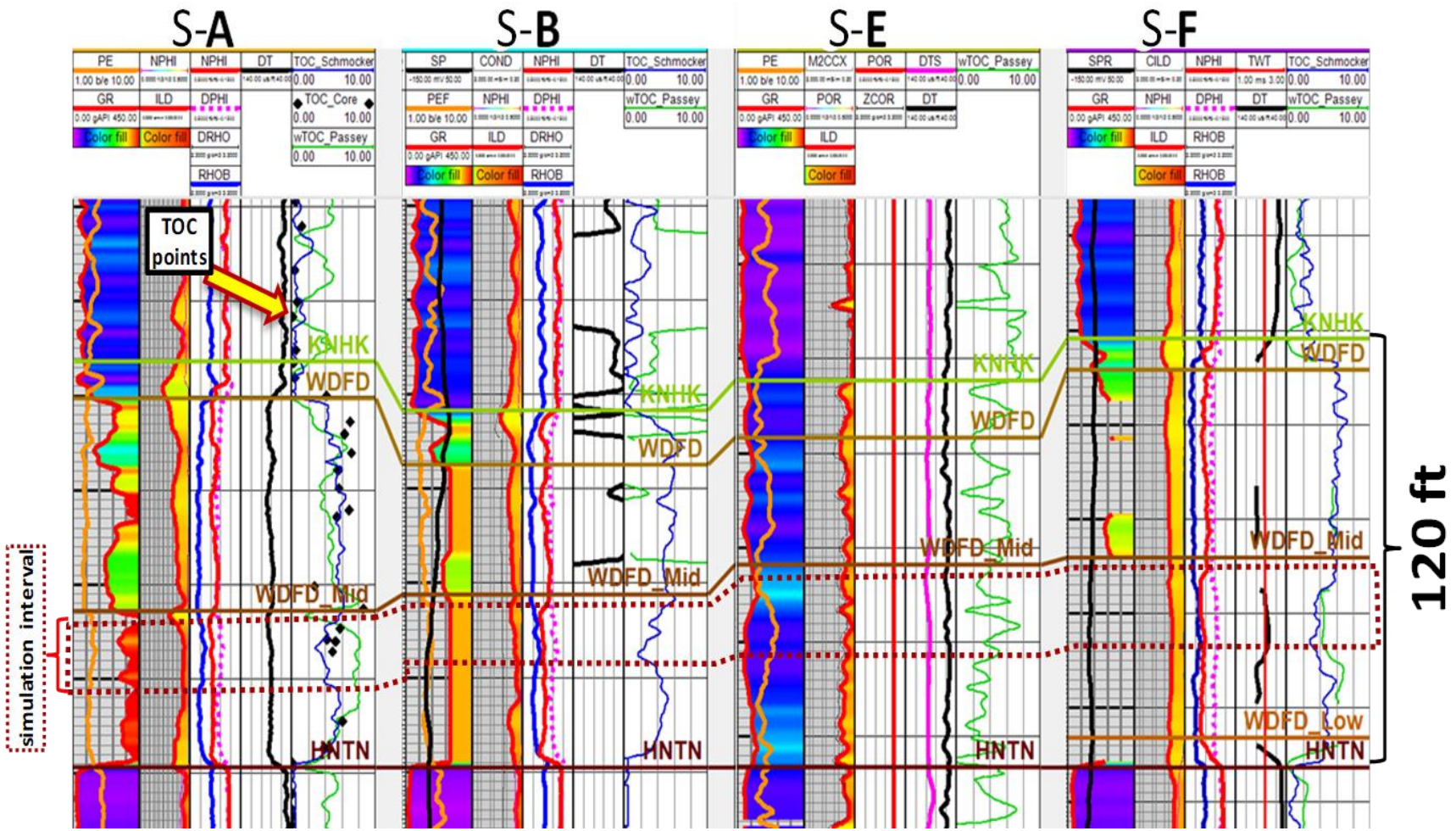

Figure 4.5. Stratigraphic correlation of the Woodford Shale (WDFD) along the study area flattened on the Hunton (HNTN) group top. Well S-A has a cored section with measured %TOC [wt.%] that covers the entire Woodford Shale (black diamonds in well S-A). We used equation 4.11 to compute %TOC at the wells lacking core data points. The %TOC calculations in the right log track in each well used both Passey et al. (1990; light green curve) and Schmoker (1979, 1981; dark blue %TOC curve) methodologies. Note that in the right track in well S-A, the Schmoker's %TOC matches better the core points (black points), whereas the Passey curve (light green) overestimates %TOC below the Hunton top (HNTN horizon) and above the Woodford top (WDFD horizon), giving a better confidence in the Schmoker (1979, 1981) methodology for the study area.

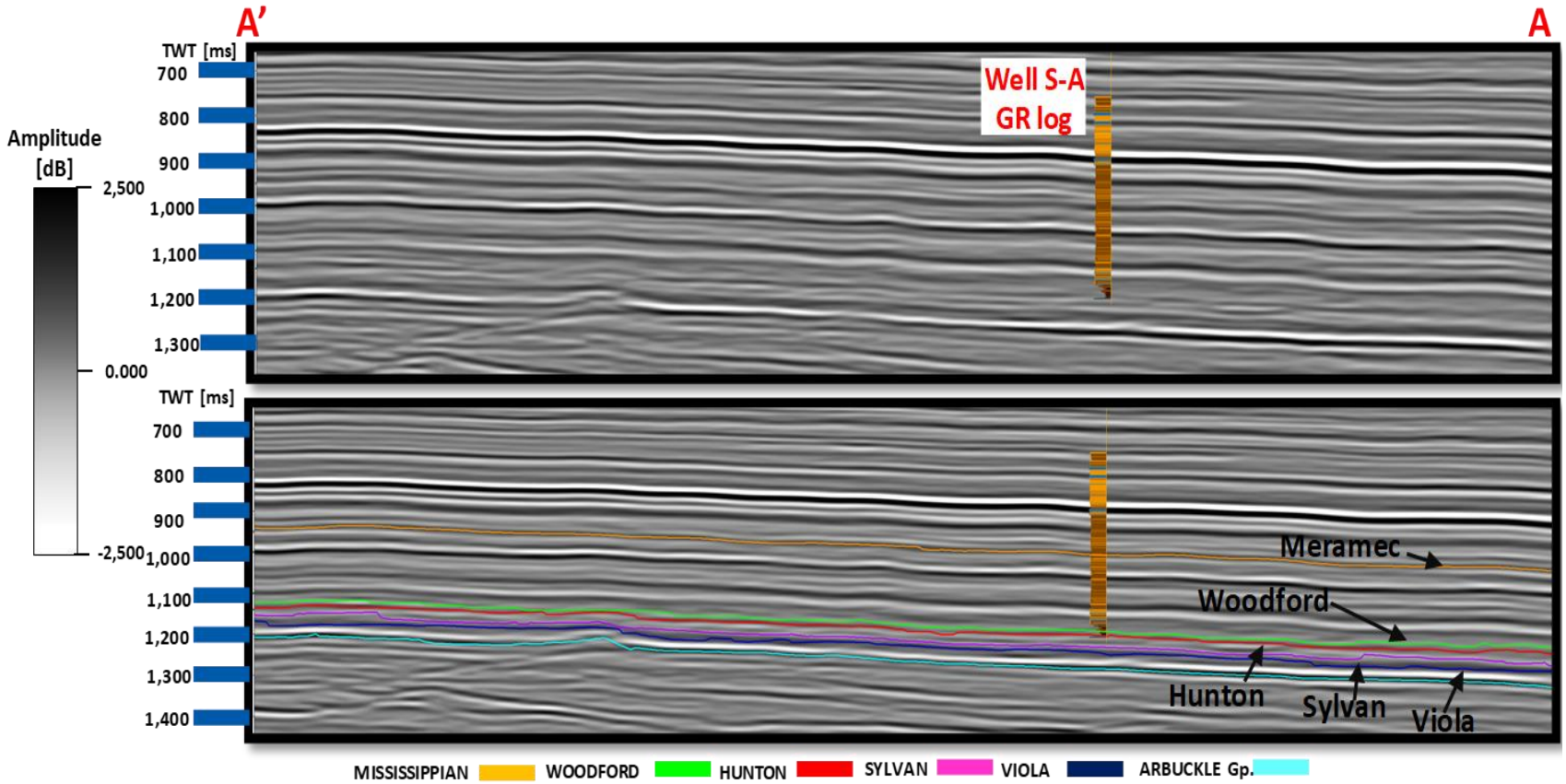

Figure 4.6. (a) A representative vertical slice through the seismic data volume and (b) with interpretation showing the Woodford Shale top, tied with well S-A. The Woodford Shale top is a seismic trough (negative amplitude). The Woodford Shale base (Hunton Group top) is a bright, positive amplitude horizon. Location of the line shown in Figure 4.7.

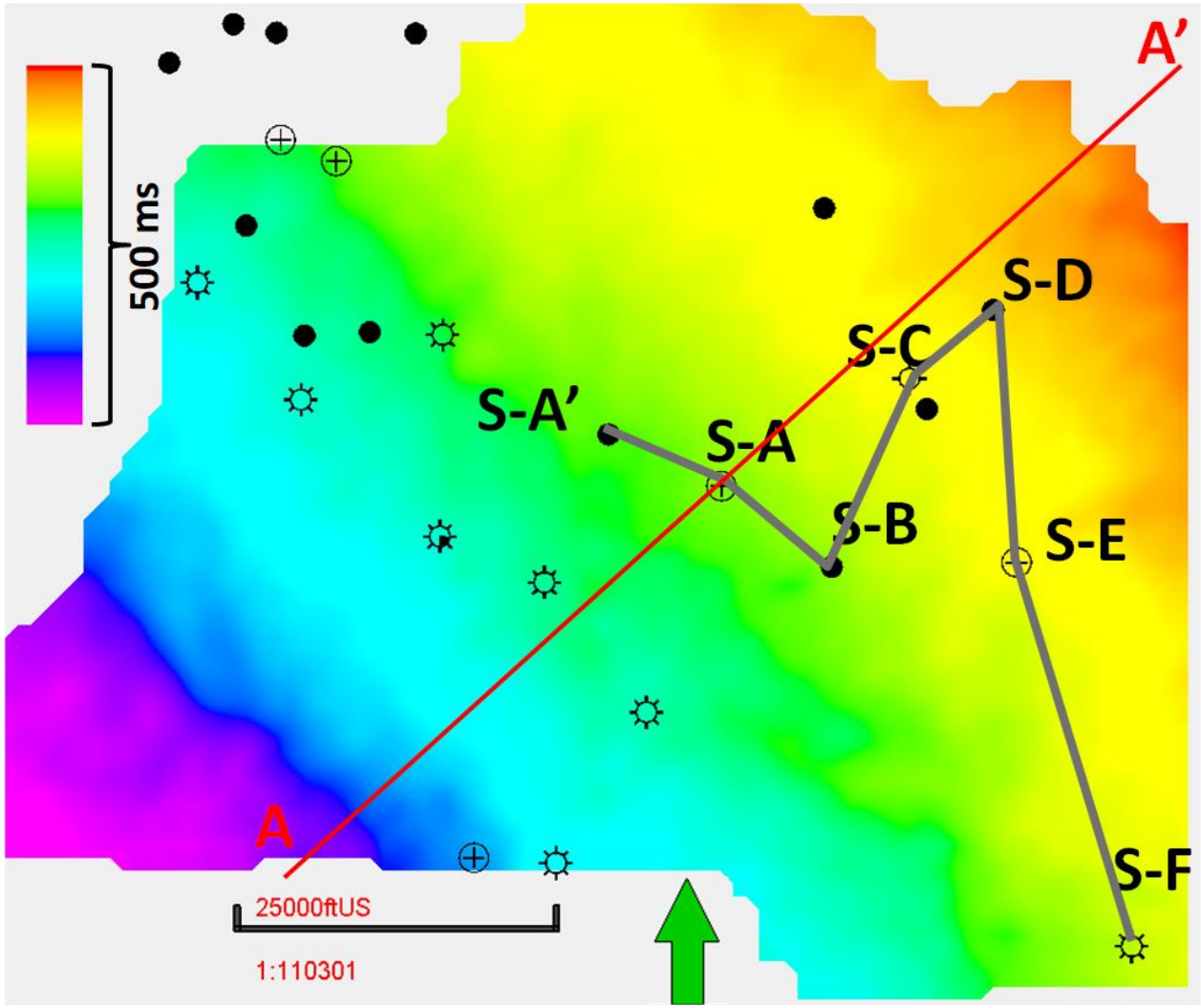

Figure 4.7. Woodford Shale time structure map [ms] in the study area. The time structure maps were converted to depth and used to define our geocellular model. The red line corresponds to the seismic vertical slice in Figure 4.6. Relative times used to protect data sensitivity.

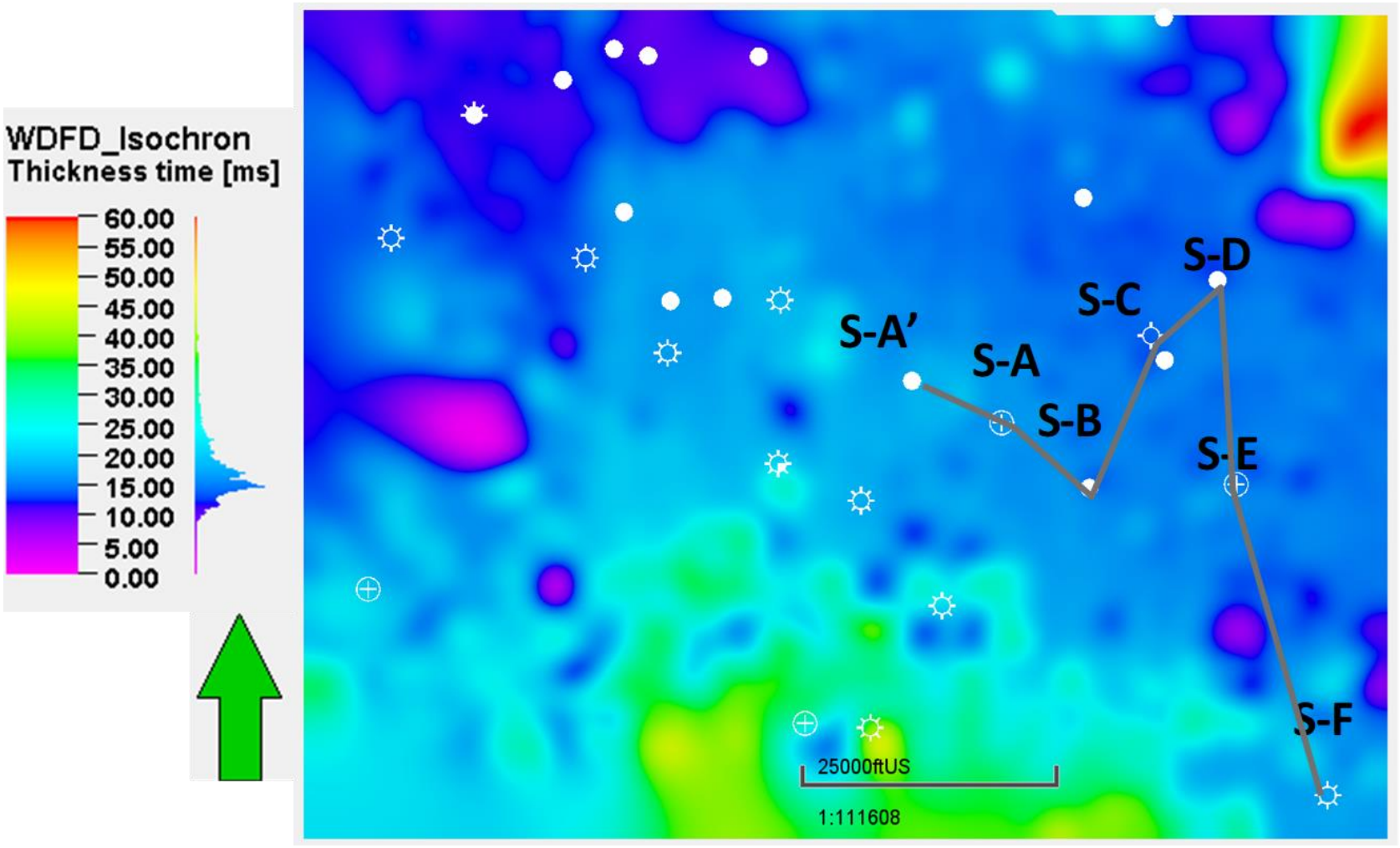

Figure 4.8. Woodford Shale time thickness map [ms]. Note the increased thickness in the northeast and south of the study area (thickness higher than 45 ms). Wells from stratigraphic correlation shown in Figure 4.5.

Because it uses a seismic wavelet using the well log information, Z_p inversion revealed a higher vertical resolution and lateral impedance changes within the Woodford Shale than the seismic amplitude itself(Figure 4.10 and Figure 4.11). The generated seismic %TOC volume was then applied to the reservoir modeling to laterally and vertically guide the calculated %TOC and density-porosity calculated at each well location. We performed the property guidance using the Z_p volume as probability trend maps with collocated cokriging of the petrophysical properties modeling, using a sequential Gaussian simulation algorithm.

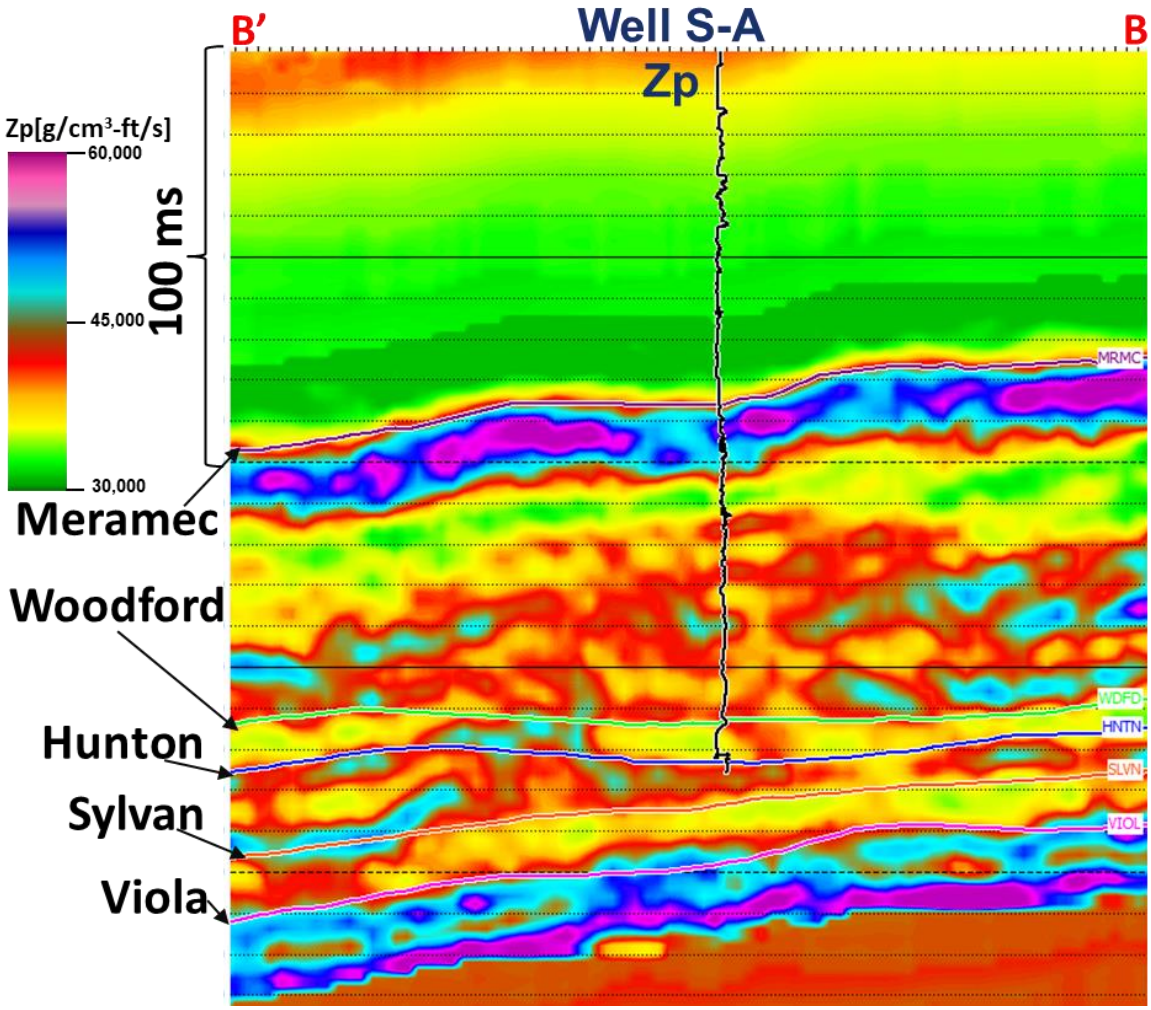

Figure 4.9. A seismic vertical slice of the low-frequency acoustic impedance (P-impedance) background model in the S-A cored well obtained using a neural network and a suite of instantaneous attributes. The well log corresponds to the P-impedance (Z_p) curve.

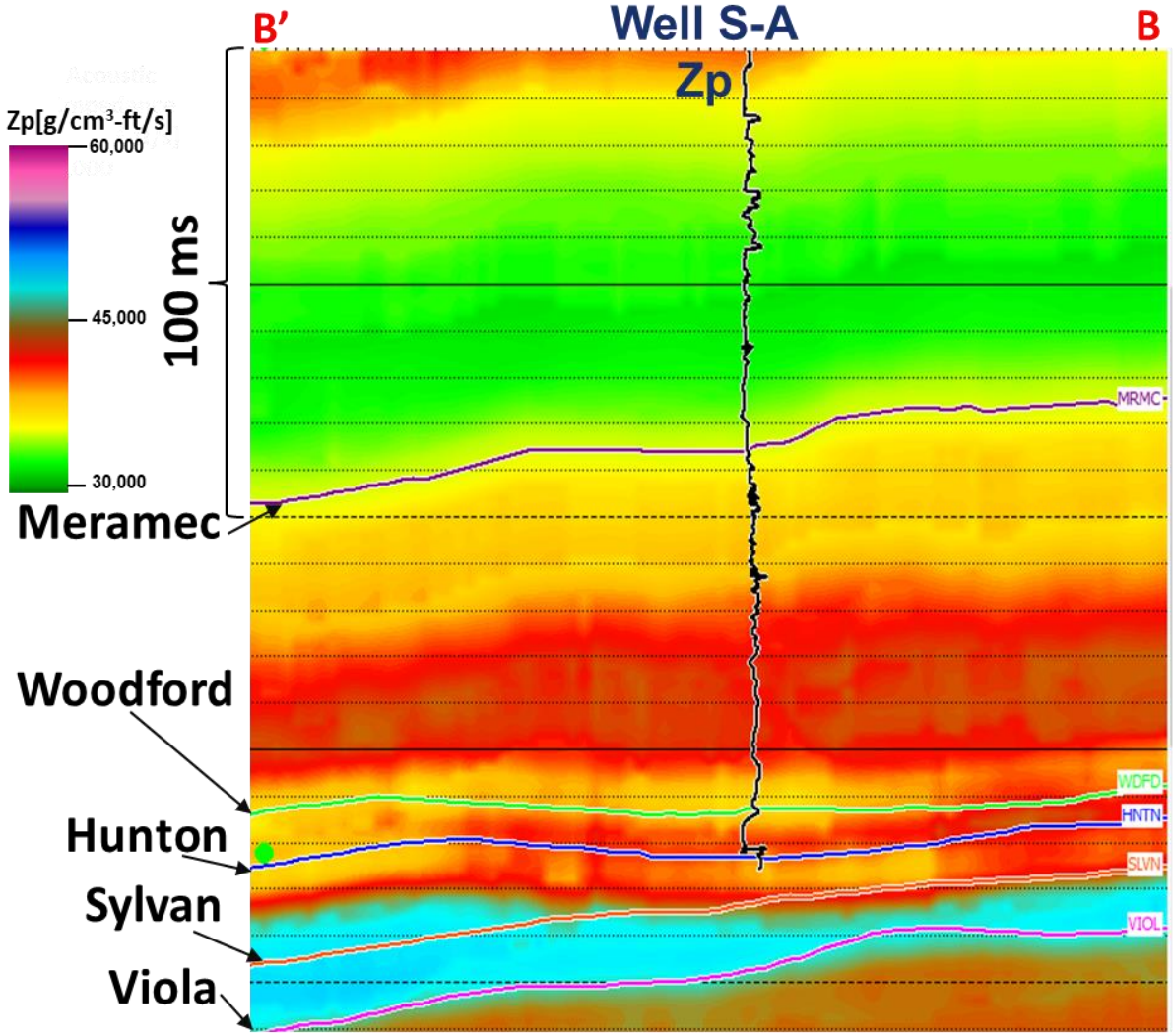

Figure 4.10. A seismic vertical slice of P-impedance volume using model-based inversion calculations. The well log corresponds to the P-impedance (Zp) curve in the projected cored S-A well.

4.5.Mapping reservoir variability using 3D seismic unsupervised machine learning

The Woodford Shale seismic characteristics in the study area make this formation amenable to semiautomated interpretation because of the flat structure without any major faulting nor structural dipping. Seismic attributes provide a means of quantifying subtle variations in stratigraphy that may easily be overlooked (Chopra and Marfurt, 2007). Machine learning provides a quantitative measure of the patterns across these attributes (Roy et al., 2013; Roy et al., 2014;

Zhao et al., 2015). A key component to machine learning is determining which seismic attributes best differentiate a feature of interest from the background (Infante-Paez and Marfurt, 2018).

SOM organizes the input attributes in a manner that voxels with similar characteristics (input attributes) are grouped and colored similarly. Following the work by Matos et al. (2011), Yenugu et al. (2011), and Zhao et al. (2015), we used RMS amplitude, gray level co-occurrence matrix (GLCM) homogeneity, GLCM entropy, peak spectral magnitude, and peak spectral frequency. Over similar colors correspond to similar rock facies in SOM, K-means, and GTM classification volumes, as shown in Figures 4.12 - 4.14.

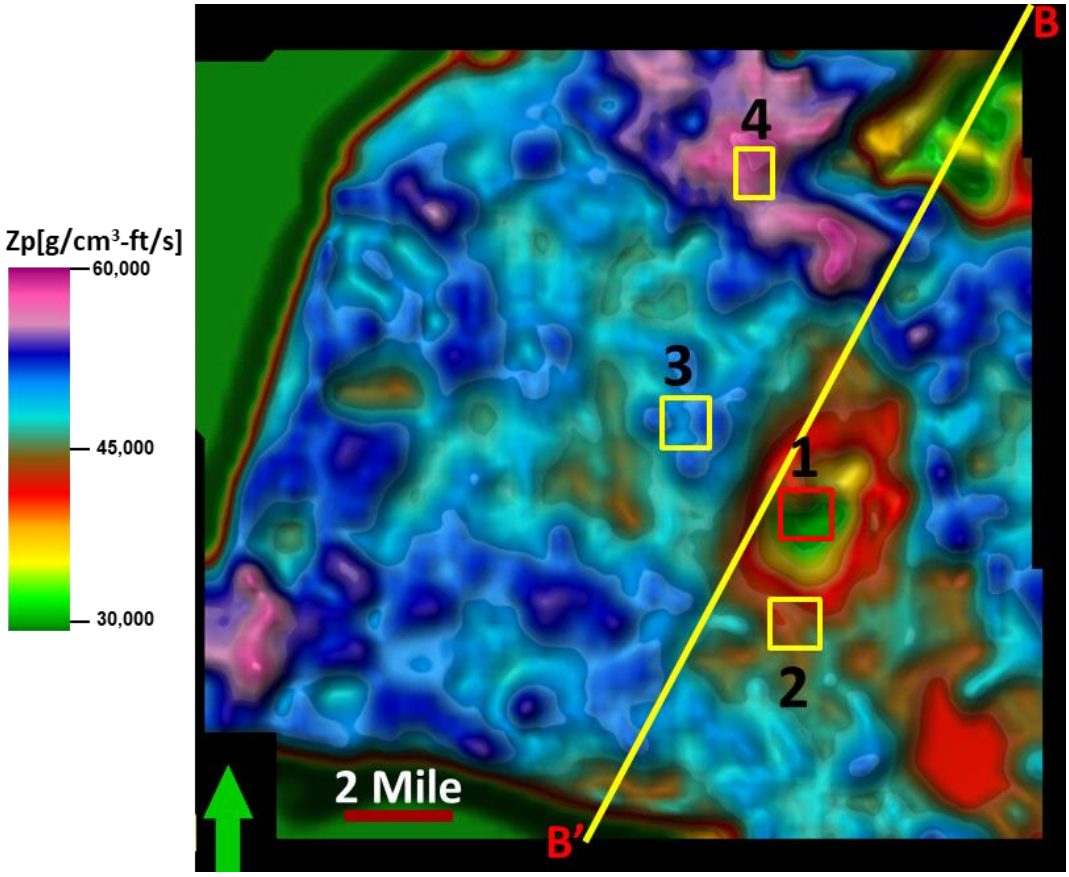

Figure 4.11. Average inverted P-impedance (Z_p) for the entire Woodford Shale stratigraphic interval (From Woodford top to Hunton group top). Extracted and interpolated along with the Woodford seismic window (10 ms above the Woodford Shale seismic top, and 10 ms below the Woodford Shale seismic base). Each of the colored boxes corresponds to one type of curve area used for reservoir simulation.

4.6.Geological and quantitative 3D seismic characterization results

Figure 4.5 illustrates the stratigraphic well log correlation that defines the target interval inside the middle Woodford member. We used the Z_p volume and SOM volumes as probability trend maps to guide the calculated reservoir properties modeling in each vertical well by applying the collocated cokriging in a sequential Gaussian simulation algorithm (Figure 4.11 and Figure 4.12). We selected SOM over the K-means (Figure 4.13) and GTM (Figure 4.14) volumes because it is the one with less patchy clusters, less variability and more similarities to the Zp volume in Figure 4.11.

The main zones of interest for the Woodford Shale in the study area are in the middle Woodford Shale member and are the ones with high %TOC, low fracture gradient, and low fracture toughness (Figure 4.15 – 4.17). We performed the reservoir simulation for the middle Woodford member in local areas (smaller model sub grids of 2-mile x 1-mile size) using publicly reported industry standards of operations and completions in adjacent areas (Barzin and Mattar, 2017). Key geological factors to include in the simulations are the Young modulus, Poisson's ratio, shear modulus, Biot modulus and the variability of organic matter.

Starting with our 3D geocellular grid of 20-mile x 9-mile built in the previous step, we extracted a series of smaller sub-grids for the simulation (Figure 4.15 and Figure 4.16). Each sub-grid is a 2 square mile (mi^2) for each specific reservoir property for subsequent reservoir simulations. The size of each sub-grid is based on standard drilling spacing unit (DSU) size of operated sections in the state of Oklahoma for a 1-mile lateral wellbore length. The grid cell properties were upscaled to a 5 ft vertical resolution and maintained as 110 ft laterally.

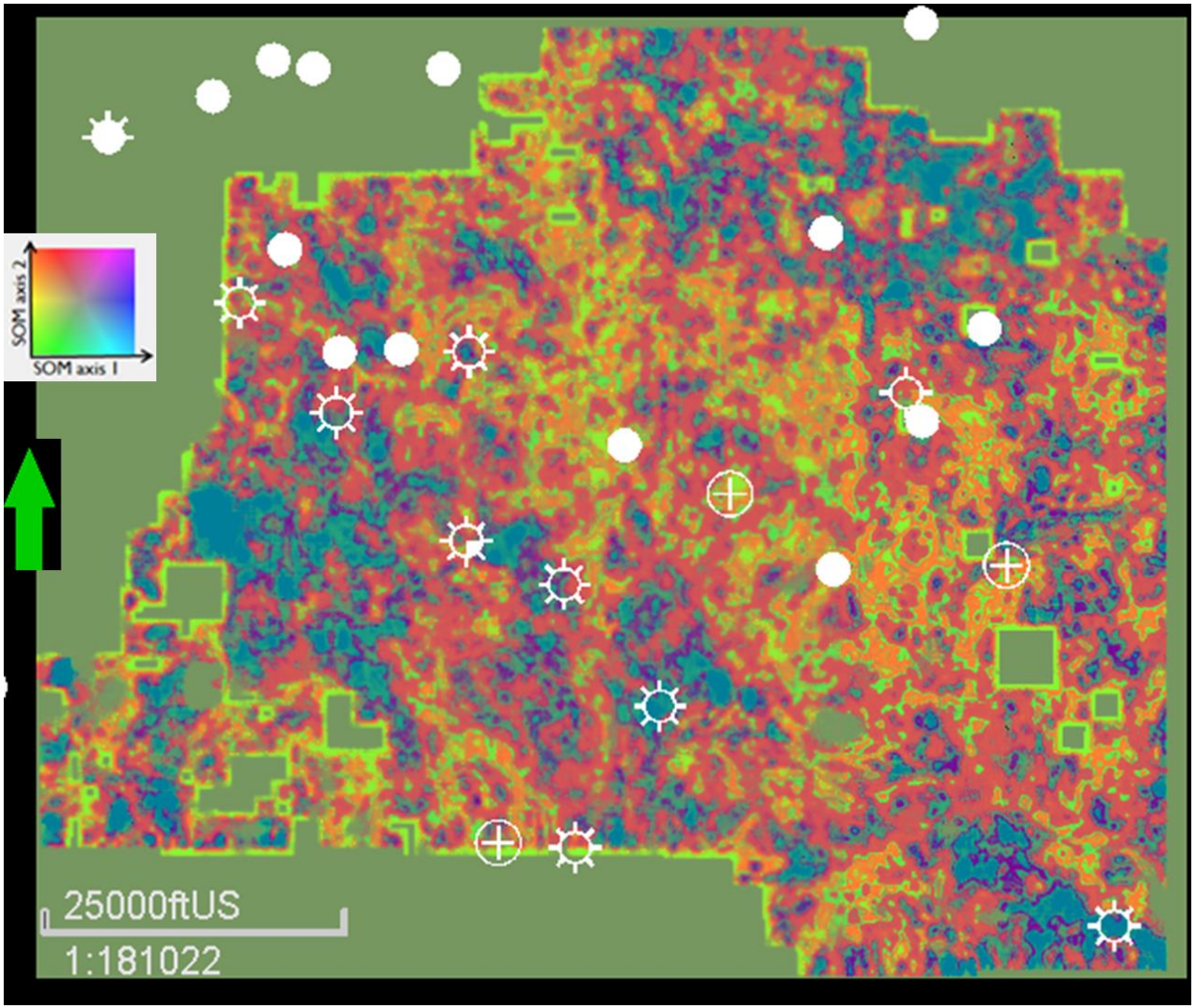

Figure 4.12. Horizon slice along the top of the Woodford Shale SOM classification volume. Average values extracted in the Woodford Shale seismic window. Input attributes are GLCM homogeneity, GLCM entropy, peak frequency, peak magnitude and RMS amplitude. Similar colors correspond to similar seismic facies. We selected SOM over the K-means and GTM volumes because it is the one with less patchy clusters, less variability and more similarities to the Z_p volume in Figure 4.11.

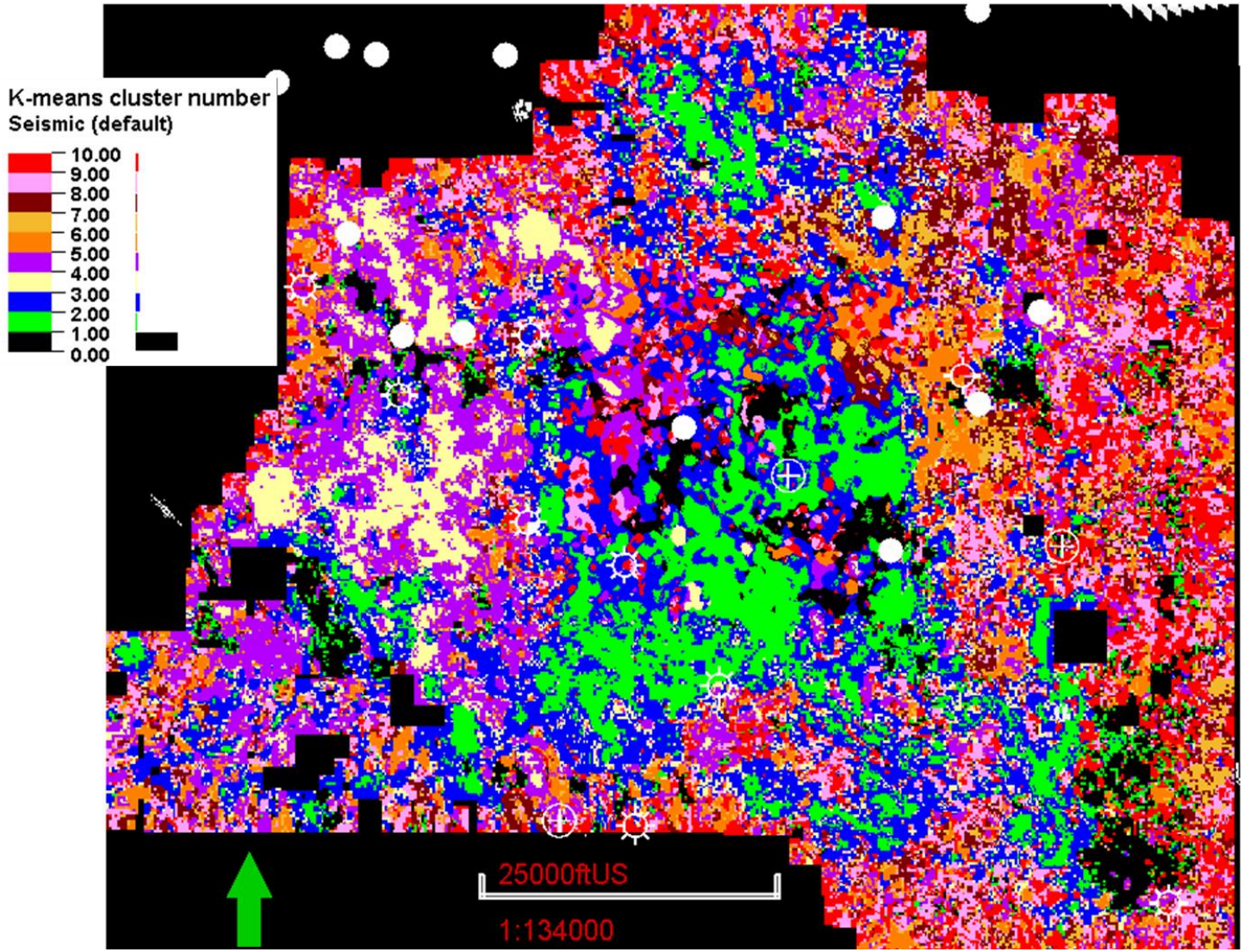

Figure 4.13. Horizon slice along the top of the Woodford Shale unsupervised K-means cluster classification volume. Average values extracted in the Woodford Shale seismic window. Input attributes are GLCM homogeneity, GLCM entropy, peak frequency, peak magnitude, RMS amplitude. Similar colors correspond to similar seismic facies.

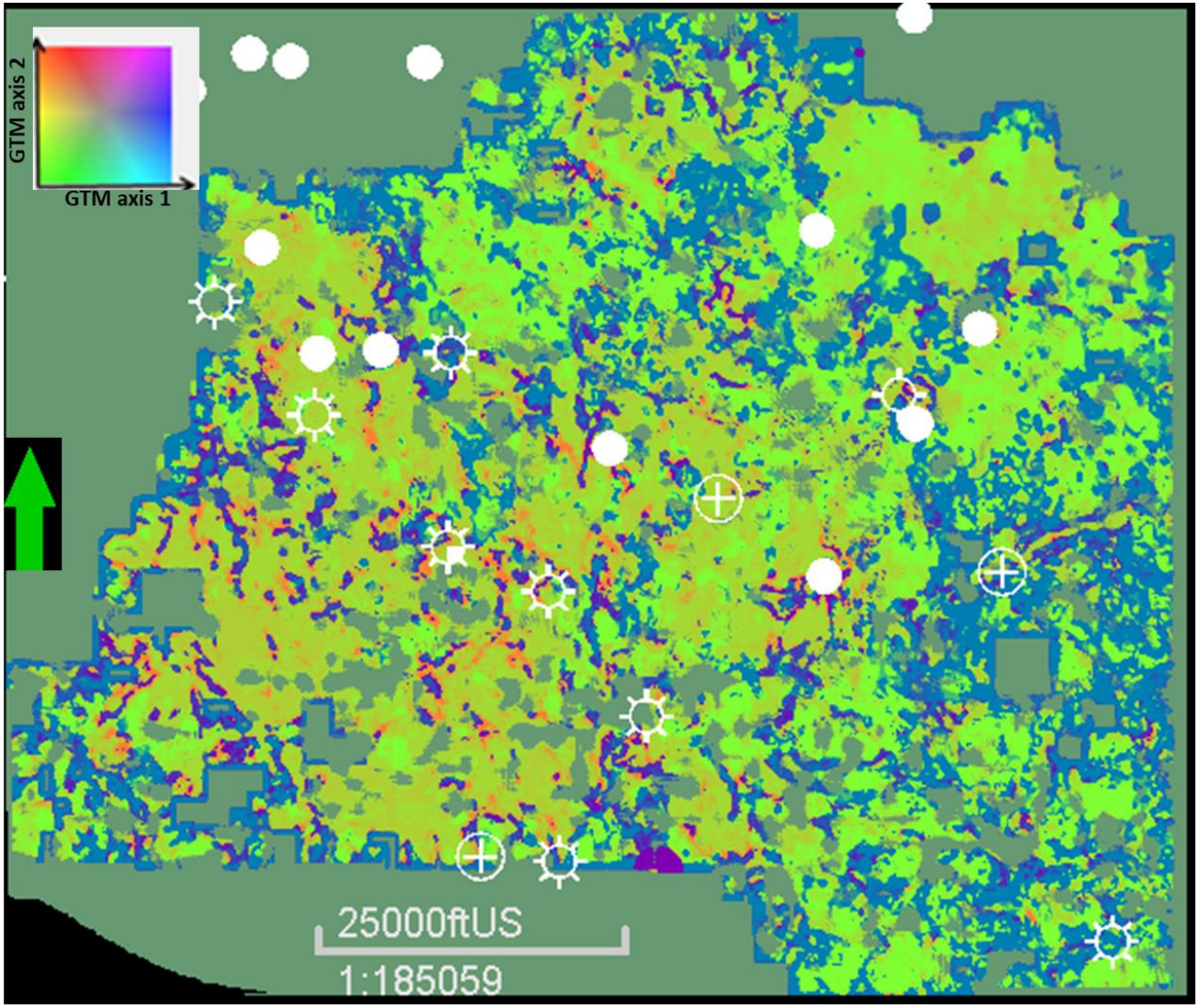

Figure 4.14. Horizon slice along the top of the Woodford Shale GTM classification volume. Average values extracted in the Woodford Shale seismic window. Input attributes are GLCM homogeneity, GLCM entropy, peak frequency, peak magnitude, RMS amplitude. Similar colors correspond to similar seismic facies.

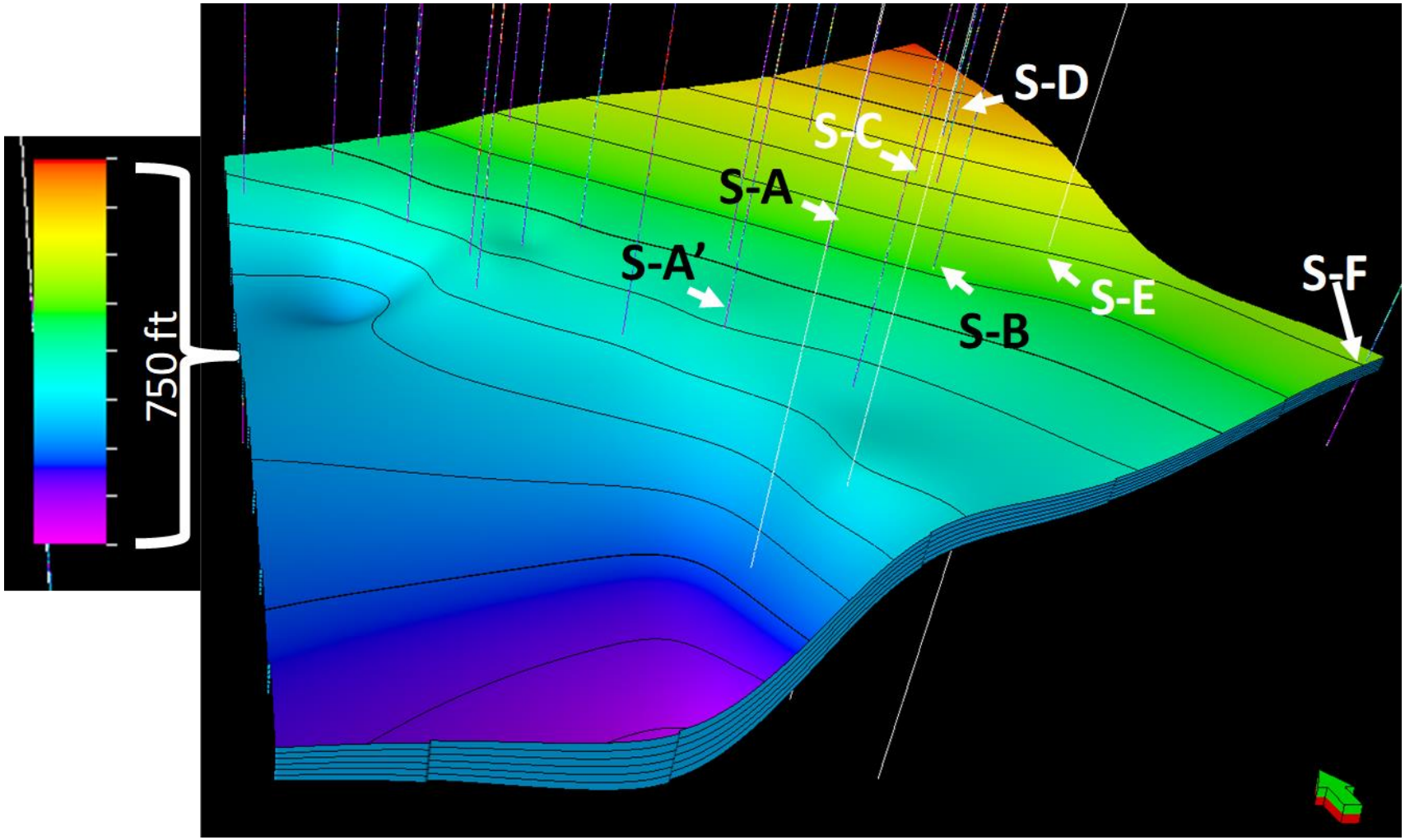

Figure 4.15. Woodford reservoir model 3D grid. Wells displayed in the study area have bulk shear and compressional sonic logs. Reservoir grid from seismic-well tie and depth domain conversion of Woodford seismic top and bottom maps. Vertical exaggeration 1:10.

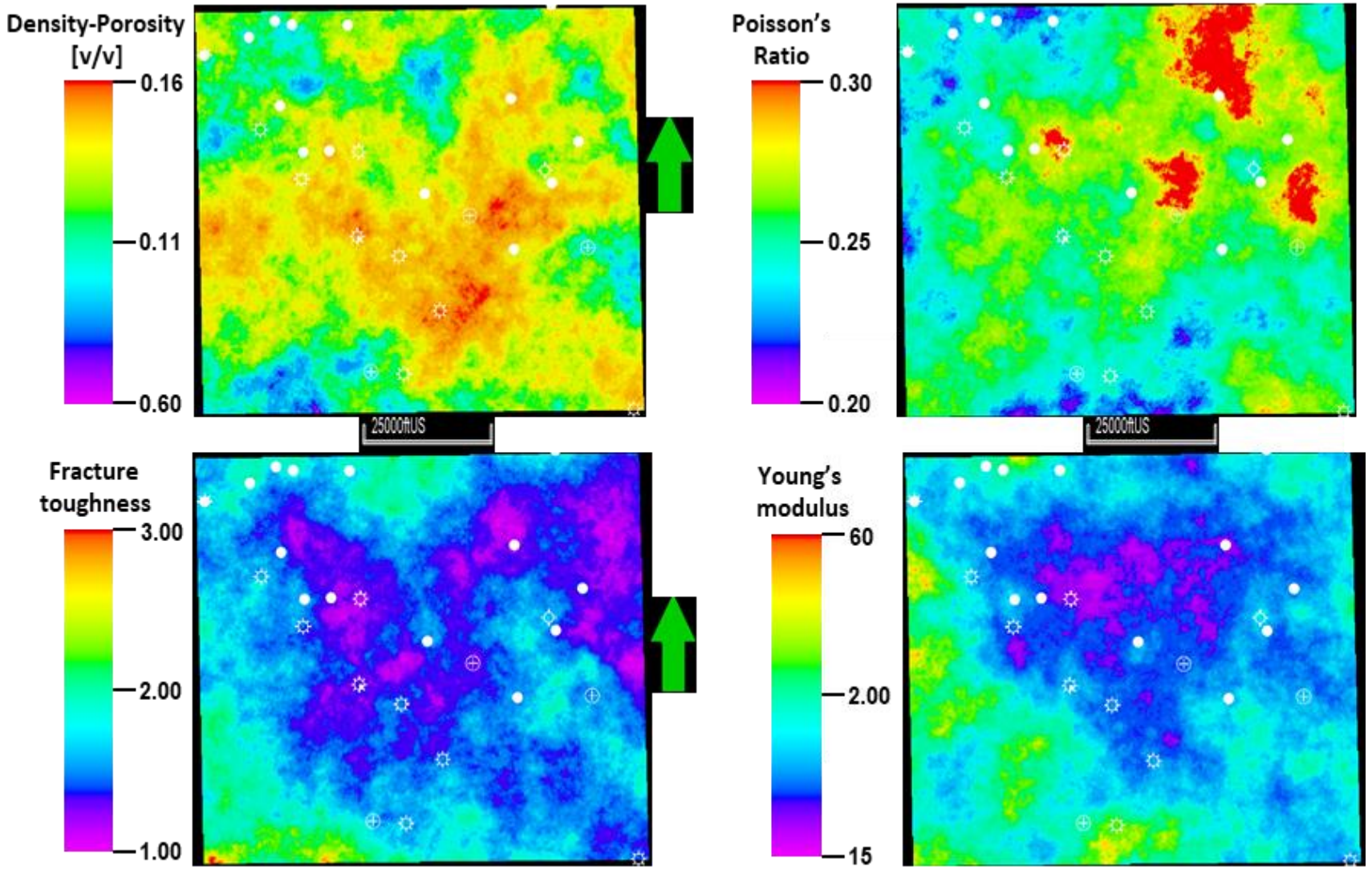

Figure 4.16. Average values of the middle Woodford member interval of interest shown in Figure 4.5 of density-porosity, calculated Young's modulus, Poisson's ratio, and fracture toughness. We calculate the lateral property variation using collocated cokriging using SOM classification volume and Z_p inversion volumes as probability maps.

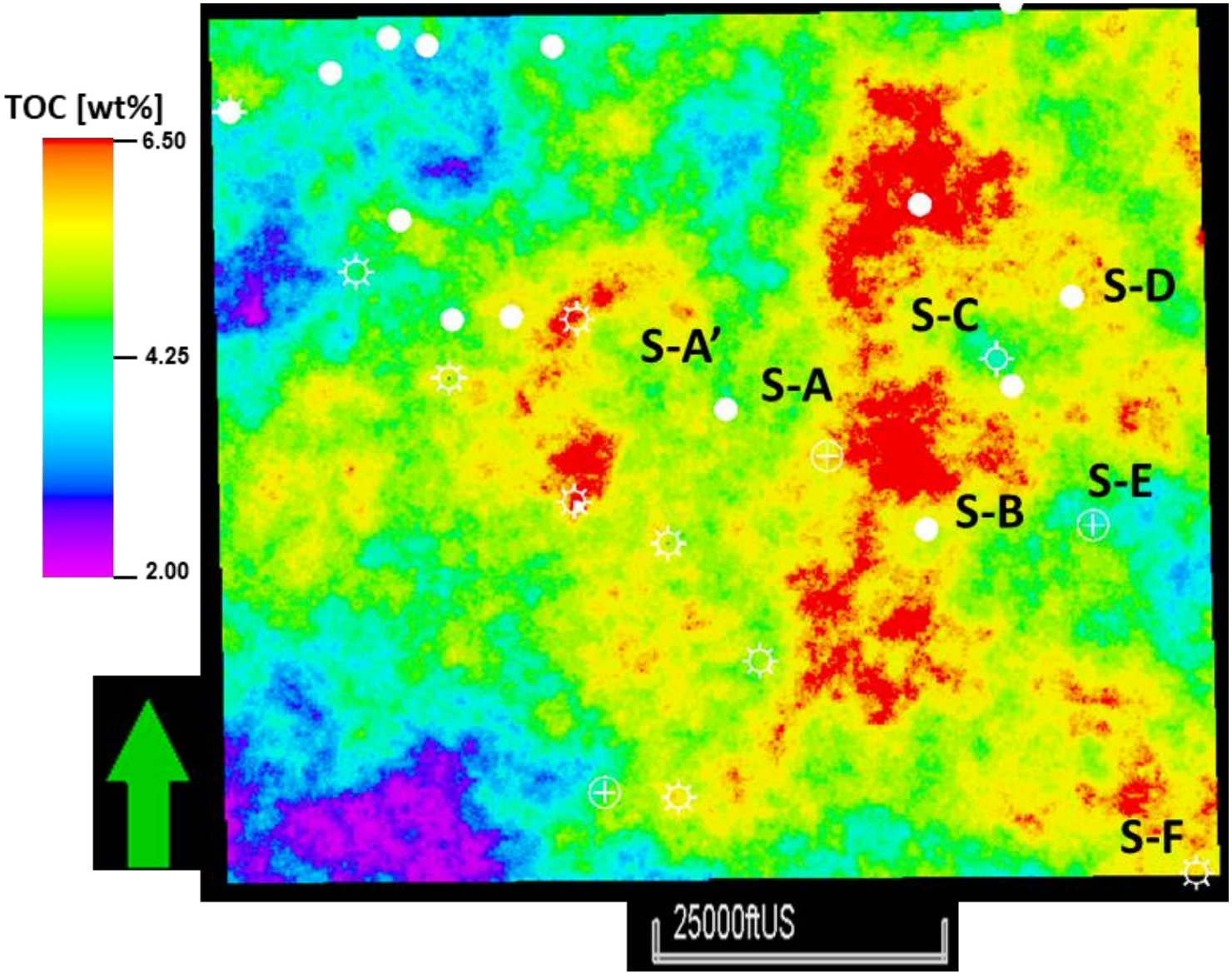

Figure 4.17. Collocated cokriging Schmoker (1979 and 1981) %TOC using the SOM as the probability volume.

4.7.Reservoir simulation

We use a fully coupled geomechanical equation of state (EOS) simulator (Bandis et al., 1983) to establish the baseline production type curve for 5,200 ft lateral wellbores. We identified four different clusters and hence four type curve areas. The four type curve areas defined four major average production curves, each one representing different geological properties. To better understand these four type curve areas, the equation of state simulator estimates the stimulated rock volume as a function of stress as well as cumulative production for a rich condensate high maturity oil. Two of the simulated areas represented enclosed mini-basin fills with a thicker Woodford Shale, overlaying the eroded Hunton group. The other two TC areas represent interpreted open marine conditions of the Woodford Shale, where the calculated average %TOC is lower than the mini-basin fill areas and the average acoustic impedance is higher than areas with mini-basin fills. The stimulated rock volume is commonly used for history matching of existing production data and EUR forecasting (Nayaran and Truax, 2017). Our results support that the standard integration of core, logs, and seismic to production scale not only allows highlighting areas with mini-basin fills but also provides excellent control on the unconventional reservoir characterization and bolsters confidence in the static reservoir models.

For the geomechanical coupling, we use a fully coupled dual-porosity Barton-Bandis model (Bandis et al., 1983). In this model (Figure 4.18), the permeability of the natural fractures is coupled to minimum effective stress. Increasing injection volumes in hydraulic fracturing results in decreasing the minimum effective stress decreases, eventually increasing the permeability of the natural fractures.

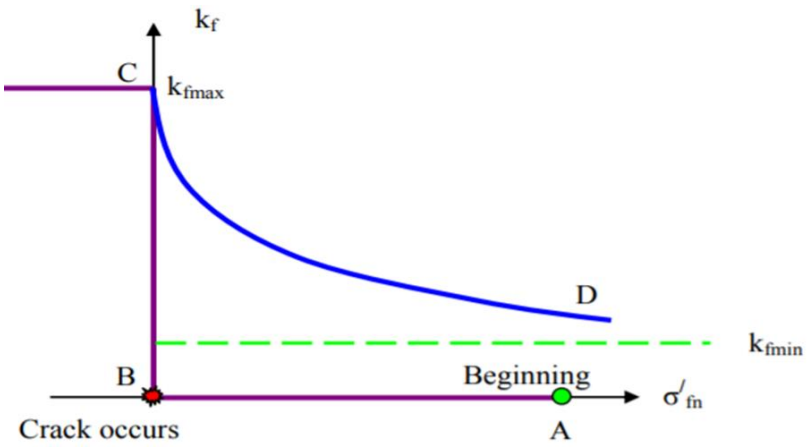

Figure 4.18. Conceptual implementation of Barton – Bandis model (after Tran et al., 2009). Initially, the bottom hole conditions are at the beginning point. As injection continues, the effective stress decreases, and at a certain point, when it reaches the minimum stress, the natural fracture opens, and the permeability increases. As injection stops and well is put on production, due to fluid withdrawal, the permeability decreases again due to a rise in stress. The well ultimately reaches a permeability of K_{fmin} and continues to produce at that permeability. In our case, we keep the K_{fmin} = 25 mD for the fractures.

As the injection is stopped, the effective stresses increase, thus leading to the closure of the natural fracture system, reducing to lower permeability. The initial high permeability corresponds to the flash production in the wells, while the latter stable permeability corresponds to the long-term production in the wells (10 to 20 years). We used the Poisson's ratio map, Young's modulus map, and fracture toughness as geomechanical controls for the production simulation.

4.7.1. Applied completions design to the reservoir simulation

Our methodology performed a fully coupled geomechanical equation of state simulator to establish the baseline production type curve for 5,280 ft lateral wellbores (~1 mile of horizontal length). We used reported operators Woodford Shale completion values of 45 barrels of slickwater per lateral foot, for a total of 230,000 gallons of slickwater, 2,500 lb./ft of proppant and fracture stage in the lateral wellbores every 220 ft for all of the four type curve areas. We kept the completions design constant for all four type curve areas along with fluid and the lateral length of the well.

To fully capture the fluid effects, we use a fully compositional rich condensate representative PVT in the four type curve areas. The applied API gravity of the fluid is 55º, the dew point is 4,200 psi and 0.65 of specific gravity. We use the same fluid properties with the primary aim to identify the EUR variations in the type curve areas based on reservoir properties that can be known ahead of the drilling and not to the fluid properties, which can vary and alter the production recovery factors. Figure 4.19 shows the well bottom-hole pressures during the injection.

The simulation results show a fall in bottom hole pressure (BHP) after the natural fractures open. Figure 4.19 shows the cumulative production, BHP, and gas rates after we set the well on production.

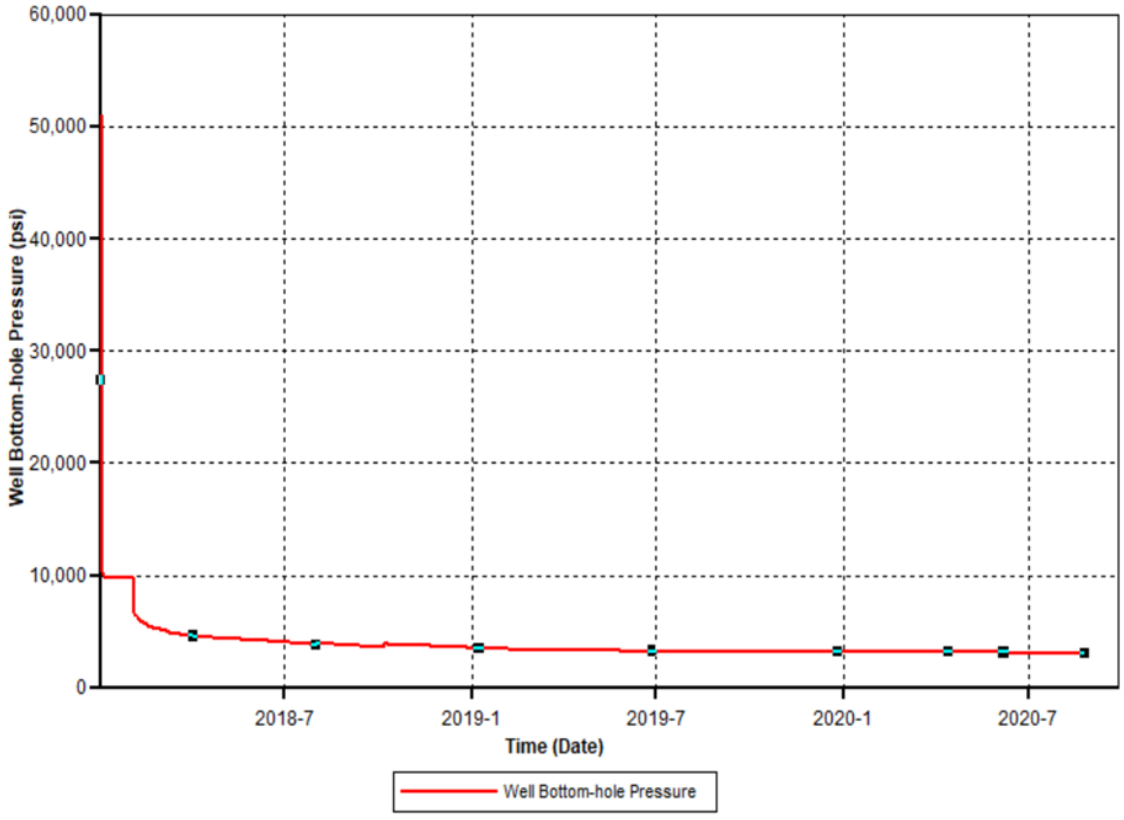

Figure 4.19. Well bottom-hole pressure for the injection. Notice that when a crack occurs at 0 months in time, the stimulated pressure falls rapidly.

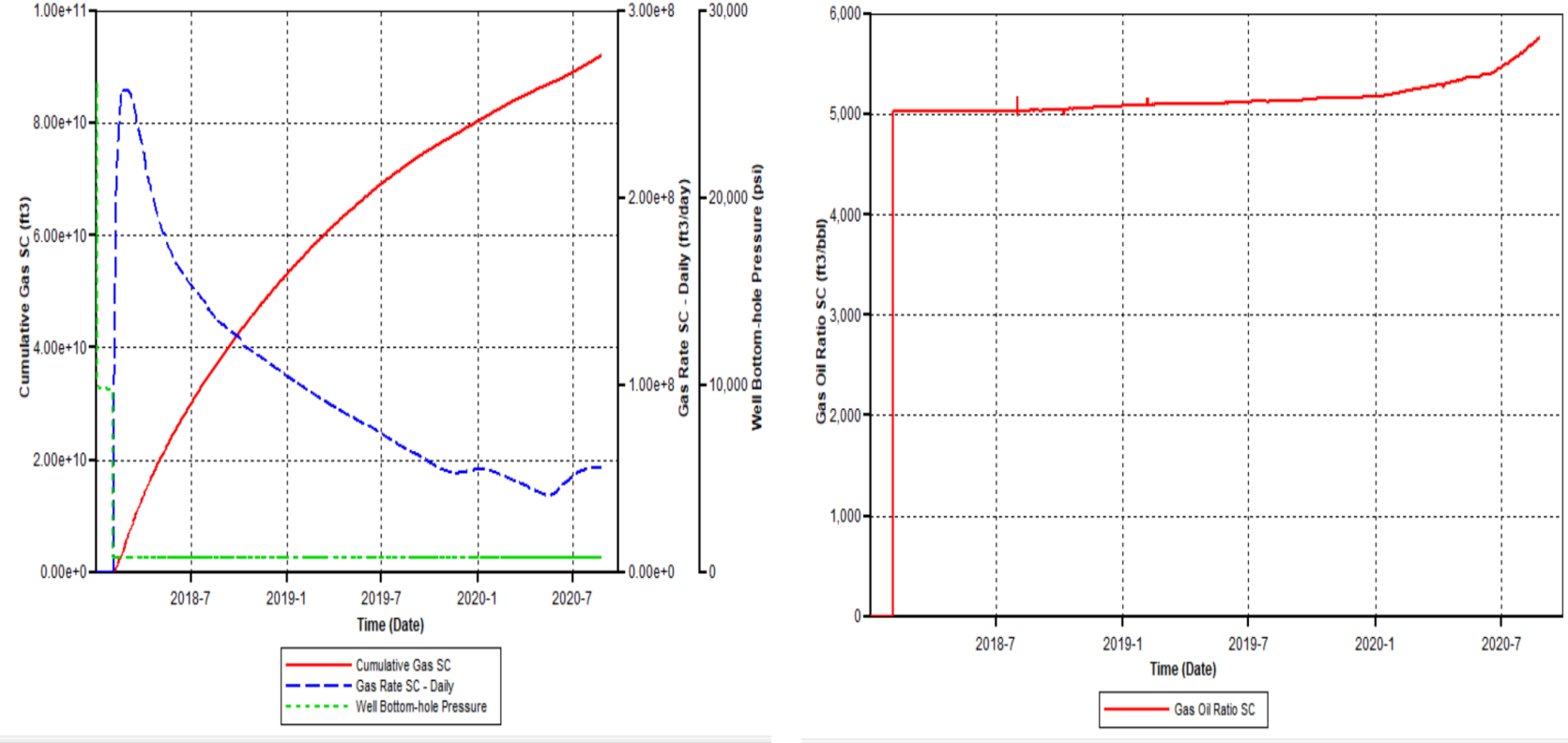

Figure 4.20. (A) Gas rate, bottom-hole pressure (BHP) and (B) cumulative gas for a simulated well EUR in type curve area 1.

The initial high bottom-hole pressure (BHP) shows the injection of slickwater and proppant as the well is hydraulically fractured. We approximated the expected ultimate recovery to be the five years' cumulative gas and condensate production. We repeated the same procedure for the remaining three type curve areas and summarized the results in Table 4.1. We attribute the difference in EUR's for the corresponding completion and fluid to the reservoir properties. Specifically, a high-resolution characterization including petrophysical and geomechanical properties, allows an operator to identify high-value type curve areas, lateral landing zones, well interference issues and ultimately optimize well spacing and capital investments. In Table 4.1, the type curve areas 1 and 2 correspond to interpreted enclosed mini-basin fill that exhibit thicker Woodford and higher %TOC content.

Simulation Results	
Area	TC Well EUR (MBOE)
1	1,802
2	1,624
3	803
4	729

Operator xx Results	
Area	TC Well EUR (MBOE)
1	2,033
2	1,702
3	1,385
4	509

Table 4.1. Cumulative oil EUR in million of barrels for the four simulated type curve areas.

4.8. Limitations

For the simulation part, we recognize the type curve areas from the cornerstone for the conventional reservoir (Fetkovich, 1973; Soliman et al., 1984; Mattar, 1999) and an unconventional shale reservoir (Duda et al., 1991; Xiong et al., 2018). Type curve areas are used as a petroleum industry standard to calculate and report reserves of developed and underdeveloped

resources (Mattar, 1999). In unconventional hydrocarbon assets, a type curve area is generally defined using from an extensive well data set the reservoir true vertical depth (TVD feet), thickness (feet), maturity, gas-oil ratios (GORs), wellbore lateral length, amount of proppant, and completions design (Barzin and Mattar, 2017; Joshi et al., 2019). Due to proprietary data, our main limitation is that we have a restricted wellbore production database to build the type curve areas with standard industry practices and obtain a precise history match. For this reason, we argument the PDNP reports we don't have with simulated data. We use machine learning of 3D seismic attributes to define the production type curve areas, which, based on our workflows and results, are geologically consistent.

4.9. Summary and Conclusions

This study identifies geological sweet spots and production type curve areas in the Woodford Shale along with significant facies variations. We conducted simulation in areas interpreted as mini-basin fill settings and areas recognized as entire open marine deposits (or with very thin mini-basin fills).

Our analysis shows that the uppermost middle Woodford Shale member is the interval with the best reservoir porosity, permeability, and thickness. The thicker and the higher %TOC intervals correspond to the mini-basin fill interval, close to the change to open marine conditions. As expected, Young's modulus exhibited higher values in the highest silica-rich reservoir of the Upper-middle Woodford Shale intervals than other areas of the Woodford Shale stratigraphic sequence. The 3D seismic multi-attribute and cluster analyses allow us to populate the geocellular model.

Geomechanical simulation allows us to model a gradual closing of fractures. Rather than conventional history matching of the production with multiple permeability zones, we use a time-

variant "shrinking" simulated rock volume to match well EURs. The proposed natural fracture model, along with hydraulic fractures, provide estimates of pressure distribution in the four Woodford Shale type curve areas as these models can then be used to optimize well spacing for future enhanced oil recovery (EOR) projects.

The mini basin fill type curve areas 1 and 2 have the highest EUR simulation results and closely match the EUR data provided by the operator.

4.10. Acknowledgments

Special thanks to Pathfinder Exploration LLC., **Mr. Gerald Wilson (*in-memoriam*)** and the Wilson family for providing the 3D seismic surveys and the well-log data for this exercise. Special thanks to the kind assistance of the geologists, geophysicists, reservoir engineers and sponsors of both the University of Oklahoma Institute of Reservoir Characterization (IRC) and Attribute Assisted Seismic Processing and Interpretation (AASPI) consortiums for the well cumulative production and EUR calculation data sets. Special acknowledgments to Schlumberger and CGG for allowing us the academic licenses of their software.

4.11. Cited References

- Allen, D.B., Pranter, M. J., 2016. Geologically constrained electrofacies classification of fluvial deposits: An example from the Cretaceous Mesaverde Group, Uinta and Piceance Basins. AAPG Bulletin 100, 12, 1775-1801.
- Babak, O., Bergey, P., Deutsch C.V., 2014. Facies trend modeling for SAGD application at Surmont. Journal of Petroleum Science and Engineering 119, 2014, 85-103.
- Bandis, S.C., Lumsden, A.C, and Barton, N, R., 1983. Fundamentals of Rock Joint Deformation. International Journal of Rock Mechanics and Mining Sciences 20, 6, 249–68.
- Barree, R.D., and Gilbert, J.V., 2009. Stress and rock property profiling for unconventional reservoir stimulation. SPE Hydraulic Fracturing Technology Conference, The Woodlands, Texas, USA, 2009. SPE 118703.

- Baruch, E., Elebiju, O., and Perez, R., 2009. Geophysical evidence of basement-controlled faulting in the Ellenburger group and Viola Limestone, Fort Worth basin, Texas. 79th Annual International Meeting, SEG 2009 Expanded Abstracts, 995–999.
- Barzin, Y., Mattar, L., 2017. Limitations of current type curves in characterizing SRV; and development of EFR type curves. Unconventional Resources Technology Conference URTeC 2017, SPE-185038-MS, p. 25.
- Bishop, C.M., Svensen, M., Williams, C.K.I., 1998. The generative topographic mapping. Neural Computation 10, 1, 215-234.
- Cardott B. J., 2009. Woodford gas-shale plays of Oklahoma. Louisiana oil & gas symposium, May 20, 2009. Oklahoma Geological Survey OGS.
- Cardott, B.J., 2012. Thermal maturity of Woodford Shale gas and oil plays, Oklahoma, USA. International Journal of Coal Geology 103, 1-13.
- Castagna, J.P, Batzle M. L., and Eastwood R. L., 1886. Relationships between compressional-wave and shear-wave velocities in clastic silicate rocks. Geophysics Journal, Society of Exploration Geophysicists 50, 4, 571-581.
- Castagna, J.P, and Backus M.M., 1993. AVO analysis—Tutorial and review. Offset-dependent reflectivity: Theory and practice of AVO analysis. SEG Investigations in Geophysics 8, 3-36.
- Castillo, D.A., and Moos, D., 2000. Reservoir geomechanics applied to drilling and completion programs in challenging formations: northwest shelf, Timor Sea, North Sea, and Colombia. APPEA Journal, 2000.
- Cervantes-Velazques, A., 2019. Reservoir characterization and modeling of a Cretaceous triple porosity carbonate reservoir. Contribution of pore types to hydrocarbon pore volume and production, Campeche Sound, Gulf of Mexico, Mexico. Doctoral dissertation manuscript, The University of Oklahoma, p. 184.
- Chopra, S., Marfurt, K.J., 2007. Seismic attributes for prospect identification and reservoir characterization. SEG Geophysical Developments.
- Chopra, S., Marfurt, K.J., 2014. Seismic facies analysis using generative topographic mapping. SEG Denver 2014 Annual Meeting extended abstracts.
- Comer, J.B., 2005. Facies distributions and hydrocarbon production potential of the Woodford Shale in the southern midcontinent: in B.J. Cardott, eds., Unconventional energy resources in

the southern midcontinent, 2004 symposium. Oklahoma Geological Survey, Circular 110, 51-62.

- Coburn, T. C., Yarus, J. M., Chambers, R.L., 2006. Geostatistics and stochastic modeling: Bridging into the 21st century, in T. C. Coburn, J. M. Yarus, and Chambers, R. L. eds., Stochastic modeling and geostatistics: Principles, methods, and case studies, volume II: AAPG Computer Applications in Geology 5, 3-9.
- Daly, C., Quental, S., Novak, D., 2010. A faster, more accurate Gaussian simulation. American Association of Petroleum Geologist, Search and Discovery Article 90172.
- Deutsch, C., 2002. Geostatistical reservoir modeling. Oxford University Press, p. 385.
- Deutsch, C., 2006. A sequential indicator simulation program for categorical variables with point and block data: BlockSIS. Computers & Geosciences 32, 2006, 1669–1681.
- Duda, J.R, Salamy. S.P., Aminian, K., Ameri, S., 1991. Pressure analysis of an unstimulated horizontal well with type curves. Society of Petroleum Engineers SPE Journal 1991, August, 988-993.
- Fetkovich, M.J., Fetkovich, E.J., Fetkovich, M.D., 1996. Useful concepts for decline-curve forecasting, estimation and analysis. Society of Petroleum Engineers SPE, Journal of Reservoir Engineering 1996, 13-22.
- Franti, P., Sieranoja, S., 2019. How much can k-means be improved by using better initialization and repeats? Journal of Pattern Recognition, 93, 2019, 95-112.
- Ghassemi, A., Tao, Q., Diek, A., 2009. Influence of coupled chemo-poro- thermoelastic processes on pore pressure and stress distributions around a wellbore in swelling shale. Journal of Petroleum Science and Engineering 67, 57-64.
- Ghassemi, A., Rawal, A., Zhou, X., 2013. Rock failure and micro-seismicity around hydraulic fractures. Journal of Petroleum Science and Engineering 108, 118-127.
- Goovaerts, P., 1994. Comparative performance of indicator algorithms for modeling conditional probability distribution functions. Mathematical Geology 26, 3, 385–410.
- Goovaerts, P., 1997. Geostatistics for Natural Resources Evaluation. Oxford University Press, New York, p. 496.
- Hampson, D. J., Schuelke, S., Quirein, J., 2001. Use of multiattribute transforms to predict log properties from seismic data. Geophysics, 66, 220–236.

- Havens, J. B., and Batzle, M.L., 2011. minimum horizontal stress in the Bakken formation. 45th US Rock Mechanics / Geomechanics Symposium held in San Francisco, CA, 2011.
- Havens, J.B., and Batzle, M.L., 2010. A geomechanical model of the Bakken petroleum system. American Rock Mechanics Association 44th US Rock Mechanics Symposium and 5th U.S.-Canada Rock Mechanics Symposium, held in Salt Lake City, UT, 2010.
- Heggland, R., 2004. Definition of geohazards in exploration 3D seismic data using attributes and neural network analysis. AAPG Bulletin, 88, 857–868.
- Infante-Paez, L.E., Cardona L.E., McCullough, B., Slatt, R.M., 2017. Seismic analysis of paleotopography and stratigraphic controls on total organic carbon: Rich sweet spot distribution in the Woodford Shale, Oklahoma, USA. Interpretation 5, 1, T33-T48.
- Infante-Paez, L.E., 2018. Seismic expression of igneous bodies in the sedimentary basin and their impact on hydrocarbon exploration: Examples from a compressive tectonic setting, Taranaki basin, New Zealand. Doctoral thesis manuscript, The University of Oklahoma, p. 196.
- Infante-Paez, L.E., Marfurt, K.J., 2018. Using machine learning as an aid to seismic geomorphology, which attributes are the best input?: Interpretation 7, 3, SE1-SE18.
- Issaka, M., Ambastha, A., 1996. Decline curve analysis for composite reservoirs. SPE 47th Annual Technical Meeting, 96-15, p. 11.
- Jarvie, D.M., Hill, R.J., Pollastro, R.M., 2005. Assessment of the gas potential and yields from shales: the Barnett Shale model. In: Cadott, B., eds., Oklahoma Geological Survey Circular 110: Unconventional gas of the Southern mid-continent symposium, March 2005. Oklahoma City, Oklahoma, 37-50.
- Jarvie, D.M., Hill, R.J., Ruble, T.E., Pollastro, R.M., 2007. Unconventional shale-gas systems: the Mississippian Barnett Shale of North-Central Texas as one model for thermogenic shale-gas assessment. AAPG Bulletin 91, 4, 475-499.
- Joshi, K., Lee, J., 2013. Comparison of various deterministic forecasting techniques in shale gas reservoirs. SPE Hydraulic Fracturing Technology Conference 2013, SPE 163870, p. 12.
- Joshi, K., Muralidharan, V., Patel, D., 2019. Production diagnostic type curves for performance evaluation: An extension of the universal type curve approach. Unconventional Resources Technology Conference (URTeC) 2019, 31, p. 16.

- Kelkar, M., Perez, G., 2001. Applied geostatistics for reservoir characterization. Society of Petroleum Engineers SPE, p. 273.
- Kirkland D.W., Denison, R.E., Summers, D.M., and Gormly, J.R., 1992. Geology and organic geochemistry of the Woodford Shale in the Criner Hills and western Arbuckle Mountains, Oklahoma. Oklahoma Geological Survey, Circular 93, 38-69.
- Kohonen, T., 2001. Self-Organizing Maps. Springer Series in Information Sciences, Volume 30. Springer, Berlin, Heidelberg, New York, 3rd edition, p. 268.
- Kohonen, T., Kaski, S., Lagus, K., Salojarvi, J., Honkela, J., Paatero, V., Saarela, A., 2000. Self-organization of a massive document collection. IEEE Transactions on Neural Networks 11,574-585.
- Kumar, D., Ghassemi, A., 2018. Three-dimensional poroelastic modeling of multiple hydraulic fracture propagation from horizontal wells. International Journal of Rock Mechanics and Mining Sciences 105, 192–209.
- Li, F., Verma, S., Zhou, H., Zhao, T., Marfurt, K.J., 2016. Seismic attenuation attributes with applications on conventional and unconventional reservoirs. Interpretation 4, 1, SB63-SB77.
- Liu, J., 2017. Geomechanical reservoir characterization and applications. M.Sc. thesis manuscript, The University of Oklahoma, p. 97.
- Manchuck, J.G., Clayton, V.D., 2012. A flexible sequential Gaussian simulation program: USGSIM. Computers & Geosciences 41, 2012, 208–216.
- Matos, M., Yenugu, M., Angelo, S.M., Marfurt, K.J., 2011. Integrated seismic texture segmentation and cluster analysis applied to channel delineation and chert reservoir characterization. Geophysics 76, 11-21.
- Meldahl, P., Heggland, R., Bril, B., and de Groot, P., 2001. Identifying fault and gas chimneys using multi-attributes and neural networks: SEG The Leading Edge 20, 474–482.
- Miceli-Romero, A.A, 2010. Geochemical characterization of the Woodford Shale, central and southeastern Oklahoma. M.Sc. thesis manuscript, The University of Oklahoma, p. 149.
- Miceli-Romero, A.A., and Philp, R.P., 2012. Organic geochemistry of the Woodford Shale, southeastern Oklahoma: How variable can shale be? AAPG Bulletin, 96, 3, 493-517.
- Molinares, C. E., 2013. Stratigraphy and palynomorphs composition of the Woodford Shale in the Wyche farm Shale pit, Pontotoc County, Oklahoma. M.Sc. Thesis Manuscript. The University of Oklahoma, School of Geology and Geophysics, pp. 104.

- Molinares, C. E., 2019. The Frasnian/Famennian (F/F) transition in the Woodford Shale, south-central Oklahoma – a multiproxy approach. Doctoral dissertation manuscript, The University of Oklahoma, p. 117.
- Mullen, M., Roundtree, R., Barree, R., and Turk, G., 2007. A composite determination of mechanical rock properties for stimulation design (What to do when you do not have a sonic log). SPE Rocky Mountain oil and gas technology symposium, Denver, CO. SPE 108139.
- Muralidharan, V., Joshi, K., 2018. Myths and facts of forecasting horizontal well production in unconventional reservoirs – Are we complicating a simple analysis? Unconventional Resources Technology Conference (URTeC) 2018, 2897088, p. 19.
- Nayaran, N., Truax, J., 2017. Comparing and estimating initial production of fractured wells using vertical well logs. SPWLA 58th Annual Logging Symposium, June 2017, p. 17.
- Northcutt, R.A., Johnson, K.S., and Hinshaw, G.C., 2001. Geology and petroleum reservoirs in Silurian, Devonian, and Mississippian rocks in Oklahoma. In: Johnson K. S., eds., Silurian, Devonian, and Mississippian geology and petroleum in the southern midcontinent, 1999 symposium. Oklahoma Geological Survey Circular 105, 1-29.
- Passey, Q. R., Creaney, S., Kulla, J.B., Moretti, F.J., and Stroud, J.D., 1990. A practical model for organic richness from porosity and resistivity logs. AAPG Bulletin 74, 1777-1794.
- Passey, Q. R.., Bohacs, K. M., Esch, W. L., Klimentidis, R., and Sinha, S., 2010. From oil-prone source rock to gas-producing shale reservoir-geologic and petrophysical characterization of unconventional shale-gas reservoirs. 2010 CPS/SPE International Oil & Gas Conference and Exhibition in China, 29 p.
- Portas, R., 2009. Characterization and origin of fracture patterns in the Woodford Shale in southeastern Oklahoma for application to exploration and development. M.Sc. thesis manuscript, The University of Oklahoma, p. 113.
- Qi, J., Lin, T., Zhao, T., Li, F., and Marfurt, K.J., 2016. Semisupervised multiattribute seismic facies analysis. Interpretation 4, 1, SB91-SB106.
- Qiao, J., Cai, X., Xiao, Q., Chen, Z., Kulkarni, P., Ferris, C., Kamarthi, S., Sridhar, S., 2019. Data on MRI brain lesion segmentation using K-means and Gaussian Mixture model-expectation maximization. Journal Data 27, 2019, 104628, p. 9.
- Rickman, R., Mullen, M., Petre, E., Grieser, B., and Kundert, D., 2008. A practical use of Shale petrophysics for stimulation design optimization: All shale plays are not clones of the Barnett

Shale: Proceedings from the SPE Annual Technical Conference and Exhibition ATC, SPE 115258.

- Roy, A., Dowdell, B., and Marfurt, K.J., 2013. Characterizing a Mississippian tripolitic chert reservoir using 3D unsupervised and supervised multiattribute seismic facies analysis: An example from Osage County. Interpretation 1, 2, SB109–SB124.
- Roy, A., Romero-Peláez, A.S., Kwiatkowski, T.J., Marfurt, K.J., 2014. Generative topographic mapping for seismic facies estimation of a carbonate wash, Veracruz Basin, southern Mexico. Interpretation 2, 1, SA31-SA47.
- Sabeti, H., Javerian, A., 2009. Seismic facies analysis based on the K-means clustering algorithm using 3D seismic attributes. EAGE International Petroleum Conference and Exhibition extended abstracts.
- Schmoker, J.W., 1979. Determination of organic content of Appalachian Devonian Shales from formation density logs. AAPG Bulletin 63, 9, 1504-1537.
- Schmoker, J.W., 1981. Determination of organic matter content of the Appalachian Devonian Shales from Gamma-Ray logs. AAPG Bulletin 65, 7, 1258-1298.
- Shepherd, M., 2009. Reservoir modeling and geostatistics, in M. Shepherd, Oil field production geology: AAPG Memoir 91, p. 157.
- Strecker, U., Uden, R., 2002. Data mining of 3D post-stack attribute volumes using Kohonen self-organizing maps. The Leading Edge 21, 1032-1037.
- Sierra-Perez, R., 2011. Integrated geomechanics and geological characterization of the Devonian-Mississippian Woodford Shale. M.Sc. thesis manuscript, The University of Oklahoma, p. 123.
- Slatt, R.M., 2016. Institute of Reservoir Characterization (IRC), Woodford-Mississippian consortium, phase III technical report. The University of Oklahoma, p. 202.
- Slatt, R. M., Buckner, N., Abousleiman, Y., Sierra, R., Philp, R.P., Miceli-Romero, A., Portas, R., O'Brien, N., Tran, M., Davis, R., and Wawrzyniec, T., 2012. Outcrop/behind outcrop (quarry), multiscale characterization of the Woodford gas shale, Oklahoma, in J. Breyer, eds., Shale reservoirs-giant resources for the 21st century: American Association of Petroleum Geologists AAPG Memoir 97, 1–21.
- Snyder, J., 2016. Correlating rate of penetration and bit trips to 3D surface seismic data, Anadarko shelf, Oklahoma. M.Sc. thesis manuscript, The University of Oklahoma, p. 184.

- Sone, H., and Zoback, M.D., 2013. Mechanical properties of shale-gas reservoir rocks - Part 2: Ductile creep, brittle strength, and their relation to the elastic modulus. Geophysics 78, D393-D402.
- Sullivan, K.L., 1985. Organic facies variation of the Woodford Shale in western Oklahoma. Shale Shaker 35, 76-89.
- Tran, D., Shrivastava, V., Nghiem, L., and Kohse, B., 2009. Geomechanical risk mitigation for CO_2 sequestration in saline aquifers. Proceedings of SPE Annual Technical Conference and Exhibition 2009, 1–18.
- Turner, B., 2015. The use of chemostratigraphy to refine ambiguous sequence stratigraphic correlations in marine shales: An example of the Woodford Shale, Oklahoma. AAPG education directorate, Woodford Shale forum: Focus on optimization. Oklahoma City, Oklahoma, 2015. AAPG Datapages Search and Discovery Article 90241.
- Turner, B., Molinares, C., and Slatt, R.M., 2015. Chemostratigraphic, palynostratigraphic, and sequence stratigraphic analysis of the Woodford Shale, Wyche Farm quarry, Pontotoc County, Oklahoma. Interpretation 3, 1, SH1-SH9.
- Verma, S., Guo, S., Marfurt, K.J., 2016a. Data conditioning of legacy seismic using migration-driven 5D interpolation. Interpretation 4, 2, SG31-SG40.
- Verma, S., Zhao, T., Marfurt, K.J., Devegowda, D., 2016b. Estimation of total organic carbon and brittleness volume. Interpretation 4, 3, T373-T385.
- Vermylen, J.P., 2011. Geomechanical studies of the Barnett Shale, Texas, USA. Doctoral dissertation manuscript, Stanford University, p. 143.
- Wang, Z., 2000. Dynamic versus static elastic properties of reservoir rocks. Seismic and acoustic velocities in reservoir rocks. SEG Geophysics Reprint Series 19.
- Wang, C., Zeng, Z., 2011. Overview of geomechanical properties of Bakken formation in the Williston basin, North Dakota. 45th US Rock Mechanics / Geomechanics Symposium held in San Francisco, CA, June 26–29, 2011.
- Xiao, M., Zhang, G., Breitkopf, P., Villon, P., Zhang, W., 2018. Extended co-kriging interpolation method based on multi-fidelity data. Applied Mathematics and Computation 323, 120-131.
- Xiong, H., Zhu, T., Forest, J., Yang, C., Wook Lee, J., Kumar, H, Li, C., 2018. A practical way to prepare physical-based type well performance curves for unconventional reservoirs in the

Permian basin. Unconventional Resources Technology Conference (URTeC) 2018, 2888118, p. 13.

- Yale, D.P., Jamieson Jr., W.H., 1994. Static and dynamic mechanical properties of carbonates. In: 1st North American Rock Mechanics Symposium. American Rock Mechanics Association.
- Yarus, J. M., 1994. Selected readings on geostatistics, in Yarus, M.J., Chambers, R.L eds., Stochastic modeling and geostatistics. Computer Applications 3, AAPG Special Volumes, 369-370.
- Yasar, E., Erdogan, Y., 2004. Correlating sound velocity with the density, compressive strength, and Young's modulus of carbonate rocks. International Journal of Rock Mechanics and Mining Sciences 41, 5, 871-875.
- Ye, Z., Sesetty, V., Ghassemi, A. 2018. Experimental and numerical analysis of shear stimulation and permeability evolution in shales. Hydraulic Fracturing Journal 5, 3, p. 2841.
- Yenugu, M., Marfurt, K. J., Matson, S., 2011. Seismic texture analysis for reservoir prediction and characterization. The Leading Edge 29, 1116-1121.
- Zhao, T., Jayaram, V., Roy, A., Marfurt, K.J., 2015. A comparison of classification techniques for seismic facies recognition. Interpretation 3, SAE29–SAE58,
- Zhao, T., Zhang, J., Li, F., and Marfurt, K.J., 2016. Characterizing a turbidite system in Canterbury basin, New Zealand, using seismic attribute and distance-preserving self-organizing maps. Interpretation, 4, 1, SB79–SB89.
- Zhao, T., Li, F., and Marfurt, K. J., 2017. Seismic attribute selection for unsupervised seismic facies analysis using user-guided data-adaptive weights. Geophysics 83, 2, 1–62.
- Zeng, Z., and Jiang, A., 2006. Geomechanical Study of Bakken formation for improved oil recovery. ISRM - Sponsored International Symposium on Rock Mechanics: Rock characterization, modeling, and engineering design methods, 2006.
- Zoback, M. D., Barton, C., Brudy, M., Castillo, D., Finkbeiner, T., Grollimund, B., Moos, D., Peska, P., Ward, C., and Wiprut, D., 2003. Determination of stress orientation and magnitude in deep wells. International Journal of Rock Mechanics and Mining Sciences 40, 1049 – 1076.

5. Dissertation summary and conclusions

In this dissertation, I show how on the regional and local scales, the enclosed mini-basin fill settings can be identified. The mini-basin fill started to develop at the onset of a major marine transgression (sea level rise), where the erosion of pre-existing strata form concave-down silled areas. These restricted areas served as accommodation space of highly restricted deposits during the oceanic transgression events. On the persistent transgression events, the highly restricted conditions ended when filling these previously eroded pockets. I propose, for the case of the Woodford Shale, the mini-basin fill settings started at the base of the Lower member, into the Middle member time (upper part of the Middle Woodford member). The uppermost Woodford Shale (uppermost Middle Woodford member and entire Upper Woodford member) was deposited after the maximum flooding event (MFS) of the Woodford ocean, as a significant continuous, well-circulated open marine deposits. These uppermost Woodford open marine deposits occurred blanketing the filled pockets of Lower and Middle Woodford strata (the Woodford enclosed mini-basin fill). The open water conditions allowed the interaction with upwelling currents, providing nutrient-rich waters and developed algal, radiolarian and planktonic blooms that allowed more biogenic activity and more oxidant agents. The oxidant agents in the Upper Woodford member disallowed higher preservation of the organic matter when compared to the Lower and Middle Woodford Shale enclosed mini-basin fill. I recognize how the geological and geochemical characteristics of the Woodford shale deposits can also be recognized in the seismic data and have a direct impact on the simulation of unconventional production of hydrocarbons and wellbore operational planning and forecasts of production performance. I also showed how distinctive patterns in seismic data could be exploited using machine learning algorithms to identify and map the vertical and lateral stratigraphic variabilities of enclosed mini basin fill and open marine

Woodford Shale deposits. For this reason, I mention the crucial outcomes of my integrated analyses as the following:

Seismic characteristics of enclosed mini-basin fill.

- Thicker basal sections that trend to pinch out towards paleo structural highs of the pre-existing strata. In this case, the seismic resolution was enough to image internal reflectors of the Woodford Shale.
- Incoherent seismic data at the base of the Woodford Shale, caused by erosion or karstification of pre-existing strata
- Most negative curvature values in the areas of these deposits that indicate accommodation space and sedimentation filling the enclosed mini-basin fill pockets.
- Low (or the lowest) acoustic impedance that correlates with higher accumulations of organic matter (%TOC) in the lowermost parts of the Woodford Shale seismic window. This is due to a deeper water column in these areas and more restricted water circulation, therefore, a restricted interaction with upwelling currents that preserve the %TOC.

Principal geological and geochemical indicators for a highly restricted enclosed mini-basin fill settings in the Woodford Shale.

- The Lower Woodford member's gross thickness is, on average, greater than 90 ft. A much higher thickness of this specific member when compared to other Woodford Shale locations in the Oklahoma petroleum provinces. Therefore, more accommodation space was available for these basal Woodford Shale to deposit in the enclosed mini-basin fill settings.
- Locations surrounded by a lot of faulted provinces that can be the reactivation of pre-existing fault grabens could have acted as paleo structural lows. These graben depocenters allowed more accommodation space, higher sedimentation rates if proximal to the sediment supply of a

specific petroleum province. These paleo depocenters would favor the development of restricted conditions to the water chemocline for preventing open water circulations and oxidation processes in the organic matter.

- From the saturate and aromatic biomarker analysis, the indicators of a rise in the gammacerane index, a decrease in sterane/hopane ratios, high content of aryl isoprenoids and C_{40} carotenoids indicate that the Lower Woodford and upper portion of the Middle Woodford member are characterized by isolated and persistent episodes of photic-zone euxinia (PZE). This PZE points to oxygen minimum zones and higher restricted conditions as critical characteristics of the enclosed mini-basin fill settings. These fills are between 150-200 ft thick, which include both Lower and Middle Woodford intervals.

- For the uppermost Middle member and complete Upper Woodford member, the biomarker analyses have provided evidence for a potential mechanism for mass extinctions involving eutrophication of shallow marine settings, followed by increased bio productivity, oxygen consumption and subsequent global euxinic seas. I concluded that after the maximum flooding surface and before the Middle-Upper Woodford member's boundary, the Woodford develops the highstand system tract (HST), which is the setting for typical open marine deposits.

- The enclosed mini-basin fill is critical for allowing the higher accumulation, restriction and preservation of organic matter, which is observed by a higher total organic carbon (%TOC), high hydrogen index (HI) and low oxygen index (OI). Also, the bulk %TOC regional maps indicate that the enclosed mini-basin fill present higher average %TOC values for the Woodford Shale when compared to areas with open circulation conditions.

- The enrichment in the Upper Woodford member of organically related proxies U, Mo, V, are likely to reflect more open water circulation conditions. The enrichment in heavy elements

occurs when the open marine deposits capture them transported by upwelling current supplies. The heavy elements are concentrated principally in phosphate concretions and chert-rich lithofacies in the Upper member. It is essential to recognize this enrichment in U, Mo, and V for avoiding a false-positive interpretation of anoxia related proxies in the Upper Woodford member.

I propose as an easy initial screening step of possible enclosed mini-basin fill rock intervals to perform Rock-Eval pyrolysis analyses. This methodology should be useful for screening if there are possible changes in the type of organic matter of a stratigraphic section, ideally undertaken on low maturity samples and minimized weathering for the outcrop samples (tough to obtain for the outcrop samples). The identification of highly restricted anoxic deposits, as the enclosed mini-basin fill can be focused and preferentially done to samples with high %TOC (>5% wt.), high HI (HI>600 mg HC/g rock), low OI and generally high sulfur (S[ppm] from XRF) content. These initial interpretations of mini-basin fill settings should be correlated with the chemostratigraphy data proxies with a multi-linear regression for identifying possible restricted areas that might correspond to accumulations under anoxic proxies (high U, V and Mo form XRF).

It is essential to clarify that the Lower, Middle and Upper Woodford Shale members described in the chapters of this manuscript might vary across the state of Oklahoma. So a direct one-to-one detailed comparison must be made when interpreting if the same enclosed mini-basin fill deposits are present in other areas where the Woodford members are identified or labeled with the same nomenclature (e.g., the Lower and Middle Woodford Shale members might be lithologically different and thinner, or not present, in other areas of Oklahoma, and present lower %TOC because of depletion caused by higher maturity levels or organic facies variations).

6. Appendices

Appendix A: Proposed workflow for screening dynamic geomechanics parameters in unconventional resource shales (Young modulus, Poisson's ratio, fracture gradient, and fracture toughness) based on density (RHOB) and sonic (DTC/DTS) curves.

Authors: Emilio J. Torres-Parada[1] and Jean D. Amorocho-Sanchez[2].

[1] The University of Oklahoma, School of Geology and Geophysics.

[2] Ecopetrol S.A. Gerencia de Yacimientos, Bogotá, Colombia.

Procedures for estimating unconventional shale sweet-spot geomechanical properties

Reservoir geomechanics is the integrated study of the state of stress, pore pressure, and physical properties of reservoirs, natural fractures/faults, cap rocks, and the formations in the overburden (Kumar and Ghassemi, 2018). It provides a context within which to understand the interactions between Geological conditions and engineering and production practices (Sierra-Perez, 2011).

The primary parameters controlling these interactions are the state of in-situ stress, rock strength, bedding orientation and properties, pore pressure, distribution of fractures and faults, wellbore trajectory, and mud weight (Mullen et al., 2007; Rickman et al., 2008). The state of stress in a hydrocarbon reservoir is defined in terms of the vertical stress (Sv) and the two mutually perpendicular horizontal stresses (S_{hmax} and S_{hmin}; Kumar and Ghassemi, 2018). It is highly recommended to apply the equations proposed in this appendix for the Woodford Shale, that are calibrated from the rock measurements done by Sierra-Perez (2011) and Slatt et al. (2012) in Oklahoma USA., and include the work of Zoback et al. (2003), Mullen et al. (2007), Rickman et al. (2008), Barree and Gilbert (2009), and Sone and Zoback (2013) for unconventional resources, along with the compressional and shear velocity calculations methods proposed by Castagna et al.

(1986) and Castagna and Backus (1993). Their equations are compiled and described in this document as a handy but straightforward methodology for screening brittle vs. less brittle intervals within the Woodford Shale.

Force and stress

Force is defined by Newton's second law as:

$$F = ma \ , \qquad \text{(A-1)}$$

where *F* is the force, *m* is mass, and *a* is the acceleration.

Stress is defined as the force per unit area (Zoback et al., 2003):

$$\sigma = \frac{F}{A} \ , \qquad \text{(A-2)}$$

where σ' is the stress measured in Pascal. F is the force measured in Newton, and A is the area in m^2.

Because rocks react to stresses and not to forces, the rock mechanics theory uses only stresses.

Displacement and strain

Displacement, *ΔL*, is the change in length:

$$\Delta L = L_2 - L_1, \qquad \text{(A-3)}$$

where L_1 and L_2 are the original and displaced lengths respectfully.

Strain, *ε*, is the displacement divided by the original length:

$$\varepsilon = \Delta L / L_1, \qquad \text{(A-4)}$$

Poro-elastic properties

Poisson's ratio (ν), named after **Siméon Poisson**, is the ratio when a sample object is stretched of the contraction or transverse strain (perpendicular to the applied load), to the extension or axial strain (in the direction of the applied load). When a material is compressed in one direction, it usually tends to expand in the other two directions perpendicular to the direction of compression (Kumar and Gassemi, 2018). This phenomenon is called the **Poisson effect**. Poisson's ratio ν ("nu") is a measure of the Poisson effect. The Poisson ratio is the ratio of the fraction (or percent) of expansion divided by the fraction (or percent) of compression for small values of these changes (Kumar and Gassemi, 2018).

Young's modulus, also known as the tensile modulus, is a measure of the stiffness of an elastic material and is a quantity used to characterize materials (Schlumberger Oilfield Glossary, 2019). It is defined as the ratio of the uniaxial stress over the uniaxial strain in the range of stress in which **Hooke's Law** holds. In solid mechanics, the slope of the stress-strain curve at any point is called the tangent modulus. The tangent modulus of the initial, linear Young's modulus portion of a stress-strain curve is called Young's modulus. It can be experimentally determined from the slope of a stress-strain curve created during tensile tests conducted on a sample of the material (Kumar and Gassemi, 2018). In anisotropic materials, Young's modulus may have different values depending on the direction of the applied force to the material's structure (Kumar and Gassemi, 2018). It is also commonly called the elastic modulus or modulus of elasticity because Young's modulus is the most common elastic modulus used, but there are other elastic moduli measured, too, such as the bulk modulus and the shear modulus. Young's modulus is named after **Thomas Young**, a 19th-century British scientist.

Bulk modulus *K* of a substance measures the substance's resistance to uniform compression and according to Mullen et al. (2007), Rickman et al. (2008) and Barree and Gilbert (2009) is the ratio of the infinitesimal pressure increase to the resulting relative decrease of the volume. The bulk modulus is measured in Pascal, is always positive, and is defined by:

$$K = -V\frac{\mathrm{d}P}{\mathrm{d}V}, \tag{A-5}$$

where *P* is pressure, *V* is volume, and *dP/dV* denotes the derivative of pressure with volume. Equivalently,

$$K = \rho\frac{\partial P}{\partial \rho}, \tag{A-6}$$

where ρ is density, and $\delta P/\delta \rho$ denotes the derivative of pressure concerning density. The inverse of the bulk modulus gives a substance's compressibility. Other moduli describe the material's response (strain) to other kinds of stress: the shear modulus describes the response to shear stress, and Young's modulus describes the response to compressive stress.

Shear Modulus, *G*: In materials science, the **shear modulus** or **modulus of rigidity**, denoted by *G*, or sometimes *S* or μ, is defined as the ratio of shear stress to the shear strain:

$$G \stackrel{\text{def}}{=} \frac{\tau_{xy}}{\gamma_{xy}} = \frac{F/A}{\Delta x/l} = \frac{Fl}{A\Delta x}, \tag{A-7}$$

where $\tau_{xy} = F/A$= shear stress,

F is the shear, A is the area on which the force acts, $\Delta x$is the transverse displacement, $l$is the initial length,

In engineering, $\gamma_{xy} = \Delta x/l = \tan\theta$= shear strain.

Shear modulus is measured in Pascal (Pa), gigapascals (GPa), or thousands of pounds per square inch (kpsi). The shear modulus is always positive. Rickman et al. (2008) mention that the shear modulus is one of several quantities for measuring the stiffness of materials. All of them arise in the generalized Hooke's law:

- **Young's modulus** describes the material's response to linear strain (such as pulling on the ends of a wire),
- the **bulk modulus** describes the material's response to uniform pressure, and
- The **shear modulus** describes the material's response to shearing strains.
- The shear modulus is concerned with the deformation of a solid when it experiences a force parallel to one of its surfaces while its opposite face experiences an opposing force (such as friction). In the case of an object that's shaped like a rectangular prism, it will deform into a parallelepiped.
- Anisotropic materials such as wood, paper, and nearly all single crystals exhibit a differing material response to stress or strain when tested in different directions. In this case, one may need to use the full tensor-expression of the elastic constants, rather than a single scalar value.

Compressional and shear velocities

In anisotropic material, the compressional wave (P-wave) is a wave whose displacement vector is parallel to the wave's propagation vector. In contrast, the shear wave (S-wave) is a wave in which its displacement vector is perpendicular to the wave's propagation vector (Castagna et al., 1986). For anisotropic materials, there is only one quasi P-wave and two quasi S-waves (Castagna and Backus, 1993). The compressional wave velocity, *Vp*, is higher than the shear wave velocity, *Vs*; therefore, the P-wave arrival time is smaller than the shear wave arrival time (about half the value). Castagna et al. (1986) and Castagna and Backus (1993) used sonic and density logs to derive empirical relations for shale and dolomite rocks.

Castagna et al. (1986 and 1993) for shale lithologies:

$Vp = [\rho/1.75]^{3.77}$, (A-9a)

$Vs = 0.804^{*} Vp - 0.8559$, (A-9b)

Where density is measured in g/cm^3, and velocities in Km/s.

Castagna et al. (1986, 1993) for dolomite lithologies:

$Vp = [\rho/1.74]^{3.97}$, (A-10a)

$Vs = 0.583^{*} Vp - 0.078$, (A-10b)

The velocities can also be expressed in terms of density, shear modulus, and the bulk modulus as:

$$V_p = \left[\frac{K + 4/3G}{\rho}\right]^{1/2}, \quad \text{(A-11a)}$$

and $$V_s = \left[\frac{G}{\rho}\right]^{1/2}, \quad \text{(A-11b)}$$

The stress and strain recorded in the quasi-static measurements enable us to calculate Young's modulus and Poisson's ratio:

$$E = 2G(1+\upsilon), \quad \text{(A-12a)}$$

$$\nu = \varepsilon_x / \varepsilon_z, \quad \text{(A-12b)}$$

where ε_x, and ε_z are a lateral strain and axial strain for an isotropic medium.

Alternatively, it can be computed:

$$\nu = \frac{Vp^2 - 2Vs^2}{2\left(Vp^2 - 2Vs^2\right)}, \tag{A-13}$$

Likewise, the bulk modulus, *K* can be computed, and the shear modulus, *G* using the following relationship:

$$K = \frac{E}{3(1-2\nu)} \ , \tag{A-14a}$$

$$G = \frac{E}{2(1+\nu)}, \tag{A-14b}$$

Dynamic moduli from velocities

In order to compute the elastic properties of a sample using a dynamic measurement, it is necessary to calculate the sample density (ρ) directly from the RHOB well log. The P-wave velocities can be computed from the DT log. These measurements provide dynamic rather than static estimations:

$$E = \frac{\rho V_s^2\left(3V_p^2 - 4V_s^2\right)}{\left(V_p^2 - V_s^2\right)} \ , \tag{A-15a}$$

$$\nu = \frac{\left(V_p^2 - 2V_s^2\right)}{2\left(V_p^2 - V_s^2\right)} \ , \tag{A-15b}$$

$$K = \rho V_p^2 - \frac{4}{3}\rho V_s^2, \tag{A-15c}$$

$$G = \rho V_s^2, \tag{A-15d}$$

$$\alpha = 1 - \frac{K}{K_s} \quad ; \text{Ks = 83GPa for south Oklahoma (Sierra-Pérez, 2011).} \tag{A-15e}$$

The Unconfined stress in MPa is:

$UCS = 7.22E^{0.712}$ for shale intervals. (A-16)

$UCS = 25.1E^{0.3}$ for dolomite-rich intervals. (A-17)

and the Tensile stress

$T_o = 10\%UCS$, (A-18)

In-situ stresses and the fracture gradient (FG)

Depending on the in-situ stress state, there may exist an optimal drilled near-balanced or under-balanced trajectory that can be to minimize the rock damaging effects due to mud infiltration on the completed open-hole. Optimal trajectories may require more aggressive drilling and completion parameters. A well-constrained stress field can help determine the appropriate mud window that controls compressive failure leading to the development of wellbore breakouts (in both isotropic and anisotropic rock) and at the same time, prevent catastrophic tensile failure leading to formation breakdown (Zoback et al., 2003),. The unconventional shale reservoirs exhibit considerable variability in composition and geologic history. However, the major shale reservoirs in the United States are all characterized by extremely small grain sizes, low natural permeability, and elevated total organic carbon (Mullen et al., 2007). After the organic-rich rock was buried and heated, first to temperatures high enough to generate oil and then to temperatures high enough to generate natural gas, a significant amount of the generated liquid and gas hydrocarbons remained.

Procedures for estimating in-situ stresses and fracture gradient reservoir before hydraulic fracturing occurred.

The geological and geomechanical data must be integrated in order to characterize the rock properties in a specific study area in order to model the stresses. Ideally, the hydraulic fracturing and micro-seismicity data from that study area provide a means to build a geomechanical model of the reservoir that includes the mechanical rock properties along with the state of in situ stresses.

This model is particularly useful in understanding the evolution of stress before, during, and after hydraulic fracturing. Zoback et al. (2003), Zeng and Jiang (2006), and Sone and Zoback (2013), recommended measurements of the orientation and magnitudes of the principal stresses in the reservoir, where common rock properties used in the stress determination are based on well logs, lab tests, and published literature on different unconventional shale reservoirs.

The **fracture gradient** is defined as the pressure required to induce fractures in rock at a given depth. The Schlumberger Oilfield Glossary (2019) defines the fracture gradient as: "*the factor used to determine formation fracturing pressure as a function of well depth in units of psi/ft. For example, a fracture gradient of 0.7 psi/ft [15.8 kPa/m] in a well with a true vertical depth of 8000 ft [2440 m] would predict a fracturing pressure of 5600 psi [38.6 MPa]".*

The **fracture toughness** is defined as the ability of a material containing a crack to resist further fracture and is one of the most important properties of any material for virtually all design applications. The linear-elastic fracture toughness of a material is determined from the stress intensity factor (K_I) at which a thin crack in the material begins to grow and is measured in $Pa*m^{1/2}$. It is denoted as K_{IC}.

The Plastic-elastic fracture toughness is denoted by J_{Ic}, with the unit of J/cm^2 or lb.-ft/in^2 and is a measurement of the energy required to grow a thin crack. The subscript *Ic* denotes "mode I" crack opening under a normal tensile stress perpendicular to the crack since the material can be made deep enough to stand with shear (mode II) or tear (mode III) failure (Kumar and Ghassemi, 2018). Fracture toughness is a quantitative way of expressing a material's resistance to brittle fracture when a crack is present. If the material has sufficient fracture toughness, it will probably undergo ductile fracture. In contrast, brittle fracture is very characteristic of materials with less fracture toughness.

In the Chapter III, the fracture gradient and fracture toughness model was made for the Woodford Shale, using estimates of these mechanical properties from well logs and previous work by Zoback et al. (2003), Havens et al. (2010), Sierra-Perez (2011), Wang et al. (2011), and Sone and Zoback (2013). The recommended equations are the following:

The fracture toughness $K_{ic} = 0.05E$, (A-19)

The minimum horizontal Stress $S_h = \left(\frac{v}{1-v}\right) S_v + \left(\frac{1-2v}{1-v}\right) \alpha\rho$, (A-20)

And the fracture gradient $FG = \frac{S_h + T_o}{Depth(m)}$, (A-21)

The in-situ pore pressure within unconventional shales like the Woodford Shale is difficult to measure accurately due to its very low intrinsic permeability (Sierra-Perez, 2011; Slatt et al., 2012). For this reason, the pore pressure is often assumed to be roughly equal to the mud weight when there is neither gas intrusion nor loss of circulation at that weight.

Cited References

- Castagna, J.P, Batzle M. L., and Eastwood R. L., 1886. Relationships between compressional-wave and shear-wave velocities in clastic silicate rocks. Geophysics Journal, Society of Exploration Geophysicists 50, 4, 571-581.
- Castagna, J.P, and Backus M.M., 1993. AVO analysis—Tutorial and review. Offset-dependent reflectivity: Theory and practice of AVO analysis. SEG Investigations in Geophysics 8, 3-36.
- Barree, R.D., and Gilbert, J.V., 2009. Stress and rock property profiling for unconventional reservoir stimulation. SPE Hydraulic Fracturing Technology Conference, The Woodlands, Texas, USA, 2009. SPE 118703.
- Havens, J. B., and Batzle, M.L., 2011. Minimum horizontal stress in the Bakken formation. 45th US Rock Mechanics / Geomechanics Symposium held in San Francisco, CA, 2011.
- Kumar, D., Ghassemi, A., 2018. Three-dimensional poroelastic modeling of multiple hydraulic fracture propagation from horizontal wells. International Journal of Rock Mechanics and Mining Sciences 105, 192–209.
- Mullen, M., Roundtree, R., Barree, R., and Turk, G., 2007. A composite determination of mechanical rock properties for stimulation design (What to do when you don't have a sonic log). SPE Rocky Mountain oil and gas technology symposium, Denver, CO. SPE 108139.
- Rickman, R., Mullen, M., Petre, E., Grieser, B., and Kundert, D., 2008. A practical use of Shale petrophysics for stimulation design optimization: All shale plays are not clones of the Barnett Shale. Proceedings from the SPE Annual Technical Conference and Exhibition ATC, SPE 115258.
- Sierra-Perez, R., 2011. Integrated geomechanics and geological characterization of the Devonian-Mississippian Woodford Shale. M.Sc. thesis manuscript, The University of Oklahoma, p. 123.
- Slatt, R. M., Buckner, N., Abousleiman, Y., Sierra, R., Philp, R.P., Miceli-Romero, A., Portas, R., O'Brien, N., Tran, M., Davis, R., and Wawrzyniec, T., 2012. Outcrop/behind outcrop (quarry), multiscale characterization of the Woodford gas shale, Oklahoma, in J. Breyer, eds., Shale reservoirs-giant resources for the 21st century: American Association of Petroleum Geologists AAPG Memoir 97, 1–21.
- Schlumberger Oilfield Glossary, 2019. https://www.glossary.oilfield.slb.com/

- Wang, C., and Zeng, Z., 2011. Overview of geomechanical properties of Bakken formation in the Williston basin, North Dakota. 45th US Rock Mechanics / Geomechanics Symposium held in San Francisco, CA, June 26–29, 2011.
- Zeng, Z., and Jiang, A., 2006. Geomechanical Study of Bakken formation for improved oil recovery. ISRM - Sponsored International Symposium on Rock Mechanics: Rock characterization, modeling, and engineering design methods, 2006.
- Zoback, M. D., Barton, C., Brudy, M., Castillo, D., Finkbeiner, T., Grollimund, B., Moos, D., Peska, P., Ward, C., and Wiprut, D., 2003. Determination of stress orientation and magnitude in deep wells. International Journal of Rock Mechanics and Mining Sciences 40, 1049 – 1076.

Appendix B: Applied biomarker analysis workflow and analytical techniques

Soluble organic matter extraction and precipitation

For obtaining the biomarkers from the soluble organic matter (rock extracts), the rock samples were initially prepared by scrubbing and rinsing in deionized water to remove dirt or contamination from the surface. With sterilized metal tongs, each sample was dipped into methanol three times and left to dry for several hours. Then, the same procedure was repeated with dichloromethane; these processes remove organic impurities that might cause erroneous analyses of contamination effects. Samples were left to dry for 24 hours in a vent hood. Approximately 50-60 grams of each sample was weighed and crushed using a mortar and pestle until each sample was clean enough to be sieved through a US standard mesh No. 40 (0.425 mm) screen. For samples with the lower the TOC, more amount of sample was used, and vice-versa.

The Forty-five samples out of the 536 available were selected for extraction, and for effectively removing the soluble bitumen from each sample, using Soxhlet extraction. The glass apparatus, thimble, glass wool, and boiling chips that are used in this methodology were pre-extracted for 24 hours with approximately 500 mL of a 1:1 mixture of dichloromethane and methanol before the start of each extraction. The Soxhlet was allowed to cool; the solvent was removed and replaced, keeping the boiling chips in place. The ground sample (50-60 g) was poured into each thimble and covered with the pre-extracted wool for avoiding sediment (of powdered rock sample) to contaminate the organic matter extract. The condenser was placed back on the Soxhlet with the sample and cycled on medium heat for 24 hours, or until the solvent in the thimble was clear, indicating that the majority of the soluble organic matter (soluble bitumen) has been extracted from the rock.

Bitumen fractionation

The Soxhlet extracts from the previous step were concentrated using a rotary evaporator until they were nearly dry. The extracts were removed from the flask using dichloromethane and placed in a pre-weighed 20 mL vial, evaporated to dryness using nitrogen gas, and reweighed to obtain the total extractable organic matter (EOM). The asphaltene fraction was removed from the Soxhlet extract before performing column chromatography. The high polarity component of the asphaltene fraction does not permit it to identify detailed molecularly lighter hydrocarbon in the maltene fraction via GC, nor GC-MS.

In order to do this, the bitumen was transferred into 40 mL centrifuge tubes, taking care to transfer as much bitumen as possible, since much of the sample tended to adhere to the side of the container. Using a nitrogen dryer, the excess solvent was blown off from each sample. Approximately 1 milliliter of dichloromethane (DCM) was added to each centrifuge tube before it was placed in the sonicator, to ensure maximum dissolution into the n-pentane. Next, the sonicator was turned on for 15 minutes, while n-pentane was added dropwise to the centrifuge tube to break up the organic material until the tube was filled. Tubes were placed standing up overnight in a freezer set to -5 °C. After 24 hours, the samples were centrifuged for 10 minutes, so the asphaltenes were collected at the bottom of the tube. The solvent was decanted and filtered through 1 inch of packed glass wool in a glass pipette while making sure not to disturb the asphaltene pellet at the bottom. The product was collected in a 100 mL round bottom flask and dried via rotary evaporation, then transferred with 2 mL of dichloromethane into a pre-weighed 4 mL vial, dried under nitrogen, and reweighed to assess maltene weight. The remaining asphaltene was also removed from the centrifuge tube and weighed.

Liquid column chromatography of the maltene fractionation

In a new 4 mL vial, 15-20 mg of the maltene fraction was weighed out and diluted with 200 microliters of hexane. For samples that had limited extract, as little as 10 mg of sample were used for fractionation. In a glass pipette, a half-centimeter of glass wool was packed into the bottom, and 3.8 grams of powdered $AlSiO_2$ was measured on aluminum foil and poured into the pipette. The pipettes were tapped until the powder was settled and leveled. Air was used for packing the liquid chromatography alumina column. Approximately 40 mL of hexane was pushed through the column. By doing this while avoiding drying out the column, the alumina forms a continuous substrate on which the various compound classes could be fractionated.

The obtained 200 microliter maltene/hexane solution was then introduced to the column for performing compound separation by liquid chromatography. The aliphatic fraction was eluted using 8.5 mL of hexane; the aromatic fraction with 25 mL of a 3:7 mix dichloromethane and methanol; the remaining polar fraction with 100% dichloromethane. Each of these products was collected in separate heated 100 mL round bottom flasks and dried via rotary evaporation. The dried fractions were diluted with approximately 1 mL of their respective solvents and transferred to pre-weighed 4 mL vials. The final weight of each biomarker fraction was recorded. A summary of the entire laboratory workflow used to analyze samples is illustrated in Figure B.1.

Gas Chromatography

The gas chromatography (GC) is used to analyze the maltene fraction of all samples on an Agilent 6890 series GC system with a split/splitless capillary injection system equipped with a 30 m by 0.32 mm i.d. J&W scientific HP-5 fused silica capillary column with a 0.25 μm liquid film. Samples were also analyzed in splitless injection mode with a temperature program set to an initial

temperature of 40 °C with a 10 min holding time. The temperature of the system is increased to 300 °C at 4 °C/min rate and held isothermal for 24 min with a detector temperature of 310 °C. Helium is used as the carrier gas with a flow rate of 2.0 ml/min.

Gas Chromatography-Mass Spectrometry

The saturate and aromatic fractions of the maltenes were analyzed by gas chromatography-mass spectrometry (GC-MS) using an Agilent 7890A GC coupled with a 5975C mass spectrometer detector (MSD) running in the splitless injection mode. The GC-MS used a 60 m by 0.25 mm i.d. J&W scientific DB-5MS fused silica capillary column coated with a 0.25 μm liquid film. Single ion monitoring (SIM) is used with specific ions for biomarker analyses. The temperature program for the analyses started at 40 °C with a 1.5 min hold time, and the oven temperature was programmed to 316 °C at 4 °C/min rate and held isothermal for 50 min with helium as the carrier gas at a flow rate of 1.4 ml/min.

Gas Chromatography-Mass Spectrometry-Mass Spectrometry

Eight selected samples were analyzed using Thermo Scientific TRACE 1310 GC coupled with an 8000 triple stage quadrupole (TSQ) operating in splitless injection mode. For more detailed analyses, the GC/MS/MS was equipped with a 60 m by 0.25 mm J&W scientific DB-5MS fused silica capillary column coated with a 0.25-micrometer liquid film. Helium was used as the carrier gas at a rate of 1.4 mL/min; the oven was programmed with a 1.5-minute hold at 40 °C, with a 4 °C per minute ramp to 300 °C, where it was held isothermally for 34 minutes. The identities of the compounds were determined by utilizing parent → daughter ion relationships and literature comparisons for identifying the presence of tricyclic polyprenoids (TPP) using the m/z 414→259 and m/z 358→ 217 rations.

Compound quantification and identification

Agilent Technologies Mass Hunter workstations software B.0.8208.0 (2016) was used as a qualitative analysis navigator to identify and quantify each sample. The peak identities were determined by their retention time, relative position to the standard, and by comparison to the literature. Mass spectra were also used and compared to literature in order to verify compound identities. For samples quantified, chrysene in the ion m/z 228.3 (Figure B.2) was used as an external standard of known concentration, to calculate concentrations in micrograms/gram of extractable organic matter (EOM).

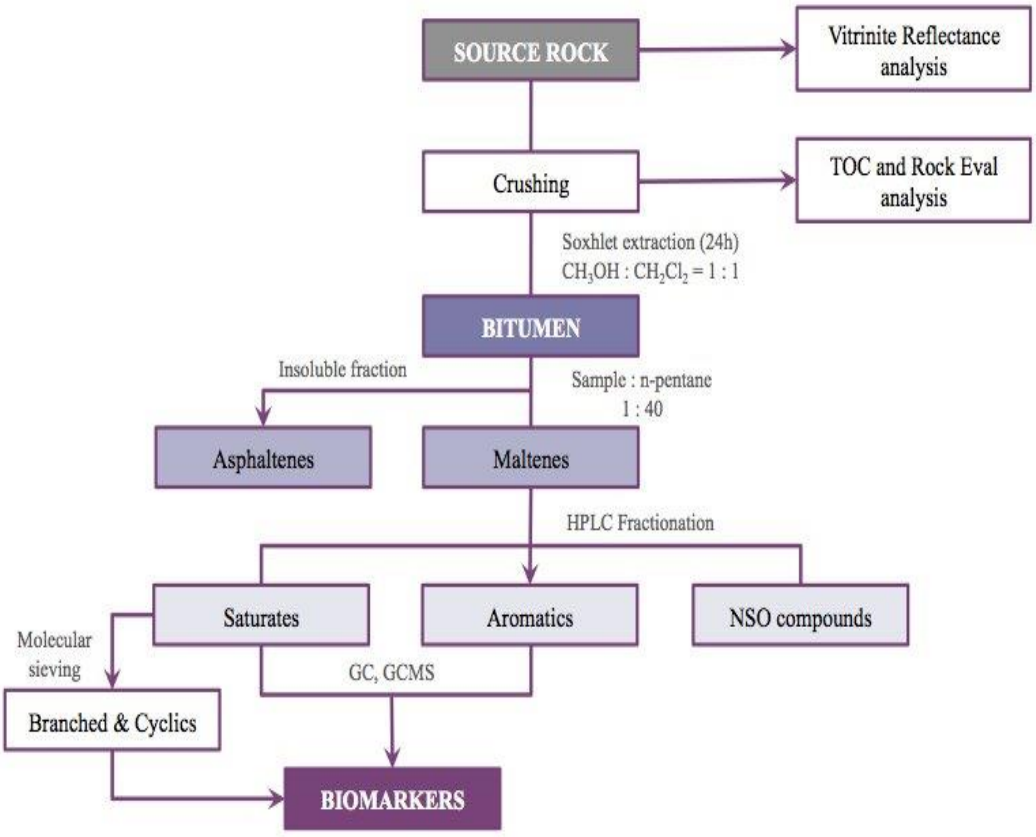

Figure B.1. Schematic workflow used in the laboratory analysis. Methodology from the OU Organic Geochemistry Group (OG2). Diagram modified from Miceli-Romero (2014).

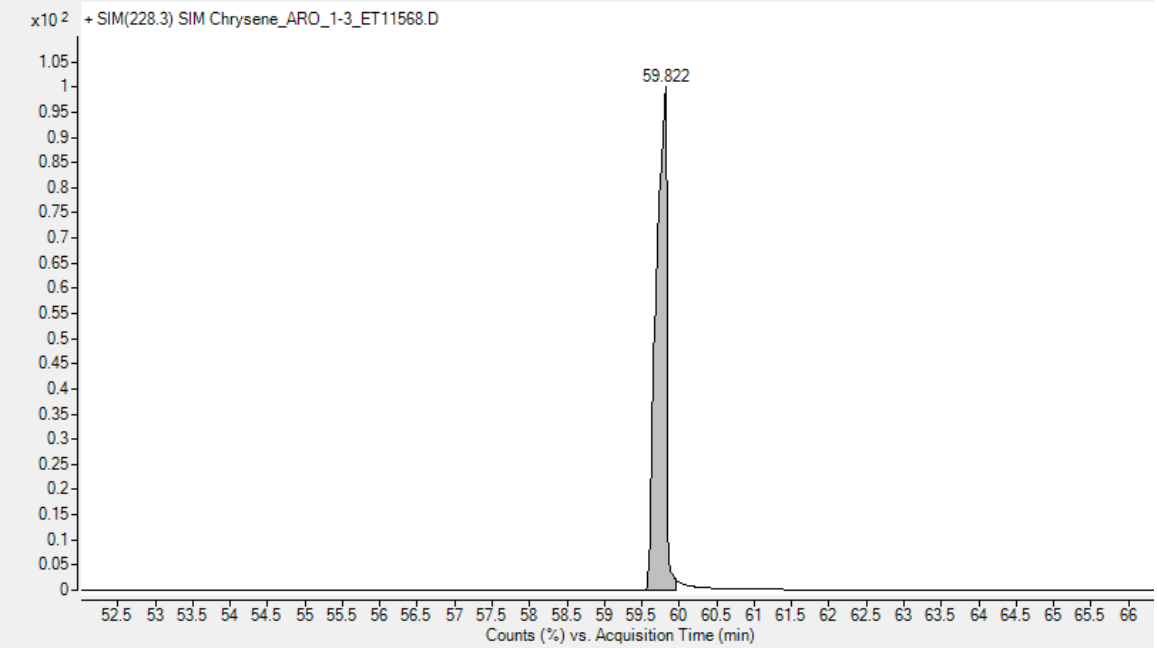

Figure B.2. Chrysene of 107 ppm as an external standard, recognized in ion m/z 228.3

Appendix C: Rock-Eval pyrolysis characterization of Woodford Shale core, cutting, and outcrop samples. Organic facies identification and its variations in the different study areas of the Institute of Reservoir Characterization (IRC).

Torres-Parada, E.J.

A unique statewide organic matter and thermal maturity study of The Woodford Shale was conducted between the Institute of Reservoir Characterization (IRC) and Organic Geochemistry Group (OG2) of the University of Oklahoma, USA. This analysis allowed us to identify critical variabilities between the different Oklahoman Petroleum Provinces. Slatt and Rodriguez (2012), and Miceli-Romero and Philp (2012) mention that at original immature conditions, the prolific Woodford Shale intervals are usually characterized by type II kerogens (oil and gas prone) with high organic richness (usually > 3% Total Organic Carbon -TOC-) and Hydrogen Index (HI) values > 350 (mg HC/g rock). Peters and Cassa (1994) defined for a common source rock that the threshold for typical immature oil-prone kerogen has high TOC (>2% wt.), High HI (>400 mg HC/g rock), low Oxygen Index (OI) and generally low sulfur (S) content.

These screening parameters aid in identifying possible zones of higher unconventional pay (sweet spots of oil vs. gas), where the rock intervals with these characteristics will screen the probable GOR level of any specific producing acreage location. Analyses were performed by the Institute of Reservoir Characterization (IRC) consortium members on thousands of samples of core, cuttings, and outcrops and donated to the IRC database, and additional 600 measured samples from graduate thesis. These measurements were corrected to original (immature) TOC and HI conditions (Jarvie, 2012). Analyses were performed on approximately 2g of each sample and represented the screening parameters of organic facies, and thermal maturity reached in hundreds of locations. The TOC values reflect the amount of organic carbon, including kerogen and bitumen,

in a source rock and are interpreted into the regional depositional IRC model of The Woodford shale for understanding the differences in burial histories (thickness and present-day depths) and organic facies distribution in the state of Oklahoma (kerogen type lateral and vertical variability within the Woodford Shale beds; Figure B.3, and Figure B.4).

In conclusion, in the state of Oklahoma, the Woodford Shale members have: (1) for the Lower member TOC from 0.07% to 16.90% (7.06% TOC average); (2) the Middle Woodford member from 0.09% to 15.60% (average of 6.31% TOC); and (3) for the Upper member from 0.07% to 15.70% (with average 6.00% TOC). Some anomalous values in the Upper Woodford Shale member at specific outcrops range from 12-31% of TOC and are related to Woodford sourced hydrocarbon migration, and as was confirmed by fluid inclusion analysis (Woodford Shale charging itself from deeper to shallower locations). A total statistical average of 6.38% for all samples is indicative of very good to the excellent potential for oil and gas generation, and that there still exists remaining areas to explore and develop that economically vary due to the maturity, depths (pressured or under pressured reservoirs) and thickness in specific petroleum province locations.

Woodford shale organic facies by Rock-Eval pyrolysis data analysis

Peters and Cassa (1994) defined the threshold for values typical of immature type I kerogen as high TOC (>2% wt.), high atomic H/C (>1.5), low O/C (<0.1), high HI (>600 mg HC/g rock), low oxygen index (OI) and generally low sulfur (S) content. The type I oil-prone kerogens are dominated by amorphous organic matter (*Botryococcus* and similar lacustrine algae), with liptinite macerals and vitrinite and inertinite macerals in lesser amounts and appear to be derived from extensive bacterial reworking of lipid-rich algal organic matter, commonly but not always deposited under lacustrine settings (Peters and Cassa, 1994). These screening parameters provide

a crucial factor for identifying possible enclosed mini-basin fill deposits, where the rock intervals with these kerogen characteristics will screen a possible lacustrine provenance towards the enclosed mini-basin fill, but in reality, can be a low OI marine kerogen. A comprehensive series of geochemical analyses were performed on 553 Woodford Shale samples corresponding to the core, cuttings, and outcrop samples of the IRC database. The Rock-Eval pyrolysis (RE) and Total Organic Carbon (TOC) were performed on approximately 2g of each sample and represented the screening parameters of organic facies and thermal maturity previously discussed. Table C.1 summarizes the Rock-Eval pyrolysis parameters applied in the characterization of source rocks. All of the raw data that was gathered and analyzed in this document is available in the IRC Woodford-MSSP digital database upon request. Access can be granted by emailing Dr. Roger M. Slatt to rslatt@ou.edu or Emilio J Torres to emilianitto@gmail.com. A total statistical average of 6.38% for all 553 samples and also for each member is indicative of very good to excellent potential source rock intervals (Peters, 1986; Peters and Cassa, 1994).

Table C.1. Parameters and terms derived from Rock-Eval pyrolysis (modified from Peters and Cassa, 1994; Jarvie et al., 2005 and 2007).

TOC	Total Organic Carbon	wt.%
S_1	Free volatile hydrocarbons thermally flushed from a rock sample at 300°C (free oil content)	mg HC/g rock
S_2	Products that crack during standard Rock-Eval pyrolysis temperatures (remaining potential)	mg HC/g rock
S_3	Organic carbon dioxide released from rock samples	mg CO_2/g rock
T_{max}	The temperature at peak evolution of S_2 hydrocarbons	°C
HI	Hydrogen Index = S_2 x 100/TOC	mg HC/g TOC
OI	Oxygen Index = S_3 x 100/TOC	mg CO_2/g TOC
S_1/TOC	Normalized Oil Content = S_1 x 100/TOC	
S_2/S_3	Describes the type of hydrocarbons generated	Values from 0.00 to >5.00
PI	Production Index = $S_1/(S_1 + S_2)$ (or transformation ratio)	Values from 0.00 to 1.00

Woodford shale kerogen type

The organic matter quality was determined through Rock-Eval pyrolysis parameters, which provided additional information regarding hydrocarbon generative potential for the Woodford Shale (Table C.1). The most commonly used parameters for determining kerogen type are the Hydrogen Index (HI) and Oxygen Index (OI), which are plotted on a modified or Van Krevelen-type diagram developed by Tissot et al. (1974) and is illustrated for all the 553 samples in Figure B.3 and Figure B.4. These samples are different from the 536 samples measured for the Speake Ranch and discussed in Chapter III. This appendix presents the locations different than the Speake Ranch for showing an overview in different areas and petroleum provinces of Oklahoma. A diagram of RE S2 versus TOC constitutes another approach to determine kerogen quality in source rock samples (Figure B.9). According to Cornford et al. (1998), this plot is more reliable for establishing organic matter type, especially for rocks with high carbonate contents that tend to yield dubious OI values.

The thermal maturity of the 553 Woodford Shale samples was assessed through calculated vitrinite reflectance (%Ro) values and Rock-Eval pyrolysis. According to Miceli-Romero (2010), Slatt et al. (2011a) and Dahl et al. (2012), in a shale gas/shale oil exploration framework, %Ro values besides being useful for determining source rock maturity, have also been used to help estimate and predict gas flow rates. Jarvie et al. (2007) and Dahl et al. (2012) suggested %Ro as a geochemical parameter for locating high gas flow rates in the Barnett Shale and Woodford Shale. These authors indicated that areas of low %Ro (low maturity) usually exhibit low gas flow rates, probably due to low volumes of gas generated and because residual liquid hydrocarbons obstruct pores. The areas of high %Ro commonly show high gas flow rates due to more significant amounts of gas generated from cracking of kerogen and bitumen in high-maturity source rocks. It is

essential to correlate %Ro values with other maturity parameters such as Tmax and transformation ratios in order to make a more accurate estimation of organic matter conversion.

According to Peters and Cassa (1994) and Peters et al. (2005), since Tmax and production index (PI) are dependent on organic matter type, they are used to make rough estimates of thermal maturity, which need to be correlated with more reliable maturity parameters. In general, it is expected to observe an increase in PI with Tmax, where PI constitutes a measure for hydrocarbon retention (Peters, 1986; Cornford et al., 1998; Peters et al. 2005). The 553 Woodford samples show PI values ranging from 0.02 to 0.89 and Tmax values for immature intervals (<435° Tmax) and some samples beyond 500°C indicating high maturity organic matter beyond the dry gas window.

The S1 vs. TOC plot (Figure B.5) was useful to determine that the samples analyzed in this study were not contaminated or stained with non-indigenous hydrocarbons such as drilling fluids from oil-based drilling mud (Miceli, 2010; Albaghdady, 2013). In Figure B.5, the red dashed lines separate samples with and without contamination. There are some possibilities for a sample to yield under the contamination area of this S1 vs. TOC plot, and these are due to:

- Relatively low TOC samples (< 1% in the plot) with high S1 (mobile and volatile hydrocarbons measured by Rock-Eval pyrolysis; S1 from 1 to 10 in the plot) *may* contain some of this contamination, because if the TOC is low and if the thermal maturity is low, then something additional is adding mobile hydrocarbons (possibly drilling fluids in core and cuttings, but no contamination of this type in outcrop samples).
- Samples with very high S1 with high TOC (TOC from 1% to 10%). If the S1 is high, the rock has generated hydrocarbons from the kerogen, and TOC should decrease. Again, some external addition of mobile hydrocarbons is indicated; Low TOC (< 1%) with S1 from 0.1 to 1.

- Low TOC, but some S1 means that something can be caved in (in the case of cuttings) that decreases the TOC, or the original TOC is low (low generation potential), but the S1 is due to drilling fluid contamination.

Drilling fluids are hard to wash out from samples, especially those that soak the rock during drilling. Shales tend to retain drilling fluids. Contamination can also occur when cores are stored for a long time after being cleaned for organic geochemistry. In this current compilation of Rock-Eval data, the deeper wells, especially the Ridenour well, have samples that indicate contamination, but this can also be a misinterpretation due to the very high maturity (dry gas window) with remaining minimal TOC and S1 (which both should have been depleted at an elevated level of thermal maturity).

As proposed by Miceli-Romero (2010) for the Woodford Shale, and Lo Monaco (2012) for the Barnett Shale, a plot of HI versus Tmax provides information about the maturity of the samples if the type of organic matter is known or can indicate the type of organic matter if maturity is the known parameter. Hydrocarbon generation, as a consequence of thermal maturity, results in a decrease of HI, so the trends represented by gray dotted lines in Figures B.6 and B.5 indicate the remaining hydrocarbon potential of the rock (Cornford et al., 1998). In Figures B.8 and Figure B.9 most of the Woodford Shale samples plot within the type I/II kerogen field and along the maturity line for vitrinite reflectance < 1.2 % Ro (peak oil window) indicating that these samples reached high maturity levels for the generation of oil and wet gas, but not for dry gas.

The interpretation of the yield of mixed organic matter between types II/III kerogen could be due to a thermal maturation effect where only solid bitumen is left in the rock, and HI, S1 and S2 are depleted. This mixing could be due to a thermal maturation effect where chemical structures present in the kerogen rearrange and become more aromatized (Miceli-Romero, 2010) or the

supply of continental organic matter to these members is higher. In Figure B.3, Figure B.8, and Figure B.9, most of the immature samples plot within the Type I and type II kerogen field and along the maturity line for vitrinite reflectance 0.5%Ro (early oil window) indicating that these samples are immature to marginally mature.

The purely lacustrine deposits have typical Type I kerogen which can be distinguished by having high TOC (>2% wt.), high atomic H/C (>1.5), low O/C (<0.1), very high hydrogen Index (HI >600), very low Oxygen Index (OI<20) with general low sulfur content. These apparent type I kerogen intervals from Figure B.4, Figure B.8, and Figure B.9 plots will be screened with future biomarker analysis for a more detailed characterization if any lacustrine origin organic matter is present (Chapter 3). This screening analysis, followed by a more detailed characterization of the organic matter type (Chapter III), will determine if rocks of a marine environment under very controlled conditions can additionally support the accumulation of lacustrine organic matter within the Woodford Shale. If so, where the marine rock intervals are in high thermal maturity, the liquid hydrocarbons are cracked to gas, but in a similar maturity level for the lacustrine organic matter in the enclosed mini-basin fill deposits, the sourced oil will be preserved or more resistant to thermal cracking, thus providing previously unidentified exploration and prospectivity targets within the Woodford Shale.

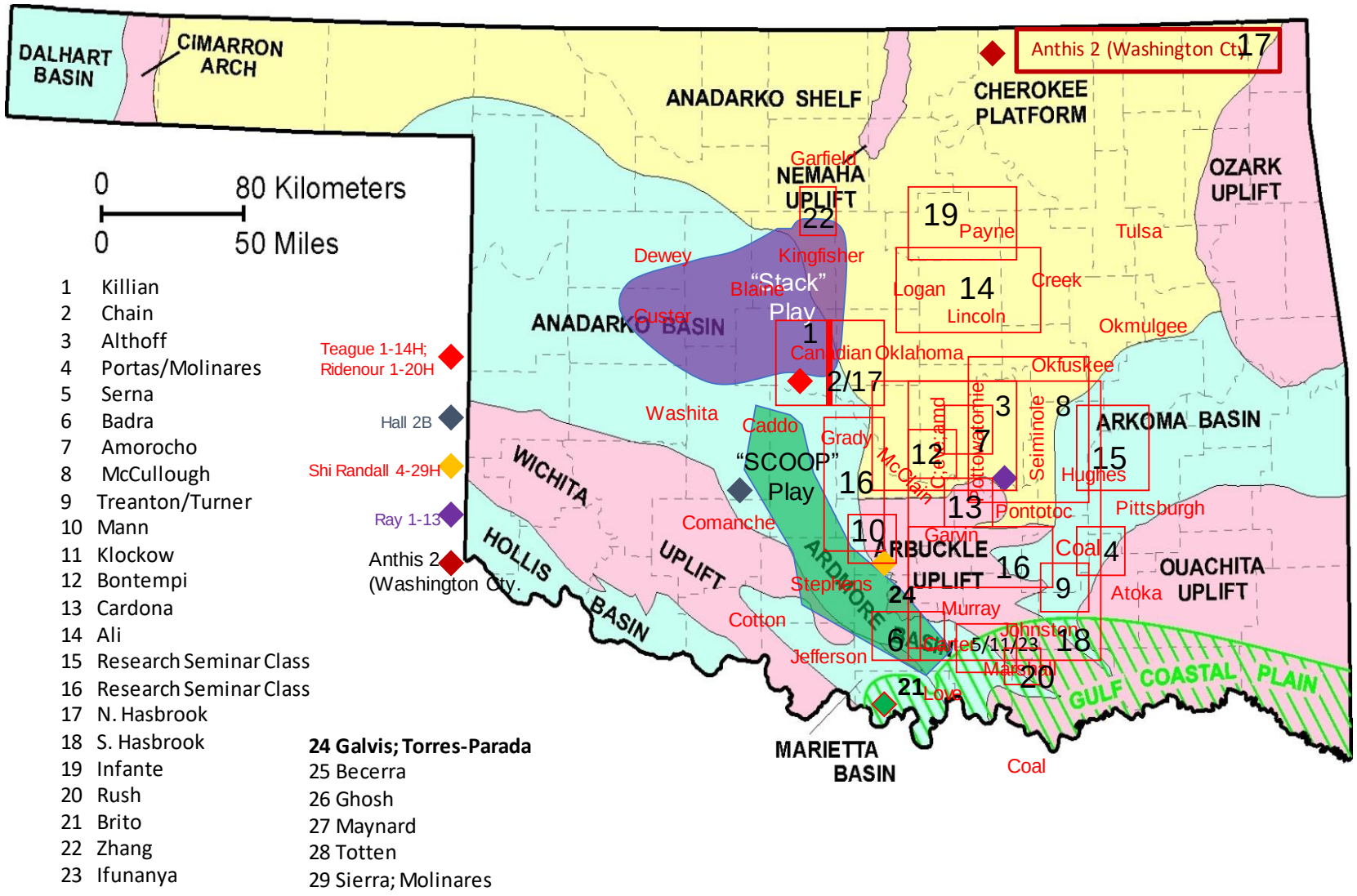

Figure B.3. Location of the different masters and doctorate theses where the Rock-Eval pyrolysis data was gathered and organized for an organic facies' analysis of the Woodford Shale in Oklahoma.

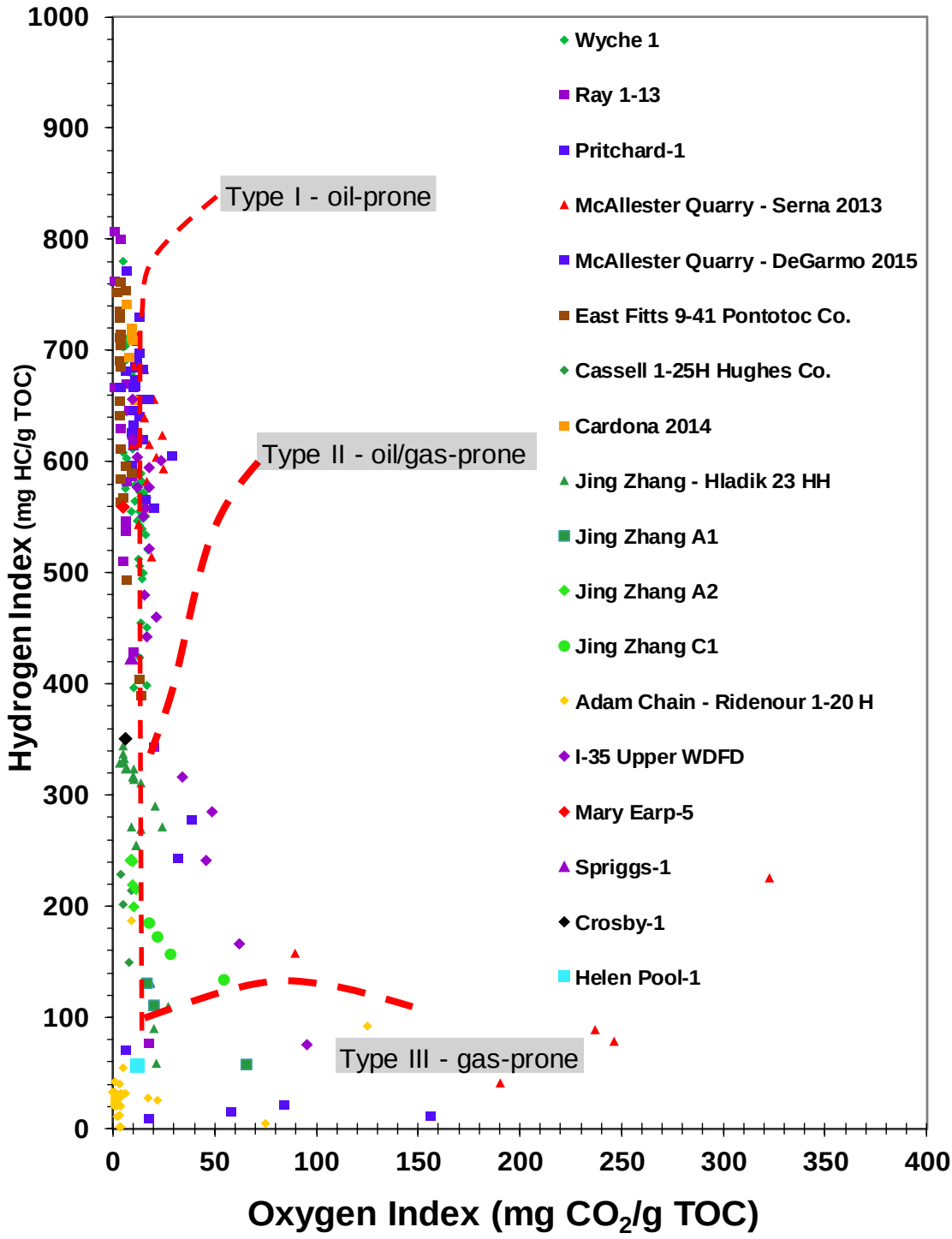

Figure B.4. Modified pseudo van Krevelen diagram for all the 553 Woodford Shale core, cuttings, and outcrop samples. The diagram shows that the source rock intervals are dominated by apparent type I and type II kerogen. Some intervals are in the type III zone because of the type of organic matter and also due to the high thermal maturity, such as the well Ridenour 1-20H. Tmax average of 435 ºC.

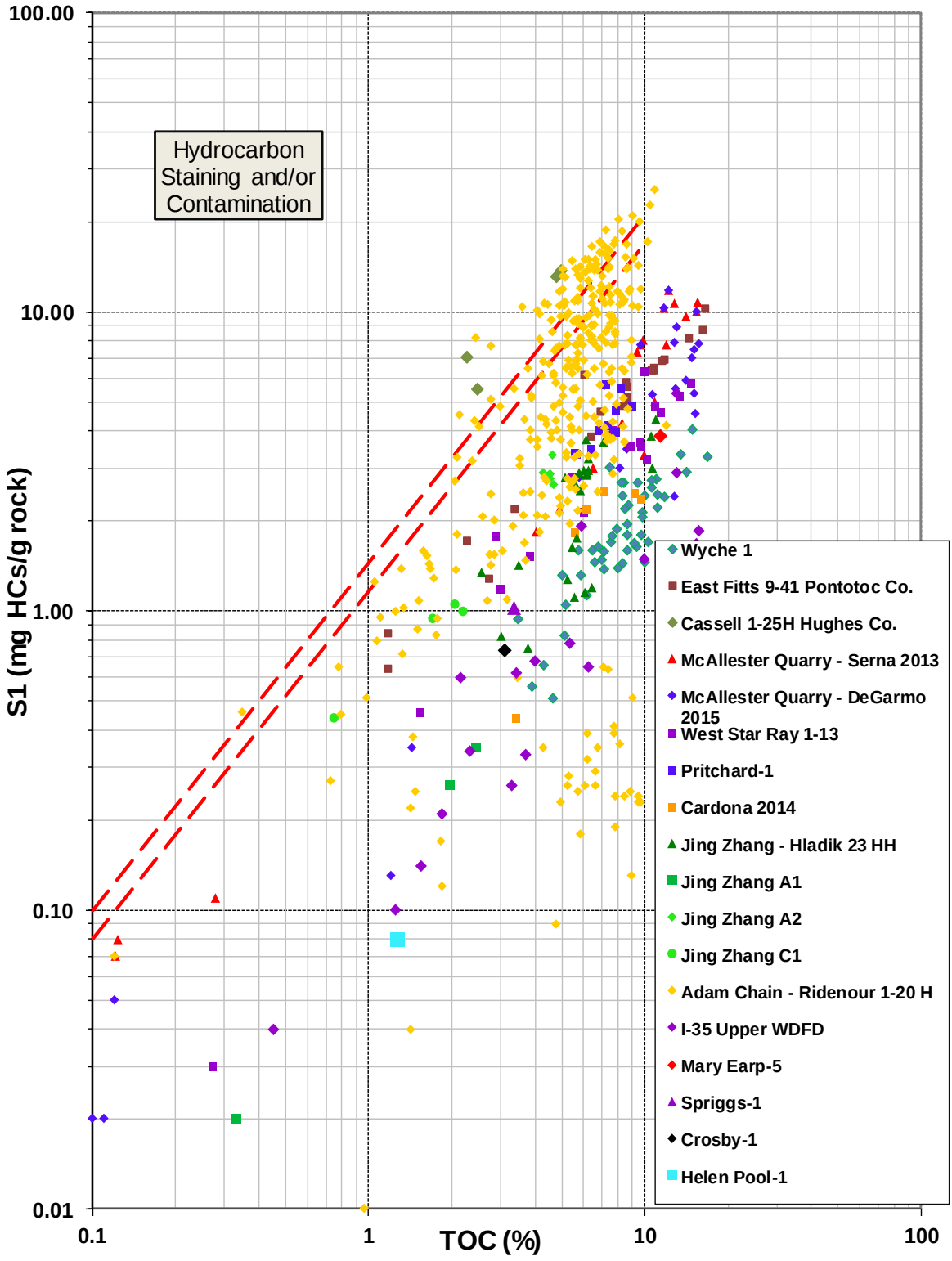

Figure B.5. S1 vs. TOC plot for identifying the hydrocarbon staining and contamination for all the 553 Woodford Shale samples. The wells Ridenour 1-20H and Cassell 1-25H are the only ones that seem to have been affected by contamination with the drilling mud fluids. Plot modified from Miceli-Romero (2010) and Albaghdady (2013).

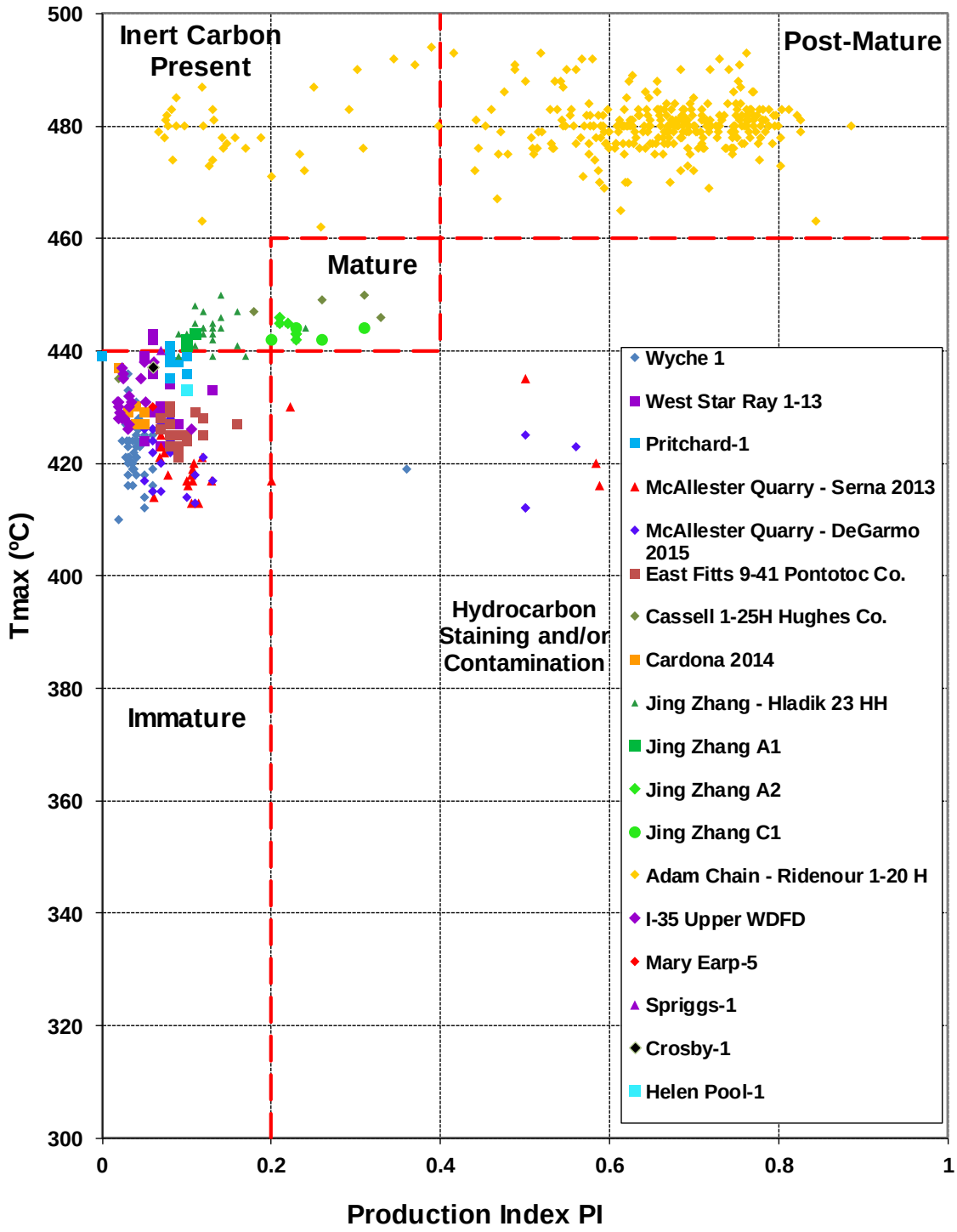

Figure B.6. Tmax vs. Production Index (PI) plot for estimating thermal maturity for all the 553 Woodford Shale core, cuttings, and outcrop samples. The only samples with high maturity levels are from the Ridenour 1-20H well. All other samples are immature or in the early oil generation window. Plot modified from Miceli-Romero (2010) and Albaghdady (2013).

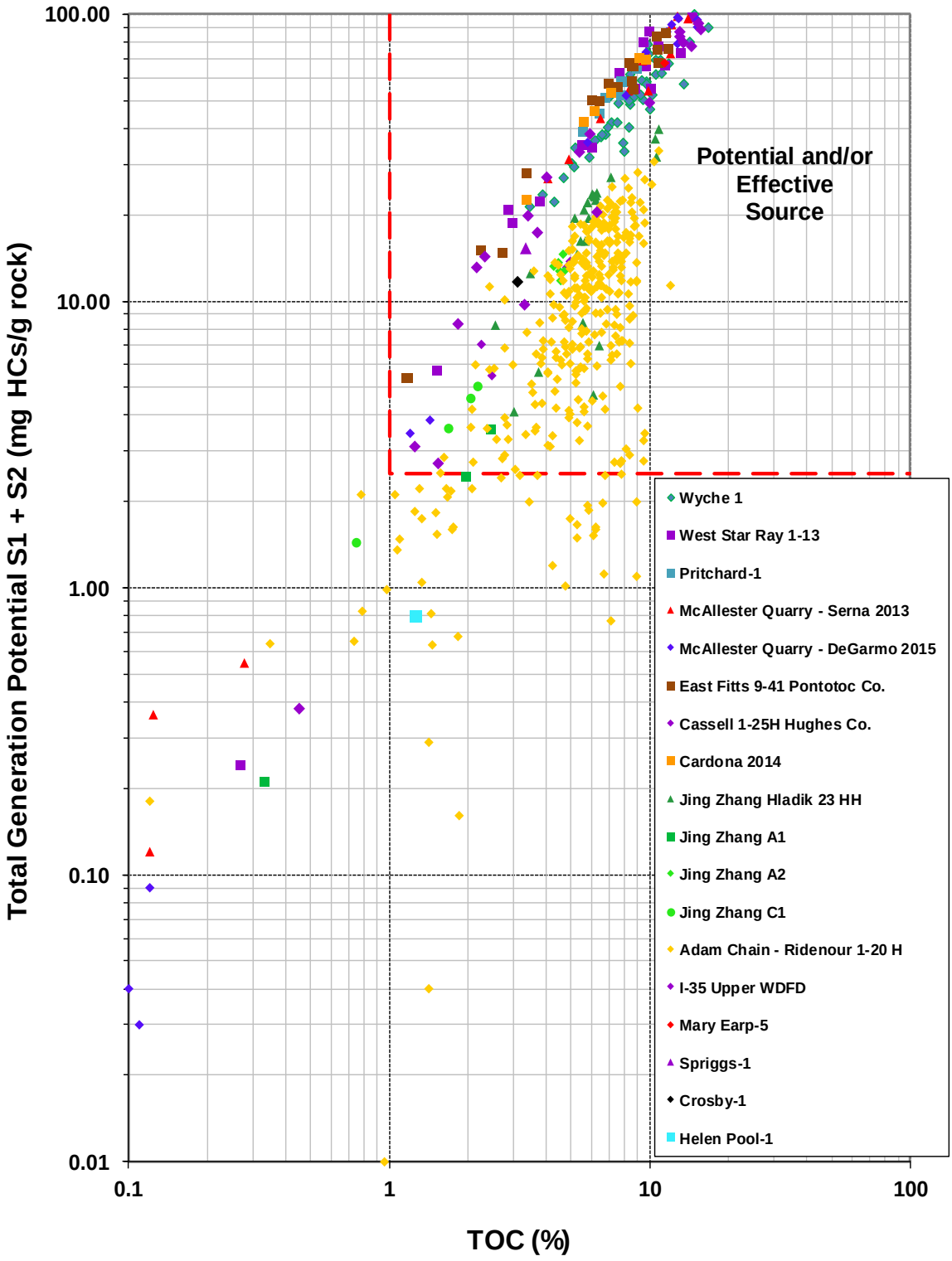

Figure B.7. Diagram of TOC vs. total generation potential (S1+S2), which illustrates the source rock intervals that reached the hydrocarbon generation conditions (potential or active source rocks). All locations analyzed have rock intervals that reached the conditions of enough organic matter and maturity to generate hydrocarbons.

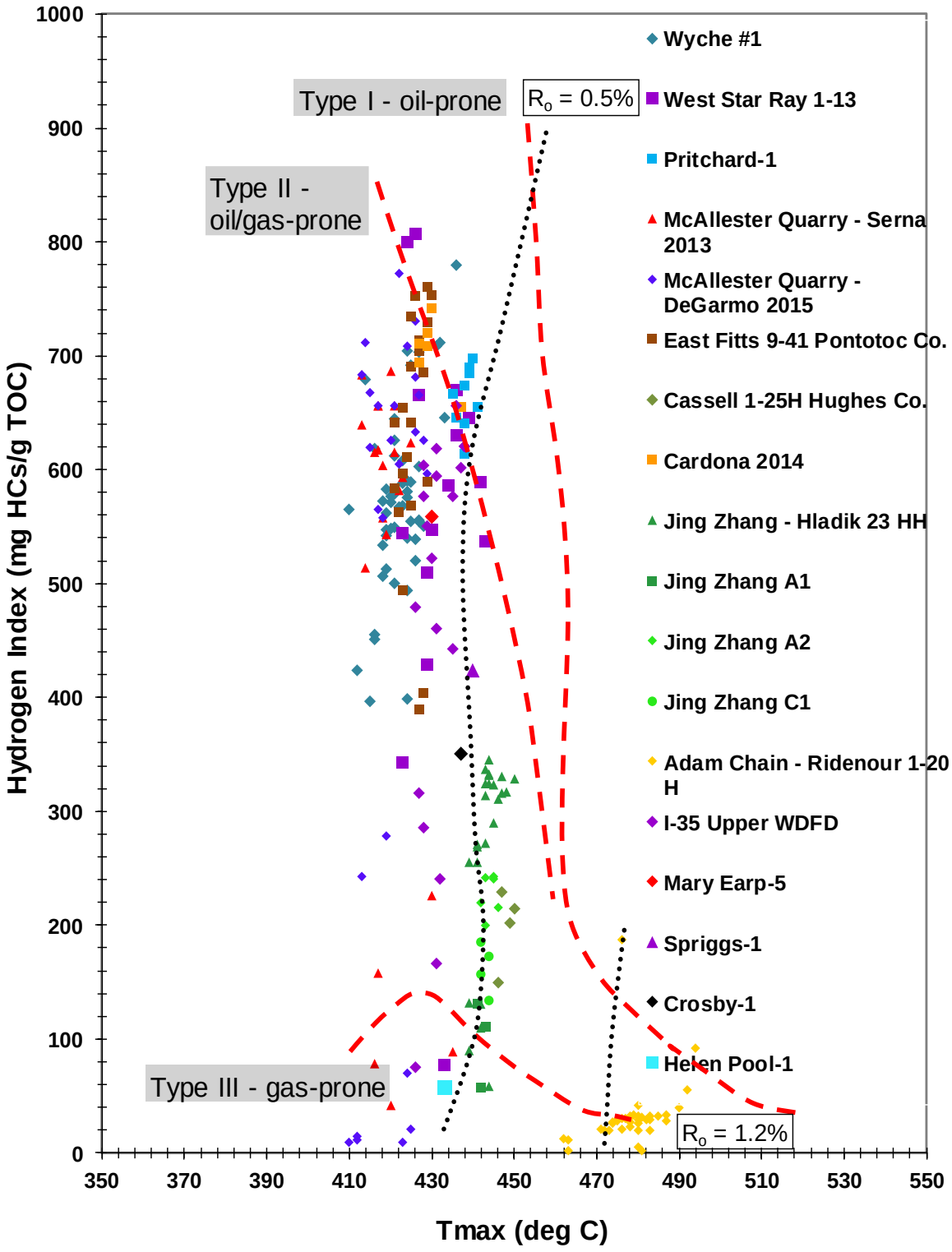

Figure B.8. HI vs. Tmax plot showing maturity and kerogen type for all the 553 Woodford Shale core, cuttings, and outcrop samples. Most of the samples plot on the type II kerogen yield, some in the type I kerogen, some in type III. The Ridenour 1-20H well shows a high maturity level and apparent type III kerogen because of the depletion of HI by thermal cracking.

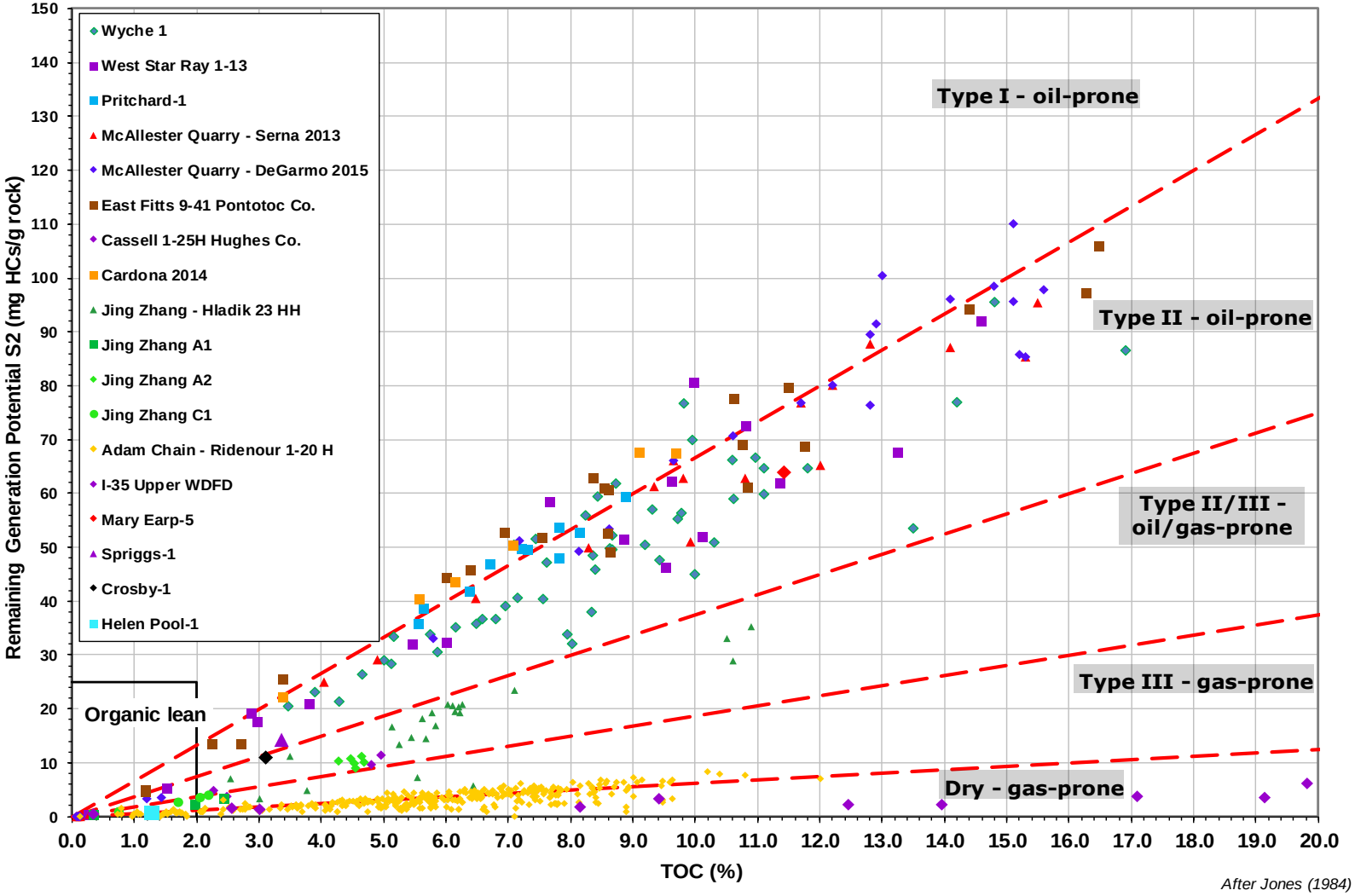

Figure B.9. Rock-Eval remaining hydrocarbon potential (S_2) vs. TOC plot for determination of kerogen type and maturity for all the 553 Woodford Shale core, cuttings, and outcrop samples. Note that most of the samples plot in the type II Kerogen area, but some are in the type I kerogen yield. The Ridenour 1-20H well shows a high maturity level and apparent type III kerogen because of the depletion of S2 by thermal cracking.

Specific location Woodford Shale characterization

Individual locations of wells for Rock-Eval Pyrolysis characterization are shown in this chapter for a more detailed analysis per well or outcrop location. A total of eighteen different locations across Oklahoma have key sample measurements. From these different data sets, only seven significant locations are composed of enough data to show a significant variation within the Woodford Shale internal vertical stratigraphy. The total data corresponds to 440 core sample measurements, 46 cutting sample measurements, and 67 sample outcrop measurements for a total of 553 Rock-Eval data points.

Wyche-1 Core. Pontotoc Co.

The Wyche-1 core is a core drilled behind an outcrop in the Wyche Farm quarry located in Pontotoc Co, Oklahoma. TOC varies from 3.67% to 16.9%. Data points from Miceli (2010) and Connock (2015).

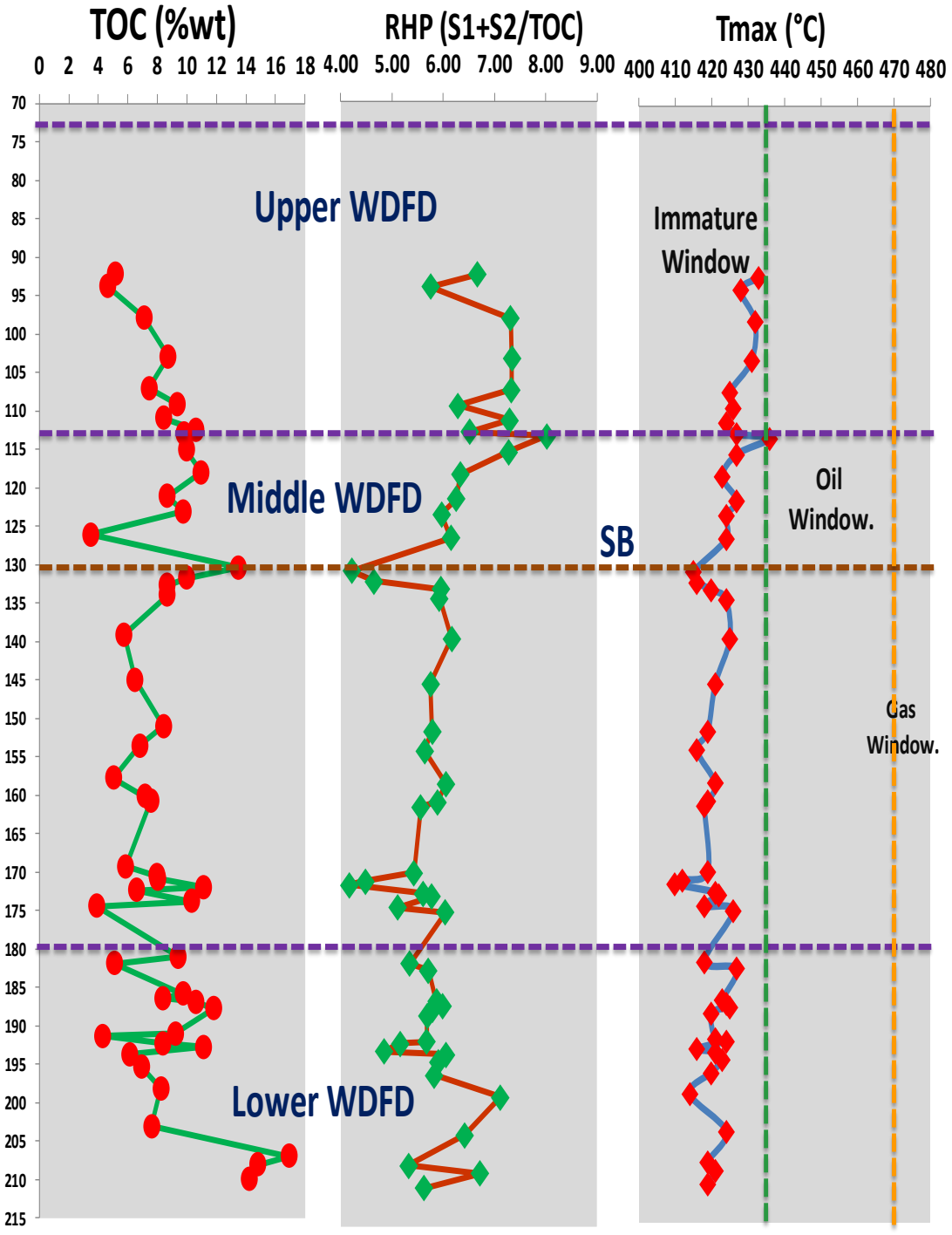

Figure B.10. TOC, relative hydrocarbon potential (RHP), and Tmax maturity variations along with the Wyche-1 core. The purple dashed horizontal lines correspond to Woodford Shale member tops, and brown dashed horizontal line corresponds to the top of a maximum flooding surface (SB) and start of the highstand system tract (HST) facies towards the Woodford Shale top. All samples are immature (Tmax < 435 °C) with an average of 422°C of Tmax.

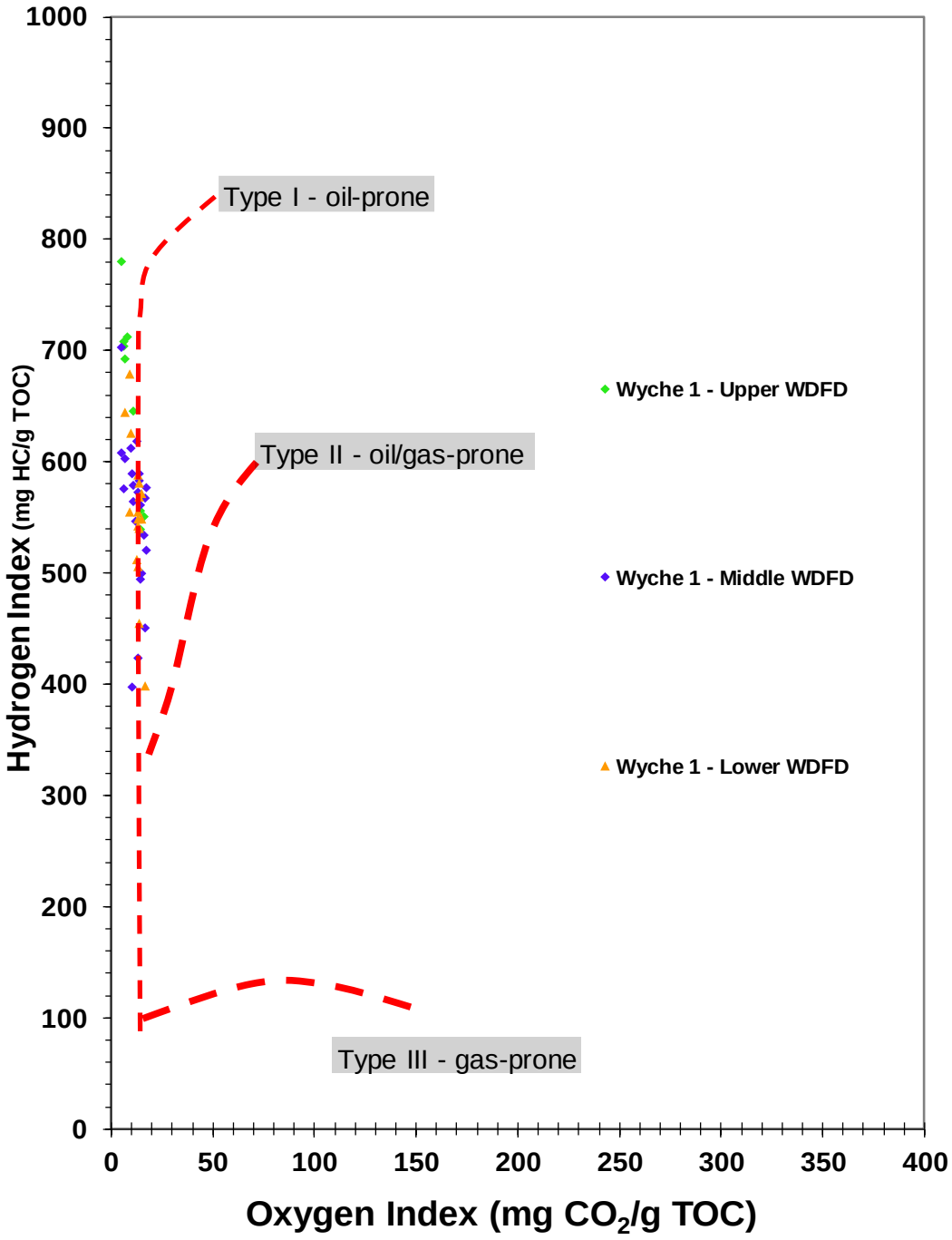

Figure B.11. Modified pseudo van Krevelen diagram for all the 59 core samples of Woodford Shale Wyche-1 core. The diagram shows that the source rock intervals are dominated by apparent type I and type II kerogen. There are no samples which plot in the type III area, maybe because the core is immature and usually the hydrogen index gets depleted with thermal cracking, and these core samples are showing original conditions of the organic matter types. All three Woodford Shale members have apparent type I kerogen samples. Tmax average of 422 ºC.

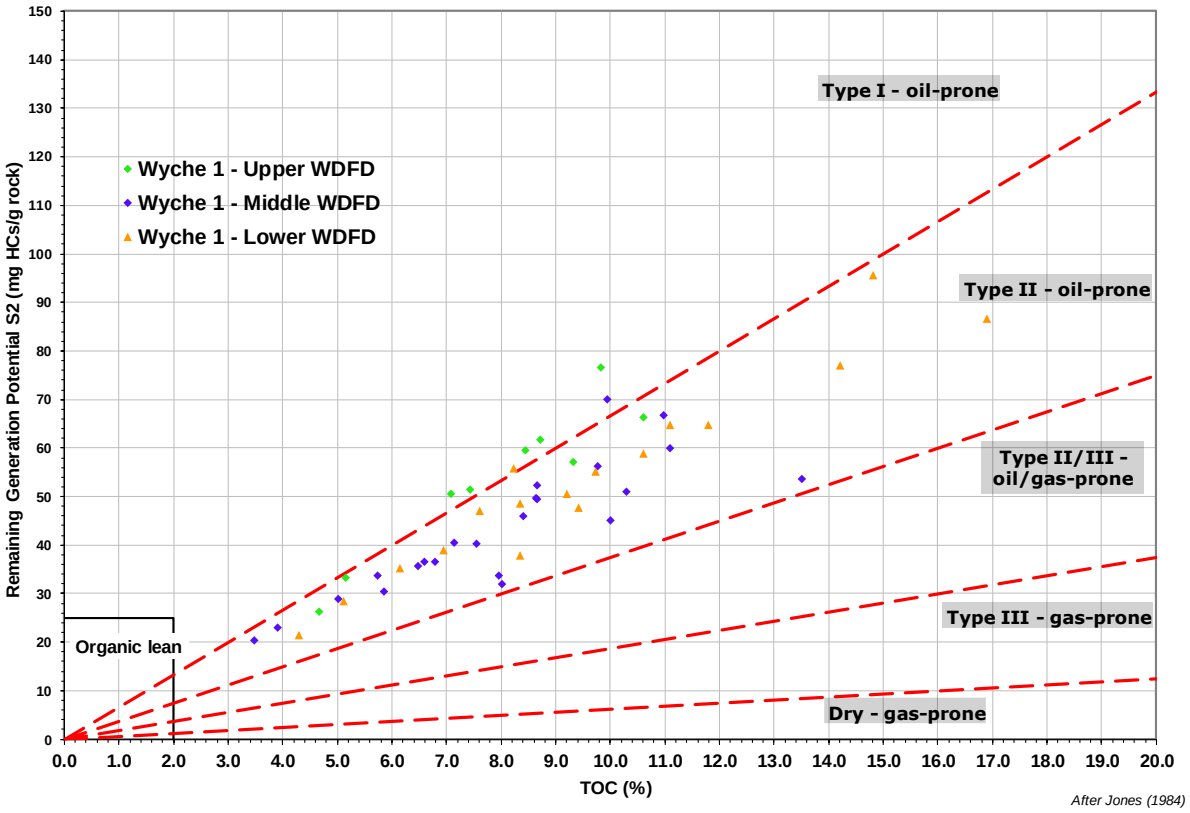

Figure B.12. Rock-Eval remaining hydrocarbon potential (S2) vs. TOC plot for determination of kerogen type and maturity for all the 59 Wyche-1 Woodford Shale core samples. Note that most of the samples plot in the type II kerogen area, but some are in the type I kerogen yield, mainly for the Upper Woodford member and one for the Middle and one sample for the Lower member. There is not any apparent type III kerogen because of the depletion of S2 by the thermal cracking. Also, no samples plot in the lean organic area.

East Fitts 9-41 well. Pontotoc Co.

The East Fitts 9-41 core is located in Pontotoc Co, Oklahoma. Only samples from the Woodford Shale Middle and Lower members were obtained and measured by Miceli-Romero (2010). TOC varies from 1.18% to 16.48% wt. (Figure B.13).

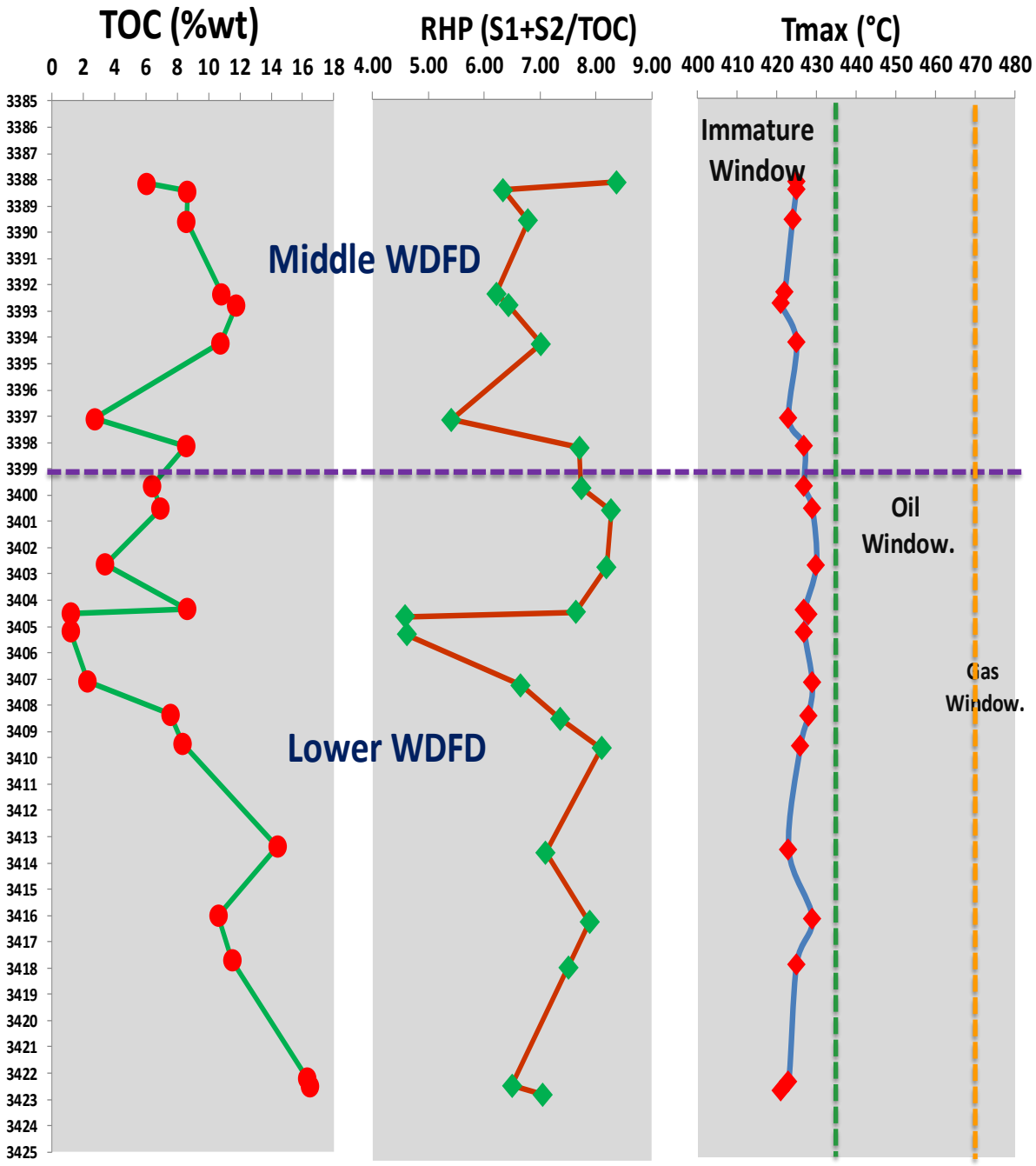

Figure B.13. TOC, relative hydrocarbon potential (RHP), and Tmax maturity variations along with the East Fitts 9-41 well core. The purple dashed horizontal lines correspond to Woodford Shale's Lower member. All samples are immature (Tmax < 435 °C), with an average of 425.63°C of Tmax.

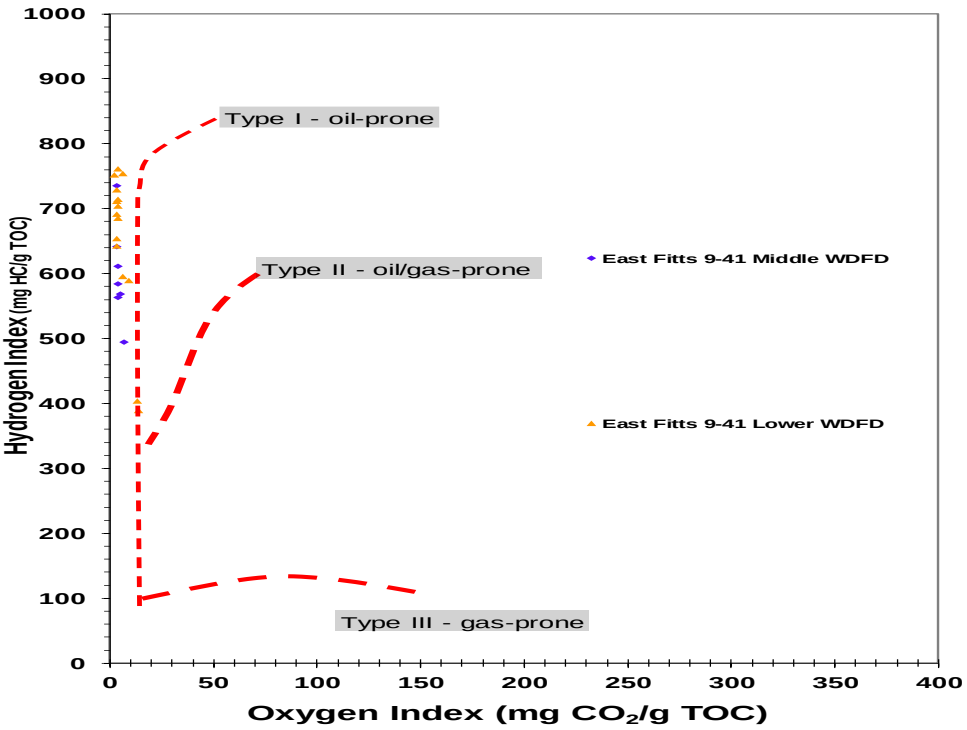

Figure B.14. Modified pseudo van Krevelen diagram for all the 59 core samples of Woodford Shale East Fitts 9-41 core. Note that all the samples plot in an apparent type I kerogen.

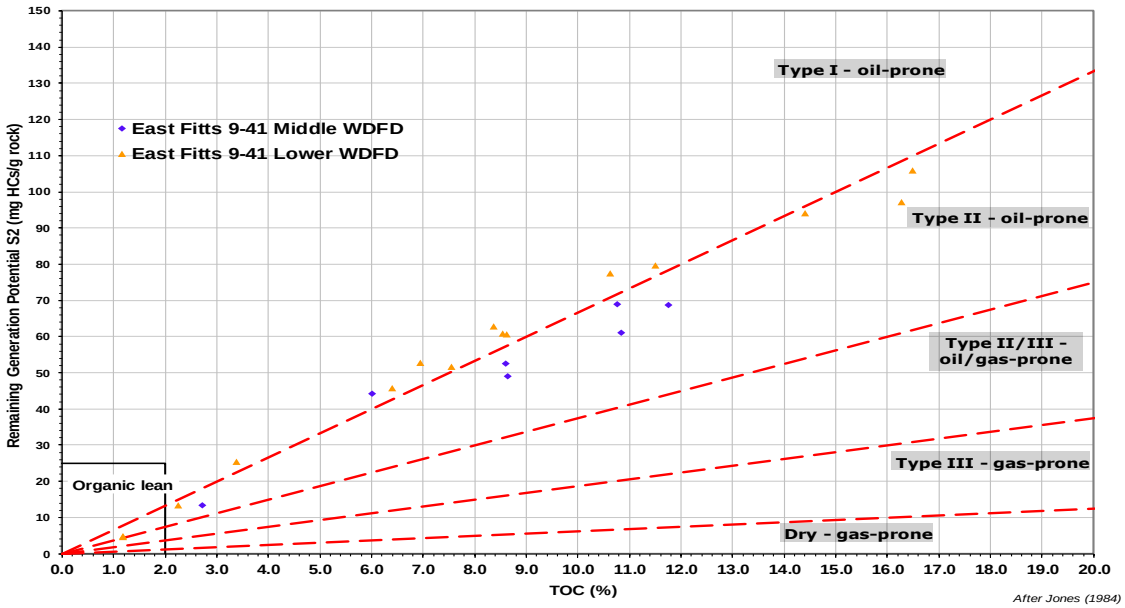

Figure B.15. Rock-Eval remaining hydrocarbon potential (S2) vs. TOC plot for determination of kerogen type and maturity for all the 22 East Fitts 9-41 Woodford Shale core samples. Note that most of the samples plot in the type I kerogen for the Lower Woodford member, and type II kerogen yield mainly for the Middle Woodford member. There is not any apparent type III kerogen because the depletion of S2 by the thermal cracking is absent due to the low maturity of the samples. Also, there is one sample that plots in the lean organic area of the Lower Woodford member.

Ridenour 1-20H. Canadian Co.

The Ridenour 1-20H core is located in Canadian Co, North Central Oklahoma. Samples from the Woodford Shale Upper, Middle, and Lower members were obtained and measured by Chain (2012) and Marathon Oil Co. TOC varies from 0.78% to 12% wt. Average Tmax of 480 °C indicates that the dry gas window was reached. The high maturity levels are a key restriction to interpreting organic facies variations with this Rock-Eval Pyrolysis data because the pyrolysis analysis products (especially Hydrogen Index, S1, and S2 peaks) might be depleted due to the thermal cracking of organic compounds. Not all the TOC samples were provided with Hydrogen Index and Oxygen index values, which is why the Figure B.17 plot has fewer data points than Figure B.16 vertical plots.

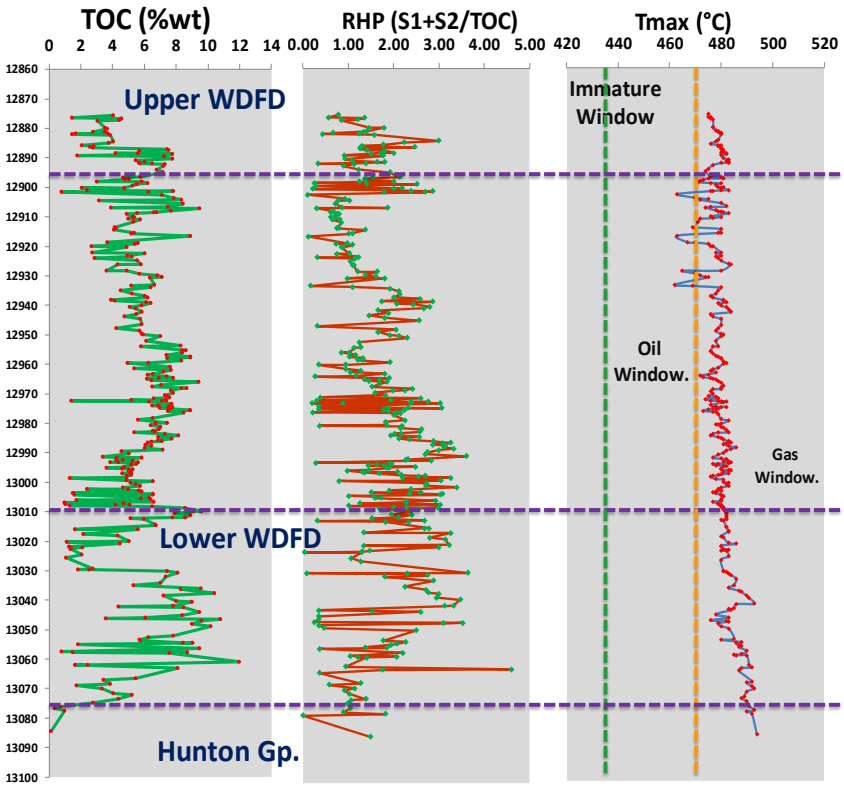

Figure B.16. TOC, relative hydrocarbon potential (RHP), and Tmax maturity variations along with the Ridenour Hill 1-20H well core. The purple dashed horizontal lines correspond to Woodford Shale member tops and at the base to the contact with the Hunton group. All samples are over-mature (Tmax > 470 °C) with an average of close to 480°C of Tmax.

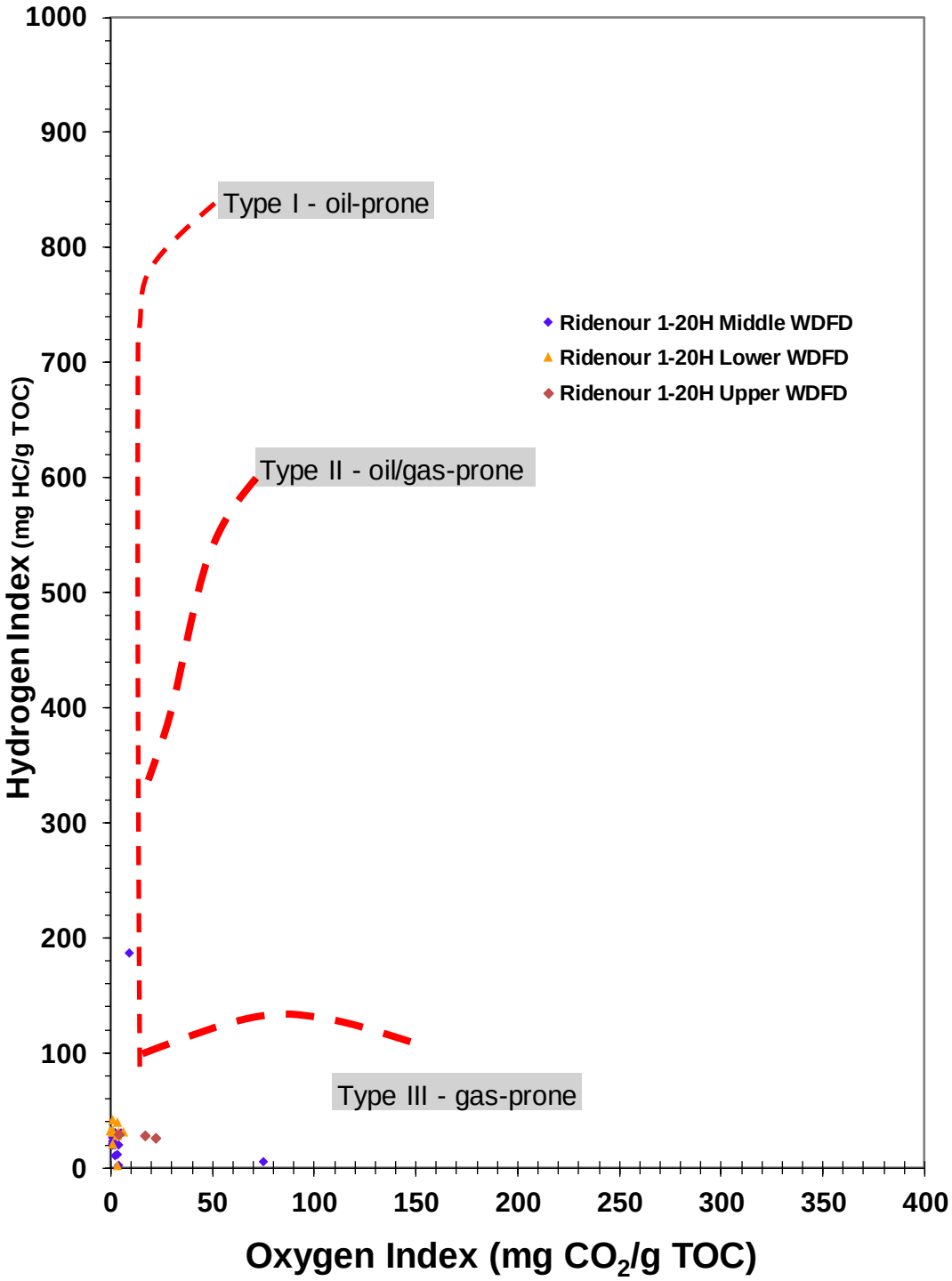

Figure B.17. Modified pseudo van Krevelen diagram for the core samples of Woodford Shale Ridenour Hill 1-20H core. The diagram shows the source rock intervals are dominated by apparent type III kerogen, but this is an artifact due to the high thermal maturity level reached in this location. Usually, the hydrogen index becomes depleted with thermal cracking, and these core samples are not showing original conditions of the organic matter types. For this reason, the Rock-Eval pyrolysis analysis is not a good indicator of organic facies within this core.

McAlister Quarry, Carter Co.

The McAlester quarry is an outcrop that exposes the complete Woodford Shale section. This outcrop is located in Carter County, southeast Oklahoma, in the McAlister Cemetery quarry, Criner Hills uplift, Ardmore basin Oklahoma. TOC varies from 0.07% to 15.6% [Data points from Serna-Bernal (2013) and DeGarmo (2015)]. The average Tmax is 419.78 °C.

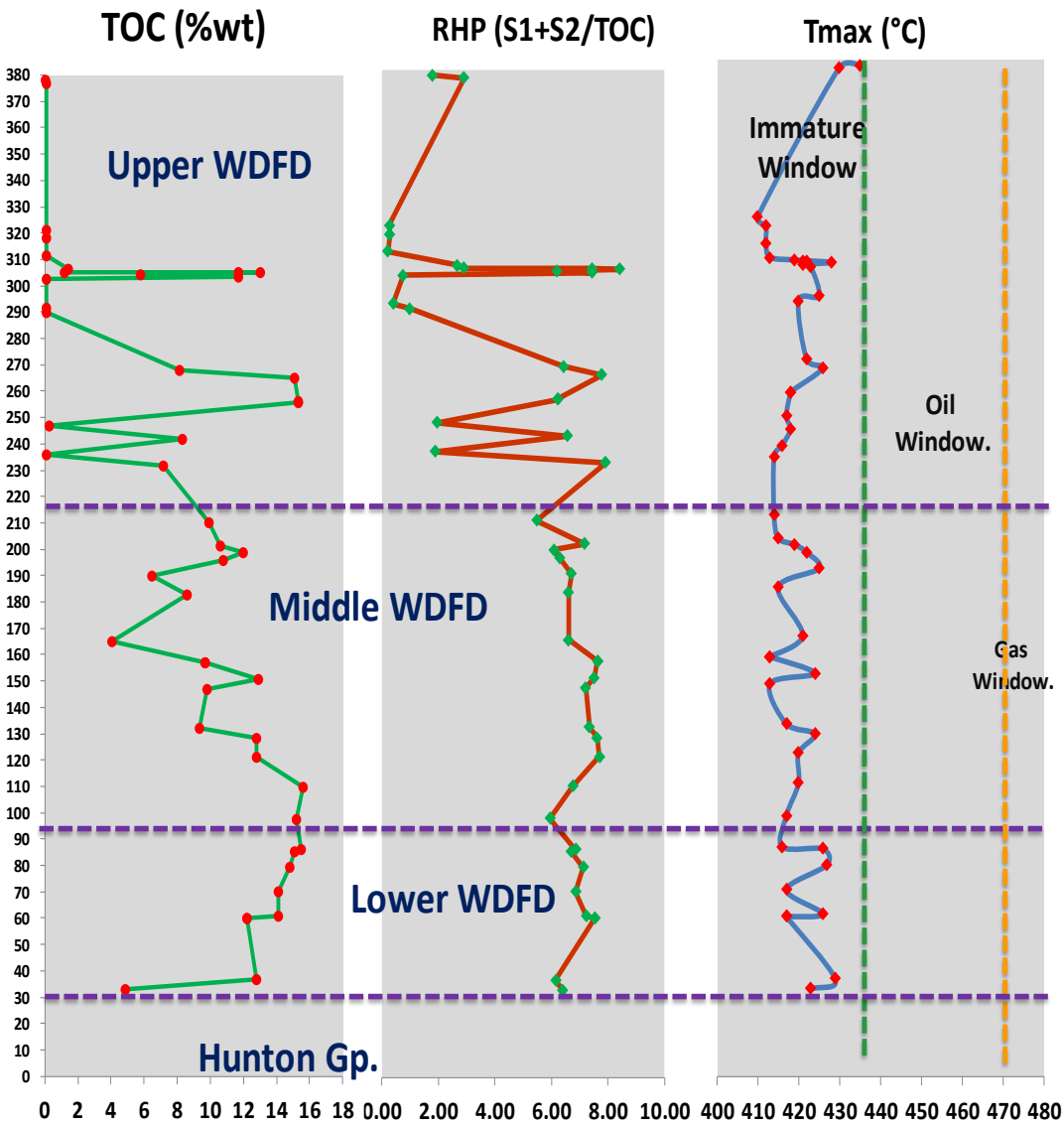

Figure B.18. TOC, relative hydrocarbon potential (RHP), and Tmax maturity variations along the McAlister quarry outcrop. The purple dashed horizontal lines correspond to Woodford Shale member tops and at the base to the contact with the Hunton group. All samples are immature (Tmax <435 °C) with an average of close to 420°C of Tmax.

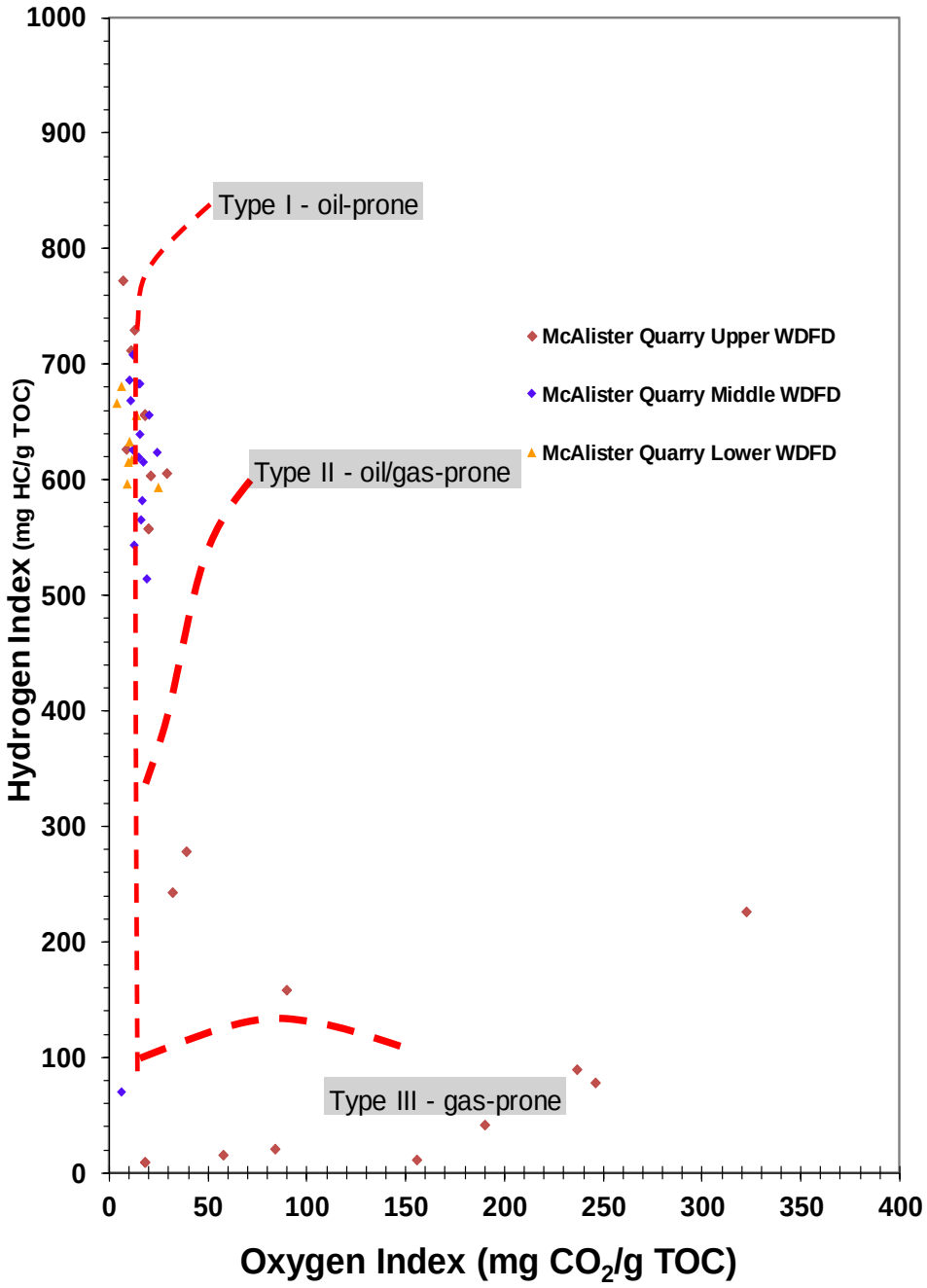

Figure B.19. Modified pseudo van Krevelen diagram for the outcrop samples of Woodford Shale McAlister quarry. The diagram shows the source rock intervals are dominated by apparent type I and type II kerogen. Also, type III kerogen occurs primarily in the Upper member is not an artifact due to the high thermal maturity level reached in this location because samples are immature. Usually, the hydrogen index becomes depleted with thermal cracking, and these core samples are not showing original conditions of the organic matter types. For this reason, the rock eval pyrolysis analysis is a good indicator of organic facies within this outcrop section.

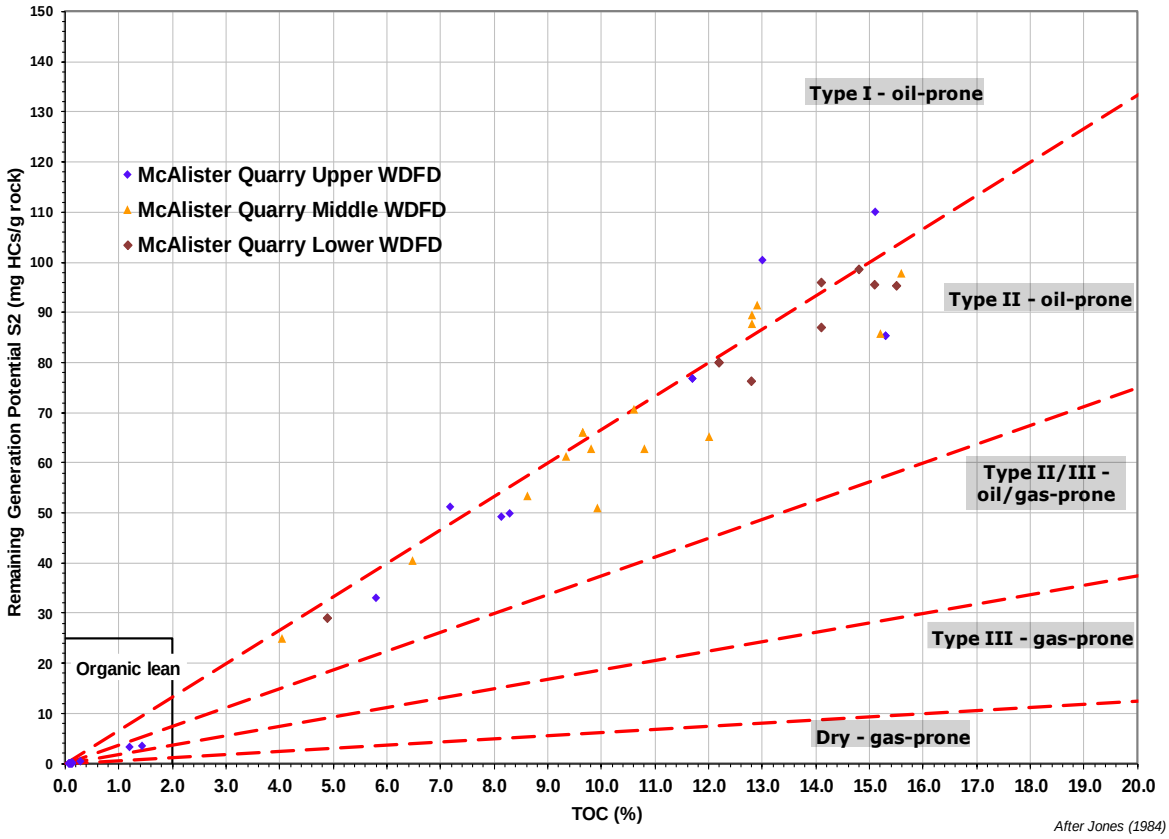

Figure B.20. Rock-Eval remaining hydrocarbon potential (S2) vs. TOC plot for determination of kerogen type and maturity for all the 47 McAlister quarry Woodford Shale outcrop samples. Note that most of the samples plot in the type II Kerogen range for the Lower and Middle Woodford members, and some type I kerogen yield mainly for the Middle Woodford and Upper member. There are not many apparent type III kerogen samples because of a lack of depletion of S2 by thermal cracking, due to the low maturity of the samples. Also, a few samples are plotting in the lean organic area of the Upper Woodford member.

West Star Ray 1-13 well, Pottawatomie Co.

The West Star Ray 1-13 is a 150 ft core located in the southeast Pottawatomie county in Oklahoma. TOC varies from 0.27% to 14.59%. Data points are from Althoff (2012) and Villalba (2016). Average Tmax of 430.13 °C, close to the oil window generation. Figure B.21 illustrates the variation of TOC, which is high at the base of the Lower Woodford member, starts to decrease towards the contact with the Middle Woodford member, then increases again in the Middle Woodford towards the contact with the Upper Woodford and finally decreases towards the

Woodford Shale top. The relative hydrocarbon potential (RHP; Figure B.21) varies along the Woodford Shale but drastically drops from the base of the Upper Woodford towards the top of the Woodford Shale, indicating more oxic conditions and sea-level drop upward in the section.

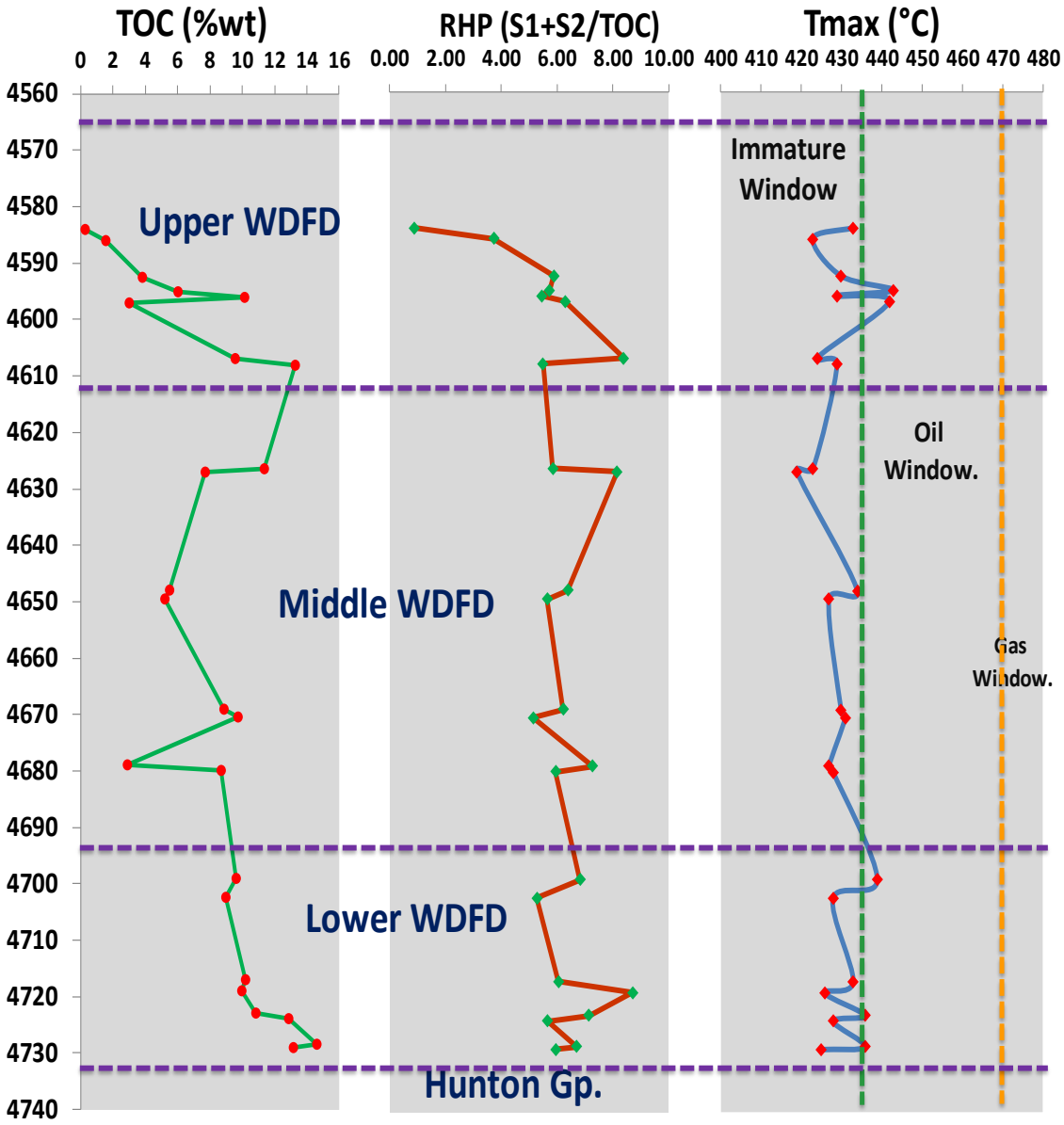

Figure B.21. TOC, relative hydrocarbon potential (RHP), and Tmax maturity variations along with the West Star Ray 1013 core. The purple dashed horizontal lines correspond to Woodford Shale member tops and at the base to the contact with the Hunton group. Most of the samples are immature (Tmax <435 °C), with an average of 430°C of Tmax. Some samples show new oil generation thermal maturity.

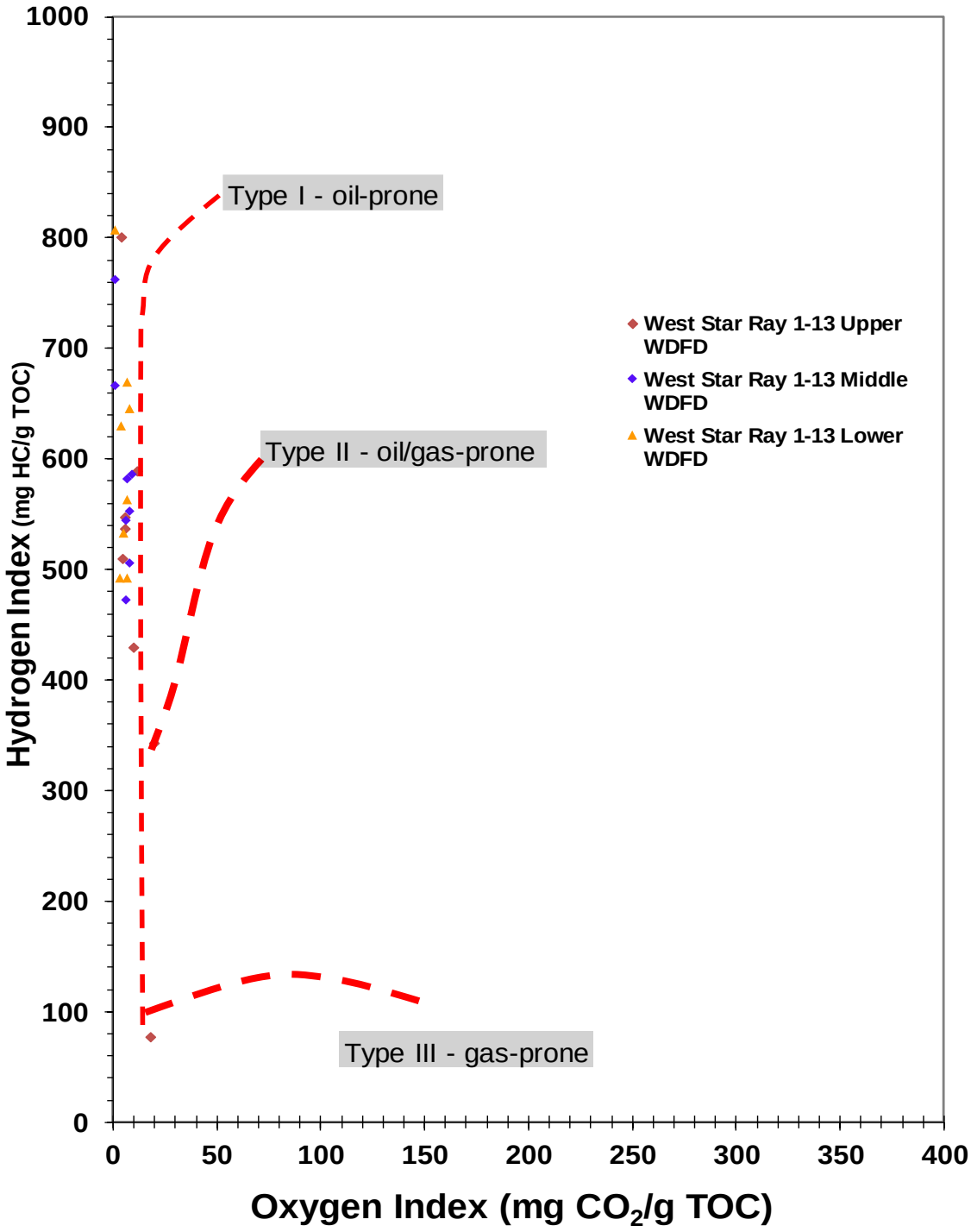

Figure B.22. Modified pseudo van Krevelen diagram for the samples of Woodford Shale West Star Ray 1-13 core. The diagram shows the source rock intervals are dominated by apparent type I kerogen. This apparent type I yield is due to the very low oxygen index content that plots the samples on the type I yield. Special consideration must be considered to see if these samples are correct to type I kerogen, or there is a possibility of high molecular sulfur within the organic matter which sequestrates the atomic oxygen, therefore, obtaining low OI values from the Rock-Eval pyrolysis analyses.

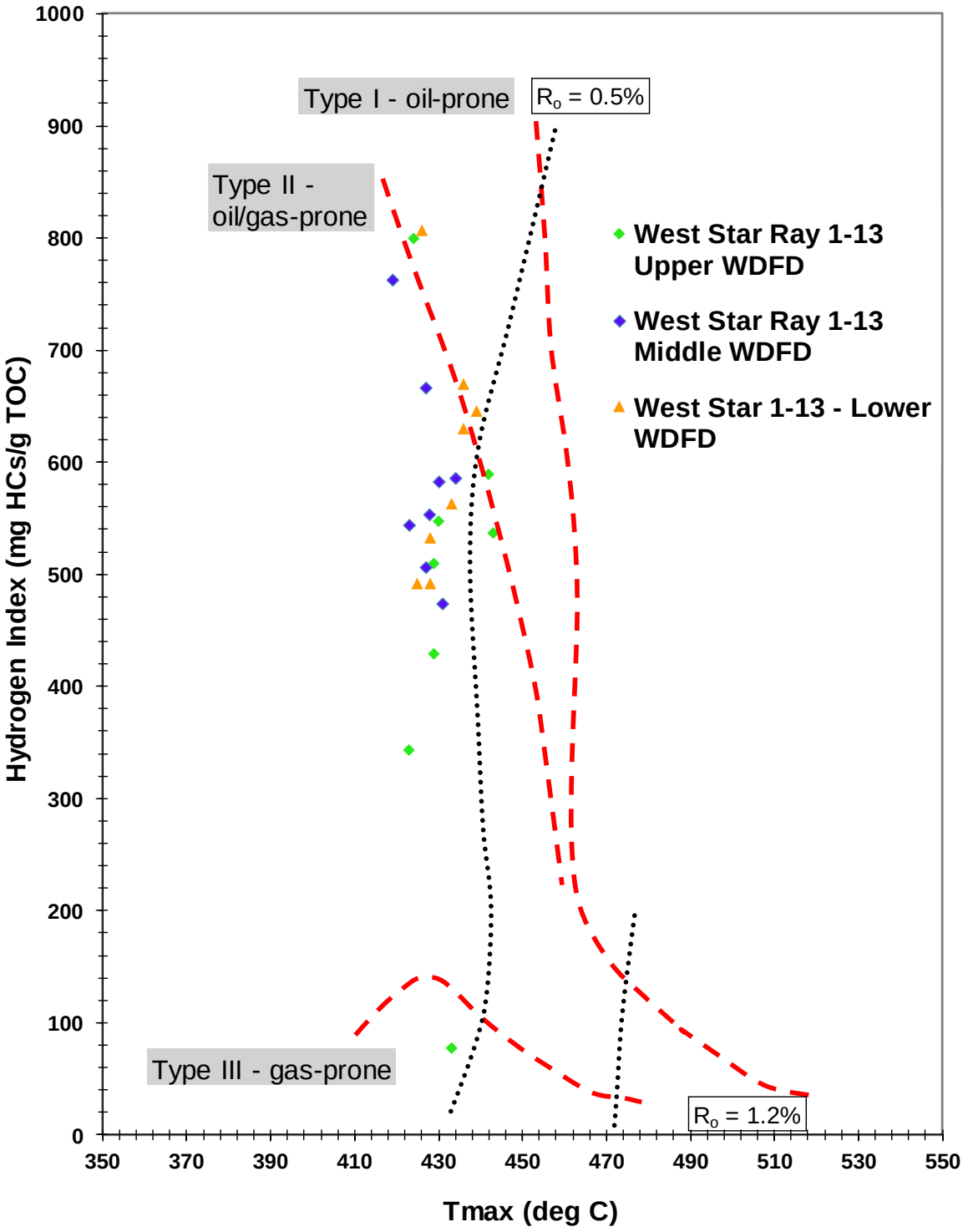

Figure B.23. HI vs. Tmax plot showing maturity and kerogen type for all the 24 Woodford Shale core samples of the West Star Ray 1-13 well. Most of the samples plot on the type II kerogen yield, some in the type I kerogen, most of which are from the Lower Woodford member. All samples are of low thermal maturity; therefore, the kerogen type yields might illustrate depositional organic facies conditions.

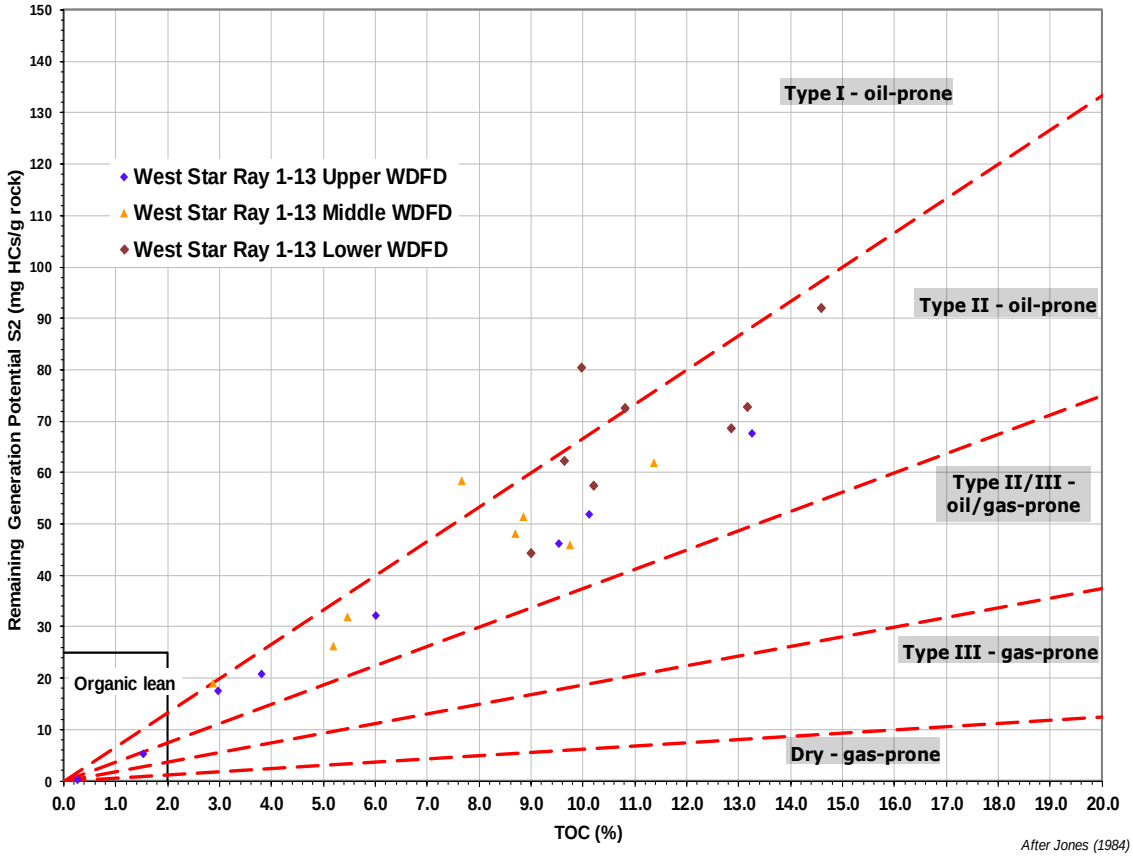

Figure B.24. Rock-Eval remaining hydrocarbon potential (S2) vs. TOC plot for determination of kerogen type and maturity for all the 47 West Star Ray 1-13 Woodford Shale outcrop samples. Note that most of the samples plot in the type II kerogen yield for the Lower and Middle Woodford members, and some type I kerogen yield mainly for the Middle Woodford and Upper member. There are not many apparent type III kerogen samples because of the lack of depletion of S2 by thermal cracking and the low maturity of the samples. Also, there are a few samples that plot in the lean organic area of the Upper Woodford member.

I-35 Upper Woodford outcrop, Carter County.

The outcrop is 3 miles north of Ardmore. TOC varies from 0.45% to 15.7%. Data points are from Becerra-Rondon (2017) and Galvis (2017). The average Tmax of 431.15 °C is close to the oil generation window. Figure B.25 illustrates the variation of TOC, which is high at the base of the Upper Woodford member and starts to decrease towards the middle portion of the Upper member, then increases again in the middle portion and finally decreases towards the Woodford shale top.

The relative hydrocarbon potential (Figure B.25) varies along with the Woodford shale Upper member but drastically increases towards the Upper Woodford top with a final gentle drop, indicating oxic to anoxic depositional conditions in this area.

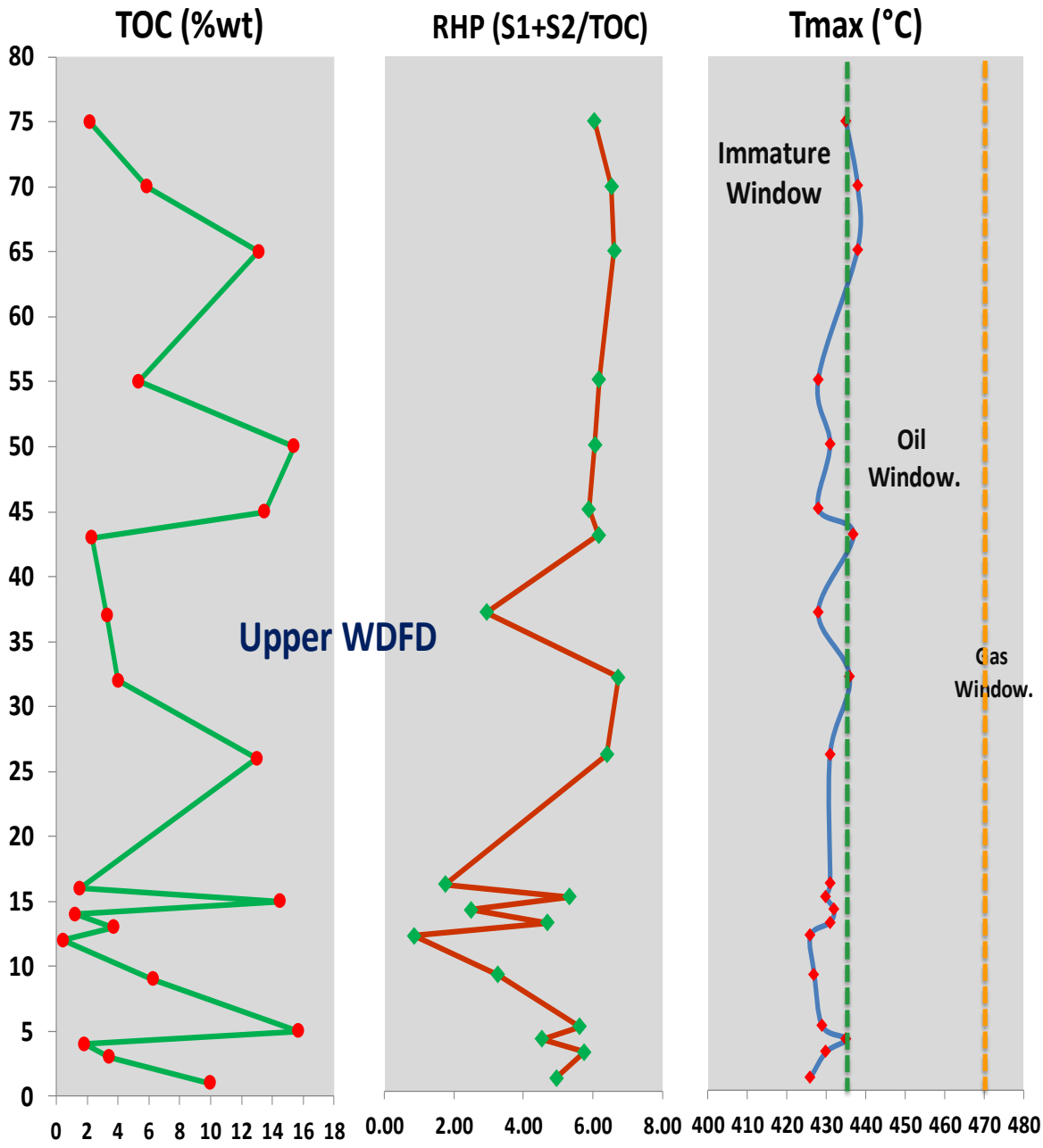

Figure B.25. TOC, relative hydrocarbon potential (RHP), and Tmax maturity variations along the I-35 Upper Woodford member outcrop. Most of the samples are immature (Tmax <435 °C), with an average of 431°C of Tmax. Some samples show early oil generation thermal maturity, especially towards the top.

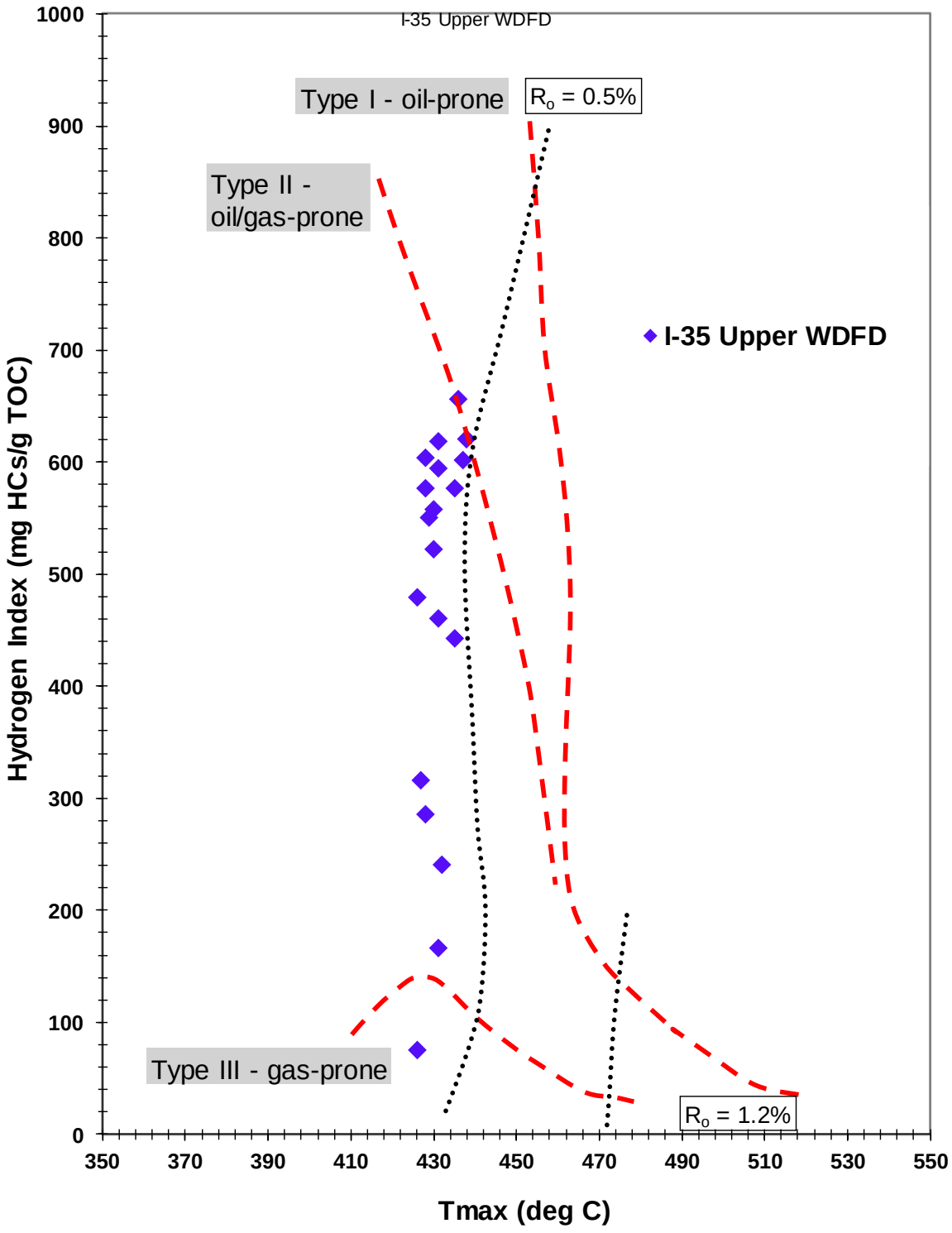

Figure B.26. HI vs. Tmax plot showing maturity and kerogen type for all 20 Woodford shale outcrop samples of the I-35 section. Most of the samples plot on the type II kerogen yield, and two in the type I kerogen. All samples are of low thermal maturity; therefore, the kerogen type yields might illustrate depositional organic facies conditions.

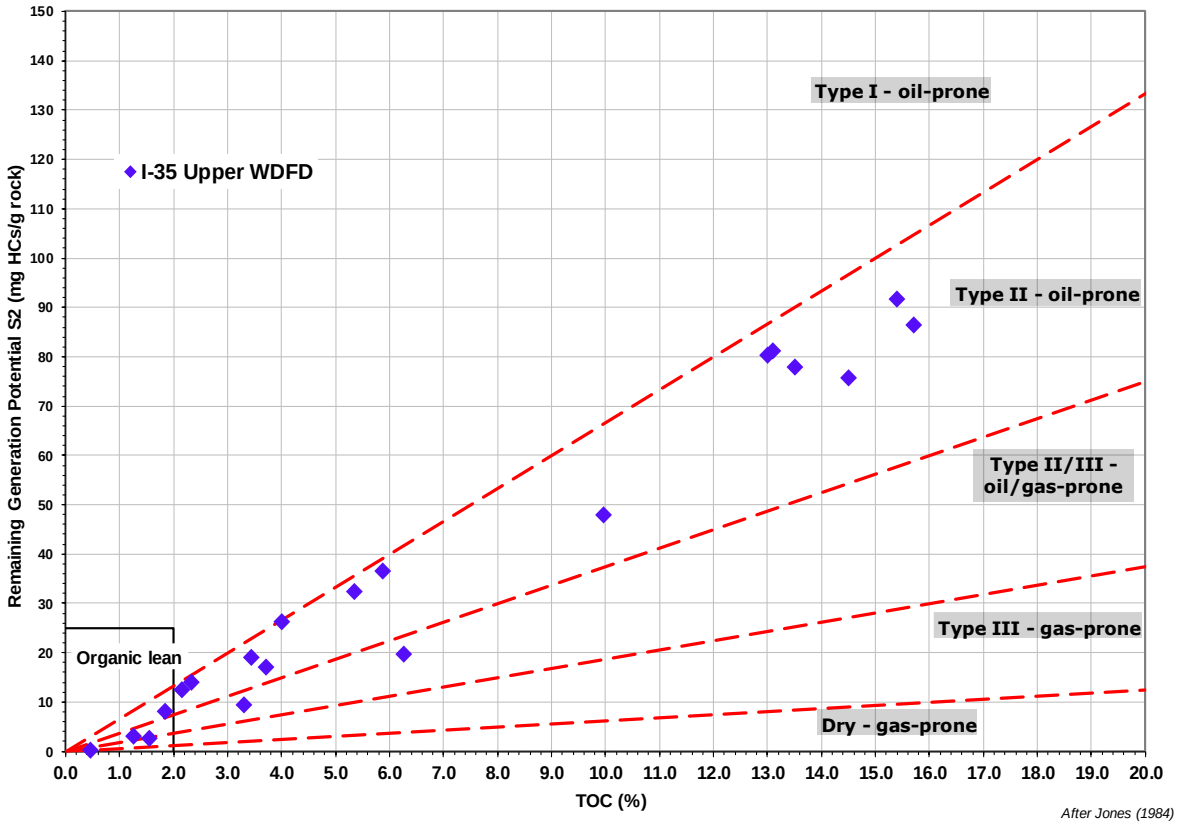

Figure B.27. Rock-Eval remaining hydrocarbon potential (S2) vs. TOC plot for determination of kerogen type and maturity for all the 20 I-35 Woodford Shale outcrop samples. Note that most of the samples plot in the type II kerogen yield, and some are close to the type I kerogen yield. There are some type III kerogen samples attributed to being part of mixed organic matter, because of the lack of depletion of S2 by the thermal cracking and the low maturity of the samples. Also, some samples plot in the lean organic area of the Upper Woodford member.

I-35 Hladik 23 H, Kingfisher Co. Zhang (2016).

These samples are from a 1,300 ft horizontal well of the Woodford Shale, located in south Kingfisher County in Oklahoma. TOC varies from 2.55% to 10.9%. Data points are from Zhang (2016). The average Tmax of 443.5 °C, indicates oil and wet gas window generation. Figure B.28 illustrates the variation of TOC, which is lower at the toe of the well and increases towards the heel of the horizontal well. Relative hydrocarbon potential (Figure B.28) varies along the

Woodford Shale and increases close to the toe of the well, where the horizontal well was landed in the Lower Woodford member (Zhang, 2016).

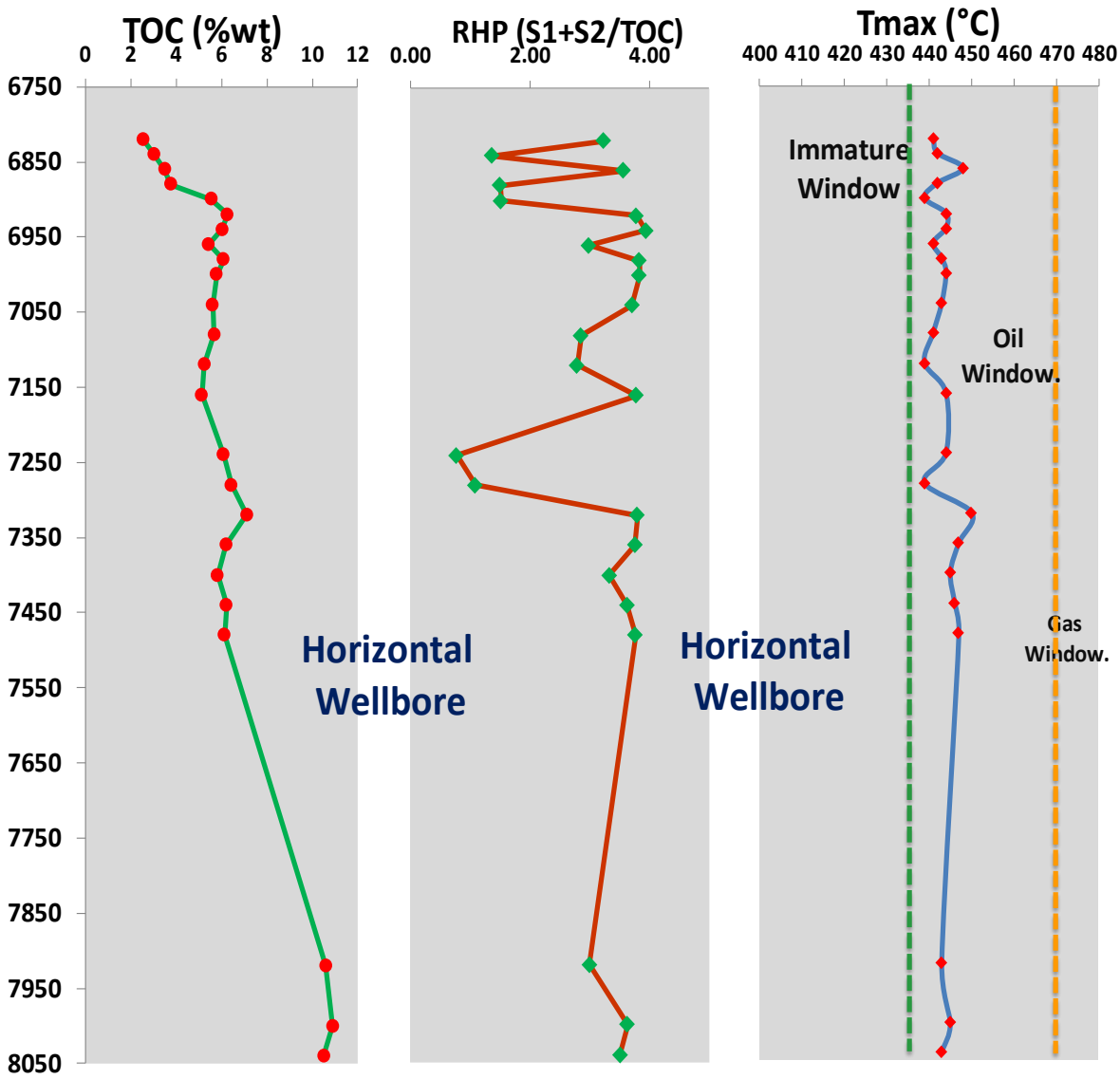

Figure B.28. TOC, relative hydrocarbon potential (RHP), and Tmax maturity variations along the Hladik 23 horizontal well. Horizontal well geosteering profile was not available; it was difficult to understand if the horizontal trajectory kept the wellbore most of the time inside the target zone and therefore, the variations in TOC, RHP, and Tmax can be attributed to lateral facies change, or if this observed changes when increasing the measured depth (MD) correspond to a vertical disparity of the wellbore horizontal section that crosses the Woodford Shale vertical stratigraphic variations. Most of the samples are mature (Tmax >435 °C), with an average of 443.5°C of Tmax. All the samples show early oil generation thermal maturity to peak oil maturity, especially towards the end of the horizontal wellbore.

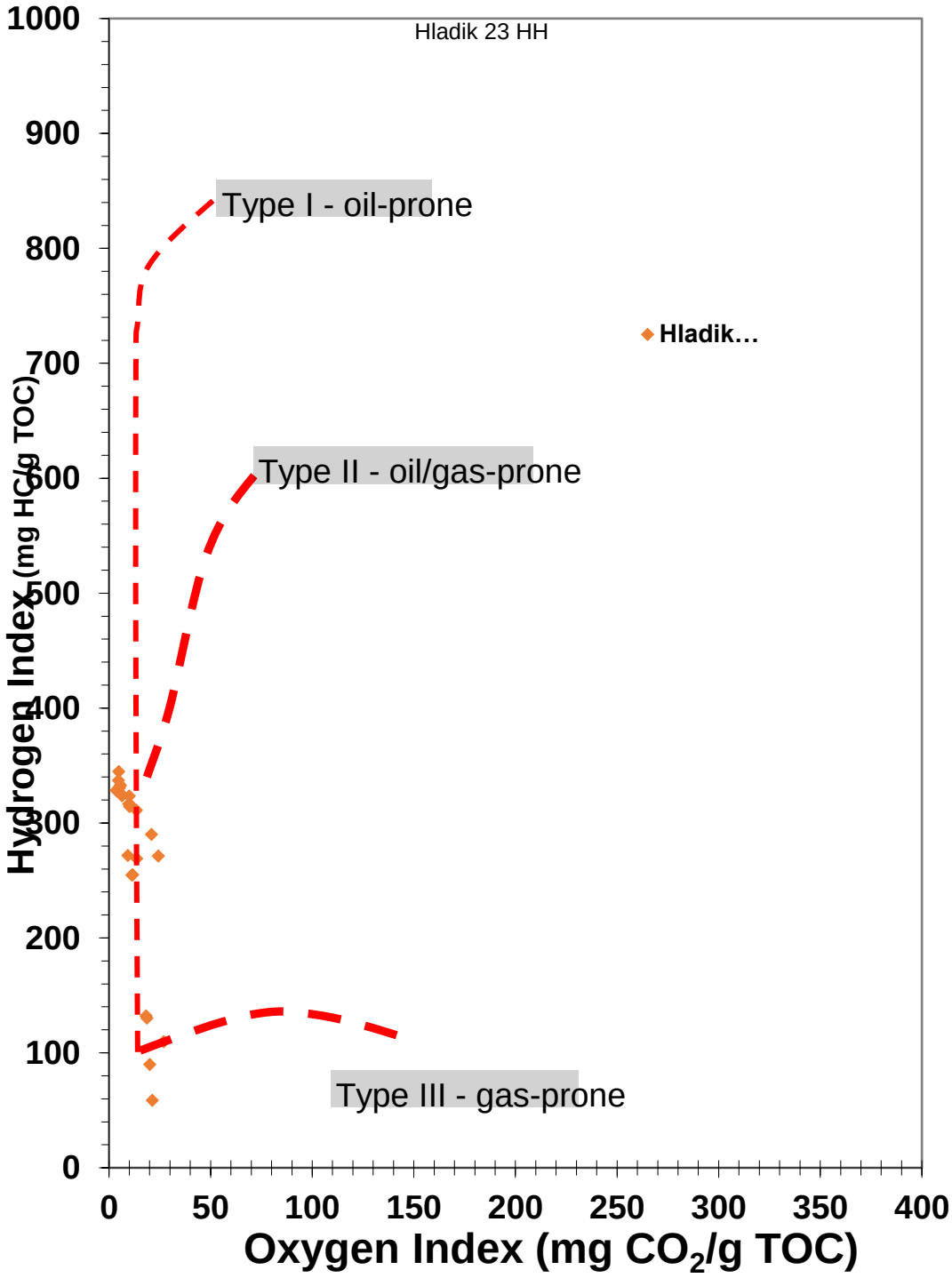

Figure B.29. Modified pseudo van Krevelen diagram for the cutting samples of the horizontal well Hladik 23. The diagram shows the source rock intervals are dominated by apparent type II kerogen — some samples plot in the type III area.

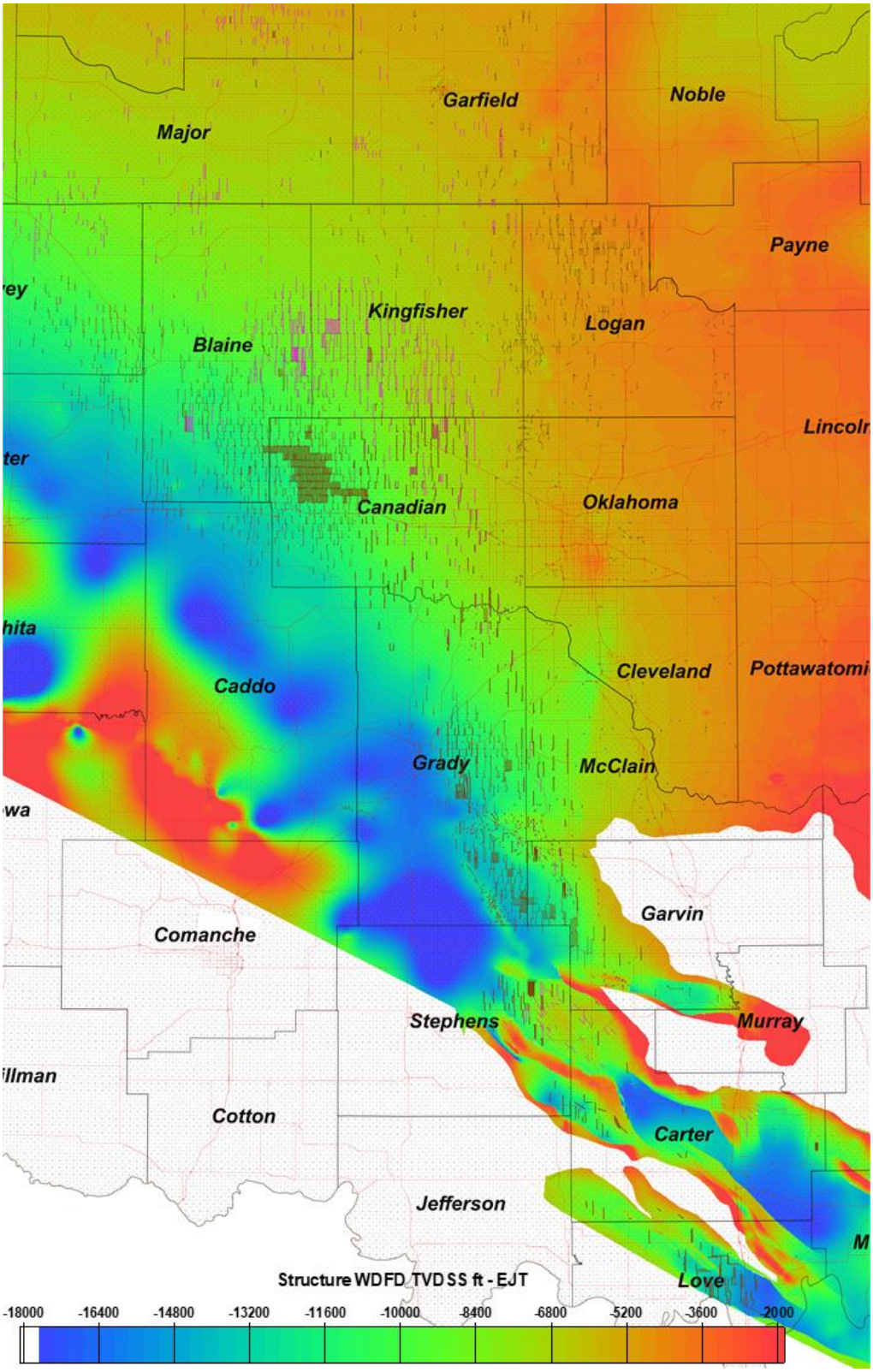

Figure B.30. Regional Woodford Shale structure map [TVDSS ft]. Magenta lines correspond to Mississippian reservoir horizontal wells. Brown lines correspond to Woodford Shale horizontal wells.

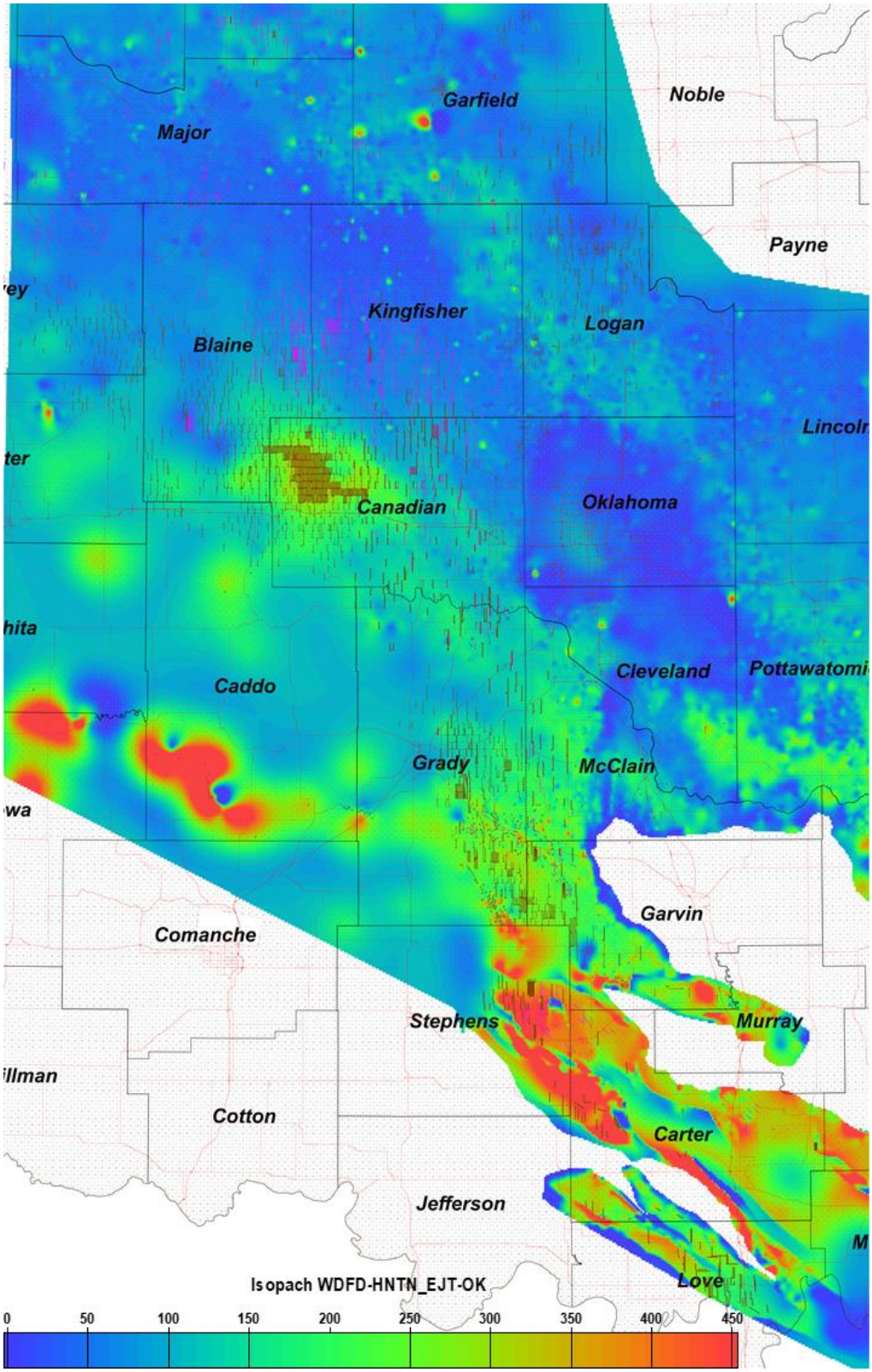

Figure B.31. Regional Woodford Shale gross thickness map [ft]. Magenta lines correspond to Mississippian reservoir horizontal wells. Brown lines correspond to Woodford Shale horizontal wells.

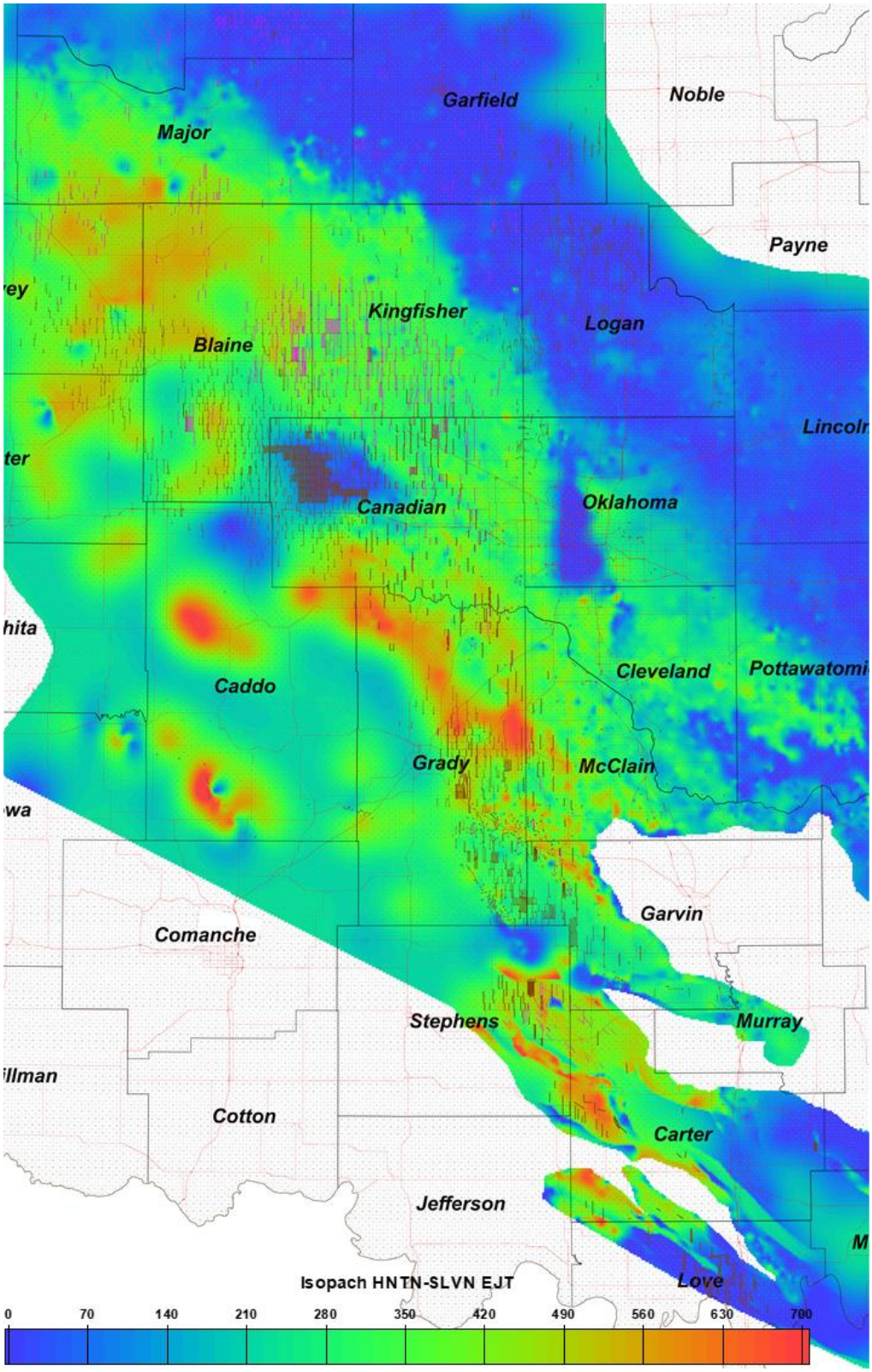

Figure B.32. Regional Hunton group (pre-Woodford Shale) gross thickness map [ft]. Magenta lines correspond to Mississippian reservoir horizontal wells. Brown lines correspond to Woodford Shale horizontal wells.

Conclusions

There are some samples that on the plots seem to contain apparent type I kerogen, indicating a possible lacustrine depositional origin, especially for the Lower and Upper Woodford Shale members in the I-35 outcrop, for the Ray 1-13 core, McAlister Quarry and the Wyche-1 core locations. These samples co-vary with the relative hydrocarbon potential (RHP) as high anoxic intervals. For the other locations, the Woodford Shale organic facies seem to correspond to only type II and type III. These can also be related to the low oxygen content and higher free sulfur that replaces oxygen molecules, therefore indicating an area of apparent lacustrine type organic matter inside the marine Woodford Shale.

Cited References

- Albaghdady, A., 2013.Organic geochemical characterization of source rocks (Sirt Shale) and crude oils from the Central Sirt basin, Lybia. Doctoral dissertation manuscript, The University of Oklahoma, p. 259.
- Chain, A.R., 2012. Stratigraphy and composition of the Woodford Shale in depositionally updip and downdip wells, Anadarko Basin, Oklahoma. M.Sc. thesis manuscript, The University of Oklahoma, p. 138.
- Connock, G.T., 2015. Paleoenvironmental Interpretation of the Woodford Shale, Wyche Farm shale pit, Pontotoc County, Arkoma Basin, Oklahoma With Primary Focus on Water Column Structure. M.Sc. thesis manuscript, The University of Oklahoma, p. 266.
- Connock, G.T., Nguyen, T.X., and R.P. Philp, 2018. The development and extent of photic-zone euxinia concomitant with Woodford Shale deposition. AAPG Bulletin 102, 6, 959-986.
- DeGarmo, D., 2015. Geochemical characterization of the Woodford Shale (Devonian-Mississippian), McAlister cemetery quarry, Criner Hills uplift, Ardmore basin, Oklahoma. M.Sc. thesis manuscript, The University of Oklahoma, p. 223.
- Demaison G.J., and Moore G.T., 1980. Anoxic environments and oil source bed genesis. American Association of Petroleum Geologists Bulletin 64, 8, 1179-1209.

- Fang, H., Jianyu, C., Yongchuan, S., and Yaozong, L., 1993. Application of organic facies studies to sedimentary basin analysis: a case study from the Yitong Graben, China. Organic Geochemistry 20, 1, 27-42.
- Hunt J. M.,1996. Petroleum Geochemistry and Geology, 2nd ed. Freeman, New York.
- Hunt, J.M., Philp, R.P., and Kvenvolden, K.A., 2002. Early developments in petroleum geochemistry. Organic Geochemistry 33, 1025–1052.
- Jones, R.W. 1984. Comparison of carbonate and shale source rocks in petroleum geochemistry and source rock potential of carbonate rocks. In: Palacas, J.G., eds, AAPG Studies in Geology 18, 163-180.
- Lo Monaco, G.A., 2012. Characterization of the Mississippian Barnett Shale formation well, using organic geochemistry parameters and their relationship with different lithofacies, Fort Worth basin, Texas. M.Sc. thesis manuscript, The University of Oklahoma, p. 106.
- Magoon L. B. and W. G. Dow, 1994. The petroleum system, in L. B. Magoon and W. G. Dow, eds., The petroleum system - from source to trap: AAPG Memoir 60, p. 3-24
- Magoon, L. B., and G. E. Claypool, 1983. Petroleum geochemistry of the North Slope of Alaska - Time and degree of thermal maturity. In: Bjorøy, M., eds., Advances in organic geochemistry, Chichester, U.K., Wiley Heyden, 28-38.
- Miceli-Romero, A.A, 2010. Geochemical characterization of the Woodford Shale, central and southeastern Oklahoma. M.Sc. thesis manuscript, The University of Oklahoma, p. 149.
- Miceli-Romero, A.A., and Philp, R.P., 2012. Organic geochemistry of the Woodford Shale, southeastern Oklahoma: How variable can shales be? AAPG Bulletin, 96, 3, 493-517.
- O'Brien, N. R., and Slatt, R. M.,1990. Argillaceous Rock Atlas, Springer-Verlag, N.Y., p. 141.
- Peters, K.E., and Cassa, M.R., 1994. Applied source rock geochemistry. In: Magoon, L.B., and Dow, W.G., eds., The petroleum system – from source to trap, American Association of Petroleum Geologists Memoir 60, 93-117.
- Peters, K.E., Walters, C.C., and Moldowan, J.W., 2005a. The biomarker guide, Volume 1, Biomarkers, and isotopes in the environment and human history. Cambridge University Press, New York, second edition, p. 1155.
- Peters, K.E., Walters, C.C., and Moldowan, J.W., 2005b. The biomarker guide, Volume 2, Biomarkers, and isotopes in petroleum exploration and earth history. Cambridge University Press, New York, second edition, p. 471.

- Peters, K. E., Magoon, L. B., Valin, Z. C., and Lillis, P.G., 2007, Source-rock geochemistry of the San Joaquin basin province, California. In: Hosford-Scheirer, A., eds., Petroleum systems and geologic assessment of oil and gas in the San Joaquin basin, California. U.S. Geological Survey Professional Paper 1713, 11, 1-102.
- Philp, R.P., 2003. Formation and geochemistry of oil and gas. Treatise on Geochemistry 7, p. 223-256.
- Serna-Bernal, A., 2013. Geological characterization of the Woodford Shale, McAlister Cemetery quarry, Criner Hills, Ardmore basin, Oklahoma. M.S. Thesis manuscript, The University of Oklahoma, p. 141.
- Slatt, R. M., and Rodriguez, N. D., 2012. Comparative sequence stratigraphy and organic geochemistry of gas shales: Commonality or coincidence? Journal of Natural Gas Science and Engineering 8, 68-84.
- Tissot, B. P., 1984. Recent advances in petroleum geochemistry applied to hydrocarbon exploration. American Association of Petroleum Geologists Bulletin 70, 5, 545 – 563.
- Tissot, B.P., and Welte, D.H., 1984. Petroleum formation and occurrence. Berlin Springer-Verlag, p. 699.
- Tyson, R.V., and Pearson, T.H, 1991. Modern and ancient continental shelf anoxia: an overview. Geological Society of London, Special Publications 58, 1-24.
- Villalba, D.M., 2016. Organic geochemistry of the Woodford Shale, Cherokee platform, Oklahoma, and its role in a complex petroleum system. M.Sc. thesis manuscript, The University of Oklahoma, p. 126.
- Welte, D. H., 1972. Petroleum exploration and organic geochemistry: Journal of Geochemical Exploration 1, 117-136.
- Zhang, J., 2016. Comprehensive reservoir characterization of the Woodford Shale in parts of Garfield and Kingfisher Counties, Oklahoma. M.S. thesis manuscript, The University of Oklahoma, p. 144.

Appendix D: Organic compound structures in literature and in Chapter III biomarker analysis.

I: C_{17} n-Alkane

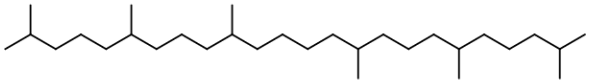

II: Squalene (tail-to-tail example)

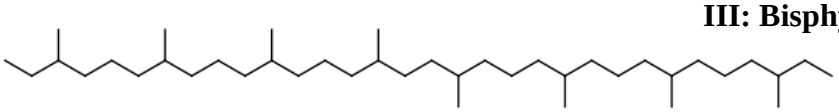

III: Bisphytane (head-to-head)

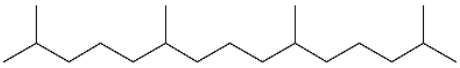

IV: Pristane

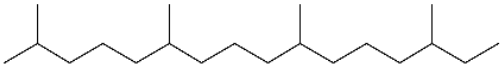

V: Phytane

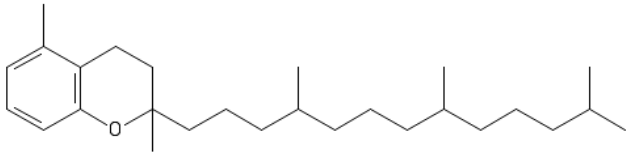

VI: MTTC

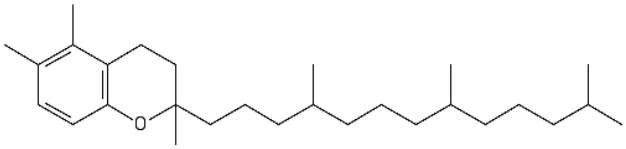

VII: diMe-MTTC

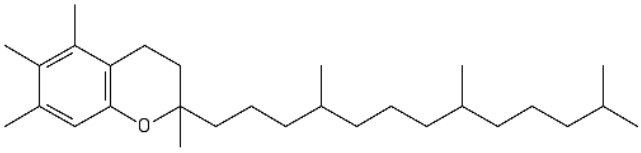

VIII: triMe-MTTC

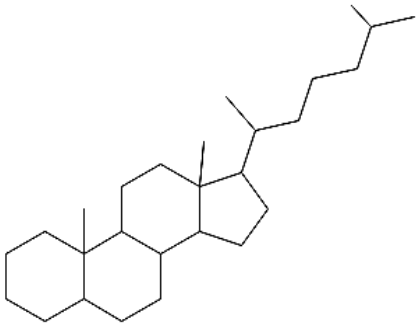

IX: C_{27} Sterane

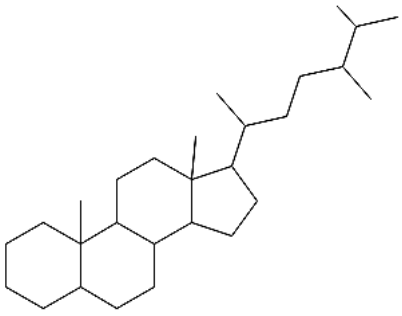

X: C_{28} Sterane

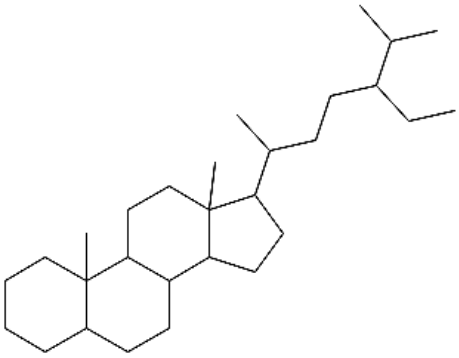

XI: C_{29} Sterane

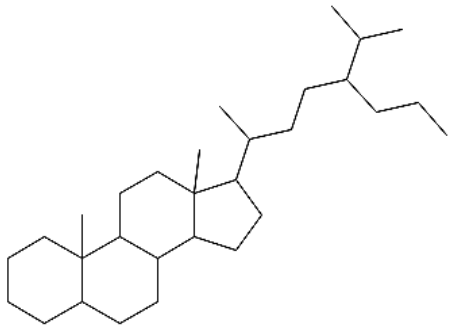

XII: C_{30} Sterane

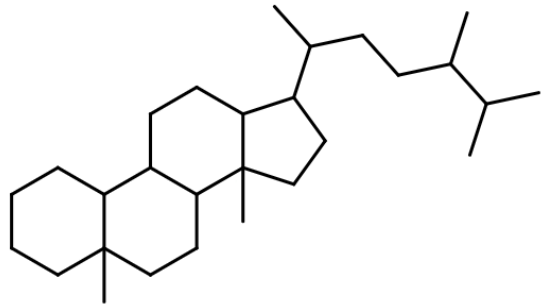

XIII: C27 Diasterane

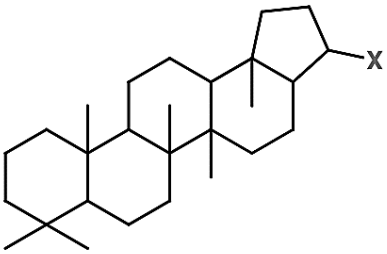

XIV: Hopane

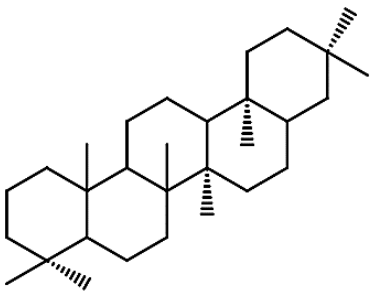

XV: Gammacerane

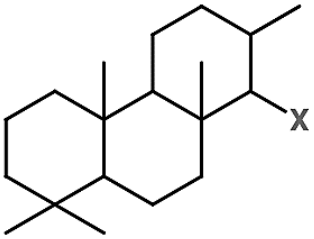

XVI: Tricyclic Terpane

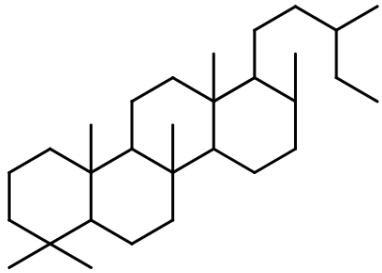

XVII: Tetracyclic Polyprenoid (C_{30})

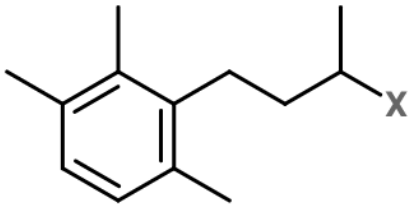

XVIII: 2,3,6- trimethylbenzene

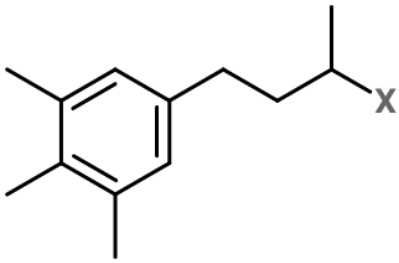

XIX: 3,4,5- trimethybenzene

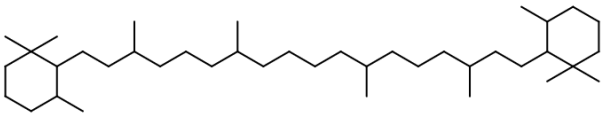

XX: B-Carotane

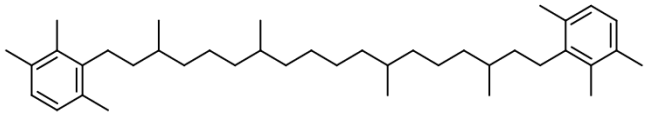

XXI: Isorenieratane

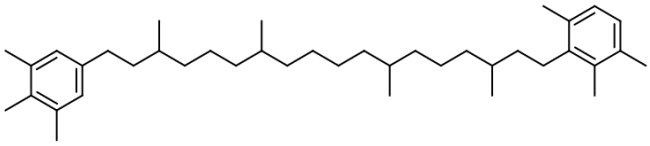

XXII: Paleorenieratane

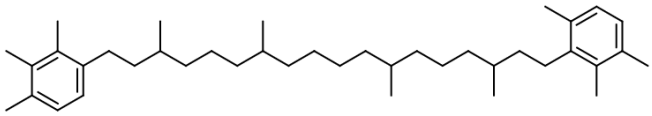

XXIII: Renieratane

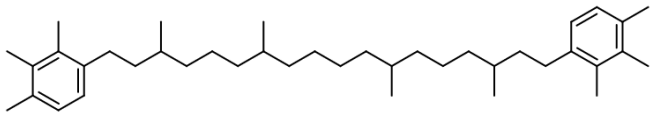

XXIV:

Renierapurpurane

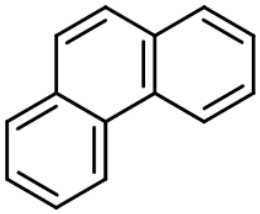

XXV: Phenanthrene

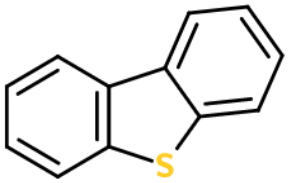

XXVI: Dibenzothiophene

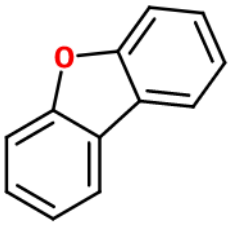

XXVII: Dibenzofuran

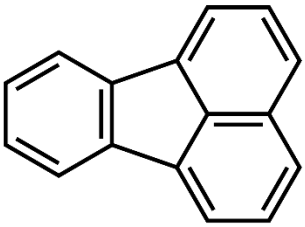

XXVIII: Fluoranthene

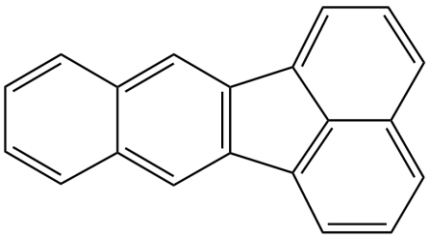

XXIX:

Benzo(k)fluoranthene

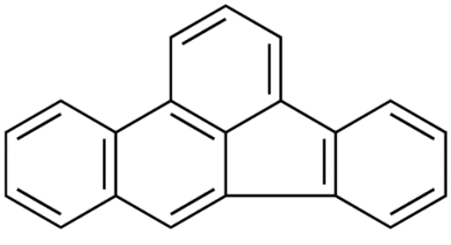

Benzo(b)fluoranthene

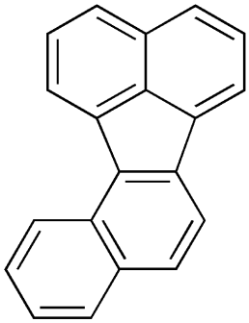

Benzo(j)fluoranthene

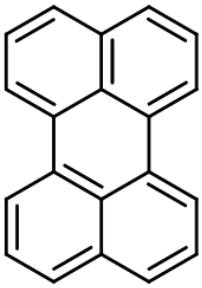

XXX: Perylene

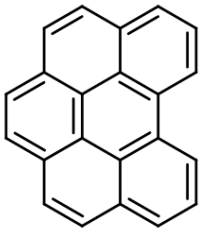

XXXI: Benzo(g,h,i)perylene

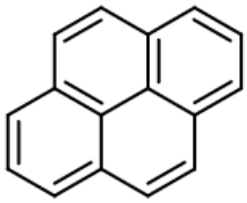

XXXII: Pyrene

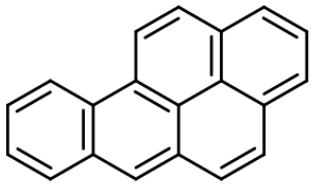

XXXIII: Benzo(a)pyrene

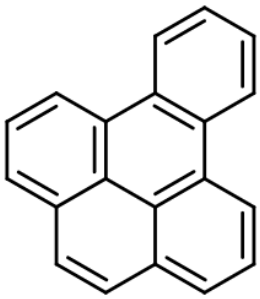

Benzo(e)pyrene

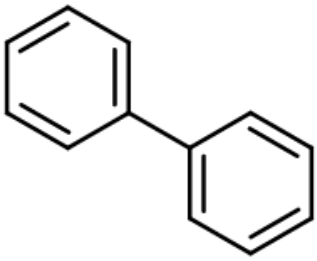

XXXIV: Biphenyl

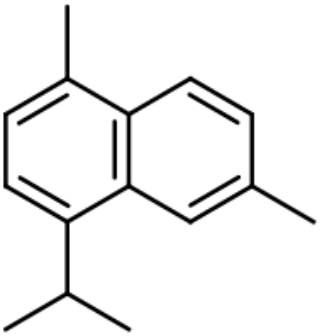

XXXV: Cadalene

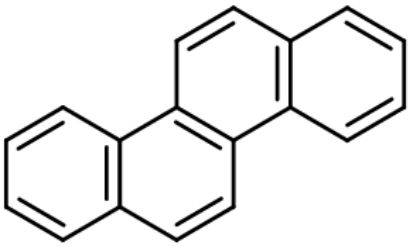

XXXVI: Chrysene

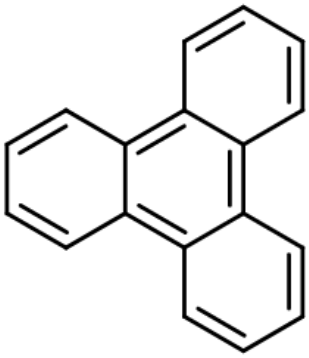

XXXVII: Triphenylene

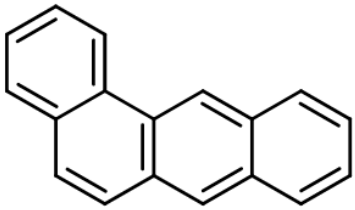

XXXVIII: Benzoanthracene

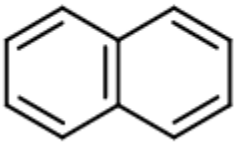

XXXIX: Naphthalene

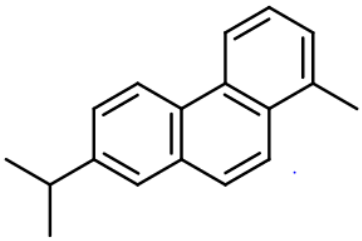

XXXX: Retene